THE STRUCTURE AND PETROLOGY OF THE SAN JOSÉ PLUTON NORTHERN BAJA CALIFORNIA, MEXICO

Thesis by

Jay Dennis Murray

In Partial Fulfillment of the Requirements

for the Degree of

Doctor of Philosophy

California Institute of Technology

Pasadena, California

1978

(Submitted February 22, 1978)

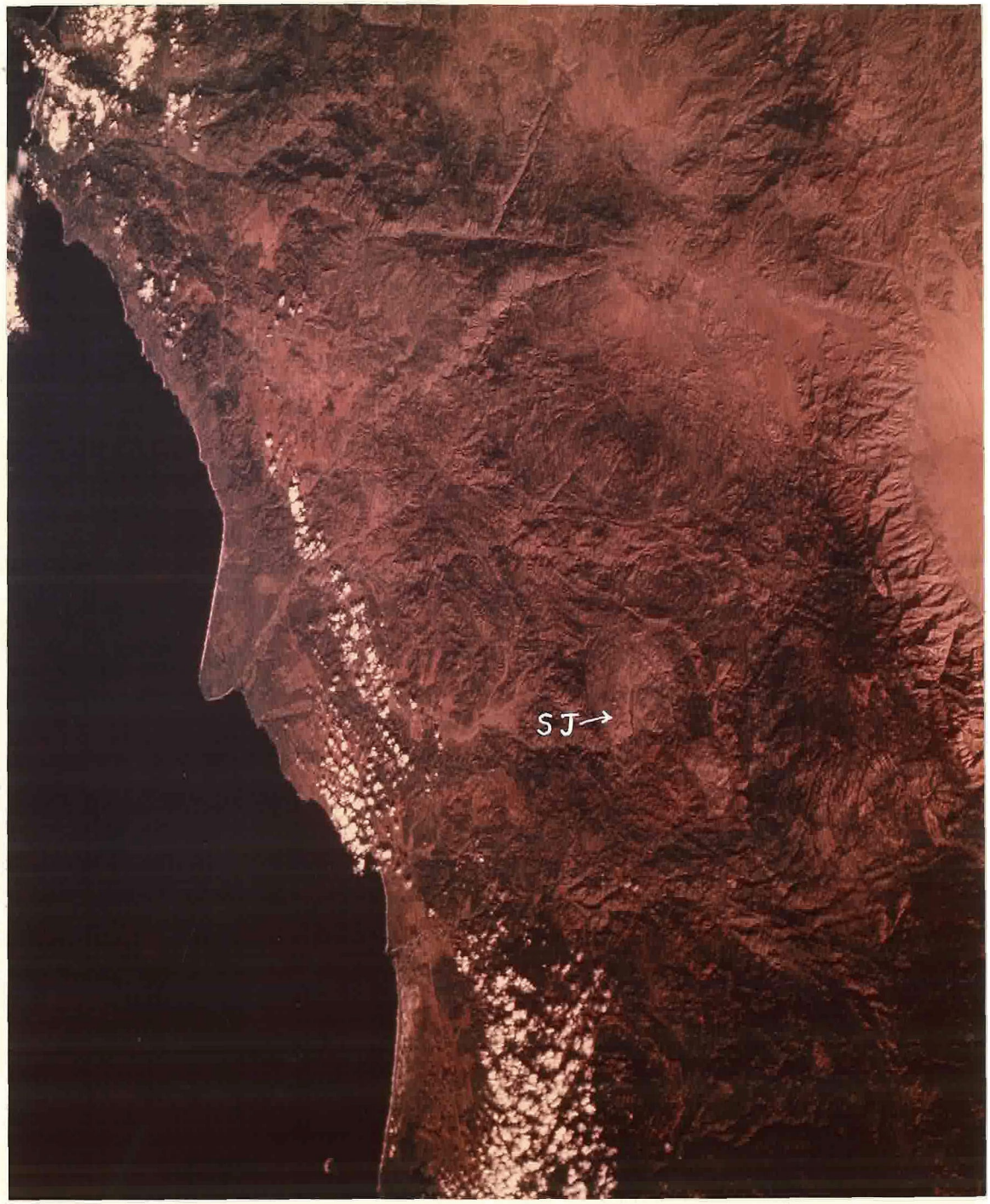

San José and surrounding areas of northern Baja California as seen from the Apollo 7 satellite (frame AS7-7-1795). North is parallel to the sides of the photograph, and Ensenada is in the northwestern corner. The area of the photograph is outlined in Figure 1. The prominent light-colored ovoid body (SJ) in the center of the frame is the San José pluton. Several other plutons are visible north and east of San José. Northwest-southeast linear features in the center of the photograph are parallel to bedding in the pre-batholithic strata.

To Donald B. Potter
who introduced me to geology,

and to W. Scott Baldridge and Clay M. Conway
each of whom has contributed his knowledge
and personal friendship.

ACKNOWLEDGMENT

Foremost, I wish to express my gratitude to Professor Leon T. Silver, who introduced me to the San José area, and whose geologic insight, guidance, and enthusiasm were instrumental in the successful completion of this project. Clay M. Conway and Thomas H. Anderson also deserve special thanks for many long and animated discussions of the structural and petrologic ideas, as does L. Peter Gromet, whose frequent discussions of magmatic genesis and differentiation, particularly the application of trace element geochemistry to these problems were especially valuable.

Many individuals assisted on brief excursions in the field, including W. Scott Baldridge, Raymond L. Joesten, Clay Conway, Peter Gromet, Tom Anderson, George R. Rossman, Robert Root, Michael Meling, and James Hopper. Their interest and help is greatly appreciated. I am also grateful to Douglas L. Smith and Robert F. Roy for providing drill core from a heat-flow hole in the center of the pluton, and to Doug Smith for several productive expeditions on mule-back and foot through the Sierra San Pedro Mártir.

Janet Boike assumed the task of typing the manuscript, perhaps not fully anticipating the magnitude of this undertaking, and I greatly appreciate her cheerful cooperation and effort. Guidance in the preparation of illustrations was provided by Janet Scott, who also personally drafted numerous illustrations during the final days of manuscript preparation. Ricardo Dagonel printed many of the photographs.

Finally, I extend my very warm thanks to Aida Meling Barré and

Mary Meling Saldana of Rancho Meling (San José) who truly provided a second home and family for me during many months in Mexico. My days at Rancho Meling, with its many other residents and visitors, will remain among the most memorable in my life.

Field work was funded in part by Penrose Bequest Research Grants 1310-69 and 1449-70. The remaining field work and the laboratory studies were supported by a variety of grants to Leon T. Silver: National Science Foundation Grants EAR76-23153, GA-40858, and GA-15989; National Aeronautics and Space Administration Contract NAS-9-13960; and The United States Atomic Energy Commission Contract AT(04-3)-767. A combination of National Science Foundation Fellowships and both research and teaching assistantships provided tuition and subsistence support.

ABSTRACT

The San José pluton, a 117-km^2 body of medium-grained biotite-hornblende tonalite in the foothills of the Sierra San Pedro Mártir, northern Baja California, Mexico, is one of the more westerly plutons in the Cretaceous Peninsular Ranges batholith. The pluton has a teardrop form in plan view, elongate north-south and outlined by commonly well-exposed contacts. To the north the outline is remarkably hemi-circular and concordant to isoclinally folded, highly stretched strata. Traced southward, the form becomes increasingly discordant and tapers irregularly to a point. The wall rocks consist of tuffs, tuffaceous sedimentary rocks, and lesser amounts of marble, volcanic flows, and hypabyssal intrusive rocks of primarily basaltic to andesitic composition. Aptian and Albian fossils place the strata in the lower Cretaceous. Hornblende-hornfels facies assemblages are developed near the pluton contacts, but lower greenschist facies assemblages prevail outside the contact aureole.

Detailed field and laboratory studies indicate that the pluton is chemically and mineralogically very uniform. The mapping has revealed, however, three texturally distinguishable lithologies each of significant areal extent and coherent form. (1) An interior core of prismatic hornblende tonalite (PHbT) is characterized by elongate prismatic hornblende, thin platy biotite, and a seriate grain-size distribution. (2) An outer horseshoe-shaped partial shell of stubby hornblende tonalite (SHbT) characterized by equant, equigranular, and anhedral poikilitic hornblende and biotite surrounds the PHbT.

Together these units comprise the northern two thirds of the body. (3) A seriate porphyritic tonalite (SPT) phase distinguished from the PHbT by the presence of sparse phenocrystic plagioclase grains 6-20 mm in size forms the discordant southern wedge.

These major lithologic types represent two, or possibly three, distinct intrusive pulses. Conclusive evidence of the relative ages of the SHbT and PHbT intrusive units is lacking. However, the relationships of both units to several narrow zones of diorite and inclusion-rich tonalite associated with their mutual contact in the northeast, together with the scattered occurrence throughout the interior PHbT unit of inclusions of wall-rock lithologies similar to those around the northern and eastern margins of the pluton, strongly suggest that the SHbT is the younger mass and was emplaced around the perimeter of a pre-existing PHbT pluton. The SPT is completely gradational, both structurally and petrographically, into the PHbT, but is not exposed in contact with the SHbT. The SPT appears to be the youngest of the three units and may be either a late phase of the PHbT intrusive pulse or a separate pulse intruded prior to complete solidification of the PHbT.

The SHbT and PHbT units appear to have been emplaced almost entirely by forceful shouldering aside of the wall rocks. The effects of the penetrative deformation and distension of the wall rocks accompanying intrusion (and enhanced by externally-imposed deformation) are intense around the northern contact. These effects decrease gradually southward, giving way to predominantly brittle deformation within the wall rocks around the southern and particularly the south-

western margins. Emplacement of the SPT involved large-scale stoping as well as lateral displacement of the strata. Altogether, stoping appears to have contributed no more than 5-10% to the exposed area of the pluton.

Magmatic flow plus marginal protoclasis produced an unusually regular pattern of northward-convex, arcuate foliation in the northern two thirds of the pluton. Foliation is gneissose and conformable to the contact near the pluton margins and decreases to weak in the interior. The dip of foliation changes systematically from steeply outward around the margins through vertical to inward dipping in the interior. Traced southward into the SPT, foliation becomes faint or unrecognizable, the dip increases gradually again to vertical, and the pattern becomes only vaguely concentric and not obviously related everywhere to the local contacts. There is a suggestion of closure (in plan view) of vertical foliation attitudes around the probable center of latest intrusion in the interior of the SPT.

This foliation pattern suggests a funnel-shaped geometry of intrusion of PHbT and SPT magmas rising through relatively narrow conduits and expanding primarily to the north and east at essentially the final level of emplacement. The center of intrusion apparently migrated slightly southward with time from the interior of the PHbT into the center of the SPT. The SHbT was emplaced separately around the margins of the PHbT prior to intrusion of much or all of the SPT. Again expansion was preferentially to the north and east.

The pattern of deflection of wall rocks around the pluton also indicates predominantly northward and eastward expansion; lesser

southward expansion was limited to late fracture-controlled breaking out of the SPT magma from the concordant confines of the northern masses.

Petrographic and structural observations indicate that preferred mineral orientation developed primarily by rotation of crystals in the magma rather than by solid-state deformation and recrystallization. However, flow deformation may have continued locally after the completion of magmatic crystallization, particularly in the protoclastic gneissose rocks.

Variations in the intensity of foliation and protoclasis in the tonalite and of penetrative deformation and distension in the wall rocks are attributed in large part to the history of progressive intrusion and asymmetric expansion. However, the pluton was apparently syntectonic, and externally-imposed deformation not directly related to emplacement of the San José pluton also contributed to the deformation of the wall rocks and outer parts of the tonalite, particularly around the northern and eastern margins. Systematic lineation patterns developed in both the wall rocks and the marginal gneissose tonalite in the latter areas suggest two sources of externally-imposed deformation: (1) southward expansion or shoving of the nearby Las Cochas pluton towards the northern margin of the San José pluton, and (2) deformation directed apparently upward and southwestward from the northeast and east, possibly in response to plutonic emplacement or regional uplift in the Sierra San Pedro Mártir.

Although the oval outline and striking concordance of the pluton may be superficially suggestive of *en masse* diapiric emplacement,

as opposed to gradual rise of magma through narrow channelways and balloon-like expansion at the final level of emplacement, the asymmetry of both the foliation pattern in the tonalite and the deformation of the wall rocks appears inconsistent with such a mechanism.

Mineralogically, the tonalite consists on the average of 64% plagioclase, 16% quartz, 11% hornblende, 5-6% biotite, and <0.3% alkali feldspar. Plagioclase, zoned from cores of An_{40-45} to rims of An_{20-30}, was the principal liquidus phase, accompanied by minor clinopyroxene in the SHbT and by hornblende and locally minor clinopyroxene in the PHbT and SPT. Biotite crystallized as a late interstitial or poikilitic phase primarily in coexistence with hornblende rather than as a reaction product. The trace amounts of late interstitial alkali feldspar (sanidine-orthoclase) are unusually potassic (Or_{90-95}) and do not appear to have crystallized in equilibrium with plagioclase; much or all of the potassium feldspar and possibly some of the biotite may have crystallized from a late-stage exsolved vapor phase.

The assemblage of opaque minerals -- nearly pure magnetite coexisting with complex lamellar intergrowths of titano-hematite and ferrian-ilmenite -- implies crystallization under unusually oxidizing conditions apparently approaching those of the $MnO-Mn_3O_4$ buffer during much of crystallization, and increasing to those of the hematite-magnetite buffer at near-solidus conditions. Low Fe/(Fe + Mg) ratios in biotite (0.40-0.44), hornblende (0.32-0.36), and relict clinopyroxene (0.23-0.26) and low whole-rock $FeO/(Fe) + Fe_2O_3$) ratios (0.408-0.515) also record unusually oxidizing conditions. Textural characteristics distinguishing the SHbT phase, on the one hand, from the PHbT and SPT phases, on the other, appear to be

due to slight differences in f_{O_2}, f_{H_2O}, and possibly temperature throughout all but the late stages of crystallization (SHbT magma drier, less oxidizing, and possibly slightly hotter).

Both the modal and chemical data confirm the petrologic significance of the textural units defined in the field. Together the PHbT and SPT define one set of variation trends which, for a given SiO_2 or modal quartz content, are characterized by slightly higher normative or modal plagioclase content and slightly lower normative or modal color index than the combined trends of the SHbT and its gneissose border phase. The SPT samples show a much more restricted range of modal and chemical compositions than do the PHbT samples, supporting the identification of the SPT as a third unit closely related to the PHbT. The composition of the outer gneissose phase of the SHbT is also distinctive, being slightly more felsic rather than more mafic than the rest of the tonalite.

Despite the systematic compositional distinctions and the evidence for at least two, possibly three separate pulses of intrusion, both the modal and chemical compositions are remarkably uniform. SiO_2 contents range from 59.4 to 65.2% (exclusive of the gneissose border rocks). Variations in other elements are correspondingly much smaller. The SHbT and SPT, in particular, are both exceptionally homogeneous, with SiO_2 contents consistently in the ranges 60.1-62.0 and 61.8-64.1%, respectively. Yet both the strong compositional zoning in plagioclase and the sequence of mineral crystallization indicate that the composition of the melt changed considerably as crystallization proceeded. The homogeneity of the tonalite, particularly within the individual textural units, therefore implies highly viscous magmas in which processes of

segregation or differential migration of crystals relative to melt (e.g., gravity settling or flow differentiation) were generally ineffective except on a small scale (local schlieren). Multiple emplacement of such large volumes of homogeneous magmas, rising essentially through the same conduit, without visible association of materials with other compositions argues strongly that the tonalite magmas were generated as primary magmas.

Chemically, the tonalite is characterized by a calcic alkali-lime index (63); high Na_2O and low K_2O contents (average: 4.82 and 0.74%, respectively), hence high Na_2O/K_2O ratios (average: 6.51); high Al_2O_3 and normative plagioclase contents (18.17 and 66.37%, respectively); and low $FeO/(FeO + Fe_2O_3)$ ratios (average: 0.463). The pluton is depleted in Rb, U, Th, and rare earth elements, and the $^{87}Sr/^{86}Sr$ initial (0.7036) and Pb isotopic ratios (206/204 = 18.56, 207/204 = 15.58, and 208/204 = 38.19) are relatively unradiogenic. The low concentrations of K and other incompatible elements and the relatively unradiogenic Sr initial and Pb isotopic ratios rule out significant contribution from older sialic crust or related sedimentary rocks. Partial melting of a material chemically similar to ocean floor (ocean ridge or abyssal) basalt, whether subducted oceanic crust or basaltic areas in the overlying mantle or lower crust, appears to best satisfy all of the compositional constraints.

TABLE OF CONTENTS

Table of Contents (continued)

Table of Contents (continued)

Table of Contents (continued)

Table of Contents (continued)

Table of Contents (continued)

LIST OF FIGURES

LIST OF TABLES

LIST OF PLATES
(in Pocket)

PART I

INTRODUCTION AND REGIONAL SETTING OF THE SAN JOSÉ PLUTON

Chapter 1

INTRODUCTION

1.1 Purpose and Scope of the Study

Large volumes of calcic and calc-alkaline igneous rocks, both volcanic and plutonic, are characteristic of many island arcs and continental margins. There are no better examples of the plutonic manifestation of calcic and calc-alkaline magmatism than the large Mesozoic batholiths of western North America. Although much information has been gathered on these batholiths, particularly on the Sierra Nevada batholith, detailed studies of individual plutons are few. The present investigation combines detailed field work with extensive petrographic, modal, and chemical study of a single tonalite pluton, the San José pluton.

The principal topics considered in this study are: (1) The field relationships of the pluton and the mechanisms and history of emplacement; (2) the nature and origin of preferred mineral orientation in the pluton and how this relates to both the regional tectonic regime and the degree of crystallization of the magma at the time of emplacement; (3) the modal and chemical variations in the pluton and how they relate to textural and structural variations; (4) the trend and controls on magmatic differentiation, including the sequence of mineral crystallization, the effectiveness of mechanisms of separation of crystals from melt, and the apparent effects of such intensive parameters as f_{O_2} and f_{H_2O}; and (5) the implications of these data for the possible origins of the tonalite magma. The ultimate goal is to better

understand the emplacement, crystallization, differentiation, and genesis of tonalitic and related magmas and the relationship of these magmas to the general tectonic and petrologic evolution of magmatic arcs on continental margins.

The Peninsular Ranges of southern California and Baja California (Figure 1) provide an excellent site for studying these topics. Much of the area is underlain by a thick section of meta-sedimentary and meta-volcanic strata which has been subjected to only one major cycle of deformation, metamorphism, and plutonism. Except along the eastern margin of the ranges, pre-Mesozoic rocks have not been unequivocally recognized; in fact, there may be no pre-Jurassic rocks in most of Baja California del Norte. The Cretaceous Peninsular Ranges batholith, which is intruded into these strata, has experienced relatively little subsequent modification other than weathering, erosion and late Cenozoic faulting. Thus the processes and events in the evolution of a magmatic arc and the chemical, petrographic, and structural characteristics of the rocks comprising the arc can be recognized without the serious complications which may result from multiple cycles of magmatism or orogeny.

The San José pluton is a particularly attractive intrusive to study. It is one of many geographically separate plutons intruded into lower Cretaceous volcanic and volcaniclastic strata in the western foothills of the Sierra San Pedro Mártir (inset map on Plate 1). As can be seen on the aerial photomosaic and the accompanying overlay map (Figure 2A, 2B), the margins of the body are well defined and have, for

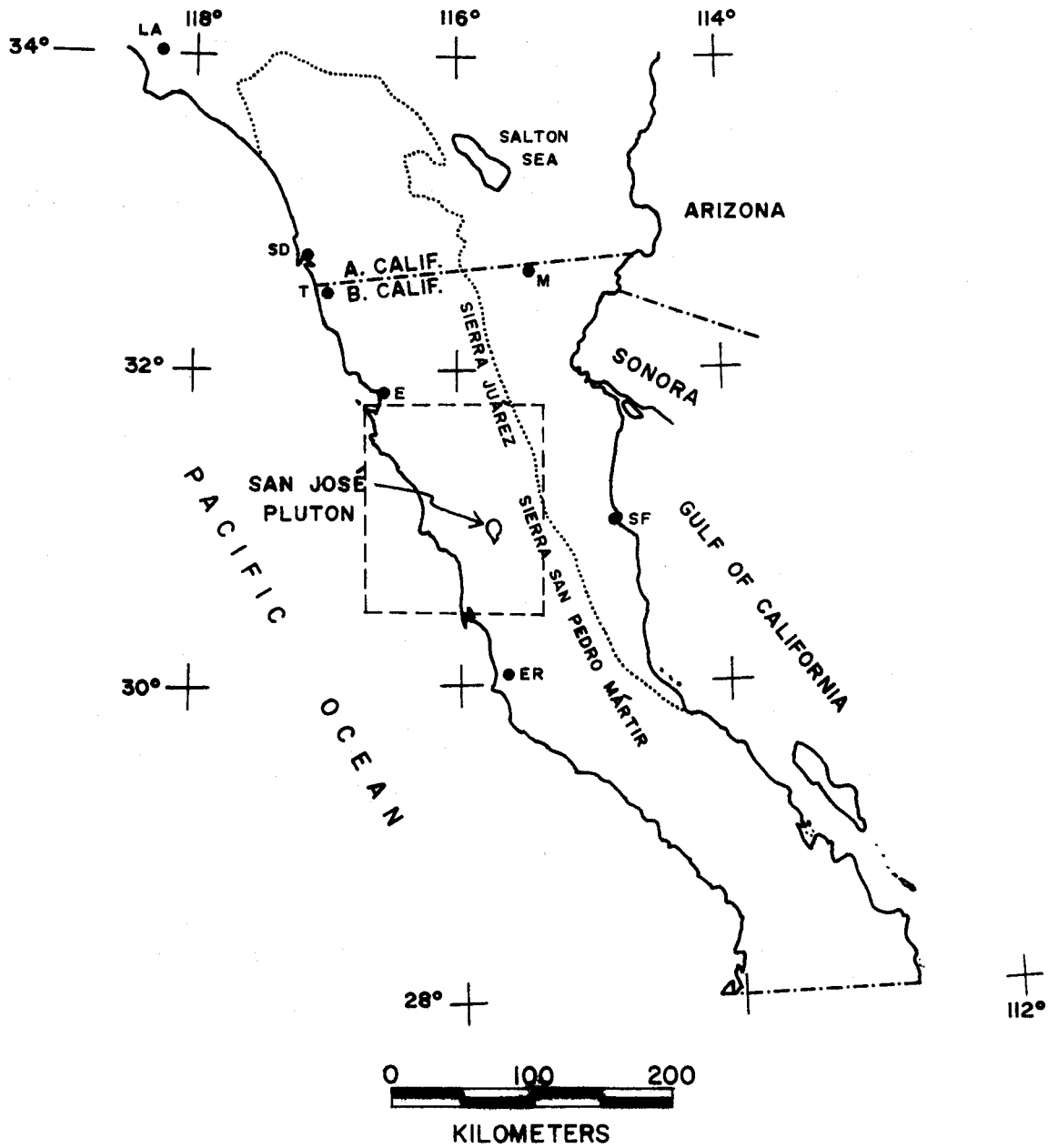

Figure 1. Index map of the northern half of the Peninsular Ranges, showing the location of the San José pluton. The dotted line marks the approximate northern and northeastern limits of the Peninsular Ranges. The dashed rectangle outlines the approximate area covered by the Frontispiece Apollo photograph.
E, Ensenada; ER, El Rosario; LA, Los Angeles; M, Mexicali; SD, San Diego; SF, San Felipe; T, Tijuana.

Figure 2. Aerial photomosaic (A) and generalized geologic map (B) of the San José area. The scales of the photomosaic and map are identical, although the map covers a slightly larger area to the southeast and southwest.

Map symbols:

Crosses denote tonalite and quartz diorite, locally with some more felsic or mafic intrusive rocks or some pre-batholithic rocks.

Stippled pattern denotes gabbro and diorite, locally with minor tonalite or quartz diorite.

Pattern of subparallel dashed lines in the areas surrounding the plutons represents the trace of bedding and metamorphic foliation in the pre-batholithic rocks traced from the photomosaic.

Strike and dip symbols indicate the local attitude of bedding.

CLJM - mafic complex of Cañon La Jolla

WCP - Willow Creek pluton

Note the clear definition of the San José pluton and the north-south asymmetry in contact geometry and in relationship to bedding and foliation in the wall rocks. The arcuate topographic grain visible in the northern half of the pluton is a manifestation of magmatic flow foliation and coplanar jointing.

Figure 2A

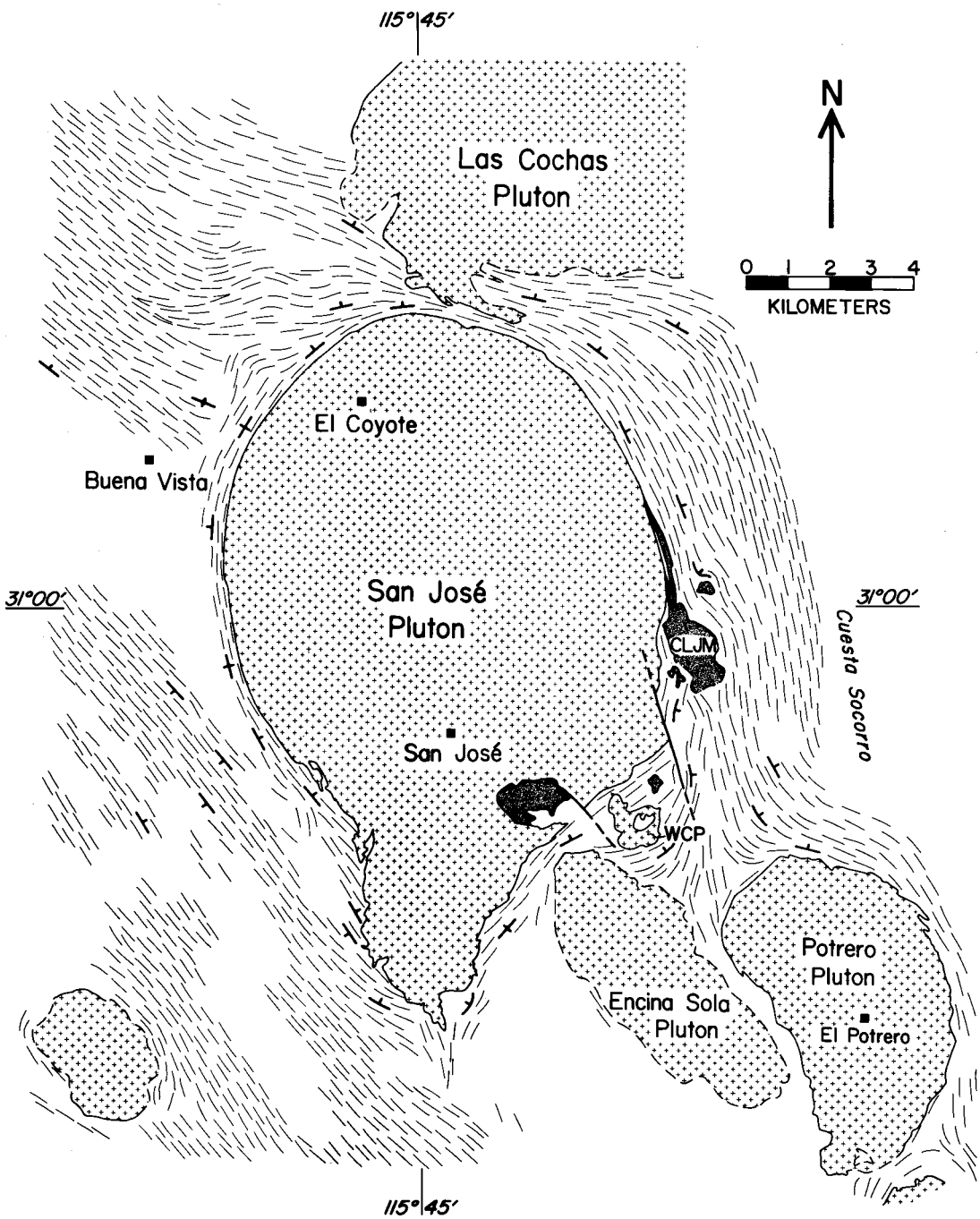
115°45′
N
0 1 2 3 4
KILOMETERS
Las Cochas
Pluton
El Coyote
Buena Vista
31°00′
San José
Pluton
CLJM
31°00′
Cuesta Socorro
San José
WCP
Potrero
Pluton
Encina Sola
Pluton
El Potrero
115°45′

Figure 2B

the most part, been disrupted relatively little by other plutons. Exposure is good, and the terrane is relatively free of dense vegetation and easy to work in. Consequently, opportunities for examining the structural relationships of the pluton to wall rocks and for determining the mechanism of intrusion are excellent. Furthermore, tonalite, which comprises 96% of the pluton, is the dominant plutonic rock type in the Peninsular Ranges (Larsen, 1948; Gastil et al., 1975). Thus, petrologic conclusions reached in this study should have widespread applicability.

A total of 10 months were spent in the field, mapping and collecting samples in the San José pluton, the surrounding pre-batholithic rocks, and several nearby smaller plutons. An additional 17 days were spent examining and collecting over a wide area of the Sierra San Pedro Mártir to the east. Mapping was concentrated on relationships within the San José pluton and at the contacts with wall rocks. Mapping in the pre-batholithic rocks and adjacent plutons was less detailed.

Most of the field work was done between August, 1968 and May, 1972, but brief excursions continued up to September, 1976. With a few exceptions, the work was restricted to the cooler months from November through May.

Laboratory studies included examination of approximately 450 thin sections and polished sections representing all of the map units and many of the minor rock types and petrographic variants. Modal analyses, each based on from 3700 to 11,000 points in 3 to 8 thin sections, were

obtained on 28 tonalite samples representing each of the textural units, and whole-rock chemical analyses were obtained on 22 of those samples. Ten of the chemical analyses were obtained using a technique, discussed in Appendix D, of electron microprobe analysis of glasses prepared by fusion of rock powders fluxed with lithium tetraborate. Eight of the other analyses were done by standard wet chemical techniques at the Japan Analytical Chemistry Research Institute and the remaining four were done by both techniques. In addition, L. T. Silver kindly provided standard wet chemical analyses of the two tonalite samples which he has dated by U-Pb isotopic techniques, raising the total number of chemically analyzed samples to 24. Finally, electron microprobe analyses of all of the major minerals, plus magnetite and several other accessory phases, were obtained on eight of the modally and chemically analyzed rocks.

1.2 Location and Accessibility

The San José pluton is located in the very sparsely populated interior of the peninsula of Baja California (Figure 1), roughly 45 km from the Pacific Ocean and 115 km southeast of Ensenada. The area lies in the western foothills of the Sierra San Pedro Mártir, 10-15 km west of the western escarpment of the sierra. Elevations range from 400-1400 m (Plate 7), as compared with 1500-2800 m atop the westward-sloping plateau of the Sierra San Pedro Mártir and 3095 m on Picacho del Diablo, the highest peak in the peninsula, at the eastern edge of the range. Local relief is moderate or high in much of the pre-batholithic terrane and in some parts of the San José pluton, but

comparatively low or moderate over much of the area of the pluton.

Principal cultural and physiographic features of the area are shown in Plate 6. In accordance with local usage, I have applied the names Cañon La Jolla, Arroyo San José, and Cañon Las Cabras to local segments of the continuous arroyo forming the main branch of the Rio San Telmo drainage. Again following local custom, I have used the English name for Willow Creek Canyon. Inasmuch as there are no formal road names, I have chosen appropriate informal names solely for the purpose of this report.

Slightly south of the center of the pluton, in the broad north-south Arroyo San José, is Rancho San José, a cattle and guest ranch now more widely known as the Meling Ranch, after the family which has owned it since 1924. Several small ranches occur within a 15-km radius of San José, but the nearest village, San Telmo de Arriba, with a population of several hundred persons, is 30 km by road to the west.

In spite of the remote location, accessibility is remarkably good. For years a dirt road branching off the peninsula's principal highway, Mexico 1D, near the Pacific coast has provided access to the area from the west. This road divides east of San Telmo, one route winding directly over the hills to the Meling Ranch (San José-San Telmo Road), the other diverging northeastward and entering the northern part of the area through Ranchos Buena Vista and El Coyote. The southern branch continues eastward to the top of the Sierra San Pedro Mártir (San José-Observatorio Road). Because of the recent establishment of an astronomical observatory on the eastern crest of the sierra by the

Universidad Nacional Autonoma de Mexico, the entire road from the observatory to highway 1D is being widened, graded, and, in many places slightly rerouted[1]; it may eventually be paved. In 1970 a road was extended northward from the pluton to join a major route through the Valle de la Trinidad and Paso San Matías to Mexico highway 5 along the Gulf, thus for the first time providing access to the field area from the north and east as well as from the west.

Within the pluton, minor dirt roads are common, and no part of the body is more than 4 km from a passable track. In contrast, roads in the surrounding metamorphic terrane are few, making access difficult and time consuming. Most parts of the high plateau country of the Sierra San Pedro Mártir are accessible only on foot or muleback.

1.3 Compilation and Presentation of the Geologic Maps

Because no topographic maps exist for the area on a scale less than 1:250,000, mapping was done on aerial photographs with stereoscopic coverage. The geologic maps were compiled using an uncontrolled but carefully prepared photomosaic (Figure 2A) as a base. The horizontal scale (ca. 1:24,100) and north orientation were determined by careful measurement, using a 100-foot tape measure and a brunton compass, along a straight, flat, 4860-foot (1481.3-meter) stretch of airstrip and road 1-2 km east-northeast of Rancho San José. Two separate measurements of this distance agreed to within 0.3 m. Secondary checks of

---

[1] I have not yet mapped the exact route of the newly graded road in the areas outside of the San José pluton; however, the new road deviates only slightly from the old route shown on Plates 2, 6 and 7.

scale and north orientation at several locations agree satisfactorily with the principal measurements.

Various aspects of the field data have been presented separately on five maps. Plate 1 shows the generalized regional geology of the San José area. The geology of the areas surrounding the San José pluton is based primarily on photogeologic interpretation and local ground observations. Plate 2, the main geologic map of the San José pluton, shows the distribution of rock types and the principal structural features. Plates 3-5 show the detailed patterns of (3) foliation and bedding, (4) lineation, and (5) joints, dikes, and veins, respectively. Roads and drainages, as well as the patterns and letter symbols distinguishing the various map units, have been omitted from Plates 3-5 to avoid obscuring the structural patterns. For the same reason, the thin (≤8 m thick) units of marble, quartzite, and meta-volcanic wacke and pebbly wacke designated by special symbols on Plate 2 have been omitted from the other maps.

Names of cultural and topographic features shown on Plate 2 or cited in the text can be found on Plate 6. Topography is shown on Plate 7. To produce the topographic map, Army Map Service 1:250,000 San Felipe and Mission Santo Domingo topographic map sheets were enlarged and superimposed on the planimetric base of Plate 6, traced from the aerial photomosaic. At this scale, the planimetric control of the AMS maps is only approximate, and some adjustment of contour positions was necessary to conform to the photomosaic base.

Double-line borders oriented exactly north-south and east-west have been drawn around Plates 2-5 and divided at 1-km intervals.

Sequential numbers (west to east) and letters (north to south) assigned to each interval provide a coordinate system permitting localities referred to in the text to be found quickly on the maps (generally on Plate 2, unless otherwise noted). For example, Rancho El Coyote (area E-6) is located 5.1 km from the western border of the map (i.e., in km-interval 6) and 4.2 km from the northern margin (interval E). Rancho San José (area L,M-8) lies in east-west interval 8, on the boundary between north-south intervals L and M.

Slight planimetric distortion in the geologic maps is inevitable, due to topographically controlled distortion within individual photographs and to mismatch along photo junctures in the mosaic. Such distortion is generally insignificant. High local relief and up to 400 m of photo mismatch in the immediate vicinity of Cañon Las Cabras and Cerro El Molino southwest of the pluton (areas P-5 and Q-5; see also Plate 6) have introduced a slight uncertainty in the relative locations of measured bedding attitudes on the crest and southern slope of Cerro El Molino and an uncertainty of perhaps ±5-10° in the trends of two fold axes as they project away from the pluton. However, this distortion has little effect on the positions and trends of nearby contacts, all of which lie outside the region of greatest distortion.

1.4 Previous Work

In comparison to the dearth of detailed data in much of Baja California, the San José area (Plate 1) has been treated at least briefly in numerous studies ranging from reconnaissance geologic mapping to specialized geochemical and geophysical measurements. Woodford and

Harriss (1938) established the general character and distribution of rock types in a 40-km by 80-km area (area 4 in Figure 3, p 19) across the Sierra San Pedro Mártir and its western foothills, including the San José area. Their pioneering reconnaissance map, constructed without the benefit of topographic maps or aerial photographs, contains inevitable planimetric distortion; nevertheless, as a general guide to the geology of the area, it is reasonably reliable. Smith (1972) further subdivided the plutonic rocks in the sierra on the basis of textural, modal, and radioactivity data, but he did not alter the the basic map patterns or identification of rock types established by Woodford and Harriss.

Covering a much larger area (area 3 in Figure 3, p. 19) from Ensenada south to San Quintín and east across the Sierra San Pedro Mártir, Silver et al. (1956, 1963) showed that strata in the San José area, designated by Woodford and Harriss as the San Telmo formation, are correlative and continuous with the Alistos formation of upper Lower Cretaceous age (Aptian-Albian) along the Pacific coast at Punta China, 110 km northwest of San José. Fossils found in the hills north of Rancho Buena Vista (near area E-1 on Plate 2) indicate that the strata intruded by the San José pluton include rocks at least as young as lower to middle Albian age (Larsen et al., 1958; Silver et al., 1963).

Birkbahn (1969) studied the structural and petrographic characteristics of the San José pluton in reconnaissance. His discussion of the geomorphology and erosional history is brief, but generally quite good. Unfortunately, his field and petrographic studies were necessarily

limited by the restricted time and effort which can be devoted to a senior thesis. Many of his observations and conclusions are not supported by the present study.

Most recently, R. G. Gastil and his coworkers (1973b, 1975) at San Diego State University completed the monumental task of compiling a reconnaissance geological map of the entire state of Baja California del Norte, accompanied by a lengthy discussion of the regional geology and geologic history of the state. This important work and several shorter related publications (Gastil, 1975; Gastil et al., 1974; Krummenacher et al., 1975) help to provide a broader geologic context for understanding the San José pluton and for applying the results of the present local detailed study to other parts of the batholith. Whereas the most detailed pre-existing geologic map of Baja California (Beal, 1948) distinguishes the various post-batholithic sedimentary and volcanic lithologies, but lumps the pre-batholithic and batholithic rocks into a single crystalline complex, the map of Gastil et al. provides, for the first time, a comprehensive picture of the distributions of the various plutonic and metamorphic rock types which underly at least half of the state.

Although the map of Gastil et al. is an outstanding improvement over pre-existing geologic maps, several significant omissions and errors in the representation of the San José area should be pointed out. (1) The Encina Sola pluton, immediately southeast of the San José pluton (see Plate 1), was mapped in reconnaissance by Woodford and Harriss (1938), yet it is not shown on the map of Gastil et al.

(2) The Potrero pluton in the southeastern corner of Plate 1 is shown as granodiorite by Gastil et al., whereas, in fact, it consists of K-feldspar-poor hornblende-biotite tonalite similar in many respects to the seriate porphyritic phase of the San José pluton. (3) The small Santa Cruz pluton just south of the Potrero mass was mapped by Gastil et al. as granodiorite (?), but a brief examination by the writer indicates that it consists largely or entirely of quartz diorite and possibly diorite. (4) The general outline of the San José pluton shown by Gastil et al.is approximately correct, but the position and geometry of the contact around the southern third of the pluton are noticeably inaccurate, and the contact is locally misplaced by as much as 700 m.

Geochemical studies include U-Pb isotopic age data obtained by L. T. Silver (unpublished data) on zircons from two samples which he collected from the pluton. Sample BC-I-12 from the interior of the pluton (area K,L-6; transitional between the prismatic hornblende and seriate porphyritic textural units) gave an age of 112 ± 2 m.y., and sample BC-I-5 from the gneissose border rocks (area D-4,5) gave the analytically indistinguishable age of 111 ± 2 m.y. T. O. Early and L. T. Silver (unpublished data) determined the initial Sr^{87}/Sr^{86} ratio (0.7036) and the total Rb and Sr contents (12 ppm and 623 ppm, respectively) on sample BC-I-12. Taylor and Epstein (1962) and Taylor (1968) reported O^{18}/O^{16} ratios for the major phases in BC-I-12, and Hoefs and Epstein (1969) reported O^{18}/O^{16} and C^{13}/C^{12} data on a small mass of orbicular diorite in the wall rocks at the southern tip of the pluton (locality 64, area S-7).

Smith (1972, 1974) reported the first heat-flow measurement from the Peninsular Ranges in Baja California, from a hole drilled in the center of the San José pluton (locality 240, area I-7). Smith (1972) also presented K, Th, and U concentrations and heat generation values from 17 samples of the prismatic hornblende unit and from a much larger number of samples collected on top of the Sierra San Pedro Mártir.

Chapter 2

REGIONAL GEOLOGIC SETTING OF THE SAN JOSÉ PLUTON

2.1 General Character and Setting of the Peninsular Ranges Batholith

Baja California and adjacent southern California, U.S.A. (referred to hereafter as southern Alta California) can be divided into two major physiographic provinces: The Peninsular Ranges and the Gulf of California-Salton Sea Depression. The peninsula can be further divided on geologic grounds into a northern half and a southern half, with the natural boundary coinciding approximately with the political boundary between the states of Baja California del Norte and Baja California Sur (28° N latitude). This discussion will deal principally with the northern half of the Peninsular Ranges, which can be defined as that part of Baja California del Norte and adjacent Alta California south of the Transverse Ranges and the Los Angeles Basin (about 34° N latitude) and west of the steep eastern escarpments of the Sierra San Pedro Mártir and Sierra Juárez in Baja California and their northern extension in southern Alta California (Figure 3). The Gulf of California-Salton Sea Depression and the southern half of the peninsula have experienced much more complicated Cenozoic histories which are not directly relevant to the subject of this thesis.

The Sierra Juárez and Sierra San Pedro Mártir together form the "backbone" of the peninsula. Both are high westward-sloping plateaus bounded on the east by steep escarpments generally 1000 m to 2500 m high. The plateaus give way westward to commonly rugged foothills which extend with decreasing elevation to a generally narrow Pacific coastal

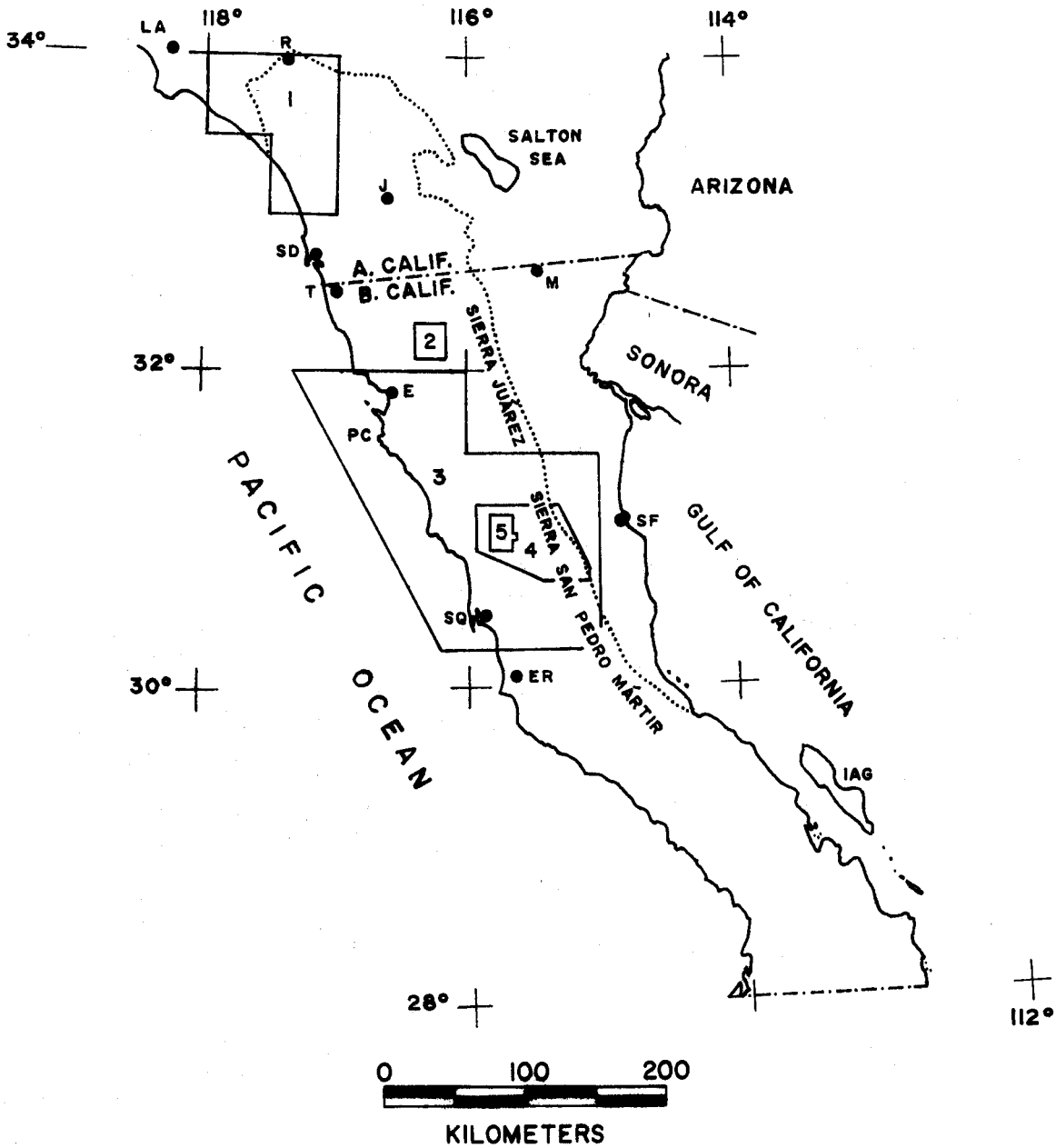

Figure 3. Index map of the northern half of the Peninsular Ranges, showing the locations of several key studies. The dotted line marks the approximate northern and northeastern limits of the Peninsular Ranges.

1: Larsen (1948)
2: Duffield (1968)
3: Silver et al.,(1956, 1963)
4: Woodford and Harriss (1938)
5: This study; San José area

E, Ensenada; ER, El Rosario; IAG, Isla Angel de la Guarda; R, Riverside; SD, San Diego; SF, San Felipe; SQ, San Quintín; T, Tijuana.

plain. The situation is basically similar in southern Alta California, but somewhat more complicated due to Cenozoic faulting which has broken the area into numerous ranges and high plateaus.

Numerous summaries have been published on the geology of Baja California and adjacent southern Alta California. Foremost among these is the recent Geological Society of America memoir (Gastil et al., 1975) and the accompanying reconnaissance geologic map (Gastil et al., 1973b) covering the state of Baja California del Norte. Other summaries include Larsen (1948) and Jahns (1954) in southern Alta California, and Beal (1948), Wisser (1954), Durham and Allison (1960), and Allison (1964) in Baja California. Many additional papers have dealt with local areas or particular aspects of the geology of the peninsula; nevertheless much of Baja California has yet to be examined in detail. The locations of several studies of particular interest, including the present study, are outlined in Figure 3.

The rocks of the northern Peninsular Ranges can be divided into three basic groups: pre-batholithic, batholithic, and post-batholithic. My interest here centers on the pre-batholithic and batholithic rocks. The Cretaceous Peninsular Ranges batholith is exposed almost continuously for a distance of about 770 km from the latitude of Riverside, California, U.S.A. (34°N) southeastward to the boundary between the states of Baja California del Norte and Baja California Sur (28°N). The largest exposed areas of plutonic rocks underlie the Sierra San Pedro Mártir and Sierra Juárez (inset map, Plate 1) and their northern extensions in southern Alta California. Several widely scattered areas

of plutonic rock occur farther south, particularly in the Sierra Victoria near the southern tip of the peninsula (Beal, 1948). However, most of the southern half of the peninsula is mantled by Cenozoic volcanic and sedimentary rocks.

Westward from the crests of the ranges, the size and abundance of plutons decreases; the Pacific coastal areas are underlain largely by pre-batholithic and post-batholithic rocks, with relatively few scattered plutons (Allen et al., 1960; Silver et al., 1963; Gastil et al., 1975). The batholith also extends eastward across the Gulf of California Depression into western Sonora (Anderson et al., 1969; Gastil et al., 1972, 1975), but the eastern portions have been severely disrupted by Cenozoic faulting and extensively covered by Cenozoic deposits.

Tonalite is the predominant rock type in the batholith. Larsen (1948) found that tonalite comprises 63%, granodiorite 28%, gabbro 7%, and granite 2% of the batholithic rocks in the northwestern part of the Peninsular Ranges (area 1 in Figure 3). Similarly, tonalite comprises about 75% of the batholithic rocks in a 40-km by 80-km area across the Sierra San Pedro Mártir (area 4 in Figure 3), with granodiorite comprising all but a few percent of the remainder (Woodford and Harriss, 1938). Over the much larger area from Ensenada south to San Quintín and inland across the Sierra San Pedro Mártir (area 3 in Figure 3), quartz diorite (including tonalite) constitutes more than 80% and granodiorite most of the remainder of the plutonic rocks (Silver et al., 1963).

From the reconnaissance geologic map of Gastil et al. (1973b), it is clear that the relative proportions of plutonic rock types are

roughly comparable to the various estimates given above along the entire length of the Peninsular Ranges from Riverside to the southern margin of the state of Baja California del Norte. However, Gastil et al. (1974) pointed out that the relative proportions of the major plutonic rock types varies systematically across the width of the batholith. In particular, gabbro is largely restricted to the "gabbro sub-belt" in the western foothills, where it generally "constitutes less than 20% of the granitic rocks and tonalite makes up about 60%" (Gastil et al., 1974, p. 74). Also, quartz monzonite and granite occur abundantly with granodiorite and tonalite only in the less extensively studied eastern part of the batholith in Sonora, Mexico (Anderson et al., 1969; Gastil et al., 1974). Despite these variations, it is important to emphasize that tonalite and petrographically similar potash-poor granodiorite predominate across the entire width of the Peninsular Ranges and are present east of the Gulf as well.

The pre-batholithic rocks also vary systematically across the Peninsular Ranges. Gastil et al. (1975) have summarized the available data. Slightly metamorphosed volcanic and volcaniclastic rocks are the principal country rocks in the western part of the ranges. In the western foothills of the Sierra San Pedro Mártir, these rocks are assigned to the Alisitos formation of Santillán and Barrera (1930), which consists of at least 6500 m of volcanic breccia, tuff, flows, and tuffaceous mudstone and wacke, with sparse biostromal limestone (Silver et al., 1956, 1963; Allison, 1955, 1964, 1974). Neither the top nor the bottom of the formation has been found. The volcanic rocks

range in composition from basalt to rhyolite, but andesite and dacite are most abundant. Silver et al. (1963) found no detritus of non-volcanic origin, other than organic carbonate debris, in the Alisitos rocks between San José (area 5 in Figure 3) and Punta China (PC) along the Pacific coast 35 km south of Ensenada. They (1963, 1969) pointed out that the Alisitos strata constitute a classical eugeosynclinal suite with the characteristics of a typical volcanic archipelago. Gastil et al. (1972, 1975) have extended this concept and reconstructed the possible paleogeometry of the archipelago, which they named the Alistos arc.

Marine fossils collected at a number of locations in the Alisitos formation are all of Aptian to Albian (upper Lower Cretaceous) age (Allison, 1955, 1974; Larsen et al., 1958; Silver et al., 1956, 1963), but the presence of older and/or younger rocks cannot be ruled out. East and southeast of El Rosario, similar strata containing some of the same diagnostic fossils (Silver et al., 1956, 1963) were designated as the San Fernando formation by Beal (Anonymous, 1924; Beal, 1948). Allison (1964) pointed out that the name "San Fernando" is preoccupied and should be dropped in favor of the name Alisitos.

Even farther south, in Arroyo San José about 220 km southeast of El Rosario, Minch (1969, p. 42) discovered a thick fossiliferous section of slightly metamorphosed, relatively undeformed clastic and pyroclastic strata unconformably below fossiliferous "Upper-Lower Cretaceous strata equivalent to the lower part of the Alisitos Formation." The fossils suggest a Jurassic to possibly Early Cretaceous age for the section beneath the unconformity. This is the only documented occurrence

of probable Jurassic rocks in Baja California.

Pre-batholithic volcanic and volcaniclastic rocks along the western flank of the Peninsular Ranges in southern Alta California were assigned by Larsen (1948) to the Santiago Peak Volcanics (equivalent to the Black Mountain Volcanics of Hanna, 1926). According to Larsen, andesite and quartz latite are the predominant volcanic rocks, but rhyolite and probably basalt are also present. Fossils are rare, but Fife et al. (1967) found latest Jurassic (Portlandian) fossils at three localities north of San Diego. At least part of the Santiago Peak Volcanics is therefore significantly older than any of the paleontologically-dated Alisitos strata.

Slightly metamorphosed volcanic flow, pyroclastic, and epiclastic rocks predominate in the western foothills of the Sierra Juárez (Hawkins, 1970; Gastil et al., 1975). Neither paleontologic nor stratigraphic data are available to establish the relationship of these strata to either the Alisitos formation or the Santiago Peak Volcanics.

The volcanic and volcaniclastic rocks give way eastward near the center of the Peninsular Ranges to generally higher-grade schists and gneisses in which volcanic contribution, if appreciable, is obscure (Gastil et al., 1975). In the Sierra San Pedro Mártir, these rocks were called the Santa Eulalia formation by Woodford and Harriss (1938). They consist of medium-grained and coarse-grained muscovite- and/or biotite-rich quartzo-feldspathic schist and gneiss, with some amphibolite, quartzite, marble, and calc-silicate rock. Similar lithologies apparently dominate the pre-batholithic section along the crest of the

Sierra Juárez (Fries and Schmitter, 1945; Hirschi and de Quervain, 1927; Gastil et al., 1975).

In southern Alta California, the meta-sedimentary rocks have been given several local names. In the Santa Ana Mountains southwest of Riverside, a thick section of argillite, slate, phyllite, and quartzite (metamorphosed graywacke and shale), with minor conglomerate, limestone, chert, and volcanic rocks was named the Bedford Canyon formation by Larsen (1948). Fossils are very rare. Larsen reported that the formation unconformably underlies the Santiago Peak Volcanics and considered it to be Triassic in age. However, more recent work has shown that much of the formation is of Middle to early Late Jurassic (Bajocian to Callovian) age (Imlay, 1964; Silberling et al., 1961). It is not known whether Triassic rocks are also present.

Schwarcz (1969) assigned the pre-batholithic rocks in the Winchester area (about 35 km southeast of Riverside in Figure 3) to the French Valley formation. He showed that this formation "generally composed of interlayered schist, feldspathic to arkosic quartzite, amphibolite, meta-chert, and meta-conglomerate" (p. 9) is not of Paleozoic age, as previously thought (e.g., Webb, 1939; Larsen, 1948; Jahns, 1954), but rather conformably overlies the section assigned by Larsen to the Bedford Canyon formation.

Farther south, the metamorphic rocks hear Julian consist of quartz-mica schist and gneiss, quartzite and some amphibolite (Hudson, 1922). These rocks, known as the Julian schist, are widespread in eastern San Diego County and are also similar to the schists and gneisses in the

Sierra Juárez (Jahns, 1954; Gastil et al., 1975). The Julian schist has yielded a single ammonite impression believed to be a Triassic form (Hudson, 1922), but the fossil has apparently been lost, and the Triassic assignment cannot be verified (Gastil et al., 1975).

Along the northeastern side of the Peninsular Ranges in southern Alta California (Jahns, 1954) and in several areas along the eastern side of the Sierra San Pedro Mártir and the smaller ranges farther south (Gastil et al., 1975), pre-batholithic sections consist principally of metamorphosed limestone, shale, and sandstone, with some conglomerate, bedded chert, and volcanic rock. Similar sections are found in isolated ranges in the Gulf of California-Salton Sea Depression (Gastil et al., 1975). McEldowney (1970) discovered Paleozoic ("possibly Carboniferous") fossils in the northern Sierra Pinta west of the northern tip of the Gulf. Subsequently, Gastil et al. (1973a) reported the occurrence of angular boulders of fossiliferous Permian limestone in a basal conglomerate bed underlying Miocene volcanic rocks and overlying granitic basement in the Sierra Santa Rosa near San Felipe. They concluded that the boulders could not have been transported very far. Paleozoic (?) fossils have also been found at two localities "northeast of El Marmol" near the southern end of the Sierra San Pedro Mártir (Gastil et al., 1975, pp. 24 and 26). The latter workers therefore suggested that a belt of Paleozoic meta-sedimentary rocks parallels the eastern margin of the Peninsular Ranges; however, the age of most of the carbonate-sandstone-shale sections has yet to be established. No other pre-Mesozoic rocks have yet been recognized in the Peninsular

Ranges. In fact, aside from the probable Jurassic strata which Minch (1969) discovered in Arroyo San José, no other pre-Cretaceous rocks have been documented in Baja California del Norte.

Schwarcz (1969) concluded that metamorphism in Winchester area of southern Alta California was of the high-temperature, low-pressure Abukuma type of Miyashiro (1958). The general mineral assemblage reported by Duffield (1968) in the El Pinal area of northern Baja California (area 2 of Figure 3) is also consistent with Abukuma-type metamorphism, as are the assemblages in the San José area (see Section 4.3 and Table 1) and on top of the Sierra San Pedro Mártir (Woodford and Harriss, 1938; also this study, Appendix E).

Gastil (1975) and Gastil et al. (1975) interpreted the schists and gneisses in the interior and eastern parts of the Peninsular Ranges as constituting a thick wedge of Paleozoic to Jurassic meta-sedimentary rocks upon the western part of which the Jurassic and Cretaceous volcanic and volcaniclastic rocks accumulated. This model may be correct, but it is as yet unproven. The base of the meta-volcanic pile is generally unexposed, and the nature of the underlying rocks is unknown along most of the belt. Nor has direct evidence been found concerning the structural, stratigraphic, or temporal relationships of the schists and gneisses in the Sierra San Pedro Mártir and Sierra Juárez to the less metamorphosed volcanic and volcaniclastic rocks. These relationships are difficult to decipher because of the severe metamorphism, deformation, and disruption of stratigraphic and structural continuity by plutonic intrusion in the interior of the peninsula. Nor are the relationships

between the various meta-volcanic and meta-sedimentary sections well established in southern Alta California. Finally, one cannot rule out the possibility of appreciable tuffaceous and/or epiclastic volcanic contribution to the parent lithologies of the high-grade quartzo-feldspathic schists and gneisses. Such contribution would be difficult to recognize through the metamorphic overprint. Thus no definite break has been shown to exist either in age or lithology between the meta-volcanic and meta-sedimentary belts.

Regardless of the exact age and stratigraphic relationships of the volcanic and sedimentary belts, their systematic distribution allows one to crudely reconstruct the overall paleogeometry of the volcano-sedimentary arc, as was done by Gastil et al. (1972). The distribution of lithologies suggests the existence of a sialic landmass to the east, shedding debris into the eastern part of the arc, while volcanism predominated in the western part of the arc.

In scattered places along the Pacific coast of the Peninsular Ranges and on nearby islands, many workers have recognized rocks of Franciscan aspect -- commonly including blueschists, greenschists, graywacke, bedded chert, serpentinite, saussuritized gabbro, and basalt -- either as primary deposits or as reworked debris derived from the west (for example, Woodford, 1925; Beal, 1948, Cohen et al., 1963; Bailey et al., 1964; Minch, 1967; Yeats et al., 1971). These rocks suggest the existence of a low temperature-high pressure metamorphic belt of Franciscan-type lithologies west of the volcanic arc and the belt of high temperature-low pressure metamorphism (Yeats et al., 1971).

Thus, the northern Peninsular Ranges appear to possess all of the components of a complete Jurassic-Cretaceous island arc-subduction zone system into which the Peninsular Ranges batholith was emplaced. The arc was apparently bounded by open ocean to the west and possibly by a sialic land mass at an undetermined distance to the east.

Since emplacement of the batholith, the northern half of the Peninsular Ranges has behaved as a relatively stable block contrasting with the tectonically complex regions of the Gulf of California-Salton Sea Depression and the southern half of the peninsula. Tectonic activity has been limited mainly to broad-scale vertical motions and to horizontal and vertical displacement on major faults which bound or transect the ranges.

Post-batholithic igneous activity has been similarly limited, being represented almost entirely by middle Miocene (20 m.y.) and younger flows and pyroclastic rocks generally no more than several hundred meters thick (Gastil et al., 1975). In contrast, up to several thousand meters of similar rocks are locally present in the Gulf of California Depression (Gastil et al., 1975) and in Baja California Sur (Beal, 1948). Middle Miocene to Pliocene volcanic rocks ranging in composition from basalt to rhyolite mantle much of the southern half of Baja California del Norte (Beal, 1948; Gastil et al., 1975). Middle to late Miocene volcanic rocks with a similar compositional range cover the southern part of the Sierra Juárez and a few isolated areas in the northern Sierra Juárez and the ranges in southern Alta California (Allen et al., 1960; Miller, 1935; Gastil et al., 1975). Basaltic rocks comprise

a major part of the middle Miocene Rosarito Beach formation covering much of the coastal strip from Tijuana to Ensenada (Minch, 1967; Minch et al., 1970). Two other prominent volcanic fields occur along the Pacific coast: the Pleistocene to Recent (?) basalt field at San Quintín (Woodford, 1928) and the Plio-Pleistocene basalt field capping Mesa San Carlos 35-45 km southeast of El Rosario (Gastil et al., 1975). Surprisingly, no post-batholithic volcanic rocks have been found in the northern half of the Sierra San Pedro Mártir or its western foothills.

Many workers (e.g., Santillán and Barrera, 1930; Silver et al., 1963; Allison, 1964) have recognized that the Pacific shoreline throughout the Late Cretaceous and Cenozoic time was generally close to the modern shoreline. Gastil and Allison (1966) pointed out that the eastern limits of the coastal strip of Upper Cretaceous marine strata define a remarkably straight line traceable for 650 km from northern San Diego County in Alta California southward to the southern boundary of Baja California del Norte. This line, which marks the Late Cretaceous shoreline, was first recognized in Baja California by Santillán and Barrera (1930) and has therefore been named the Santillán y Barrera line by Gastil et al. (1975). Cenozoic marine strata are likewise restricted mainly to this narrow coastal strip (Gastil et al., 1975). Thus, the Santillán y Barrera line has been an important tectonic hinge line closely controlling the coastline since Late Cretaceous time (Gastil and Allison, 1966; Gastil et al., 1975).

Tertiary non-marine sedimentary strata underlie much of the inland area capped by Miocene and younger volcanic rocks. Additional gravel

deposits cap scattered areas in the western foothills of the Sierra San Pedro Mártir, in the Sierra Juárez, and in the western half of the ranges in southern Alta California. These sedimentary and volcanic strata rest on old erosion surfaces recognizable throughout much of southern Alta California (Gastil, 1961) and preserved extensively along the crest of the Sierra Juárez (Minch, 1970). An old erosion surface also extends across the top of the Sierra San Pedro Mártir at elevations of 2000-3000 m (Woodford and Harriss, 1938) and descends gradually southward to extend under the cover of Cenozoic sedimentary and volcanic rocks in the southern half of the state (Gastil et al., 1975). Scattered remnants of an old surface are preserved in the western foothills of the Sierra San Pedro Mártir.

The non-marine strata capping the erosion surfaces are unfossiliferous, and their ages are for the most part uncertain. However, in the San Diego area of Alta California, Moore and Kennedy (1970) showed that the non-marine Poway Conglomerate grades westward into the Eocene marine La Jolla formation. Also, Abbott et al. (1973) reported that deep soil profiles are preserved beneath Eocene strata in places along the western side of the ranges. Farther inland, near Ramona and Elsinore in Alta California and on top of the Sierra Juárez, scattered linear gravel deposits were interpreted by Minch (1970) as the remnants of westward-flowing river courses of probable Eocene age.

These observations led Gastil et al. (1975) to conclude that the erosion surfaces developed during Paleocene and Eocene time and, furthermore, that the broad area now occupied by the Peninsular

Ranges was then near sea level and was characterized by low rolling relief, with many westward-flowing streams depositing gravels derived from terrane apparently east of the peninsula. This interpretation may well be correct. However, over most of their extent, the surfaces can be positively dated only as younger than early Late Cretaceous (i.e., post-batholithic) and pre-middle Miocene (i.e., older than the overlying volcanic rocks).

Whatever the age or ages of the erosion surfaces, their widespread development and preservation attests to the remarkable stability of the northern Peninsular Ranges in early to middle Tertiary time. The volcanic rocks capping the southern Sierra Juárez and scattered areas near the international border are truncated or downfaulted along the eastern escarpment of the Sierra Juárez (Allen et al., 1960; Gastil et al., 1975). Thus, much or all of the uplift of this range, and presumably of the ranges to the north and south, occurred subsequent to middle or late Miocene time. Young fault scarps in alluvium at the eastern base of the Sierra San Pedro Mártir imply that uplift may still be occurring (Gastil et al., 1975).

2.2 Age of the Batholith

The batholith is intruded into volcanic and volcaniclastic strata at least as young as Late Jurassic (Portlandian; Fife et al., 1967) in southern Alta California and late Early Cretaceous (lower to middle Albian; Larsen et al., 1958; Silver et al., 1963) in Baja California. Because of the duration and possible temporal overlap of the volcanic and plutonic episodes, the stratigraphic and paleontologic evidence

place an apparent older limit on the age of the batholith only as Early Cretaceous or possibly Late Jurassic. The volcanic and sedimentary rocks were deformed, and plutonic rocks were emplaced, crystallized, and locally exposed by erosion, all before deposition of the marine upper Upper Cretaceous (Campanian-Maestrichtian) Rosario formation along the Pacific coast (Allison, 1964; Silver et al., 1963).

Studying U-Pb isotopic relationships in zircons and monazites, Silver et al. (1956, 1963, 1969, 1975) and Banks and Silver (1966, 1969) obtained ages for numerous plutons from southern Alta California, Baja California, and Sonora, Mexico. These studies revealed (Silver et al., 1975, p. 376) "a space-time progression of plutonic emplacement, largely independent of lithologies, eastward from the Pacific margin (110-130 m.y.) to the east side of the Peninsula (90-100 m.y.), and across to eastern Sonora (60-70 m.y.)."

Evernden and Kistler (1970) and Armstrong and Suppe (1973) reported K-Ar age determinations, mainly on hornblende and biotite, for plutonic rocks in southern Alta California. Krummenacher et al. (1975) combined these data with a great number of new analyses for northern Baja California and southernmost Alta California. The latter workers interpreted these ages, which range from 143 to 61 m.y., but fall mostly between 75 and 115 m.y., as cooling ages rather than ages of magmatic emplacement and crystallization. They also showed that the ages decrease systematically from west to east.

In summary, the bulk of the batholithic rocks in the northern Peninsular Ranges were apparently emplaced over a time span of 30-40 million years in the Cretaceous, from about 130 to 90-100 m.y. The

area may have remained hot, however, for a considerably longer period of time, particularly in the eastern part of the ranges and in the Gulf of California-Salton Sea Depression. At least along the western side of the batholith, uplift and subsequent tectonic stability were apparently achieved in late Cretaceous time, i.e., within about 60 million years or less after the initiation of plutonism. This single, relatively brief episode contrasts markedly with the repeated episodes of plutonism in the Sierra Nevada batholith, covering an apparent span of 130 million years from Middle and Late Triassic to Late Cretaceous (Evernden and Kistler, 1970), and is one of the factors making the northern Peninsular Ranges an attractive area for studying the characteristics and development of a volcano-plutonic arc complex.

2.3 Local Setting of the San José Pluton

The San José area (Plate 1), which lies in the western part of the batholith, near the eastern limits of the "gabbro sub-belt" of Gastil et al. (1974), is underlain by predominantly northwest-striking, steeply dipping, mildly to moderately metamorphosed sedimentary and volcanic rocks intruded by numerous concordant to sub-concordant plutons, the largest of which is the San José pluton. Tonalite is by far the principal plutonic rock type. Numerous small bodies of quartz diorite, diorite, and gabbro are scattered throughout the area, particularly along the eastern side of the San José pluton. Only the largest of these are distinguished on Plate 1. Except for numerous small dikes and one small metamorphosed hypabyssal granite body in the pre-batholithic section, granite, quartz monzonite, and granodiorite are absent.

At the present level of exposure, the larger plutons in the San José area are everywhere separated from each other by metamorphic strata. In contrast, plutons in the high plateau country farther east and generally throughout the eastern half of the Peninsular Ranges are commonly intruded into one another and are only locally separated by pre-batholithic rocks (Gastil et al., 1975).

Woodford and Harriss (1938) grouped the quartz diorite and tonalite into two formational units based upon petrographic and structural characteristics: (1) the slightly metamorphosed Encina Sola quartz diorite occupying the Encina Sola pluton and several small plutons outside the San José area "doubtfully correlated with the Encina Sola quartz diorite" (p. 1314), and (2) the San José "gneissoid quartz-biotite-hornblende diorite" (mostly tonalite) comprising the San José, Potrero (called "Upper Valladares mass" by Woodford and Harriss), and Las Cochas plutons and all of the tonalite on the high plateau to the east. Because the genetic relationship and contemporaneity implied by the grouping of intrusive masses into formations have not been substantiated, individual names for each pluton rather than formational names will be used in this report.

The pre-batholithic strata in the San José area, shown by Silver et al. (1956, 1963) to be largely or entirely correlative with the Alisitos formation of Santillán and Barrera (1930), consist of metamorphosed volcanic and hypabyssal intrusive rocks, volcanogenic sedimentary strata, and minor limestone and calc-silicate rock. The volcanic rocks are mainly basaltic to dacitic, but rhyolitic rocks also occur. Tuff, tuffaceous and siliceous mudstone, and volcanic wacke,

pebbly wacke, and breccia predominate, but metamorphosed hypabyssal dikes, sills, and plugs similar to the extrusive rocks are locally abundant. Some volcanic flows may also be present.

The pre-batholithic strata are consistently steeply dipping, and metamorphic foliation is generally parallel to bedding. Patterns of light and dark "striping" visible on the aerial photographs northwest, north, and east of the pluton indicate that the strata have been thrown into numerous large-scale isoclinal folds.

Contact metamorphic mineral assemblages characteristic of the hornblende-hornfels facies are developed around the margins of the San José and Las Cochas plutons. Outside the contact aureoles to the west and southwest, strata are only slightly metamorphosed. Likewise, strata along the San José-Observatorio road from about 2 km to about 5 or 6 km east of the pluton consist of greenschist facies assemblages. Eastward from there, metamorphic grade increases rapidly, and upper amphibolite facies assemblages are widespread on top of the Sierra San Pedro Mártir.

Aplitic and pegmatitic dikes abound throughout much of the plutonic and high-grade metamorphic terrane farther east, but are only locally abundant in the San José area. Some are undeformed and unmetamorphosed, but others, including some which cut the San José pluton, have been intensely sheared and faulted during regional deformation and/or deformation associated with continuing emplacement of the pluton. Undeformed and unmetamorphosed dikes of intermediate to mafic composition are also locally abundant in both the plutons and metamorphic rocks.

Other than Quarternary alluvium, the only post-batholithic deposits recognized in the San José area consist of unconsolidated, poorly sorted, round-cobble gravels forming a discontinuous veneer over wide areas mainly west and northwest of Rancho Buena Vista.

Perhaps the most spectacular feature observable on the aerial photographs (Figure 2) is the sharp bending of structural and stratigraphic trends in the country rocks conformably around the plutons, particularly around the San José and Potrero bodies. The overall pattern is geometrically reminiscent of foliation bending around augen in a gneiss, but on an enormous scale. Country-rock trends are least disturbed by the Encina Sola and Willow Creek plutons. These two bodies also differ from the others in being largely discordant and in lacking well-developed flow structure even along their margins. Woodford and Harriss recognized that the Encina Sola pluton has been weakly metamorphosed and is older than the San José pluton; contact metamorphism by the San José pluton produced abundant clinopyroxene in the northwestern part of the Encina Sola mass. The Willow Creek pluton, on the other hand, is apparently younger than the San José pluton. The age relationships of the other plutons to the San José are generally uncertain, but the Las Cochas pluton is probably slightly younger.

PART II

FIELD RELATIONSHIPS OF THE SAN JOSÉ PLUTON

Chapter 3

GENERAL CHARACTER OF THE PLUTON

This chapter is intended to serve as an expanded abstract, summarizing the key characteristics of the pluton as revealed by the field studies and introducing some of the principal questions and concepts towards which the subsequent discussion of the field relationships will be directed.

The San José pluton has a teardrop cross-section in plan view, elongate north-south and outlined by commonly knife-sharp contacts remarkably hemi-circular and concordant to isoclinally folded, highly stretched and thinned strata in the north, becoming discordant and tapering irregularly to a point in the south. The pluton lies generally at a slightly lower elevation than the surrounding metamorphic rocks and, except in a few areas, shows low to moderate local relief in contrast to the moderate to high local relief in the metamorphic terrane. The outcrop pattern in the pluton is typical of tonalite in the semi-arid Peninsular Ranges, i.e., most of the rock is exposed as rounded bouldery outcrops and fewer broad exfoliated surfaces scattered over grus-covered hills (Figure 4). Exposure, however, is unusually good in comparison to many plutons in the batholith.

Light gray or tannish-gray biotite-hornblende tonalite containing 1-2% of mafic inclusions and leucocratic and mafic schlieren constitutes about 96% of the pluton; dioritic rocks make up almost 3%, and mela-tonalite, lime-contaminated tonalite, gabbro, and various dike and vein

Figure 4. Panoramic views across the San José pluton.

The upper panorama looks towards the west and northwest from the San José-Observatorio road 3.3 km due east of Rancho San José (area L-11). The ranch is located among the trees along the axis of the broad north-south Arroyo San José towards the left side of the central frame. The western margin of the pluton follows the base of the skyline ridges. The scattered boulders and rounded exfoliation surfaces are typical of the outcrop pattern in most of the pluton. Broad remnants of the low-relief Peterson erosion surface are conspicuous just below the skyline in the central and right-hand frames.

The lower view is towards the north from the northern slope of Cerro Hechicera (area R-6). The broad valley in the center-foreground is El Alisito canyon, which intersects Arroyo San José at Rancho El Molino in the center-left. The southwestern contact of the pluton (partially hidden by a thin veneer of reddish colluvium) is marked by the highest occurrences of light-colored grus. Complex interfingering of tonalite and wall rock is visible in the lower left-hand corner of the view. The skyline ridges in the center of the panorama are 1-2 km north and northeast of the pluton. The northwestern tip of the high plateau of Sierra San Pedro Mártir is faintly visible at the right-hand edge of the photographs. The poor exposure apparent in this view is typical of the southern third of the pluton. The prominent topographic bench in the right-hand frame is a remnant of the Peterson erosional surface; a second remnant appears as a short dark horizontal line slightly above this bench.

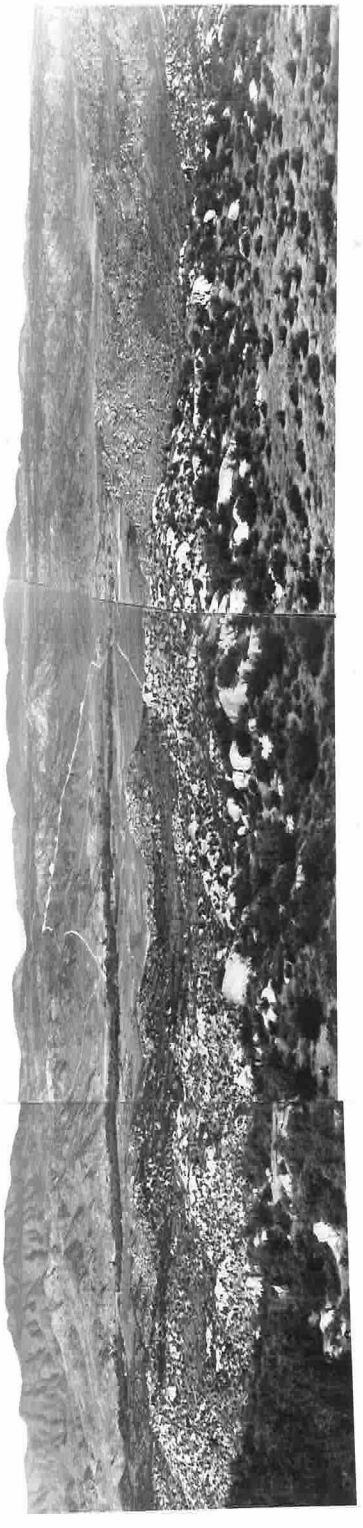

rocks total 1-2%. The tonalite is medium-grained and contains consistently 15-25% mafics, 10-25% quartz, and 55-70% plagioclase. Hornblende generally exceeds biotite, but both are conspicuous. Potash feldspar is not visible in hand specimen and typically constitutes <0.25% of the rocks, although much of the western third of the pluton contains 0.5-2%.

Weak to strong flow foliation recognizable throughout most of the pluton led Woodford and Harriss (1938) to describe the San José tonalite as typically "gneissoid". This term implies to me a stronger fabric than is present in most of the rocks, and I use it only for some of the marginal rocks of the pluton.

Overall, the pluton is remarkably uniform, both petrographically and chemically. Abundant schlieren and/or inclusions produce a small-scale inhomogeneity in some areas, but in general, the large-scale uniformity is duplicated on the outcrop scale. Despite this striking uniformity, detailed mapping revealed three texturally distinct units (Plate 2) formed by two or possibly three intrusive pulses. Two units, an interior prismatic hornblende tonalite (PHbT) and an outer horseshoe-shaped stubby hornblende tonalite (SHbT), make up the northern two thirds of the pluton. A seriate porphyritic tonalite unit (SPT) comprises the southern wedge. The PHbT is characterized by elongate prisms of hornblende, thin plates of biotite, and a seriate grain-size distribution of all major minerals. The SHbT, whose horseshoe shape is open to the south, is distinguished primarily by subequant forms and equigranular grain-size distribution of hornblende and biotite.

The SHbT grades outward into a gneissose border phase (GBT) developed near contacts with country rocks. The SPT is distinguished from the PHbT only by the presence of very sparse large euhedral plagioclase crystals, generally 6-15 mm but up to 20 mm in size.

Along much of its length, the contact between the SHbT and PHbT is gradational across a zone 1-100 m wide, but in the east and northeast, a zone of heterogeneous dioritic rock and inclusion-rich tonalite separates the two units and is intruded by both. Similar zones occur within the adjacent SHbT. The relationships of the two tonalite units strongly suggest that the SHbT is a younger pulse emplaced around the margins of the PHbT. Other relationships indicate that the two units were closely spaced in time, possibly in part contemporaneous.

The SPT is completely gradational, both petrographically and structurally, into the PHbT; it is not exposed in contact with the SHbT. The SPT appears to be the youngest of the three units and may be either a late phase of the PHbT or a separate pulse intruded prior to complete solidification of the PHbT.

Although the pluton is clearly a single structural and petrologic entity composed of intrusive pulses which are closely related in time as well as space, the structure and style of emplacement differ markedly in the northern and southern parts of the body. The two northern units share a single structural pattern; together they appear to form a steeply north-northeast-plunging, concordant cylindrical body emplaced almost entirely by forceful shouldering aside of the strata. Penetra-

tive deformation and distension of wall rocks are extreme around the northern contact, but decrease gradually southward. In contrast, intrusion of the southern wedge of SPT involved large-scale stoping and much less deflection and distension of the strata. The southwestern contact of the SPT crosscuts strata irregularly at an acute angle. The southeastern contact is also discordant, but it is more nearly parallel to bedding on a large scale.

The igneous foliation pattern (Plate 3) shows a similar asymmetry from north to south. A northward-convex, arcuate pattern of foliation conformable to the contacts is the dominant internal structure in the northern two thirds of the pluton. The pattern is unusually regular and systematic in comparison to the foliation patterns in most mapped batholithic plutons. Foliation intensity decreases inward from gneissose and protoclastic near the pluton margins to faint in the center of the body. There is generally a distinct increase in foliation intensity near the SHbT-PHbT contact zone, particularly in the PHbT.

As with the horseshoe shape of the SHbT, the arcuate foliation pattern does not close to the south, but rather, as the more interior and southern parts of the mass are considered, the center of curvature is displaced progressively southward. Concurrently, foliation becomes progressively less distinct and systematic until, within the southern wedge, foliation is faint at best, the pattern is irregular and only vaguely concentric, and there is little, if any, increase in intensity near most contacts. There is, however, a suggestion of closure of foliation attitudes in plan view around the probable latest source of up-welling

magma near the center of the SPT.

The transition from concordant to discordant contact geometry occurs rather abruptly at and just south of the tips of the SHbT horseshoe. In contrast, the transition in intensity of both the magmatic foliation and the penetrative deformation of wall rocks is gradual and continuous.

There is thus a gradation between two greatly differing structural styles, one concordant and indicative of emplacement in a regime dominated by penetrative regional deformation, the other discordant and indicative of a fracture-dominated, seemingly post-tectonic or sheltered regime. Similarly, there is complete petrographic and structural gradation from the PHbT in the northern regime to the SPT in the south. The origin of this north-south asymmetry without discontinuity is one of the important structural problems to be considered. Closely related to this are several other important questions.

(1) What were the mechanisms of emplacement -- that is, forceful intrusion *versus* stoping, "en masse" diapiric rise *versus* gradual up-welling and lateral expansion of magma?

(2) What was the physical state of the tonalite during emplacement -- i.e., melt-rich magma, crystal-rich magma, or solid rock? Directly related to the second question is the problem of

(3) how does one distinguish between magmatic *versus* solid-state origin of flow structures?

(4) How does one recognize the timing of batholithic intrusion relative

to regional deformation and the extent to which the structural and textural characteristics of a pluton and its country rocks are dependent upon the nature of the tectonic regime during emplacement? Examination of a single pluton cannot provide answers of universal applicability to all of these questions; however, evidence presented in the following chapters suggests that the San José pluton is illustrative of the types of structures and textures which develop in response to syntectonic forceful emplacement of crystal-rich magmas, involving gradual up-welling and lateral expansion rather than "en masse" diapiric rise.

Chapter 4

PRE-BATHOLITHIC ROCKS

4.1 General Statement

The goal of the limited mapping in the country rocks was to determine the basic types of rocks present and, in particular, to determine their contact relationships to the pluton. Except along roads and around the Willow Creek pluton, mapping was largely restricted to within 1.5 km or generally less of the San José pluton. Where lithologic units are readily distinguishable, I have subdivided the section and mapped their distribution, but throughout most of the area I have not attempted to establish either stratigraphic or structural details. Superposition of severe deformation and locally intense recrystallization and magmatic injection on a section apparently characterized by originally discontinuous stratigraphic units and local facies changes, especially in the volcanic and calcareous units, makes subdivision and mapping of lithologies and structure a challenging project outside the scope of the present study.

Silver et al. (1963) found no non-volcanic detritus other than fragmental organic carbonate material in the Alisitos formation throughout the area from San José northwestward 110 km to Punta China on the coast. Other than a single fragment of gabbro in a conglomeratic wacke, I also found no identifiable contribution from a non-volcanic, non-carbonate source. There is no evidence that a batholithic or cratonic terrane was exposed in the source region during deposition of the pre-batholithic rocks surrounding the San José pluton.

4.2 Lithologies and Distribution

For tens of kilometers northwest of the San José area, the Alisitos strata maintain a relatively uniform southeastward trend toward the pluton (Silver et al., 1963; see Frontispiece). As seen in Figure 2 and Plate 1, the section divides northwest of the pluton near Rancho Buena Vista. One element of the section, consisting of interbedded volcanic wacke and pebbly or conglomeratic wacke, plus several masses of basalt[2] and andesite, one small body of hypabyssal granite, and some marble, calc-silicate rock, mudstone, and tuff, continues along the regional southeastward strike down the western side of the pluton. The other portion of the section, consisting mostly of tuffaceous and siliceous mudstone, plus some tuff, volcanic wacke, pebbly wacke, breccia, and andesitic to rhyolitic porphyry, is bent abruptly eastward and northeastward and is wrapped around the northern and eastern sides of the pluton; marble and calc-silicate rock are minor but stratigraphically important rock types in this part of the section.

Consider the section west of the pluton. Metamorphosed volcaniclastic wacke and pebbly wacke, with some interbeds of mudstone and rare calc-silicate rock, form a thick unit which extends along much of the western margin of the pluton (Plate 2). The western contact of the SPT steps gradually across this unit and truncates it just north of Cerro Hechicera (area R-6). Truncation of fold axes (area Q,R-6) and

---

[2]The term basalt refers to all dark porphyries (>20% phenocrysts) or aphanitic igneous rocks having a color index >30 and containing plagioclase phenocrysts whose average An content is ≥50. In a chemical classification system, some or all of the "basalts" might be basaltic andesites or andesites.

of metamorphic foliation indicates that the section was tightly folded prior to intrusion of the SPT.

Beds in the wacke and pebbly wacke range from a few centimeters to many meters thick. In good exposures, pebbly or conglomeratic layers commonly can be seen to wedge out along strike. Cross-bedding and, less commonly, graded bedding and sedimentary slump structures are locally conspicuous. Together with the resistant nature of the unit and its distinctiveness from other strata in the San José region, these sedimentary structures make this unit potentially very important for regional mapping and correlation.

In the least metamorphosed and least deformed pebbly wacke, clasts are generally one to several centimeters in diameter -- rarely greater than 10 cm -- and subangular to subrounded. Mineral grains are also angular to subrounded and could not have been transported very far. Rock types in the coarse clast population include, in approximate order of decreasing abundance: dark gray basalt (and/or andesite) similar to that forming the large masses shown on Plate 2; fine-grained light gray marble, dark gray mudstone and/or tuff; massive fine-grained epidote; and minor jasper, bull quartz, light-colored felsite, and fine- to medium-grained hypabyssal granitic rock. A single 6-cm fragment of gabbro or diorite with a 3-4 mm grain size and about 40% mafics is the only plutonic rock fragment identified in the country rocks immediately around the pluton.

The matrix of the volcanic wacke and pebbly wacke varies from a dark gray mudstone or fine-grained tuff with abundant 1-2 mm plagioclase crystals to a gray or gray-green wacke with abundant volcanic rock

fragments and detrital grains of plagioclase, pyroxene and/or amphibole, quartz, and chert. Several percent of fine-grained interstitial orthoclase is visible in thin sections of the more metamorphosed samples, but detrital K-feldspar is rare or absent.

Within a few hundred meters of the pluton, clasts have been greatly stretched into triaxial ellipsoids. Clasts of marble have generally been converted to calc-silicate rock. Extreme stretching of clasts in the thin strip of pebbly wacke bordering most of the pluton contact in the north and northwest produced ellipsoids with axial ratios commonly reaching about 15:5:1. These ellipsoids define spectacular lineations at many places (see Figure 11, p. 88). Stretching decreases southward along the contact and westward away from the pluton; it is slight in the rocks more than 1 km west of the pluton.

At least two large masses of metamorphosed basalt and basalt porphyry occur within the area of wacke and pebbly wacke west of the pluton. One body is centered around Arroyo de las Encinas (area L,M-2,3). The second mass, examined only at its southern end, is exposed 1-2 km farther north.

The meta-basalt around Arroyo de las Encinas is a dark gray aphanitic or porphyritic rock containing 0-35% (generally 15-20%) of euhedral plagioclase phenocrysts of variable size and up to several percent of recrystallized 0.5-2 mm pyrabole phenocrysts. Plagioclase phenocrysts most commonly average 1-3 mm in size, but in some of the rocks they average 1 mm or less, and locally they exhibit a seriate range from 1-15 mm. Thin-section examination of two samples shows that the body has been metamorphosed to greenschist grade. Actino-

litic amphibole is abundant in the groundmass, but pilotaxitic texture defined by plagioclase laths is well preserved. Rare mafic phenocrysts have been recrystallized to actinolitic amphibole, or, in a few cases, to aggregates of biotite + opaques + quartz. In contrast, plagioclase phenocrysts are unrecrystallized and consist of weakly zoned bytownite ($\sim An_{75-85}$), with thin rims and some replacement patches of andesine ($\sim An_{40-45}$). The color index is about 30-35. The paucity of mafic phenocrysts, the relatively low color index, and the abundance of plagioclase (60-70%) suggest that the rock corresponds chemically to high-aluminum basalt, basaltic andesite, or possibly andesite.

Near its eastern margin, this mass is moderately sheared and foliated due to intrusion of the San José pluton, but the interior is nearly undeformed. Reconnaissance examination revealed neither magmatic flow structures nor vesicules, nor unequivocal pyroclastic or sedimentary structures or interbeds. Consequently, the origin of the body is uncertain. The simple elliptical geometry suggests that the mass is intrusive. On the other hand, the variable proportion and size of phenocrysts suggest a composite, perhaps pyroclastic, origin.

The southern end of the meta-basalt mass 1-2 km north of Arroyo de las Encinas (area K-2), is amygdaloidal, and the groundmass is slightly coarser-grained; otherwise, this body is similar to the one just described. Amygdales are filled with calcite, quartz, epidote, actinolitic amphibole, and minor sphene.

Non-vesicular meta-basalt with variable proportions of plagioclase phenocrysts occurs as clasts in the adjacent pebbly wacke as well as in marble and calc-silicate layers elsewhere around the pluton.

It is also abundant as pyroclastic and/or epiclastic interlayers and admixed debris in the undifferentiated pre-batholithic rock near the pluton both north and especially south of the Buena Vista-Coyote road.

The principal units surrounding the southern tip of the pluton are a thick section of metamorphosed dark gray volcanic and volcaniclastic rocks, plus a layer of highly variable thickness consisting of marble plus calc-silicate rock. South and southwest of Cerro Hechicera, there are also thick zones of mudstone and tuff and a small body of metamorphosed hypabyssal granite which have not been sufficiently mapped to distinguish on Plate 2.

The meta-volcanic unit at the southern end of the pluton is quite variable. Meta-basalt and meta-andesite containing 15-40% of 1-5 mm subhedral and euhedral plagioclase phenocrysts and several percent of 0.5-2 mm recrystallized pyrabole phenocrysts predominate, but are mixed with and grade into abundant dark gray, fine-grained tuff or tuffaceous mudstone lacking megacrysts. Meta-felsite -- mostly sodic dacite[3] and rare rhyolite or rhyodacite -- is a minor constituent. Sedimentary lenses and interbeds -- particularly lenses of epidote and calc-silicate rock <1 m thick and up to several meters long -- are common throughout the unit, but volumetrically minor. Several slightly larger mappable layers and lenses of marble and calc silicate rock are also scattered through the unit (Plate 2).

Some of the meta-volcanic rocks, especially the meta-felsites,

---

[3]The term sodic dacite refers to those porphyries or aphanitic igneous rocks in which quartz comprises >5%, alkali feldspar comprises <1/3 of the total feldspar, and plagioclase has an average An content <20. No dacite or sodic dacite was found containing >5% alkali feldspar.

near the southern end of the pluton are flow-banded, but much of the unit is massive and lacks obvious layering or flow structures. The intermixing of volcanic and sedimentary material indicates that much of the meta-volcanic rock is pyroclastic and/or epiclastic. The massive and flow-banded porphyries are probably flows and/or tuffs. Except for a few obvious dikes, I saw little evidence that much of the unit is intrusive.

The suggested westward wedging-out of the meta-volcanic unit south of Cañon Las Cabras (area Q-4) is based upon photogeologic observations, suggesting convergence of the volcanic wacke and marble + calc-silicate units, and upon the absence of a meta-volcanic unit between the marble and volcanic wacke about 500 m southeast of the San José-San Telmo road (area N,O-2). I am confident that the map pattern is grossly correct, but the exact geometry and structure need to be determined by ground observations.

The main calcareous zones near the southern end of the pluton range from predominantly marble to nearly pure calc-silicate rock. Variable amounts of admixed volcanic debris are also present, and locally the calcareous layers grade both along and across strike into calc-silicate-rich variants of the surrounding meta-volcanic unit. The principal calc-silicate minerals are garnet, epidote, and diopside, but wollastonite and scapolite are each locally abundant. Quartz, plagioclase, and sphene are other common constituents.

The thickness of the marble and calc-silicate exposures varies from 1 or 2 m to possibly more than 200 m (on Cerro Hechicera). Locally the beds pinch out completely. Both sedimentary facies changes, on

the one hand, and tectonic thickening and thinning and minor faulting, on the other, contribute to the variations, but it is difficult as yet to determine the relative importance of the two. Stretching of clasts in both the pebbly wacke and the calcareous beds rarely exceeds about 3 or 4:1 and is commonly much less. Penetrative deformation was therefore much less intense around this part of the pluton than it was farther north. However, the country rocks around the southern end of the pluton have been pervasively fractured along three major steeply-dipping joint sets: one striking northeast, one approximately north, and one northwest (Plate 5). Minor faulting is common along these sets and may have contributed to the discontinuity of the units. On the other hand, sedimentary facies variations of this scale may not be unreasonable. From studies in areas where deformation and metamorphism are less severe than in the San José area, Silver et al. (1963, p. 2055) found that the limestones "range from thin beds of mixed volcanic clasts and marine shell debris to massive biohermal accumulations" which "locally form sections 300-500 feet thick with only minor clastic interbeds". Metamorphism and deformation have apparently destroyed whatever fossils may have existed in the limestone immediately around the San José pluton. However, Silver (oral communication) found fossils in the limestone unit just south of the San José-San Telmo road (area N,O-2,3). It seems possible, therefore, that the welt of marble and calc-silicate rock on Cerro Hechicera is a biohermal or biostromal mass rather than the product of extreme tectonic thickening, and that the lenticular character of many of the calcareous beds is a primary sedimentary feature. The depositional

environment appears to have been one in which discontinuous beds and locally thick biohermal or biostromal masses of limestone accumulated amid areas of active volcanism and were subjected to frequent influx of pyroclastic and epiclastic volcanic debris and perhaps some flows and shallow intrusives.

The zone of marble plus calc-silicate rock on Cerro Hechicera and up to at least 1.5 km to the west (area R,S-5,6) is bounded on the southwest by about 70-250 m of metamorphosed dark-gray mudstone or tuff not differentiated on Plate 2. The rock is poorly exposed, and bedding is obscure. It may be a phenocryst-poor facies of the meta-volcanic rocks or a separate unit. Southwest of this zone, approximately 1.5 km west of Cerro Hechicera (at and around locality 697, area R-5), there is an unmapped body of metamorphosed hypabyssal granite. The granite is slightly gneissose and has an average grain size of about 0.5-1.5 mm. One sample examined in thin section consists (by estimate) of 30-35% quartz, 60% antiperthite, 5% plagioclase (An_{0-5}), 2% biotite, and 1-2% accessory minerals. Micrographic texture is incipiently developed.

At the southern edge of the map area, the meta-volcanic unit is bounded on the southwest by a section of fine-grained siliceous and tuffaceous mudstone and tuff of unknown thickness and distribution. These rocks, which are thinly bedded and commonly laminated, are reminiscent of the strata comprising most of the section around the northern and eastern sides of the pluton.

Hypothetical projection of the thick section of volcanic wacke and pebbly wacke from west of the pluton southeastward along strike

across the pluton suggests that an equivalent northwestward-striking section of similar rocks should border the SPT on the southeast. However, the area where the volcanic wacke and pebbly wacke would be expected is underlain primarily by meta-volcanic rocks and marble plus calc-silicate rock striking northeastward roughly parallel to the pluton contact. Only the marble plus calc-silicate units are distinguished on Plate 2. Volcanic wacke and pebbly wacke similar to the section west of the pluton appear to be restricted to small incompletely mapped areas on either side of the Willow Creek fault zone, and again the strata strike to the northeast. Thus the section of volcanic wacke and pebbly wacke apparently does not continue directly southeastward away from the pluton. Likewise, the main zone of marble plus calc-silicate rock appears to be wrapped around the southern tip of the pluton rather than to continue southward or southeastward. These observations strongly suggest that the southern tip of the pluton was intruded into the limb of a major steeply-plunging isoclinal fold. This hypothesis and possible alternative interpretations of the large-scale structure in the pre-batholithic rocks will be discussed in Chapter 11.

Now consider the section enclosing the northern and eastern side of the pluton. Figures 5 and 6 show two generalized stratigraphic sections between the San José and Las Cochas plutons: one along Arroyo El Tepetate (area B-6,7) and one from Rancho Cerro Costilla (area C-9) to the crest of Cerro Costilla (area B-10,11). Similar rocks, particularly the tuffaceous and siliceous mudstone and fine-grained tuff, predominate within 1-2 km of the San José pluton and the entire

Figure 5. Generalized stratigraphic section from Rancho Cerro Costilla to the crest of Cerro Costilla. This is a composite of observations along three traverses: (1) on the Concepción road; (2) on an abandoned road branching north off the Concepción road 2.5 km east of Rancho Cerro Costilla, and (3) on a traverse from Rancho Cerro Costilla N 40° E to the crest of Cerro Costilla. Thicknesses are very rough estimates for the third traverse. The section thickens greatly from west to east.

Thickness (m)	Rock type and description
---	Tonalite. Contact of San José pluton at Rancho Cerro Costilla.
1 - 8	Marble plus calc-silicate rock. Fine-grained, light gray marble and fine to coarse-grained garnet- and epidote-rich calc-silicate rock. Probably correlative with map unit M-1.
0 - 15	Slaty tuffaceous siltstone. Present west of Rancho Cerro Costilla. Dark gray, reddish-brown weathering. Poor slaty cleavage.
1 - 5	Schistose leucotonalite(?) sill(?). Discontinuous or poorly exposed, locally branching and discordant. Fine- to medium-grained, light gray to tan, plagioclase-quartz-diopside schist.
650	Slaty mudstone and fine-grained tuff, with layers and lenses of wacke. Poorly cleaved quartz-biotite, quartz-hornblende-biotite, and quartzo-feldspathic slates, phyllites, and very fine-grained schists, frequently very siliceous. Dark gray overall and weathers reddish brown or dark brownish gray; often banded with closely spaced light gray and tan laminae which weather tan or rusty. Sparse thin layers and lenses of marble, calc-silicate rock, and amphibolite. Rare amphibolite masses up to 25 m thick (meta-porphyry and/or meta-diorite). Locally intruded by quartz diorite and gabbro or diorite from Las Cochas pluton.
250	Schist. Northern boundary not well located. Fine- to very fine-grained, dark gray to medium gray or grayish brown biotite and hornblende quartzo-feldspathic schists, locally with garnet, frequently very siliceous. Weathers brownish gray to reddish brown. Some schistose meta-conglomerate or breccia and lithic tuff.
300?	Slaty mudstone and fine-grained tuff, with layers and lenses of wacke. Southern boundary not well located. Similar to thick mudstone and tuff unit nearer the San José pluton.
50	Schist. Fine-grained, dark gray or brownish-gray mica and hornblende schists similar to the previous schist unit.
400	Schist and gneiss. Fine to medium-grained, thick resistant layers of poorly foliated, schistose and gneissose, medium gray volcanic breccia, light gray rhyolite porphyry, and light gray to creamy rhyolitic tuff. Also some medium gray quartzo-feldspathic biotite schist (meta-breccia or lithic tuff), dark brownish-gray mica schist, and dark gray andesite(?) porphyry. Schists are coarser than those nearer the San José pluton.

Figure 6. Generalized stratigraphic section in Arroyo El Tepetate between the San José and Las Cochas plutons. Thickness estimates are approximate. The section thickens greatly to the west and both thins and is truncated by gabbro or diorite and quartz diorite to the east.

Thickness (m)	Rock type and description
---	Tonalite. Contact of San José pluton
1	Stretched-pebble meta-wacke. Pinches out within 100 m to the west. Thickens gradually to 10-15 m at and east of the Tepetate road. Resistant, orange-brown weathering gneiss; medium to dark gray or greenish gray on fresh surface. Grain size in pebbles and matrix is fine or very fine. Pebbles have been flattened and stretched into ellipsoidal plates with axial ratios commonly as extreme as 15:5:1, giving the rock a gneissose appearance. Maximum dimensions of stretched pebbles, variable from 1 to 30 cm define a spectacular east-plunging lineation (Figure 11, p. 88). Some interbeds of wacke and mudstone. Locally cut by abundant thin patches and stringers of light-colored granitic rock with hornblende (rarely diopside).
5 - 8	Marble and calc-silicate rock (map unit M-1). Pinches out abruptly east of road. Variable proportions of fine-grained, light gray marble and fine- to coarse-grained garnet- and epidote-rich calc-silicate rock.
850	Slaty mudstone and fine-grained tuff, with lenses and interbeds of wacke. Medium to dark gray, poorly cleaved slates and phyllites, frequently siliceous; similar to thick zones of mudstone and tuff in the Cerro Costilla section. Weathers reddish brown and dark brownish gray. Within 200 m of the San José pluton and in the northernmost part of the section, laminated slates predominate; laminae are light to medium gray or tan and weather tan to rusty. Laminae commonly produce a pin-stripe or tiger-stripe appearance. Some thin lenses and layers of calc-silicate rock. Minor meta-conglomerate and lithic tuff. Sparse andesitic and dacitic dikes. Towards the center of the section, meta-siltstone and fine-grained wacke increase in abundance, and lamination is less pronounced. The northern part of the unit is intruded and truncated by diorite or gabbro and quartz diorite from Las Cochas pluton.
70	Slaty tuffaceous siltstone and wacke. Probably gradational with adjacent mudstone and fine-grained tuff. Medium to dark gray tuffaceous meta-siltstone, like that in the previous unit, and light to medium gray, fine- to medium-grained wacke (and tuff?) predominate. Weakly laminated and slightly gneissose. Some laminated slate like that in the adjacent unit, and some light gray or tan, fine- to medium-grained, gneissose meta-felsite. Intruded and truncated by gabbro or diorite and quartz diorite from the Las Cochas pluton.
---	Tonalite, quartz diorite, and gabbro or diorite. Contact of Las Cochas pluton.

northern and eastern sides between the Buena Vista-Coyote and San José-Observatorio roads. South of the latter road, the section of mudstone and tuff appears to diverge slightly away from the pluton, and marble, calc-silicate rock, meta-volcanic rocks, and locally volcanic wacke and pebbly wacke predominate within several hundred meters of the pluton.

Small masses of dark gray meta-basalt or meta-andesite with abundant plagioclase phenocrysts occur locally in the mudstone and tuff between the San José-Observatorio road and Cañon La Jolla (area K-13), but there are no large areas of meta-volcanic rocks immediately north or east of the pluton such as exist around the western and southern margins. Dikes and sills or extrusive layers of basaltic to dacitic composition are scattered through the section, but are volumetrically minor. Small bodies of diorite and/or gabbro are intruded locally into the section; some are strongly deformed and metamorphosed and may be part of the pre-batholithic section, but others appear undeformed and may postdate the San José pluton. In the southeastern part of the area, aplitic dikes striking generally N 35-80° W are abundant in the country rocks and also cut the San José pluton (Plate 5). Many of these dikes are deformed.

Woodford and Harriss (1938) chose the strata exposed in "Arroyo San Telmo" between the San José and La Jolla plutons as the type section for their San Telmo formation. This section corresponds to the stretch of Cañon La Jolla from area J-14 eastward for about 4 km. They (p. 1306) reported that the section consists of "slates or phyllites, quartzite, meta-conglomerate, meta-porphyry, and meta-tuff, mostly dipping steeply northeast, and with an apparent thickness

of 10,000 feet or more". Measured on the aerial photographs, the apparent thickness is approximately 4000 m. I have examined only the westernmost 800 m of this section; the rocks are comparable to those described in Figures 5 and 6. The abundant fine-grained "quartzite" to which they referred apparently corresponds to the siliceous slate and phyllite which I interpret to be metamorphosed cherty mudstone and tuff. I found no clear evidence of detrital quartz in these rocks.

Three zones of feldspathic quartzite, each several meters thick, outcrop southeast of the pluton: (1) a layer traced for 100 m northeastward from the northeastern contact of the Willow Creek pluton (area N-13), (2) a fault-disrupted segment between the southwestern margin of that pluton and the Willow Creek fault zone (area O-11,12), and (3) a bed extending at least 330 m southwestward from the Willow Creek fault zone 0.5-1 km west of the Willow Creek pluton (area O-11). The quartzite in zone 2 is composed of laminae several millimeters to several centimeters thick of nearly pure recrystallized gray quartz interspersed with laminae of light tan or pinkish-tan feldspathic quartzite showing various degrees of preservation of an original medium-grained (0.5-1 mm) detrital texture. Thin-section examination of a feldspathic layer revealed (by estimate) 75% quartz, 10% microcline, 5% plagioclase (oligoclase), 4-5% deep blue-green (Fe-rich) hornblende, 2-3% epidote, and accessory biotite, sphene, clinopyroxene, opaque, apatite, and zircon. Spotty preservation of the original detrital texture reveals equant anhedral to subhedral or rarely euhedral bipyramidal quartz grains and sparse subhedral plagioclase crystals in a matrix consisting mostly of molded and interstitial microcline. The

parent rock appears to have been a reworked felsic volcanic in which quartz phenocrysts were strongly concentrated. The bipyramidal form of quartz and the absence of identifiable granitic or metamorphic rock fragments seems to rule out a plutonic or metamorphic source. The microcline probably formed by recrystallization of clays or of a potassic volcanic groundmass, although there may also have been some detrital alkali feldspar.

The quartzite in zone 1 appears similar in outcrop to that just described, except that some layers contain abundant garnet, presumably indicative of a calcareous component in the parent rock. The quartzite in zone 3 is a light gray, poorly bedded rock whose original detrital textures and structures have been largely destroyed by shearing and recrystallization. A thin section of the latter zone revealed approximately 90% quartz, 4-5% plagioclase (albite), 3-4% actinolitic (?) amphibole, and accessory epidote, carbonate, apatite, sphene, biotite, white mica, chlorite, and zircon, but little or no potash feldspar.

Quartzite zones 1 and 2 on opposite sides of the Willow Creek pluton are almost certainly correlative; they strike very nearly towards one another and indicate an absence of significant lateral offset across the pluton. Correlation with quartzite zone 3 southwest of the Willow Creek fault zone implies an apparent right-lateral offset of about 475 m on the fault. If other similar quartzites are present in the section (or if a single bed has been duplicated by folding or by faulting independent of the Willow Creek fault), the estimate of offset is clearly invalid; however, I have found no other detrital quartzites, nor indeed any suggestion that more are likely. Moreover, the estimated offset

agrees well with the minimum 350 m of apparent right-lateral offset of the incompletely mapped volcanic wacke and pebbly wacke and with the 440 m of apparent right-lateral offset of the intrusive rock-country rock contact of the San José pluton farther west (see Section 5.4 for a more detailed discussion of faulting).

4.3 Metamorphism

In a general way, metamorphic grade increases greatly from west to east across the western foothills and the Sierra San Pedro Mártir (Woodford and Harriss, 1938; Silver et al., 1963). Strata west and northwest of the San José pluton consist of greenschist facies assemblages mixed with relict sedimentary and volcanic material; many are virtually unmetamorphosed. Hornblende-hornfels facies assemblages are developed in contact aureoles around the San José and neighboring plutons, but greenschist facies assemblages again prevail along the San José-Observatorio road from about 2 km to 5 or 6 km east of the pluton. Eastward from there, metamorphic grade increases rapidly; locally abundant sillimanite and/or cordierite in quartz-biotite-muscovite-plagioclase schists and gneisses indicate development of upper amphibolite facies of regional metamorphism or K-feldspar-cordierite-hornfels facies of contact metamorphism (Winkler, 1967) on the high plateau of the Sierra San Pedro Mártir.

Throughout much of the area from San José eastward, but especially on the high plateau, contact metamorphic aureoles overlap, and distinction between contact and regional metamorphism is extremely difficult and perhaps not meaningful. Except for some calc-silicate

masses, the rocks all possess a cleavage or schistosity indicative of dynamothermal metamorphism, regardless of their proximity to intrusive contacts. The calc-silicate rocks are commonly coarse- or very coarse-grained (garnet, epidote, or wollastonite crystals up to several centimeters in size); otherwise, the average grain size in the rocks surrounding the San José pluton is consistently $\leq$0.5 mm. Despite recrystallization and severe deformation, sedimentary and volcanic structures and textures (e.g., bedding, lamination, and porphyritic or conglomeratic textures) are generally recognizable. However, repeated intrusion and metamorphism, combined with complex shearing, faulting, and migmatization, caused nearly complete destruction of primary structures and textures in some of the rocks between the San José, Willow Creek, and Encina Sola plutons.

Characteristic assemblages in the major pre-batholithic rock types are listed in Table 1. The rocks have been divided loosely into three groups: (1) low-grade rocks outside or in the periphery of the contact aureole of the San José pluton, (2) moderate- to high-grade rocks northeast of the pluton, where the contact aureoles of the San José and Las Cochas plutons overlap, and (3) moderate- to high-grade rocks within the San José contact aureole. No attempt has been made to accurately delineate the limits of the contact aureole. Assemblages observed in schists and gneisses on top of the Sierra San Pedro Mártir are listed in Appendix E.

The various rock types differ notably in the extent to which they show metamorphic effects. In particular, the volcanic and hypabyssal intrusive rocks appear to equilibrate less readily than do the wackes,

Table 1

Principal Metamorphic Assemblages in the San José Area.

(1) low-grade regional and outer contact-aureole assemblages (widespread west and locally present east of the San José pluton)

Limestone and calcareous mudstone
carb-qtz-hb/act-bio-plag-op + relict volcaniclastic material
carb ± relict volcaniclastic material

Volcanic and hypabyssal intrusive rocks
meta-felsite (microgranite)
antiper-qtz-plag (ab)-bio-op-ep-sph-w mica-zir

meta-andesite and meta-basalt
plag (original igneous composition)-act-op-qtz ± ep ± bio ± alk feld ± sph ± carb ± chl ± w mica

Volcanic breccia
ep-act-qtz-leuc + relict volcaniclastic material
act-carb-qtz-plag-bio-op-sph-ep + relict volcaniclastic material
bio-chl-qtz-carb-cz + relict volcaniclastic material

Volcanic wacke and pebbly wacke
act-qtz-bio-carb-ab (?) + relict volcaniclastic material

Mudstone and fine-grained tuff
act-bio + relict tuffaceous and epiclastic volcanic material.

(2) higher-grade regional or contact-regional mineral assemblages (northeast of the San José pluton)

Mudstone, fine-grained tuff, and wacke
qtz-bio-hb-plag (An=30-40)-op-sph
qtz-bio-plag(An=30-40)-hb-op±alk feld±ga(alm/sp)±sph±ap±zir
qtz-bio-plag (An=35-40)-op-ga (alm/sp)-w mica-ap(?)-zir(?)
qtz-w mica-plag-op
qtz-bio-w mica-plag-andal-op-ep-alk feld

(3) higher-grade contact metamorphic mineral assemblages

Marble and calc-silicate rock
carb-ga (gr/an)-woll(?)
woll-ga (gr/an)-cpx-carb-vesuv(?)-sph-zir
ga (gr/an)-qtz-thul-vesuv(?)-cpx-zeol(?)-al
ga (gr/an)-qtz-ep ± plag
scap-cpx-ga (gr/an)-plag (An ≈ 35)-carb-woll-sph-op

Table 1 (continued)

Calcareous mudstone
qtz-cpx-ga (gr/an)-orth ± ep ± carb ± plag ± op ± sph(?)
qtz-cz-ga (gr/an)-op-plag ± cpx(?) ± orth ± sph
qtz-woll(?)-ep-ga(?)-op-carb-cpx-sph(?)
qtz-ga (gr/an)-op-cpx-ep-alk feld-ap-sph-w mica
ga (gr/an)-qtz-plag (lab)-ep-sph(?)-op-cpx-ap-alk feld-chl-w mica

Volcanic and hypabyssal intrusive rocks
meta-felsite
alk feld (micr/antiper)-qtz-plag(ab)-hb-op-bio-sph-ap-zir±ep
plag (ab)-qtz-bio-hb-op-ap-sph-ep-alk feld-carb
plag (An=10-20)-qtz-bio-w mica-ga (alm/sp?)-ap±alk feld±sph±zir

meta-andesite and meta-basalt
plag (ads and/or original igneous composition)-hb-qtz-bio-op-alk feld ± ap ± ep ± sph
plag (ads)-bio-hb-op-alk feld-sph-ap

Volcanic wacke and pebbly wacke
plag (ads)-hb-qtz-cpx-op-ap±orth±sph±ep±bio±zir±ga (alm/sp?) ±trem±tourm
qtz-plag (ads)-hb-cpx-orth-ep-op-sph-ap ± bio ± al
plag (lab)-hb-qtz-alk feld-ap-ep-bio ± op ± sph
plag (ads)-hb ± bio ± qtz ± alk feld ± op ± cpx ± scap ± ep sph ± ap
qtz-plag (An ≈ 40)-bio-hb-op-ep-alk feld-sph-ap-zir
plag (An ≈ 40-45)-cpx-hb-op-sph-ap-alk feld-zir
plag (An ≈ 40)-hb-qtz-sph-orth-ap

Mudstone, fine-grained tuff, and wacke
plag (ads)-hb-qtz-orth-op-bio ± ep ± carb ± w mica ± sph
plag (byt)-hb-qtz-op ± ep ± cpx ± sph ± bio ± carb ± ap
qtz-bio-plag-hb-alk feld-op ± carb ± ap ± ep
qtz-plag (ads)-hb-bio-op ± alk feld ± ap(?) ± ep(?)
qtz-plag (ads/olig)-w mica-ep(?)-op-bio-sph(?)-ap

Feldspathic quartzite
qtz-plag (ab)-hb/act-ep-carb-ap-sph-bio-w mica-zir
qtz-micr-plag (olig)-hb-ep-cpx-sph-bio-ap-op-zir

Explanation of abbreviations:

act:	actinolite	antiper:	antiperthite
al:	allanite	andal:	andalusite
alk feld:	alkali feldspar	ap:	apatite
orth:	orthoclase	bio:	biotite
micr:	microcline	carb:	carbonate

Table 1 (continued)

Explanation of abbreviations (continued)

chl:	chlorite	qtz:	quartz
cpx:	clinopyroxene	scap:	scapolite
cz:	clinozoisite	sph:	sphene
ep:	epidote	thul:	thulite
ga:	garnet	tourm:	tourmaline
gr/an:	grossularite/andradite	trem:	tremolite
alm/sp:	almandine/spessartine	vesuv:	vesuvianite
hb:	hornblende	w mica:	white mica
leuc:	leucoxene	woll:	wollastonite
op:	opaque	zir:	zircon
plag:	plagioclase	zo:	zoisite
ab:	albite		
olig:	oligoclase		
ads:	andesine		
lab:	labradorite		
byt:	bytownite		
An:	anorthite content		

mudstones, and calcareous rocks. In the andesites and basalts, the mafic component of the groundmass is typically converted to fine-grained actinolitic amphibole (or hornblende) ± epidote, biotite, sphene, and chlorite, but plagioclase phenocrysts commonly show little or no modification, and porphyritic textures are frequently well preserved. In the felsic rocks, metamorphic effects are even less conspicuous; not only may the plagioclase phenocrysts appear unmodified, but the leucocratic groundmass tends to change very little in grain size or mineral assemblage. Consequently, where volcanic or hypabyssal intrusive rocks prevail, as around much of the southern end of the pluton and locally along the western side, metamorphic grade is difficult to determine.

The low-grade rocks outside or in the periphery of the contact aureole (group 1) will be discussed first, then the strata north and northeast of the pluton between the San José and Las Cochas plutons (group 2), and finally the strata within the contact aureole of the San José pluton (group 3).

A calcareous mudstone collected about 470 m northwest of the pluton (area C-4) contains several percent of weakly oriented hornblende (or actinolitic amphibole) porphyroblasts in a very fine-grained matrix. This sample appears to be near the periphery of the San José contact aureole. The aureole is significantly wider west and southwest of the pluton. Hornblende-hornfels facies assemblages are developed in the wacke and pebbly wacke for at least 400 m from the pluton contact, and weak foliation parallel to the contact can be seen as much as 1-1.5 km west of the pluton. However, recognizable contact effects are slight in the rocks 1 km or more from the pluton.

Outside the contact aureole in the west and northwest, the rocks consist of variable proportions of greenschist assemblages plus relict sedimentary and volcanic material. In many cases, relict material appears to greatly predominate, and primary textures and structures are well preserved. The principal metamorphic minerals are actinolitic amphibole, epidote, biotite, quartz, and carbonate. Sphene, chlorite, clinozoisite, and opaques also occur. Metamorphic albite is apparently minor or absent; plagioclase generally appears to be relict.

Two samples collected 650 m apart along the San José-Observatorio road about 4 km east of the pluton were examined in thin section. One is a laminated slate containing 1-2% of 0.1-0.5 mm amphibole porphyroblasts in a very fine-grained, virtually unrecrystallized (?) matrix. The other is a calcareous meta-volcanic breccia composed of very fine-grained, intergrown actinolitic amphibole, carbonate, quartz, and plagioclase, with some biotite and epidote and much relict material. Comparably low-grade rocks prevail all along the road from about 2 to 5 or 6 km east of the pluton.

The existence of low-grade rocks east of the pluton has important implications. Clearly, the regional grade of metamorphism prior to intrusion of the San José and neighboring plutons was low not only to the west, but also for at least 5-6 km to the east of the San José pluton. If, across this part of the foothills and sierra, there is a regional metamorphic gradient which is independent of contact metamorphic effects, the gradient must be very slight west of Cuesta Socorro (Plate 1). Conceivably, the general eastward increase in metamorphic grade is due entirely to increasing intensity, breadth,

and coalescence of contact metamorphic aureoles.

Throughout the area between the Las Cochas and San José plutons, and for several kilometers along the Concepción road east of Rancho Cerro Costilla, the strata consist of slates and fine-grained schists and gneisses containing biotite and/or blue-green or yellow-green hornblende irregularly zoned in some cases to patches or rims of actinolite. Characteristic assemblages are given in Table 1, part 2. Some of the plagioclase is relict, but the recrystallized plagioclase is generally andesine ($\sim An_{30-40}$), except in the meta-felsite. Pinkish-red garnet, presumably almandine or spessartine, is locally present. The assemblages are characteristic of the hornblende-hornfels facies of contact metamorphism or of the upper greenschist or lower amphibolite facies of regional metamorphism (Winkler, 1967). Fine-grained andalusite comprises several percent of a narrow zone of phyllite 730 m northeast of the San José pluton (locality 850; area D-11). This is the only known occurrence of alumino-silicate in the San José area.

Now consider the higher-grade rocks in the inner part of the San José contact aureole (Table 1, part 3). Calc-silicate rocks intermixed with marble are the most spectacular metamorphic rocks in the area. Grossularite/andradite is the most abundant mineral in the calc-silicate rocks, but epidote and quartz are also generally present, and wollastonite, diopside, scapolite, thulite, and plagioclase (variably andesine to bytownite) are major phases at one or more localities. Accessory minerals include sphene, clinozoisite, orthoclase (or microcline), opaques, apatite, white mica, and chlorite. Nearly pure red-brown garnet occurs with minor epidote and quartz in masses tens

or hundreds of square meters in size. Well-formed garnet crystals up to 1-2 cm in size are common in these masses, and excellent dark green epidote crystals up to 1-2 cm are locally developed. A nodule 30 cm or more in diameter of nearly pure white wollastonite in blades 1-4 cm long was found along the northern contact about 30 m west of the Tepetate road (area C-6,7). Wollastonite also occurs with scapolite, garnet, diopside, and plagioclase as much as 270 m southeast of the pluton (in the marble + calc-silicate layer north of El Alisito canyon, area Q-9).

In the wackes and mudstones within the San José contact aureole, the principal minerals are quartz, hornblende, biotite, clinopyroxene, plagioclase, and alkali feldspar. Epidote, sphene, opaque, apatite, zircon, and rarely white mica, allanite, and tourmaline (?) are accessory minerals. Carbonate, garnet, and scapolite are present in some of the originally calcareous rocks. Plagioclase is generally andesine, although labradorite or bytownite occurs in a few originally calcareous rocks. Clinopyroxene, apparently salite, is pale or very pale green and shows little or no pleochroism; the 2V estimated in several samples by the method of Kamb (1958) is about 60-62° ± 5°, similar to that of the clinopyroxene in the calc-silicate rocks and of the trace amounts of relict clinopyroxene in the tonalite. Hornblende is typically deep yellow-green to blue-green and has a large negative 2V. Biotite is orange-brown or red-brown and strongly pleochroic. Alkali feldspar, where coarse enough to see clearly, generally appears untwinned and has a moderate or sometimes large 2V. Wavy extinction or distinct twinning indicative of microcline is present in some or all of the

alkali feldspar in a few samples.

The various minerals in the volcanic wacke respond quite differently to metamorphism. For example, in low-grade rocks along the San José-San Telmo road 2 km southwest of the pluton, plagioclase, quartz, mafic grains, carbonate, and rock fragments all exhibit clear detrital (or relict phenocrystic) shapes, but mafic grains have been converted to actinolite, whereas some, possibly most, of the plagioclase retains its original magmatic zoning and composition. In the hornblende-clinopyroxene-rich assemblages within 400 m of the pluton, detrital mafic grains have been entirely destroyed, but some detrital plagioclase, quartz, and carbonate grains are generally still recognizable except in the most intensely sheared and recrystallized rocks within 100-150 m of the contact. However, in the hornblende-clinopyroxene-rich rocks, even those plagioclase grains which preserve detrital shapes are unzoned, uniform in composition from grain to grain, and identical in composition to the obviously recrystallized plagioclase; these detrital grains have apparently equilibrated without major textural modification.

Schwarcz (1969) showed that regional metamorphism in the Winchester-Hemet area of southern California is similar to the low pressure-high temperature type described by Miyashiro (1958) from the Abukuma Plateau in Japan. The general assemblage reported by Duffield (1968) for the pre-batholithic rocks around the El Pinal pluton 150 km northwest of San José is also consistent with Abukuma-type metamorphism. However, Winkler (1967, pp. 123-124) pointed out that Abukuma-type regional metamorphism and relatively deep-seated

contact metamorphism produce identical mineral assemblages.

Cordierite, an important indicator of this type of metamorphism in both the Winchester-Hemet and El Pinal areas was not found in the San José area, but it occurs locally with sillimanite in the Sierra San Pedro Mártir (Appendix E). Also, Woodford and Harriss (1938, p. 1310) tentatively identified cordierite as a major mineral in a hornfels "on the San Telmo-San José road, 10 miles east of San Telmo village" (about 16 km west of Rancho San José).

The presence of andalusite 730 m northeast of the pluton (locality 850) requires pressures less than that of the alumino-silicate triple point. Estimates of the pressure of the triple point vary widely and include, among others: 6.5 kb (Althaus, 1967), 5.5 kb (Richardson et al., 1969), and 3.76 kb (Holdaway, 1971). In general, all of the assemblages found in the San José area are consistent with low pressure-high temperature contact or Abukuma-type regional metamorphism.

In the ensuing discussion of contact metamorphic facies and conditions, I have followed the classification system and many of the arguments of Winkler (1967, see especially pp. 69-79 and 116-124). Figure 7, modeled after Figure 16 of Winkler, superimposes Winkler's estimates of the P-T limits of the major metamorphic facies upon the experimentally determined P-T curves for a number of important reactions. All of the curves are for $P_{fluid} = P_{total}$, and, except for reactions involving CO_2, all of the curves are for $P_{H_2O} = P_{total}$.

Winkler considered the first appearance of hornblende, diopside, and grossularite/andradite garnet, as well as several minerals not found in the San José area, as diagnostic of the lower limits of the

Figure 7. Important reactions and pressure-temperature fields of contact metamorphic facies ($P_{fluid} = P_{total}$). Field 1 (below heavy curve C): albite-epidote-hornfels facies; field 2 (between heavy curves C and F): hornblende-hornfels facies; field 3 (above curve F): K-feldspar-cordierite-hornfels facies. Estimates of the facies limits are those of Winkler (1967), except that boundary curve F between the fields of the hornblende-hornfels and K-feldspar-cordierite-hornfels facies is based on the experimental data of Althaus et al. (1970) and is at slightly lower temperatures than those given by Winkler (p. 74 and Table 4). Curves B_1 and B_2 for the reaction tremolite + calcite + quartz $\rightleftharpoons$ diopside + CO_2 + H_2O are given for two CO_2-H_2O mixtures: $X(CO_2) = 0.25$ and $X(CO_2) = 0.75$. Curve B_2 gives the maximum temperatures at which this equilibrium will occur; i.e., for $X(CO_2) > 0.75$, the equilibrium temperatures must be lower than those for $X(CO_2) = 0.75$ (Winkler, pp. 30-31). Curves E_1-E_5 (italicized print) for the reaction calcite + quartz $\rightleftharpoons$ wollastonite + CO_2 are given for $P(CO_2) = P(total)$, i.e., $X(CO_2) = 1.0$, and for four CO_2-H_2O mixtures: $X(CO_2) = 0.8$, 0.6, 0.4, and 0.2. The reaction for curve D changes for P > 2 kb: anorthite appears as an additional product, and the exact reaction is uncertain (Choudhuri and Winkler, 1967). Several independent determinations (stippled boundaries) are shown for the polymorphic transition reactions kyanite $\rightleftharpoons$ andalusite and andalusite $\rightleftharpoons$ sillimanite.

Sources of data:

curve A after Althaus (1966a) as reported by Winkler (1967, p. 70); reaction temperatures drop as much as 90°C in the presence of HCl or H_2SO_4 (Althaus, 1966b);
curves B_1 and B_2 after Metz and Winkler (1964) and Metz (1966) as reported by Winkler (1967, pp. 30-31) and by Metz and Trommsdorff (1968);
curve C from Winkler (1967, p. 72);
curves D, H, and I from Choudhuri and Winkler (1967);
curve E_1 from Harker and Tuttle (1956);
curves E_2, E_3, E_4 and E_5 from Greenwood (1967);
curve F from Althaus et al. (1970);
curve G from Akella and Winkler (1966);
curve J from Tuttle and Bowen (1958).

Abbreviations:

Ab:	albite	en:	enstatite	or:	orthoclase
an:	anorthite	ged:	gedrite	pyph:	pyrophyllite
andal:	andalusite	hb:	hornblende	Q, qtz:	quartz
anth:	anthophyllite	hyp:	hypersthene	sill:	sillimanite
cc:	calcite	Kf:	K-feldspar	trem:	tremolite
chl:	chlorite	ky:	kyanite	v:	vapor
cord:	cordierite	musc:	muscovite	woll:	wollastonite
di:	diopside	opx::	orthopyroxene		

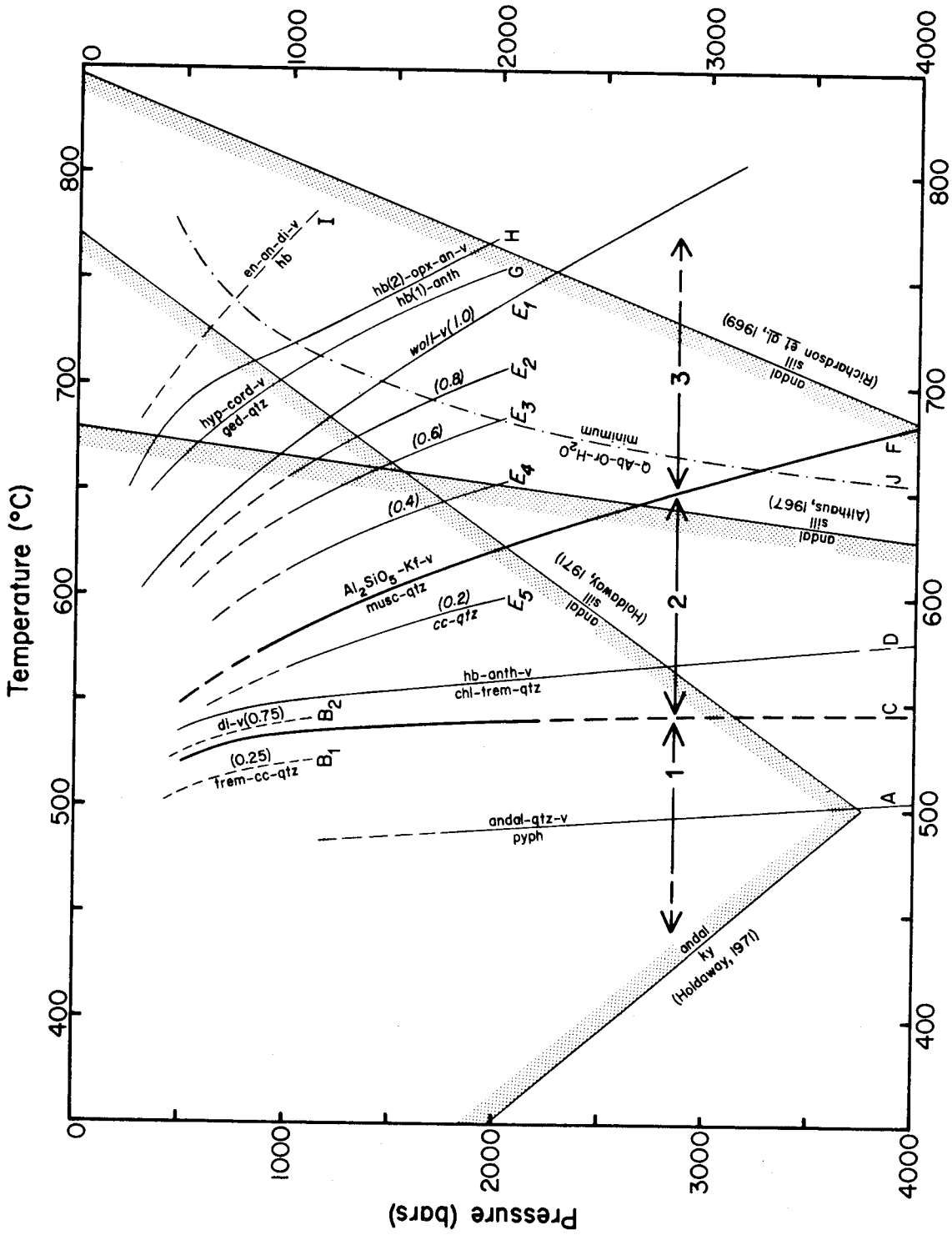
Temperature (°C)
Pressure (bars)
0
1000
2000
3000
4000
400
500
600
700
800
en-an-di-v
hb
I
hb(2)-opx-an-v
hb(1)-anth
H
G
wol-v(1.0)
E1
(0.8)
E2
hyp-cord-v
ged-qtz
E3
(0.6)
Q-Ab-Or-H2O
minimum
F
J
E4
(0.4)
Al2SiO5-Kf-v
musc-qtz
(0.2)
cc-qtz
E5
hb-anth-v
chl-trem-qtz
D
di-v(0.75)
B2
C
(0.25)
trem-cc-qtz
B1
andal-qtz-v
pyph
A
andal
ky
(Holdaway, 1971)
andal
sill
(Holdaway, 1971)
andal
sill
(Althaus, 1967)
andal
sill
(Richardson et al., 1969)
1
2
3

stability field of the hornblende-hornfels facies. Reactions producing these phases occur over a range of temperatures; the curve drawn for the lower-temperature stability limits of the hornblende-hornfels facies is an average, given by Winkler, of a number of experimentally investigated reactions. Winkler placed an uncertainty of about ±20° on the position of this boundary at any given pressure. None of the above minerals, however, is unique to this facies; all can also occur in assemblages characteristic of at least the lower half of the higher-temperature stability field of the K-feldspar-cordierite-hornfels facies. Near the contacts of the San José and Las Cochas plutons, albite and sodic oligoclase appear to be restricted to the Ca-poor meta-felsites, whereas labradorite and bytownite were found only in calc-silicate rocks, in originally calcareous wackes and mudstones, and in unequilibrated (?) meta-basalts and meta-andesites.

Winkler defined the transition from the hornblende-hornfels facies to the K-feldspar-cordierite-hornfels facies by the breakdown reactions:

$$\text{muscovite} + \text{quartz} \rightleftharpoons \text{alumino-silicate} + \text{K-feldspar} + H_2O$$

$$\text{muscovite} + \text{quartz} + \text{biotite} \rightleftharpoons \text{cordierite} + \text{K-feldspar} + H_2O$$

He (p. 74) reported that both reactions proceed at nearly identical conditions. Coarse prograde muscovite coexists with quartz and biotite in a sodic dacite only 35 m northeast of the pluton (in Cañon Campo Buena Vista, area G-12,13). Therefore, at least around this part of the pluton, metamorphism did not exceed the stability limits of the hornblende-hornfels facies, except possibly within a few meters of the contact. Unfortunately, none of the assemblages involved in

these two reactions was found elsewhere near the pluton margin.

In the presence of a CO_2-rich fluid phase, wollastonite is stable only in the K-feldspar-cordierite-hornfels facies. However, Figure 7 shows that wollastonite can occur in the hornblende-hornfels facies if the fluid phase was water-rich (X_{CO_2} < ca. 0.25-0.3). Because the calcareous rocks in the San José area are commonly impure and make up only a small proportion of the pre-batholithic section, and because the particular calcareous zones in which wollastonite was found are generally <10 m thick, rarely 30-40 m thick, the fluid phase in the areas where wollastonite formed may well have been water-rich.

In summary, all of the assemblages in the interior of the contact aureole are consistent with the hornblende-hornfels facies. It is possible that metamorphism locally exceeded the lower stability limits of the K-feldspar-cordierite-hornfels facies, but none of the observations requires this. Orthopyroxene, which is characteristic of the upper part of the P-T field of the K-feldspar-cordierite-hornfels facies, was not found in any of the metamorphic rocks.

Figure 7 permits an estimate of the range of temperatures reached in the wall rocks near the contact. One must keep in mind that the experimental curves for the formation of diopside and of hornblende + anthophyllite provide only a rough estimate of the minimum P-T conditions at which clinopyroxene and hornblende could have formed in the San José assemblages. The stability limits of these phases depend not only on P_{H_2O} and P_{CO_2}, but also on the exact compositions of the pyroxene and hornblende, and on the identities and compositions of the other minerals in the assemblages (i.e., on the possible

reactions which can occur). Nevertheless, assuming the presence of an H_2O-rich fluid phase and assuming pressures in excess of 1 kb, which assumptions seem reasonable, it seems that temperatures in the pre-batholithic rocks at the pluton contact and locally for at least 400 m west and southwest of the contact almost certainly exceeded about 525-550°C.

The upper limit on the possible temperatures is much harder to place. If pressures were in the range 1-3 kb, the stability of the mineral pair muscovite + quartz indicates that the temperature in the meta-dacite 35 m northeast of the contact did not exceed the range 580-660°C. Closer to the contact, temperatures may have been higher, but probably not by much. At pressures greater than 3.2 kb, the stability curve for muscovite + quartz intersects the curve for the initiation of melting in the Q-Ab-Or-H_2O system. Because addition of anorthite to this system raises the temperature of initial melting (von Platen, 1965), curves for the beginning of anatexis in the country rocks around the San José pluton should be higher, perhaps by a few tens of degrees. However, there is no evidence of anatexis at the present level of exposure. Igneous-textured patches and veins in the country rocks typically contain 15-30% mafic minerals (generally hornblende ± biotite, rarely clinopyroxene), as well as relatively calcic plagioclase (generally andesine). Such veins may have formed by metasomatism and/or by injection of magma from the pluton or from other smaller intrusive masses, but apparently not by anatexis. Therefore, 700°C seems to be an upper limit on the maximum temperature attained in the wall rocks. Actual temperatures were probably lower.

Chapter 5

THE PLUTON CONTACT AND RELATIONSHIPS TO WALL ROCKS

5.1 Introduction

The San José pluton was emplaced into strata which had already been deformed into northwest-striking tight or isoclinal folds. Bedding is moderately or steeply dipping throughout the entire area. Except in a few important areas to be considered later, bedding and metamorphic foliation are parallel. In most outcrops, beds are uncontorted or only slightly folded, but small-scale crumpling, isoclinal folding, and boudinage are locally spectacular (Figure 8) and argue for similar deformation on a large scale. Apparent bedding trends inferred from patterns of light and dark striping on aerial photographs also suggest large-scale isoclinal folding northwest, northeast, and east of the pluton. Except for the nose of one northwest-plunging isoclinal synform well exposed along the San José-Observatorio road (area N-15), none of these structures has been mapped. Woodford and Harriss (1938, p. 1324) reported that "southwest of San José the San Telmo slates seem to have been anticlinally folded". Judging from their map, this structure is west of the area I have covered, but reversals of dip and sparse information on the directions of tops of beds in the metamorphosed volcanic wacke and pebbly wacke nearer the pluton also indicate major folding. For the most part, the structural trends in the wall rocks are wrapped concordantly around the pluton, but the southwestern contact of the SPT locally truncated pre-intrusive fold axes (Plate 2).

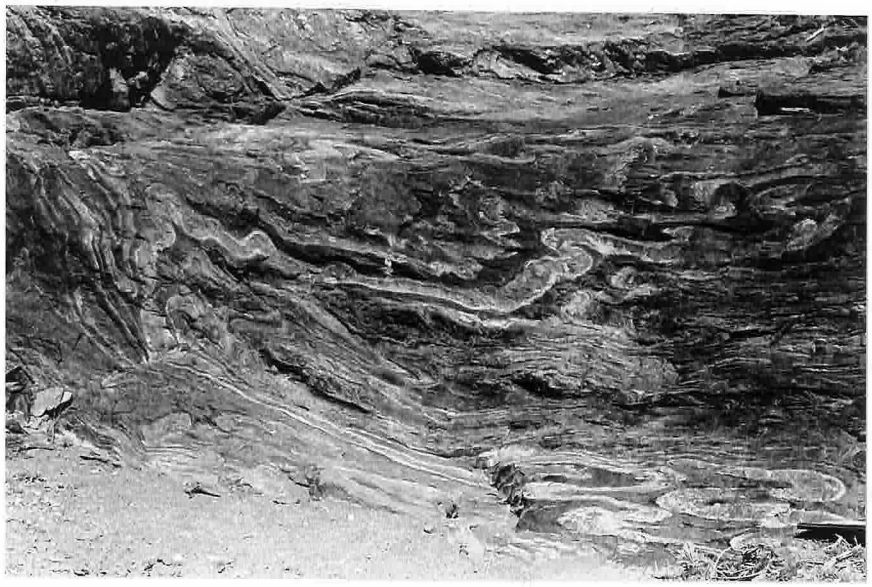

Figure 8A

Figure 8B

Figure 8. Severe flow folding and boudinage of metamorphosed tuffaceous mudstones and tuffs. The hammer in the right center of (A) and at the top of (B) shows scale. Note the thickening and thinning of beds in the noses and limbs of folds. Folds in (A) plunge 55° to the left (N 5° E); the axial planes strike N 20° W and dip 72° northeast (away from the camera) parallel to the pluton contact and to the regional trend of bedding and foliation. Localities: (A) 70 m east of the large mafic sheet along the eastern margin of the pluton, 1 km southeast of Cañon Campo Buena Vista (area H-13); (B) several meters east of the pluton contact, 500 m south of Cañon La Jolla (area K-13).

The simple tear-drop outline of the pluton has been complicated only locally on the eastern side by the Cañon Socorro and Willow Creek fault zones and by shoving of small adjacent intrusive masses against the pluton. However, structures and textures in both the tonalite and wall rocks around the margins of the northern two thirds of the pluton have been influenced by superimposed regional deformation accompanying and perhaps continuing after emplacement of the pluton. The contact around the northern two thirds of the pluton seems to have served as an important regional surface of shearing and tectonic discontinuity during this deformation.

Many major regional lineaments other than the Cañon Socorro and Willow Creek fault zones cross but do not offset the pluton contact. In some cases, these lineaments are related to dikes or dike swarms (e.g., the northeast-striking set north of Cañon Campo Buena Vista, area G-11,12). In other cases, they appear to be simply the expression of regional joint systems. Further mapping and stratigraphic subdivision is required before the importance of faulting in the wall rocks can be fully determined.

The SHbT and SPT are exposed against wall rocks along roughly 29 km and 16 km, respectively, of the 47-km exposed perimeter of the pluton. The PHbT occurs against wall rocks only along a 1.6-km stretch near the San José-San Telmo road in the west.

Variations in the geometry of the contact, in the pattern and intensity of flow structures in the tonalite near the contact, and in the style of deformation of the wall rocks define a striking north-south asymmetry with three main elements.

(1) The pluton contact is remarkably sharp, concordant, and smoothly curving around the margins of the SHbT, but becomes abruptly more irregular and discordant immediately south of the SHbT, especially along the southwestern margin.

(2) The outer part of the SHbT is gneissose and protoclastic. The intensity and width of the gneissose zone are greatest around the northern and northeastern margins and decrease progressively southward. Foliation is generally weak or absent around the margins of the southern third of the pluton.

(3) Penetrative deformation in the wall rocks is extreme near the northern and northeastern margins of the pluton, but also decreases southward and gives way to fracture-dominated deformation around the southern end of the pluton. This north-south asymmetry is of profound importance to understanding the mechanisms and history of emplacement of the pluton.

5.2 Contact of the Stubby Hornblende Tonalite with Wall Rocks

Typical exposures of the SHbT against wall rocks are shown in Figures 9 and 10. The contact is smoothly curving and commonly knife-sharp, especially around the northern margin. In individual outcrops it is generally perfectly concordant or, rarely, discordant by a few degrees. The dip of the contact, of foliation in the tonalite, and of bedding and foliation in the adjacent wall rocks averages 65-75° outward around the eastern and northeastern margins of the SHbT and changes very gradually through 75-85° outward around the northern margin to vertical and locally 85-90° inward on the western side of the SHbT.

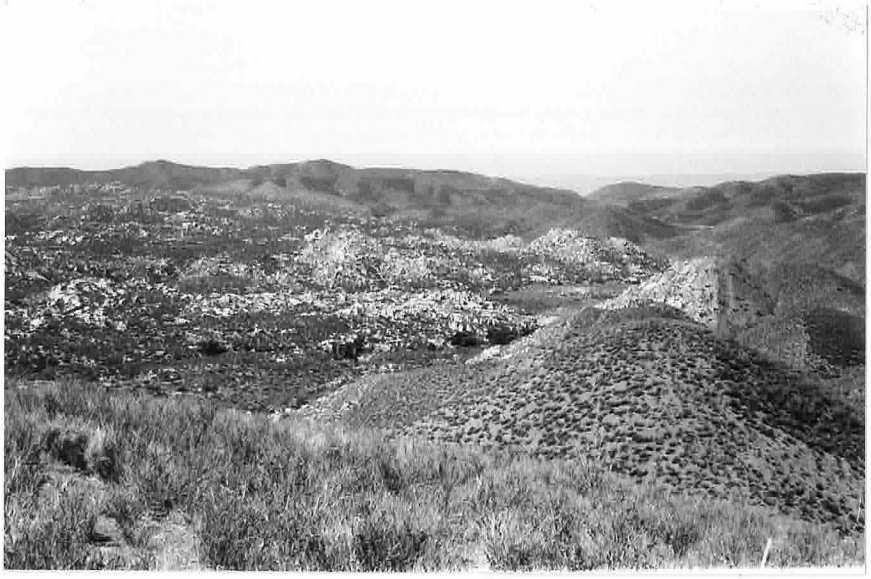

Figure 9A

Figure 9B

Figure 9. Northwestern margin of the pluton. (A) Overview from just west of the Tepetate road (foreground) to just south of Arroyo de las Parritas (left background). (B) Closer view of the contact in the right-central part of (A) about 850 m west of the Tepetate road (area C-6). The extremely sharp, smoothly curving and dike-free contact is consistently parallel to foliation in the tonalite and to bedding in the adjacent wall rocks. The prominently exposed beds nearest the contact in (B) consist of marble plus calc-silicate rock (map unit M-1).

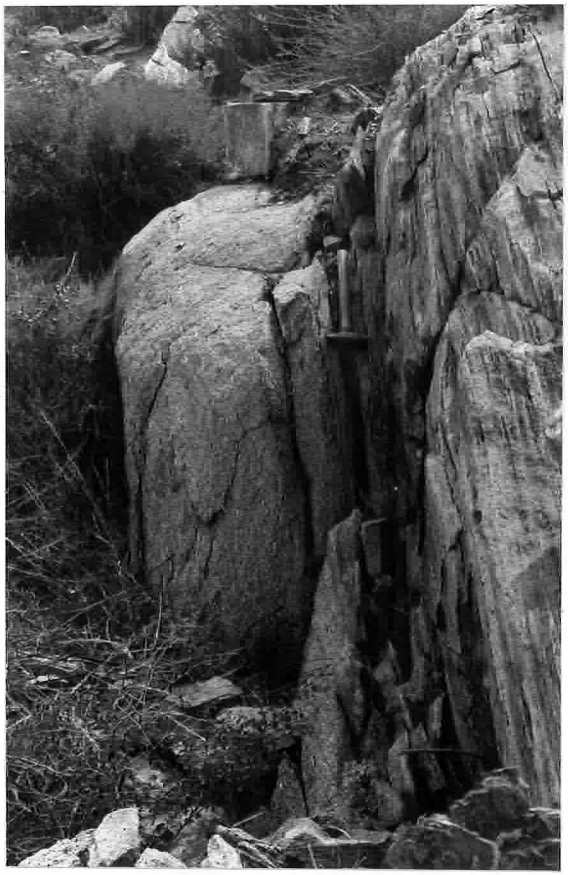

Figure 10A

Figure 10B

Figure 10. Gneissose tonalite in sharp concordant contact with intensely foliated and injected country rocks. The hammer in (A) and the pocket knife at the top of the outcrop in (B) give scale. The zone of injection is 1-3 m wide in each case. Localities: (A) northern contact near locality 71, about 370 m west of the Tepetate road (area C-6) and (B) eastern contact in Cañon Socorro, about 900 m south of the intersection with Cañon La Jolla (area L-13).

The dips around any given part of the SHbT are extremely consistent and independent of topography, suggesting that the contact geometry does not change rapidly downward, nor originally upward. The same pattern of dips continues southward along the short stretch of PHbT-wall rock contact on the western side of the pluton, although the latter contact is more irregular and discordant. The consistency and symmetry of dips suggest that the northern two-thirds of the pluton, *at this level of exposure*, may be an ovoid or cylindrical body plunging at about 80° to the northeast or north-northeast. Other evidence discussed later (Chapters 9 and 11) suggests that this geometry probably does not continue to any great depth in the crust, but rather that the SHbT and PHbT contacts curve inward, and the pluton pinches down at depth, perhaps to a narrow root zone.

Recrystallized mafic inclusions generally comprise several percent of the outer gneissose tonalite, but identifiable inclusions of pre-batholithic rocks are rare. Even if the inclusions were all derived from the wall rocks, the amount of stoping and assimilation indicated is very slight.

White, lime-contaminated tonalite containing hornblende and/or clinopyroxene, but no biotite, forms a rind a few centimeters to a meter thick around much of the margin of the SHbT (see Figure 27, p. 158). The rind is best developed at contacts with marble and calc-silicate rock, but it also commonly occurs where stretched-pebble wacke separates the calcareous zones from the tonalite. It is rarely present at contacts with metamorphosed mudstone and tuff.

Injection or metasomatism of wall rocks was also very minor. Much

of the calc-silicate material apparently formed by metamorphism of mixed calcareous and detrital or pyroclastic debris rather than by metasomatism. Igneous-textured patches and stringers generally of dioritic or quartz dioritic composition locally occur up to several meters into the wall rocks, but they are typically no more than a few tens of centimeters in maximum dimension and are generally of minor abundance. The amount of injection and the width of the injected zone increase southward around the margins of the SHbT, but, except locally along the eastern side, where small masses of diorite, quartz diorite, and gabbro have complicated the situation, the zone of conspicuous injection, if present, is rarely more than 1-2 m wide.

Except for the small stringers and patches described above, dikes or sills derived from the northern two thirds of the pluton are very rare. In fact, there appear to be no dikes or sills clearly derived from the SHbT; tonalite and quartz diorite in the two intrusive sheets south of Cañon Campo Buena Vista in the northeast, and in a few other small unmapped dikes and sills, may all have been derived from the PHbT, then separated from that unit by later emplacement of the SHbT (see discussion of diorite and gabbro, section 7.2.2). If so, the apparent structural continuity of the two larger intrusive sheets with the SHbT is due simply to incomplete exposure and the low angle at which these sheets have been truncated.

On a larger scale, the concordance of the contact is apparent not only from the trends of bedding, but also from the continuity of lithologies around much of the contact. The generalized stratigraphic section in Arroyo El Tepetate (Figure 6, p. 58) shows an especially

important sequence of rock types beginning with stretched-pebble wacke at the margin of the San José pluton, followed directly by marble plus calc-silicate rock, followed in turn by a thick section of slate and fine-grained schist (predominantly metamorphosed mudstone and fine-grained tuff). This particular zone of marble plus calc-silicate rock will be referred to as M-1 to distinguish it from other calcareous zones near the pluton in the northwest. As shown on Plate 2, both M-1 and the stretched-pebble wack locally pinch out, and neither can be traced continuously for more than a few kilometers at a time. However, the exposed segments of each unit overlap in such a way that they can be correlated over a distance of more than 12 km along the pluton contact from 1.1 km west of Rancho Cerro Costilla (area C-8) to the main body of volcanic wacke and pebbly wacke west and southwest of the pluton. Along this entire distance, M-1 is nowhere more than 100 m from the pluton contact. Where the stretched-pebble wacke pinches out, M-1 crops out directly against the tonalite. The *apparent* discordance of the pluton to wall rocks along this 12-km distance is therefore about 100 m and is very gradual. However, the apparent discordance is not a direct measure of the *intrusive* discordance; rather it is a product of the combined effects of intrusive crosscutting, tectonic thinning, and possible primary depositional variations in thickness of the wall rocks. Clasts in the pebbly wacke have been deformed into discoidal and spatuloid shapes, giving the rock the appearance of a finely banded gneiss whose foliation is parallel to bedding. Along the northern contact of the pluton, where deformation was most intense, many of the pebbles have been stretched into triaxial ellipsoids with axial ratios as extreme as

15:5:1. Strong alignment of these ellipsoids defines a spectacular lineation at many outcrops (Figure 11). Assuming that the pebbles were initially spherical, thinning by a factor of about 4 or 4.5 would be necessary to produce ellipsoids with axial ratios of 15:5:1. Thus the original intrusive discordance could have been as much as 400-450 m. However, many pebbles are less spectacularly stretched. Moreover, both the tectonic thinning itself and any sedimentary facies changes may have contributed appreciably to the pinching out of the pebbly wacke. Therefore, the total intrusive discordance over the entire 12-km distance was probably much less than 400 m.

Beginning about 300 m west of Rancho Cerro Costilla (area C-9), a similar zone of marble and calc-silicate rock reappears along the contact and borders the pluton for a distance of 1600 m to the southeast (Plate 2). This zone is either correlative with unit M-1 or is in a nearly equivalent stratigraphic position. Short segments of marble and calc-silicate rock possibly correlative with M-1 occur at several other places along the eastern contact as far south as the San José-Observatorio road. Stretched-pebble wacke (not distinguished on Plate 2) is recognizable in the sliver of country rocks between the pluton and the large mafic sheet south of Cañon Campo Buena Vista (area G,H-13.)

Although I have not mapped lithologies within the thick pre-batholithic section north and east of the pluton, the general parallelism of bedding to the pluton contact supports the interpretation that the pluton does not cut significantly across section. Furthermore, it indicates that the isolated lenses of marble and calc-silicate rock

Figure 11. Strongly lineated stretched-pebble wacke at the northern contact of the pluton. The lineated surface is nearly vertical and coincides with the plane of bedding and foliation in the wacke. The light-colored rock at the bottom of the photograph is the gneissose margin of the tonalite, whose contact extends horizontally across the picture just behind and above the hidden head of the hammer. The wacke has slumped forward several centimeters to cover the contact in the right half of the picture. The lineation, which is also pronounced in the tonalite, plunges 26° towards the east-northeast, nearly parallel to the strike of the contact. Locality 71, 370 m west of the Tepetate road (area C-6).

and of stretched-pebble wacke east of the pluton, if not exactly correlative with the similar units along the northern and northwestern contacts, are in a roughly equivalent stratigraphic position.

The position where the marble and calc-silicate zone (M-1?) along the northeastern contact disappears southeast of Rancho Cerro Costilla is approximately opposite the position where a zone of dioritic rocks and inclusion-rich PHbT appears between the PHbT and SHbT (Plate 2). That is, if the SHbT were removed and the country rocks were contracted to enclose the PHbT, the southeastern end of the marble and calc-silicate zone would coincide roughly with the northwestern end of the mafic zone. Inclusions of calc-silicate rock and fine-grained schistose amphibolite are locally abundant in the dioritic rocks, in the inclusion-rich outer part of the PHbT, and rarely in the adjacent SHbT. Inclusions of thin-bedded mudstone and tuff also occur, but are less common. Additional evidence will be presented later which suggests that the southeastward extension of the calcareous zone was intruded, hybridized, and incorporated into the outer margin of the PHbT and the dioritic rocks. Subsequently, the SHbT was apparently intruded along the very slightly discordant contact between the PHbT pluton and the pre-batholithic rocks, leaving only small scattered remnants of the stretched-pebble wacke and calcareous rocks along the present eastern margin of the pluton.

The evidence therefore suggests that the entire northern half of the pluton, from just north of Arroyo de las Encinas in the west to as far south as Cañon Socorro fault zone and possibly farther in the east, is enveloped in an almost perfectly concordant sheath consisting, in succession outward from the contact, of stretched-pebble wacke

(locally absent, followed by marble and calc-silicate rock (locally absent), followed in turn by metamorphosed mudstone and tuff, with some marble, wacke, pebbly wacke, and andesite or basalt porphyry.

Structural relationships are very complex in the area northwest of the pluton, where the thick northwest-striking section of Alisitos strata divides around the pluton. The generalized structural pattern can be best seen from Plate 1 and Figure 2. Traced westward, most of the strata north of the pluton are bent smoothly northwestward away from the pluton to join the main northwest-striking section. However, the strata nearest the northern contact do not diverge away from the pluton, but rather are wrapped southwestward around the pluton as a continuation of the concordant sheath. Attitudes of bedding differ by about 90° across a N 30° E stretch of Arroyo El Tepetate from the intersection with Arroyo de las Parritas northeastward for 1.5 km. This part of the arroyo therefore follows the trace of a major local structural discontinuity between the concordant strata and the northwest-striking section. Reconnaissance mapping and aerial photograph interpretation indicate that the zone of discontinuity continues northward up a tributary arroyo for about 750-800 m from Arroyo El Tepetate, then appears to end abruptly or die out. The nature of this discontinuity has not been determined.

South of Cañon San Jorge and Arroyo de las Parritas, there is a large wedge-shaped area in which manifestations of bedding are not clearly visible on aerial photographs (Plate 1 and Figure 2). This area, which narrows southward and pinches out near Arroyo de las Encinas, lies between the concordant sheath of strata near the pluton and a thick

section of metamorphosed volcanic wacke and pebbly wacke striking northwestward away from the pluton. The southern part of wedge-shaped area is underlain by masses of meta-basalt separated by volcanic wacke and pebbly wacke (Plate 2). Most of the rest of the area has not been covered on foot, but a short traverse along the ridge crest immediately south of Cañon San Jorge revealed an area underlain by extremely broken and jumbled strata beginning about 900 m west of the pluton and extending at least 600 m westward towards Rancho Buena Vista. Several metamorphosed mudstone and tuff lithologies similar to those in the outer 200 m of the concordant sheath to the east appear to be chaotically interspersed as blocks several meters or tens of meters in size. Attitudes of bedding vary erratically and apparently abruptly among the blocks.

Part of the wedge-shaped area therefore appears to be underlain by a tectonic mega-breccia involving lithologies correlative with some of those which are wrapped concordantly around the pluton. L. T. Silver (personal communication) reports that there are also large areas of hypabyssal intrusive in the area south of Rancho Buena Vista.

The structural complexities northwest of the pluton appear to be due to northward and outward expansion of the pluton, causing a concordant sheath of strata to be split off from the main Alisitos section, rotated counterclockwise as much as 180°, and doubled back on itself with the hinge of rotation located near or slightly north of Arroyo de las Encinas. The resulting structure appears to be a very tight V-shaped fold open to the north and locally complicated by faulting and large-scale brecciation. These relationships will be discussed further

in Chapter 11.

Gneissose foliation around the entire outer margin of the SHbT is parallel to the pluton margin and decreases inward. The width of the gneissose zone diminishes gradually southward and westward from about 150-250 m in the north and northeast to about 10-20 m at the southeastern tip of the SHbT and to practically nothing at the southwestern tip. In the surrounding country rocks, a strong penetrative metamorphic foliation is parallel to the pluton contact and decreases in intensity away from the contact. Foliation is generally parallel to bedding, but there are important exceptions. Northwest of the pluton, where the regional trends of strata are only partially bent towards parallelism with the pluton contact, strong fracture cleavage parallel to the contact crosses bedding at moderate to steep angles (Plate 3). The crosscutting cleavage is locally apparent as much as 1800 m from the contact and possibly farther. Similarly, where bedding in the volcanic wacke and pebbly wacke west and southwest of the pluton dips westward away from the contact, flattening of pebbles defines a steep crosscutting foliation parallel to the smoothly curving contact of the northern two thirds of the pluton or to the southeastward-projected extrapolation of this contact. This foliation is recognizable as much as 1500 m west of the pluton in Arroyo de las Encinas; only a few of the localities where it was recognized are recorded on Plate 3. Finally, just north of the diorite-gabbro complex in Cañon La Jolla (area I-13,14), strata diverge abruptly from the regional trend, but cleavage remains parallel to the regional bedding trend and to the pluton contact and cuts sharply across the beds. This is a local

phenomenon near the axis of one of the many tight or isoclinal folds suggested by light and dark striping visible on the aerial photographs. Similar local divergence of bedding from foliation must exist near other fold axes.

Penetrative deformation was especially severe in the section between the Las Cochas and San José plutons. Extreme stretching of clasts in the pebbly wacke along the northern contact has already been mentioned. Photo-interpretation of bedding trends (Figure 2 and Plate 1) suggests that a section which is about 4.5 km thick north of Rancho Buena Vista is pinched down to as little as 1.2 km thick between the plutons. Southeast of Cerro Costilla the thickness appears to increase again to about 2.5 or possibly 3.5 km. The plunges of lineations in the gneissose tonalite around the northern margin of the San José pluton and in the country rocks between the two plutons (Plate 4) converge downward towards an area beneath the southern margin of the Las Cochas pluton. Plunges are steepest where the country-rock section is thinnest (i.e., from the Tepetate road eastward for 3-4 km). Southeastward and especially westward from that area, lineations become more shallowly plunging and also generally more intense and consistently developed. Apparently, where thinning was greatest, stretching and flattening were predominantly planar, but with a moderate net vertical elongation, whereas westward and, to a lesser extent, southeastward from the zone of greatest thinning, stretching was more unidirectional and had a greater horizontal component. The converging lineation pattern and the severe thinning of the wall rocks suggest squeezing of strata upward and outward from between the San José and Las Cochas

plutons after the northern part of the San José pluton was sufficiently solid to behave as a rigid mass relative to the wall rocks.

Southward from the Concepción road, lineations in both the gneissose tonalite and wall rocks become slightly steeper and rotate gradually from northwesterly through more northerly to northeasterly trends. Consistently northeastward-plunging lineations are developed all along the eastern and southeastern margins of the pluton south of Cañon Campo Buena Vista. Reconnaissance observations revealed similar lineation orientations in both the pre-batholithic and batholithic rocks at a number of places up to 10 km east of the San José pluton, indicating that the lineations are part of a regional system not directly related to emplacement of the San José pluton.

Several observations in addition to the regional lineation patterns and the intense deformation of the gneissose tonalite and wall rocks indicate that the outer contact of the SHbT served as a regional surface of shearing and tectonic discontinuity during superimposed deformation. In numerous places around the northern and northwestern contacts, quartz veins and mafic, aplitic, or pegmatitic dikes which crosscut foliation and lineation in the gneissose tonalite or wall rocks are themselves offset or strongly foliated and lineated along directions parallel to the flow structure in the host rock. In an unusual exposure along the northern contact 340 m west of the Tepetate road (locality 71, area C-6; see Figure 34, p. 198), typical gneissose foliation in the tonalite more than 40 cm from the contact trends at a 20° angle to the contact. This oblique foliation is abruptly truncated by an unusually strong protomylonitic foliation parallel to the pluton contact in the outer

40 cm of tonalite. A similar relationship exists on a larger scale along the southeastern margin of the SHbT for about 650 m northeast of the Willow Creek fault zone (Plate 3, area N-11). Also, along the northern contact 1.1 km west of Rancho Cerro Costilla (area C-8), local intrusive discordance resulted in an abrupt deviation of the contact from the regional smoothly-arcuate trend; however, a zone of shearing and injection bounds the protruding mass of wall rocks on its northern side, which zone coincides with the hypothetical interpolated position of the contact and indicates that deformation along the contact ignored this minor local discordance. Finally, regional deformation may also have been responsible for shoving the small mafic intrusives in the Cañon La Jolla area against the eastern margin of the pluton, producing the smoothly curving indentations in the pluton contact. However, the indentations in the pluton contact could also indicate that the mafic masses were obstacles to the expansion of the pluton.

5.3 Contact of the Seriate Porphyritic and Prismatic Hornblende Tonalites with Wall Rocks

A change in the geometry of the pluton contact from consistently smooth and concordant around the northern two thirds to more irregular and commonly discordant around the southern third coincides approximately with the southern tips of the SHbT. Some penetrative deformation is apparent in the wall rocks around the entire pluton, but the intensity decreases progressively southward. The intensity of flow structures in the tonalite also diminishes southward, becoming generally weak or unrecognizable around the margins of the SPT. Concurrently, the country

rocks become progressively more fractured and cut by minor faults. Much of the fracturing and minor faulting around the southern third of the pluton preceded or accompanied intrusion of the SPT and contributed to stoping, diking, and the irregular contact geometry. Figures 12 and 13 show, on a small scale, the type of fracture-controlled injection characteristic of the contacts of the SPT with wall rocks.

Discordance and complex injection are most pronounced along the southwestern contact, where large masses of metamorphosed volcanic wacke and pebbly wacke were removed by stoping. Several large, incompletely stoped blocks are apparent on Plate 2. Much of the discordance occurs along a relatively straight, 3.5-km stretch of contact trending north-south, parallel to a major joint and dike system (Plate 5) and to the structurally controlled, north-south drainages well developed in this area. Thus the north-south fracture system appears to have been a major factor contributing to the discordance and stoping. Unfoliated tonalite crosscuts foliation and lineation trends as well as fold axes in the volcanic wacke and pebbly wacke along this north-south contact. Inasmuch as foliation in the wacke is parallel to the hypothetical southeastward-projected position of the smoothly curving margin of the northern two thirds of the pluton and decreases in intensity away from the pluton, the foliation appears to be the result of penetrative deformation around the margins of the northern two thirds of the pluton. Intrusion of the SPT caused little or no penetrative deformation or forceful deflection of these strata.

The southeastern contact crosscuts strata at a low angle and is irregular in detail, but the degree of discordance and stoping is much

Figure 12. Southwestern margin of the seriate porphyritic tonalite: I. Meta-volcanic wacke (blocky outcrops and darker soil) is complexly cut by and included in decomposed tonalite (smooth light-colored soil). The view is toward the north, and relatively homogeneous tonalite begins at the right-hand edge of the photograph. The complex relationships, poor exposure, and deep weathering are typical of the southwestern and southern contacts of the SPT, where the zone of intense injection generally varies from 5 to 50 m wide. The southeastern contact is less discordant, and the zone of injection is much narrower. Locality: 1.5 km south of Rancho El Molino (area Q,R-6).

Figure 13A

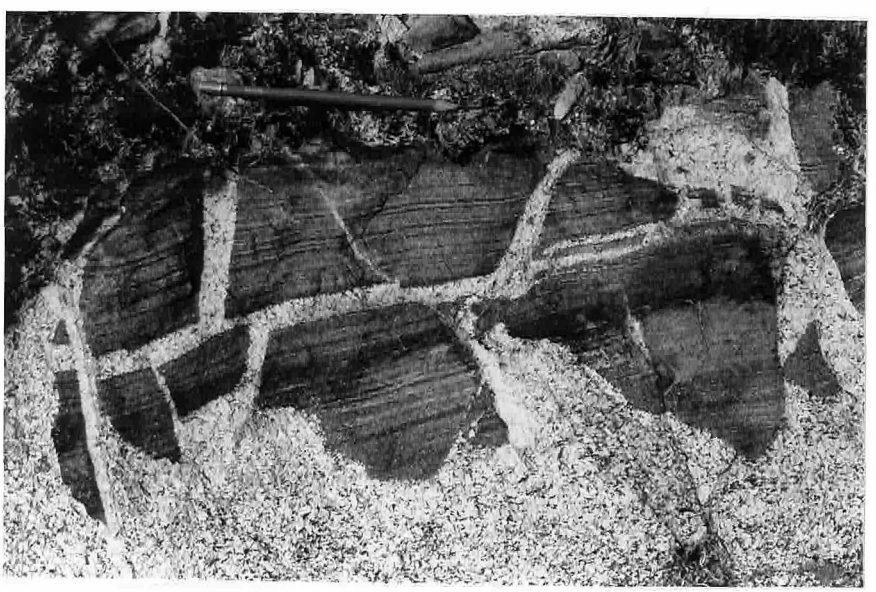

Figure 13B

Figure 13. Southwestern margin of the seriate porphyritic tonalite: II. These photographs show, on a small scale, the irregular and fracture- and bedding-plane-controlled injection and stoping characteristic of the SPT, particularly along the southwestern contact. The pocket knife near the center of (A) and the pencil above the exposure in (B) give scale. Locality: 600 m south-southwest of Rancho El Molino (area P,Q-6).

less than along the southwestern contact. The inlier of pre-batholithic and mafic intrusive rocks south of Willow Creek Canyon (around area N-10) is an especially large, partially stoped block almost completely surrounded by tonalite at the present level of exposure.

Strata were broken and rotated clockwise around one or more well-defined hinge lines along the southeastern contact. One hinge line is represented on the maps by two short northwest-trending faults cutting the marble and calc-silicate rock just east of the southern tip of the pluton (area S-8). There appears to be very little offset on the faults, but bedding attitudes change abruptly from N 5° W and nearly vertical southwest of the faults, to about N 55° E and inward-dipping between the breaks, then back to roughly N 45° E and inward-dipping northeast of the faults. Traced northward for 1.5 km, the beds swing gradually back to north-south and north-northwest trends while maintaining inward dips. Near the arroyo called El Alisito (area R-8,9), the marble and calc-silicate zone appears to be discontinuous, and bedding trends again change abruptly to N 40-50° E and roughly vertical or steeply outward-dipping. This change probably represents another hinge line. At present, mapping is too preliminary to permit detailed analysis of the structure along this side of the pluton, but it seems clear that outward displacement of the strata around the intruding SPT was accomplished as much or more by brittle failure as by penetrative deformation and plastic flow, in contrast to the relationships around the northern two thirds of the pluton.

Along almost the entire southwestern margin of the pluton, the immediately adjacent strata dip steeply and consistently to the north-

east towards the pluton. Near the pluton contact in Cañon Las Cabras (Plate 3, locality 63, area P-5,6), cross-bedding indicates that the strata are right-side-up. There is no guarantee that the entire east-dipping section is similarly right-side-up, but the uniformity of attitudes is suggestive. Over a wide area near the San José-San Telmo road, strata in the western half of the volcanic wacke and pebbly wacke unit dip moderately or steeply to the west. Along the road near the western margin of the unit (locality 780, area N-2), excellent cross-bedding and graded bedding indicate clearly that the tops of beds are to the west. Poor graded bedding in one outcrop near the center of the unit about 500 m north of the road (Plate 3, area M-2,3) also tentatively suggests that the west-dipping section is right-side-up. This pattern suggests a major northwest-trending anticlinal fold traceable for more than 2 km northwest of the road and for at least 1 km to the southeast. The meta-basalt masses north of the road are near the core of this fold, but the exact location of the fold axis is undetermined. Limited observations 2 km southeast of the road suggest a possible synclinal axis southwest of the anticlinal axis.

South of Cañon Las Cabras (area Q-5,6), reversals of dip define an anticlinal axis followed southwestward by a sharp synclinal axis. Both fold axes are truncated by the pluton. The previously-mentioned cross-bedding in Cañon Las Cabras suggests that the eastern limb of the anticline is right-side-up. Suggestions of graded bedding and cross-bedding at many outcrops on either side of the synclinal axis are all compatible with a right-side-up orientation, but the evidence is inconclusive.

Around the southern tip of the pluton, the outcrop pattern of the marble plus calc-silicate zones flanked on either side by metavolcanic rocks is most readily interpreted as defining the nose of a nearly isoclinal fold into which the SPT was intruded. This hypothesis and possible alternative interpretations of the large-scale structure in the pre-batholithic rocks will be discussed in Chapter 11.

5.4 Major Faulting of the Pluton Contact

Two major fault zones offset the eastern margin of the pluton -- the Cañon Socorro and Willow Creek fault zones.

The trace of the Cañon Socorro fault zone is prominent on aerial photographs (Figure 2) and runs N 15-20° W in a straight line independent of topography, indicating a roughly vertical dip. This fault zone offsets the pluton contact in two or more steps for a total apparent left-lateral displacement of about 970 m. Part of the offset appears to be accumulated from small displacements along secondary *en echelon* fractures striking about N 40° W and dipping steeply southwest. The true displacement is undetermined; the small *en echelon* offsets and the change from steep outward dips of magmatic foliation, country-rock bedding, and the pluton contact northeast of the fault, to more erratic but generally vertical dips of these structures southwest of the fault, suggest an oblique upward and southeastward motion on the southwestern side.

The Willow Creek fault zone strikes N 40-45° W; again the trend seems to ignore topography, suggesting a steep dip. An apparent 475 m

of right-lateral offset of an unusual feldspathic quartzite bed (Plate 2, area O-11,12) has already been discussed (end of Section 4.2). Highly deformed and recrystallized volcanic wacke and pebbly wacke comprising the partially stoped inlier of wall rocks southwest of the Willow Creek fault zone is also displaced at least 350 m to the east on the northeastern side of the fault; because the full aerial extent of the wacke northeast of the fault has not been mapped, the exact displacement is undetermined.

The pluton contact also appears to be displaced 440 m in a right-lateral sense, but typical SHbT does not reappear anywhere southwest of the fault zone; in place of the SHbT is a heterogeneous complex of diorite, gabbro, and quartz diorite. However, a 5-10 m by 20 m lens of gneissose tonalite, which appears to be a possible offset equivalent of the gneissose border phase of the SHbT, crops out next to the wall rocks immediately southwest of the fault (area N-10,11). In addition, some of the diorite and quartz diorite in the mafic complex is characterized by equant, poikilitic and molded hornblende grains reminiscent of the SHbT. In the northern part of the complex, this diorite occurs as abundant inclusions in a medium- to fine-grained hornblende diorite which was intruded into the SHbT, PHbT, and metamorphic rocks along 500 m or more of the length of the fault zone. The mafic complex may therefore consist in part of a hybridized equivalent of the SHbT. Considering the rapid southward thinning of the SHbT north of the fault, the SHbT may have originally pinched out no more than 500 m or so south of the present truncated tip, and the offset extension may have been small and readily obscured by later intrusion of diorite and gabbro.

Alternatively, if the tip of the SHbT pinched out rapidly upward or downward, a vertical component of faulting could have hidden the offset extension above or below the present level of exposure.

Neither the Cañon Socorro nor the Willow Creek fault zone can be traced with confidence very far into the tonalite. The Cañon Socorro fault zone or a major branch thereof probably bends slightly westward to follow the straight N 35° W trend of the unusual, deep, throughgoing canyon formed by the intersection of the opposing but colinear drainages of Arroyos San José and Cerro Costilla. The extension of the Willow Creek fault zone into the pluton is partially obscured by the intrusion of hornblende diorite along the fault. Because neither the northern nor the western margin of the pluton is offset, both the Cañon Socorro and Willow Creek fault zones must die out within the tonalite.

Between the Cañon Socorro and Willow Creek fault zones, the country rocks up to 700 m from the pluton contact are intensely fractured and cut by minor faults. Extensive injection of gabbro, diorite, quartz diorite, and locally aplite or pegmatite into this fractured zone, and local reaction with the metamorphic rocks, produced a complex and often poorly exposed zone of mixed rocks. The structure is further complicated by locally severe penetrative deformation and metamorphic recrystallization which have converted much of the rock between the San José and Willow Creek plutons into fine- to medium-grained, lineated schists in which primary sedimentary structures are largely obscured. Much of the fracturing and injection occurred along planes parallel to the Willow Creek fault zone (Plate 5).

Joint sets and mafic and aplitic dikes subparallel to the Willow

Creek fault zone are conspicuous in the SHbT for 1-2 km northeast of the fault zone (Plate 5). Northwest-trending fractures, minor faults, and aplitic or granitic dikes are much more abundant throughout the mafic complex and the inlier of metamorphic rocks southwest of the fault. Thus, the Willow Creek fault zone is flanked on both sides by a broad region of related fracturing and minor faulting. However, dikes of this orientation are rare in the small wedge of SPT southwest of the fault zone and in the metamorphic rocks southeast of that wedge, although northwest-trending joints are conspicuous (Plate 5). Dikes also appear to be rare or absent in the Willow Creek pluton northeast of the fault zone.

As mentioned earlier, fine- to medium-grained hornblende diorite comprising an important part of the mafic complex along and south of Willow Creek Canyon has been injected southeastward for hundreds of meters along the fault zone. Intrusion along fracture zones subparallel to the Willow Creek fault zone also appears to have exerted a major control on the discordant northern and southwestern contacts of the Willow Creek pluton and on the trend of numerous diorite and quartz diorite dikes branching off from that pluton. These observations indicate that offset along the Willow Creek fault zone and widespread fracturing parallel to that zone preceded emplacement not only of minor dikes, but also of the Willow Creek pluton and of some of the diorite in the mafic complex. However, many of the dikes, including some derived from the Willow Creek pluton, are themselves disrupted by minor faulting and show variably-intense lineation and foliation, but generally little or no recrystallization. Deformation apparently associated with the

Willow Creek fault zone therefore continued during and/or after emplacement of those rocks, but neither the Willow Creek pluton nor the diorite along the fault is metamorphosed or severely deformed.

Aplitic, pegmatitic, and fine-grained mafic dikes were also emplaced into the tonalite and country rocks along the Cañon Socorro fault zone and associated fractures. Many of these dikes are themselves sheared along the plane of injection. Thus, the Cañon Socorro fault zone also appears to be an old structure, but the age of offset is less well determined than for the Willow Creek fault zone.

Chapter 6

MAJOR TEXTURAL UNITS OF THE TONALITE

6.1 Introduction

Recognition and mapping of the three major textural units of the pluton -- the stubby hornblende tonalite (SHbT) together with its gneissose border phase (GBT), the prismatic hornblende tonalite (PHbT), and the seriate porphyritic tonalite (SPT) -- was based entirely upon megascopic characteristics observed in the field and summarized in Table 2. Figure 14 permits comparison of the typical appearance of each textural type. This chapter covers these distinguishing characteristics, plus the distributions and mutual contact relationships of the units. Modal and chemical data will be discussed in Part III, but it is important to note here that these data support the subdivisions as defined by field observations. In particular, Harker variation diagrams for several elements (Figure 86, pp. 485-489) and plots of modal quartz versus modal plagioclase, hornblende, biotite, and color index (Figure 84, pp. 471-475) show distinct groupings for the SHbT, GBT, and SPT. The plots also show a close affinity between the PHbT and SPT, which define one set of variation trends, and the SHbT and GBT, which define a parallel but separate set of trends.

6.2 Stubby Hornblende Tonalite (SHbT)

The SHbT forms a northward-convex horseshoe shape, broadest in the north and northeast and narrowing gradually southward along each prong of the horseshoe (Plate 2). Together with its gneissose variant along the pluton margin, the unit underlies 42 km^2, equal to 36% of the pluton.

Table 2

Distinctive Megascopic Characteristics (Mapping Criteria) of the Major Tonalite Units

Stubby Hornblende Tonalite	Prismatic Hornblende Tonalite	Seriate Porphyritic Tonalite
Mafic Minerals equant and equigranular Hornblende generally anhedral and poikilitic; margins commonly molded Biotite books thick, anhedral, poikilitic, and molded Maximum:minimum dimensional ratios of individual mafic crystals rarely >1.5 Most mafic crystals in an outcrop fall within a 2-3 mm size range	Mafic minerals inequant and seriate Hornblende generally subhedral to euhedral prisms; rarely poikilitic; margins rarely molded; commonly elongate 2 or 3:1 or more Biotite books broad and thin (platy); anhedral, poikilitic and molded Abundant mafic crystals of all sizes from <<1 mm to 4 mm or more	Same as for the PHbT, except for the presence of sparse (<0.5%) large blocky euhedral plagioclase crystals 6-20 mm in maximum dimension
Rock light gray, with pale tannish tinge Some plagioclase crystals are brownish gray to light orange due to faint, extremely fine-grained clouding and/or to inclusion of sparse tiny euhedral hematite flakes	Rock light gray, with no tannish tinge Plagioclase light gray or white; clouding absent and hematite flakes very rare	
Quartz generally <2 mm, interstitial and inconspicuous	Quartz commonly 2-3 mm, subequant, and conspicuous	
Leucocratic schlieren exceed mafic schlieren	Mafic schlieren exceed leucocratic schlieren	

Figure 14. Comparison of the appearance in outcrop of the major textural units of the tonalite and the gneissose border phase of the stubby hornblende tonalite.

(A, B) gneissose border phase (GBT) of the stubby hornblende tonalite. Note the schlieren and highly flattened inclusions oriented parallel to the planar mineral orientation. Locality: about 65 m from the northwestern contact of the pluton, 40 m south of the Buena Vista-Coyote road (area D-4).

(C, D) stubby hornblende tonalite (SHbT). Note the equant shapes and equigranular grain-size distribution of hornblende and biotite. Foliation appears weak in outcrop, but preferred orientation of plagioclase tablets is very pronounced in thin section. Locality: 145 m west-southwest of Rancho El Coyote (area E-5).

(E, F) prismatic hornblende tonalite (PHbT). The abundance of inclusions and faint schlieren is slightly greater than in most PHbT exposures; otherwise this outcrop is typical of the more foliated parts of the PHbT. Note the thin elongate shapes and the wide range of grain sizes of hornblende and biotite. Locality: on the North-South road, 360 m south of the SHbT-PHbT contact zone (area F-6).

(G, H) seriate porphyritic tonalite (SPT). The abundance of faint schlieren is slightly greater than usual; otherwise this outcrop is typical of the more foliated parts of the SPT. Except for the characteristic presence of a few large subhedral to euhedral plagioclase crystals, the SPT is megascopically indistinguishable from weakly foliated PHbT. Locality: eastern side of Arroyo San José, 800 m south-southeast of Rancho San José (area M-8).

A

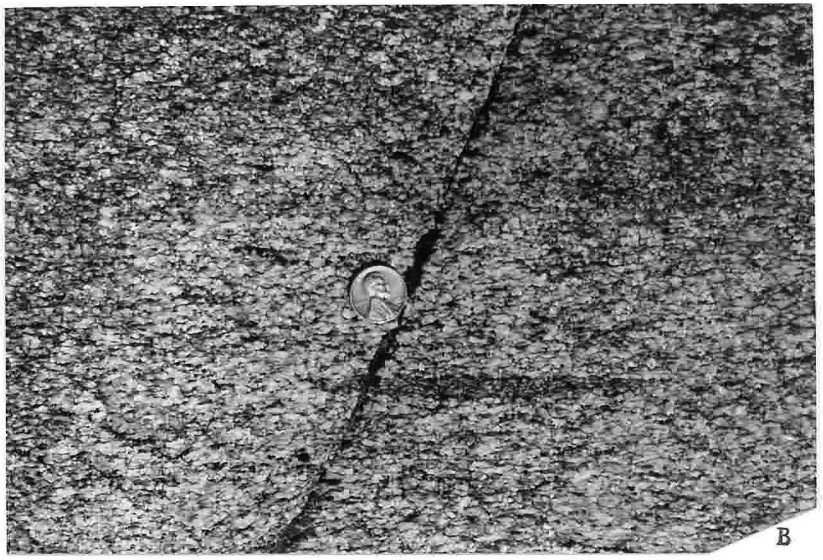

B

C

D

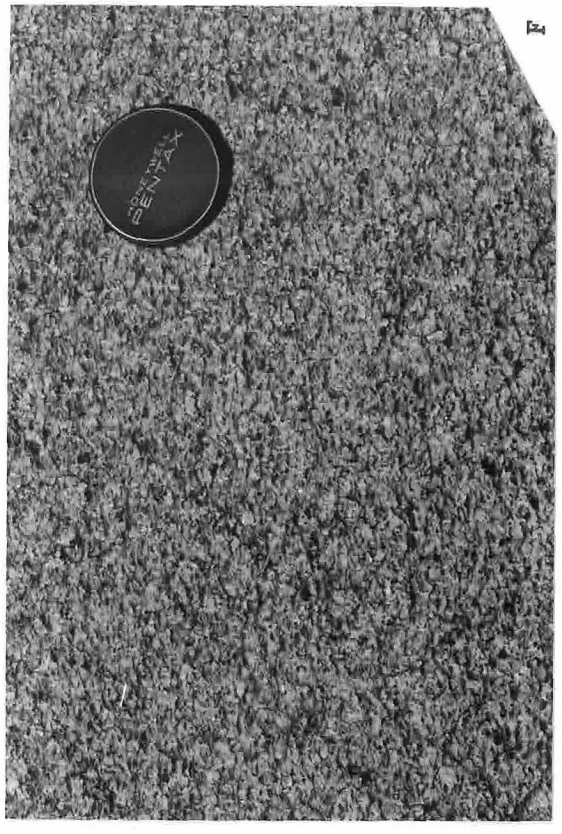

F

H

E

G

The western prong terminates by simultaneously thinning, losing its textural uniqueness, and intermingling with and grading into the PHbT within 250-1000 m north of the San José-San Telmo road. The eastern prong is terminated by the Willow Creek fault zone. However, like its western counterpart, this prong has narrowed greatly and begun to lose its textural characteristics and to grade into the PHbT within 500 m north of the fault. Typical SHbT has not been recognized southwest of the fault, but some of the diorite in the mafic complex immediately to the southwest is texturally similar to the SHbT and may be a hybridized equivalent. Excellent exposures of typical SHbT can be seen along the Buena Vista-Coyote and Concepción roads, especially west and northwest of Rancho El Coyote.

The SHbT is distinguished from other units in the field principally by three criteria (Table 2 and Figure 14C,D).

(1) Hornblende and biotite grains are roughly equant and anhedral or rarely subhedral; maximum:minimum dimensional ratios of individual crystals rarely exceed 1.5:1. In addition, many hornblende crystals poikilitically enclose one or more 0.2-1 mm plagioclase grains and/or are partially molded around plagioclase.

(2) Hornblende and biotite exhibit a consistently equigranular grain-size distribution in the SHbT, compared with a seriate distribution in the other units. The grain size of both minerals varies from 2-3 mm in some parts of the SHbT up to 6-8 mm in others, but most of the crystals in a given hand specimen and commonly within a given outcrop and region have the same diameter to within ±30%.

(3) The rock is very light gray, but has a consistently pale tannish tint absent from the rest of the tonalite. This color arises from the plagioclase, some of which is light gray or white, but some of which is distinctly brownish gray to tan or orange due to faint clouding by extremely fine-grained material and/or to inclusion of sparse tiny euhedral flakes of hematite (or hydrous Fe oxide).

There are several less prominent, but consistent characteristics of the SHbT. Quartz is finer-grained and generally less conspicuous than in the other units. Leucocratic schlieren exceed mafic schlieren, whereas the reverse is true in the rest of the pluton. Schlieren have the same texture and mineralogy as the host rock. Preferred mineral orientation appears weak in many SHbT outcrops because of the equant shape of the mafic minerals. However, close examination shows that planar orientation of plagioclase tablets is commonly more pronounced than in many PHbT outcrops showing a much more obvious orientation of mafic minerals.

The SHbT grades outward into a gneissose protoclastic phase (GBT) present around the entire contact of the SHbT with pre-batholithic rocks. The GBT is well exposed at Rancho Cerro Costilla and also along the contact 700-800 m north of the Buena Vista-Coyote road. As shown schematically on Plate 2, the zone of gneissose rocks is widest (150-250 m) in the north and northeast and narrows progressively southward. The gneissose zone is restricted to the SHbT and the northeasternmost tip of the SPT southwest of the Willow Creek fault zone.

At its strongest development the GBT is a flaser gneiss (Figure

14A,B). Foliation is defined both by crude layers of planar-oriented hornblende and biotite alternating with layers of quartz and plagioclase and by preferred orientation of thin discoidal or ellipsoidal mafic inclusions commonly 20-100 cm long, but only 1-5 cm wide. Relatively finer average grain size (1-3 mm) gives the GBT a more mafic appearance than the typical SHbT, but the actual mafic content is, if anything, slightly lower in the GBT (17-21%) than in the non-gneissose SHbT (18-25%). Many hornblende and plagioclase crystals are abraded and ellipsoidal. Biotite has been recrystallized into aggregates of fine-grained crystals forming flat circular or elliptical patches about one centimeter in diameter (Figure 15A). Lineation, where present, is defined most strikingly by streaks of recrystallized biotite separated by streaks of leucocratic minerals (Figure 15B). Mafic inclusions are commonly elongate parallel to the biotite lineation; recognizable alignment of hornblende grains is less common and rarely pronounced.

Mafic inclusions increase in abundance towards the contact, where they typically constitute several percent of the rock, rarely even 25% or more. Schlieren, mostly mafic, also constitute several percent. Concordant joints (defined as joints parallel to foliation) and transverse joints (steeply dipping joints perpendicular to foliation) are spaced one half to several meters apart throughout the GBT and combine with foliation to produce slab-shaped, block-rich outcrops. Figure 16 shows an exceptionally striking example of this outcrop pattern.

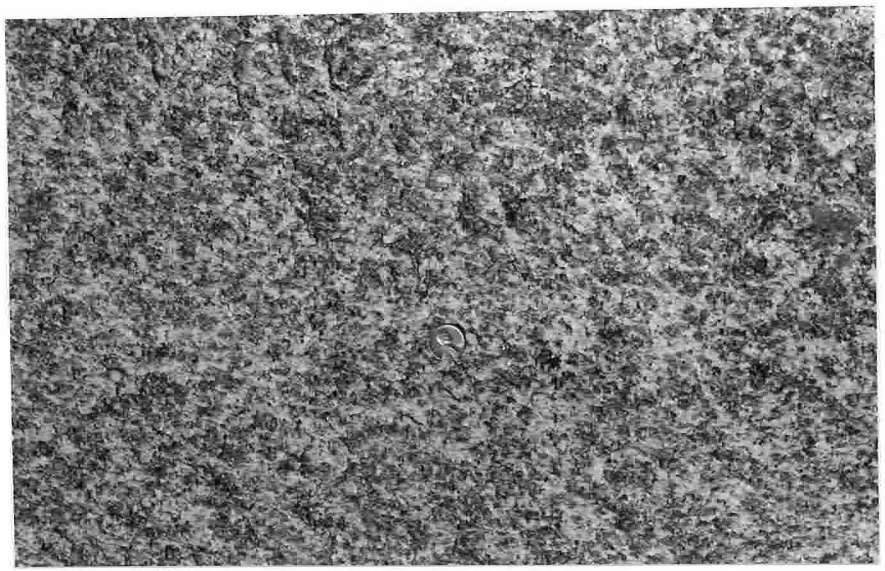

Figure 15A

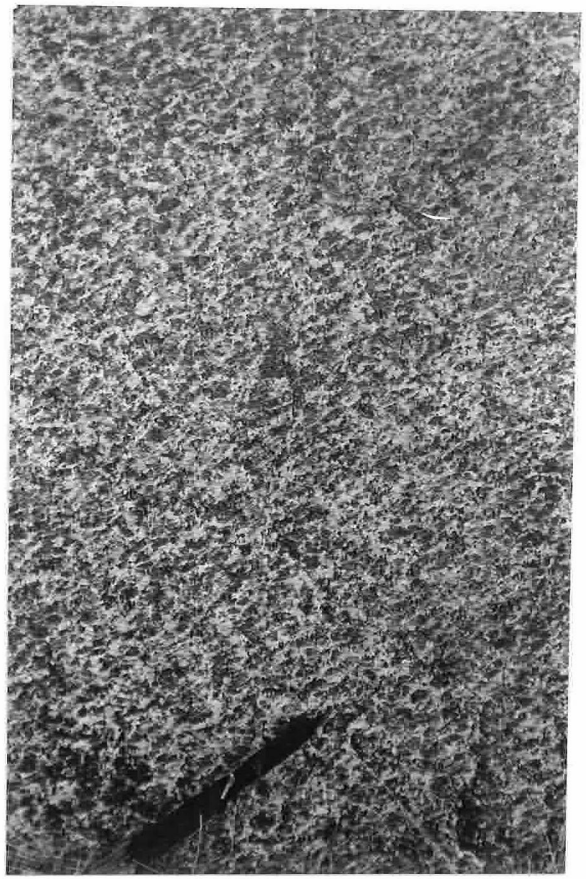

Figure 15B

Figure 15. Appearance of the gneissose border tonalite on surfaces parallel to the plane of foliation. The strong lineation parallel to the stick (about 15 cm long) in (B) is defined by thin elongate aggregates of biotite separated by streaks of feldspar plus quartz. Both localities are near the northwestern margin of the pluton: (A) about 900 m northeast of the road (area C,D-5) and (B) about 20 m south of the Buena Vista-Coyote road (area D-4).

Figure 16. Slabby outcrops of gneissose tonalite along the northeastern margin of the pluton. Igneous foliation and jointing are parallel to the pluton contact and to bedding and foliation in the wall rocks. View south from locality 807, about 900 m south of Cañon Campo Buena Vista (area H-13).

6.3 Prismatic Hornblende Tonalite (PHbT)

The PHbT is restricted to the interior of the pluton except along the southwestern margin where, for a short distance, the unit extends to the contact with country rocks (Plate 2). Because the PHbT and SPT appear gradational, and the distinction between the two is subtle, the position of their mutual contact is only approximately located. The PHbT underlies approximately 51 km^2, equal to 44% of the pluton. If the SPT is included, the combined area of the two masses is accurately fixed at 72 km^2, equal to 61% of the pluton.

The PHbT is slightly less uniform in texture and modal composition than the SHbT, but its distinguishing characteristics are still quite consistent (see Table 2 and Figures 14 E,F and G,H). Like the SHbT it contains consistently 15-25% mafics, but the color is very light gray rather than pale tannish gray. Hornblende is typically subhedral or euhedral and prismatic, with length:width ratios of 2 or 3:1. Few hornblende grains are poikilitic, and margins are very rarely molded or interstitial. Biotite is always platy and generally anhedral. As in the SHbT, much biotite is poikilitic, with molded or interstitial margins. The average grain size of the rock is 2-4 mm, but all major minerals have a seriate size distribution. Thus crystals $\leq$1 mm in size are abundant, and, in most samples, a very small proportion of plagioclase grains range up to 5-10 mm, rarely even 15 mm. In some areas, hornblende and/or biotite show a similar range, but generally they do not exceed 5-6 mm. Anhedral quartz grains 2-3 mm in size are commonly conspicuous, especially on weathered surfaces. Mafic schlieren are more abundant than in the SHbT, but they rarely comprise more than

a few percent of an outcrop and are commonly absent. Leucocratic schlieren, on the other hand, are rare in most of the mass.

Three sorts of megascopic variations are superimposed on the first-order homogeneity.

(1) The ferromagnesian minerals vary from almost entirely hornblende to approximately equal proportions of hornblende and biotite. In the zones of lower hornblende:biotite ratio, much of the biotite commonly occurs as conspicuous poikilitic plates, 6-12 mm in diameter, disseminated through the tonalite and locally through mafic inclusions as well. The variations are generally subtle and gradational, and attempts to map them proved difficult. The representation in Figure 17 is therefore very incomplete, but I am convinced that, given sufficient time and effort, patterns of slight modal and textural variations could be recognized in the PHbT, which would define discontinuous arcuate zones roughly parallel to the flow foliation.

(2) Leucocratic and mafic schlieren, commonly accompanied by abundant mafic inclusions, are concentrated in discontinuous zones parallel to foliation. The most prominent zone forms a nearly continuous concordant arc, 4.5 km long and roughly 50-300 m wide, located 5 km north of Rancho San José (Plate 2 and Figure 17). Schlieren typically 1-20 cm wide and 30-500 cm long, containing either 25-35% or 5-15% mafic minerals, dominate many outcrops in this zone. Mafic inclusions are concentrated in some outcrops. Schlieren are also locally concentrated in the inclusion-rich zones along the northwestern and northeastern margins of the PHbT (Figure 17) and in scattered small areas throughout the unit.

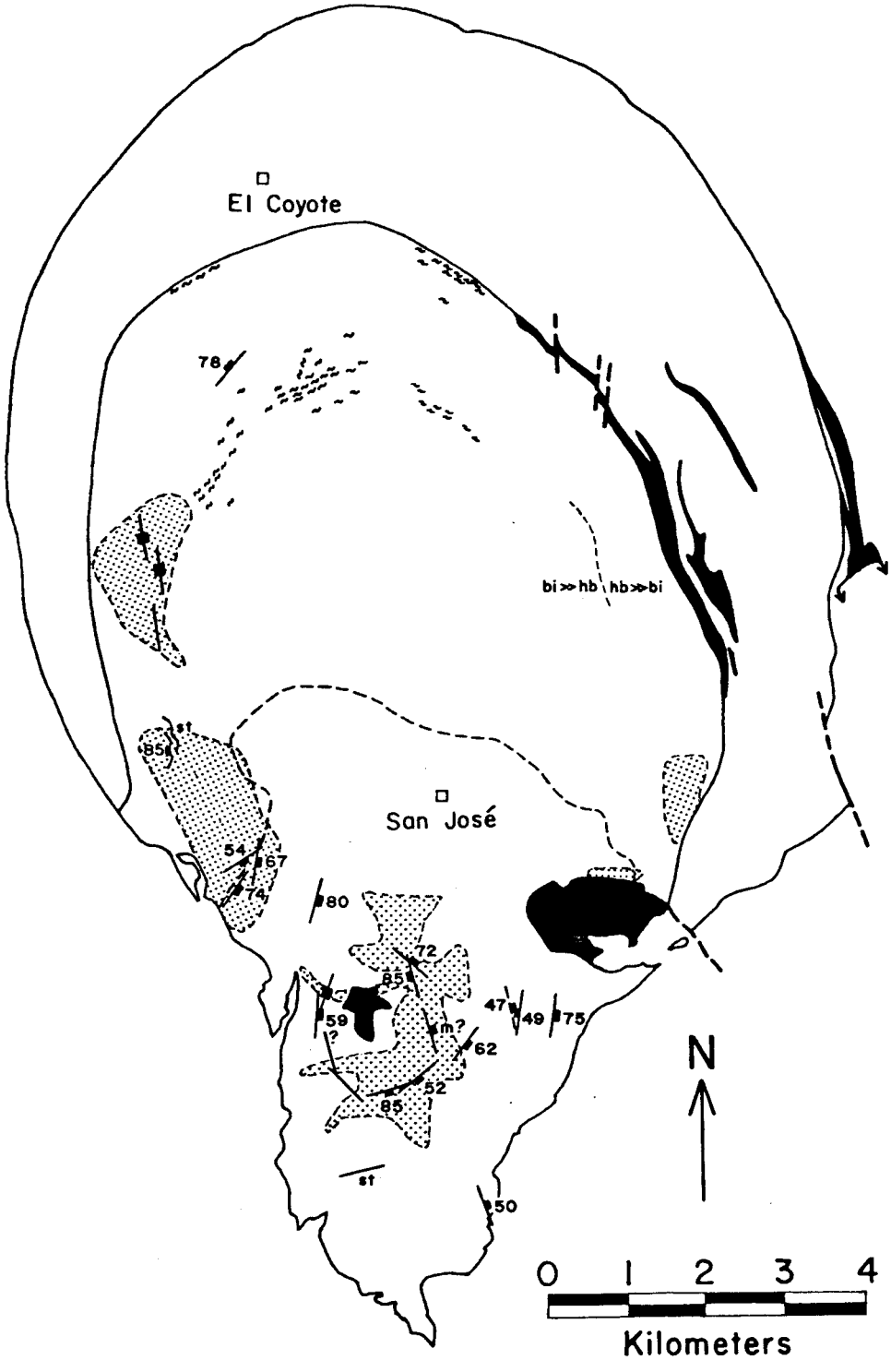

Figure 17. Distribution of conspicuous coarse poikilitic biotite, of biotite tonalite layers, and of principal schlieren-rich zones in the prismatic hornblende and seriate porphyritic tonalites.

(3) Straight or slightly wavy layers of tonalite containing 10-20% biotite and only trace amounts of hornblende are abundant in some outcrops in the western and especially the southwestern parts of the PHbT (Figure 17 and Plate 5). The layers, which are generally 2-4 cm wide and several or more meters long, may be parallel to or at a low angle to foliation and appear to follow early-formed joint planes. Their distribution overlaps considerably with that of tonalite characterized by disseminated coarse poikilitic biotite.

It is important to re-emphasize that these three types of variations are second-order phenomena. In the PHbT as in the other two textural units, uniformity is the outstanding characteristic.

6.4 Seriate Porphyritic Tonalite (SPT)

Tonalite showing little or no preferred mineral orientation makes up the southern part of the pluton. Except for the characteristic presence of a few stout euhedral plagioclase crystals 6-20 mm in size, the rock looks identical to the least foliated outcrops of the PHbT (Figure 14 E,F and G,H) into which it grades both structurally and petrographically. Phenocrysts invariably comprise less than 0.5% of the rock, but they can be easily recognized in most outcrops, especially on weathered surfaces. There is a continuous range in grain size from the largest phenocrysts down to the average of 2-4 mm, hence the term seriate porphyritic.

The SPT underlies approximately 21 km^2, equal to 17% of the pluton. Rocks containing the largest and most abundant phenocrysts occupy an area extending 1.5 km south and southeast of Rancho San José,

particularly on the eastern side of Arroyo San José. Excellent exposures can be seen just east of a narrow road extending south along the eastern edge of the arroyo.

The distribution of SPT was mapped by estimating the abundance of conspicuous large (>6 mm) euhedral plagioclase crystals as (1) more than one per square foot of exposure, (2) less than one per square foot, but noticeably present, and (3) very few or none in an outcrop. The greatest abundance seen is about five per square foot. Phenocrysts tend to decrease in size and abundance not only northward towards the PHbT, but also eastward and westward towards contacts with country rocks, especially in the northern half of the unit. Phenocrysts are small and commonly absent in the northeastward-projecting wedge of slightly hybridized tonalite south of Willow Creek Canyon (area O-10).

Unlike the PHbT, the SPT contains very few schlieren, either mafic or leucocratic. Inclusions are also very sparse in much of the unit. However, disseminated coarse poikilitic biotite and thin biotite tonalite layers similar to those in the PHbT are locally abundant in the SPT (Figure 17). As in the PHbT, there is a crude spatial correlation between the abundance of coarse disseminated biotite and the presence of biotite tonalite layers.

6.5 Contact Relationships Among the Major Textural Units

6.5.1 Stubby Hornblende-Prismatic Hornblende Contact Zone

Both the SHbT and PHbT maintain distinctly different and relatively uniform textures throughout practically their entire outcrop areas.

A screen of heterogeneous diorite and inclusion-rich tonalite separates the units for nearly 6 km in the east. Elsewhere, the contact between the two units varies from sharp to generally gradational across a zone several meters to slightly more than 100 m wide.

Gradational contacts are characterized by interlayering of textural types (as in Figure 18) and by the development of intermediate-textured rocks. Interlayers, which range from a few centimeters to several meters wide and may have sharp or gradational margins, are invariably parallel to foliation. Where layers pinch out, foliation passes smoothly from one textural type to the next (Figure 19). In no case did these layers provide clear evidence of intrusive relationships. If crosscutting relationships were originally present, they were smeared out into conformity by combined flow of the two tonalite masses. The texturally intermediate rocks are characterized in some cases by a mixture of equant poikilitic hornblende and biotite grains plus elongate hornblende prisms and platy biotite crystals and, in other cases, by an abundance of fine-grained equant mafic crystals in otherwise typical SHbT.

The contact zone is consistently narrowest along the northern stretch from Arroyo de las Parritas in the northwest (area F,G-4) to the northern end of the mafic screen in the northeast (area F,G-9). Locally the contact appears sharp or gradational over no more than a few meters, but close examination generally reveals sparse interlayers of PHbT in the SHbT and, less commonly, of SHbT in the PHbT for up to tens of meters from the contact. Southwest of Arroyo de las Parritas, and also south of the mafic zones in the east, the zone of

Figure 18

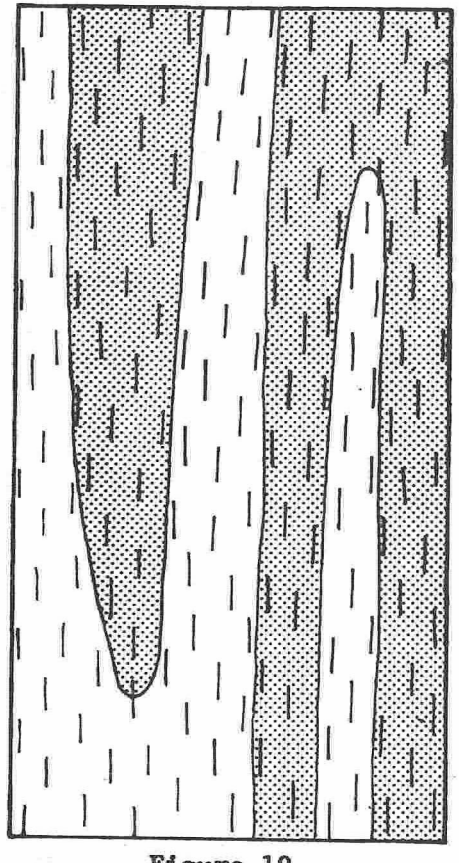

Figure 19

Figure 18. Interlayered stubby hornblende and prismatic hornblende tonalites in the contact zone between the two units. Note the sharp contacts and the conformity of foliation to layering. Locality: 10 m east of the North-South road (area E-6).

Figure 19. Schematic illustration of the relationship of foliation (short dashed lines) to the lenticular interlayering between the stubby hornblende (stippled) and prismatic hornblende tonalites in the contact zone between the two units. The area shown would be about 1 m by 2 m.

gradation widens rapidly to 50 or 100 m. Locally in the west, PHbT layers occur in the SHbT as much as 300 m from the contact.

Within 0.5-1 km of the southern tips of the SHbT horseshoe, the contacts with the PHbT become broadly gradational and difficult to define. The gradational contacts as mapped separate areas where some typical SHbT occurs from areas where none was seen.

Consider the western prong. Typical SHbT is the principal rock type in the SHbT along Arroyo de las Encinas. The transitional zone eastward into typical PHbT is slightly over 100 m wide. Southward to the tip of the prong much SHbT persists, but the proportion of PHbT and of intermediate textural types increases. Exposure is poor, and the rock types are complexly gradational and intermingled on a scale of meters and tens of meters. The textural gradation from SHbT towards PHbT is marked by: (1) a decrease in the average grain size from 3-6 mm in the SHbT to 2-4 mm in the PHbT and the intermediate type; (2) a change in the shape of the equant poikilitic hornblende crystals from the smoothly molded, angular shapes characteristic of the SHbT to more rounded, ragged shapes; (3) an increase in the abundance of elongate subhedral or euhedral hornblende prisms, especially in vaguely defined layers parallel to foliation; and (4) an increase in the abundance of small equant hornblende crystals.

Texturally intermediate tonalite lacking SHbT interlayers extends as the principal rock type for 100-200 m to the east and several hundred meters to the south of the mapped contact before grading into typical PHbT. Foliation intensity varies from weak to strong throughout the area, and steeply plunging lineation is distinct at many outcrops.

Thin-section observations suggest that the ragged outlines of hornblende crystals are due to moderately strong protoclasis, plus considerable replacement of hornblende by biotite.

Similar relationships exist along the southern 500-600 m of contact between the PHbT and the eastern prong of the SHbT, except that the SHbT and PHbT are not interlayered or complexly intermingled here as they are in the southern part of the western prong. In the outer 200 m of the pluton, typical SHbT and GBT extend unmodified to the abrupt termination against the Willow Creek fault zone; however, the western 200-300 m of the unit consist of an intermediate textural type similar to that just described. This intermediate type extends for several hundred meters to the west of the mapped contact and grades into the PHbT and SPT. Again protoclasis, possibly associated with movement on the Willow Creek fault zone and definitely associated with the frequently strong, northeastward-plunging lineations observed at most outcrops in this area, was responsible for the rounded, ragged outlines of hornblende.

Direct evidence of the relative ages of the SHbT and PHbT is scarce and ambiguous. At localities 312 and 588 in the west (areas H-3 and J-3, 300 m and 150 m respectively, west of the mapped contact), the SHbT contains a roughly equant inclusion several meters in diameter of tonalite texturally similar to the PHbT. On the other hand, tonalite texturally similar to the SHbT occurs as rare masses several to many square meters in size in the outer few hundred meters of the PHbT in the east and northeast. The latter masses are poorly exposed; whether they are intruded into or included in the PHbT is unclear.

Several less direct lines of evidence combine to strongly suggest that the present margins of the PHbT coincide approximately with the margins of an original PHbT pluton, around the periphery of which the SHbT was later emplaced. These lines of evidence, which shall be discussed in sequence, are:

(1) An increase in foliation intensity and in the development of concordant joints towards the SHbT-PHbT contact zone, especially in the PHbT;

(2) a concentration of inclusions of pre-batholithic rocks near the contact, especially in the PHbT, plus the scattered occurrence of large (>1 m) inclusions of pre-batholithic rocks throughout the PHbT; and

(3) relationships of the "mafic zones" of dioritic rock and inclusion-rich tonalite to the two tonalite units.

(1) Foliation intensity. Foliation intensity increases in the PHbT within several hundred meters of the margins everywhere except perhaps along the broadly gradational southernmost stretches of contact. Concurrently, concordant joints become more prevalent and closely spaced (Plate 5). These effects are most pronounced along the northern margin, where the PHbT is locally gneissose, and jointing locally produces slab-shaped outcrops (Figure 20) approaching those developed in the GBT. Inclusions in the PHbT are flattened into discs with dimensional ratios commonly 5 or 6:1 and locally up to about 15:1. The SHbT also shows an increase in foliation intensity and in the frequency of concordant joints towards its inner contact, but the effects are less pronounced;

Figure 20. Strongly foliated prismatic hornblende tonalite about 35 m south of the SHbT-PHbT contact zone. Note the pronounced concordant jointing and extreme flattening of inclusions. Locality: 30 m east of the North-South road (area E-6).

Figure 21. Sharp concordant contact (center of photograph) between the stubby hornblende (left) and prismatic hornblende tonalites. The outer 1-3 m of the PHbT contains abundant layers and lenses of finer-grained, slightly darker gray tonalite cut by and included in typical foliated PHbT. Sparse inclusions of fine-grained schistose amphibolite (e.g. at the bottom of the photograph) commonly occur in the outer few meters of the PHbT, especially in association with the finer-grained tonalite layers. Locality 110, 1.7 km southwest of Rancho El Coyote (area F-4,5).

some discoidal inclusions locally have dimensional ratios up to 5 or 6:1, but most are more equant.

Foliation in both units is generally conformable to the mutual contact, but there are several important exceptions (Plate 3): (1) along a 700-m stretch of contact southwest of Arroyo de las Parritas in the northwest (area G,H-4), (2) along a shorter stretch of contact in the northeast (area F-8), and (3) at the southwestern tip of the SHbT. In each of those places, foliation passes smoothly across the contact and clearly records combined synchronous flow of the two masses.

(2) Inclusions. Excluding the GBT, identifiable inclusions of pre-batholithic rocks are very rare throughout most of the SHbT, but they are slightly concentrated in places along the inner margin of the unit mainly in the northeast. In contrast, country-rock inclusions from several centimeters up to several meters in size, are sparsely scattered throughout the PHbT and are distinctly concentrated in the outer part of the unit, especially where mafic inclusions or zones of dioritic rocks are prominent. In particular, small inclusions of calc-silicate rock and of fine-grained schistose amphibolite comprise up to several percent of a distinctive medium gray, relatively fine-grained, slightly porphyritic tonalite which occurs as lenses and layers at many places around the northern and eastern margins of the PHbT, exclusively in the outer few meters of that unit (Figure 21) or in the zone of diorite and inclusion-rich tonalite separating the PHbT and SHbT. Thin-section observations suggest that the fine-grained tonalite is a more rapidly cooled and perhaps slightly hybridized

variant of the PHbT. The distribution of this rock type and the consistent association with inclusions of pre-batholithic rocks strongly suggest that the rock is a border phase of the PHbT once in contact with the country rocks.

A former extensive contact of the PHbT with country rocks also explains the distribution of large country-rock inclusions in the interior of the PHbT. These inclusions all consist of thin-bedded mudstone, tuff, and calc-silicate rock identical to the strata which are wrapped around the entire northern and eastern margins of the pluton.

(3) Zones of Diorite and Inclusion-Rich Tonalite and their Relationships to the Stubby Hornblende and Prismatic Hornblende Tonalites. A narrow "mafic zone" (MZ-1) of heterogeneous diorite and inclusion-rich tonalite and quartz diorite separates the SHbT and PHbT for a distance of nearly 6 km in the east. Similar subparallel zones (MZ-2 and MZ-3) occur within the SHbT immediately to the east. The diorite ranges in average grain size from <1 mm to 2-3 mm and in mafic mineral content from 30-45%. Hornblende and plagioclase are the principal minerals. Biotite, quartz, and K-feldspar are minor or absent. Textures range from hypidiomorphic-granular to allotriomorphic-granular or granoblastic, with intermediate textures prevailing. Some of the rock is megacrystic and consists of up to 20% subhedral plagioclase tablets and 5% subhedral hornblende prisms, both 2-5 mm in size, enclosed in a fine-grained groundmass.

Injection and assimilation of diorite by the PHbT and, to a lesser

degree, by the SHbT produced all gradations from hornblende diorite through quartz diorite and mafic tonalite to normal biotite-hornblende tonalite with 15-20% mafic minerals. The mafic zones branch and pinch out irregularly, and the proportions of rock types vary widely from predominately inclusion-rich tonalite or quartz diorite (Figure 22A) to predominately hornblende diorite cut by minor dikes and stringers of tonalite and quartz diorite (Figure 22B). Inclusions of thin-bedded metamorphic rocks, especially calc-silicate rock and fine-grained schistose amphibolite, are scattered throughout the western zone; locally they are abundant, but overall they make up <<1% of the zone. Moderate foliation defined by preferred orientation of minerals and inclusions and by the average trend of branching dikes and irregular contacts among the various rock types is parallel to the length of the zones and to the foliation in the adjacent SHbT and PHbT.

Each zone appears to pinch out abruptly at its southern end. Traced northward, zone MZ-1 divides into two branches about 400 m south of Arroyo San José. The main branch separating the two tonalite units continues northwestward across the arroyo for about 1.7 km, then gives way gradually to a zone of inclusion-rich PHbT which continues, with decreasing inclusion abundance, northwestward along the SHbT-PHbT contact zone for another 1.5-2 km. The eastern branch, MZ-1A, apparently gives way northward beneath the arroyo to a zone of inclusion-rich and schlieren-rich SHbT which continues northwestward parallel to foliation and to zone MZ-1 for at least 3 km, possibly farther (not mapped). The other large zone, MZ-2, divides northward into several thin branches which pinch out or are lost

Figure 22A

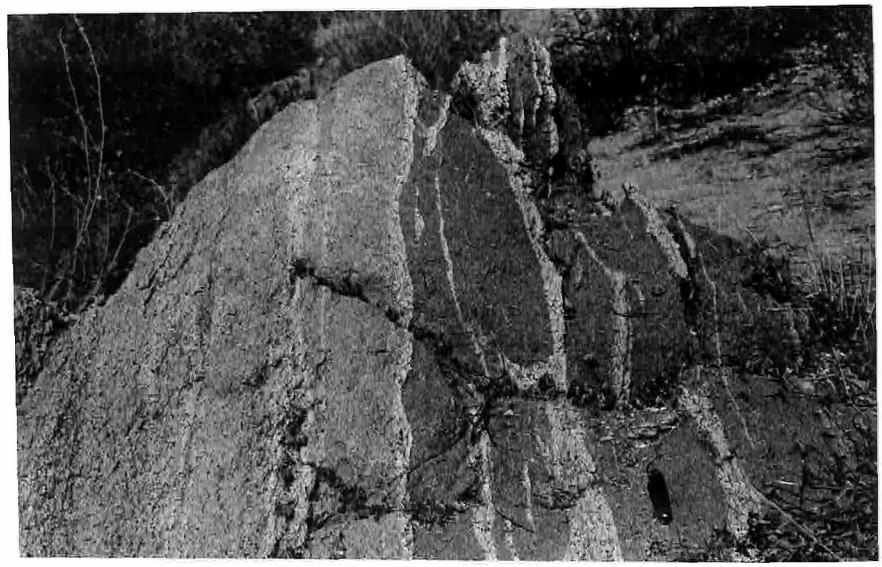

Figure 22B

Figure 22. Two exposures in the zone (MZ-1) of diorite and inclusion-rich tonalite separating the prismatic hornblende and stubby hornblende units. (A) inclusion-rich PHbT; (B) diorite and hybridized tonalite cut by dikes of PHbT. Mafic inclusions, tonalite dikes, and planar mineral orientation in the mafic zone are all parallel to the margins of the zone and to foliation in the adjacent PHbT and SHbT. Localities: (A) 600 m north of the San José-Observatorio road (area J-11) and (B) 1100 m northwest of the intersection of Arroyos San José, Cerro Costilla, and Campo Buena Vista (area G-9,10).

beneath Arroyo San José.

Mafic zone MZ-1 grades consistently westward over tens of meters into the PHbT; no real contact exists. As one approaches and enters that zone from the west, the PHbT becomes progressively richer in dioritic inclusions of all sizes up to many meters until, in the most mafic outcrops generally in the eastern part of the zone, diorite predominates and only thin dikes and patches of tonalite remain (Figure 22B). Concurrently, the mafic mineral content of the tonalite commonly increases to 25-30%, and the quartz content commonly decreases, so that much of the rock is strictly quartz diorite (Streckeisen, 1973). Typical relationships in the resulting complex mixture are heterogeneous diorite (1) included in and cut by either mafic or normal PHbT or (2) included in and cut by mafic PHbT, and the two together included in or diked by normal, light gray PHbT.

Some tonalite in mafic zones MZ-2 and MZ-3, both of which are wholly in the SHbT, is clearly recognizable as normal or slightly hybridized PHbT. However, much of the tonalite in these two zones has assimilated sufficient amounts of finer-grained diorite so that its parentage is difficult to assign. Most of the latter tonalite contains abundant 2-4 mm elongate hornblende prisms and some platy biotite, but generally has few if any 3-6 mm equant poikilitic hornblende and biotite crystals such as characterize the surrounding SHbT; thus most of this hybridized tonalite is probably also derived from the PHbT.

Contacts of the SHbT with the mafic zones, although broadly gradational in some places, are generally much sharper. In many out-

crops, the contact can be defined to within 1-2 m, locally even 1-2 cm. Except for a local increase in the abundance of dioritic inclusions (rarely up to 5-10% of an outcrop) or of leucocratic and mafic schlieren (at most a few percent of the rock), the appearance of the SHbT remains generally unchanged up to the contact. However, dikes and patches cutting the mafic zones consist not only of normal SHbT, but also of leucocratic and mafic variants petrographically similar to schlieren in the SHbT, as well as of hybridized SHbT containing abundant small (0.5-2 mm) equant grains and elongate prisms of hornblende apparently derived from the mafic rocks. Most of the SHbT dikes appear to be restricted to the outer few meters of the mafic zones.

These general relationships strongly suggest that the SHbT is intruded into and has partially broken up a large pre-existing mass of complexly mixed and hybridized diorite and PHbT. Several small-scale crosscutting relationships support this interpretation. At locality 744 near the southern end of zone MZ-1 (area K-11), a narrow dike of variably leucocratic to mafic tonalite or quartz diorite texturally similar to the SHbT cuts sharply across mixed foliated diorite and typical to slightly mafic PHbT (Figure 23). The dike is in the western part of the mafic zone, where the PHbT in the mixed rock can be readily traced into the main body of PHbT. Several smaller tonalite and hornblende-rich quartz diorite (?) dikes with typical SHbT texture occur within 10 m of this outcrop. At locality 343 along the eastern margin of the same mafic zone 350 m to the north, small dikes of leucocratic tonalite are complexly intruded into mixed diorite

and PHbT (Figure 24). The leucocratic dikes appear megascopically similar to leucocratic schlieren in the SHbT; mafic minerals are mostly equant, equigranular, and in some cases, poikilitic, although elongate subhedral hornblende prisms also occur and locally predominate. Traced towards the SHbT, the leucocratic dikes approach parallelism with the margin of that unit and either grade abruptly into the SHbT or are truncated at a low angle by that unit. Either relationship implies that the PHbT into which the leucocratic dikes are intruded is older than the SHbT. Finally, at locality 443 near the southern end of zone MZ-2 (area J-11,12), a rotated boulder shows foliation in normal PHbT truncated by weakly foliated or unfoliated SHbT (Figure 25).

The small-scale relationships thus corroborate the large-scale impression that the SHbT is younger than both the mafic rocks and the PHbT. However, I cannot rule out the possibility that the two tonalite units are so closely spaced in time that reversals of these relationships may exist. The relationships observed where the two units grade into one another -- specifically, the concordant interlayering of the two textural types without recognizable crosscutting relationships; the development of intermediate-textured rocks; the absence of a finer-grained border phase in the SHbT, and generally in the PHbT as well; and the development of a common foliation in both units, locally crossing the contact -- imply that both tonalite masses were hot and capable of at least limited flow and intermingling at the time of juxtaposition. All of these observations can be explained by a model invoking intrusion of the SHbT around the margins of the PHbT while crystallization, and possibly intrusion, of the latter was still in progress.

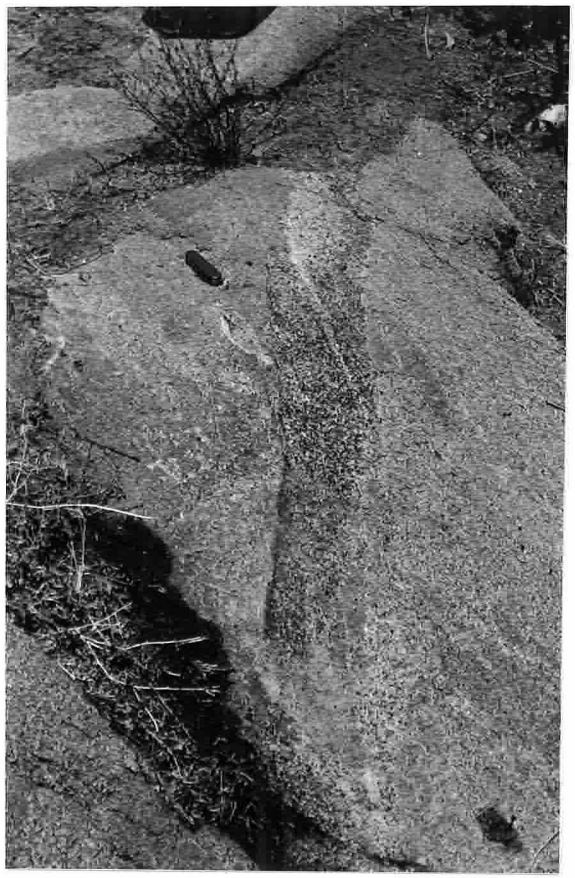

Figure 23A

Figure 23B

Figure 23. Inhomogeneous quartz diorite or melatonalite dike crosscutting foliation in mixed diorite and hybridized prismatic hornblende tonalite. Foliation in the mixed host rock is parallel to the pocket knife. Note that the mafic minerals (mostly hornblende) in the dike have the anhedral to subhedral, equant and poikilitic forms characteristic of the stubby hornblende unit. Locality 744, near the southern end of mafic zone MZ-1 separating the PHbT and SHbT units, 65 m west of the San José-Observatorio road (area K-11).

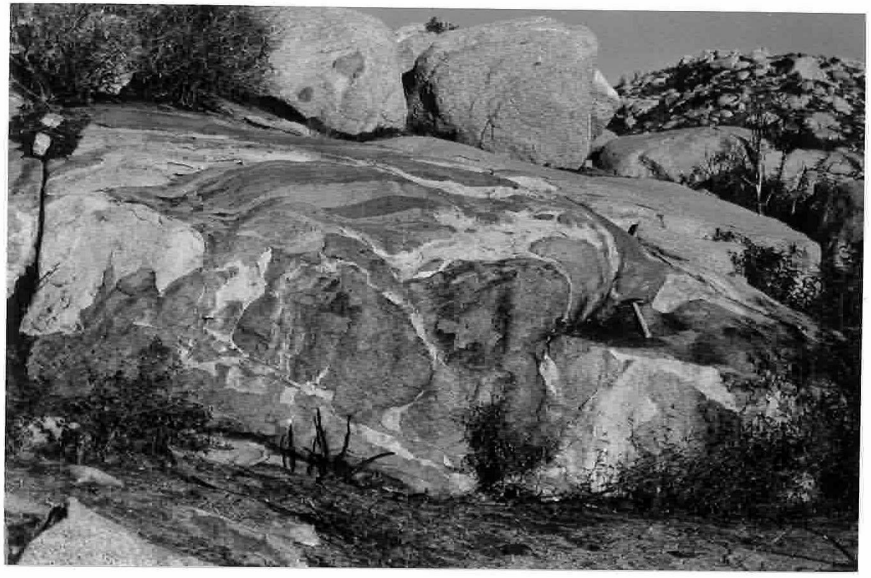

Figure 24

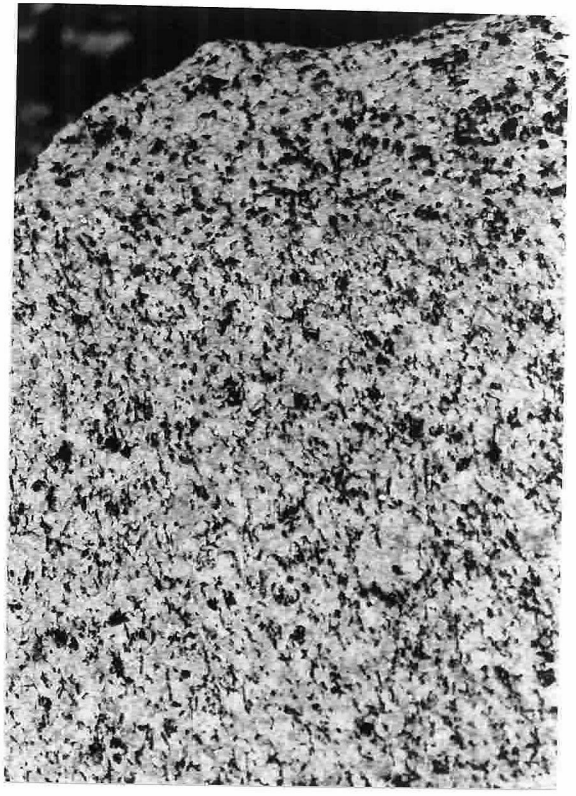

Figure 25

Figure 24. Leucotonalite dikes cutting inclusion-rich prismatic hornblende tonalite at the eastern edge of mafic zone MZ-1 separating the SHbT and PHbT. The dikes, which are megascopically similar to leucocratic schlieren in the SHbT, appear to be derived from, or possibly intruded by, the adjacent SHbT. Either relationship implies that the PHbT is older than the SHbT. Locality 343, 40 m east of the San José-Observatorio road, 500 m north of the southern tip of zone MZ-1 (area K-11).

Figure 25. Foliated prismatic hornblende tonalite truncated at the top of the boulder by unfoliated or weakly foliated stubby hornblende tonalite. Locality 443 near the southern end of mafic zone MZ-2 in the SHbT just east of zone MZ-1 separating the SHbT and PHbT units (area J-11,12).

U-Pb isotopic age determinations on zircons from two samples also indicate contemporaneity within the limits of the precision of the data. Sample BC-I-12 from the transitional zone between the PHbT and SPT and sample BC-I-5 from the gneissose border phase of the SHbT gave ages of 112 ± 2 m.y. and 111 ± 2 m.y., respectively (L. T. Silver, unpublished data).

6.5.2 Prismatic Hornblende-Seriate Porphyritic Contact Zone

The PHbT and SPT are completely intergradational. Both foliation (Plate 3) and joint (Plate 5) patterns cross the zone of textural transition without change in trends or intensities. Southeast of Rancho San José, a gradual northward decrease in size and abundance of large plagioclase crystals defines a contact zone averaging 100-300 m wide, and there is generally no doubt to which unit the rocks on opposite sides of the zone belong. Similarly, in the outer kilometer along the southwestern side of the pluton, the transition zone is several hundred meters wide. However, in the intervening area the contact zone is poorly defined; in many outcrops in a 7-km^2 area in the western part of the PHbT (stippled in Figure 26), sparse coarse plagioclase crystals are more conspicuous than elsewhere in the PHbT, but neither as abundant nor as consistently large as in the typical SPT. The rocks in this area grade smoothly into both the PHbT and SPT; their assignment to the PHbT is somewhat arbitrary, but not critically important.

Two models can account for the gradational relationship between the two textural units. (1) They may be variants from a single magmatic

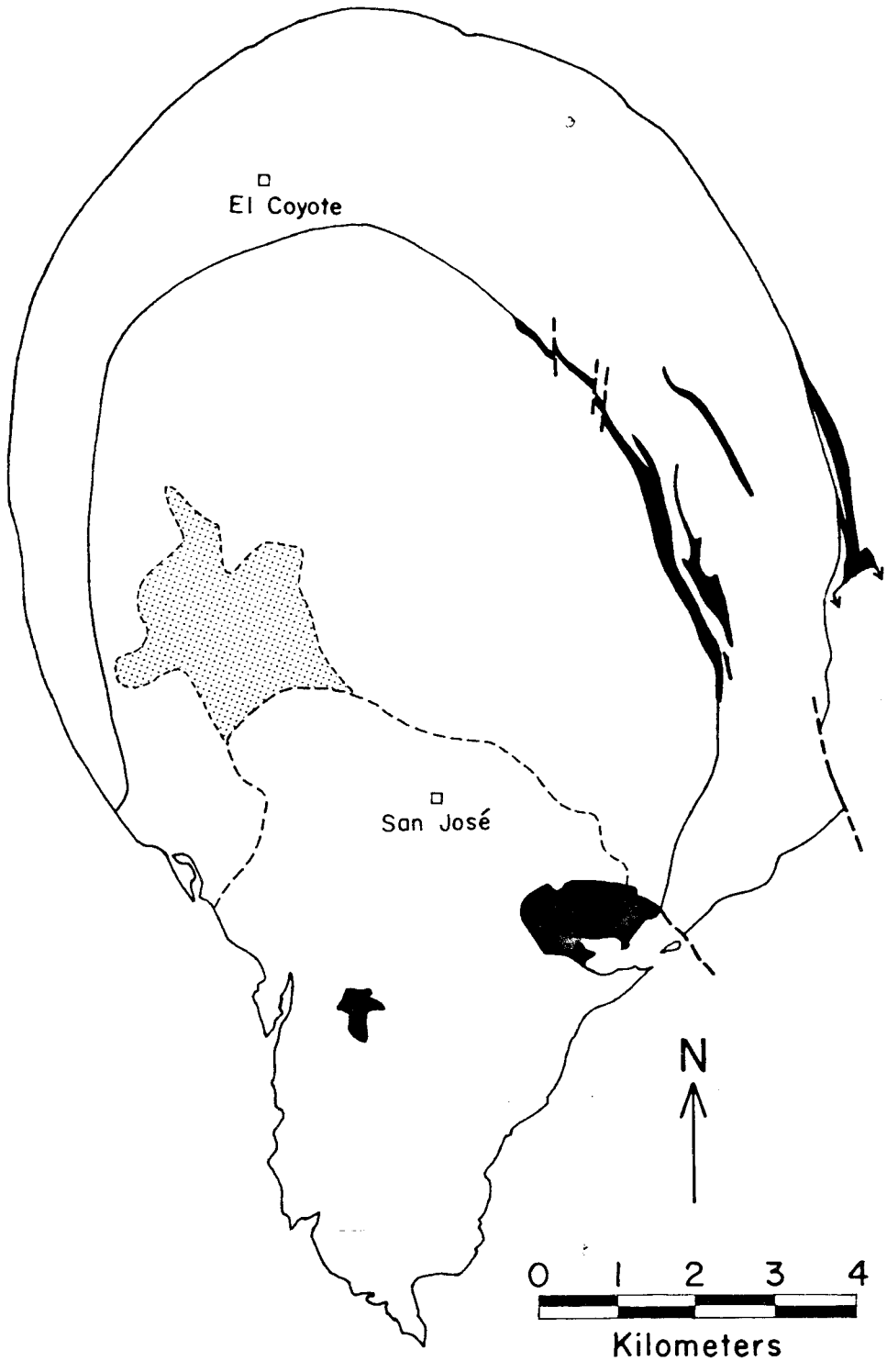

Figure 26. Area (stippled) of tonalite texturally intermediate between the prismatic hornblende and seriate porphyritic tonalites. The area was mapped as PHbT.

pulse. (2) They may have formed from two pulses, closely spaced in time, which mixed extensively at their margins. In either case, the foliation patterns and other structural evidence discussed in Chapter 11 indicate that the SPT was the last of the tonalite units to be emplaced and expanded northward into the partially molten interior of the PHbT. Density considerations discussed in Appendix F indicate that plagioclase would have tended to sink rather than float in the tonalite magma if gravity-dependent segregation was at all effective. Thus the PHbT and SPT magmas may have been derived from shallower and deeper levels, respectively, of a single magma chamber.

Chapter 7

MINOR ROCK TYPES AND PETROGRAPHIC VARIANTS IN THE PLUTON

7.1 General Statement

A variety of rock types and petrographic variants of the tonalite altogether comprise several percent of the pluton. In approximate order of decreasing abundance these are: dioritic and gabbroic rocks, various dike and vein rocks, inclusions, mafic quartz diorite and tonalite, schlieren, lime-contaminated tonalite and quartz diorite, and mafic-layered tonalite. Schlieren will be discussed in conjunction with flow structures, of which they are one form.

7.2 Diorite and Gabbro

In addition to the zones of diorite and inclusion-rich tonalite discussed in Chapter 6, heterogeneous dioritic and gabbroic rocks occur in three principal areas in or connected to the pluton (Plate 2): (1) in a long narrow zone crossing Cañon Campo Buena Vista in the middle of the eastern prong of the SHbT (area G-11 to I-12), (2) in sheets connecting the eastern margin of the pluton to the gabbro-diorite complex in Cañon La Jolla (area G-12 to I-13), and (3) in an oval mass along and south of Willow Creek Canyon (area N-9 to N-10). Each area consists of complexly mixed and intergradational diorite, gabbro, quartz diorite, and tonalite. Excluding the sheets and the associated mafic complex in Cañon La Jolla, dioritic and gabbroic rocks altogether comprise nearly 3% of the pluton.

7.2.1 Gabbro-Diorite Zone Crossing Cañon Campo Buena Vista

This zone, which averages 70-80 m wide and extends for at least 2 km

parallel to t he N 35° W trend of foliation in the host SHbT, is highly complex and variable along its length. The narrow northern end consists mostly or entirely of fine-grained dikes of complexly mixed and intergradational hornblende diorite and leucodiorite (?), some of which contain sharply angular, fracture-bounded inclusions of unmodified SHbT. A subparallel narrow zone of fine-grained mafic dikes 700-900 m along strike to the northwest may be an extension of this mafic zone, but mafic rocks are not conspicuous in the intervening area.

Just north of Cañon Campo Buena Vista, the zone jogs slightly eastward and widens. Here recognizable mafic dikes are minor or absent, and the zone consists of normal to slightly mafic (up to 25-30% mafic minerals) SHbT containing abundant medium-grained dioritic inclusions up to several meters in size.

From Cañon Campo Buena Vista southward, the mafic zone consists of abundant gabbro, diorite, and inclusion-rich mafic quartz diorite. These rocks are complexly intermingled, and contacts with the surrounding SHbT are gradational. Fine-grained diorite dikes containing angular inclusions of SHbT are again present, but volumetrically minor. Most of the diorite is medium-grained (1-3 mm), contains 30-40% mafic minerals, and is included in or grades into quartz diorite and tonalite. The gabbro is dark brownish gray and contains about 35-40% mafics and 60-65% plagioclase (labradorite to calcic andesine). Grain size averages 0.5-2 mm, but tabular plagioclase crystals range up to 6-8 mm. Extremely poikilitic, anhedral hornblende crystals 1-2 cm in diameter make up several percent of many outcrops and impart a spotty appearance to

weathered surfaces. The one sample examined in thin section is a pyroxene-hornblende gabbronorite containing at least 5% each of augite hypersthene, hornblende, and pale amphibole (both actinolite and cummingtonite). The mafic zone appears to pinch out abruptly 1100 m southeast of Cañon Campo Buena Vista, although several large inclusions of gabbro occur in the SHbT 200-300 m farther south.

The mafic zone is thus a composite of at least two generations of mafic rocks. Some or all of the fine-grained diorite dikes were clearly emplaced when the SHbT was relatively cool and rigid, whereas some or all of the medium-grained diorite and gabbro grades into or is included in the SHbT. The gabbro and medium-grained diorite may constitute a septum of older wall rock partially assimilated by the SHbT. The occurrence of a few scattered inclusions of calc-silicate rock in the SHbT just west of the zone supports this interpretation. Alternatively, the gabbro and diorite may have been intruded into the SHbT while the latter was still partially molten and capable of disrupting and partially assimilating the mafic material. The approximate coincidence of the mafic zone with the hypothetical northward projection of the Cañon Socorro fault zone suggests that intrusion could have been localized along fracture or shear zones related to the fault.

7.2.2 Mafic Sheets and the Gabbro-Diorite Complex in Cañon La Jolla

Two intrusive sheets connect the eastern margin of the San José pluton to the gabbro-diorite complex in Cañon La Jolla (Plate 2). The smaller western sheet consists predominantly of intensely foliated and lineated tonalite and quartz diorite. The larger eastern sheet, which extends

for 3 km and varies from about 70-180 m wide, consists of a heterogeneous mixture of diorite, gabbro, and lesser amounts of tonalite or quartz diorite, with up to 10% inclusions and small septa of metamorphic rocks. Contacts of both sheets are grossly concordant, but low-angle discordance and interfingering with metamorphic rocks are common. Neither sheet has been mapped in detail.

Most of the rocks in the larger sheet contain 30-45% mafic minerals, but the range is from 25-70%. Hornblende is the only conspicuous dark mineral in the gabbro and mafic diorite, but biotite makes up several percent of some diorite and tonalite. Patchy concentrations of hornblende or plagioclase are locally common on a scale of centimeters. Grain size ranges from 0.5-1.5 mm in some rocks to 3-4 mm in others; small pegmatitic patches and stringers occur in the more mafic rocks. Protoclasis and preferred mineral orientation -- variably linear, planar or both -- are very strong in some rocks, but weak in others. Textures in the less sheared rocks range from hypidiomorphic-granular to nearly granoblastic and from generally seriate to rarely equigranular. Hornblende prisms are typically elongate about 2:1 or 3:1, but in some equiangular rocks the grains are equant.

The gabbro-diorite complex in Cañon La Jolla is similar to and appears to have been the source for much of the rock in the larger sheet. The slightly irregular ovoid complex is about 2.3 km long, averages 1 km wide, and is oriented with its long axis approximately N 30° W. Except along the western margin, I have examined very little of the body; the eastern and southern contacts are roughly drawn from aerial photographs. The northwestern and western margins of the mass consist mostly of fine-

to medium-grained inhomogeneous hornblende diorite, plus some hornblende gabbro and some quartz diorite or tonalite. The interior of the body consists mostly of fine- to medium-grained gabbro generally containing subequal amounts of hornblende and plagioclase, but with many small patches and stringers of nearly pure hornblende or plagioclase. Arcuate masses of metamorphic rocks up to 10 m or more in length and several meters in width are sparsely scattered through the interior of the body.

Strata are wrapped around the Cañon La Jolla body in a grossly concordant fashion, but the mapped parts of the contact are commonly discordant in detail. Foliation and lineation attitudes in the mafic complex, as well as in the two intrusive sheets and in several mafic and aplitic dikes which cut the mafic complex, are parallel to those in the adjacent pre-batholithic strata and the gneissose border phase of the San José pluton. All of the rock types have therefore been subjected to a similar pattern of deformation. The margin of the San José pluton is smoothly indented directly west of the Cañon La Jolla body and, to a lesser degree, west of the northern half of the large mafic sheet. These indentations were probably caused by shoving of the older, more rigid mafic intrusives towards the partially molten San José pluton during superimposed regional deformation. Alternatively, the indentations may indicate that the mafic masses were obstacles to the expansion of the pluton.

The two intrusive sheets have many similarities to the zones of diorite and inclusion-rich tonalite associated with the SHbT and PHbT contact zone. If the SHbT was emplaced around the margins of a pre-existing PHbT pluton, as the observations discussed in Chapter 6 strongly

suggest, it seems likely that the two sheets, the gabbro-diorite complex in Cañon La Jolla, and the mafic zones associated with the SHbT-PHbT contact zone were originally part of a single mafic complex. Alternatively, the sheets may be zones of mixed material from the SHbT and Cañon La Jolla masses.

If the first hypothesis is correct, the sheets must be truncated at their junctures with the pluton. The contact zone of the large mafic sheet with the SHbT in and north of Cañon Campo Buena Vista is at most 4-5 m wide, but it is not actually exposed. The SHbT does not appear to grade into the mafic rocks, but clear evidence of structural discontinuity is also lacking. The southern end of the smaller sheet divides, one branch merging with the larger mafic sheet and the Cañon La Jolla complex, the other projecting southwestward back towards the pluton. The latter branch does not appear to merge with the pluton, but whether it is truncated by the SHbT or pinches out before reaching the pluton contact is unclear. More detailed field and microscopic examination of the intrusive sheets, especially of the hybridized tonalite and quartz diorite, is needed to determine the structural and petrologic relationships of the sheets to the tonalite units.

7.2.3 Diorite-Gabbro Complex Along Willow Creek Canyon

This complex is an east-west oval mass 1.5 km long and 0.8 km wide, consisting of several textural varieties of diorite, a lesser amount of gabbro, and minor tonalite and quartz diorite. The diorite and gabbro generally contain 25-45% hornblende, up to 2-3% pale amphibole (mostly cummingtonite, some actinolite), and trace amounts of biotite, clinopy-

roxene and possibly orthopyroxene. Small stringers and patches of nearly pure hornblende are locally abundant. The quartz diorite grades into diorite, but generally contains 20-25% mafic minerals; hornblende exceeds biotite, but both are abundant.

All of these rocks exhibit hypidiomorphic-granular textures. In contrast to the areas of mafic rock previously described, granoblastic or allotriomorphic-granular textures are rare or absent. The rocks range from fine- to medium-grained (average grain size up to 3-4 mm) and from seriate to equigranular. In much of the equigranular rock, hornblende crystals are equant and often poikilitically enclose small plagioclase grains; some of the equigranular diorite is texturally similar to the SHbT.

Magmatic flow structure -- either linear, planar, or both -- and protoclasis are locally strong, but generally weak or absent. Shearing is locally intense in narrow zones parallel to the major fault, fracture, and dike directions, especially in the northwest-striking direction, but there is no evidence of metamorphism or pervasive penetrative deformation.

Local crosscutting relationships indicate at least three generations of diorite. Fine-grained diorite (1) containing 35-40% hornblende is intruded by and included in various types of medium-grained diorite, (2) which may or may not all be of one generation. The latter are in turn intruded by and abundantly included in relatively homogeneous, fine- to medium-grained, slightly porphyritic diorite (3) containing about 35% hornblende. The third diorite type is abundant mainly in the northeastern quarter of the complex, although dikes of similar diorite occur elsewhere in the mass. Similar diorite is also an important dike rock

in the extensively injected pre-batholithic rocks on both sides of the Willow Creek fault zone, throughout the area west of the Willow Creek quartz diorite pluton.

As mentioned earlier, some of the medium-grained (type-2) diorite is texturally similar to the SHbT. Inclusions of this diorite type are locally abundant in the type-3 diorite along Willow Creek Canyon. Also, just south of the Willow Creek fault zone, in the northeastern corner of the complex, a 5-10 m by 20 m lens of gneissose tonalite probably correlative with the border phase of the SHbT occurs along the contact with pre-batholithic rocks. Less gneissose quartz diorite and diorite with raggedly equant and equigranular mafic minerals is poorly exposed along the contact with metamorphic rocks for several hundred meters to the southwest. These observations suggest that much of the rock in the mafic complex may be an offset hybridized extension of the SHbT.

Aplite, pegmatite, and fine-grained diorite dikes (generally similar to type-3 diorite) abound in the mafic complex and in the adjacent metamorphic rocks. Most strike N 15°-60° W -- parallel to major fracture, fault, and photo-lineament directions -- and generally dip at moderate to shallow angles to the southwest (Plate 5). Quartz veins are also locally abundant.

Contacts of the mafic complex with pre-batholithic rocks are sharp in and just south of Willow Creek Canyon, but elsewhere injection is extensive, and contacts with metamorphic rocks are commonly gradational across several meters or more. The combination of straight contact segments and abrupt changes in contact orientation implies that intrusion was controlled by bedding and fracture planes in the metamorphic rocks.

Six small mappable masses of pre-batholithic rocks capping hills in the central and southern parts of the complex (Plate 2) are probably pendants. Inclusions of pre-batholithic rocks are abundant in the diorite and gabbro around these masses.

South of Willow Creek Canyon, contacts with the SPT are gradational generally over 10-30 m. Sparse, smoothly elliptical mafic inclusions occur in the adjacent SPT, but there are no sharp crosscutting relationships. Much of the northern contact is hidden under alluvium in Willow Creek Canyon. The northeastern contact is slightly irregular in detail, but coincides roughly with the northwestward extension of the Willow Creek fault zone. The mafic complex here consists mainly of unfoliated, unsheared type-3 diorite which was intruded along the fault zone apparently after most or all of the displacement had occurred. This diorite is intruded into not only the other mafic rocks and the pre-batholithic rocks, but also the SHbT and PHbT. A dike of similar diorite in the interior of the complex contains angular inclusions of typical PHbT or SPT. Typical PHbT or phenocryst-poor SPT forms a north-south mass at least 100 m long and 15 m wide surrounded by gabbro and type-2 diorite in the interior of the mafic complex. The contacts of this mass are poorly exposed; it could be either a dike or an elongate inclusion.

Within 150-400 m of the contacts, foliation in the PHbT and SPT is wrapped conformably around the mafic complex. Where recognizable, foliation in the outer part of the mafic complex is also parallel to the contact. Dips of foliation are steeply northward away from the complex on the northern side, swing to vertical or very steeply outward on the western side, then to steeply northward under the complex on the southern

side. This pattern suggests that the body is an ovoid cylinder plunging steeply northward or northeastward.

7.3 Heterogeneous Quartz Diorite and Diorite in Arroyo San José

Heterogeneous biotite-hornblende quartz diorite grading to hornblende diorite and partially intermixed with typical SPT forms an irregularly shaped mass about 0.2 km^2 in area along Arroyo San José slightly west of the center of the SPT (Plate 2). The rocks are medium to dark gray and contain generally about 30%, but up to 50% mafic minerals, mostly hornblende. Preferred mineral orientation is very weak or absent. The average grain size is 1-3 mm, compared to 2-4 mm in the surrounding tonalite. However, subhedral to euhedral plagioclase crystals 4-10 mm in size range from sparse to as much as 5-10% of the rock and produce a markedly seriate porphyritic texture in many outcrops. A few hornblende crystals also reach 6-7 mm. Although the plagioclase phenocrysts are smaller than those in the surrounding SPT, the seriate porphyritic texture is commonly more striking because of the finer average grain size and darker color of the quartz diorite. Variability in the abundance and distribution of plagioclase phenocrysts and of mafic versus leucocratic minerals commonly produces a mottled appearance on a scale of centimeters.

Hornblende is subhedral to euhedral and commonly acicular, but some prisms are stout. Anhedral biotite flakes 3-6 mm in diameter make up about 5% of most of the rocks, but are minor or absent in the more mafic variants. Quartz is fine-grained and inconspicuous in hand specimen, but it comprises 10-15% of the one sample examined in thin section and may be similarly abundant throughout all but the most mafic

parts of the mass.

Typical SPT is scattered throughout the mafic body as vaguely-bounded stringers and patches 10-20 cm in size and as larger, poorly-exposed masses up to many meters in diameter. Contacts of the larger masses, where seen, are gradational. The margins of the entire mafic body are poorly exposed, except in one small outcrop where the contact is sharp.

Mafic inclusions are generally scarce in the interior of the SPT, but they abound in the quartz diorite and in the intermixed and immediately adjacent tonalite. Some of the inclusions are fine-grained schistose amphibolite; many others are fine- to medium-grained, unfoliated gabbro or diorite (or amphibolite) characterized by 30-50% acicular hornblende crystals. Many of the inclusions are diffusely bounded and partially disaggregated; assimilation of these inclusions appears to have been a source of both the acicular hornblende crystals and the mottled textures in the quartz diorite.

Thin-section examination of a single sample reveals approximately 10-15% quartz, 55% plagioclase, <1% K-feldspar, 20% hornblende, 5% biotite, 1-2% cummingtonite, and 5-6% accessory and alteration phases. Plagioclase occurs as fat, subhedral to euhedral tablets similar in shape to those in the tonalite, but consisting typically of corroded, saussuritized cores of weakly zoned or unzoned calcic labradorite surrounded and extensively replaced by strongly zoned, unaltered rims. The rims generally show sharp, euhedral, two-step zoning, the inner zone averaging An_{50-60} and the outer zone decreasing from about An_{40} at the inner edge down to An_{15-20} at the grain margin. Repeated oscillatory zoning is

absent. In contrast, plagioclase in the surrounding SPT shows strong oscillatory and progressive zoning from cores of An_{40-45} to rims of An_{19-23}; calcic cores and stepwise zoning are absent. The pattern and broad range of zoning distinguish the plagioclase in the quartz diorite from that in any of the other rocks studied.

Hornblende is optically similar to that in the tonalite, but the crystals are highly corroded, and some are faintly mottled. Quartz is irregularly interstitial, and the larger grains are consistently full of hornblende and plagioclase inclusions. Cummingtonite occurs as (1) subhedral crystals and anhedral interstitial grains usually, but not always, enclosed in quartz and (2) homoaxial areas in composite hornblende-cummingtonite grains, again preferentially, but not exclusively, where those grains are in contact with quartz. Proximity to quartz appears to have stabilized cummingtonite relative to hornblende, presumably by a reaction such as:

hornblende + siliceous melt $\rightleftharpoons$ plagioclase + cummingtonite + H_2O.[4]

The interstitial cummingtonite apparently crystallized directly from the melt. A few cummingtonite grains are partially rimmed or replaced by hornblende, so the stabilization was locally or subsequently reversed.

The plagioclase zoning, the pronounced corrosion of hornblende, and the abundance and late magmatic growth of cummingtonite point to an unusual complex history. The mafic body is apparently a mass of horn-

---

[4]For example: $7\ NaCa_2(Mg,Fe)_4Al_3Si_6O_{22}(OH)_2 + 7\ Al_2O_3 + 39\ SiO_2 \rightleftharpoons$

$7\ NaAlSi_3O_8 + 14\ CaAl_2Si_2O_8 + 4\ (Mg,Fe)_7Si_8O_{22}(OH)_2 + 3H_2O$

blende diorite and/or gabbro partially assimilated by the SPT, but whether it is an older mass included in the tonalite or a slightly younger mass emplaced into the incompletely solidified interior of the SPT is unclear. The body is located near the center of the crudely concentric pattern of faint flow foliation in the SPT (Plate 3 and Figure 39), i.e., near the axis of latest up-welling in the SPT, but the significance of this coincidence is uncertain.

7.4 Dike and Vein Rocks

Altogether a variety of dike and vein rocks constitute perhaps 1-2% of the pluton. They parallel each of the major joint directions in the pluton, but those parallel to concordant joints (i.e. parallel to foliation) are few. The volume of dike rocks is greatest in the southwestern part of the SPT, where they comprise perhaps 5% of the rock. On Plate 5, dikes have been classified on the basis of field appearance as mafic (m), intermediate (i), granitic (g), aplitic (a), and pegmatitic (p). Distinctions among the categories are gradational, and some dikes are of composite character: e.g., aplo-pegmatite (a-p) and mafic-intermediate (m-i) dikes. Most veins consist of quartz (q), epidote (e), or both minerals (q-e).

Mafic dikes (m): All dark-colored dikes were put in this group. They are the predominant type of dike throughout most of the SHbT and PHbT, but are sparse in much of the SPT. Most are hornblende or biotite-hornblende microdiorite or melanocratic microdiorite, commonly porphyritic; acicular hornblende is the usual phenocryst phase, sometimes accompanied by plagioclase (generally zoned from andesine to oligoclase).

Dark-colored andesite and possibly dacite porphyry dikes also occur and were grouped with the mafic dikes; hornblende and plagioclase (andesine-oligoclase) are the phenocryst phases. Mafic dikes generally contain >30% dark minerals.

Some mafic dikes show two or three distinct generations of euhedral amphibole and, in some cases, plagioclase, giving them a lamprophyric character. For example, the long northwest-trending dike mapped in the center of the PHbT (Plate 5, area J-7) contains 25% altered, 0.5-2 mm mafic phenocrysts (pseudomorphed by chlorite plus minor actinolite and epidote) and <1% unaltered, 0.5-1 mm amphibole phenocrysts in a fine-grained groundmass of plagioclase (andesine), acicular amphibole, and minor quartz, opaque, sphene and apatite. Both the groundmass and phenocrystic amphibole is zoned from orange-brown kaersutitic (?) cores to thin green hornblende rims. A parallel dike in Arroyo de las Parritas near the northwestern margin of the PHbT (Plate 5, area G-4) consists of 15-20% strongly zoned, 0.5-2 mm, acicular amphibole phenocrysts (kaersutitic (?) cores, hornblende rims), 2-3% plagioclase phenocrysts (andesine) 1-6 mm in size, and 25-30% andesine microphenocrysts in an aphanitic groundmass of amphibole, plagioclase, and opaques. The phenocrysts and microphenocrysts in the latter dike are all strikingly euhedral.

Numerous north-south striking, steeply-dipping, dark-colored porphyry dikes called "malchite" dikes by Woodford and Harriss (1938, p. 1322) are intruded into both the SPT and wall rocks near Cerro Hechicera (areas R-7 and S-7). The dikes consist of variable proportions of euhedral 1-5 mm hornblende and plagioclase phenocrysts and rare,

0.5-3 mm, rounded quartz xenocrysts (?) in a very fine-grained or aphanitic groundmass. The one sample examined in thin section is similar to the one described by Woodford and Harriss; it is simply an andesite porphyry, with 10-15% euhedral hornblende phenocrysts (brownish green, weakly zoned), 6-7% euhedral plagioclase phenocrysts (andesine-oligoclase, with very thin zones of labradorite near the rims), and rare corroded quartz megacrysts in a fine-grained groundmass consisting mostly of plagioclase, hornblende, and biotite, plus minor opaques, quartz, apatite, and epidote.

Dikes of intermediate composition (i): This category includes mainly fine-grained or barely medium-grained (0.5-2 mm), medium or light gray dikes consisting of quartz, plagioclase, 10-30% dark minerals (hornblende and/or biotite), and perhaps alkali feldspar in some cases. Some fine-grained, medium- to light-colored, hornblende-plagioclase dikes lacking macroscopic quartz are also included, although some of these may be leucodiorite.

Dikes of intermediate composition are relatively rare except in the southwestern part of the SPT. Two from that area were examined in thin section: one is a porphyritic microtonalite and the other a fine- to medium-grained seriate porphyritic tonalite. Both are essentially identical to the host rock in all respects except grain size.

Granitic dikes (g): These are medium- to coarse-grained (2-10 mm), equigranular, leucocratic dikes consisting of quartz, plagioclase, alkali feldspar, and <10% mafics, generally biotite. Most are no more than a few centimeters wide. They are concentrated along with aplitic and peg-

matitic dikes, near the southwestern tip of the SHbT and occur sporadically along the western edge of the PHbT and SPT south to Arroyo San José; elsewhere, they are rare.

Aplitic (a) and pegmatitic (p) dikes: All fine-grained or barely medium-grained (0.5-2 mm), equigranular, quartz-feldspar dikes containing <10% mafics were classed as aplite. Mineralogically similar dikes of very coarse or widely varying grain size were mapped as pegmatite. The two are intergradational and commonly composite. They also grade texturally into granitic dikes. Two typical aplitic dikes examined in thin section consist of subequal amounts of quartz, plagioclase (zoned from andesine to oligoclase), and orthoclase or microcline, plus 2-8% biotite and minor opaques, apatite, epidote, and sphene.

Aplite and pegmatite dikes are less abundant, generally smaller, and mineralogically simpler in the San José area than throughout much of the sierra and foothills to the east and northeast. Pegmatites in the latter area commonly contain abundant black tourmaline crystals locally up to 10-15 cm long; some also contain coarse biotite, muscovite, garnet, ilmenite, diallage, clinozoisite, or andalusite (Woodford and Harriss, 1938, p. 1320). In the San José pegmatites, tourmaline is rare and does not exceed 2-3 cm in length, ilmenite is extremely rare, and biotite and muscovite are minor minerals, generally less than a few centimeters in size. Epidote occurs in some of the San José pegmatites, but none of the other minerals listed above was observed. Pronounced mineralogic zoning is common in the pegmatites farther east, but rare in the San José pegmatites.

Aplite and pegmatite dikes are concentrated locally, especially along the western margin of the pluton and along the SHbT-PHbT contact zone in the west. In those areas, the dikes are generally more abundant in the tonalite than in the pre-batholithic rocks, although numerous large aplite and pegmatite dikes cut the wall rocks near the contact around Cañon Las Cabras. Aplite and some pegmatite dikes are also abundant in the diorite-gabbro complex near Willow Creek Canyon and in the pre-batholithic rocks immediately southeast of the pluton, but few occur in the adjacent tonalite.

Quartz (q), epidote (e), and composite quartz-epidote (q-e) veins occur throughout the pluton and less abundantly in the wall rocks. Most are <30 cm wide and can rarely be traced more than 10 m. A small amount of gold was extracted from pyritiferous quartz veins at the abandoned Peterson gold mine near the southern end of the North-South road (Plate 6).

Both vein minerals tend to be concentrated locally, often in the same areas. Epidote is a major constituent in a few exceptionally veined and pervasively epidotized areas of tonalite hundreds of square meters in size, mainly in the SPT and the western part of the PHbT. Various types of dike rocks, themselves often veined and partially altered to epidote, are commonly associated with the zones of intense epidotization.

Intrusion of the various types of dikes overlapped in time; I recognized no consistent age sequence. Some mafic dikes crosscut and others are intruded by intermediate or aplitic dikes. Dikes of intermediate composition, including the fine-grained tonalite dikes which

were the last phase of SPT magmatism, in some cases cut and in other cases are crosscut by aplitic dikes.

Some dikes and veins of all types exhibit varying degrees of deformation. In particular, many of those cutting the wall rocks and tonalite around the northern two thirds of the pluton exhibit a strong fabric parallel to that in the host rocks, but others are undeformed and were apparently intruded after both the emplacement of the pluton and the cessation of regional deformation. In several outcrops along the arroyo called El Alisito (area Q-6 to R-7), the SPT contains abundant inclusions of porphyry megascopically indistinguishable from the "malchite" dikes which are intruded into the tonalite and wall rocks less than 1 km to the south. The "malchite" porphyry dikes are therefore synplutonic.

A swarm of northeast- and northwest-striking, moderately- to steeply-dipping, microdiorite dikes cuts the northeastern part of the SHbT near Cañon Campo Buena Vista (areas G-11 and G-12, dikes marked "m" and "m-i"). These dikes, many of which actually consist of a complex intergradational mixture of microdiorite cut by and included in more-leucocratic microdiorite or microtonalite, commonly contain sharply angular, fracture-bounded inclusions of unrecrystallized SHbT and must therefore have been intruded after the host rock had cooled sufficiently to behave as a brittle solid. How much younger these dikes are than the pluton is unknown.

7.5 Lime-Contaminated Tonalite

Creamy white, medium-grained hornblende tonalite and clinopyroxene

tonalite form numerous masses from a few up to thousands of square meters in area scattered through the southernmost part of the SPT and in the country rocks at the southern tip of the pluton. The largest masses are shown on Plate 2.

The white tonalite consists of 60-70% plagioclase, 10-20% quartz, and 10-20% mafic minerals (hornblende and/or clinopyroxene and/or actinolitic amphibole). The rocks appear megascopically similar to the typical SPT, except for the creamy white rather than light gray color, the absence of biotite, the generally gray-green rather than black color of the mafic minerals, and the common occurrence of sparse 0.5-1.5 mm sphene crystals. The white color of the rocks arises from the milky white appearance of the plagioclase rather than from a paucity of mafic minerals. However, the plagioclase is fresh, not altered. The minerals exhibit a seriate grain-size distribution averaging 1-3 or 2-4 mm, but a few euhedral plagioclase crystals up to 12 mm in size impart a faint seriate porphyritic texture.

The distribution of the white tonalite is closely related to the distribution of marble and calc-silicate rock. Masses of white tonalite too small to map border and are injected into the small pendant of marble and calc-silicate rock near the southern tip of the pluton (area S-7); four slightly larger masses shown on Plate 2 occur within 100 m to the east and north of the pendant. Likewise, a small unmapped sill of white tonalite occurs against marble and calc-cilicate rock 300 m south of the tip of the pluton (area T-7,8), and two larger mappable linear masses are intruded into the calc-silicate-bearing meta-volcanic rocks 100-200 m to the northwest, roughly along the projected extension of the marble

Figure 27. Thin rind of white lime-contaminated hornblende tonalite along the sharp contact of gneissose tonalite against marble. A 1-2 cm wide layer of garnet plus some epidote and thulite is developed between the lime-contaminated tonalite and the marble. Locality: northwestern contact of the pluton, 1.6 km north-northwest of Rancho El Coyote (area C-5).

plus calc-silicate unit. A roughly circular mass of white tonalite 40-50 m in diameter caps a hill in the pluton immediately southeast of the arroyo called El Alisito (area R-8), only 230 m from the southeastern contact of the SPT with a thick mass of calc-silicate rocks.

Gneissose, but otherwise similar, white hornblende tonalite and clinopyroxene tonalite form a discontinuous rind varying from 2 cm to slightly more than a meter thick around much of the margin of the northern half of the pluton (Figure 27). The rind is most consistently developed at contacts with marble and calc-silicate rock, but it also occurs against stretched-pebble wacke. In the latter occurrences, marble is generally exposed no more than 80 m from the tonalite, and lenses of calc-silicate rock occur in the wacke itself.

The gneissose white tonalite is similar in texture to the normal GBT and grades into the latter over distances of a few millimeters or centimeters. Contacts with the metamorphic rocks are sharp. Where the rind is thin and occurs against marble or calc-silicate rock, a systematic sequence of rock types is often developed across a zone 5-10 cm wide: typical GBT → gneissose white hornblende tonalite → pure epidote or epidote-rich calc-silicate layer, locally coarse-grained → pure garnet or garnet-rich calc-silicate layer, locally coarse-grained → marble or calc-silicate rock. In some places, either the garnet-rich or epidote-rich zone is thin or missing. Pink thulite locally occurs with or instead of epidote.

7.5.1 Evidence of Lime Contamination

In addition to the close spatial association with marble and calc-

silicate rocks, the mineralogical and textural characteristics of the white hornblende and clinopyroxene tonalites imply introduction of CaO during magmatic crystallization. Six representative samples were examined in thin section. The contaminated rocks differ from the uncontaminated tonalite in six major respects.

(1) Plagioclase appears milky white in hand specimen. However, in thin section, the plagioclase appears unaltered and, except in one sample to be discussed below, is indistinguishable in texture, composition, and zoning patterns from that in the uncontaminated tonalite. The cause of the milky appearance is undetermined.

(2) Biotite occurs at most in trace amounts and is invariably very fine-grained. In its place there is commonly 1-4% K-feldspar, but some of the white tonalite contains very little of any potassic phase.

(3) Clinopyroxene is commonly abundant and, in some cases, clearly rimmed and replaced hornblende. The presence in the unsheared rocks of strikingly euhedral clinopyroxene outlines, especially against quartz, and of repetitive thin euhedral zoning in some crystals indicates magmatic rather than metamorphic crystallization.

(4) Hornblende is generally paler green, less pleochroic, and slightly more birefringent than in the uncontaminated tonalite; these properties suggest a more actinolitic composition. Deep green hornblende, if present, occurs as rare small inclusions in plagioclase and, in one sample, as large relict crystals partially

rimmed and replaced by clinopyroxene and actinolitic amphibole.

(5) Actinolitic amphibole is an important constituent of some or all of the southern masses. Some may be deuteric, but euhedral overgrowths on hornblende and clinopyroxene in one sample apparently crystallized from the magma.

(6) Opaque minerals occur only in trace amounts as tiny inclusions in plagioclase, hornblende, or sphene. Sphene, on the other hand, is abundant (generally 1-3%), forming anhedral to euhedral crystals up to 1.5 mm in size. Many sphene crystals contain small anhedral patches of an orange-brown, high-relief mineral, probably rutile.

Lime contamination can account directly for the late magmatic crystallization of clinopyroxene and actinolitic amphibole and for the crystallization of sphene in place of opaque Fe-Ti oxides. Disappearance of biotite, however, may have been due less to introduction of CaO than to influx of CO_2 causing a decrease in f_{H_2O}. The persistence of hornblende in many of the contaminated rocks is reasonable because hornblende contains not only considerable CaO, but also less hydroxyl than does biotite. However, a sufficient decrease in f_{H_2O}, along with an increase in CaO activity, must also favor replacement of hornblende by the anhydrous, more calcic mineral clinopyroxene. Surprisingly, carbonate is just as rare in the contaminated tonalite as in the uncontaminated rocks. The contaminated rocks preserve no direct evidence of the hypothesized high CO_2 pressures.

Especially striking evidence of lime contamination prior to the completion of magmatic crystallization is provided by sample 777 from

one of the relatively large linear masses of white tonalite intruded into the pre-batholithic rocks at the southern tip of the pluton (area T-7). The rock consists of 70% plagioclase, 10% quartz, 9-10% very pale green clinopyroxene, 7% blue-green actinolitic amphibole, 1% green hornblende similar to that in the uncontaminated tonalite, 1-2% sphene, and 1% accessory and deuteric minerals including, in rough order of decreasing abundance, apatite, K-feldspar, zeolite (veins), rutile (?), epidote, clay minerals (?), chlorite, opaques, zircon, carbonate, and limonite or hematite. Clinopyroxene and actinolitic amphibole occur both as rims and patches replacing hornblende and as scattered crystals which are often strikingly euhedral, especially against quartz. These euhedral grains crystallized from the magma apparently before crystallization of much or all of the quartz. Some euhedral clinopyroxene crystals exhibit repetitive thin euhedral zoning. Opaques occur as rare tiny inclusions in plagioclase and hornblende or as tiny relicts occurring with rutile (?) in sphene.

Most of the plagioclase exhibits the same pattern of euhedral oscillatory and normal zoning as observed in typical SPT; interiors of An_{36-38}, in some cases with scattered patches and thin zones as calcic as An_{60}, zone down to rims of An_{20-25}. However, some grains have sharp, often discontinuous rims of mottled plagioclase consisting mostly of An_{28-32}, with patches of An_{20-25} (Figure 28). The inner contacts of these reversed rim zones with the adjacent sodic zones are sharp and slightly irregular in detail, but grossly euhedral; the rims are magmatic overgrowths which replaced the pre-existing plagioclase to only a slight degree. The outer margins of the overgrowths are frequently irregular,

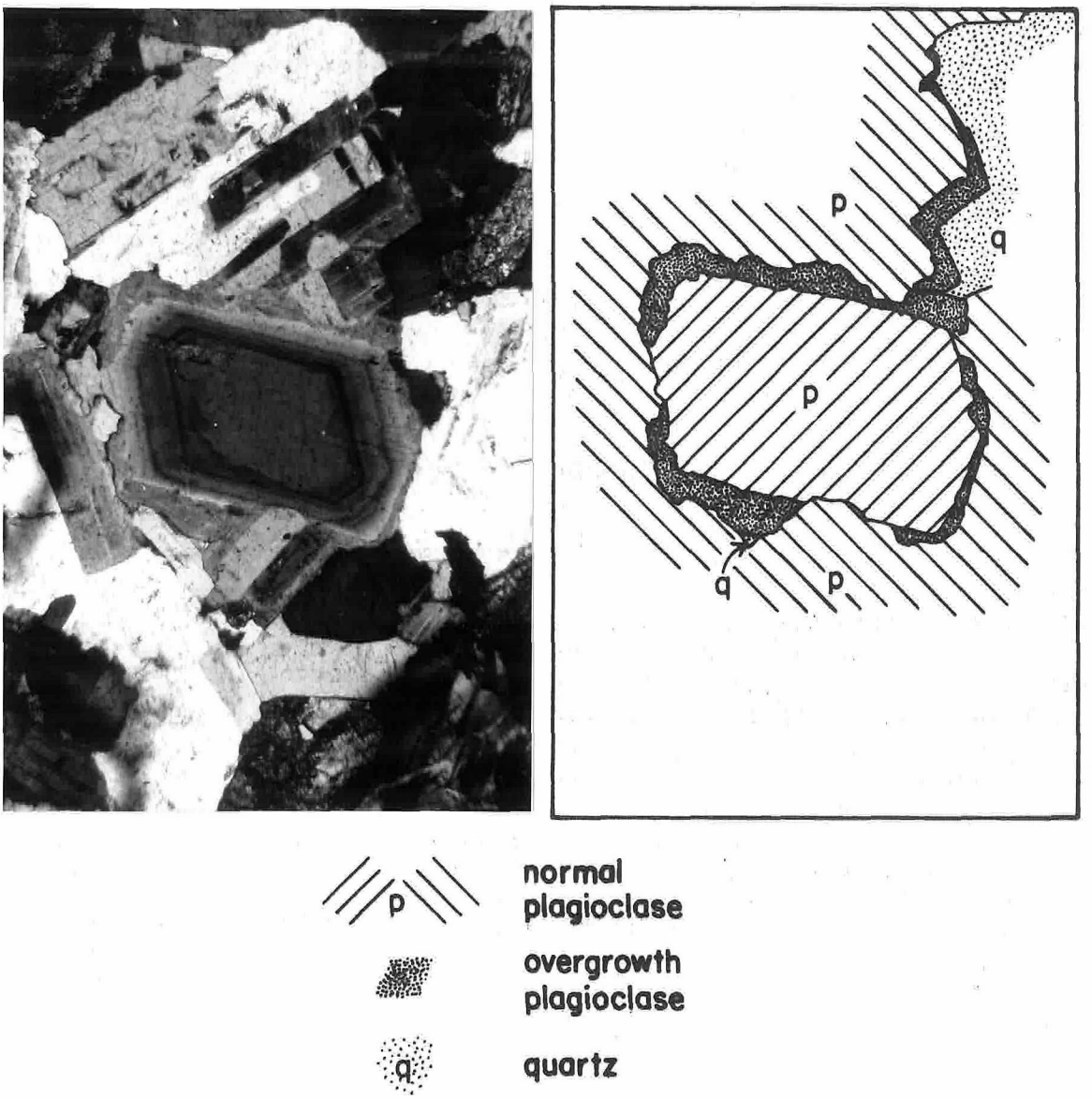

Figure 28. Lime-contaminated tonalite showing mantled plagioclase. The simplified drawing covers the same area as the photograph. An irregularly shaped, medium gray overgrowth surrounds nearly the entire margin of the central plagioclase crystal. An euhedral but otherwise similar overgrowth rims the plagioclase crystals in the upper right part of the photograph, where these crystals are bounded by interstitial quartz. The overgrowths consist of An ≈ 28-32, with tiny patches of An ≈ 20-25. The zones immediately inside the overgrowths are generally An ≈ 20-25. Note the strong euhedral zoning and the sharp, relatively smooth and uncorroded euhedral boundaries at the inner margins of the overgrowths. Sample Ba-JM-777 from the largest mass of lime-contaminated tonalite 200 m southwest of the southern tip of the pluton (area T-7).

and the width of the overgrowth around the margins of a given grain varies as a function of the interstitial space available during crystallization. The overgrowths are generally broadest, and the outer margins are typically euhedral, against interstitial quartz. Thus, the plagioclase overgrowths, like the euhedral pyroxene and actinolite amphibole crystals, crystallized prior to much or all of the quartz. Overgrowths make up as much as 25-35% of a few crystals, but overall they comprise 5% or less of the total plagioclase.

Complex aggregates of very fine-grained, anhedral actinolitic amphibole, clinopyroxene, sphene (?), minor K-feldspar, and occasional euhedral apatite crystals, all immersed in a matrix of quartz, comprise several percent of this sample and suggest the former existence of another mafic phase. Quartz generally makes up 40-60% of the aggregates, commonly as a single grain sharing optical continuity with adjacent interstitial areas of pure quartz. The size (0.5-2 mm) and elongate interstitial outlines of the aggregates suggest that the original mafic phase was biotite.

In summary, this rock preserves a clear record of an abrupt change in the stable magmatic mineral assemblage from hornblende + opaque + biotite (?) + plagioclase with composition of An_{20-25} to clinopyroxene + uralite + sphene + plagioclase with a composition of An_{28-32}. The change occurred after roughly 95% of the plagioclase, plus several percent hornblende and several percent of another mineral mafic (biotite?), had already crystallized, but before crystallization of much or all of the quartz. The magma appears to have been approximately 75-90% crystalline when exposed to the contaminating material.

7.6 Mafic-Layered Tonalite

An unusual mass of layered tonalite is exposed at locality 532 in the arroyo called El Alisito near the southwestern margin of the pluton (area Q,R-7). The layered rock appears to be an inclusion at least 6 m by 6 m in area, but only the northern contacts are exposed. The mass is characterized by curving, steeply dipping layers of biotite-hornblende melatonalite 1-15 cm wide, which alternate with and grade into layers 1-50 cm wide of typical biotite-hornblende tonalite (Figure 29). Except for the absence of conspicuously large plagioclase crystals, the light layers appear identical to the surrounding SPT. The dark layers are consistently finer-grained (0.5-2 mm) and contain typically 35%, but up to 50% mafic minerals, as compared with 15-20% in the light-colored layers.

Both the mafic and intervening layers show a weak planar mineral orientation parallel to layering and a moderate lineation plunging down-dip; preferred orientation is slightly more pronounced in the dark layers. Some contacts between layers are sharp, but most mafic layers grade in one or both directions into the light-colored tonalite by simultaneous decrease in mafic mineral content and increase in grain size. There is a statistical preference for sharp contacts on the eastern sides of mafic layers and gradation westward. Splitting of layers into two or three branches is common.

Deformation of two types has affected the layers. Figure 30 shows truncated mafic layers within the mass itself. The truncation did not disturb adjacent layers and clearly formed while the lighter layers were still mobile. Minor offset of layers also occurs. The second

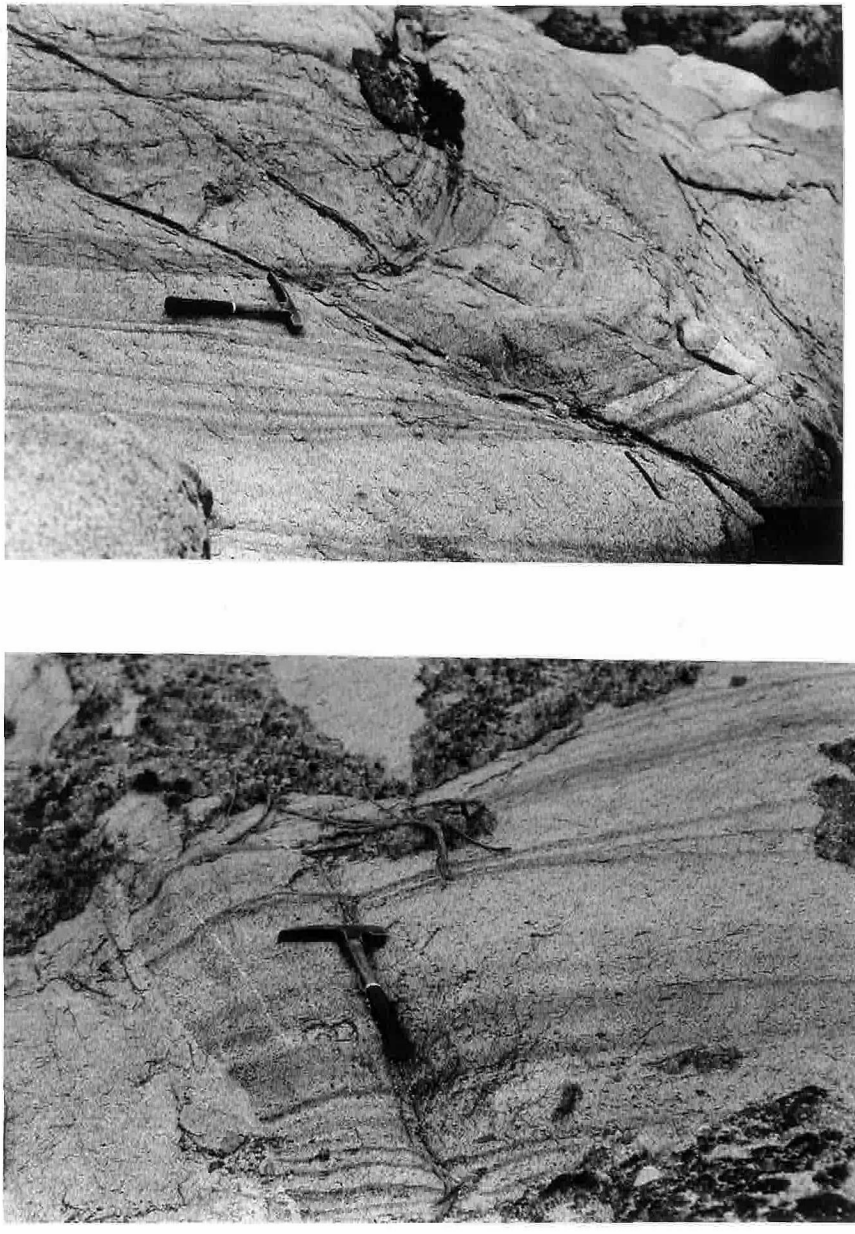

Figure 29. Mafic-layered tonalite in the southwestern part of the seriate porphyritic unit. Note the truncation and local bending of layers against the host tonalite. The layered rock appears to be an isolated block included in normal SPT. Locality 532 in the arroyo called El Alisito, 1.7 km south-southeast of Rancho El Molino (area Q,R-7).

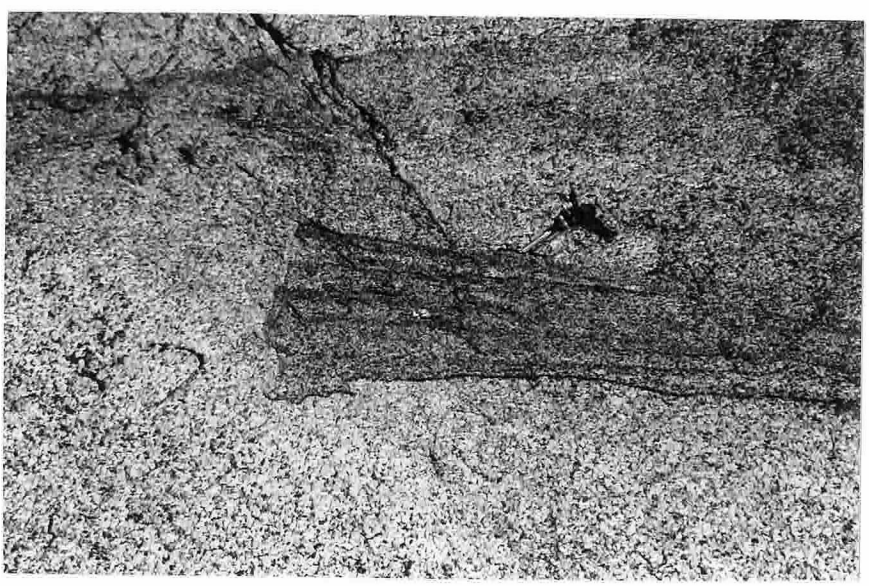

Figure 30. Truncated layers in the mafic-layered tonalite. Note that both the surrounding lighter tonalite and the mafic layer at the top of the photograph appear completely undisturbed. No offset equivalent of the truncated layers is exposed in the outcrop. Locality: same as in Figure 29.

type of deformation is strong bending of layers adjacent to the sheared contact with the host SPT (Figure 29). The bending was itself accomplished without visible shearing, so it also occurred while the layered rock was soft, presumably as a result of disruption and transport of the layered block from its site of formation. Along part of the northern contact, a dike of fine- to medium-grained SPT truncated, but did not deform, the layering, the host SPT, and the sheared contact of the layered block with the SPT.

Modes and average grain sizes (excluding deuteric phases) estimated from three thin sections of a relatively homogeneous, 5-cm-wide mafic layer and one thin section of the homogeneous interior of a 15-cm-wide light-colored layer in sharp contact with the mafic layer are compared in Table 3. Except for a greater biotite-hornblende ratio, the light-colored layer is indistinguishable from the typical SPT. Plagioclase in both layers exhibits normal and oscillatory zoning from average interiors of An_{35-40} to thin discontinuous rims of An_{20-25}. Partially altered calcic patches, cores, and thin zones of An_{50-60} are common, but volumetrically minor. These zoning characteristics are the same as those in typical SPT.

The principal modal difference between the mafic and lighter tonalite layers lies in the concentration of hornblende and opaques in the mafic layer and of plagioclase and quartz in the light-colored layer. Potash feldspar, sphene, chlorite, and possibly epidote are slightly depleted in the mafic layer, but biotite is of similar abundance in both layers. A few hornblende and biotite grains in the mafic layer reach about the same maximum size as in the lighter tonalite layer, but

Table 3

Comparison of Light and Dark Layers in the Mafic-Layered Tonalite

	Light-Colored Layer		Mafic Layer	
	Estimated Mode	Average Grain Size	Estimated Mode	Average Grain Size
Quartz	17	1-3 up to 5	11	0.3-1 up to 1.5
Plagioclase	65	2-4 up to 6	55	0.3-1 up to 1.5
K-feldspar	0.5	---	tr.	---
Hornblende	4	0.5-2 up to 3	17	0.3-1 up to 2.5
Biotite	11	1-3 up to 4	12	0.5-1 up to 3
Chlorite	0.5	---	<0.5	---
Opaques	1	0.2-0.6	3	0.2-0.6
Sphene	<0.5	---	<<0.5	---
Epidote	<<0.5	---	tr.	---
Apatite	<<0.5	0.5-0.2	<0.5	0.05-0.15
White Mica and Clay	0.5-1	---	0.5	---
Zircon	tr.	0.1-0.2	tr.	0.1-0.2
Zeolite (Chabazite?)	tr.	---	---	---

the average grain size of each of the major minerals is notably finer in the mafic layer. Thin sections were cut normal to both foliation and lineation; hence, grain orientations should be similar in all sections, and the grain-size comparison should be reliable.

Textures in both layers are hypidiomorphic-granular, but hornblende and plagioclase are more frequently subhedral or euhedral in the light-colored layer. Smoothly bounded interstitial textures are also well developed in the light-colored layer, just as in typical SPT, but are rare in the mafic layer. These smooth interstitial areas are occupied mainly by quartz and minor K-feldspar. In the mafic layer, most plagioclase, hornblende, and even quartz grains are subequant and frequently somewhat rounded, but there is no evidence of protoclasis or recrystallization. Much biotite in both layers is poikilitic or raggedly interstitial and grew late, partially at the expense of hornblende and plagioclase; this is especially true in the light-colored layer. Some biotite has been recrystallized into aggregates, particularly in the light-colored layer.

Much of the chlorite, sphene, zeolite, and white mica in both layers is clearly secondary. However, in the light-colored layer, each of these minerals, particularly chlorite and sphene, also occurs as small, smoothly bounded , interstitial grains and aggregates which appear to have filled available open spaces (probably vapor-phase microcavities) rather than to have replaced pre-existing minerals. Similar primary interstitial grains and aggregates are widely distributed, but volumetrically very minor, throughout the southern part of the pluton (see Section 12.10).

The more leucocratic composition, particularly the higher quartz and K-feldspar content, and greater development of euhedral textures and of smoothly interstitial chlorite, sphene, zeolite, and white mica imply concentration of residual, volatile-rich melt in the light-colored layers compared to the mafic layers.

7.6.1 Origin of the Mafic-Layered Tonalite

The mafic-layered rock appears to be a large block included in the SPT and formed initially in a different environment elsewhere in the pluton. Similar structures were not seen anywhere else in the pluton, nor does the SPT in this vicinity exhibit more than the faintest flow structure of any sort. The layering is very similar to that described by Wilshire (1969) in the Twin Lakes granodiorite in Colorado and by Wilson (1961) in the Alta stock in Utah. It is also similar to the type la-lb layering described by Smith (1975) in the granitic rocks in southwestern Nova Scotia. However, each of those occurrences is in granodiorite. The layered masses in the Alta stock are definitely inclusions, whereas those in both the Twin Lakes and Nova Scotia occurrences reportedly formed *in situ*, in the first case along steep margins of the body, and in the second case apparently near the roof of the pluton.

Two principal mechanisms can be proposed for the origin of this type of layering: gravitational accumulation (invoked by Wilson) and grain-size-dependent sorting of crystals in a flowing magma (invoked by Wilshire and by Smith).

Several observations conflict with the hypothesis of gravitational accumulation. First, although there is a slight preference for layers

to grade from finer-grained and mafic on the east to coarser and more leucocratic on the west, numerous layers grade in the opposite direction or in both directions. Secondly, as emphasized by Wilshire for the Twin Lakes layering, the observed grain-size grading and mineral-density grading are in opposite directions. That is, if the mafic layers represent the bottoms of density-graded beds, the grain-size dependence on settling rates should have led to concentration of the coarsest mafic grains at the sharp base of each mafic layer, but, in fact, the finest mafic grains are invariably concentrated there, and the coarsest grains are in the light-colored layers. Alternatively, if the light-colored layers are the coarser-grained bottoms of gravity-accumulated, grain-size-graded beds, the density dependence of settling rates should have caused the coarsest mafic crystals to accumulate preferentially towards the sharp bottom of each light-colored layer, but, in fact, the coarsest mafic grains are uniformly distributed through the light-colored layers. Furthermore, opaques, which are of similar size in both the mafic and light-colored layers, are concentrated in the mafic layers; this observation seems totally incompatible with interpretation of the mafic layers as the tops of gravity-accumulated beds.

Thus, whichever side of a mafic→leucocratic graded sequence one interprets as the base, the details of the modal and grain-sized grading conflict and argue strongly against gravitational accumulation.

A third set of considerations seems inconsistent with a gravity-settling model. Preservation of layering during disruption and transport of the block from its site of origin indicates that the layered rock was more solid and coherent than the host magma and must therefore

have had a slightly greater density. Considering its size, the block was more likely sinking from a higher initial position rather than being rafted upward from a deeper level, where gravity accumulation would be most probable. This conclusion, which would seem to apply equally well to the mafic-layered inclusions described by Wilson (1961) in the Alta stock, is consistent with the *in-situ* layering described by Wilshire (1969) and by Smith (1975) near and parallel to the steep walls and the roof of their respective plutons.

Bhattacharji and Smith (1964) and Bhattacharji (1967) have shown experimentally that particles in a flowing suspension tend to migrate away from the walls of the conduit -- i.e., away from regions of high shear stress. Under at least some conditions, the rate of migration is directly proportional to particle size for similar particle shapes (Bhattacharji and Smith, 1964; Komar, 1972a, 1972b). By analogy with these experiments, both Wilshire and Smith proposed that the mineral layering in their respective plutons formed by grain-size-dependent sorting of crystals in response to shear flow of crystal mush. Specifically, they concluded that mafic layers formed by concentration of finer crystals in zones of high relative shear stress as a result of migration of coarser crystals towards zones of lower shear stress. Although this hypothesis is not free of defects, as acknowledged by Wilshire (1969, p. 258), it also seems to best account for the characteristics of the mafic-layered block in the San José pluton.

7.7 Inclusions

Inclusions ranging in maximum dimension from 1 cm up to several

meters, but averaging 10-30 cm, comprise 1% or less of most outcrops. By far the majority consist of fine- to medium-grained hornblende-plagioclase rock of dioritic composition. These inclusions correspond in petrographic character to the "autoliths" of Pabst (1928), but whether they are cognate or foreign inclusions is open to question.

Identifiable xenoliths of pre-batholithic rocks -- generally calc-silicate rock or thin-bedded tuffaceous mudstone -- are next in abundance, but very minor volumetrically. Inclusions of gabbro and tonalite are very rare.

Where the tonalite shows a recognizable planar mineral orientation, inclusions are consistently oriented with their long axes within the foliation plane. In the weakly foliated interior and southern parts of the pluton, dioritic inclusions are only slightly elongate ($\leq$2:1) and smoothly ellipsoidal; a few are angular or subangular. As the intensity of planar mineral orientation increases in the tonalite, dioritic inclusions become increasingly flattened. Those in the GBT and in some outcrops along the northern margin of the PHbT have been greatly flattened into discs for which the axial ratios in cross-sections perpendicular to foliation are between 4:1 and 15:1 or even 20:1. Cross-sections in the plane of foliation vary from circular to elongate as much as 5:1 parallel to other elements of lineation.

The distribution of inclusions is fairly uniform throughout most of the pluton, but dioritic inclusions and, to a lesser extent, identifiable xenoliths of pre-batholithic rock are notably concentrated near the pluton margins. Inclusions comprise typically several percent, rarely even 25% of more, of the GBT, but the abundance drops off to ~1%

in most outcrops 100 m or more from the margins.

Inclusions are even more notably concentrated along the northeastern and eastern margins of the PHbT, beginning about 1.8 km east of the North-South road and continuing southeastward to the southern end of the screen of diorite and inclusion-rich tonalite separating the SHbT and PHbT (Plate 2). In those areas, the abundance of dioritic inclusions in the outer 100-150 m of the PHbT increases progressively towards the margins of the unit, so that the tonalite grades into the screen of diorite and inclusion-rich tonalite. Local swarms of dioritic inclusions comprising 10-20% of an outcrop are also scattered through this part of the PHbT as much as 500 m from the margins. In contrast, there is generally little or no concentration of dioritic inclusions near the inner margin of the SHbT.

Xenoliths of pre-batholithic rock are concentrated with the dioritic inclusions, but to a much lesser degree (<<1%), along the eastern and northeastern margins of the PHbT and in the screens of diorite and inclusion-rich tonalite. Fragments of calc-silicate rock and of fine-grained, black schistose amphibolite, both generally <20 cm in maximum dimension, are most common, but blocks up to several meters in size of thin-bedded mudstone or calc-silicate rock also occur. A few inclusions of country rock also occur in the inner 200 m of the SHbT locally in the northeast. Fragments of calc-silicate rock and schistose amphibolite are again slightly concentrated (<1%) in the outer few meters of the PHbT in the northwest, but there is no visible concentration of either dioritic or pre-batholithic inclusions along the western part of the SHbT-PHbT contact zone south of Arroyo de las Parritas.

Inclusions up to several meters in size of calc-silicate rock and metamorphosed thin-bedded mudstone and tuff, identical to the strata which are wrapped around the entire northern and eastern margins of the pluton, are distributed sparsely throughout the interior of the PHbT. In contrast, identifiable xenoliths of pre-batholithic rock are rare in the SHbT and SPT, except near contacts.

The distribution of wall-rock xenoliths implies that the PHbT at one time had extensive contacts with the pre-batholithic strata north and east of the pluton. This conclusion is one of several lines of evidence, presented in the discussion of the SHbT-PHbT contact zone, that the SHbT is slightly younger than the PHbT and was emplaced around the perimeter of the latter. According to this interpretation, the zones of diorite and inclusion-rich tonalite associated with the SHbT-PHbT contact zone and the mafic sheets and other mafic rocks along the eastern margin of the pluton were originally part of a single heterogeneous complex of gabbro, diorite, hybridized tonalite, and metamorphic rocks around the margins of the original PHbT pluton.

The mineralogy of the dioritic inclusions is generally the same as that of the host rock, but the modal abundances and textures are different. Typical modal ranges are: 50-70% plagioclase; 20-40% hornblende; 1-4% biotite; generally <1%, but up to 15-20% quartz; 1-4% opaques; and 1-2% others. Potash feldspar is always a trace constituent. There is a complete range from wholly granoblastic, recrystallized textures to practically unmodified, igneous-appearing, hypidiomorphic-granular textures, with intermediate textures common. Granoblastic inclusions are fine-grained (0.1-0.5 mm), whereas inclusions with hypi-

diomorphic-granular texture generally have an average grain size of 0.5-2 mm and sometimes contain abundant subhedral to euhedral megacrysts of hornblende and plagioclase 2-5 mm, locally up to 10 mm, in size.

Hornblende and biotite in the dioritic inclusions are consistently similar in optical properties to their counterparts in the host rock. In contrast, plagioclase is quite variable. In inclusions dominated by granoblastic texture, plagioclase is unzoned or weakly zoned andesine (An_{35-40}). Twinning in these grains is simple and mainly on the albite law; oscillatory zoning is very rare. In inclusions dominated by hypidiomorphic-granular texture, the fine-grained plagioclase is mostly anhedral, weakly zoned andesine (An_{35-45}) derived at least in part by recrystallization or fragmentation of larger zoned crystals. The latter are subhedral and show complex twinning and zoning characteristics similar to those in the host tonalite. Combined albite-Carlsbad and albite-pericline sets are well developed. The zoning commonly consists of oscillatory or mottled cores and normal-zoned rims. The oscillatory-zoned crystals typically range from An_{35-45} in the interiors to An_{22-25} in rims, but many contain thin calcic zones (generally An_{60-70}) usually located in the intermediate parts rather than the centers of the crystals. The mottled crystals show the same range of zoning, but the calcic zones have been partially replaced by andesine and occur as diffuse patches and discontinuous zones in the andesine.

Pabst (1928, p. 358) noted a frequent correlation between the distinctive characteristics of mafic autoliths and those of the enclosing granitic rock in many parts of the Sierra Nevada batholith. Analogous

correlations exist in the San José pluton. For example, inclusions containing euhedral plagioclase megacrysts 5-10 mm in size occur mainly in the SPT. The megacrysts exhibit complex oscillatory zoning similar in pattern and compositional range to that of the plagioclase phenocrysts in the host tonalite. Inclusions in the SHbT are characterized by anhedral hornblende which is molded around and poikilitically encloses plagioclase grains, whereas inclusions in the other two units are characterized by non-poikilitic subhedral prisms or granoblastic grains of hornblende. Where coarse (5-10 mm) poikilitic books of biotite are conspicuous in the western and southwestern part of the PHbT, similar books occur in and rarely bordering some of the mafic inclusions. These crystals replaced plagioclase extensively and hornblende to a lesser degree; they appear to be poikiloblasts which grew in response to permeation of the inclusions and host rock by late residual melt or hydrothermal fluids. Perhaps some or all of the plagioclase and hornblende megacrysts grew in a similar manner, but direct textural evidence for this is lacking, and the complex oscillatory zoning in the plagioclase is difficult to envisage as a product of metasomatic growth. I interpret them, therefore, as relict phenocrysts.

Numerous workers (e.g., Piwinskii, 1968a, 1968b; White and Chappell, 1977) have suggested that most mafic inclusions may be masses of unmelted residuum carried up from a region of partial melting where the host magma was generated. If so, petrographic evidence of derivation from much greater depths has been destroyed. On the other hand, the mafic screens associated with the SHbT-PHbT contact zone, the mafic intrusive complexes around Cañon La Jolla and Willow Creek Canyon,

and possibly other mafic masses at deeper levels, provide a more immediate and very reasonable source for dioritic inclusions. A few unusual dioritic inclusions, themselves containing even darker, sharply bounded dioritic inclusions, can be readily explained as fragments of inclusion-bearing diorite or hybridized tonalite incorporated into the tonalite magma. Inclusion of hybridized variants of the tonalite can also account for the frequent correlation of distinctive characteristics between inclusions and host rock -- particularly, the occurrence of oscillatory-zoned plagioclase megacrysts mainly in inclusions in the SPT. However, some mafic inclusions were clearly formed by disruption of "synplutonic" mafic dikes intruded into the incompletely crystallized tonalite magma, as, for example, the inclusions of "malchite" dike rock in the SPT along the arroyo called El Alisito (see p. 156). The volumetric importance of synplutonic dikes as a source for mafic inclusions is unknown. It is also possible that many mafic inclusions, especially those with granoblastic or megacrystic textures, are reconstituted fragments of sedimentary or volcanic country rocks. However, the occurrence of totally unreacted blocks of metamorphosed mudstone and tuff even in the center of the PHbT several kilometers from any apparent source and the rarity of identifiable metamorphic-rock inclusions in varying stages of conversion to typical dioritic inclusions make incorporation and assimilation of meta-sedimentary or meta-volcanic rocks seem an unlikely explanation for most of the inclusions.

Chapter 8

POST-BATHOLITHIC DEPOSITS

8.1 Lithologies and Distribution

The only known post-batholithic deposits within or immediately around the San José pluton consist of at least two generations of alluvium, both of which were recognized by Woodford and Harriss (1938) and by Birkbahn (1969). Recent alluvium (al_1) flooring present drainage channels consists almost entirely of locally derived material: grus and occasional cobbles of tonalite within the pluton, metamorphic rocks plus minor granitic material in the country rocks. Country-rock contribution to Recent alluvium within the pluton is appreciable only near contacts. In contrast, readily distinguishable remnants of older alluvium (al_2) widely scattered around the margins and throughout the interior of the pluton consist, regardless of where they occur, of reddish-brown, poorly sorted gravels derived from the country rocks, with relatively little contribution from the tonalite. The age of this older alluvium is uncertain; nor is it all necessarily of one age.

Over wide areas west and especially northwest of the San José area, the hills are capped by poorly sorted, unconsolidated, round-cobble gravels whose age is determined only as post-batholithic. These round-cobble gravels do not appear to extend into the area mapped in this study. However, a large poorly sorted gravel deposit mapped as "al_2" covers a smooth broad hilltop along the San José-San Telmo road at the western edge of the map area (Plate 2). The cobbles in this deposit are predominately subangular to subrounded, but the erosion surface on which

they lie may well be correlative with that on which the round-cobble gravels were deposited. Whether these deposits are of the same age or older than any of the reddish alluvium within the pluton is undetermined.

The older deposits within and at the margins of the pluton have three modes of occurrence.

(1) Small isolated hills and thin veneers of reddish alluvium up to 10 m thick are scattered at numerous places along the sides of Arroyo San José, Willow Creek Canyon, and the arroyo called El Alisito, all at elevations of 20 m or less above the present channel floors. They consist of angular to subrounded pebbles and cobbles of metamorphic rocks and rare tonalite in a matrix of reddish-brown silt and clay, with minor tonalite grus.

(2) Ribbons and sheets of reddish colluvium up to several meters thick locally mantle hillsides around the margins of the pluton, commonly concealing the pluton contact. Such mantles, which are presently being stripped away, are most widespread around the margins of the SPT, but remnants of similar deposits, many too thin and discontinuous to map, occur sporadically elsewhere around the pluton contacts. The colluvium is composed of reddish soil and angular rock fragments derived from the country rocks higher up on the hillsides. Lithologic similarity and close spatial association of the colluvium to the scattered patches of reddish alluvium in Willow Creek and El Alisito canyons leaves little doubt that the patches in the valleys, including those scattered along Arroyo San José in the center of the pluton, were formerly continuous with and fed by more extensive colluvial mantles.

(3) A long narrow strip of reddish alluvium occupies the axis of a broad shallow east-west depression east of Rancho El Coyote. This deposit, which I will call the Coyote gravels, appears to be the remnant of an abandoned stream bed. The alluvium consists of subangular to subrounded pebbles and cobbles, up to 50 cm across, of metamorphic rocks and sparse aplo-pegmatite in a matrix of reddish-brown silt and clay. The deposit varies from 15 m to 170 m wide and extends continuously over a distance of 2.4 km. Scattered deposits west and northwest of Rancho El Coyote, including patches too thin to map along the Buena Vista-Coyote road 800-900 m northwest of the ranch, indicate that the stream continued westward along the present path of the road for nearly 1 km from the ranch, then probably swung northward to join Arroyo El Tepetate near the pluton contact.

At their eastern limit, the Coyote gravels are abruptly truncated by Arroyo Cerro Costilla, leaving the old stream bed perched nearly 100 m above the rapidly eroding canyon floor only 100 m to the east and roughly 200 m above the alluviated and graded floor of the same arroyo less than 2 km to the southeast. The thickness of gravels is about 15 m at the eastern end of the deposit (Birkbahn, 1969) and probably 7-8 m in the isolated patch 200 m west of Rancho El Coyote, but it appears to be much less in some of the intervening areas.

Post-depositional erosion has resulted in a slight inversion of topography along much of the length of the Coyote gravel deposit, with the upper surface of the gravels standing as much as 10 m above the adjacent land. However, east of the North-South road, that surface

itself is, for the most part, relatively smooth and graded, with little evidence of dissection. Elevations measured on this surface with a Paulin altimeter are 958 m at the eastern end and 923 m at a point about 170 m east of the North-South road, giving a gradient of approximately 19 m/km downslope to the west[5].

8.2 Preliminary Observations on the Erosional History of the San José Area

The abandoned Coyote stream bed crosses an old erosion surface, called the Peterson surface by Woodford and Harriss (1938), which is preserved over wide areas in the western and northern part of the pluton (Plate 7 and Figure 4, p. 40; note that the contour interval on Plate 7 and on the AMS 1:250,000 map sheets is too large to show the low-relief surface satisfactorily). The surface "is characterized by broad, open valleys (and terraces) above which rise rather smooth hills and ridges" (Woodford and Harriss, p. 1328). The average elevation of the surface decreases gradually from about 1000 m in the northeastern part of the pluton to slightly below 800 m along the western margin of the pluton less than 9 km to the southwest. Isolated remnants of this surface occur along the southeastern side of the pluton between Cañon Socorro and Willow Creek Canyon (1000-1100 m elevation) and between Willow Creek

---

[5] Uncertainty in the absolute elevations is estimated at ±10 m. However, because measurements were made only 40 minutes apart to a precision of ±0.3 m, and corrections were made for atmospheric changes by measuring the elevation at the intersection of the North-South and Buena Vista-Coyote roads before and after measuring the gravel surface, uncertainty in the relative elevations is believed to be no greater than ±4 m, corresponding to an uncertainty of ±4 m/km in the gradient.

Canyon and the arroyo called El Alisito (800-900 m; right side of lower panorama in Figure 4).

Birkbahn (1969) observed that the Peterson surface appears to be developed on the tonalite, giving way at the pluton contacts to generally higher and more rugged terrane in the country rocks. However, Woodford and Harriss (p. 1328) noted that the surface appears to be present at a level "200 to 300 feet higher in the metamorphic rocks at the southern end of San José basin". Possibly the gravel-capped surfaces west and northwest of the San José area are also correlative with the Peterson surface.

Arroyo San José and its major tributaries have eroded deeply into the Peterson surface. From south to north, Willow Creek Canyon, Cañon Socorro, Cañon La Jolla and Cañon Campo Buena Vista all drop abruptly 100 m or more upon entering the pluton from the east, producing steep rock cascades and dry waterfalls. In contrast, Arroyo Cerro Costilla maintains a relatively constant low gradient across the pluton contact and south to Las Encinas Corral, but over the next 1.5 km, the canyon swings sharply to the southeast and drops nearly 200 m to reach the flat alluviated valley floor northwest of the intersection with Cañon Campo Buena Vista and Arroyo San José. The elevation at Las Encinas Corral, where a few large cobbles of metamorphic rock mark the remnant of a thin gravel deposit, is approximately the same as that of the truncated eastern end of the Coyote gravel surface, suggesting that the Coyote gravels were deposited by an ancestral Arroyo Cerro Costilla which drained westward into Arroyo El Tepetate and Cañon San Jorge. Headward erosion by the deep southeast-draining tributary to Arroyo San José

diverted the Cerro Costilla drainage into the Arroyo San José system. Capture occurred recently enough so that the present bed of Arroyo Cerro Costilla upstream from Las Encinas Corral is incised only 5 m or less into the apparent pre-capture surface, yet long enough in the past to permit rejuvenated erosion downstream from the corral to leave the Coyote gravels perched nearly 100 m above the adjacent canyon floor.

The small isolated hills and veneers of reddish alluvium scattered along the sides of the major arroyos, and the partially dissected patches of reddish colluvium locally mantling hillsides around the pluton margins appear to be remnants of a once-continuous sheet of country-rock debris which covered the floors of the arroyos and blanketed parts of the intervening higher country as well. As recognized by Woodford and Harriss (1938), pebbles and cobbles of metamorphic rock are sparsely scattered over much of the Peterson surface, suggesting that that surface was also partially blanketed by reddish alluvium.

Development of the Peterson surface required a long episode of slow erosion and tectonic stability. A major episode of stream rejuvenation recognized by Woodford and Harriss and by Birkbahn (1969) led to deep dissection of this surface by Arroyo San José and its tributaries. Deposition of some of the reddish alluvium on the Peterson surface may have preceded this rejuvenation; however, deposition of the reddish alluvium preserved along the sides of the major arroyos and of at least some of the colluvium mantling the Peterson surface and the hillsides around the margins of the pluton marks a second episode of reduced erosion which followed the first rejuvenation and the nearly complete development of the present topography. A second

episode of stream rejuvenation, which is apparently still active, swept away most of the reddish alluvium. The latter episode undoubtedly contributed to further erosion of the major arroyos into the Peterson surface, and may have been the episode responsible for capture of the ancestral westward-draining Arroyo Cerro Costilla by the Arroyo San José drainage system; however, along most of the length of the major arroyos within the bounds of the pluton, this second rejuvenation has led to no more than 10-20 m of erosion beneath the surface on which the scattered hills of reddish alluvium were deposited.

The San José area has thus experienced a complex post-batholithic erosional history which has not been adequately studied. A detailed geomorphological study of the area, especially of the age of the Peterson surface and its relationships to both the gravel-capped surfaces west and northwest of San José and the erosion surface on top of the Sierra San Pedro Mártir, might provide considerable information on the post-batholithic history of uplift and erosion of this part of the peninsula.

Chapter 9

STRUCTURES IN THE PLUTON

9.1 Flow Structures

Preferred planar orientation of inclusions, schlieren, and minerals, especially hornblende and biotite, defines a foliation which varies from gneissose around the margins of the northern two thirds of the pluton to weak or absent in the interior and especially the southern part of the pluton. Preferred linear orientation of minerals and inclusions is less consistently developed, but locally it is pronounced. Foliation and lineation patterns are shown on Plates 3 and 4, respectively.

9.1.1 Use of the Terms Protoclasis and Protoclastic

In his professional paper on cataclastic rocks, Higgins (1971, p. 13) stated that "it (protoclasis) applies to cataclasis of an igneous body, or parts of an igneous body, due to late intrusive movements of, or within, that body, generally before it has completely crystallized. The products of protoclasis are called protoclastic rocks, and may be indistinguishable texturally from other cataclastic rocks, except for their intimate association with, or localization within, the parent igneous body." In the case of the San José pluton, several lines of evidence indicate that the deformations recorded by the foliations, lineations, and crushed or recrystallized textures began during magmatic flow and may have continued after emplacement and solidification of much of the northern two thirds of the pluton. Thus, the cataclasis may not have been exclusively protoclastic; that is, it may not have occurred entirely

while some melt remained in the deforming tonalite. However, because nearly all of the cataclasis (1) occurred along the same directions as those defined by magmatic mineral orientations, (2) was accompanied by extensive recrystallization of the granulated material, and (3) appears to have been an integral part of the emplacement and cooling history of the pluton, it may be impossible to fully distinguish the separate effects and relative importance of magmatic versus high-temperature solid-state deformation in the more strongly foliated and lineated rocks. Therefore, the terms protoclasis and protoclastic will be applied to all of the cataclasis and all of the cataclastic textures and structures, respectively, produced while the tonalite was still partially molten or at least hot enough to permit extensive recrystallization of the granulated material. Evidence of appreciable low-temperature cataclasis has not been recognized.

I have one objection to the definition by Higgins. Protoclasis, even in its strict magmatic definition, is not necessarily due entirely to "intrusive movements of, or within" a pluton. If a pluton is emplaced during regional deformation, that superimposed deformation may cause protoclasis even after intrusion has ceased. Distinction between intrusive and superimposed sources of protoclasis may be extremely difficult, but it is also extremely important in understanding not only the origin of the flow structures and protoclastic textures themselves, but also the emplacement and crystallization history of the pluton and the deformational history of the country rocks.

9.1.2 Foliation Patterns in the Pluton

The foliation patterns have eight principal characteristics summarized below.

(1) Foliation is gneissose and protoclastic around the northern two-thirds of the pluton and decreases to weak in the interior. Foliation is weak or absent throughout most of the southern third of the pluton, and only locally is there a noticeable increase towards the pluton contact.

(2) With a few local exceptions, foliation around the margins of the northern two-thirds of the pluton is conformable to the contact and to bedding and foliation in the adjacent wall rocks. Around most of the southern part of the pluton, foliation, if recognizable, is roughly parallel to the eastern contact, but is at best only crudely conformable to the western margin.

(3) Foliation intensity increases towards the SHbT-PHbT contact zone. Foliation is generally parallel to that contact, but locally it crosses the contact at a low angle.

(4) Neither the pattern nor the intensity of foliation shows any relationship to the gradational contact zone between the PHbT and SPT.

(5) Foliation attitudes and intensity are generally uniform over distances of tens of meters, but some outcrops exhibit local complexities such as truncating sets of foliation, swirling, narrow zones of more intense foliation, or complex shear or mylonitized zones.

(6) Foliation is expressed in part by generally sparse schlieren composed of the same minerals as the host rock, but containing

notably higher or lower concentrations of mafic minerals. Leucocratic schlieren predominate in the SHbT, and mafic schlieren in the PHbT; neither type is common in the SPT. Some leucocratic schlieren are discordant and have been folded, generally along planes parallel to foliation.

(7) Foliation attitudes change in a regular pattern suggestive of an asymmetric, funnel-shaped pattern of flow, elongate north-south and crudely centered around the west-central part of the SPT.

(8) Foliation (and locally lineation) is developed not only in the tonalite, but also in dikes and veins which are intruded into the marginal parts of the SHbT and PHbT.

(1) Variations in Foliation Intensity.

Around the margins of the northern two thirds of the pluton -- i.e., around the outer margins of the SHbT -- the tonalite is a flaser gneiss (Figure 14, A,B, pp. 108 and 109, and Figure 31). Segregation of mafic and leucocratic minerals into crude lenticular layers 1-3 mm thick and several centimeters long has produced a pronounced fissility. Biotite has been completely recrystallized into platy aggregates of fine- to medium-grained crystals which impart a spotty or streaked appearance to foliation surfaces. Mafic inclusions have been flattened into smooth ellipsoids with axial ratios frequently as extreme as 15 or 20:1. Concordant joints (joints parallel to foliation) are commonly spaced 0.5-1 m apart; they combine with the gneissosity to produce markedly slab-shaped, block-rich outcrops. The width of the

gneissose zone is greatest around the northern and northeastern margins of the pluton and decreases gradually southward as shown schematically on Plate 2.

The gneissose foliation is remarkably regular both in orientation and intensity. With rare local exceptions, the gneissosity is neither contorted nor generally variable in intensity, except gradually over tens of meters. Mylonitic zones or zones of stronger foliation indicative of discrete planes or zones of failure are rare. The GBT was clearly homogeneous in its resistance to shearing and flow and remained so as deformation proceeded.

Thin-section examination of the GBT reveals partially recrystallized protomylonitic textures (Figure 31). Biotite occurs as platy aggregates of crystals which are less uniformly oriented than the aggregates themselves and appear randomly oriented in some cases. In many rocks, the biotite crystals are predominantly anhedral or subhedral and commonly deformed, but, in other rocks, most crystals are subhedral or euhedral and undeformed (Figure 32). Some recrystallization of biotite clearly continued after deformation had largely or entirely ceased.

Most plagioclase and hornblende grains are rounded and abraded, and some are bent or broken. However, the frequent preservation of euhedral oscillatory zoning and, in some cases, of subhedral to nearly euhedral tabular crystal shapes (Figure 31), and the rarity of aggregates of plagioclase replacing original magmatic crystals all show that crushing and recrystallization were restricted largely to the margins of the plagioclase. Hornblende has been more extensively

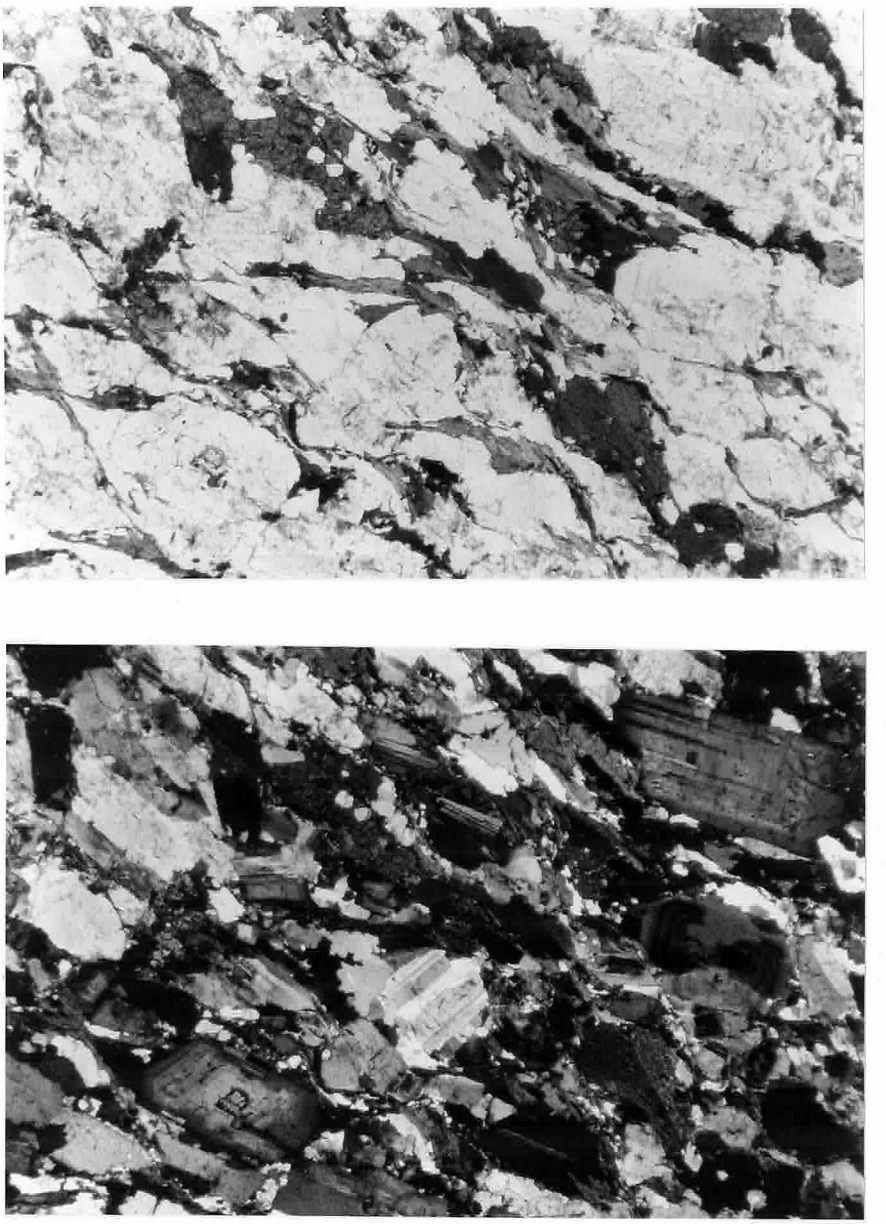

Figure 31. Photomicrographs of the gneissose border phase of the stubby hornblende tonalite. Upper photo, plane light; lower, same area in crossed nicols. Intense protoclasis produced the ovoid abraded outlines of many plagioclase and hornblende crystals and the wavy interstitial stringers of recrystallized biotite and granulated quartz and feldspar. Despite the deformation, some plagioclase crystals retain euhedral magmatic zoning and/or subhedral to nearly euhedral outlines. Sample Ba-JM-27a, 15 m from the northeastern margin of the pluton along the Concepción road, ~40 m east of Rancho Cerro Costilla (Plate 2, area C-9).

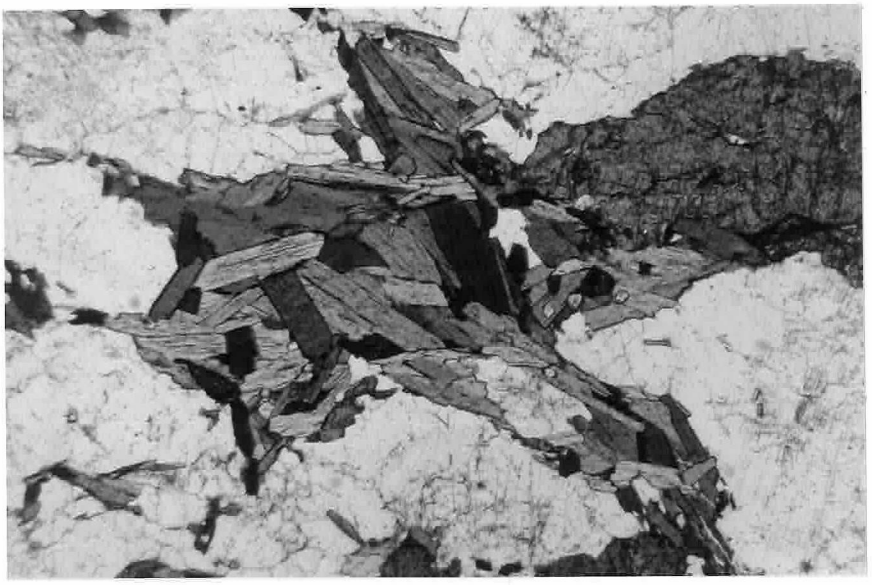

Figure 32. Aggregate of undeformed, variably-oriented, subhedral and euhedral biotite crystals in the gneissose border tonalite. The aggregate is the product of recrystallization, which apparently continued after cessation of deformation. Sample Ba-JM-807, ~30 m from the eastern margin of the pluton, ~900 m south of Cañon Campo Buena Vista (Plate 2, area H-13).

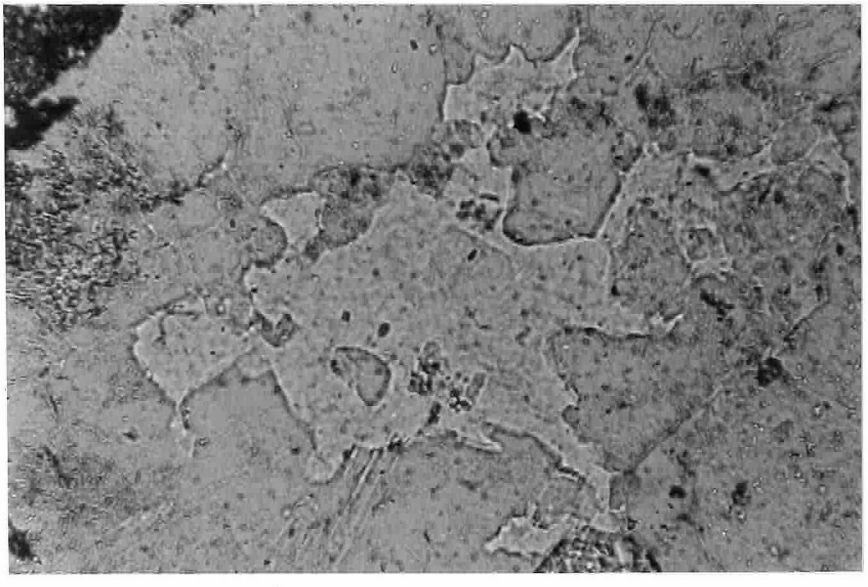

Figure 33. Interstitial branching K-feldspar (bright areas) in the gneissose border tonalite. The photograph was taken under reduced lighting and poor focus in order to accentuate the appearance of relief. The irregular unbroken branches projecting from the central grain suggest crystallization after cessation of intense deformation. Sample Ba-JM-568a, 45 m from the northwestern margin of the pluton in Arroyo de las Parritas (Plate 2, area F-3).

crushed and fractured than plagioclase; the molded or interstitial shapes characteristic of the margins of large hornblende grains in the SHbT are absent in the GBT, where grain boundaries are rounded or ragged. However, hornblende has not been as extensively recrystallized as biotite. Quartz is interstitial and frequently occurs in thin lenses parallel to foliation. It exhibits moderate to strong undulatory extinction and is commonly polygranular, but it is not extensively granulated.

The GBT typically exhibits a continuous range from the average 1-3 mm grain size down to the finest interstitial material averaging 0.02-0.1 mm. The latter, comprising at most 5-10% of the rock, contains all of the major minerals, but has consistently a high biotite/hornblende ratio and commonly contains an unusually high proportion of sphene. The 1-3% of K-feldspar and associated myrmekite in the GBT around the western half of the SHbT are restricted almost entirely to the finer-grained crushed and recrystallized areas.

Textures in the finer-grained material range from irregularly interlocking to granoblastic, with the exception of biotite and accessory minerals, which may be subhedral or euhedral. Some fine-grained plagioclase shows deformed twin lamellae, but recrystallization has destroyed most strain features. In particular, K-feldspar forms interstitial patches averaging 0.1-0.5 mm in size, many of which are poikilitic and send off thin branches and networks into the surrounding material (Figure 33). These patches commonly consist of several extinction domains, but they show little other evidence of deformation; they apparently crystallized after most of the deformation.

Deformation clearly occurred while the GBT was sufficiently hot to allow recrystallization of the granulated material and growth of interstitial K-feldspar. Although it is uncertain whether some residual melt -- or only deuteric fluids -- remained in the GBT throughout the entire period of deformation, the development of the gneissosity and of the crushed and recrystallized textures appears to have been an integral part of the emplacement history of the pluton.

The intensity of foliation decreases progressively from the GBT inward into the interior of the SHbT, but at least a weak orientation of minerals, inclusions, and sparse schlieren is visible throughout the unit. In the least foliated SHbT outcrops, inclusions are commonly flattened 2 or 3:1 in the plane of foliation.

In thin section, foliation is seen to be more pronounced in the SHbT than is apparent megascopically. Tabular plagioclase crystals show a pronounced orientation throughout the unit. Some bending and fracturing of plagioclase and hornblende is visible in most thin sections, and a small amount of interstitial mortar is commonly present. Biotite generally shows incipient recrystallization into aggregates, and the larger patches of quartz generally consist of several grains.

Foliation intensity increases in the SHbT near the SHbT-PHbT contact zone, then decreases gradually into the interior of the PHbT and southward into the SPT. In much of the southern part of the pluton, flow structures are faint or absent; consequently, measurements of foliation and lineation attitudes are fewer, and many are queried. In some outcrops, a crude planar orientation of inclusions, generally

elongate 2:1 or less, is the only visible expression of flow structure. In thin section, slight protoclasis is locally apparent even in the interior of the PHbT and the northern part of the SPT. Except along discrete shear or fracture zones, protoclastic textures are absent throughout the southern half of the SPT.

Foliation intensity in the northeastern part of the SPT increases slightly towards the contacts with the diorite-gabbro complex, but nowhere is the foliation strong, nor are protoclastic effects apparent. In the tongue of finer-grained, less-porphyritic tonalite projecting northeastward into the pre-batholithic rocks southeast of the mafic complex, the intensity of foliation, lineation, and protoclasis approaches that of the outer gneissose phase of the SHbT. However, the intensity of flow structures decreases rapidly southwestward along the contact and westward into the interior of the SPT. There is generally little if any increase in foliation or lineation intensity towards the contacts elsewhere around the margins of the SPT.

(2) Relationship of Foliation Orientation to the Pluton Contact.

Both on the map scale and within individual outcrops, the gneissose foliation around the northern two thirds of the pluton is remarkably conformable to the pluton contact and to bedding and foliation in the adjacent pre-batholithic rocks (Plate 3). Where the eastern margin of the pluton has been indented adjacent to the diorite-gabbro complex in Cañon La Jolla, foliation in the tonalite is similarly deformed and remains parallel to the contact. Only where the contact has been offset by the Cañon Socorro and Willow Creek fault zones does foliation trend

at a high angle to the contact.

The foliation pattern in the eastern part of the SPT is grossly conformable to the southeastern contact with pre-batholithic rocks and is wrapped conformably around the diorite-gabbro complex of Willow Creek Canyon. Weak foliation in the PHbT and SPT for 3 km south of the western prong of the SHbT is also parallel to the general trend of the contact, but attitudes of faint foliation in the southwestern part of the SPT are variable and show at best only a very crude relationship to the contact.

The difference in degree of conformability of foliation to the contacts around the entire pluton correlate directly with the degree of concordance of the contacts to bedding and foliation in the wall rocks.

There are several local exceptions to the general pattern of conformability around the northern two thirds of the pluton: (1) at locality 71, along the northern contact 340 m west of the Tepetate road, (2) along the northern contact 1.1 km west of Rancho Cerro Costilla, and (3) locally along the southeastern contact between the Cañon Socorro and Willow Creek fault zones.

(1) In a small exposure at locality 71 (Figure 34), foliation in typical GBT more than 40 cm from the pluton contact trends at a 20° angle to the contact. This oblique foliation is abruptly truncated about 40 cm from the contact, and the outermost tonalite has an unusually intense protomylonitic foliation parallel to the contact. A thin sheared vein of quartz separates the disconformable and conformable zones. In exposures along the contact several meters on either side,

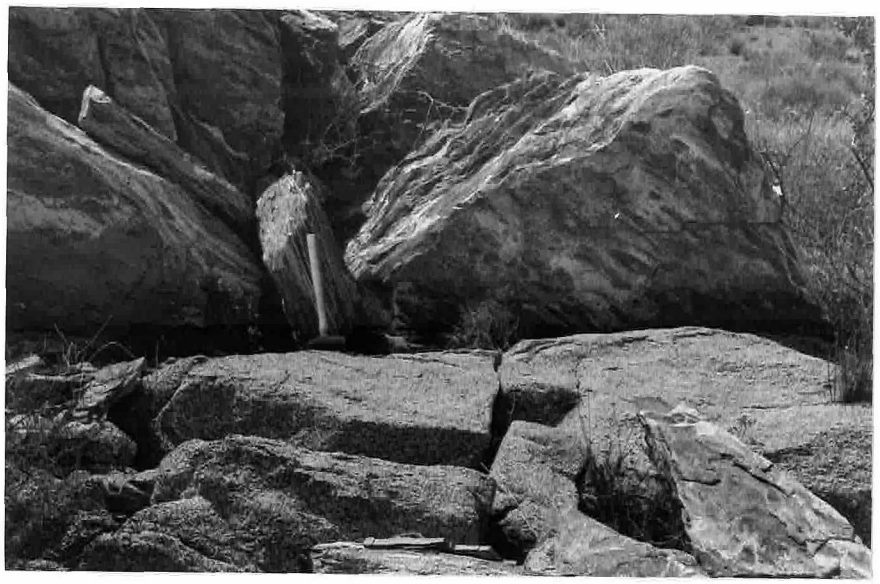

Figure 34A

Figure 34B

Figure 34. Disconformable foliation in gneissose tonalite at the contact with profoundly lineated stretched-pebble wacke. The photograph in (B) is a close-up of the area just below and to the right of the hammer head in (A). Gneissose foliation trending at a 20° angle to the contact is abruptly truncated 40 cm from the contact. Intense shearing parallel to the contact has reduced the outer 40 cm of the tonalite to a protomylonitic and mylonitic gneiss whose foliation is conformable to the contact. Locality 71 along the northern margin of the pluton, 360 m west of the Tepetate road (area C-6).

the outer 40 cm of tonalite is again intensely protomylonitic, but it grades into typical GBT, and foliation is consistently parallel to the contact. These relationships record a history of flow producing a gneissose and protoclastic foliation parallel to the contact, followed by local disruption and rotation of rigid blocks of apparently solid tonalite, followed in turn by continued extreme deformation of the tonalite along the contact. The time involved between these successive events is undetermined; the latest shearing could be due to continued emplacement of the pluton or to external deformation superimposed on the pluton or both.

(2) Along the northern contact 1.1 km west of Rancho Cerro Costilla, there is an unusual deviation from the nearly perfect circular outline of the northern part of the pluton. Traced eastward, the stretched-pebble wacke bordering the tonalite thickens rapidly from 5 m to 25-30 m and protrudes in a bulging mass 25 m into the pluton (Plate 2). Traced farther to the east, the wacke pinches out abruptly, and the pluton contact returns to its regional circular geometry. Bounding the protruding mass on the northern side is a zone of shearing and injection which coincides with the hypothetical position of the pluton contact interpolated between the opposite ends of the protruding mass. The shearing recorded by the gneissose foliation in the tonalite apparently ignored this local deviation of the contact from the regional smoothly arcuate geometry.

(3) From the Willow Creek fault zone northeastward for at least 750 m, foliation in the SHbT nearest the pluton contact is gneissose and protoclastic and follows the curving path of the contact. Just a short

distance into the pluton, foliation is weak or moderate, only slightly protoclastic, and follows a regional N 25-40° E trend, whereas the adjacent contact locally trends as much as 40° more easterly. Good exposures 350 m northeast of Willow Creek Canyon show that the transition from the conformable gneissose foliation in the outer 15-20 m of tonalite to the more northerly relatively weak foliation in the rocks farther from the contact occurs across a zone no more than 5-10 m wide.

Both the divergence of the regional N 25-40° E trend of foliation in the SHbT from the wavy trend of the adjacent pluton contact (averaging N 50-55°E) and the abrupt increase in foliation intensity towards the contact are apparent everywhere between the Willow Creek and Cañon Socorro fault zones. However, exposures are inadequate to reveal whether or not the gneissosity in the tonalite nearest the contact consistently parallels the local trend of the contact. The zone of discontinuity in foliation intensity appears to define a relatively straight shear zone roughly parallel to the average trend of the pluton contact, but the width of the gneissose zone is variable, reaching 100 m or more where the pluton margin bulges outward, and decreasing to 10-15 m where the wall rocks protrude inward.

The N 25-40° E foliation appears to record flow controlled by the regional shape and curvature of this part of the SHbT rather than by the local geometry and orientation of the pluton contact. The discordance between the N 25-40° E foliation and the contact suggests that the pluton and the immediately adjacent wall rocks at one time were partially or entirely locked together across the contact and deformed as a unit. However, the pluton and wall rocks were later de-

coupled, and a major zone of intense crushing and shearing developed approximately along the contact when at least the outer part of the SHbT was either solid or sufficiently crystal-rich to have a definite strength and rigidity.

(3) Relationship of Foliation to the SHbT-PHbT Contact Zone.

Foliation intensity in both the SHbT and PHbT increases towards their mutual contact zone, especially in the PHbT. In the SHbT, the most conspicuous expression is a slight or moderate increase in the flattening of mafic inclusions; the accompanying increase in mineral orientation is not apparent in all outcrops.

In the outer part of the PHbT, foliation varies from moderately strong to slightly gneissose. Foliation is particularly strong along the northern margin of the unit, where stretching of mafic inclusions locally approaches that in the GBT, and concordant jointing is conspicuous (Figure 20, p. 126).

The contact between the two tonalite units therefore appears to have been an important surface of increased magmatic flow and protoclasis, i.e., an intrusive contact. The outer margin of the PHbT appears to be analogous to the present margin of the pluton, although foliation, protoclasis, concordant jointing, and recrystallization of biotite into aggregates are nowhere as intense in the PHbT as in the outer gneissose phase of the SHbT. As around the margins of the pluton, the increase in foliation intensity along the SHbT-PHbT contact decreases southward, becoming inconspicuous near the southwestern and southeastern tips of the SHbT.

Foliation in both the SHbT and PHbT is consistently parallel to their mutual contact zone except in three areas. (1) Along a 700 m stretch in the northwest (Plate 3, area G-4), where the contact bends rapidly from a northeast-southwest trend to a north-south trend, foliation bends more gradually and strikes 15-25° more easterly than the contact zone. (2) Foliation in both units also appears to strike at a 10-15° angle to the contact zone in a very local area 1.7 km south-southwest of Las Encinas Corral (area F-8). (3) Where the SHbT pinches out in the southwest, foliation passes smoothly from the SHbT to the PHbT, with no change in orientation. These observations imply continued flow of the two textural units as a single mass after juxtaposition and development of the contact zone.

On a smaller scale, foliation also ignores the lenticular geometry of the interlaying between the two textural types. That is, where one layer pinches out, foliation strikes straight across the boundary of that layer into the adjacent one. Again this implies combined synchronous flow of the two textural units.

(4) Relationship of Foliation to the Gradational PHbT-SPT Contact Zone.

In general, the pattern and intensity of foliation (and also the pattern of jointing) ignore the existence of the gradational contact zone between the PHbT and SPT. It is clear that, if the two units formed from separate magmatic pulses, they must have been closely spaced in time, and they must have flowed eventually as a single mass to produce the present foliation pattern. If any flow structure developed parallel to the contact zone it was obliterated.

(5) Local Complexities in Foliation Orientation and Intensity.

Within local areas and individual outcrops, the attitude and intensity of foliation are generally uniform. Foliation attitudes commonly vary by no more than 5 or 10° over distances or tens of hundreds of meters. However, several types of complexity locally occur. Severe local swirling of foliation and/or intense minor faulting and shearing were seen in two areas, both in the GBT: (1) along the southeastern contact of the pluton between the Cañon Socorro and Willow Creek fault zones, especially in Willow Creek Canyon, and (2) along the western contact 300-800 m south of Arroyo de las Parritas (area L-3). In neither area is crushing or recrystallization of the tonalite severe; the deformation apparently occurred while the tonalite was hot, relatively mobile, and perhaps still partially molten.

A slightly more common complexity, especially in the western part of the PHbT, is variation of up to 20-25° in foliation attitudes over distances of tens of meters (denoted by sinuous strike symbols on Plate 3). The changes may be curving and gradual, or they may involve abrupt truncation of one foliation direction by another. In some cases, the truncating sets of foliation are due to flow parallel to local shear zones, whereas, in other cases, they may indicate breaking up and rotation of blocks of nearly solidified tonalite.

In some outcrops, foliation intensity increases markedly in conformable zones ranging from several centimeters to several meters wide. Apparently, as crystallization proceeded and the magma developed sufficient shear strength, continued flow and shearing was locally concentrated in narrow zones between more rigid masses. One might expect

Figure 35A

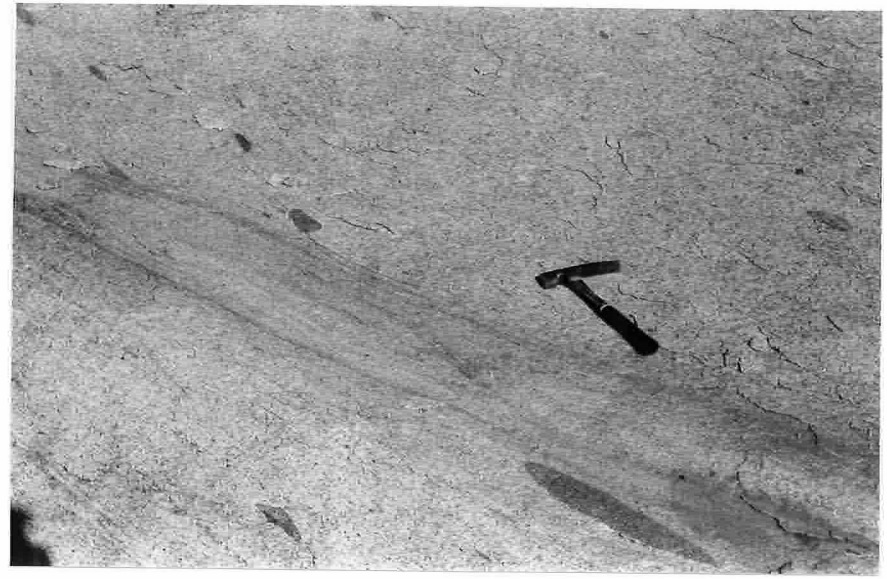

Figure 35B

Figure 35. Protoclastic shear zone in the prismatic hornblende tonalite. Foliation and inclusions (parallel to the hammer handle) are truncated at a 20° angle on one side of the shear zone, but are parallel to the zone on the other side. Note the sharply truncated inclusion at the upper left in (B). Locality 46, about 40 m west of the Quatal road, 1.3 km north-northeast of Rancho Quatal (area J-5).

this phenomenon to be widespread, but it is not evident in most exposures.

In some parts of the pluton, particularly in the western third of the PHbT, weakly or moderately foliated tonalite is cut by rare zones of intense protoclasis or mylonization ranging from single layers several millimeters wide up to complex splaying or anastomosing zones one meter wide (Figure 35). In some zones, the sheared rock is a fine- to medium-grained protoclastic tonalite in which the granulated material has been largely recrystallized. In other zones, little recrystallization has occurred, and the sheared rock consists of relict broken and abraded crystals in a very fine-grained groundmass. Many of the zones sharply truncate foliation and, in some cases, inclusions in the adjacent rock. However, minerals and inclusions in the tonalite within several meters on one or both sides of other zones have been reoriented parallel to the trends of the zones, implying that deformation occurred prior to complete solidification of the surrounding rock. A few zones developed parallel to earlier foliation. Most or all of these sheared or mylonitized zones apparently formed as an integral part of the intrusive history of the pluton, after the main flow foliation in the surrounding rock had been "locked in", but, in some cases, while sufficient melt remained to allow local flow parallel to the shear zones.

(6) Schlieren.

Mafic and leucocratic schlieren occur throughout the pluton, but they are sparse or absent in most outcrops. Mafic schlieren are more abundant than leucocratic schlieren in the PHbT, whereas leucocratic schlieren greatly predominate in the SHbT. Neither type is common

in the SPT.

I apply the term schlieren to straight or wavy, occasionally contorted, streaks, layers, and lenses, either vaguely or sharply bounded, which are composed of the same minerals as the host tonalite, but contain distinctly higher or lower concentrations of mafic minerals than the host rock. Mafic schlieren typically contain 25-35%, in some cases as much as 50%, dark minerals; hornblende generally exceeds biotite. Plagioclase is the principal mineral, and quartz is generally minor. Leucocratic schlieren typically contain 5-10% mafic minerals, mostly subequal amounts of hornblende, biotite, and epidote-group minerals. Plagioclase is again the dominant phase, but quartz is also abundant. Only a slight trace of K-feldspar is present in either the mafic or leucocratic schlieren.

Textures in the schlieren are hypidiomorphic-granular and correlate with those of the host rock; that is, schlieren in the SHbT contain equant, anhedral grains of hornblende and biotite, some of which are molded around or poikilitically enclose plagioclase, non-poikilitic prisms of hornblende, and thin plates of biotite. Leucocratic schlieren in the SHbT are slightly finer-grained than the host rock; otherwise, there are no obvious consistent differences in grain size between schlieren and host. The optical properties of the minerals are also similar in the schlieren and host rock. Compositions and zoning patterns of plagioclase are comparable to those of the host rock; interiors average An_{35-45}, rims average An_{23-29}. Plagioclase in the leucocratic schlieren in the SHbT may average slightly more sodic than in the host rock.

Most schlieren, such as those in Figure 36, are 1-10 cm wide and from 0.5 m to many meters long; however, sparse lenticular leucocratic schlieren as much as 0.5-1 m wide and several meters long occur in the SHbT (Figure 38B). Many schlieren taper out gradually, but some pinch out abruptly, and others interfinger with the host rock. Both the schlieren and the component mineral grains typically parallel other elements of foliation in the tonalite, but locally the schlieren are contorted into complex, non-systematic patterns or, more commonly, into folds whose axial planes coincide with host-rock foliation. Most contorted schlieren are leucocratic. Foliation is commonly stronger in the schlieren, particularly the leucocratic schlieren, than in the host rock. Some leucocratic schlieren exhibit a foliation as strong or stronger than in any of the rocks examined, including the GBT, yet protoclasis is relatively minor and granoblastic textures are rare. Some discordant leucocratic layers megascopically indistinguishable from the schlieren can be recognized as dikes intruded into the tonalite; other rare, sharply bounded, ellipsoidal masses of equally indistinguishable leucocratic rock found in the SHbT are clearly fragments included in the host rock.

Schlieren are scattered rather uniformly through the SHbT; often they occur singly, and only rarely are there many in an outcrop. There may be a slight concentration near the inner margins of the SHbT. In some SHbT outcrops, mafic schlieren are closely associated with leucocratic schlieren, but, more commonly, the latter have no recognizable mafic counterpart. Except in the GBT, there is no apparent correlation between the abundance of schlieren and of inclusions in the SHbT.

Figure 36. Prismatic hornblende tonalite with abundant lenticular mafic schlieren oriented parallel to foliation. Locality: about 40 m west of the North-South road, 4.1 km south of Rancho El Coyote (area I-5).

Figure 37. Prismatic hornblende tonalite exhibiting exceptionally pronounced development of interlayered concordant mafic and leucocratic schlieren. Locality: about 50 m east of the Quatal road, 4.1 km south of Rancho El Coyote (area I-5).

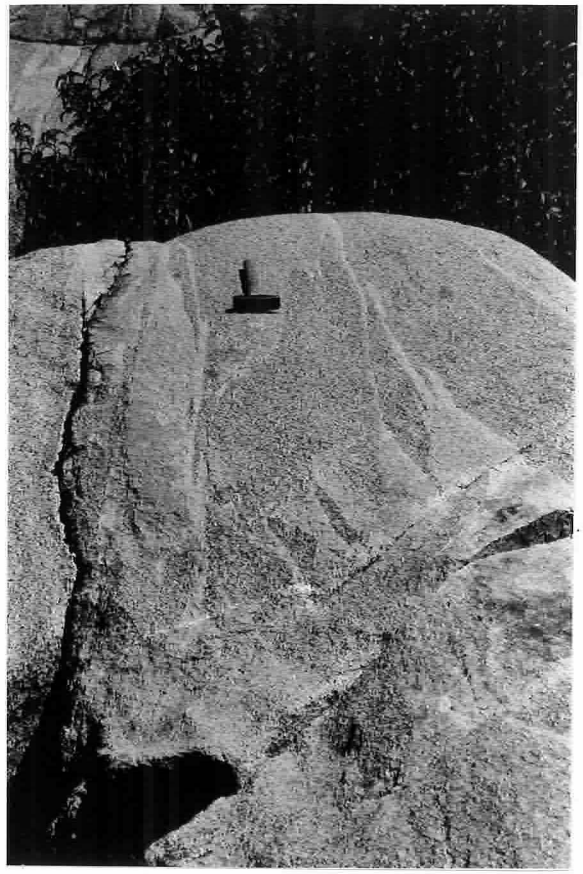

Figure 38A

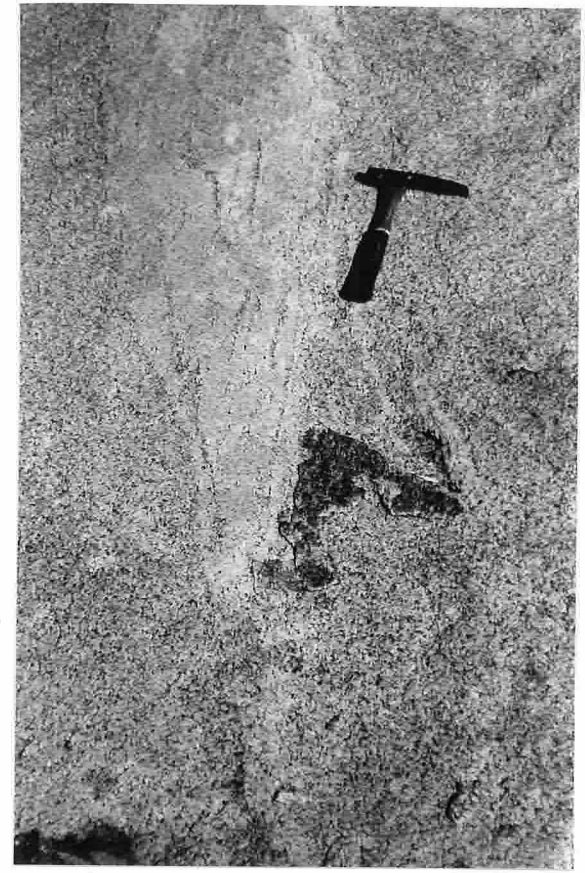

Figure 38B

Figure 38. Leucocratic schlieren in the stubby hornblende tonalite. The long thin schlieren in (A) are the most common form in the SHbT, but the thicker lenticular masses in (B) are not unusual. However, the schlieren in (A) are unusually abundant and complex. Localities: (A) about 300 m east of the San José-Observatorio road, 630 m northeast of the southern tip of the mafic zone separating the SHbT and PHbT (area K-11,12); (B) central part of the western prong of the SHbT, 4.3 km southwest of Rancho El Coyote (area H-3).

In contrast, schlieren in the PHbT commonly occur in swarms, accompanied in some cases by abundant mafic inclusions. The most striking schlieren swarms define a discontinuous, concordant, arcuate zone 4.5 km long and roughly 50-300 m wide, located about 5 km north of San José (Plates 2 and 3). Most exposures in this zone are similar to the one in Figure 36, in which schlieren constitute 20% or less of the rock. However, where most spectacularly developed, interlayered leucocratic and mafic schlieren 2-10 cm wide and up to many meters long so dominate outcrops as to make definition of typical host rock impossible (Figure 37).

At many places in this schlieren-rich zone, flow structure is complex. Leucocratic schlieren are locally contorted and, at several places, two directions of foliation were observed (Plate 3), with one direction striking as much as 60° off the typical trend for the area. Linear alignment of hornblende prisms and dioritic inclusions, generally plunging at moderate angles to the northeast and east, is more prevalent in the western half of this zone than elsewhere in this part of the pluton. Evidently, the development of the schlieren swarms is related in some way to an especially complex local history of flow.

(7) Funnel-Shaped Flow Pattern.

Foliation attitudes in the northern two thirds of the pluton define a pattern of northward-convex arcs which, like the crescentic outline of the SHbT, do not close on the southern side. The pattern, shown schematically in Figure 39, is remarkably uniform and smoothly curving, but it is not centrosymmetric. Rather, the approximate center of

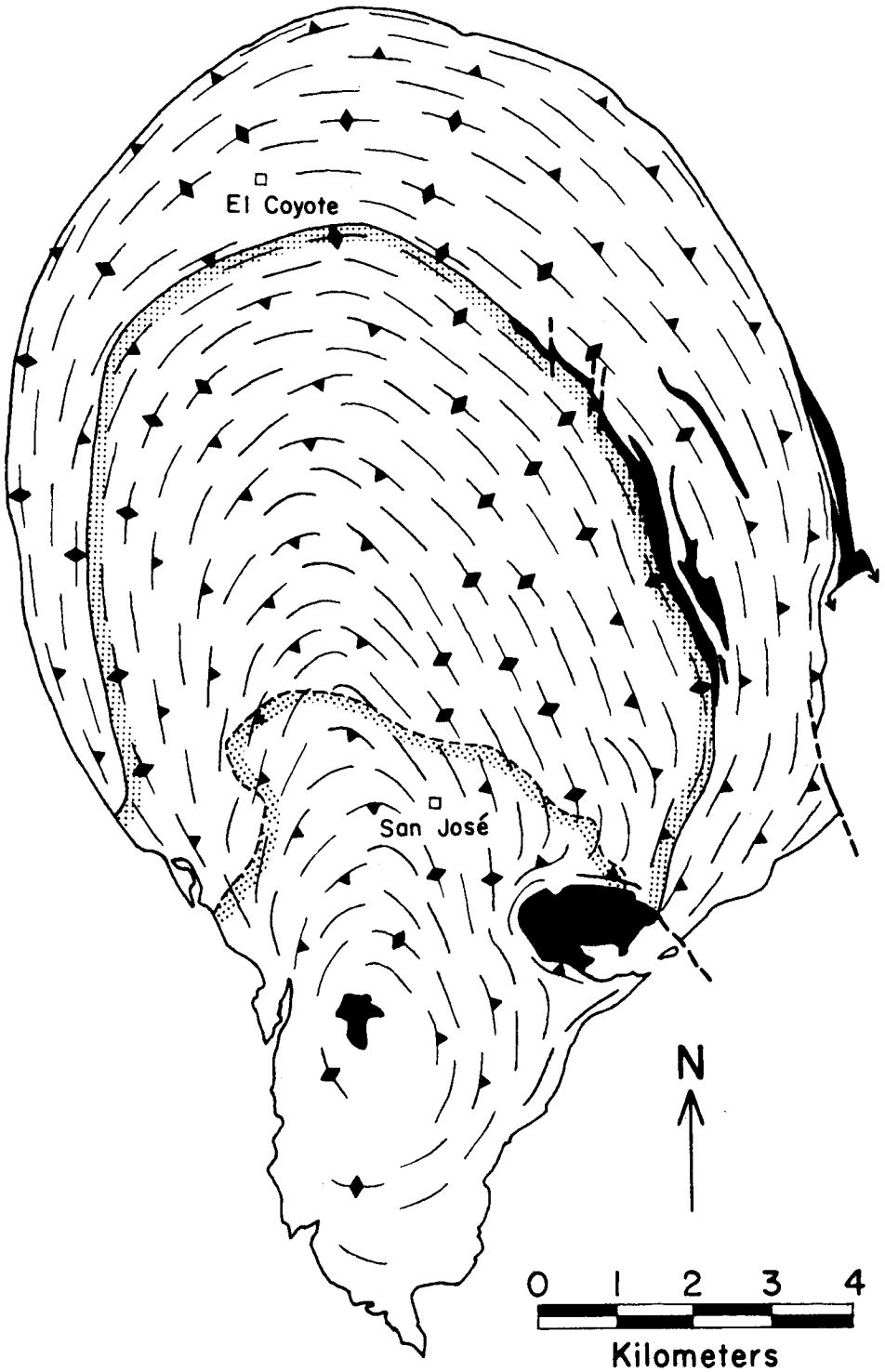

Figure 39. Generalized foliation patterns in the San José pluton.

curvature of arcuate foliation trends (in plan view) at successively greater distances inward from the pluton margins plots progressively farther south. This migration of successive centers of curvature continues southward into the interior of the SPT, where the attitudes of weak foliation vaguely suggest closure of strikes around a point in the west-central part of that unit. Flow of the SPT around the diorite-gabbro complex near Willow Creek Canyon, and a local strong westward curvature of the foliation pattern in the eastern part of the PHbT 1.5-2 km north of Willow Creek Canyon (Plate 3), are the only significant deviations from the general uniform pattern.

The dip of foliation varies systematically both around the margins of the northern two thirds of the pluton and from those margins inward and southward towards the apparent center of closure of foliation trends in the SPT. Around the northern two thirds of the pluton, the dip of the pluton contact, of the outer gneissose foliation, and of bedding and foliation in the adjacent wall rocks changes gradually from 65-75° outward on the east and northeast to 75-85° outward on the north, and finally to vertical or locally 80-90° inward on the west. Although this progressive westward steepening of dips correlates in a general way with decreasing topographic elevation of the pluton contact, from 1000-1100 m in the northeast to 800-900 m in the west (Plate 7), the dips show no systematic relationship to local relief, which reaches 100-150 m in some places. This pattern argues against rapid variations in foliation or contact orientation either downward or originally upward and can be interpreted as evidence that the northern two thirds of

the pluton, *at this level of exposure*, has a roughly cylindrical outline plunging about 80° to the northeast or north-northeast. However, considerations discussed in the next several paragraphs suggest that the pluton probably does not maintain such a northward-plunging geometry to any great depth in the crust.

From the margins inward, the dip of foliation changes consistently, throughout the northern two thirds of the pluton, from steeply outward (or vertical) through vertical to inward in the interior of the PHbT. In the west-central part of the PHbT, inward dips average from 50 to 70°, but they are locally as shallow as 40° and as steep as 80°.

Followed southward into the SPT, the dips increase gradually again to vertical around the apparent center of closure of foliation trends in the west-central part of the unit. Combined with the southward migration of the successive centers of curvature in plan view, the changes in dip suggest a funnel-shaped pattern of flow of magma upward and expanding predominantly northward and eastward from a conduit shifting progressively southward with time from the interior or southern part of the PHbT into the west-central part of the SPT. If the pattern of flow recorded by foliation is related at all closely to the geometry of the intrusive contacts in the vertical plane, then this flow pattern implies that the SHbT and PHbT contact zone, and probably the outer contact of the SHbT as well, curve

gradually inward at depth, and that the pluton narrows downward, although probably not immediately below the present level of exposure.

(8) Crosscutting Foliation in Dikes.

At numerous localities near the contact around the northern two thirds of the pluton, dikes and veins cutting the pluton and the wall rocks are strongly foliated and, in some cases, offset along planes parallel to the foliation in the tonalite and to foliation and bedding in the pre-batholithic rocks. Strong lineation parallel to the host-rock lineation is also apparent in some dikes veins. A few dikes and veins in the tonalite appear to be truncated at the contact.

Figure 40 shows strong foliation crosscutting one of several fine-grained quartz gabbro or mafic quartz diorite dikes which are intruded into the GBT along the northeastern contact about 100 m east of Rancho Cerro Costilla (area C-9,10). The dikes strike parallel to host-rock foliation and to the pluton contact, but dip 40-45° to the south, i.e., at a 55-60° angle to the 80°-northward dip of the pluton contact and of foliation in both the tonalite and the dikes. Locally the margins of the dikes are sharp and planar; in other places, post-intrusive shearing parallel to foliation produced contorted interfingering of the dike and host rock on a scale of several centimeters. A thin section of the photographed dike reveals strong mineral orientation parallel to the crosscutting foliation. Textures imply strong protoclasis accompanied by recrystallization of the granulated material as well as of biotite and possibly much of the hornblende. Thus the deformation recorded by the gneissose foliation in the GBT continued

Figure 40A

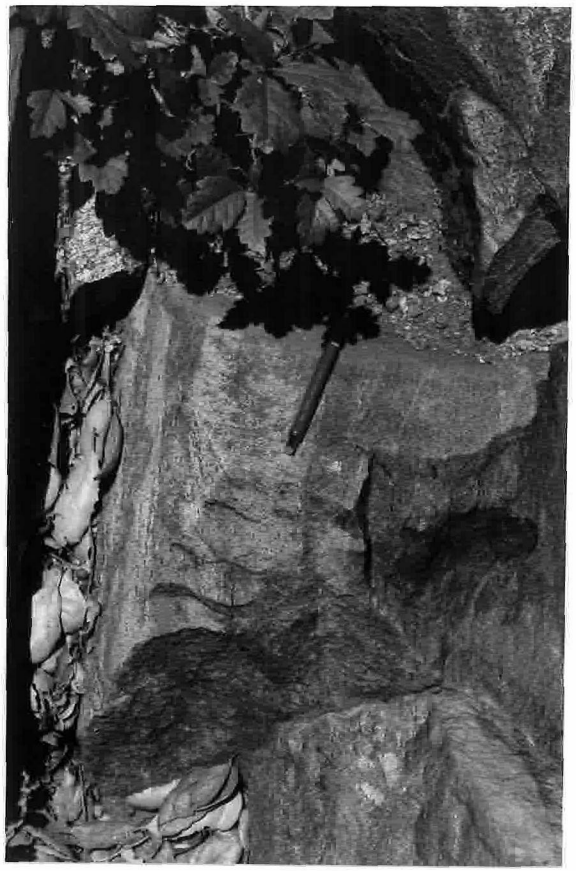

Figure 40B

Figure 40. Foliated mafic dike cutting gneissose tonalite at the northeastern margin of the pluton. The dike strikes parallel to the pluton contact and dips at a 45° angle into the pluton. Strong foliation in the dike (parallel to the conspicuous cleavage planes in (A) and to the pencil in (B)) coincides with foliation in the tonalite, but is nearly perpendicular to the walls of the dike. Locality 27 in Arroyo Cerro Costilla, about 100 m east of Rancho Cerro Costilla (Plate 5, area C-9,10).

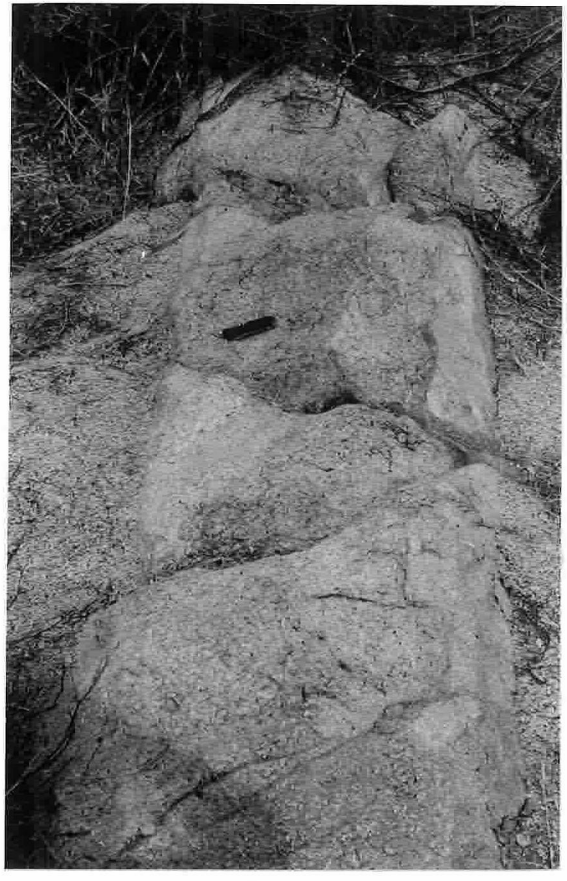

Figure 41A

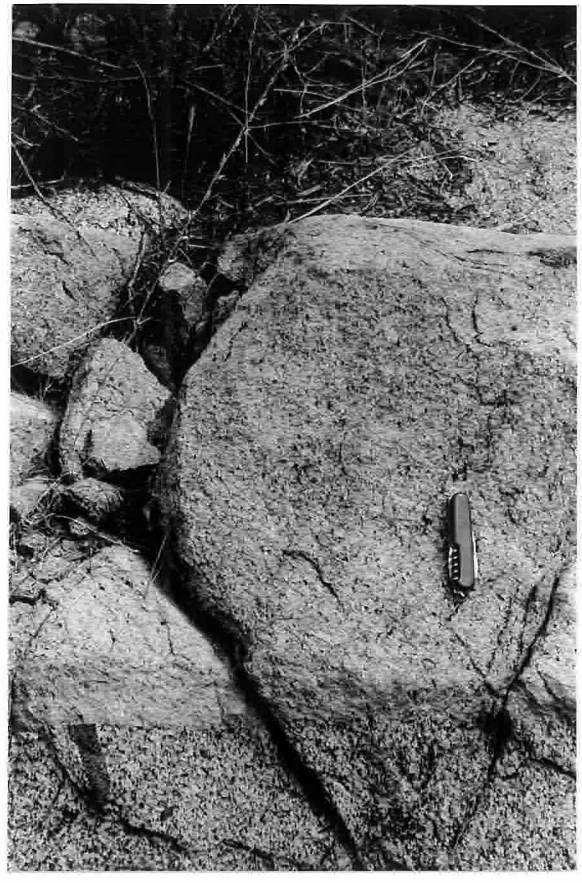

Figure 41B

Figure 41. Granite dike intruded into normal to interlayered stubby hornblende and prismatic hornblende tonalite in the contact zone between the two tonalite units. Note the sharp planar contacts and fine-grained margins of the dike and the truncated mafic inclusion in the tonalite. Preferred orientation of biotite flakes in the dike defines a faint foliation (parallel to the pocket knife) which coincides with that in the tonalite, but is perpendicular to the walls of the dike. Locality 302, 4.3 km southwest of Rancho El Coyote (Plate 5, area H-3,4).

not only after the GBT was sufficiently solid to fracture, but also apparently after crystallization of the dikes which fill the fractures.

Host-rock foliation also crosses a granitic dike at locality 302 along the SHbT-PHbT contact zone in the northwest (Plate 5, area H-3,4). The dike, which strikes normal to foliation and to the contact zone in the host rocks and dips about 70° northward, is traceable almost continuously for about 80 m. At its eastern end in the PHbT, the dike is about 1.2 m wide, has a 1-3 mm grain size, and contains about 10% biotite and minor hornblende. The dike thins gradually westward to about 30 cm, then branches and pinches out in the western part of the zone of interlayered SHbT and PHbT. As the dike thins, the average grain size decreases to about 0.5-2 mm, hornblende disappears, leaving 5-10% biotite, and conspicuous fine-grained (0.1-0.5 mm) rapidly-cooled zones 1-5 cm wide appear at the contacts. The dike walls are sharp, relatively planar, and locally truncate mafic inclusions in the host rock (Figure 41). The fine-grained margins are equally well developed against both the SHbT and PHbT layers in the host rock.

Two faint planar mineral orientations are developed in the dike. Rapid cooling in the fine-grained margins locked in an intrusive flow foliation parallel to the dike walls and defined by the orientation of subhedral plagioclase phenocrysts 0.5-1 mm in size. In the more slowly cooled interior of the dike, preferred orientation of sparse 2-6 mm, anhedral biotite books and, to a lesser degree, of anhedral to subhedral plagioclase crystals up to 2 mm and anhedral ragged quartz grains up to 3-4 mm defines a weak foliation trending at a high angle to the dike walls, but parallel to the foliation in the host tonalite (parallel to

the pocket knife in Figure 41). Thus, the movements recorded by the host-rock foliation continued during emplacement and crystallization of the dike, but were insufficient to deform the dike margins. Furthermore, the interlayered SHbT-PHbT host rock was sufficiently cool at the time of emplacement of the dike to cause rapid cooling of the dike margins.

All known dikes and veins exhibiting foliation and/or lineation parallel to the host-rock fabric occur near either the pluton contact or the SHbT-PHbT contact zone. All dikes and veins seen in the SPT or in the interior of the SHbT or PHbT truncate the planar and linear fabric of the host rock.

9.1.3 Lineation Patterns in the Pluton and Country Rocks

Lineations in the tonalite (Plate 4) are generally most intense and consistently developed near the pluton contacts, especially around the northern and eastern margins. Lineations generally plunge within the plane of foliation, but are rarely downdip. In some outcrops, particularly in the western and southern parts of the SPT, lineation is the only visible flow structure.

In the GBT, lineations are defined most strikingly by streaks of recrystallized biotite separated by streaks of the leucocratic minerals (Figure 15B, p. 114). Long axes of hornblende and plagioclase crystals and of mafic inclusions are aligned parallel to the biotite lineation, but their orientation is often less distinct. These are protoclastic lineations closely related in time and origin to the gneissose foliation.

In the rest of the tonalite, biotite is mostly or entirely un-

recrystallized and has not been streaked out; lineation, where visible, is generally faint and is defined by alignment of unrecrystallized mafic minerals and of mafic inclusions. These are magmatic flow lineations generally accompanied by little or no protoclasis.

The lineations can be roughly divided into two groups.

(1) Those developed around the northwestern, northern, and eastern margins of the pluton and locally for as much as 2 km into the pluton have systematic orientations and belong to regional systems equally well or better developed in the surrounding country rocks.

(2) Those in the interior and along the southwestern margin of the pluton are less consistently developed; some may be related to the regional systems, but most appear to be due to local intrusive flow patterns.

Group (1) lineations can be further subdivided into two systems. One system is developed along the eastern side of the pluton from Cañon La Jolla southward to the tip. Lineations in this system plunge consistently at angles of 40 to 75° towards N 30-75° E. The orientations are the same in the tonalite and country rocks regardless of the orientations of foliation bedding or the pluton contact. Plunges are downdip only in rare circumstances where the strike of bedding or foliation is normal to the regional trend of lineation. The second system is developed around the northern half of the pluton and consists of lineations whose plunges vary as a function of the location around the pluton margin. Specifically, the lineations around the northeastern and northwestern margins plunge consistently northward; followed north-

ward around the margins, the lineations rotate gradually, and the plunges converge towards an area beneath the southern margin of the Las Cochas pluton. The converging pattern is well developed southwest of the Tepetate road, where the lineations trend nearly parallel to the pluton contact and plunge at angles as low as 24°, and southeast of Rancho Cerro Costilla. In the intervening area, lineations are generally less intense, less consistently developed, and more erratic in orientation. Plunges are downdip only in the area around and north of Rancho Cerro Costilla. Lineations are especially strong in the stretched-pebble wacke between the Tepetate and Buena Vista-Coyote roads, where clasts have been stretched into extremely thin spatuloid shapes elongate as much as 5:1 in the plane of foliation (Figure 11, p. 88).

Northward-plunging lineations belonging to the northward-converging system continue with decreasing intensity southward in the wall rocks west of the pluton nearly to Arroyo de las Encinas; south of there the attitudes are erratic. Northward-plunging lineations are also well developed at least locally in the adjacent GBT for 5-6 km south of the Buena Vista-Coyote road; the paucity of attitudes in the GBT reflects mainly a scarcity of prominent tonalite outcrops along this part of the contact and consequent difficulty in obtaining dependable lineation readings.

Southward along the northeastern contact, lineations belonging to the northward-converging system rotate gradually to more easterly trends and merge with the northeastward-plunging pattern. Inasmuch as I found no evidence of discontinuity in orientation between the two

systems or of superposition of one system on the other, the two systems may be contemporaneous and closely related.

Both regional lineation systems are most intense near the pluton margin. The northward-converging system generally extends no more than a few hundred meters into the pluton; as gneissosity disappears, so generally do the lineations. All along the northeastern contact and in the vicinity of the Tepetate road along the northern margin, the northward-converging system gives way abruptly (?) inward to downdip or nearly downdip lineations defined by alignment of unrecrystallized mafic minerals and of inclusions. Thus, there are two generations of lineations in this part of the SHbT: an older set of downdip lineations formed by magmatic flow with little or no protoclasis, and a superimposed set of northward-converging lineations which formed in the GBT (and the country rocks) during intense shearing and protoclasis.

Near Cañon La Jolla, the northeastward-plunging system likewise extends only a few hundred meters into the tonalite, but farther south it is recognizable across the entire width of the SHbT and locally in the outer part of the PHbT. In both units within several hundred meters north of the Willow Creek fault zone, lineations are unusually strong and locally obscure foliation. Unlike elsewhere in the interior of the pluton, the northeastward-plunging lineations in this area are accompanied by moderate to strong protoclasis and are defined in part by streaks of recrystallized biotite as in the GBT.

Except in the northeastward-projecting wedge of strongly foliated and lineated SPT intruding the pre-batholithic rocks south of Willow Creek Canyon (Area 0-10), lineation is faint or unrecognizable in the

SPT along the southeastern margin of the pluton. However, the northeastward-plunging lineation system is well developed in the adjacent wall rocks. Several approximate or queried attitudes in the outer part of the SPT near the arroyo called El Alisito (areas Q-8 and R-8) also conform to this system, although their plunges may tend to be more shallow; these lineations are defined entirely by alignment of unrecrystallized mafic minerals and mafic inclusions and are not accompanied by any protoclasis. Faint flow lineations near the southern tip of the SPT plunge more consistently eastward; they may or may not be part of the regional system.

In the pre-batholithic rocks, lineations are defined megascopically by preferred orientation of hornblende, micas, and rarely plagioclase, by stretching of rock fragments, by low-relief ridges and troughs on foliation surfaces, and locally by boudinage structures. Although the intensity of lineation in the wall rocks decreases away from the pluton, weak lineations parallel to the northeastward-plunging system are visible along and south of the San José-Observatorio road as much as 3-4 km east of the pluton. Similarly, the northward-converging system is developed at least as much as 2 km to the northeast and 700-800 m to the northwest and west of the pluton.

Around the southwestern margin of the pluton from Arroyo de las Encinas southward, lineation patterns are much more complex. Lineations are weak or absent in the tonalite along most of the contact; they exhibit some local systematics, but they bear no consistent relationship to the lineations in the adjacent wall rocks. The latter are also less intense and more erratic in trend than elsewhere around the pluton; they

show little if any relationship to either of the regional systems previously described, and they appear to die out quickly south of Cañon Las Cabras.

In the interior of the pluton, lineations are generally weak and frequently hard to recognize. The patterns are quite variable, and plunges range from vertical to horizontal. However, several systematics are apparent. (1) Lineations generally plunge down the dip of foliation in the northeastern interior of the SHbT, in the southwestern part of the SHbT and PHbT, and in a small area in the eastern part of the PHbT 1.5-3 km north of Willow Creek Canyon. Elsewhere, lineation plunges are almost invariably oblique to the downdip direction. (2) Lineation intensity, like foliation intensity, tends to increase towards the outer part of the PHbT and perhaps also along the inner margin of the SHbT. (3) Lineations around the northern and northwestern margins of the PHbT generally plunge northward or eastward subparallel to the local orientation of the SHbT-PHbT contact zone. (4) Most lineations in the SPT and the western part of the PHbT plunge at moderate or steep angles to the northeast or east, whereas sparse lineations in the eastern half of the PHbT vary in plunge from horizontal to moderately or steeply northwestward. (5) Lineations in the southeastern part of the SHbT and in the adjacent outer part of the PHbT plunge consistently northeastward at angles of 40 to 80°.

As stated earlier, the northeastward-plunging lineations in the southeastern part of the SHbT and PHbT and probably those in the southeastern part of the SPT as well, are part of the regional northeastward-plunging system developed around the eastern margin of the pluton.

Lineations elsewhere in the interior of the pluton probably record local patterns of intrusive flow. In particular, the opposed northeastward and northwestward plunges in the western and eastern halves of the PHbT, respectively, suggest a pattern of upward and outward flow combined with varying degrees of lateral extension parallel to foliation. I cannot rule out the possible influence of regional deformation on the local flow patterns and the resulting lineations.

There are several points to emphasize about the two regional lineation systems.

(1) They are developed in all three textural units of the pluton. Although the lineations are best developed in the gneissose rocks, where they formed apparently during and possibly after the latest stages of magmatic crystallization, they also occur in unfoliated rocks along the southeastern margin of the SPT, where they formed by magmatic flow with no protoclasis.

(2) The lineations are strongly developed not only in the San José pluton and pre-batholithic rocks, but also in most, if not all, of the nearby intrusive masses. The northeastward-plunging system is strongly developed in the gabbro-diorite complex and the associated mafic sheets and small dioritic and gabbroic bodies immediately east of the pluton near Cañon La Jolla. Even an aplitic dike and a fine-grained mafic dike which are intruded into the gabbro-diorite complex exhibit strong northeastward-plunging lineations. Strong foliation, crushing, and some recrystallization accompany the lineations.

Weak northeastward-plunging lineations without accompanying protoclasis are apparent in several outcrops in the outer part of the Willow Creek pluton.

An approximate attitude of weak lineation in one exposure in the little-studied interior of the Encina Sola pluton suggests a more easterly plunge than most of the lineations, but it may belong to the same system.

Lineation, gneissose foliation, and protoclasis are intense in float blocks derived from the southern margin of the Las Cochas pluton. At the one place where the lineation orientation was measured -- in mafic tonalite 600 m north of Rancho Cerro Costilla (area C-9,10), at the eastern tip of the arm projecting from the southern margin of the pluton -- the plunge is parallel to orientations in the adjacent pre-batholithic rocks and appears to be part of the northward-converging system.

(3) The northward-converging lineations are developed in several dikes and veins which cut the GBT.

(4) There is no systematic lineation pattern along the southwestern side of the pluton corresponding to the northeastward-plunging pattern on the eastern side. Possibly, the predominance of east-northeastward plunges in the southwestern part of the pluton records movements related to those which produced the northeastward-plunging lineations on the eastern side of the pluton; if so, the movements were much weaker and less systematic than on the eastern side.

(5) Reconnaissance observations indicate that lineations plunging

consistently to the northeast or east at angles of 40-85° are widely developed in both the plutons and metamorphic rocks over a 35-km^2 area farther east along and near the base of the western scarp of the Sierra San Pedro Mártir. Lineations plunging to the east-northeast at angles of 25-80° were also observed in the tonalite and wall rocks at the northern contact of the Potrero pluton (southeastern corner of Plate 1) and in the tonalite near the southeastern margin of that pluton.

The development of the two regional lineation systems was therefore one of the last major events (other than regional uplift and erosion) to affect the San José area, but it apparently overlapped with emplacement of the San José pluton. The northward-converging system seems to be uniquely attributable to squeezing of strata upward and outward from between the San José and Las Cochas plutons and southward along both the eastern and western margins of the San José pluton. The squeezing could be due to (1) intrusion and expansion of the San José pluton against the pre-existing Las Cochas pluton, (2) intrusion and expansion of the Las Cochas pluton against the pre-existing San José pluton, (3) simultaneous emplacement of the two masses, or (4) regional deformation superimposed on both plutons during the latest stages of, and possibly after, emplacement. In both the first and third possibilities, the protoclastic lineations in the GBT should give way gradually inward to non-protoclastic flow lineations of similar or gradually changing orientation, rather than giving way abruptly inward to non-protoclastic downdip lineations as appears to be the case. Also, the San José pluton is not significantly flattened or indented along that part of its contact

nearest the Las Cochas pluton, such as it is adjacent to the small mafic pluton in Cañon La Jolla. The northern margin of the San José pluton appears to have been solid or nearly solid and rigid relative to the country rocks when the squeezing occurred. Either the second or fourth possibility therefore seems more likely. In the fourth possibility, the proposed regional deformation must have had a strong north-northeast-south-southwest component.

The northeastward-plunging system is less uniquely interpretable. The lineations may either be *a* lineations, i.e., roughly parallel to the direction of principal stress and tectonic transport, or *b* lineations normal to this direction. In either case, they cannot be readily accounted for by emplacement of the San José pluton without externally-imposed deformation. That is, inasmuch as the lineations are independent of the orientation of the pluton contact, are not downdip, and are not matched by a systematic pattern along the southwestern side of the pluton, it is difficult to conceive of any direction of emplacement to which they can be attributed. Furthermore, emplacement of the San José pluton cannot account for the development of consistently northeastward- and eastward-plunging lineations in the pluton and wall rocks near the base of the Sierra San Pedro Mártir, 6-8 km east of the San José pluton, or around the margins of the Potrero pluton farther south.

If the lineations are *a* lineations, then they record deformation directed either upward and southwestward or downward and northeastward. Plutonic emplacement and/or regional uplift in the Sierra San Pedro Mártir provide a reasonable cause for the former direction of deformation

and can readily account for (1) the northeastward-plunging lineations, (2) the lack of corresponding lineation systems on the southwestern side of the pluton, because deformation would be most intense and systematic on the side of the pluton nearest the source of deformation, and possibly (3) squeezing of the strata from between the Las Cochas and San José plutons in response to southwestward or south-southwestward shoving of the Las Cochas pluton against the San José pluton. The greatest mass of batholithic rocks exposed in this part of the peninsula is in the sierra, and U-Pb isotopic age determinations on zircons indicate that much of this rock is 8-10 m.y. younger than the San José pluton (L. T. Silver, unpublished data).

There is no such obvious cause which can be invoked for deformation with principal stress normal to the northeastward-plunging lineations. The asymmetry of the patterns and intensities of lineations, foliations, and penetrative deformation around the margins of the pluton is difficult to account for by any model invoking a principal stress direction other than northeast-southwest. Furthermore, the regional structures in the pre-batholithic rocks throughout this part of the peninsula indicate northeast-southwest compression. However, the asymmetry around the pluton is difficult to understand in terms of *equally-opposed* northeast-southwest forces. Only a net tectonic transport upward and southwestward parallel to the lineations seems to fit all of the observations.

9.1.4 Correlation of Textures with the Intensity of Flow Structures

9.1.4.1 Correlation within the Prismatic Hornblende and Seriate Porphyritic Tonalites

Throughout the PHbT and SPT, both the average degree of euhedralism of plagioclase and hornblende and the abundance of perfectly smooth euhedral faces correlate inversely with the intensity of flow structure, even among rocks lacking any apparent protoclasis. As a result, the abundance and perfection of smoothly planar-bounded interstitial textures also increases as flow structure decreases. Beautifully planar-bounded interstitial areas occupied not only by quartz and K-feldspar, but also by sphene, epidote, chlorite, zeolite (chabazite?), and rarely muscovite and calcite, are common in the least foliated or lineated rocks in the central and southern parts of the SPT. Figures 42 and 43 compare the textures in a sample showing very weak foliation and no protoclasis with those in a sample showing moderately strong foliation, but again no protoclasis.

Quartz and biotite show additional textural variations correlated with the intensity of flow structures. In the rocks showing little or no flow structure, large patches of quartz are frequently equant and often consist of only one or two large extinction domains. As the intensity of flow structure increases, the number of extinction domains in the patches also increases, although some large single grains generally remain. In the most strongly foliated or lineated rocks along the northern margin of the PHbT, and in the wedge of SPT penetrating the wall rocks south of Willow Creek Canyon, much of the quartz occurs as aggregates flattened parallel to flow structure.

In the foliated and lineated rocks, biotite is anhedral, molded around and between other minerals, and commonly penetrates raggedly into

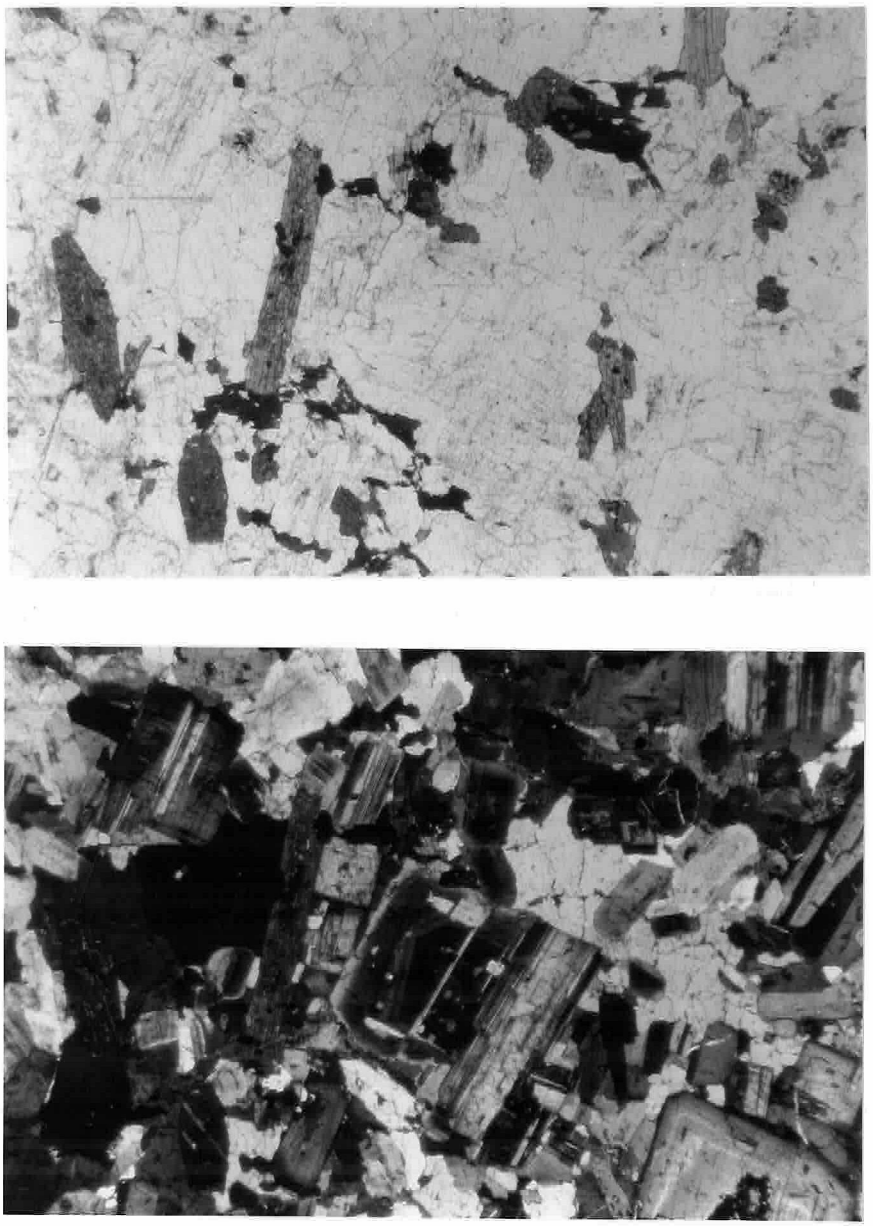

Figure 42. Photomicrographs of the seriate porphyritic tonalite showing very weak foliation and no protoclasis. Upper photo, plane light; lower photo, same view in crossed nicols. Note the abundance of euhedral hornblende and plagioclase crystals, the euhedral zoning patterns in plagioclase, and the large single poikilitic grain of quartz (light gray grain in right center of lower photograph). Sample Ba-JM-639, from the arroyo called El Alisito, 320 m from the southeastern margin of the pluton (area R-8).

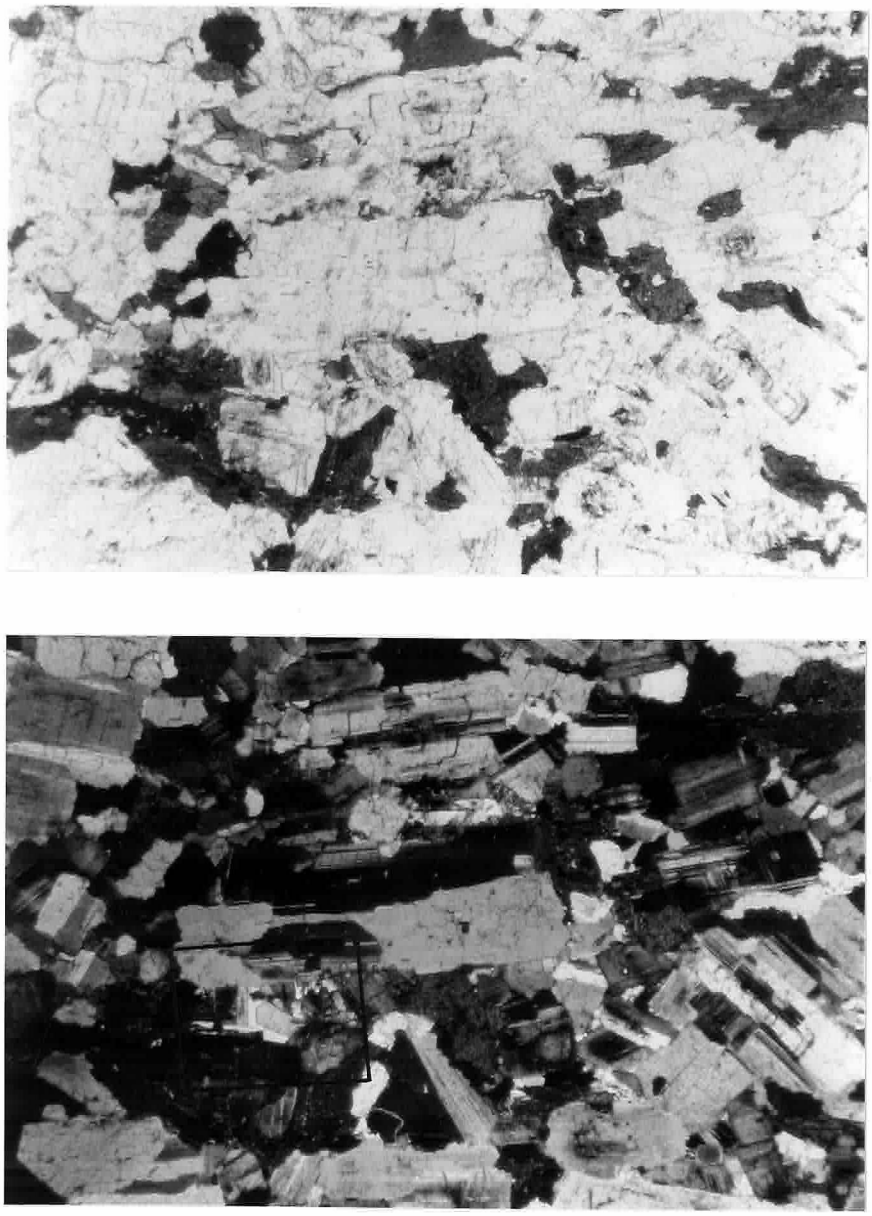

Figure 43. Photomicrographs of the prismatic hornblende tonalite showing moderate foliation, but no protoclasis. Upper photo, plane light; lower photo, same view in crossed nicols. Note the alignment, slightly ragged subhedral to euhedral form, euhedral zoning, and occasional smooth euhedral faces of plagioclase. In this orientation (thin section cut nearly normal to foliation), hornblende appears mostly anhedral, whereas in other orientations, especially parallel to foliation, slightly ragged subhedral or euhedral prisms are more conspicuous. Identifiable deformation of crystals is entirely lacking. The rectangle outlines the area shown in Figure 44. Sample Ba-JM-240 #52, from the drill hole near the center of the pluton, 3.7 km north of Rancho San José (area I-7).

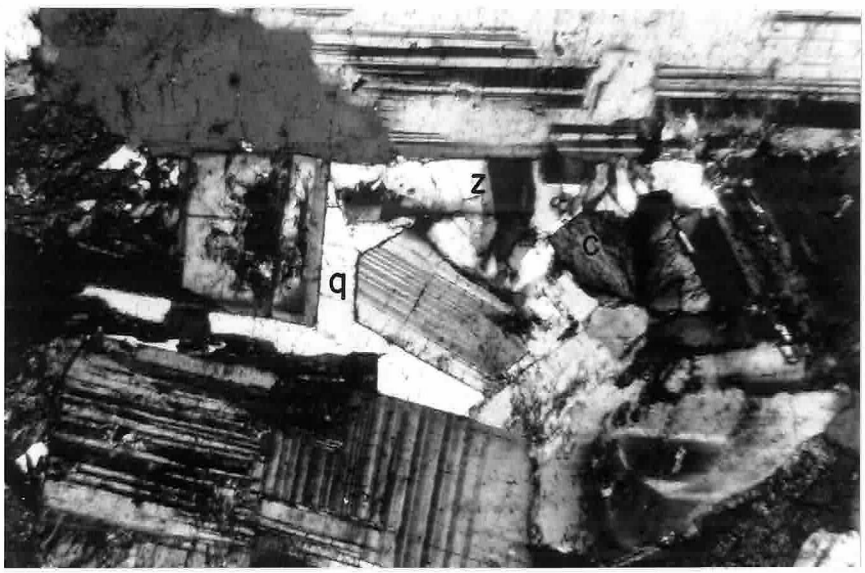

Figure 44. Detail of the area outlined in ink on Figure 43. Cross-polarized light. Smoothly euhedral plagioclase faces bound or project into an interstitial area filled by quartz (q), zeolite (z), and fanning chlorite (c). Note the euhedral zoning in the rectangular plagioclase crystal in the center-left and the complete absence of deformation.

plagioclase and locally hornblende. In contrast, biotite in the least foliated and lineated rocks in the southern part of the pluton is, in most cases, more smoothly molded around these minerals; a few biotite crystals in the latter rocks are subhedral or euhedral.[6]

Despite the clear dependence of textures on the intensity of flow structure, many well-oriented plagioclase crystals (e.g., those in Figure 43) are still nearly euhedral and preserve euhedral progressive and/or oscillatory zoning. These grains show no evidence of recrystallization, except perhaps around the outermost edges, where slight irregularities and interpenetration of crystals may be due in part to minor recrystallization, but are more likely due primarily to interference among crystals during growth. Deformation twinning of plagioclase, bending of crystals, and protoclastic or granoblastic recrystallized groundmass are all conspicuously lacking. In Figure 44, a close-up of a small area in Figure 43, note the two small, strikingly euhedral plagioclase crystals projecting into an interstitial area of quartz, zeolite, and fanning chlorite. All of these textural and zoning characteristics, which are typical of the non-protoclastic foliated and lineated rocks in the PHbT and SPT, provide very little evidence for the degree of recrystallization or mechanical rotation and granulation seemingly required to produce the preferred orientation by solid-state flow. As protoclasis becomes apparent, the principal changes are a slight increase in the raggedness or roundness of grain margins, minor

---

[6]Subhedral and euhedral biotite crystals also occur in some of the more foliated and lineated rocks, especially in the gneissose rocks, but they occur almost exclusively in aggregates resulting from recrystallization. In rocks showing little or no flow structure, subhedral and euhedral biotite crystals commonly occur as scattered grains which formed by direct crystallization from the melt.

bending or fracturing of grains, the appearance of a small amount of fine-grained mortar, partial recrystallization of biotite into aggregates, and the development of secondary twin lamellae in plagioclase.

9.1.4.2 Correlation within the Stubby Hornblende Tonalite and its Gneissose Border Phase

The correlation between textures and the intensity of flow structures is less clear in the SHbT and GBT. Figure 45 covers the range of textures in the non-gneissose SHbT. For comparison with the gneissose rocks, see Figure 31 (p.192). Some bending, fracturing, and granulation is apparent throughout the SHbT, and grain boundaries are correspondingly more ragged or rounded on a small scale than in most PHbT and SPT samples. Secondary twin lamellae are common in plagioclase, and at least incipient recrystallization of biotite into aggregates is ubiquitous. Very minor development of fine-grained granoblastic textures appears to be due to recrystallization of material abraded off the margins of the larger grains. Some granulated material has also undoubtedly recrystallized onto the margins of the larger grains, contributing to the irregularities of the grain boundaries.

Accompanying the protoclastic effects in the SHbT are a variety of deuteric reactions involving not only production of new minerals (e.g., sphene, epidote, chlorite, and sericite), but also some compositional changes in both hornblende and plagioclase. Hornblende crystals exhibit diffuse irregular zoning:[7] vaguely defined, slightly brownish-green interiors are surrounded by blue-green margins of varying width. This

---

[7] A detailed discussion of the zoning characteristics is given in Section 12.5.

Figure 45. Photomicrographs showing the variations in texture of the stubby hornblende tonalite as a function of the intensity of flow structures and protoclasis.

(A, B) Weakly foliated, slightly protoclastic SHbT. (A) plane light; (B) same view in crossed nicols. Note the preferred orientation, slightly rounded or ragged subhedral form and occasional euhedral faces of plagioclase. Zoning of plagioclase is generally weak, but euhedral zoning parallel to the present grain margins is visible in several crystals and indicates that there has been little, if any, recrystallization, except perhaps around the margins of some grains. The molded, poikilitic forms of hornblende and biotite also show little evidence of deformation or recrystallization. Sample Ba-JM-68 from the north-central part of the SHbT, 700 m northeast of Rancho El Coyote (area D-6).

(C, D) Strongly foliated, weakly protoclastic SHbT: I. (C) plane light; (D) same view in crossed nicols. Note the slightly ragged, subhedral to euhedral forms of plagioclase and the preservation of unusually strong oscillatory zoning. Biotite and quartz have been recrystallized into aggregates, but there is little or no evidence of mechanical rotation or recrystallization of the other minerals. Sample Ba-JM-149, 340 m from the northwestern margin of the pluton, 400 m north of the Buena Vista-Coyote road (area D-4,5).

(E, F) Strongly foliated, weakly protoclastic SHbT: II. (E) plane light; (F) same view in crossed nicols. Note the preservation and orientation of an unusual euhedral calcic core in the large plagioclase crystal near the top of the photographs. Most grain margins are slightly irregular, and a few biotite and plagioclase crystals are slightly bent, but there is very little evidence of granulation, mechanical rotation, or recrystallization of grains, with the possible exception of quartz. Sample Ba-JM-492, 160 m southwest of the San José-Observatorio road, ~200 m from the southeastern margin of the pluton (area M-12).

(G, H) Strongly foliated, moderately protoclastic SHbT. (G) plane light; (H) same view in crossed nicols. Grain margins are abraded, some grains are slightly bent, and most plagioclase crystals show only faint diffuse zoning. Nevertheless, most plagioclase crystals grossly retain their original tabular form, and a few, such as the large dark grain in the left center of the photographs, still possess nearly euhedral faces as well as euhedral magmatic zoning parallel to those faces. Sample Ba-JM-453 from Cañon Campo Buena Vista, 540 m from the northeastern margin of the pluton (area H-12).


B


D

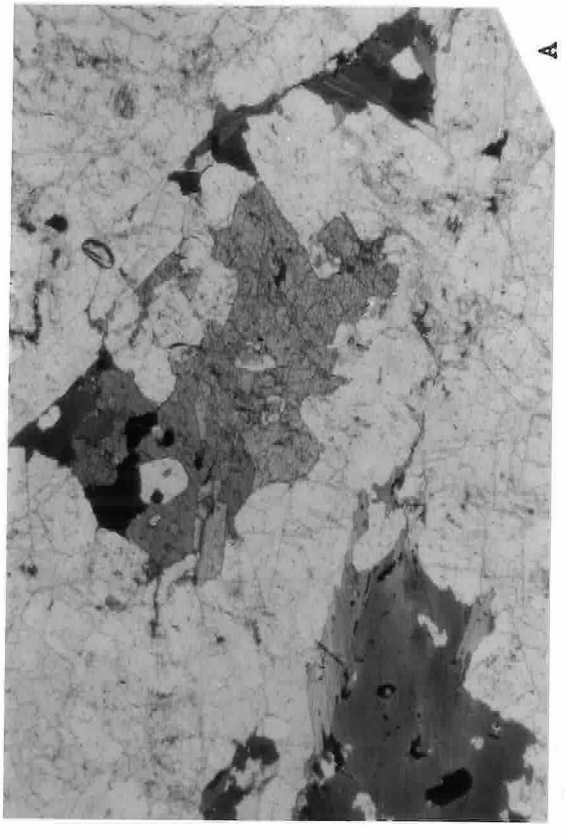
A


C

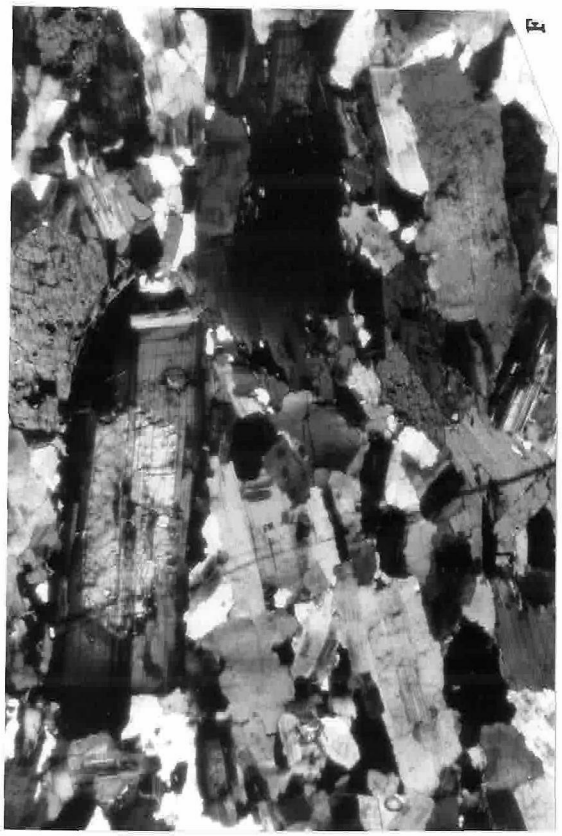

F

H

E

G

zoning does not closely parallel the grain boundaries, but rather projects irregularly into the grains, especially along cleavage directions and microfractures. Narrow blue-green halos also surround inclusions in the brownish-green interiors of hornblende grains. The color differences correlate with a pronounced decrease in the Na and Ti contents and a less striking increase in the Ca and Si contents from the brownish-green interiors to the blue-green rims (see Table 13 and Figure 65). Al^{IV}, total Al, and the Mg/Fe ratio also decrease from core to rim, whereas Al^{VI} increases slightly. Thus, the outer blue-green areas are slightly enriched in the actinolite component. The zoning appears to be an entirely deuteric phenomenon accompanying protoclasis. There is no sign of recrystallization or change of shape or orientation of the grains as a result of the reactions.

Plagioclase in the SHbT also shows several post-crystallization changes besides deformation. Zoning is typically weak and often mottled (the grain in Figure 45D is exceptional) due to partial internal homogenization of primary magmatic zoning, or, in many cases, to partial replacement of the interiors by calcic oligoclase comparable to the rims. However, relicts of original euhedral zoning are generally about parallel to the present subhedral grain margins, indicating that modification of zoning was not accompanied by a change in grain shape. A few crystals in many SHbT samples are veined by sodic to intermediate oligoclase, apparently as a result of shattering of the grains and reaction with fluids penetrating along the cracks. The same phenomenon is noticeable in several unfoliated and unlineated samples of the SPT. There is no suggestion of a significant change in shape or orientation

of the veined crystals.

Despite the protoclastic and deuteric effects, plagioclase in the SHbT is still consistently subhedral, and some crystals have one or more smooth euhedral faces. Smoothly bounded interstitial textures are less common than in the PHbT or SPT, but they occur in nearly all SHbT thin sections. Although subhedral or euhedral hornblende prisms are rare in the SHbT (again Figure 45 C,D is unusual), and the margins of many poikilitic hornblende grains are slightly rounded or abraded, the margins of many others are smoothly molded or interstitial. There is no evidence that protoclasis or deuteric reactions contributed to appreciable solid-state flow or orientation of minerals. Most of the protoclastic and deuteric effects apparently developed after the mineral orientations had been essentially "locked in". Figure 45 C-F shows excellent examples of pronounced mineral orientation accompanied by very little protoclasis and little if any of the deuteric effects.

Traced into the outer gneissose rocks, the main textural changes accompanying increasing foliation and lineation in the SHbT are similar to those in the most foliated PHbT and SPT, but more extreme: (1) increasing rounding and marginal abrasion of plagioclase and hornblende, (2) increasing recrystallization of quartz and biotite into flattened mono-mineralic aggregates, (3) increasing proportion of interstitial granululated matrix, generally extensively recrystallized, and (4) disappearance of planar-bounded interstitial textures. However, there is little or no increase in the bending, fracturing, or recrystallization of plagioclase. Nor is there greater destruction of primary magmatic zoning in plagioclase; rather euhedral progressive and oscillatory zoning appear

to be more common in the GBT than in the interior of the SHbT. Furthermore, many plagioclase crystals preserve subhedral tabular forms and occasional nearly euhedral faces. Thus, many of the primary magmatic crystallization characteristics are still recognizable in the GBT; deformation may have continued while the tonalite was solid, but there is no evidence of low-temperature cataclasis or of extensive metamorphic recrystallization.

9.2 Joints

The principal elements of the joint patterns in Plate 5 are:

(1) joints parallel to foliation (defined here as "concordant joints"),

(2) steeply dipping joints perpendicular to foliation ("transverse joints"),

(3) regional joint systems bearing no consistent relationship to foliation, and

(4) joints whose attitudes show no clear relationship either to flow structures or to regional fracture or lineament directions.

In the classical "granittektonik" system developed by H. Cloos and presented in detail by Balk (1937), two important types of joints are classified according to their relationship to lineation. In the San José pluton, joint patterns show very little systematic relationship to lineation, even where the latter is well developed. Consequently, the classical terms "cross joints" (normal to lineation) and "longitudinal joints" (parallel to lineation) are generally inapplicable, although transverse joints and concordant joints, respectively, are closely

analogous in terms of both structural role and genesis. Other terms defined by Cloos -- i.e., diagonal joints, flat-lying joints and normal faults, and marginal fissures and thrusts -- are directly applicable.

Concordant and transverse joints are consistently developed in the GBT where they contribute strongly to the slabby outcrop patterns (Figure 16, p. 115). Concordant joints are spaced generally at intervals of one half to several meters, whereas transverse joints are several meters apart.

As the intensity of foliation decreases, both concordant and transverse joints become more widely spaced or disappear. Both are generally absent or very sparsely developed in the interior and southern parts of the pluton. As foliation intensity increases towards the SHbT-PHbT contact zone, especially in the PHbT, concordant and transverse joints again become more prominent, but they are seldom less than 2 or 3 m apart.

Concordant joints are locally occupied by quartz or epidote veins or by dikes ranging in composition from mafic to aplitic, but generally they are barren. Being parallel to foliation, concordant joints are normal to the direction of maximum compression and therefore would not be expected to provide ready access for fluids or magma. Transverse joints, which are normal to the direction of maximum extension in the tonalite, are more commonly occupied by dikes and veins. Nevertheless, most transverse joints are also barren. Some dikes and veins occupying concordant or transverse joints are foliated or lineated parallel to the fabric in the host rock (e.g., the granitic dike occupying a transverse joint at locality 302; Plate 5, area H-3,4), indicating that the

joints formed before flow or deformation ceased in the tonalite.

In some cases, transverse joints related to forces originating within the pluton cannot be distinguished unequivocally from tensional joints of regional origin. This is particularly true in the northeastern part of the SHbT, where foliation strikes normal to a regional northeast-southwest joint system well developed in the eastern and southern parts of the pluton and clearly traceable in the country rocks as prominent lineaments for 7-8 km northeast of the pluton. A small swarm of mafic dikes occupies this joint system north of Cañon Campo Buena Vista (mainly area G-11). The unusually pronounced development and physiographic expression of transverse joints (visible as a trellice drainage pattern in Figure 2A, p. 6) and the intrusion of the dike swarm in this area are most likely due to coincidence of a system of regional tensional joints with the local transverse joint direction.

Joints bearing no systematic relationship to flow structures or to regional joint patterns occur throughout the pluton. Most dip at steep angles and can be classed as diagonal joints. Whether they are due to forces originating within the pluton or to external forces is difficult to determine. Flat-lying or shallowly dipping joints and dikes appear to be very sparse throughout most of the pluton. However, because of the bouldery outcrop style of the tonalite and the low relief in many parts of the pluton, shallowly dipping fractures are difficult to recognize, and some have certainly been overlooked. The most pronounced development of shallowly dipping fractures is near the western margin of the pluton, for several kilometers north and south of the

San José-San Telmo road. Numerous small granite, aplite, and pegmatite dikes occurring mainly in the tonalite rather than the wall rocks in this area strike roughly normal to foliation and dip northward at angles generally less than 30°. The fractures which they occupy may be "planes of stretching" in the Cloosian "granittektonik" terminology (Balk, 1937), or they may be local manifestations of regional stresses. Flat-lying joints are also well developed in both the metamorphic rocks and the diorite-gabbro complex around Willow Creek Canyon southeast of Rancho San José.

Joints and dikes dipping inward at moderate or shallow angles were seen at very few places around the margins of the pluton. The fine-grained, foliated mafic dikes near Rancho Cerro Costilla (area C-9,10; see p. 214) are good examples. Such joints and dikes -- the "marginal fissures" and dikes of Cloosian terminology -- have generally been interpreted as prime evidence of upward motion of plutons past their walls (e.g., Balk, 1937; Balk and Grout, 1934; E. Cloos, 1935), but there is no direct evidence for this interpretation in the case of the San José pluton.

Regionally controlled joints can be grouped into three principal systems striking N 35-60° E, N 30-65° W, and N-S ± 10°, respectively. All three systems, which are generally independent of the orientation of flow structures in the tonalite, are developed in both the pluton and country rocks. They are most conspicuous in the southern part of the area and in the interior of the pluton, where flow structures and concordant and transverse joints are generally weak. The Willow Creek fault zone is an extreme manifestation of the northwestward-

striking system.

Prominent lineament patterns on aerial photographs indicate that the northeastward and southwestward-striking systems are widely developed in both the pre-batholithic and plutonic rocks throughout the San José and surrounding areas. The north-south system is less conspicuous on the photographs more 2-3 km from the pluton. Other fracture and dike systems locally developed in different parts of the pluton are also parallel to regional lineament trends in the country rocks.

The Cañon Socorro fault zone and associated fractures, striking N 10-40° W and varying in dip from moderately westward to vertical, may constitute a more northerly-striking component of the N 30-65° W system, or they may define a fourth regional system. Prominent lineaments, mafic dikes, and minor quartz and epidote veins in the central and western parts of the PHbT, all striking N 20-40° W, may be additional expressions of this system. The dikes and veins are vertical or dip at moderate to steep angles to the west.

Dikes ranging from diorite to aplite and pegmatite follow each of the regional joint systems. Several tonalite dikes, finer-grained but otherwise similar to the host rock, are intruded into the SPT along the northeastward-striking system. Evidence presented in Chapter 5 suggests that offset on the Willow Creek fault zone and related fracturing in the surrounding areas largely preceded, but in part accompanied and followed emplacement not only of diorite, aplite, and pegmatite dikes, but also probably of the Willow Creek pluton. The north-south fracture system was apparently a major factor contributing to the local stoping of large masses of metamorphosed volcanic wacke and pebbly wacke along

the southwestern margin of the San José pluton.

Thus, each of the major intrusive and regional joint systems developed contemporaneously with plutonism. Inasmuch as the pluton appears to be syntectonic, all of the joint patterns, including the concordant and transverse joints which are genetically related to magmatic flow structures, were probably influenced by regional deformation. It is difficult to know what the joint patterns would have been like in the absence of regional deformation.

Chapter 10

MAGMATIC VERSUS SOLID-STATE ORIGIN OF THE FLOW STRUCTURES

10.1 Nature of the Problem

The physical condition of intrusive bodies during the development of planar and linear fabrics -- whether solid rock, crystal-rich magma, or melt-rich magma -- has been a perennial subject of debate. Ramberg (1967, 1970) drew close analogies between the emplacement of batholithic rocks and the buoyant rise of solid, low-density material in centrifuge experiments. He also modeled rise of crystal-free rhyolite magma through the crust and concluded that a highly liquid magma "is too weak to push the country rock aside and widen the channel in dome-like fashion, whereas its high fluidity enables it to move with little resistance in narrow channelways along zones of weakness" (1970, p. 279). He therefore interpreted emplacement of granitic batholiths -- hence, by implication, the formation of flow fabrics -- as the result of buoyant doming of solid, low-density material, but he did not seem to rule out flow and emplacement of batholithic rocks as crystal-rich magmas.

While acknowledging the possibility of solid-state development of flow fabrics, many other petrologists (e.g., Duffield, 1968; Compton, 1955) have interpreted flow structures similar to those in the San José pluton as due to orientation of minerals and stretching of inclusions during magmatic flow, locally with some protoclasis. Duffield observed that the *a* crystallographic axes of plagioclase in the El Pinal tonalite of Baja California are aligned within the plane of foliation, parallel to the lineation of hornblende prisms and triaxial inclusions, even though

the shapes of the plagioclase crystals are now generally biaxial rather than elongate. He (p. 1369) concluded, therefore, that the *a*-axis lineation (and, by implication, the planar flow fabric) "was formed early in the crystallization", when the plagioclase crystals *were* elongate, "and was preserved as crystal growth continued".

Pitcher and Berger (1972) presented an interpretation intermediate between those of Ramberg and Duffield. They interpreted the granitic rocks of the Donegal area in Ireland as the products of magmatic emplacement and crystallization, but they pointed out (p. 331) that many structures associated with foliated plutons require that "the ductility of mobile granitic material on *final* emplacement is often little different from that of its country rocks, and that flow can take place at quite a late stage in the crystallization of a plutonic unit". They, like Ramberg, argued against analogy of the behavior granitic magmas during final emplacement with the behavior of liquids and concluded further (p. 177) that foliated borders of plutons "are, for the most part, formed in the solid state" by strain and recrystallization of grains and intergranular flow, perhaps greatly aided in some cases by minor amounts of interstitial melt or late volatiles. Many of the types of structures which led them to this conclusion are also conspicuous in the case of the San José pluton: e.g., foliation crossing schlieren, crossing dikes which are intruded into the pluton, and crossing contacts among intrusive units within the pluton (PHbT-SPT contact zone in general, and the SHbT-PHbT contact zone in local areas); foliation locally oblique to the pluton contact (southeastern part of the SHbT); foliation locally ignoring minor irregularities in the geometry

of the pluton contact (1.1 km west of Rancho Cerro Costilla); extreme stretching of inclusions in the borders of the pluton; and extreme deformation of the rocks immediately surrounding the pluton.

Indeed, such observations combine to produce an extremely cogent argument in favor of flow late in the crystallization history of the tonalite, when the ductility or "liquidity" of the tonalite was severely limited. The remarkable concordance of the contact and the extreme deformation and attenuation of the wall rocks around the northern two thirds of the pluton are extremely difficult to reconcile with the concept of a highly liquid magma pushing aside the wall rocks. Furthermore, the protoclasis and recrystallization of biotite and quartz in the GBT imply considerable flow when the gneissose tonalite was solid or nearly solid. On the other hand, many structural and petrographic characteristics of the tonalite which will be reviewed in this chapter are equally difficult to reconcile with formation of the flow structures primarily or entirely in the solid or nearly solid state. Any interpretation of the origin of the flow structures must reconcile the latter characteristics with the evidence of limited ductility or "liquidity" of the tonalite during at least the last stages of intrusion and flow. The interpretation must also account for the remarkable north-south asymmetry of the pluton, not only in foliation intensity and relationship to contacts, but also in contact geometry -- hence, in apparent mobility of the magma -- and the correlative change in the style of deformation of the wall rocks.

Three basic questions are involved in interpreting the origin of granitic flow fabrics.

(1) How does one distinguish planar and linear fabrics formed by orientation of crystals in a flowing magma from those produced by solid-state deformation and recrystallization?

(2) If the fabric was principally or entirely of magmatic origin, at what stage of crystallization did the observed mineral orientations first develop? Does the development and/or preservation of flow structures require flow of a crystal-rich system?

(3) What is the relative importance of externally imposed regional deformation *versus* emplacement in producing flow structures? Does the formation of pronounced flow structure require syntectonic intrusion?

Much of the difficulty in answering the first two questions arises because solid-state flow may follow magmatic flow as part of a continuous flow history, and there are no clear criteria for distinguishing when one ended and the other began. Furthermore, if solid-state deformation unrelated to emplacement is superimposed on a pluton, the resulting flow may occur parallel to an earlier intrusive flow structure and may obscure that structure by further enhancing it.

As recognized by Pitcher and Berger, another difficulty arises in defining what is meant by flow in a "solid or nearly solid state". Little is known about the rheological properties of crystal-rich magmas, except that viscosities increase rapidly as crystallization proceeds, and the magmas do not behave as Newtonian fluids (Shaw et al., 1968; Murase and McBirney, 1973). Therefore, although the sorts of structural observations cited by Pitcher and Berger as evidence for flow of "mobile" granitic material in a "solid or nearly solid state" seem to require

that flow occurred when the granitic material was highly viscous and plastic, the observations do not prove that the material was solid; it seems very plausible that a crystal-rich granitic magma could possess the required physical properties. Indeed, Waters and Krauskopf (1941) presented numerous reasonable, if not wholly conclusive, arguments that some interstitial melt may have persisted throughout the development of the broad, intensely gneissose and protoclastic border zone of the Colville batholith in Washington. Nor does the sort of evidence cited by Pitcher and Berger prove that the preferred mineral orientations defining the observed flow structures did not begin to form when the granitic material was still relatively melt-rich and more nearly liquid in behavior. I am not arguing in favor of close analogy with liquid behavior, but only that evidence of flow in an apparently solid or nearly solid state does not eliminate the possibility of more nearly liquid behavior and initial development of magmatic flow structures during earlier stages of emplacement.

The most basic question is not so much distinguishing how much, if any, melt was present during development of flow structures, although that is important, but rather identifying the principal mechanisms of mineral orientation: whether (1) strain and recrystallization of grains plus intragranular flow in a solid or nearly solid state, or (2) relatively strain-free rotation of grains in a magma.

Possible observational criteria for answering this question fall into two categories, structural and petrographic. Pitcher and Berger have questioned whether criteria of either sort, especially petrographic criteria, are capable of proving the presence of a liquid phase during

deformation. This chapter is intended to show that criteria of both sorts can be established which show that the flow structures in the San José pluton developed primarily by rotation of grains in a crystal-rich magma, and were locally enhanced, but not initially produced, by strain and recrystallization of grains and intergranular flow in a solid or nearly solid state. Whether or not melt persisted in the protoclastic rocks throughout the entire period of flow is uncertain.

The approach taken with the petrographic evidence was to first examine the characteristics of the least foliated and lineated tonalite, for which solid-state flow appears highly unlikely, then to trace the changes in these characteristics as a function of progressively increasing development of flow structures. The resulting observations, described in Chapter 9, revealed distinctive petrographic changes, primarily in the most strongly foliated or lineated tonalite, which appear to be sensitive indicators of flow in a solid or nearly solid state. The absence of such changes in many of the rocks showing well developed preferred mineral orientation seems to be cogent negative evidence against solid-state flow in those rocks.

Structural evidence will be discussed first, to show that solid-state flow can be ruled out as a general explanation for the flow structures on the basis of macroscopic observations alone, without recourse to potentially controversial microscopic petrographic observations. The implications of the latter will then be discussed, along with an evaluation of the potential mechanisms of solid-state flow in the tonalite. The role of externally imposed deformation in the origin of the flow structures will be treated in the next chapter.

10.2 The Evidence from Structural Observations

Consider first the possibility that the fabric in the San José pluton originated entirely by solid-state flow. Such flow might be in response to either solid-state diapiric emplacement or post-crystallization regional deformation. The close relationship of the pattern and intensity of foliation in the pluton to the contact geometry and to foliation in the wall rocks is not in itself a convincing argument against solid-state (metamorphic) formation of the foliation in response to regional deformation. If the physical properties of a solid pluton and its country rocks are comparable, then a metamorphic foliation should indeed cut indiscriminately across contacts as, for example, in the case of post-crystallization regional deformation of a pluton which is enclosed in other plutons. However, the San José pluton is surrounded by well-bedded meta-sedimentary and tuffaceous rocks which are relatively water-rich and less competent than the solid tonalite; hence, it appears quite reasonable to suggest that the smoothly curving contact around the northern two thirds of the pluton could have served as an important surface of shearing and tectonic discontinuity during post-crystallization regional deformation. Such deformation would result in a foliation pattern parallel to the contact and decreasing in intensity in both directions away from the contact. Only if the pluton contact were geometrically irregular, and if foliation in the pluton conformed closely to the contact irregularities, could conformability of foliation be invoked as good evidence of a magmatic flow structure.

On structural grounds alone, there are several arguments against

both proposed mechanisms of solid-state deformation as the principal causes of the foliation and lineations. First of all, the pluton is a composite of two or possibly three intrusive pulses, and the intensity of foliation and protoclasis increases towards the margins of the inner PHbT mass in a manner analogous to, but less pronounced than, towards the gneissose margins of the pluton. Such a multi-pulse emplacement history producing a foliation shell within a foliation shell is difficult to understand in terms of either solid-state diapiric emplacement or post-crystallization regional deformation.

A second argument against solid-state origin of the fabrics is provided by the north-south asymmetry of the pluton. Both solid-state diapiric emplacement and post-crystallization regional deformation should have produced similar deformation around the entire margin of the pluton. Furthermore, the foliation pattern in the tonalite should be roughly symmetrical around the geographic center of the pluton. Neither condition is met in the case of the San José pluton.

Several smaller-scale, local structures are also more readily interpreted in terms of magmatic rather than solid-state flow. The sharp truncation of one foliation direction by another was discussed earlier. In many cases, both foliation directions are comparable in intensity and in the degree of crushing and/or recrystallization, if any. Such local variability of flow direction is most easily understood in terms of a magma which is sufficiently crystal-rich so that large masses can retain a fabric while the minerals and inclusions in the surrounding areas are reoriented without noticeable crushing or

recrystallization. The mobility implied by small-scale swirling of gneissose foliation in a few areas around the pluton margins also seems more consistent with flow of a crystal-rich magma than of a solid rock.

Undeformed, unreacted inclusions of thinly bedded meta-sedimentary rocks identical to the metamorphosed silty mudstones and tuffs around the northern and eastern margins of the pluton are scattered very sparsely throughout the weakly foliated interior of the PHbT. These inclusions, which are frequently 1-2 m wide and several meters long, are invariably oriented with their long axes parallel to the host-rock foliation. Rotation of the inclusions into parallelism with foliation, without noticeable deformation or recrystallization of either the inclusions or the tonalite, requires that the latter was much more mobile and deformable than the inclusions. This condition can seemingly be satisfied only if the tonalite were partially molten.

Orientation of recrystallized mafic inclusions parallel to host-rock foliation has also been used as evidence for the magmatic origin of foliation (e.g., Cloos, 1937; Billings, 1972). Billings (p. 379) cautioned, however, that stretching of inclusions accompanying development of a secondary (solid-state) foliation "could be so great that inclusions, regardless of their original orientation, might be elongated to such an extent that they become parallel to one another and to the secondary foliation". Such extreme solid-state deformation would seem to require severe deformation and/or recrystallization of the host rock and corresponding destruction or modification of primary magmatic textures and zoning patterns of plagioclase and therefore cannot apparently account for the strong orientation of inclusions parallel

to foliation in much of the non-gneissose tonalite.

The preceding arguments do not completely rule out the occurrence of solid-state flow in the San José pluton. Although the foliation patterns apparently formed principally in response to magmatic flow, deformation apparently continued after solidification of at least the outer parts of the SHbT and PHbT and must have contributed considerably to the development of the gneissosity and lineations in the GBT. Magmatic flow structures throughout the interior of the SHbT have also been slightly enhanced by late magmatic and/or high-temperature subsolidus protoclasis and recrystallization.

10.3 The Evidence from Petrographic Observations

The principal petrographic characteristics which can be invoked as evidence for the magmatic origin of foliation and lineation in the San José pluton are: (1) preservation of hypidiomorphic-granular textures, particularly of euhedral crystal forms and of planar-bounded interstitial textures; (2) preservation of euhedral progressive and oscillatory zoning in plagioclase, particularly of composite synneusis grains identified by multiple centers of zoning; and (3) paucity of recognizable deformational and recrystallization textures, except in the gneissose rocks. These criteria appear most convincing in the PHbT and SPT, but, even in the SHbT, it is possible to see through the minor deformational effects and recognize an original magmatic flow fabric.

I contend that these textural and zoning characteristics are magmatic in origin and would have been destroyed or much more exten-

sively modified by solid-state flow of magnitude sufficient to have produced the observed fabrics. In this connection, the Ardara pluton described by Pitcher and Berger (1972, Chapter 8) is very instructive. This pluton, which is part of the Donegal Granite Complex in Ireland, has many structural similarities to the San José pluton. The pluton has a tear-drop outline, much like that of the San José pluton, and may project downward in a funnel shape. It was emplaced forcefully into sedimentary strata which it displaced laterally and greatly distended. "The outer contact is remarkably sharp, smooth, and free from irregularities" (p. 174). Conformable foliation is strong at the margins and dies out progressively inward. A similar foliation has been imposed on the country rocks. There is even a nearly complete ring-shaped outer "component" (map unit) of foliated quartz monzodiorite surrounding a core of weakly foliated to unfoliated granodiorite and quartz monzodiorite. However, there is one fundamental difference from the San José pluton. In the foliated outer component of the Ardara pluton, the minerals have been extensively recrystallized, and it "seems that the texture as a whole is crystalloblastic and 'metamorphic' in origin" (p. 170). Plagioclase "characteristically lacks distinct zoning" (p. 170). In the interior of the pluton, the mineral relationships "are more normally igneous in character" (p. 171). In the San José pluton, crystalloblastic "metamorphic" textures are conspicuously absent in all but the most gneissose rocks. Even in the latter, recrystallization was restricted mainly to biotite, quartz, and the granulated material scraped off the margins of larger grains. Much of the primary magmatic crystallization texture and the zoning

of plagioclase is preserved.

Pitcher and Berger interpreted the structures and textures in the Ardara pluton as indicative of diapiric emplacement of a crystal-rich magma combined with radial expansion of the pluton in a balloon-like fashion.

> "The conclusion seems inescapable that this planar structure was continuously imposed by deformation of the host throughout the history of the crystallization or recrystallization and while the host was essentially solid. The disappearance of the structure inward and the restriction of cataclasis to the outermost parts indicate to us that the periphery of the pluton was consolidating and being deformed while the center was still mobile and capable of being added to by magma." (p. 177)

The evidence for this conclusion is indeed compelling. The crystalloblastic "metamorphic" textures in the foliated outer component are exactly the types of textures which should be expected to result from extensive flow of solid or nearly solid rock. Except for the much greater extent of solid-state deformation and recrystallization in the outer part of the Ardara pluton, the mechanisms and history of emplacement of the Ardara and San José plutons were apparently quite similar. However, on the basis of evidence from the Ardara and other plutons in the Donegal area, Pitcher and Berger went on to conclude (p. 177) that, in general, foliated borders of plutons "are, for the most part, formed in the solid state". They emphasized (p. 332) "that the granitic rocks which we have used in the preceding pages to argue flow in the solid state are, in general, no different in chemistry, mineralogy, and textural relationships from many other relatively high-level granites". Such an appeal to solid-state flow as a general

explanation of foliation in plutonic rocks[8] seems unnecessary and indeed contrary to the evidence in the case of the San José pluton. The paucity or absence of crystalloblastic "metamorphic" textures in the San José pluton, and in many other foliated plutons, seems to argue against extensive solid-state flow in these bodies, whereas flow of a viscous crystal-rich magma can probably produce many of the features which Pitcher and Berger invoked as evidence of solid-state flow.

Pitcher and Berger suggested that the principal mechanisms of solid-state flow *without apparent destruction of granitic texture* may be strain and recrystallization of quartz and late growth of alkali feldspar. In addition, they suggested that deuteric alteration, deformation twinning, and/or homogenization of zoning in plagioclase, and intergranular flow aided by minor amounts of interstitial melt or late volatiles may contribute. The potential importance of these and several possible related mechanisms in the case of the San José pluton will be considered in the next several paragraphs.

The fact that patches and interstitial areas of quartz commonly consist of several extinction domains, often with slightly undulose extinction, implies some strain and recrystallization. However, except in the gneissose and protoclastic rocks, grains and patches of quartz exhibit ovoid or interstitial, molded, and sometimes branching shapes which differ very little in the rocks showing pronounced mineral

---

[8]Elsewhere, Pitcher and Berger allowed for the presence of a small amount of interstitial melt or volatiles as greatly aiding flow of solid or nearly solid granitic rock, but they continued to emphasize the role of deformation and recrystallization of grains over that of relatively strain-free rotation of grains in a crystal-rich magma.

orientation from those in the fabric-free rocks. These shapes contrast strikingly with the highly flattened, lenticular aggregates characteristic of quartz in the GBT. Strain and recrystallization of quartz clearly contributed to flow of the GBT in a solid or nearly solid state, but not without leaving obvious textural evidence. Much less pronounced flattening and recrystallization of quartz into aggregates is locally apparent in the most strongly foliated, weakly protoclastic rocks around the margins of the PHbT, implying much less extensive flow in a solid or nearly solid state. The general absence of such textures, indeed of any recognizable modification of the primary magmatic shapes of quartz, throughout the rest of the pluton, seems to provide an extremely powerful argument against appreciable solid-state flow in most of the foliated and lineated tonalite.

Late growth of K-feldspar can be ruled out as an important factor in the development of the flow structures because of the negligible concentrations of this mineral -- about 0.2% or less -- in most of the tonalite. On the other hand, late growth of quartz, biotite, and/or rim plagioclase almost certainly did contribute to *late magmatic* flow and orientation of minerals, but only in an indirect manner -- not as an active mechanism of flow -- by contributing to the presence of residual interstitial melt (and/or volatiles) which would have allowed relatively strain-free rotation and orientation of crystals.

Neither deformation twinning nor homogenization of zoning in plagioclase is noticeable in much of the foliated PHbT and SPT. Where partial homogenization of zoning is apparent (mainly in the SHbT) the parallelism of relict primary zoning to the subhedral grain outlines

indicates that homogenization did not change the shape of the crystals and therefore could not have contributed significantly to solid-state flow. Likewise, where deformation twinning is noticeable, a change in grain shape is generally recognizable by bending or fracturing of the grains; in rocks lacking such visible effects, deformation twinning does not appear to have been an important mechanism of mineral orientation.

The contribution of the deuteric formation of new minerals to the development of flow structure also appears to have been insignificant. Even assuming all sphene and epidote to be deuteric, the proportion of deuteric minerals in the tonalite is typically only 2-4%, rarely as much as 6%, and shows little, if any, correlation with the intensity of flow structures. Furthermore, the most volumetrically important alterations -- replacement of biotite by chlorite and of plagioclase by sericite or epidote -- appear to have been essentially pseudomorphic and unaccompanied by strain. On the other hand, recrystallization of biotite into aggregates apparently contributed to late magmatic and/or solid-state flow in the GBT and locally in the outer part of the PHbT. Such recrystallization is minor or absent throughout the rest of the pluton and could not have been a significant mechanism of flow.

In summary, petrographic observations strongly support the conclusion, reached on structural grounds, that foliation and lineation in the San José pluton resulted principally from magmatic flow. Especially in the GBT, but also throughout the SHbT and the outer part of the PHbT, varying degrees of deformation in the solid or extremely crystal-rich magmatic state enhanced the fabric, but also left telltale

textural evidence. Processes such as deformation twinning and homogenization of zoning in plagioclase or deuteric formation of new minerals can be ruled out as important mechanisms of solid-state flow in this pluton. Strain and recrystallization of quartz and biotite also appears unimportant in the non-protoclastic rocks. Recrystallization of both minerals contributed to the enhancement of fabric in the gneissose rocks, but not without leaving a distinctive textural record. Recrystallization of biotite seems to be a particularly sensitive indicator of flow in a solid or nearly solid state. Late growth of quartz, biotite, rim plagioclase, and, locally, K-feldspar were probably important factors in the development of flow structures, but they contributed by permitting mainly late magmatic rather than solid-state flow.

10.4 Some Further Considerations on the Origin of Magmatic Flow Structures

Given that the flow structures formed primarily by magmatic flow, at what stage of crystallization did the mineral orientations first develop, i.e., crystal-rich or melt-rich magma? If preferred mineral orientation develops in a melt-rich magma, it may not be preserved unless mineral orientations can be supported in the absence of continued flow, either because the minerals form an interlocking and self-supporting mesh, or because the bulk viscosity of the crystal-melt suspension becomes sufficient to impede rotation or tumbling of crystals. If bulk flow of the magma ceases or diminishes sufficiently prior to this stage of crystallization, then phenomena such as gravity

settling, local minor flow patterns, and perhaps interference among growing crystals will tend to destroy the early-formed flow fabric. Thus, flow apparently ceased in much of the SPT prior to this stage of crystallization; if preferred mineral orientation developed during earlier flow, it was largely destroyed.

Ramberg (1970) argued persuasively from the evidence of centrifuge experiments that highly liquid granitic magma is too weak and fluid to push aside lithified country rocks and produce broad intrusive bodies such as the San José pluton. The absence of recognizable chilling effects at the pluton contacts also suggests intrusion of magma which already had a large proportion of crystals, particularly in light of the low regional metamorphic grade (hence low ambient temperature) in the wall rocks. Furthermore, the northern two thirds of the pluton exhibit many of the same characteristics which led Pitcher and Berger (1972, p. 331) to conclude that "the ductility of mobile granitic material on <u>final</u> emplacement is often little different from that of its country rocks". On the other hand, both the weakness of flow structures and the extensive stoping and injection of wall rocks in the southern part of the pluton indicate that at least the last magma to rise -- and possibly, in general, the magma rising into the pluton at any given time -- was significantly more ductile than the wall rocks and exhibited more nearly "liquid" behavior. The presence of unreacted inclusions of country rocks scattered sparsely through the interior of the PHbT implies that the magma was sufficiently liquid to allow inclusions several meters in maximum dimension to sink for a considerable distance, possibly several kilometers, in a time too short to

allow modification by the magma. Likewise, the rarity of inclusions in the SPT implies rapid sinking of stoped blocks. Quite possibly, the features indicating low ductility developed primarily after initial intrusion to the present level in the pluton. Moreover, the evidence for low ductility may be somewhat misleading. The Albian-Aptian country rocks are not much older than the tonalite, and the mudstones and tuffs surrounding the northern two thirds of the pluton may have been incompletely lithified -- hence highly plastic and deformable -- at the time of intrusion.

Considerable experimental data published over the past ten years support the interpretation that batholithic magmas, the San José included, are emplaced in the crust as crystal-rich suspensions which maintain their mobility over a wide temperature interval, hence a relatively long time period. Piwinskii (1968a, 1973a, 1973b), and Piwinskii and Wyllie (1968, 1970) have shown that, in the presence of excess water at pressures of 1-10 kb, tonalites and granodiorites melt over broad temperature intervals of 250-300°C. Such broad melting intervals result because the melting temperatures of quartz, K-feldspar, and the albite component of plagioclase are strongly depressed in the presence of H_2O, whereas the melting temperature of the anorthite component of plagioclase is less strongly depressed, and that of hornblende and biotite is affected only slightly (Robertson and Wyllie, 1971; Eggler and Burnham, 1973; Maaløe and Wyllie, 1975). This effect is shown for a biotite granite in Figure 46.

Actually the San José and other batholithic magmas probably did not approach saturation in water until the later stages of crystalliza-

tion. Experiments in water-deficient systems (e.g., Robertson and Wyllie, 1971; Whitney, 1975; Maaløe and Wyllie, 1975) show that, if H_2O is the only significant volatile constituent in the system, decrease in H_2O content below the saturation level causes the liquidus temperature to rise considerably, whereas the solidus temperature remains constant (Figure 46). Hence, the temperature interval of melting would be greater in water-deficient magmas. However, Eggler and Burnham (1973) showed that, in the presence of a volatile such as CO_2, which is relatively insoluble in the melt, H_2O must be partitioned between the melt and vapor phases; under these conditions, both the liquidus and solidus temperatures rise as the ratio of H_2O to CO_2 in the vapor phase decreases, and the temperature interval of crystallization may or may not exceed that of the water-saturated system.

Regardless of whether appreciable CO_2 was present or not, all of the experiments imply that the temperature interval of crystallization of the San José tonalite must have been very broad, at least 250-300°C. This broad interval, together with the early crystallization of much of the plagioclase and hornblende, should have provided the opportunity for a prolonged history of flow of crystal-rich magma -- a history which would seemingly have been ideal for the development and preservation of magmatic flow structures. Whereas flow apparently ceased in parts of the SPT before crystallization had proceeded to the degree necessary to either develop or preserve flow fabric, flow continued into the more advanced stages of crystallization in the more foliated rocks, perhaps locally continuing after all melt had crystallized. Unfortunately, there is no obvious way to quantitatively estimate the relative proportions

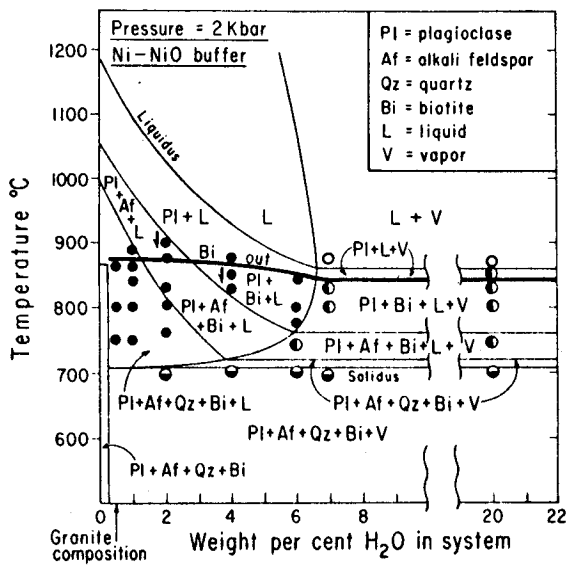

Figure 46. "Experimental results for (*biotite*) granite MG-1. ... Each experiment included two samples, one with crushed rock, and the other with crushed glass. Note the boundary between phase fields with vapor (run circles open or partly open) and those without vapor (run circles closed). The heavy line is the upper stability limit of biotite; we have not determined its position for less than 1% H_2O, nor how it reaches the subsolidus vapor-absent assemblage. The vertical arrows identify runs held first in the field of liquid. The subsolidus assemblage, listed as Pl + Af + Qz + Bi, must include as well the dehydration products of biotite, which decreases from 5.2 modal % to 0% as H_2O in the system decreases from 0.2% to 0%." From Maaløe and Wyllie (1975, Figure 1).

of crystals and melt in the magma at any stage of intrusion and flow.

Analogy with the experimental data suggests one further generality about flow structures in plutonic rocks. The compositional sequence from tonalite to granite is characterized by a progressive decrease in the proportions of hornblende (and/or clinopyroxene) and calcic plagioclase and a simultaneous increase in the proportions of quartz, K-feldspar, and sodic plagioclase. Because granites and quartz monzonites consist almost entirely of phases whose melting temperatures are depressed to similar degrees by the presence of H_2O, the temperature interval of melting is much narrower -- 50-150°C at 1-10 kb under water-excess conditions -- than for tonalites and many granodiorites under the same conditions -- generally 250-300°C (Piwinskii, 1968a, 1973b; Piwinskii and Wyllie, 1970; Stern et al., 1975). This difference should also hold, although perhaps to a lesser degree, in water-deficient systems. Hence, one might expect a general decrease in the development and preservation of *magmatic* flow structures in the sequence from tonalite to granite, provided that one compares only plutons emplaced under comparable structural and tectonic conditions. Unfortunately, I am not aware of sufficient data to satisfactorily test this suggested correlation.

10.5 Origin of the Schlieren

Four hypotheses can be proposed for the origin of the schlieren: (1) extreme stretching and recrystallization of inclusions, (2) gravitational segregation of minerals, (3) deformation and partial recrystallization and assimilation of dikes intruded before complete solidification

and cessation of flow in the host tonalite, and (4) size-dependent sorting of crystals in a flowing magma. Consider these hypotheses in sequence.

(1) Derivation from inclusions

Dioritic inclusions generally <20 cm long and elongate <3:1 are abundant in some schlieren-rich exposures in the PHbT. The inclusions vary from ellipsoidal to angular; most are sharply bounded, but some are diffuse. I recognized no such correlation of the abundances of schlieren and inclusions in the SHbT. Other than this local spatial association, I found no evidence of a direct genetic relationship between schlieren and inclusions. The consistent textural similarity of the schlieren to the host tonalite suggest that the textures in the schlieren formed by magmatic crystallization rather than by deformation and recrystallization.

Strong arguments against the first hypothesis for the origin of the leucocratic schlieren are: (1) the inability to account for discordant leucocratic layers of similar character to the schlieren, (2) the extreme rarity of leucocratic inclusions in the pluton, and (3) the rarity of appropriate potash-poor leucocratic country rocks. Table 4 shows rough calculated chemical compositions for two leucocratic schlieren from the SHbT -- sample 51b, collected 300 m south of Rancho Cerro Costilla (area C-9), and sample 835a, collected 400 m southwest of Rancho El Molino (area E-5). The average composition of four analyzed leucocratic schlieren from the Lakeview Mountains pluton in southern Alta California (Morton et al., 1969) is shown for comparison. The calculated compositions are based on visually estimated modes from one thin section of each sample and upon the assumed mineral

Table 4

Estimated Compositions of Leucocratic Schlieren from the Stubby Hornblende Tonalite Compared with Analyzed Leucocratic Schlieren from the Lakeview Mountains Pluton in Southern Alta California

	Ba-JM-51b*	Ba-JM-835a*	Leucocratic Schlieren Lakeview Mountains Pluton Mean of 4 samples**
SiO_2	72.8	63.8	63.54
Al_2O_3	15.0	20.9	23.91
FeO_t	1.7	1.9	0.68
MgO	0.6	0.5	0.41
CaO	4.9	6.7	7.72
Na_2O	4.1	5.8	3.62
K_2O	0.4	0.3	0.45
TOTAL	99.5	99.9	100.33

*Based on visual estimates of modes, plus the following assumed mineral compositions:

Plagioclase: $An_{35}Ab_{64}Or_1$

Hornblende: composite of 50% average core composition and 50% average rim composition of hornblende in the SHbT

Biotite: average composition of biotite in the SHbT (Table 17)

K-feldspar: average composition of K-feldspar in the pluton (Table 11)

Opaques: assumed 50% pure magnetite plus 50% pure $hem_{50}ilm_{50}$ solid solution

Epidote: assumed analysis No. 3, Table 8 in Deer et al. (1966)

Chlorite: assumed analysis No. 3, Table 21 in Deer et al. (1966)

Sphene, muscovite, and apatite: assumed pure stoichiometric compositions

**From Morton et al. (1969, Table 3)

compositions given at the bottom of the table. Sample 835a is petrographically typical of most leucocratic schlieren in the SHbT; leucocratic schlieren in the PHbT are generally similar, although some contain slightly more quartz and less plagioclase than 835a. Sample 51b is unusually quartz-rich, but is otherwise similar.

Two features of the calculated analyses are especially striking: (1) the unusually felsic compositions considering the moderately high CaO/Na_2O ratio and (2) the extremely high Na_2O/K_2O ratios. Other than having a higher CaO/Na_2O ratio (i.e., higher anorthite content of the plagioclase) and a slightly lower FeO_t content, leucocratic schlieren from the Lakeview Mountains pluton are chemically very similar to sample 835a. This is not surprising, inasmuch as my brief field observations in the Lakeview Mountains pluton indicate that the leucocratic schlieren are megascopically very similar in both masses, and, except for being slightly more mafic and coarser grained, the typical Lakeview Mountains tonalite is texturally and mineralogically much like the SHbT. The higher CaO/Na_2O ratio in the Lakeview Mountains schlieren is also not surprising, since the average tonalite in the Lakeview Mountains pluton has a markedly higher CaO/Na_2O ratio (6.88/2.62; Morton et al., 1969, Table 1) than does the average SHbT (6.40/4.73; Plate 9A).

Concerning the differences between schlieren and inclusions, Pabst (1928, pp. 349-350) made the following observations which seem to apply nearly as well to the San José pluton as to the granitic rocks of the Sierra Nevada which he studied:

"(1) The autoliths[9] are always more basic than the surrounding rock, while the schlieren may be either more basic or more acid.

(2) The autoliths usually have sharp boundaries, and the schlieren do not.

(3) The constituents of the autoliths are characteristically much finer than those of the enclosing rock; the schlieren have the same grain sizes as the host rock.[10]

(4) Autoliths in generaly show a much greater concentration of hornblende than biotite and this feature is lacking in the schlieren."

(2) Gravitational segregation of minerals.

This hypothesis cannot be ruled out, but there is little evidence to support it. Systematic grain-size or heavy-mineral-concentration grading is rare, except in some leucocratic schlieren in the SHbT. Schlieren have steep dips, often vertical, and are almost always parallel to foliation. If they formed by gravitational accumulation, they must be relict features which have been reoriented by extensive flow; in that case, there would be no reason to expect them to be parallel to magmatic flow foliation unless they were completely smeared out during flow. Also, sparse crosscutting leucocratic layers and some concordant leucocratic schlieren were apparently intruded into the host rock, and therefore could not have formed by gravity sorting (see next paragraph.

---

[9]Dioritic inclusions in the San José pluton are autoliths by Pabst's criteria. Rare leucocratic inclusions in the SHbT probably also qualify as autoliths and therefore indicate that the statement "always more basic" is not strictly true for the San José pluton.

[10]In the San José pluton, leucocratic schlieren tend to be slightly finer grained than the host rock, but Pabst's distinction is still basically applicable.

(3) Deformation and partial recrystallization or assimilation of dikes.

Deformed and discordant leucocratic layers petrographically similar to leucocratic schlieren were apparently intruded into the host rock. A few leucocratic layers, for example, the deformed layer in Figure 47, are discordant along part of their length, but change orientation abruptly and become concordant. If only the concordant segment were seen, it would qualify as a typical schlieren, and there would be no clue to the intrusive relationship. Thus, some leucocratic schlieren are modified dikes, but they are small compared to most dikes and probably did not move very far. Perhaps some mafic schlieren are also modified dikes, but this hypothesis seems unreasonable as a general explanation, especially for the swarms of thin schlieren which dominate some outcrops (Figure 37, p. 208). Mafic schlieren are texturally similar to the host tonalite, but very different from most dikes. I saw no evidence of partial recrystallization of mafic dikes leading towards a texture like that in the schlieren. Furthermore, mafic schlieren are consistently concordant, yet foliation planes are unlikely loci for dikes, because compression rather than tension prevails across them during flow. Some other mechanism must therefore account for most schlieren.

(4) Size-dependent sorting of crystals in a flowing magma.

Wilshire (1969 , pp. 256-259) attributed minerals layers in the Twin Lakes granodiorite in Colorado to size-dependent segregation of crystals in a dense magmatic suspension undergoing shear flow. By analogy with the experimental results of Bhattacharji and Smith (1964)

and Bhattacharji (1967), Wilshire suggested that coarser crystals tend to migrate to regions of low shear stress, leaving behind concentrations of smaller crystals. As discussed in Section 7.6, such a mechanism appears to be the most reasonable explanation for the block of mafic-layered tonalite in the San José pluton.

A flow-sorting mechanism also seems consistent with the characteristics of the schlieren. Parallelism to foliation and similarity of textures and mineral characteristics in the schlieren and host are natural consequences of the process. Likewise, the paucity of schlieren in the SPT is logical, because flow foliation is nearly absent in that mass. In the SHbT, leucocractic schlieren are definitely slightly finer grained than the host rock, and mafic schlieren are of comparable grain size or possibly slightly coarser than the host. Furthermore, some leucocratic schlieren in the SHbT are sharply bounded, finer grained (1-2 mm), and very leucocratic on one side, but grade continuously by increasing grain size and mafic content into the host rock on the other. Such asymmetric schlieren argue very strongly for *in situ* segregation of felsic constituents from the magma. The interlayered leucocratic and mafic schlieren in Figure 48 are a rare and remarkably beautiful example of sorting of the magma into finer-grained leucocratic and coarser-grained mafic schlieren.

The development in many outcrops of either leucocratic or mafic schlieren without equivalent development of the counterpart must be a function of the ratio of the area of a given schliere to the area of host rock from which the schliere drew its constituents. For example, segregation of a leucocratic schliere several centimeters wide

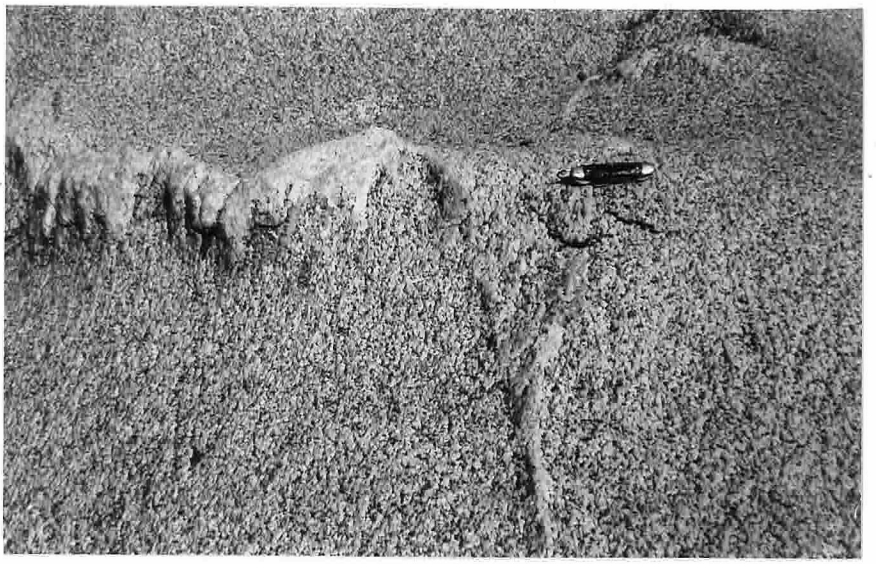

Figure 47. Deformed leucocratic schlieren in the stubby hornblende tonalite. The resistant leucocratic ridge in the upper left is oblique to foliation and is deformed along planes parallel to foliation. Near the pocket knife the schliere bends abruptly and assumes the thin concordant form typical of most leucocratic schlieren. Locality: 250 m from the northwestern contact of the pluton, ~700 m north of the Buena Vista-Coyote road (area D-5).

Figure 48. Unusual interlayered leucocratic and mafic schlieren in the stubby hornblende tonalite. Locality: 8 m east of the small zone of diorite and inclusion-rich tonalite near the inner margin of the SHbT, 200 m east of the San José-Observatorio road and 4.1 km east-northeast of Rancho San José (area K-11,12).

from a layer of crystal mush of twice that width would produce a conspicuous mafic counterpart (as in Figure 48), but segregation of the same schliere from a 1-m-wide source layer would leave behind only a faint or unrecognizable concentration of mafics.

As mentioned earlier, discordant leucocratic schlieren and some concordant leucocratic schlieren apparently formed by intrusion of melt-rich segregations into the immediate host rock. It is also possible that some leucocratic layers formed by local segregation of melt-rich material along early-formed joints in the crystal mush, rather than by injection; Morton (1969, pp. 1549-1550) invoked the latter origin for conjugate sets of discordant schlieren in the Lakeview Mountains pluton. However, the extremely low K_2O content of most of the concordant leucocratic schlieren is difficult to reconcile with formation of these schlieren from melt-rich segregations. Furthermore, the unusually pronounced planar mineral orientation in most concordant leucocratic schlieren in the SHbT suggests rotation and close packing of crystals to the virtual exclusion of melt (although development of preferred orientation should also have been enhanced by the paucity of large equant mafic crystals; in the host rock such crystals tend to disrupt orientation of plagioclase tablets). Quite possibly, there are two types of leucocratic schlieren -- those formed from melt-rich segregations containing finer-grained plagioclase and quartz crystals, and those formed from melt-poor concentrations of the same finer-grained minerals. Solution of this problem requires more extensive chemical and petrographic study.

Chapter 11

MECHANISMS AND HISTORY OF EMPLACEMENT OF THE PLUTON

11.1 Mechanisms of Emplacement

All of the structural characteristics of the pluton can be explained by a relatively simple model invoking syntectonic multiple emplacement of crystal-rich magmas, with progressive expansion outward and preferentially northward and eastward in a balloon-like fashion in response to (1) a prolonged history of magmatic up-welling in the interior and southern parts of the pluton and (2) emplacement of the SHbT around the margins of the PHbT.

The SHbT and PHbT formed in two pulses emplaced almost entirely by forceful shouldering aside of the wall rocks, accompanied by severe distension and penetrative deformation of the strata, particularly around the northern and eastern contacts.

The SPT was intruded either as a continuation of the PHbT intrusive pulse or as a third pulse utilizing essentially the same conduit up which the PHbT magma rose, although the position of this channelway apparently migrated slightly southward with time. Emplacement of the SPT involved both forceful shouldering aside of the wall rocks (along the southeastern margin) and large-scale stoping (primarily along the southwestern and southern margins). Again expansion was mainly to the north (into the partially molten interior of the PHbT) and east; lesser expansion to the south and southwest involved fracture-controlled stoping or "breaking out" of the SPT magma from the concordant confines of the rest of the pluton. Although eastward expansion

of the SPT must have caused some distension and penetrative deformation of the wall rocks along the southeastern contact, deformation of the wall rocks accompanying intrusion of the SPT was primarily by brittle fracture. There is no evidence that emplacement of the SPT caused any penetrative deformation of the wacke and volcanic rocks along the southwestern contact; in fact, the contact truncates metamorphic foliation as well as fold axes and bedding in the wacke.

Altogether, stoping can account for no more than 5-10% of the exposed area of the pluton. The remaining 90-95% or more of the area developed by concordant separation and distension of the strata. Injection and assimilation of the wall rocks around the northern two thirds of the pluton were very slight, being restricted mainly to the narrow zones of diorite and inclusion-rich tonalite between the PHbT and SHbT, and perhaps including some material in the mafic sheets and other smaller dioritic masses intruded into the pre-batholithic rocks immediately east of the pluton. Even around the southern third of the pluton, where stoping and injection were more extensive, evidence of reaction with the wall rocks is local and generally negligible.

On the basis of photogeologic mapping and reconnaissance ground observations, Gastil et al. (1971, 1975) interpreted the San José and many other subcircular plutons in Baja California as the products of *en masse* diapiric emplacement. Certainly, the subcircular geometry and the concordance and deformation around the northern two thirds of the pluton may be superficially suggestive of *en masse* diapiric rise of an ovoid or cylindrical body; however, the pattern of flow structures, the evidence of multi-pulse intrusion, and the asymmetry of deformation

in the wall rocks all seem incompatible with such a mechanism of emplacement. Rather, the northward-lobate, funnel shaped pattern of foliation in the tonalite indicates that the magmas rose through relatively narrow channelways and expanded preferentially northward in a balloon-like fashion after reaching approximately the final level of emplacement. Inasmuch as the concept of *en masse* diapiric emplacement is not applicable to the San José pluton, one of the few bodies mapped in any detail, its applicability to other subcircular plutons in the batholith must be considered uncertain until tested by more detailed individual examination. However, this does not mean that the San José and other plutons are not diapiric masses in the broad sense of the term. To the extent that it refers simply to forceful piercement of material through the overlying rocks, not necessarily by *en masse* movement, the diapiric concept is certainly applicable.

11.2 A Model for the History of Emplacement and the Development of the North-South Structural Asymmetry

Figure 49 illustrates the most reasonable interpretation of the emplacement history of the pluton. Reconstruction of the original geometry above the present level of exposure is entirely schematic. I do not know how far the SHbT extended across the roof of the body. If analogy with Ramberg's (1967) centrifuge models of viscous solid diapirs is at all valid, the roof of the pluton may have been fairly flat, and the transition from roof to steeply dipping walls may have been relatively rapid, but whether the roof of the northern two thirds of the body was smoothly domal and concordant, as drawn, or highly

Figure 49. Generalized illustration of successive stages in the emplacement history of the pluton. Upper sequence, plan view; lower sequence, north-south profiles along the vertical plane A-A'. Sequential intrusive units 1, 2, and 3 correspond to the PHbT, SHbT, and SPT, respectively. Arrows within the pluton indicate the amount of expansion of the pluton in various directions. The patterns of short arcuate lines show the orientation of magmatic foliation. Continuous lines in the wall rocks represent the generalized trends of bedding; more detailed interpretations of the evolving structure in the wall rocks are given at the end of this chapter (Figures 50 and 51). The heavy southward- and southwestward-pointing arrows in the plan views represent suggested directions and relative magnitudes of deformation superimposed on the pluton. The line of dots along the northeastern margin of the PHbT denotes areas where the PHbT complexly intruded and partially assimilated mafic intrusive rocks and minor(?) marble, wacke, and tuffaceous mudstone to produce the zones of diorite and inclusion-rich tonalite.

Reconstruction of the original geometry of the pluton appreciably above or below the present level of exposure is schematic, and the vertical scale is intended as suggestive only. Relatively rapid pinching down of the pluton to a narrow root zone under the southern half of the body is suggested by the arcuate, funnel-shaped pattern of flow structures and the evidence for the rise of the magmas through relatively narrow channelways and preferentially-northward balloon-like expansion at essentially the final level of emplacement. A combination of structural, metamorphic, and phase equilibrium considerations suggests that the rocks in the west-central part of the pluton were originally emplaced at a depth most likely in the range 3-9 km (Section 15.2.4). A depth of approximately 7 km was therefore chosen for this illustration. Two possible corresponding positions and orientations of the generalized syn-intrusive land surface are shown in the final profile, one (solid line) assuming that the syn-intrusive surface was roughly parallel to the present surface, and one (dashed line) assuming 10° of post-intrusive southward tilting of the pluton and allowing thereby for a possible difference in the original depth of emplacement of up to 3 km from north to south (southern end shallower). It is important to recognize that even an original depth of 7 km implies a relatively rapid upward change in the geometry of the pluton, i.e., a nearly flat roof, unless the pluton extended upward essentially all the way to the original land surface. The detailed geometry of the roof, whether smoothly domal and concordant or highly irregular and discordant, is conjectural, as is the nature of the structure in the wall rocks above the pluton.

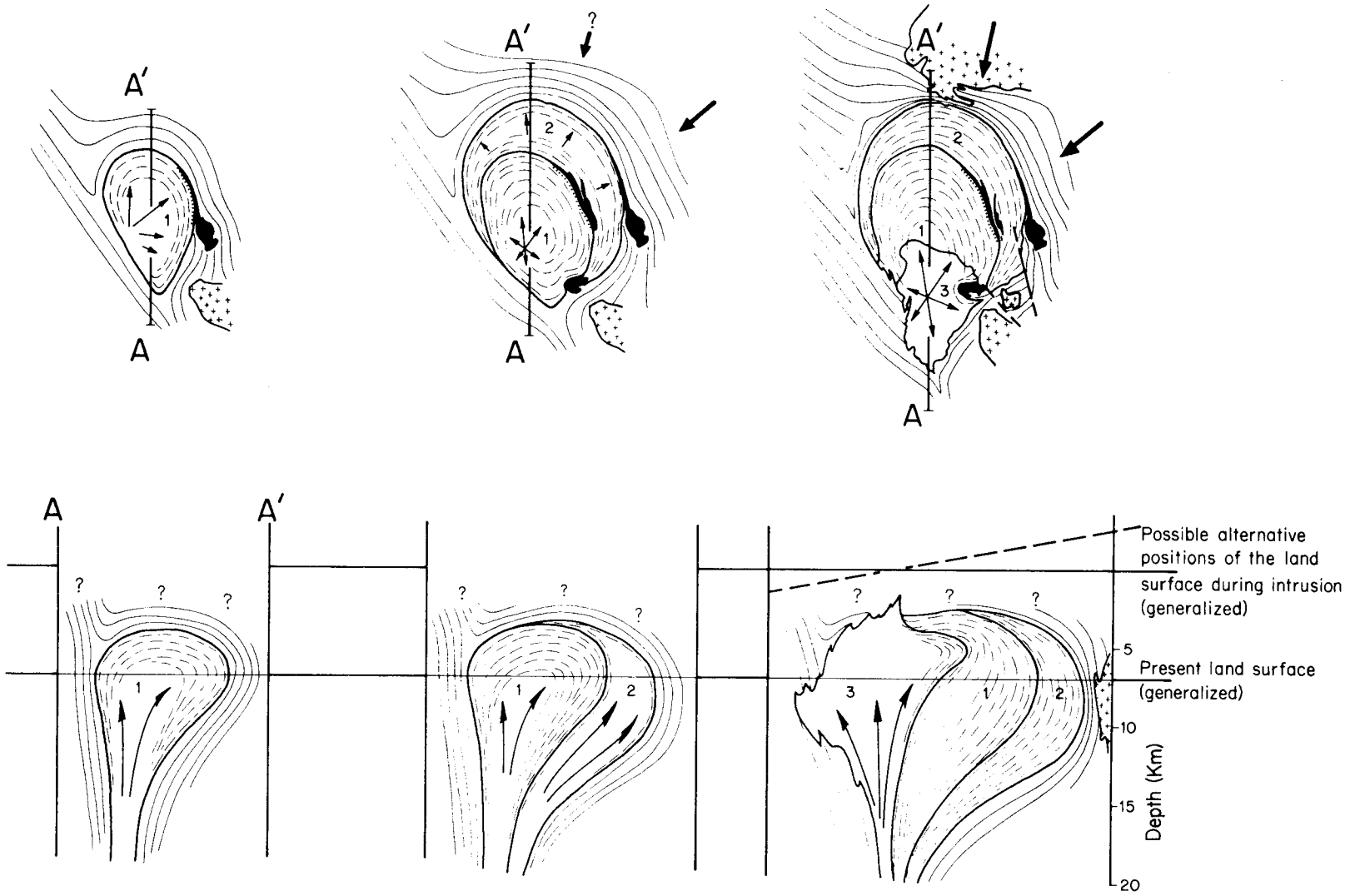
A′
A
1
2
3
?
A
A′
Possible alternative positions of the land surface during intrusion (generalized)
Present land surface (generalized)
5
10
15
20
Depth (Km)

irregular and discordant is conjectural. The shape of the body at depth is also uncertain, the hypothesized pinch-down to a relatively narrow root within the crust being based upon (1) the evidence that the magmas rose through relatively narrow conduits and expanded in a balloon-like fashion at essentially the final level of emplacement and (2) the assumption that the funnel-shaped pattern of magmatic flow recorded by the foliation patterns reflects at least crudely the changing geometry of the intrusive contacts at depth.

It is important to emphasize that, although the pluton was emplaced in two or possibly three major intrusive pulses, emplacement should not be viewed as a sequence of separate events distinct in time. Rather, the field data indicate emplacement of all three textural units of the tonalite within a very short time span, with flow and crystallization in part overlapping. This interpretation is supported by U-Pb isotopic age determinations by L. T. Silver on zircons from two samples: 111 ± 2 m.y. for sample BC-I-5 from the gneissose border phase of the SHbT and 112 ± 2 m.y. for sample BC-I-12 from the transitional zone between the SPT and PHbT.

As shown in Figure 49, intrusion apparently began with a pulse of PHbT magma expanding principally northward and eastward and developing an arcuate foliation pattern increasing in intensity towards the walls. Injection and assimilation of wall rocks -- mostly (?) diorite, plus some marble, pebbly wacke, and tuffaceous mudstone -- produced a zone up to 200-300 m wide of diorite and inclusion-rich tonalite and quartz diorite along much of the eastern side of the PHbT and was probably responsible for the presence of minor tonalite and quartz diorite in

the two intrusive sheets connecting the San José pluton to the mafic complex of Cañon La Jolla. Very slight injection and assimilation of marble and pebbly wacke also occurred along the northwestern margin of the PHbT (1-2 km west of the North-South road), and minor stoping of wall rocks gave rise to sparse blocks of metamorphosed thin-bedded mudstone and calc-silicate rock scattered through the interior of the PHbT, but stoping, injection, and assimilation of wall rocks were very minor, overall.

The PHbT is slightly flattened, with its long axis oriented about N 10° W, approaching parallelism with the regional strike of bedding in the pre-batholithic rocks. The shape of the growing mass was apparently controlled in part by the orientation of bedding and/or by regional tectonic stresses oriented northeast-southwest. However, later intrusion of the SHbT and SPT did not maintain this form, and the long axis of the entire pluton is oriented almost entirely north-south.

While the PHbT pulse was continuing, or shortly after it ceased, SHbT magma was emplaced around much of the margin of the incompletely crystallized PHbT, breaking up the zone of diorite and inclusion-rich PHbT and separating it from the intrusive sheets in the wall rocks east of the pluton. Again an arcuate foliation pattern developed parallel to and increasing towards the margins of the SHbT. At this stage of intrusion, foliation intensity in the SHbT should naturally have increased more towards the contact with pre-batholithic rocks than towards the SHbT-PHbT contact zone for several reasons. (1) The pre-batholithic rocks, being more rigid than the incompletely solidified PHbT, must have provided greater resistance to flow of the SHbT magma.

(2) The SHbT magma must have cooled and crystallized more rapidly against the pre-batholithic rocks than against the hot PHbT, thereby becoming less ductile and more prone to development of strong mineral orientation and stretching of inclusions during flow. (3) Expansion of the SHbT was primarily outward against the pre-batholithic rocks rather than inward against the PHbT; hence, the contact with pre-batholithic rocks must have been the surface of greatest extension and shearing. (4) If regional deformation was superimposed on the pluton at this time, the effects of this deformation must also have been greatest at the pluton contact.

While SHbT magma was being emplaced, it is possible that PHbT magma continued to be added to the interior and southern parts of the pluton, resulting in further expansion and combined flow of the SHbT and PHbT. Eventually, SPT magma welled up in the southern part of the pluton and expanded primarily northward into the interior of the PHbT. Most likely, this was either a third pulse of magma closely related to the PHbT or a rejuvenation of the original PHbT magmatic pulse accompanied by a slight textural change. However, it is also possible that it was simply the continuation of a steady up-welling of PHbT magma which now contained a greater abundance of large plagioclase crystals. In any case, northward and eastward expansion of the SPT magma caused continued extension and flow of the more crystalline northern and outer parts of the pluton. All three textural units flowed together at this stage, resulting in a single coherent pattern of foliation which locally crosses their mutual contacts. Eventually, the SHbT and outer parts of the PHbT became sufficiently solid so that

continued expansion caused fracturing, followed locally by intrusion of dikes and veins, some of which were themselves deformed by further flow. Except in the GBT, this latest magmatic and/or high-temperature solid-state flow resulted in minor protoclasis, but apparently only slight enhancement of earlier magmatic mineral orientation in the tonalite.

During the later stages of the intrusive history, systematic lineation patterns developed in the outer part of the tonalite and in the adjacent wall rocks. The northward-converging lineation system, which formed after development of a downdip magmatic flow lineation in the interior of the SHbT, records squeezing of strata upward and outward from between the San José and Las Cochas plutons, apparently in response either to emplacement of the Las Cochas pluton or to shoving of that pluton southward or southwestward towards the San José pluton during superimposed regional deformation. Squeezing occurred after the outer northern part of the San José pluton had crystallized sufficiently to behave as a rigid mass relative to the adjacent strata; the northern contact of the San José pluton served as a surface of intense shearing and tectonic discontinuity during this squeezing. Protoclasis, recrystallization of biotite and quartz, and development of gneissosity accompanied formation of the lineations, but these phenomena probably began before the development of the lineations.

The northeastward-plunging lineation system also formed while the outer part of the SHbT was solid or nearly solid, but at least in part while the SPT was still partially molten and relatively mobile. The southeastern interior of the SHbT and the adjacent outer part of

of the PHbT also appear to have been partially molten during at least part of the history of lineation development. Protoclasis accompanied formation of this lineation system everywhere except in the southern half of the SPT. If the northward-converging lineation system formed contemporaneously with the northeastward-plunging set, then the former was also contemporaneous with continued emplacement and crystallization of the SPT.

The northeastward-plunging lineations do not seem to be explicable in terms of emplacement of the pluton, but rather appear to record an externally imposed regional deformation, probably directed upward and southwestward from the northeast and east. Regional uplift and/or plutonic intrusion in the Sierra San Pedro Mártir may have been the driving force.

This intrusive history model can readily account for both the northward-lobate, funnel-shaped pattern of foliation and the variations in foliation intensity. Near the axis of the funnel, weak foliation must record primarily upward and outward flow of the magma. Outward and northward from this axis, lateral extension should have become progressively more important, and foliation in the northern two thirds of the pluton and perhaps also along the southeastern margin of the the SPT may have been caused as much or more by progressive horizontal extension as by upward flow of magma past the walls or past outer, more solidified tonalite. Because the pluton expanded preferentially to the north and east, the northern and northeastern margins of both the PHbT and the SHbT suffered the greatest and most prolonged extension and are correspondingly the most foliated. In proportion to the degree

to which extension decreased southward along the margins and inward into the interior of both the SHbT and PHbT, the intensity of foliation likewise decreases. The last magma to be emplaced -- comprising the central and southern parts of the SPT -- was subjected to little or no extension and completed crystallization in a static environment. Consequently, the latter rocks exhibit little or no flow structure.

In an analogous way, the model can also account for the close correlation between the intensity of penetrative deformation in the country rocks and the intensity of foliation in the adjacent tonalite.

The pattern of lineations in the northern half of the PHbT, converging eastward and westward towards the central north-south axis, are also consistent with the oblique flow directions implied by this combination of upward and outward emplacement plus horizontal extension. So is the pronounced development of transverse joints both around the outer margins of the SHbT and along the SHbT-PHbT contact zone. Although these joints could be due to cooling and contraction of the tonalite, they are more readily interpreted as extensional fractures produced during expansion of the pluton. Thus the close correlation between increasing intensity of foliation and increasing prevalence of transverse joints is logical because the development of both structures should have been greatest in those parts of the pluton which were subjected to the most prolonged and severe history of late magmatic and possibly high-temperature subsolidus extension. The paucity of inward-dipping marginal joints, thrusts, and dikes -- features which are generally interpreted as evidence for upward move-

ment of plutons past their walls (e.g., Balk, 1937; Balk and Grout, 1934; Cloos, 1935) -- and the paucity of downdip lineations, particularly in the PHbT, are also consistent with this model. If the pluton continued to rise *en masse* as it expanded, such movement appears to have been of secondary importance in the structural evolution of both the pluton and the wall rocks.

This explanation for the north-south structural asymmetry ignores the effects of externally imposed deformation. Yet such deformation must have contributed not only to the development of gneissosity and lineation in the GBT, but also to the intense deformation of the wall rocks around the northern and eastern margins of the pluton. Indentation in the eastern contact adjacent to the gabbro-diorite complex of Cañon La Jolla, and, to a lesser degree, adjacent to the two intrusive sheets connecting the Cañon La Jolla body to the pluton may have been caused by shoving of the older rigid mafic bodies against the incompletely solidified SHbT during superimposed regional deformation. However, these indentations could also have developed without regional deformation if expansion of the pluton was locally impeded by the older mafic bodies.

The role of externally imposed deformation in the development of fabrics in the interior of the pluton is more difficult to evaluate. Neither the orientations nor the intensities of flow structures appears to require externally imposed deformation, yet the pluton was apparently syntectonic, and it is therefore possible that the fabric is the product of an interplay between intrusive flow and superimposed deformation.

Strong foliation and lineation and minor protoclasis in the wedge

of slightly porphyritic tonalite intruded into the wall rocks south of Willow Creek Canyon are probably also due largely to regional deformation, but these structures die out rapidly southwestward, and weak northeastward- and eastward-plunging lineations in the southeastern part of the SPT developed without accompanying protoclasis. Considering the evidence of severe deformation superimposed on the margins of the pluton farther north, the lack either of protoclasis or of a significant increase in foliation intensity around most of the southeastern and particularly the southwestern margins of the pluton implies either that (1) regional deformation diminished or ceased before completion of crystallization of the SPT, or that (2) the southern end of the pluton was emplaced into an environment largely sheltered from synchronous regional deformation or in which regional deformation was manifested by brittle fracture. Assuming that regional deformation involved a net tectonic flow upwards and southwestward from the northeast, a tectonically sheltered environment might have existed around the southern and particularly the southwestern margins if (2a) the intensity of superimposed regional deformation decreased sufficiently southwestward due to increasing distance from the source of the deforming forces, and/or (2b) the more crystalline and rigid northern two thirds of the pluton acted as a massive buttress or shield against the deforming forces, producing a giant tectonic pressure shadow in the south and southwest. A tectonically sheltered environment could also have existed if (2c) the southern end of the pluton is nearer the original roof of the body, where lower confining pressure might have led to brittle rather than plastic deformation of the wall rocks, and

the crystallizing tonalite might have been subjected to less penetrative deformation.

The first hypothesis, that regional deformation diminished or ceased before completion of crystallization of the SPT, seems at odds with the complete structural and petrographic gradation from the seemingly post-tectonic SPT northward into the syntectonic PHbT. It is also difficult to reconcile with the evidence that deformation superimposed on the northern margin of the pluton occurred after that part of the pluton was sufficiently solid to behave as a rigid mass relative to the wall rocks and that the deformation responsible for the northeastward-plunging lineations was also a late event affecting to some degree all of the rocks along the eastern side of the pluton as well as most or all of the plutons near the western scarp of the Sierra San Pedro Mártir farther east. Emplacement in a tectonically sheltered environment therefore seems more reasonable, particularly in light of the gradual nature of the southward decrease in magmatic foliation and penetrative deformation of the wall rocks and in light of the lesser intensity of both phenomena on the southwestern side of the SPT than on the southeastern side. Tectonic sheltering may have been due to any one or combination of the three suggested causes, but the fact that deformation was weakest on the southwest seems especially compatible with hypotheses 2a and 2b.

The same considerations just presented apply equally well to the southward change in the style of intrusion and the degree of concordance of the pluton contact. Stoping and discordance at the southern end of the pluton are clearly fracture-controlled. Therefore, varying

depth of emplacement, possible tectonic shielding, and syntectonic versus post-tectonic emplacement are all possible explanations for this aspect of the asymmetry. However, several additional factors may have been involved.

(1) The SPT is strongly discordant against the comparatively competent volcanic wacke and pebbly wacke and the meta-volcanic rocks along the southwestern contact, but is only slightly discordant against the section consisting predominantly of less competent mudstone and tuff along the southeastern contact. The latter rocks, which may have been water-rich and incompletely lithified at the time of intrusion, surround nearly the entire northern two thirds of the pluton, and it may be that the concordance reflects in part the relative ease with which these strata could deform by plastic flow rather than by fracture. Furthermore, the crosscutting southwestern contact clearly follows a relatively straight north-south line which must have been an important fracture zone in the wacke.

(2) As crystallization proceeded in the northern two thirds of the pluton, the ease with which added magma could expand to the north and east must have decreased, perhaps eventually to the point that fracture-controlled expansion to the south became easier.

(3) By the time the last SPT magma was emplaced, contact metamorphism may have increased the competence of the wacke sufficiently to facilitate fracturing.

(4) The up-welling SPT magma may have been less crystal-rich than were the PHbT and SHbT magmas at the time of intrusion. Whereas this is possible, yet in view of the alternative possibilities, it does

not seem necessary to invoke a much lower crystal-melt ratio during initial up-welling to explain the crosscutting relationships, hence the apparent greater mobility of the magma, at the southern end of the pluton. It is important to note that, according to the intrusive model presented, much of the extension and deformation of the wall rocks around the northern two thirds of the pluton developed gradually as the adjacent tonalite became progressively more crystalline and less capable of stoping or injection.

One additional question remains. Why did the pluton expand preferentially northward and eastward? One possibility is that expansion to the north and east was favored by the distribution of pre-batholithic lithologies -- predominantly mudstone and tuff immediately north and east of the pluton as compared with meta-volcanic wacke, pebbly wacke and volcanic and/or hypabyssal intrusive rocks to the west and southwest. In addition, if the strata were dipping northeastward as at present, lesser confining pressure in that direction might have favored expansion to the north and east.

Regardless of the cause, preferential expansion to the north and east implies that there was no serious obstacle to northward expansion. In other words, the Las Cochas pluton was apparently intruded after emplacement of most or all of the San José pluton (but contemporaneously with or before the formation of the northward-converging lineation system). If the Las Cochas were older than the San José pluton, one might expect the San José pluton to have been flattened against it and to have expanded more to the east or northwest.

11.3 Preliminary Interpretations of the Large-Scale Structure in the Pre-Batholithic Rocks

Figure 50 shows a schematic interpretation of the large-scale pre-intrusive structure in the wall rocks and the structural evolution of these rocks during emplacement of the pluton. An alternative interpretation is shown in Figure 51. The heavy dashed lines in Figures 50A and 51A show the surface of initial concordant intrusion proposed by the respective models. Hatchured areas denote strata removed by stoping.

It must be emphasized that these are greatly simplified working hypotheses based upon preliminary mapping; conceivably, neither hypothesis is correct, but none of the several other models considered seems consistent with the observed structural patterns and lithologic distributions. Suggestions for future work to test the hypotheses will be given at the end of this section.

11.3.1 The Preferred Hypothesis: Intrusion into the Northeastern Limb of a Tight Southeastward-Plunging Anticline

According to the preferred hypothesis, the pluton was intruded into the northeastern limb of a tight southeastward-plunging anticline whose axis strikes down the center of the thick section of metamorphosed volcanic wacke and pebbly wacke west of the pluton and whose nose is represented by the V-shaped outcrop pattern of marble and calc-silicate rock south of the pluton. Preferential expansion of the pluton to the north and east caused the strata northeast of the initial surface of intrusion to be split apart from the rest of the

Figure 50. Schematic illustration of the preferred interpretation of the large-scale pre-intrusive structure in the wall rocks and the evolution of this structure during emplacement of the pluton. The main element of the proposed pre-intrusive structure is a nearly isoclinal southeastward-plunging anticline, locally overturned, whose axis trends approximately down the center of the thick section of volcanic wacke and pebbly wacke west of the pluton and whose nose is represented by the V-shaped outcrop pattern of marble and calc-silicate rock south of the pluton. The proposed present structure is shown in (D). The model assumes that the zones of marble and calc-silicate rock wrapped around the northwestern and northern margins of the pluton and those scattered along the eastern contact are correlative with the thicker zones south and southwest of the pluton.

undifferentiated pre-batholithic rocks (pbu) -- predominantly tuffaceous mudstone and tuff -- showing the general strike of bedding

marble and calc-silicate rock (pbm), showing variations in thickness

volcanic wacke and pebbly wacke (pbw); the thickness of this unit around the northern end of the pluton is exaggerated

pyroclastic, flow, and hypabyssal intrusive rocks, with local sedimentary lenses and admixed detritus

diorite, gabbro, and inclusion-rich tonalite (dg, mdg, and dti)

..... denotes areas where the PHbT complexly intruded and partially assimilated mafic intrusive rocks and minor(?) marble, wacke, and tuffaceous mudstone to produce the zones of diorite and inclusion-rich tonalite (dti)

adjacent plutons

proposed surface of initial concordant intrusion

approximate areas of wall rocks removed by stoping

Figure 51. Schematic illustration of an alternative interpretation of the large scale structure in the wall rocks. This interpretation attributes the distribution of lithologies around the southern end of the pluton to about 2 km of left-lateral offset on a northeastward-trending pre-intrusive fault rather than to large-scale folding. The corresponding present structure is shown in (D). This model also assumes that the marble and calc-silicate beds wrapped around the northwestern and northern margins of the pluton and those scattered along the eastern contact are not correlative with the thicker zones south and southwest of the pluton. Otherwise the structures implied by this model are the same as in the preferred interpretation. Symbols are the same as in Figure 50.

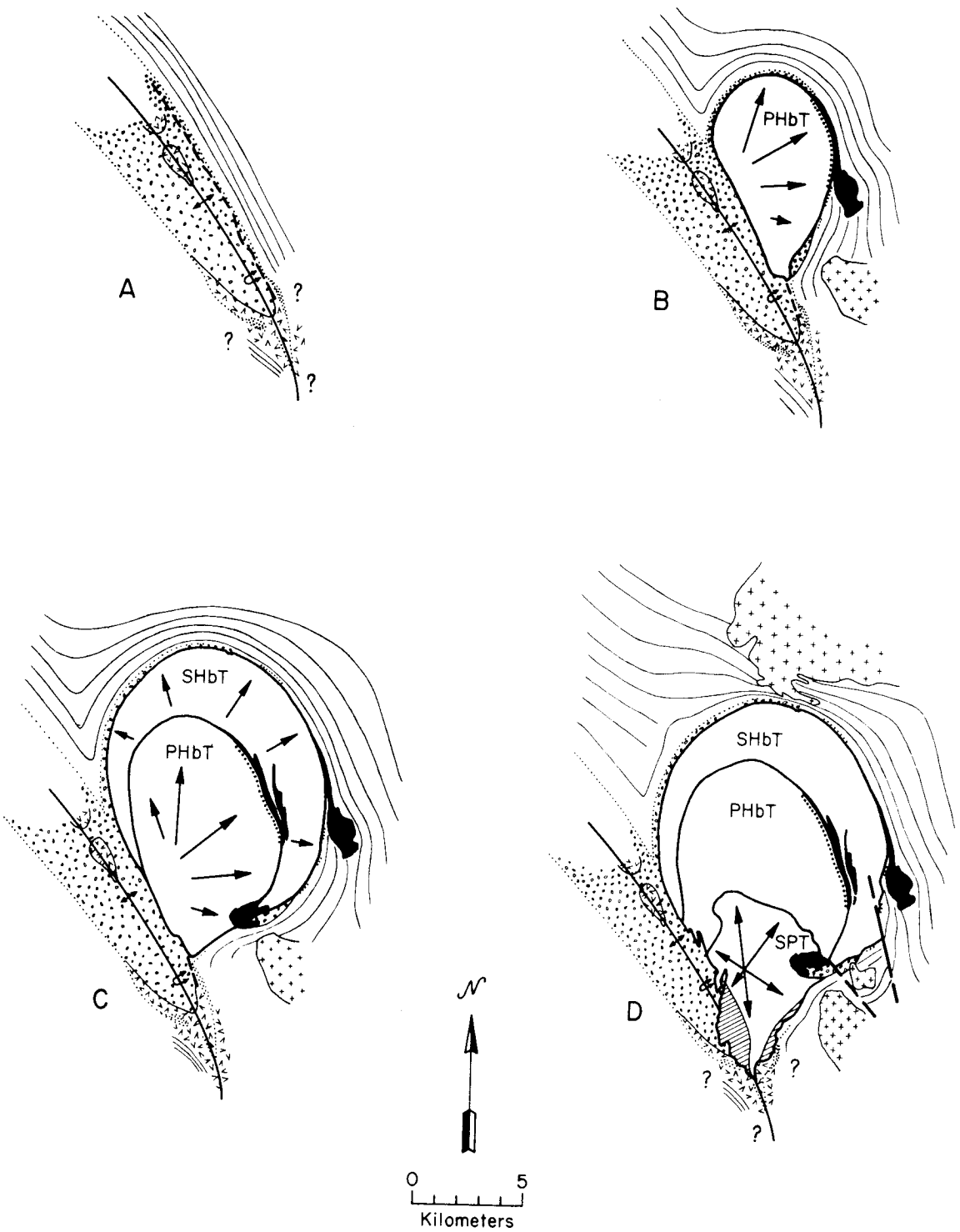

Figure 50

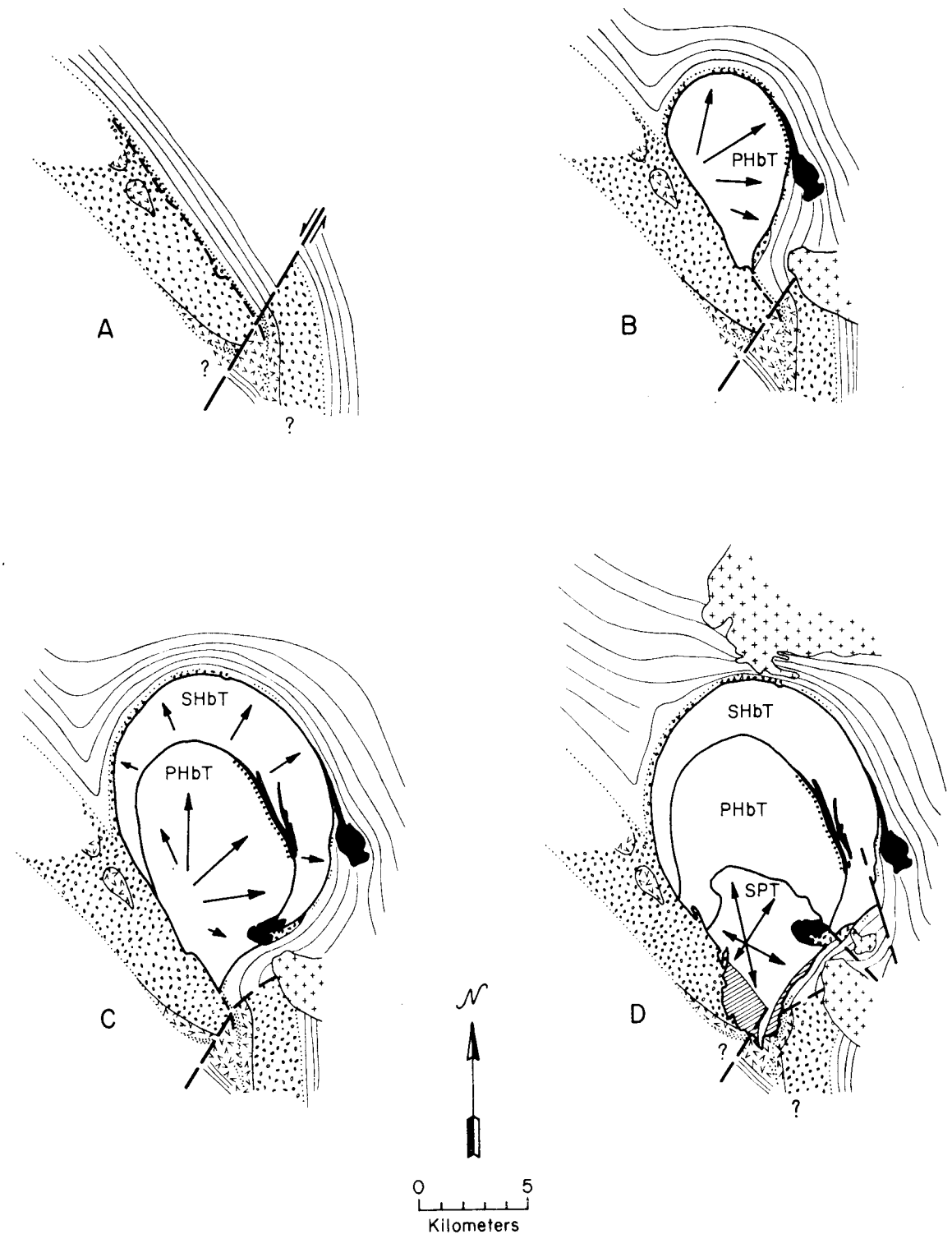

Figure 51

section, rotated progressively counterclockwise, and greatly distended. Counterclockwise rotation of up to nearly 180° produced a tight V-shaped fold west and northwest of the pluton and may have caused both the intense crumpling and brecciation inside the V and the abrupt discontinuity in structural trends across Arroyo El Tepetate. The SPT broke across the nose of the original anticline during the latest stages of emplacement, stoping large masses of wacke, plus some meta-volcanic rocks and marble.

This hypothesis readily accounts for the thin concordant sheath of stretched-pebble wacke and marble plus calc-silicate rock (unit M-1), followed in stratigraphic continuity by the thick section of predominantly mudstone and tuff, which encloses the northern and northwestern margins of the pluton. The zone of marble and calc-silicate rock bordering the pluton for 1.6 km in the northeast and several small masses of marble and calc-silicate rock scattered along the eastern margin appear to be remnants of this sheath, as does a small unmapped area of stretched-pebble wacke between the pluton and the large mafic sheet just south of Cañon Campo Buena Vista. According to this hypothesis, the carbonate beds in this sheath are correlative with the thicker zones of marble and calc-silicate rock around the southern end of the pluton. The absence of marble plus calc-silicate beds and of stretched-pebble wacke around most of the eastern margin of the pluton can be attributed to slight intrusive discordance plus extreme distension around the expanding pluton, probably combined with local pre-intrusive tectonic or depositional discontinuity.

The hypothesis also accounts for the apparent absence of a thick

section of volcanic wacke and pebbly wacke along the southeastern margin of the pluton. In fact, this absence is one of the most compelling arguments in favor of the fold hypothesis. Highly deformed and metamorphosed wacke and pebbly wacke probably correlative with the thick western section comprises much or all of the inlier of the pre-batholithic rocks southwest of the Willow Creek fault zone and of an incompletely mapped area northeast of the fault zone between the Willow Creek and San José plutons. However, these strata strike parallel to the pluton contact and appear to be restricted to a small area; they do not extend southward or southeastward away from the pluton. Thus the thick section of volcanic wacke and pebbly wacke traceable for at least 11 km along strike west of the pluton appears to stop abruptly at the pluton.

The hypothesis assumes that the marble and calc-silicate beds defining the western branch of the V-shaped outcrop pattern south of the pluton comprise the direct along-strike extension of the thicker northwestward-striking zone of marble and calc-silicate rock which appears to terminate abruptly on the eastern slope of Cerro Hechicera (area S-6,7). The occurrence of narrow masses of white lime-contaminated tonalite striking northwestward from the western branch of the V suggests that the calcareous beds in that branch originally extended farther to the northwest towards Cerro Hechicera and thus supports this correlation. The absence of marble and calc-silicate beds in the intervening area could be due to a combination of stoping and assimilation by the SPT and of sedimentary or tectonic discontinuity.

Finally, the hypothesis implies that the principal structure in

the volcanic wacke and pebbly wacke west and southwest of the pluton is a major tight anticlinal fold. Observations along and north of the San José-San Telmo road are consistent with this interpretation; they suggest a single anticlinal structure with both limbs right-side-up or vertical. The marble beds southwest of the wacke therefore appear to overlie the wacke. However, observations south of Cañon Las Cabras seem to conflict with this interpretation. That is, both the isoclinal fold hypothesis and the observations farther north imply that the northeastward-dipping section of marble and volcanic rocks southwest of the sharp synclinal axis shown on Plate 2 should be overturned. Although no direct evidence of the direction of tops of beds was seen in the calcareous and volcanic units, both the apparent pattern of folding and several examples of faint graded bedding and possible cross-bedding in the wacke suggest that the northeastward-dipping strata are right-side-up, hence, that the marble and calc-silicate beds underly the wacke and the intervening volcanic rocks.

These conflicting observations may indicate that the anticlinal fold hypothesis is incorrect. Alternatively, they may indicate that the syncline in the wacke is a minor structure and that there are additional unrecognized fold axes -- in particular, there may be an overturned anticline southwest of the syncline. Another possible, but, I believe, less likely explanation of the conflicting observations is that the reversal of dips interpreted as defining a sharp synclinal axis is actually due to abrupt steepening and overturning of the western limb of the anticline. If so, the evidence of tops from sedimentary structures southwest of the apparent synclinal axis is unreliable.

11.3.2 Alternative Interpretations

Figure 51 shows a possible alternative interpretation involving emplacement of the pluton into a section which, although certainly complicated by numerous tight or isoclinal folds, was grossly homoclinal. This hypothesis invokes pre-intrusive left-lateral offset along a major northeastward-trending fault, rather than large-scale folding, to explain the distribution of calcareous and volcanic rocks around the southern end of the pluton. According to this hypothesis, the thick zone of calc-silicate rocks extending south from El Alisito canyon along the southeastern margin of the SPT, rather than the zone defining the western branch of the V, is the original direct along-strike extension of the marble and calc-silicate beds on Cerro Hechicera. The V-shaped outcrop pattern of marble and calc-silicate rock south of the pluton can therefore be only a minor structure rather than the nose of a major fold; if so, the fact that the western branch of the V strikes northwestward towards the thick mass of marble and calc-silicate rock on Cerro Hechicera is purely coincidental.

This hypothesis predicts that there is a thick southward- or southeastward-striking section of volcanic wacke and pebbly wacke southeast of the pluton, but that this section begins several hundred meters or more east of the contact, outside the area covered on foot. The hypothesis further predicts that the zone of marble and calc-silicate rock should continue southward from the tip of the V, unless offset again by another structure or interrupted temporarily by sedimentary or tectonic pinching out. Brief examination for 300-400 m

south of the V revealed two small lenses of marble, but no clear evidence that the main mass continues southward. However, because of poor exposure, complex minor faulting, and apparent sedimentary discontinuities, no definite conclusion is possible without further work.

The second hypothesis predicts the same structural and lithologic patterns around the northern half of the pluton as does the first model, except that it interprets the marble and calc-silicate rocks around the northern and southern ends of the pluton as entirely different units separated by several thousand meters of section. Again, the absence of the marble and calc-silicate zones around most of the eastern margin of the pluton must be attributed to slight intrusive discordance, extreme distension, and probably local pre-intrusive tectonic or sedimentary discontinuities.

There are two principal weaknesses to this second hypothesis.

(1) No independent evidence of the proposed northeastward-trending fault was recognized, although mapping was not sufficient in the critical areas to rule out its existence; the northeastward-trending portion of El Alisito canyon east of the pluton could be a topographic manifestation of the fault. Although there is some leeway in the exact trend of the fault, no greatly different orientation or magnitude and direction of offset seems able to reasonably account for the trends and distributions of lithologies at this end of the pluton. On the other hand, there is direct evidence of a major fold in the wacke, and there are abundant aerial photographic indications of repeated isoclinal folding northwest, north, and east of the pluton.

(2) The V-shaped outcrop pattern of the marble and calc-silicate beds, the apparent termination of these beds at the tip of the V, the northwestward strike of the western branch of the V projecting back towards the mass of marble and calc-silicate rock on Cerro Hechicera, and the probable original northwestward extension of the western branch of the V as represented by the masses of lime-contaminated tonalite all seem to favor the fold interpretation.

Several other hypotheses can be suggested which, like the anticlinal fold model, invoke folding of the marble plus calc-silicate beds and the meta-volcanic rocks around the southern end of the pluton, but which do not involve isoclinal folding of the entire section and which, like the faulting hypothesis, interpret the calcareous zones around the northern and southern ends of the pluton as separate units. For example, one might propose a zigzag pattern of folding in which the strata southwest of the pluton are folded sharply northeastward around what is now the southern tip of the pluton, then are bent sharply back again to the southeast somewhere in the complex area between El Alisito canyon and the San José-Observatorio road. However, neither this nor any other interpretation which I can envisage seems able to account for the absence of a thick section of volcanic wacke and pebbly wacke striking southward or southeastward away from the southeastern margin of the SPT, except by invoking either an abrupt facies change across the pluton or additional complex structures for which there is presently no evidence. Inasmuch as clockwise rotation of the strata along the southeastern contact during expansion of the pluton was responsible for much of the distance now separating the truncated section of wacke west

of the pluton, the facies change would have to have occurred over a distance of at most 1-2 km. Considering that the wacke can be traced as a thick, relatively consistent lithology for at least 11 km along strike west of the pluton, such an abrupt facies change seems unlikely.

11.3.3 Suggestions for Future Work to Test the Hypotheses

There are several ways to test the preferred and alternate hypotheses. Obviously, the structure in the volcanic wacke and pebbly wacke west of the pluton must be clarified. More observations of cross-bedding, graded bedding, and other indicators of the directions of tops of beds would be especially useful. However, the most critical test would be to establish the structural and stratigraphic relationships in the complex, little-explored areas south and southeast of the pluton. South of Cerro Hechicera (area T,U-7), there is a northwestward-striking section of unknown thickness consisting of thinly bedded, siliceous and laminated mudstone and tuff very similar to the thick section north and east of the pluton. If the fold hypothesis is correct, this section may be 1000 m or more in apparent thickness and should be wrapped around the southern end of the pluton and strike northeastward to merge with the similar strata east of the pluton. It should be relatively easy to prove or disprove the thickness and wrap-around relationships and at the same time to test the predicted absence of a thick section of volcanic wacke and pebbly wacke southeast of the pluton. Continuity with the section east of the pluton may prove more difficult to verify because of the complex deformation, intrusion, and metamorphism in the intervening area. However, there are potential

marker beds. If unique and continuous, the feldspathic quartzite beds used to correlate across the Willow Creek fault zone and the Willow Creek pluton might be especially useful.

Establishing the preceding relationships might, by themselves, be sufficient to prove or disprove one or the other hypothesis. However, the suggested correlation between the marble plus calc-silicate units enveloping the northern part of the pluton and the thicker unit around the southern end of the pluton also needs to be tested. Inasmuch as the calcareous beds themselves cannot be traced through the intervening area, the correlation must be tested indirectly by mapping lithologies in the thick section of predominantly mudstone and tuff. Again the structural and intrusive complexities east and southeast of the pluton may make correlation extremely difficult.

Finally, both working hypotheses predict a V-shaped fold pattern west and northwest of the pluton, which pattern should be revealed by the distribution of the zones of marble plus calc-silicate rock. Unfortunately, none of these zones could be traced more than 3 km south of Arroyo de las Parritas, either because they are too poorly exposed (much of the area is covered by dense brush) or because of actual sedimentary or tectonic discontinuity. As pointed out earlier, discontinuous exposure is a frequently recurring problem in mapping the calcareous zones. Nevertheless, both hypotheses predict that one or more zones of marble followed by or interbedded with mudstone, tuff, and perhaps andesite or basalt porphyry should border the thick northwestward-diverging section of volcanic wacke and pebbly wacke on the northeast, i.e., within or along the western margin of the wedge-

shaped area lacking traces of bedding on aerial photographs (Figure 2 and Plate 1). If the calcareous layers have not been thoroughly obscured due to crumpling, faulting, brecciation, or intrusion of hypabyssal rocks, it should be relatively easy to test the existence of this fold.

PART III

PETROGRAPHY AND PETROLOGY

OF THE TONALITE

Chapter 12

PETROGRAPHY OF THE TONALITE AND PROPERTIES OF THE MINERALS

12.1 General Description

The mineralogy of the tonalite is very uniform throughout the pluton, and the proportions of the phases vary within restricted ranges. Plagioclase, quartz, hornblende, and biotite generally comprise about 95% of the rock, with most of the remainder consisting of opaques and alteration products of the major phases. The amount of K-feldspar is generally very small. Table 5 lists all of the minerals observed, together with their average modal abundances, ranges of abundance, and some pertinent comments. The ranges of abundance are based both on modal analyses and on visual estimates in additional thin sections and polished sections.

Textures are consistently hypidiomorphic-granular, with varying degrees of protoclastic modification. Hornblende and biotite tend to be equigranular in the SHbT; otherwise, the major minerals in all three units exhibit a seriate grain-size distribution. The average grain size is 2-4 mm, but it ranges from 1-3 mm locally near the margins of the units, particularly in the CBT, to as much as 5-8 mm locally near the inner margin of the SHbT. Nowhere does the tonalite exhibit fine-grained margins. Schlieren and inclusions are local inhomogeneities, but generally the minerals are uniformly distributed on both a hand specimen and an outcrop scale. Hornblende, biotite, and sometimes opaques tend to cluster into monomineralic or polymineralic aggregates, but this is a subordinate effect.

Table 5

Summary of the Mineralogical Characteristics of the Tonalite

	Average Mode (vol %)	Range of Abundance (vol %)*	Comments
Quartz	16.3	8 - 25	
Plagioclase	62.1	50 - 70	zoned from calcic andesine to calcic or intermediate oligoclase
K-feldspar	0.26	tr - 4	orthoclase and sanidine; locally some microcline
Hornblende	11.3	4 - 20	
Biotite	5.6	2 - 11	
Chlorite	0.59	tr - 2	alteration of biotite and sometimes hornblende; some interstitial primary** aggregates
Magnetite	1.3	0.3 - 1	
Hematite-ilmenite		tr - 1	complex intergrowths; also some hematite as alteration of magnetite and as inclusions in plagioclase
Rutile		tr	alteration of hematite-ilmenite; also in biotite, chlorite, and rarely quartz
Sulfide		sl tr	very fine-grained pyrite (?)
Sphene	0.34	tr - 1	alteration of hematite-ilmenite and ferromagnesian minerals; less common subhedral crystals and interstitial primary** grains
Apatite	0.22	tr - 0.4	small stout subhedral and euhedral prisms included in biotite, hornblende, hematite-ilmenite and sometimes plagioclase; also some free crystals

Table 5 (continued)

	Average Mode (vol %)	Range of Abundance (vol %)*	Comments
Epidote	0.45	tr - 2.5	interstitial primary** grains and replacement of plagioclase and ferromagnesian minerals
Clinozoisite or zoisite	<0.05	0 - tr	interstitial primary** grains and replacement of plagioclase
Allanite	<0.05	0 - tr	anhedral; often zoned to epidote rims
Zircon	<0.05	tr	
White mica and clay minerals	1.5	tr - 4	alteration of plagioclase and rarely biotite; rare interstitial primary** muscovite
Clinopyroxene (salite) Cummingtonite Actinolite	0.04	0 - 0.3	relict inclusions in hornblende; amphibole exceeds pyroxene
Carbonate (calcite?)	<0.05	0 - tr	alteration of plagioclase; also rare veinlets and interstitial primary** grains
Prehnite	<0.05	0 - 0.5	sheaths of platy crystals in biotite
Zeolite (chabazite?)	<0.05	0 - 0.5	veins, interstitial primary** grains, and alteration of plagioclase
Tourmaline	<0.05	0 - tr	extremely rare
Garnet	<0.05	0 - tr	one interstitial grain seen

*Excluding schlieren and altered rocks

**"Primary" denotes crystals formed by direct precipitation from either the melt or a vapor phase, rather than by "secondary" replacement of a pre-existing mineral.

To measure grain-size variations, IC numbers -- defined by Chayes (1956a, p. 72) as the "number of major mineral identity changes along a unit length of line" were determined throughout the pluton (Table 6, localities shown in Figure 52). Measurements for the four major minerals were made on thin sections at medium power, and values were normalized to a unit length of 40 mm.

IC numbers depend not only on grain size -- the smaller the grains, the higher the value -- but also on textural variations. Clustering of grains of the same mineral decreases the number, whereas poikilitic or irregular grain shapes as well as protoclastic granulation and recrystallization can significantly increase the number. Also, because the minerals generally have inequidimensional shapes, the degree of preferred orientation and the angle of the measurement traverses to the direction of orientation affect the numbers obtained. I attempted to compensate for orientation effects by measuring along traverse lines at various directions normal to foliation. The range of values obtained on individual samples typically varies by ±15-20; in the GBT the range reaches ±50-60. Nevertheless, the numbers serve as crude indices of grain-size variations.

The point to be made is that the three main textural units all have roughly the same grain size; variations in IC number within the units exceed the differences among the units. The IC numbers confirm the field observation that the seriate porphyritic texture in the southern third of the pluton is due to an increase in the abundance and size of large plagioclase crystals rather than to a decrease in the average grain size relative to the rest of the pluton. The GBT,

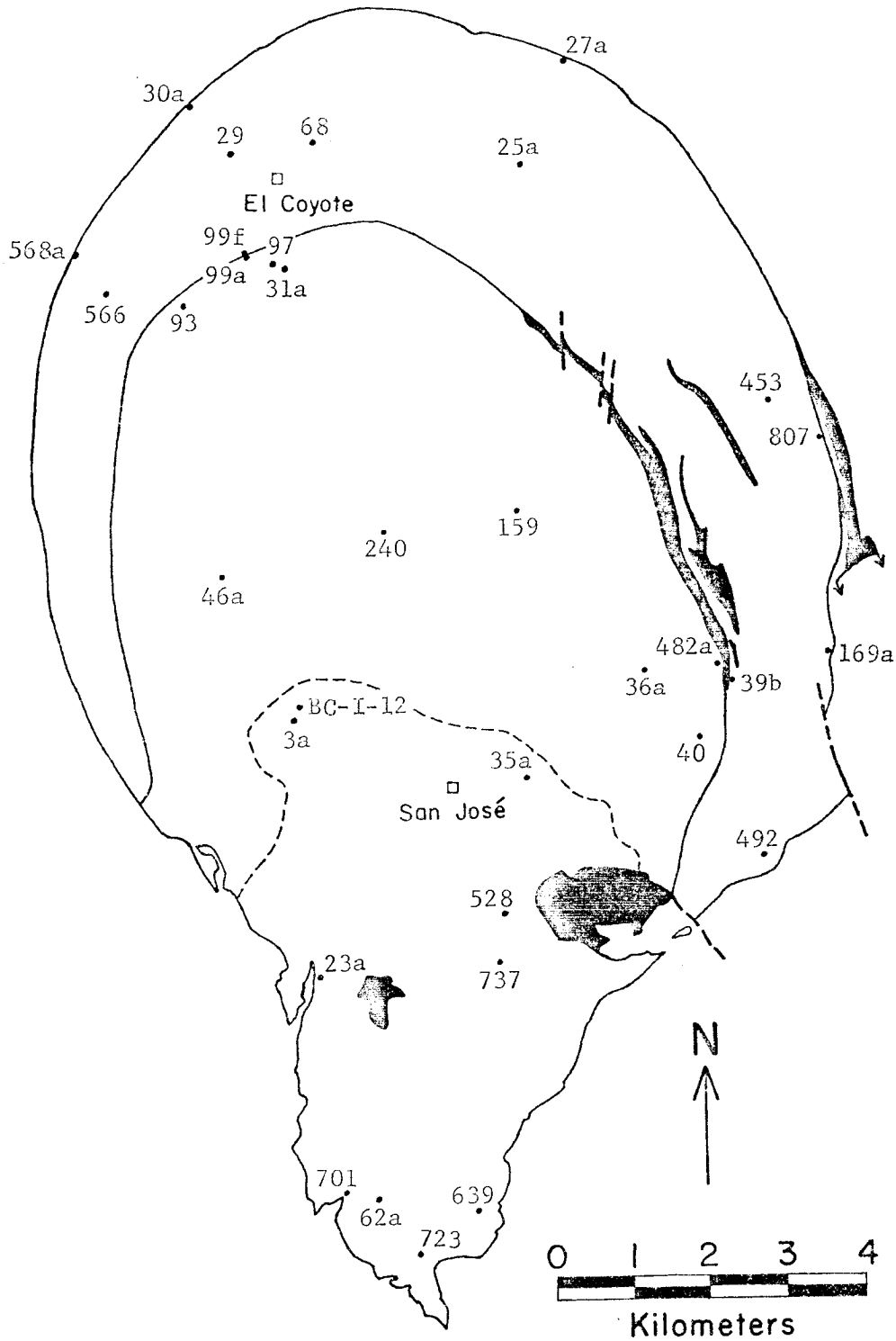

Figure 52. Location of samples examined for IC number.

Table 6

IC Numbers of the Tonalite

GBT		SHbT		PHbT		SPT	
Sample	IC	Sample	IC	Sample	IC	Sample	IC
27a	163	25a-2	73	31a	65	3a	80
30a	157	29	70	36a	70	12	86
568a	158	39b*	71*	40	73	23a	58
807	130	68	64	46a-2	78	35a	71
		99f*	80*	93	107	62a	57
		169a[a]	97[a]	97	94	528	65
		453	87	99a*	94*	639	59
		492	82	159	69	701	73
		566	76	240[b]	70[b]	723	81
				482a*	90*	737	77
Average	152	Average	75[a]	Average	81	Average	71

*Identifies samples collected within 30 m of the outer margin of the prismatic hornblende tonalite or within 10 m of the inner margin of the stubby hornblende tonalite.

[a]Sample 169a is geographically, structurally, and texturally transitional between the typical stubby hornblende tonalite and the gneissose border phase; it was omitted from the SHbT average.

[b]Average of three samples having IC = 58, 72, and 80.

however, yields much higher IC numbers, confirming the finer grain size recognized in the field. Field observations also suggest a very slight decrease in grain size in the moderately and strongly foliated outer parts of the PHbT compared to the interior of that unit, which observations are consistent with the high IC numbers of marginal PHbT samples 99a and 482a, as well as of samples 93 and 97 collected about 220 m and 200 m, respectively, from the margin of the PHbT. In contrast, the grain size of the SHbT in the field appears constant, or locally increases towards the SHbT-PHbT contact zone; no systematics are apparent in the few IC numbers.

A distinct change (decrease) in grain size is visible in the field at only a few places near the contacts of the SPT with country rocks and nowhere along the PHbT-SPT contact zone; nor do the IC numbers of samples show any systematic variations in the SPT.

Inasmuch as the finer-grained zones around the margins of the pluton and the PHbT coincide with zones of greater foliation intensity, and the general absence of finer-grained margins around the SPT correlates with the absence of appreciable flow structure, the decrease in grain size appears to have been more closely related to the intensity of magmatic shear flow than to the rate of cooling. Protoclasis and recrystallization of biotite, quartz, and, to a lesser extent, hornblende and plagioclase certainly contributed to the finer grain size. However, even in the GBT, roughly half of the plagioclase grains have ragged or rounded subhedral outlines and/or show subhedral or euhedral zoning patterns subparallel to the grain boundaries. The size of those plagioclase grains could not have been greatly reduced by crushing or

recrystallization, yet they are generally smaller than their counterparts in the interior of the SHbT. Perhaps magmatic flow differentiation (Bhattacharji and Smith, 1964) contributed to the finer grain size. Under some conditions, the intensity of the forces believed to be responsible for migration of crystals away from zones of high shear flow should be proportional to grain size (Bhattacharji and Smith, 1964; Komar, 1972a, 1972b). Thus, although the effectiveness of flow differentiation in viscous silicic magmas is debatable, the process could conceivably have led not only to an increased concentration of melt, but also to a high ratio of small crystals to large crystals in the regions of intense shear flow around the outer margins of the PHbT and especially the SHbT. Also, if there is some process favoring nucleation of more crystals in zones of high shear flow, such enhanced nucleation could have contributed to the finer grain size.

This chapter will cover the petrographic and chemical characteristics of the minerals in sequence. Tables of microprobe analyses report average compositions for the minerals in selected rocks, together with the number of grains upon which each average is based. The average compositions of the individual grains are tabulated in Appendix C along with a discussion of the analytical techniques and reliability. Analyses are believed to be accurate to within 1-2% of the amount present for oxide concentrations of several percent or more. Locations of the eight samples for which microprobe data was obtained -- samples 3a, 25a, 29, 30a, 36a, 46a, 62a, and 68 -- are included in Figure 52.

Mineral analyses are coded in the tables by mineral name, rock number, and grain number. For example, B-3a-1 identifies biotite grain

#1 in rock Ba-JM-3a. Mineral abbreviations are: P - plagioclase; KF - potassium feldspar; H - hornblende; B - biotite; M - magnetite; Cp - clinopyroxene; Cu - cummingtonitic amphibole; and A - actinolitic amphibole. Except for magnetite, total Fe is reported as FeO. Henceforth, for both the mineral and whole-rock analyses, the symbol FeO_t will be used to designate total Fe as FeO. Where the subscript is omitted, only ferrous iron is represented.

For amphiboles and biotite, the deficiency of the sum of the analyzed oxides from 100% was assigned to "H_2O". This procedure for determining H_2O and OH contents is inherently weak,
incorporate not only the actual H_2O and OH concentrations, but also the contents of all unanalyzed oxides and elements and the sum of all analytical errors. The procedure also assumes that all Fe is present as FeO. Wave-length scans on one actinolite, two biotite, and two hornblende grains indicate that the assumption of insignificant concentrations of unanalyzed components is justified; in particular, no F or Cl was detected. However, the assumption of no Fe_2O_3 is certainly incorrect, and the "H_2O" and "OH" contents are less reliable than other oxide concentrations.

A similar procedure was used to calculate Fe_2O_3/FeO ratios in magnetite. In this case, the deficiency of the sum of the analyzed oxides from 100% (assuming all Fe as FeO) was assigned to "excess oxygen"; sufficient Fe was then assigned to Fe_2O_3 to account for the "excess oxygen", and the remaining Fe was assigned to FeO. Unfortunately, the resulting Fe_2O_3/FeO ratios are very sensitive to slight errors in the oxide sum, and their reliability is uncertain.

12.2 Quartz

Quartz typically occurs as anhedral grains, or mosaics of anhedral grains, which are irregularly interstitial to plagioclase and hornblende or which are roughly equant or ovoid, with margins generally molded or interstitial. Subequant or ovoid shapes 1-3 or 4 mm in diameter are common throughout the PHbT and SPT, whereas irregularly interstitial shapes 0.5-2 or 3 mm in size predominate in the SHbT. Many of the larger grains and patches are inclusion-free, but others poikilitically enclose one or more crystals of plagioclase, hornblende, and occasionally biotite, apatite, or opaques.

Both the proportion of patches composed of mosaics and the average number of extinction domains in the mosaics increase as the development of flow structure increases. Concurrently, the patches become more flattened and lenticular, occurring as thin discoidal or elongate ellipsoidal aggregates in the GBT. Undulatory extinction is recognizable in some quartz grains in all rocks, but it is minor in the least foliated or lineated rocks. However, undulatory extinction is commonly less pronounced in the GBT than in many less foliated samples from the interior of the SHbT; evidently, the strain accumulated in quartz grains in the gneissose rocks was greatly reduced by continued recrystallization after deformation had largely or entirely ceased.

Quartz occurs rarely as inclusions in plagioclase, but only near the margins of grains; the magma apparently reached silica saturation only after a large proportion of the plagioclase had crystallized. Quartz also occurs, along with plagioclase, hornblende, and opaques, as inclusions in late-stage poikilitic biotite. In some cases, biotite

penetrates irregularly into and appears to be replacing quartz. Tiny blebs of quartz, commonly associated with actinolitic amphibole, occur in many hornblende grains in the SHbT and rarely in the PHbT. In some cases, these quartz blebs can be clearly related to replacement of clinopyroxene; possibly all of the blebs formed in this way.

In many SHbT samples, but not in the other two textural units, quartz also occurs as occasional 0.2-0.8 mm grains included in or partially enclosed by poikilitic hornblende. These inclusions are generally anhedral and equant or irregular in shape, but some exhibit rounded subhedral to euhedral bipyramidal forms (Figure 53). Most of these included grains contain abundant hairlike needles of a TiO_2 polymorph[11], presumably rutile, rarely present in the rest of the quartz (Figure 54). TiO_2 needles are also abundant in some of the rare quartz grains included in plagioclase.

The occurrence of subhedral and euhedral quartz grains in the interiors of large hornblende crystals implies nucleation of quartz in the SHbT before or shortly after the initiation of hornblende growth. Yet, most quartz in the SHbT is comparatively fine-grained and interstitial to both hornblende and plagioclase. Also, the abundance of quartz inclusions in hornblende does not appear to increase in proportion to the total modal quartz or SiO_2 content of the rocks. Furthermore, the included quartz grains are commonly rounded to some degree, and many are smoothly ovoid or irregular in form, suggesting a possible resorption prior to enclosure in hornblende. These observations, together

---

[11] Identified as Fe-bearing TiO_2 by qualitative microprobe analysis.

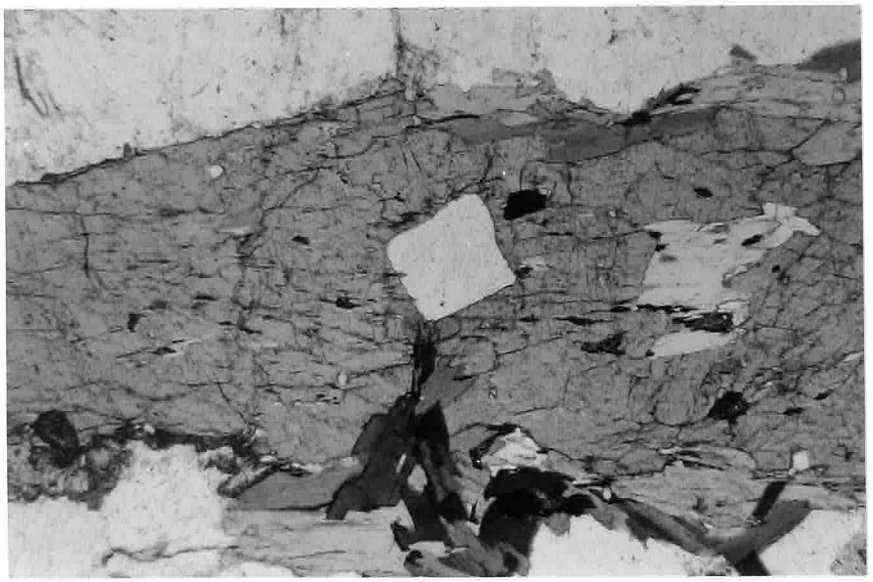

Figure 53. Euhedral bipyramidal quartz crystal in hornblende in the stubby hornblende tonalite. The extinction directions of the quartz bisect the angles between the crystal faces, but neither the extinction directions nor the margins of the quartz are parallel to either the (110) cleavage or the (100) twinning of the hornblende. Sample Ba-JM-149, 340 m from the northwestern margin of the pluton, 400 m north of the Buena Vista-Coyote road (area D-4,5).

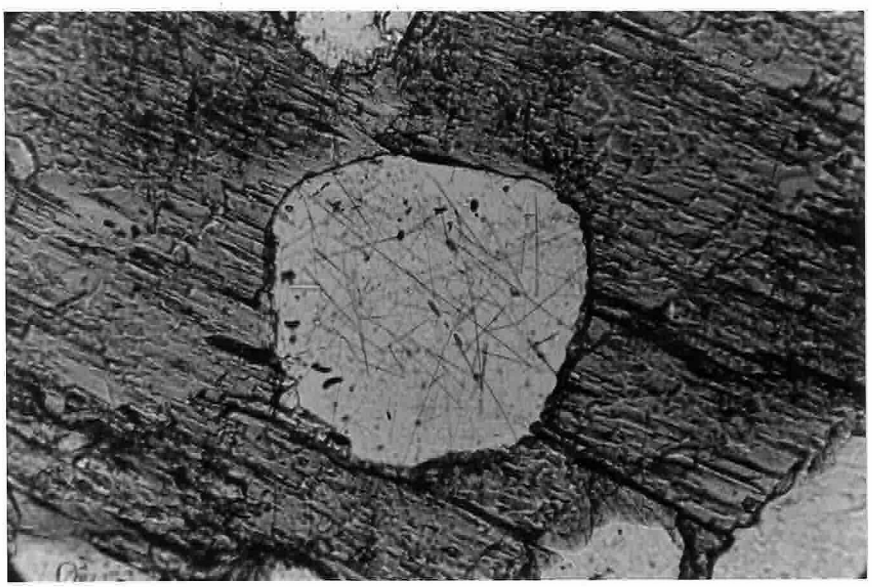

Figure 54. Rounded equant inclusion of quartz in hornblende in the stubby hornblende tonalite. The abundant hair-like needles in the quartz consist of Fe-bearing TiO_2, presumably rutile. Sample Ba-JM-454 from Cañon Campo Buena Vista, 275 m from the northeastern margin of the pluton (area J-12).

with the characteristic abundance of TiO_2 needles in the included quartz, suggest two stages of quartz growth: (1) unencumbered growth of euhedral crystals prior to extensive crystallization of hornblende and (2) continued or renewed late interstitial growth. The first stage of growth apparently occurred under sufficiently different conditions than the later quartz -- presumably higher temperature and/or pressure -- to permit appreciably greater solid solution of Ti.

There is no evidence either for or against a similar two-stage growth history for quartz in the PHbT or SPT. Nor is there clear evidence of the time of nucleation of quartz relative to hornblende in these units. As will be discussed later, the tendency for euhedralism of hornblende in the PHbT and SPT suggests that most hornblende growth occurred at a relatively earlier stage of magmatic crystallization in those units than in the SHbT. However, the large equant, non-poikilitic shape of quartz patches in the PHbT and SPT also suggest considerable growth of quartz before the magma became crowded with crystals.

12.3 Plagioclase

Plagioclase and its alteration products -- generally 1-3% of sericite, clay minerals, epidote, clinozoisite, K-feldspar, and occasionally zeolite (chabazite?) or carbonate -- comprise 60-70% of the tonalite, except in the CBT, where they total 55-60%. Most crystals are subhedral or euhedral, especially in the PHbT and SPT, and exhibit blocky forms tabular parallel to (010) and slightly elongate parallel to either the *a* or *c* axis. The average grain size is 2-5 mm, but there is a seriate distribution of sizes from <1 mm generally up to 6-7 mm.

Throughout the SPT, a small proportion of crystals reach 10-12 mm, rarely even 25 mm.

Plagioclase in the PHbT and SPT is typically light gray in color, whereas many grains in the SHbT are brownish gray, buff, or rarely light orange due to the presence of tiny euhedral inclusions of hematite (or hydrous Fe oxide) often accompanied by tiny opaque grains and needles of an unidentified high-index material. Even in the SHbT, most plagioclase crystals contain only a few of these inclusions, but some grains are sufficiently inclusion-rich to appear faintly clouded and faintly grayish orange or grayish brown in thin section. The inclusions probably formed by exsolution of Fe originally dissolved in the feldspar lattice. They are rare in plagioclase from the PHbT and SPT.

Twinning and zoning patterns in the plagioclase are quite complex. Ablite, pericline, and Carlsbad twinning are all common. According to criteria established by Vance (1961), polysynthetic twinning in the less foliated, non-protoclastic rocks is mostly primary, but secondary deformational twinning is well developed in the more foliated and protoclastic rocks. Bent and fractured crystals are common not only in the most strongly foliated rocks, but also throughout much of the SHbT, especially in the north and east.

Plagioclase grains are zoned typically from calcic or intermediate andesine (An_{37-45}) in the centers to calcic or intermediate oligoclase (An_{20-30}) at the rims. Zoning may be progressive (normal), oscillatory, mottled, or any combination of these three. Mottled zoning may be expressed as (1) scattered round or irregular patches or discontinuous

zones of more calcic plagioclase grading into and enclosed in more sodic plagioclase or as (2) irregular areas or rectangular, crystallographically controlled patches of sodic plagioclase scattered through a grain, surrounding included phases, or extending inward from grain margins, sometimes along fractures. The sodic patches are generally similar in composition to the rim plagioclase. In many cases, the calcic patches are clearly relicts of original oscillatory or progressive zoning partially obliterated either by internal equilibration or by replacement by more sodic plagioclase.

The pattern of zoning is variable throughout the pluton. Zoning is least pronounced in the SHbT. Mottled zoning and weak diffuse progressive or wavy zoning predominate in that mass, although euhedral oscillatory and progressive zoning are present in some grains. In contrast, euhedral oscillatory and progressive zoning are well developed in the SPT, and mottled zoning is minor. The large plagioclase "phenocrysts" in the latter unit show an especially complex pattern of oscillatory zoning, sometimes with several tens of thin euhedral zones (Figure 55) recording a long and complex history of crystallization. Zoning in the PHbT is similar to that in the SPT, but generally with fewer oscillations.

The frequency and complexity of oscillatory zoning increases without apparent break southward from the PHbT into the interior of the SPT. This change correlates with decreasing development of flow structures and with increasing euhedralism of crystal faces. Conversely, within the SHbT, increasing predominance of mottled or weak diffuse anhedral zoning over euhedral oscillatory and progressive zoning

Figure 55. Pronounced oscillatory zoning characteristic of the large euhedral plagioclase "phenocrysts" in the seriate porphyritic tonalite. The average size of the surrounding grains is notably smaller than the average grain size of the rock, producing an unusually marked porphyritic appearance. Sample Ba-JM-737 from the center of the SPT 2.4 km south-southeast of Rancho San José (area O-8).

correlates roughly with the increasing irregularity of grain margins and the increasing intensity of foliation and protoclasis. Although remnants of euhedral progressive or oscillatory zoning in some mottled or weakly zoned grains suggest that post-crystallization homogenization and equilibration contributed significantly to the paucity of strong euhedral zoning in the SHbT, there is no evidence that euhedral progressive and oscillatory zoning were ever as well developed in the SHbT as in the other two textural units. Furthermore, the patterns of relict zoning in the mottled and weakly zoned grains indicate that very little recrystallization or change in the size or shape of grains accompanied the destruction of zoning. This observation provides an important petrographic argument against formation of the preferred mineral orientation primarily by solid-state deformation and recrystallization.

Composite grains identified by multiple centers of zoning occur sparsely throughout the pluton. Individual units of the composite generally share prominent crystal faces, indicating that the composites formed by synneusis: "the process of drifting-together and mutual attachment of crystals suspended in a melt" (Vance, 1969, p. 24). However, some composites appear to have formed by inclusion of one or more grains in a faster-growing crystal; truncated zoning patterns indicate that the included grains in some cases are resorbed or broken fragments of crystals.

Plagioclase contains occasional inclusions of each of the other important phases. Hornblende, opaque, and apatite inclusions are most common and occur in all parts of grains. Inclusions of quartz were

observed only near the margins of crystals.

Plagioclase occurs as inclusions in hornblende, biotite, and quartz. Inclusions in hornblende are characteristic of the SHbT, but are comparatively rare in the rest of the pluton. Some of these inclusions are subhedral or even euhedral; others are rounded or irregular in form and were either partially replaced by the enclosing hornblende or partially resorbed by the magma prior to incorporation in the hornblende. Inclusions of plagioclase in biotite, common throughout the pluton and especially in the SHbT, are typically anhedral and often raggedly penetrated and replaced by the biotite. Subhedral or euhedral plagioclase grains, occasionally slightly corroded, occur as inclusions in quartz throughout the pluton, but are especially common in the SPT and the western part of the PHbT.

All of the textural observations, together with the great volumetric predominance of plagioclase over all other phases, imply that plagioclase was the liquidus or near-liquidus mineral in these rocks, possibly accompanied by hornblende (especially in the PHbT and SPT), minor pyroxene (especially in the SHbT), and/or opaques.

Most compositional data on plagioclase were obtained by extinction-angle measurements on albite and combined Carlsbad-albite twinning. Microprobe analyses were obtained on plagioclase cores and rims in eight samples (Tables 7 and 8), on sodic microveinlets in one sample (Table 9) and on plagioclase inclusions in hornblende in two samples (Table 10). Each average core and rim composition in Tables 7 and 8 is, with a few exceptions noted in the tables, based on three analyses of the more calcic parts of the interiors and three analyses of the most sodic parts of the rims of each of three grains; in some cases, small

Table 7

Average Microprobe Analyses of Plagioclase Cores in Individual Tonalite Samples

Name of Unit	GBT	SHbT			PHbT		SPT		Pluton	
Sample #	Ba-JM 30a	Ba-JM 25a	Ba-JM 29	Ba-JM 68	Ba-JM 36a	Ba-JM 46a	Ba-JM 3a	Ba-JM 62a*	Average	σ
Number of Grains	3	3	3	3	3	2	3	3	--	--
SiO_2	n.a.	56.55	n.a.	n.a.	57.63	57.67	58.01	n.a.	--	--
Al_2O_3	n.a.	27.66	n.a.	n.a.	27.06	27.32	26.67	n.a.	--	--
FeO_t	n.a.	0.12	n.a.	n.a.	0.10	0.11	0.14	n.a.	--	--
CaO	8.69	9.59	9.15	9.28	8.79	9.02	8.38	9.42	9.04	0.40
Na_2O	6.74	6.26	6.66	6.36	6.75	6.53	6.81	6.29	6.55	0.22
K_2O	0.28	0.12	0.13	0.19	0.13	0.18	0.20	0.21	0.18	0.05
TOTAL	---	100.30	---	---	100.46	100.81	100.21	---	---	---
Formula Proportions Based on Cation Sum = 5										
Si	---	2.528	---	---	2.567	2.564	2.590	---	---	---
Al	---	1.457	---	---	1.420	1.431	1.403	---	---	---
Fe	---	0.005	---	---	0.004	0.004	0.005	---	---	---
Ca	0.409	0.460	0.416	0.442	0.419	0.430	0.401	0.448	0.428	0.020
Na	0.575	0.543	0.577	0.548	0.582	0.562	0.589	0.540	0.564	0.019
K	0.016	0.007	0.008	0.011	0.008	0.010	0.011	0.012	0.010	0.003
Or/(Or + Ab + An)	0.016	0.007	0.008	0.011	0.008	0.010	0.011	0.012	0.010	0.003
Ab/(Or + Ab + An)	0.575	0.538	0.577	0.548	0.577	0.562	0.588	0.540	0.563	0.019
An/(Or + Ab + An)	0.409	0.455	0.416	0.442	0.416	0.428	0.400	0.448	0.427	0.020

*The core of grain P-62a-4 was omitted from this average -- the An content of that "core" is unusually low compared to other core values, suggesting that the thin section did not intersect the actual core of the crystal.

Table 8

Average Microprobe Analyses of Plagioclase Rims in Individual Tonalite Samples

Name of Unit	GBT	SHbT			PHbT		SPT		Pluton	
Sample #	Ba-JM 30a	Ba-JM 25a	Ba-JM 29	Ba-JM 68	Ba-JM 36a	Ba-JM 46a	Ba-JM 3a	Ba-JM 62a	Average	σ
Number of Grains	3	3	3	3	3	2	3	4		
SiO_2	n.a.	60.89	n.a.	n.a.	60.57	62.98	62.15	n.a.	---	---
Al_2O_3	n.a.	24.98	n.a.	n.a.	25.23	23.80	24.13	n.a.	---	---
FeO_t	n.a.	0.10	n.a.	n.a.	0.10	0.12	0.16	n.a.	---	---
CaO	4.88	6.35	5.71	5.79	6.51	4.69	5.09	4.83	5.48	0.71
Na_2O	9.03	8.22	8.43	8.44	8.16	9.05	8.74	8.96	8.63	0.36
K_2O	0.17	0.11	0.14	0.14	0.11	0.22	0.23	0.24	0.17	0.05
TOTAL	---	100.63	---	---	100.68	100.85	100.50	---	---	---
Formula Proportions Based on Cation Sum = 5										
Si	---	2.687	---	---	2.672	2.762	2.740	---	---	---
Al	---	1.299	---	---	1.312	1.230	1.254	---	---	---
Fe	---	0.004	---	---	0.004	0.004	0.006	---	---	---
Ca	0.228	0.300	0.270	0.273	0.308	0.220	0.240	0.226	0.258	0.034
Na	0.763	0.704	0.722	0.720	0.698	0.770	0.747	0.761	0.736	0.028
K	0.010	0.006	0.008	0.008	0.006	0.012	0.013	0.013	0.010	0.003
Or/(Or + Ab + An)	0.010	0.006	0.008	0.008	0.006	0.012	0.013	0.013	0.010	0.003
Ab/(Or + Ab + An)	0.763	0.697	0.722	0.720	0.690	0.768	0.747	0.761	0.734	0.031
An/(Or + Ab + An)	0.228	0.297	0.270	0.273	0.304	0.220	0.240	0.226	0.257	0.033

Table 9

Microprobe Analyses of Sodic Plagioclase Veinlets in Plagioclase

Name of Unit	SHbT	
Sample #	Ba-JM-29	
Grain #	P-29-3	P-29-4
Number of Points	3	3
SiO_2	n.a.	n.a.
Al_2O_3	n.a.	n.a.
FeO_t	n.a.	n.a.
CaO	4.26	3.69
Na_2O	9.35	9.70
K_2O	0.10	0.09
TOTAL	---	---
Formula Proportions Based on Cation Sum = 5		
Si	---	---
Al	---	---
Fe	---	---
Ca	0.200	0.173
Na	0.795	0.822
K	0.005	0.005
Or/(Or + Ab + An)	0.005	0.005
Ab/(Or + Ab + An)	0.795	0.822
An/(Or + Ab + An)	0.200	0.173

Table 10

Microprobe Analyses of Plagioclase Inclusions in Hornblende

Name of Unit	Stubby Hornblende Tonalite				Prismatic Hornblende Tonalite			
Sample #	Ba-JM-25a		Ba-JM-68		Ba-JM-36a			
Grain #	P-25a-4c*	P-25a-4r*	P-68-4	P-68-5	P-36a-4c*	P-36a-4r*	P-36a-5	P-36a-6
Number of Points	1	1	2	1	1	1	2	2
SiO_2	58.60	60.52	58.12	56.62	55.64	59.30	56.50	57.71
Al_2O_3	26.22	24.86	26.57	27.04	28.24	25.62	27.60	26.40
FeO_t	0.00	0.28	0.16	0.18	0.16	0.20	0.19	0.11
CaO	8.10	6.54	8.32	8.90	10.80	7.28	9.83	8.39
Na_2O	6.73	7.74	6.54	6.46	5.37	7.48	5.93	6.87
K_2O	0.11	0.10	0.09	0.09	0.07	0.09	0.06	0.09
TOTAL	99.76	100.04	99.80	99.29	100.28	99.97	100.11	99.57
Formula Proportions Based on Cation Sum = 5								
Si	2.631	2.697	2.612	2.555	2.503	2.645	2.537	2.593
Al	1.388	1.307	1.408	1.439	1.498	1.348	1.461	1.398
Fe	0.0	0.010	0.006	0.007	0.006	0.007	0.007	0.004
Ca	0.390	0.312	0.400	0.430	0.521	0.348	0.473	0.403
Na	0.586	0.669	0.570	0.565	0.468	0.647	0.516	0.597
K	0.006	0.006	0.005	0.005	0.004	0.005	0.004	0.005
Or/(Or + Ab + An)	0.006	0.006	0.005	0.005	0.004	0.005	0.004	0.005
Ab/(Or + Ab + An)	0.597	0.678	0.585	0.565	0.472	0.647	0.520	0.594
An/(Or + Ab + An)	0.397	0.317	0.410	0.430	0.525	0.348	0.477	0.401

*Letters "c" and "r" in the grain numbers designate core and rim zones.

patches or discontinuous zones of more calcic or slightly more sodic plagioclase are present. Average microprobe analyses for the cores and rims of the individual grains in each rock are tabulated in Appendix C (Table C-4). Because of the pronounced zoning in many grains, the microprobe averages depend strongly upon the choice of a few particular grains and points to be analyzed and upon the location of the thin section cut through the chosen grains. Core analyses sometimes vary as much among points in a grain or among grains in a rock as from rock to rock, and the differences in tabulated core compositions among the rocks are not statistically meaningful. In contrast, thin-section observations indicate that the differences among the tabulated rim compositions are generally meaningful and representative of the variations among the rocks.

Extinction-angle measurements indicate that the average compositions of the interiors of grains fall consistently in the range An_{35} to An_{45}, generally between An_{37} and An_{42}. Cores in the range An_{50} to An_{80} are extremely rare; most are small relicts partially replaced by andesine. These average interior compositions are naturally a bit less calcic, on the whole, than the microprobe core analyses, which were generally chosen to represent the most calcic areas in a grain. However, none of the more than 80 microprobe core analyses gave a composition more calcic than An_{52}. Anorthite contents of plagioclase cores in the GBT appear to average 2-3% lower than in the rest of the pluton; otherwise, no systematic variations in core compositions are apparent. Both microprobe and microscopic observations indicate that plagioclase crystals included in hornblende are similar in composition to the rest of the plagioclase, although rims are generally less sodic, as should be expected.

Unlike the average core compositions, rim compositions show systematic variations throughout the pluton. Rims of An_{26-32} characterize nearly the entire SHbT, although the values drop to An_{21-25} in the southwestern part of the unit and to intermediate values (An_{24-26}) in the one sample examined from the southeastern part of the mass. In contrast, rim compositions in the outer gneissose phase of the SHbT fall consistently in the range An_{21-25}. Rim compositions in the eastern three quarters of the PHbT are similar to those in the SHbT (An_{26-31}), but the values decrease to An_{20-25} in the western part of the mass. Thus, a similar increase in the soda content of plagioclase rims and in the range of zoning from core to rim occurs in both the SHbT and PHbT in the west-central part of the pluton.

Rim compositions of An_{22-26} generally prevail in the northern half of the SPT, although the rims in the one sample (35a) examined from near the northeastern margin of the unit are An_{29-32}, comparable to the values throughout the eastern part of the PHbT. Rim compositions decrease slightly to about An_{19-23} in the central and southern parts of the SPT. In general, the most sodic rim compositions in the pluton occur in the southern part of the SPT and in some samples from the western part of the PHbT.

The microprobe analyses, even those of the sodic microveinlets, invariably show <1.7% Or -- commonly <1% -- despite the presence of biotite in all samples and of K-feldspar in all but the SHbT samples. FeO_t contents, determined in half of the analyses, are consistently very low. MgO, BaO, and TiO_2 contents, not reported in the tables, were obtained on the plagioclase grains included in hornblende; the

values are too low to be analytically significant.

Some additional comments should be made concerning plagioclase zoning. Although calcic cores are extremely rare, some oscillatory-zoned grains exhibit one or more thin euhedral, often discontinuous, especially-calcic zones which occur out from the center of the crystals, sometimes even near the rims. The prevalence of these zones is closely correlated with the degree of development of euhedral progressive and oscillatory zoning. Thus, thin calcic zones are common in the SPT, less common in the PHbT, and sparse in the SHbT. Also, those in the SPT are commonly in the range An_{55} to An_{80}, whereas those in the PHbT and especially in the SHbT rarely exceed An_{55}. Although the general pattern of oscillatory zoning probably developed by a repetitive diffusion-controlled mechanism such as that proposed by Bottinga et al. (1966), the few thin, especially calcic zones probably record abrupt perturbations in the magma. Assuming that the magma was sufficiently undersaturated in H_2O at this stage of crystallization, a decrease in pressure accompanying rapid rise of the magma would seem to be the most reasonable perturbation. That is, for P_{H_2O} sufficiently less than P_{Total} -- how much less is unknown -- decreasing confining pressure should lower rather than raise the temperatures of the plagioclase crystallization loop and therefore lead to a higher An/Ab ratio of the stable plagioclase.

Rather surprisingly, euhedral oscillatory and progressive zoning are better developed and preserved in the GBT than elsewhere in the SHbT. Perhaps faster cooling near the pluton margin inhibited post-crystallization destruction of zoning, despite the intense protoclasis

and recrystallization of biotite and quartz. Alternatively, and perhaps more likely, differing physico-chemical conditions in the magma near the contact may have favored greater development of euhedral oscillatory and progressive zoning in the GBT than in the interior of the SHbT. Bottinga et al. (1966) emphasized that the development of oscillatory zoning depends upon a delicate balance between the rate of crystal growth and the relative diffusion rates of Ca, Na, Al, and Si. Because such factors as P_{H_2O}, magma composition, and cooling rate must influence this balance, it seems possible that increased cooling rate and/or influx of fluids from the wall rocks enhanced the development of zoning in the GBT. In this regard, it is interesting to note that the volatile content of the magma apparently was highest in the southern part of the pluton (see Section 12.10), where euhedral oscillatory and progressive zoning are most pronounced. Unfortunately, the physico-chemical factors controlling magmatic zoning are still poorly understood, and any hypothesis attempting to explain the variations in zoning patterns is necessarily speculative.

Consider some characteristics of the sodic rims. First of all, the rim zones are generally thin and make up only a small proportion of the grain volume; the bulk composition of plagioclase is consistently An_{35-40}. Secondly, in the western and southern parts of the pluton, the inner margins of the rims are commonly defined by an abrupt change of 5-10% in An content, from An_{19-25} in the rim to about An_{30} just inside the rim. The interiors of grains, although often showing oscillatory zoning, show a much more gradual overall increase in An content inward. This two-step zoning implies an abrupt change in the

physico-chemical conditions in the magma towards the end of crystallization in this part of the pluton. The nature of the change is open to speculation, but the simplest explanation involves an abrupt decrease in P_{H_2O}. That is, if by this stage of crystallization, the magma had closely approached or reached saturation in water, then rapid upward movement could lead to a sudden decrease in P_{H_2O}, hence a sudden increase in the Na/Ca ratio of the stable plagioclase.

Thirdly, rim zones are frequently discontinuous, and compositions vary considerably, sometimes by as much as 15% An, around the margins of individual grains. There are two explanations for this. (1) Towards the end of magmatic crystallization, crowding of grains naturally results in non-uniform growth, depending upon the availability of space around different parts of each grain. (2) Corrosion, replacement, protoclasis, and recrystallization around grain margins all contribute to discontinuities in rim zones, particularly in the SHbT, GBT, and the more foliated parts of the PHbT. Nonetheless, with the occasional exception of tiny veinlets and thin discontinuous replacement rims, the most sodic plagioclase tends to be quite uniform in composition in a given rock. It is the composition of this latest uniform material which I refer to as the rim composition and which varies systematically throughout the pluton.

Lastly, as just mentioned, some plagioclase crystals are cut by tiny veinlets of sodic plagioclase, and some have extremely thin discontinuous sodic rims, most frequently along contacts with quartz. The microveinlets, which are common in many SHbT samples and also occur in a few SPT samples, are restricted to a few scattered individual

grains and never cross grain boundaries. Fracturing -- in some cases severe shattering -- of grains was thus a very local intergranular phenomenon, and veining must have been accomplished by a pervasive intergranular fluid phase rather than by fluids introduced or concentrated along macroscopic fractures. Microprobe analyses yielded compositions of An_{17} and An_{20} for veinlets in SHbT sample 29 (Table 9). Thin-section observations suggest that these compositions, which are 7-10% less calcic than the rim compositions in the same rock (Table 8) and in the SHbT as a whole, are representative of the microveinlets and thin replacement rims in general, although extinction-angle measurements indicate rare, extremely thin replacement rims as sodic as An_{10-12} in some SPT samples. Both the microveinlets and the replacement rims are deuteric phenomena caused by interaction with a fluid phase which was out of equilibrium with the rims as well as the interiors of the plagioclase.

12.4 Potassium Feldspar

Fine-grained interstitial potassium feldspar is a consistently minor constituent of the tonalite, comprising <0.3% everywhere except in (1) the western quarter of the PHbT, (2) the adjacent southwestern part of the SHbT, and (3) the GBT around the western half of the SHbT. In those three areas, concentrations are typically 0.5-2% and may locally reach 5%. The areas of higher K-feldspar contents coincide with the parts of the SHbT and PHbT characterized by more sodic plagioclase rim compositions.

Potash feldspar appears non-perthitic and generally untwinned.

Some grid-twinned microcline occurs in the GBT and rarely in other samples. The 2V of the untwinned K-feldspar varies from <10° (possibly down to 0°) up to 50°, rarely higher, with angles <30° prevailing throughout most of the pluton. The entire range is sometimes present in a single thin section, and variations of 20° or more are found in a few individual grains, generally accompanied by a small change in birefringence. For K-feldspar of this composition (Or_{90-95}; Table 11), the variation in 2V corresponds to a range in structural state from sanidine to orthoclase (Tuttle, 1952). Conceivably, most or all of the K-feldspar crystallized initially as sanidine.

Slight systematic variations in the textures and optical properties of K-feldspar can be recognized within and among the textural units. K-feldspar in the SPT is invariably sanidine plus subordinate orthoclase (2V generally 5-25°, seldom >40°) and occurs mainly as scattered interstitial grains, up to 0.2 mm in size, bounded by euhedral hornblende or plagioclase and/or by quartz or biotite. Evidence of reaction with other phases is rare, although minor replacement of plagioclase has occurred. Those parts of the hornblende and plagioclase crystals bounding the interstitial areas are often exceptionally smooth and euhedral, indicating that the K-feldspar in the SPT filled small open spaces into which the plagioclase and hornblende had grown uncontested. In some cases, the intersititial K-feldspar is accompanied by quartz, primary muscovite, or occasionally primary chlorite, sphene, or epidote.

Throughout the eastern three quarters of the PHbT, K-feldspar is again untwinned and generally has a small (<30°) 2V. Smoothly

bounded interstitial primary grains are scarce and tiny; much of the K-feldspar forms tiny networks, veins, and patches in plagioclase and appears to be of secondary origin.

As its concentration increases westward across the PHbT, K-feldspar becomes coarser and occurs more as interstitial grains than as networks, veins, or patches in plagioclase. Most is untwinned, but some shows wavy extinction and rare grid twinning, especially in those samples showing visible protoclasis. The 2V averages 30-50°, but ranges widely from <10° to 60° within most thin sections. Although the average grain size appears in thin section to be 0.2-0.5 mm, many crystals are highly poikilitic and actually coarser; a few grains reach 2-4 mm. Margins of interstitial grains may be molded smoothly around or between euhedral faces of hornblende or plagioclase, as in the SPT, or they may be slightly irregular and may embay or vein adjacent grains. In a few samples from the southwestern part of the PHbT, some of the K-feldspar occurs as discontinuous overgrowths on subhedral or euhedral plagioclase; the overgrowths have replaced plagioclase to some degree, but they appear, for the most part, to have nucleated on the plagioclase and grown into available open space. Textures suggest concurrent growth of K-feldspar and interstitial quartz.

In the southwestern 2 or 3 km of the SHbT, K-feldspar is comparable in abundance, texture, and optical properties to that in the western part of the PHbT. Elsewhere in the SHbT, K-feldspar is much less abundant and commonly too fine-grained for positive identification. Some material identified as potash feldspar on the basis of low

refractive index could be zeolite or sodic plagioclase, and the modal abundances reported in Plate 8 -- ranging from 0.05-0.19% -- may be overestimated, especially the 0.18% reported for sample 29. The trace of K-feldspar recognized in the SHbT is untwinned, has a small 2V, and occurs almost exclusively as tiny veins, networks, and patches replacing plagioclase; interstitial grains were seen in a few thin sections. Textures suggest that much or all of the K-feldspar is of deuteric origin; except perhaps in the southwestern part of the unit, most of the SHbT magma may never have achieved saturation in K-feldspar.

Potash feldspar occurs in the GBT mostly as fine-grained granular or irregularly poikilitic material in the protoclastic and recrystallized mortar. Structural state ranges from sanidine to microcline in individual thin sections. Because of the protoclastic history and partial recrystallization of these rocks, it is unclear whether the K-feldspar is of hypersolidus or subsolidus origin.

Myrmekitic plagioclase-quartz intergrowths have partially replaced K-feldspar in the GBT and in some samples from the western parts of the PHbT and SHbT. Much of the myrmekite occurs in the granulated and recrystallized mortar of the protoclastic rocks, but some occurs as discontinuous rims on subhedral or euhedral plagioclase crystals adjacent to or enclosed in K-feldspar. Generally, such myrmekitic rims are discrete overgrowths nucleated onto sharply defined crystal faces, but in some cases, the plagioclase component of the myrmekite grades smoothly into the non-myrmekitic interior of the plagioclase grain as well as laterally, parallel to zonal boundaries, into typical non-myrmekitic

rim plagioclase (Figure 56). Refractive indices and extinction positions indicate that the plagioclase in the myrmekite is compositionally similar to, or only slightly more sodic than, the typical rim plagioclase in the same rocks: roughly An_{15-25}. These observations imply replacement of K-feldspar by myrmekite simultaneously with the crystallization of typical plagioclase rims. Thus, crystallization of K-feldspar began in some rocks before cessation of plagioclase crystallization.

Average microprobe analyses of K-feldspar in five rocks are given in Table 11. The averages are based on 38 analyses in 15 grains. Average compositions of the individual grains are listed in Appendix C, Table C-5, along with the estimated 2V angles of suitably oriented grains. The number of analyses was limited by the low abundance and fine grain size in some samples. No grains sufficiently coarse to identify and analyze were found in microprobe sections cut from SHbT samples 25a, 29, and 68, but optical properties of rare grains in other thin sections of these rocks are consistent with the compositions in Table 11.

The compositions are remarkably potassic and fall within a very restricted range from $Or_{90.5}$ to $Or_{94.8}$ (mole %) among the five rocks and $Or_{88.4}$ to $Or_{96.9}$ among all grains. BaO contents are notably higher than Na_2O; all other analyzed oxides -- FeO_t, MgO, MnO, TiO_2, and even CaO -- are present in only trace amounts. The data show real variations of up to 4.5% Or among points in a grain and of up to 6.7% Or among grains in a single thin section. The small differences in composition from rock to rock are thus of doubtful significance.

Figure 56. Part of a subhedral zoned plagioclase crystal in the gneissose border tonalite. The rim at the top of the crystal consists of a myrmekitic intergrowth of plagioclase and quartz. Refractive indices and extinction position indicate that the composition of the plagioclase in the intergrowth is the same as that of the non-myrmekitic rim (An ≈ 20-25) into which it grades laterally parallel to the grain margin. A trace of K-feldspar remains as a tiny inclusion in the myrmekite. Sample Ba-JM-568a from Arroyo de las Parritas, 45 m from the northwestern margin of the pluton (area F-3).

Table 11

Average Microprobe Analyses of K-Feldspar
in Individual Tonalite Samples

Name of Unit	GBT	PHbT		SPT		Pluton	
Sample #	Ba-JM 30a	Ba-JM 36a	Ba-JM 46a	Ba-JM 3a	Ba-JM 62a	Average	σ
Number of Grains	4	2	2	4	3		
SiO_2	64.60	62.68	64.77	63.77	63.56	63.88	0.85
TiO_2	n.a.	0.01	n.a.	0.01	0.02	0.01	0.01
Al_2O_3	18.61	18.53	18.84	18.66	17.98	18.52	0.32
FeO_t	0.07	0.07	0.06	0.04	0.03	0.05	0.02
MnO	0.00	n.a.	0.00	n.a.	n.a.	0.00	0.00
MgO	0.04	0.01	0.03	0.01	0.01	0.02	0.01
BaO	1.46	1.67	1.34	0.91	0.72	1.22	0.39
CaO	0.03	0.10	0.03	0.02	0.03	0.04	0.03
Na_2O	0.74	0.32	0.73	0.59	0.41	0.56	0.19
K_2O	15.18	14.66	15.05	15.68	15.97	15.31	0.52
TOTAL	100.73	98.05	100.84	99.69	98.73	99.61	---
Formula Proportions Based on Cation Sum = 5							
Si	2.990	2.995	2.992	2.971	2.994	2.988	0.010
Ti	---	0.000	--	0.000	0.001	0.000	0.001
Al	1.015	1.043	1.026	1.025	0.994	1.021	0.018
Fe	0.003	0.003	0.002	0.002	0.002	0.002	0.001
Mn	0.000	---	0.000	---	---	0.000	0.000
Mg	0.002	0.001	0.002	0.000	0.001	0.002	0.001
Ba	0.027	0.031	0.024	0.016	0.012	0.022	0.008
Ca	0.001	0.006	0.001	0.001	0.002	0.002	0.002
Na	0.066	0.029	0.066	0.053	0.037	0.050	0.017
K	0.896	0.894	0.887	0.932	0.959	0.914	0.031
Or/(Or+Ab+An+Ce)	0.905	0.933	0.907	0.930	0.948	0.925	0.018
Ab/(Or+Ab+An+Ce)	0.067	0.030	0.067	0.053	0.037	0.051	0.017
An/(Or+Ab+An+Ce)	0.001	0.006	0.001	0.001	0.002	0.002	0.002
Ce/(Or+Ab+An+Ce)	0.027	0.032	0.025	0.016	0.013	0.023	0.008

However, there is no evidence of systematic compositional zoning within grains, nor any variation in composition as a function of grain size, texture, or structural state, although more analyses are needed to substantiate these conclusions.

Deer et al. (1963, vol. 4) consider any feldspar containing >2% BaO to be barium feldspar. Grain KF-36a-2 (single analysis, Table C-5, Appendix C) contains 2.78% BaO (5.3 mole % celsian) and thereby qualifies as a barium sanidine or barium orthoclase; several other grains contain nearly 2% BaO. Inasmuch as BaO contents show real reproducible variations of up to 1-2% among grains in a thin section and among points in some grains, additional analyses might well reveal even higher local BaO concentrations.

12.4.1 Ternary Feldspar Relationships and the Origin of the Potassium Feldspar

Compositions of K-feldspar and plagioclase have been plotted on an Ab-An-Or triangle in Figure 57. Lines join the compositions of potash feldspar to those of plagioclase rims in the same samples. Inasmuch as the term "tie line" is strictly applicable only to phases demonstrably in equilibrium, I will refer to these lines as "apparent" tie lines.

The most striking observations from the diagram are (1) the extremely limited degree of ternary solid solution and (2) the very high Or content of the K-feldspar, hence the low angle between the apparent tie lines and the Ab-Or side of the triangle. Note also that the Or content of plagioclase does not change from core to rim. Inasmuch as plagioclase cores crystallized long before the melt attained saturation in K-feldspar, the core composions should be undersaturated in Or. In fact, the melt probably

Figure 57. Ab-An-Or plot (in mole %) for feldspars from the San José pluton. Lines connect K-feldspar compositions with the compositions of plagioclase rims in the same rock.

▲ gneissose border tonalite

△ stubby hornblende tonalite

◮ sodic microveinlets in plagioclase (sample 29, stubby hornblende tonalite)

○ prismatic hornblende tonalite

● seriate porphyritic tonalite

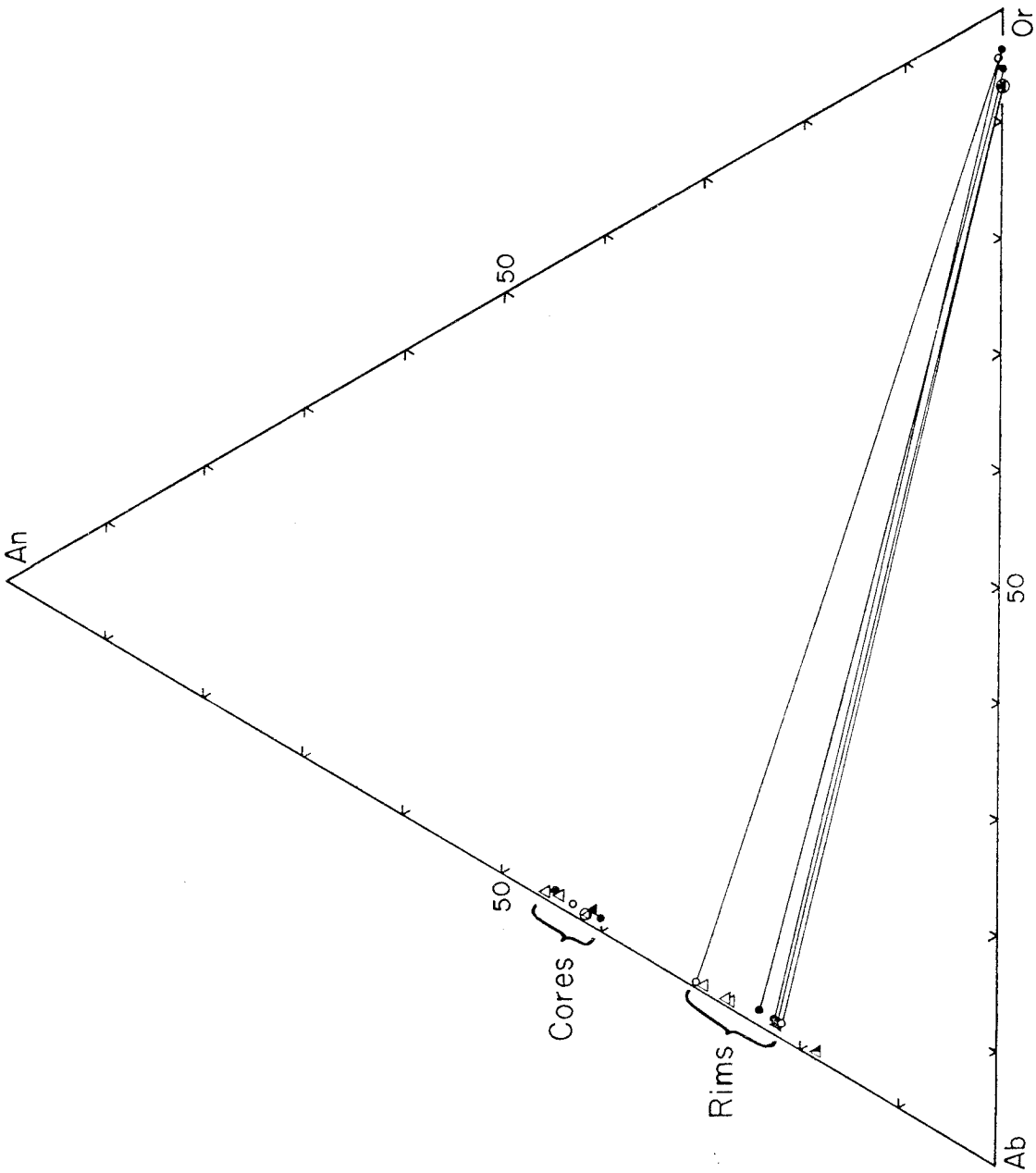
An
Or
Ab
50
50
50
Cores
Rims

did not become saturated even in biotite until after much of the plagioclase had crystallized. Likewise, plagioclase rims and microveinlets in the SHbT samples may not be in equilibrium with the trace amounts of entirely (?) deuteric K-feldspar in those rocks and may therefore also be undersaturated in Or. The question arises, do the plagioclase rim and K-feldspar compositions in the GBT, PHbT, and SPT samples represent magmatic equilibrium values -- that is, are the connecting lines in Figure 57 true tie lines joining compositions which define segments of the ternary solvus under the T, P, and P_{H_2O} prevailing at the end of magmatic crystallization? Alternative possibilities are that (1) K-feldspar crystallized as a late magmatic or high-temperature subsolidus phase from fluids not in equilibrium with the rim plagioclase, or (2) K-feldspar and plagioclase rim compositions record post-crystallization exchange. Textural evidence bearing on this question and on possible sources of Or component in the fluid phase will be discussed later. Let us first examine the evidence from analyses of coexisting feldspars in other granitic rocks and from experiments and thermodynamic considerations.

Piwinskii (1968b) and Piwinskii and Wyllie (1970) reported microprobe analyses of the cores and rims of feldspar pairs in granitic rocks of the Sierra Nevada and the Wallowa batholith (Oregon) respectively. Rim compositions reported in these two papers are plotted in Figure 58. Both sets of data are similar to the San José analyses in several respects. Solid solution of Or in plagioclase and of An in K-feldspar are very limited in each case; 0.5-2% Or and 0.4-1% An in the Sierra Nevada analyses and 0.8-1.5% Or and 0.1-0.5% An in the Wallowa batholith

Figure 58. Compositions (in mole %) of coexisting K-feldspar and plagioclase rims in (A) Sierra Nevada granitic rocks (Piwinskii, 1968b) and (B) the Wallowa batholith (Piwinskii and Wyllie, 1970).

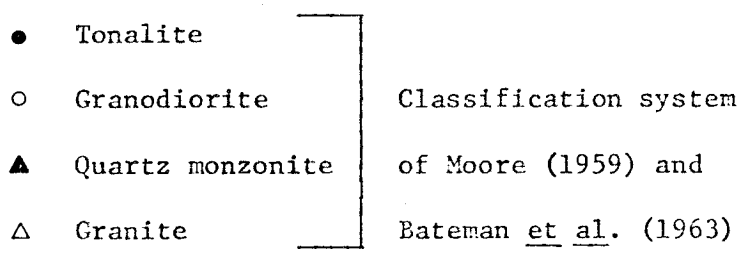

The stippled areas define the range of apparent tie lines for K-feldspar and rim plagioclase in the San José pluton.

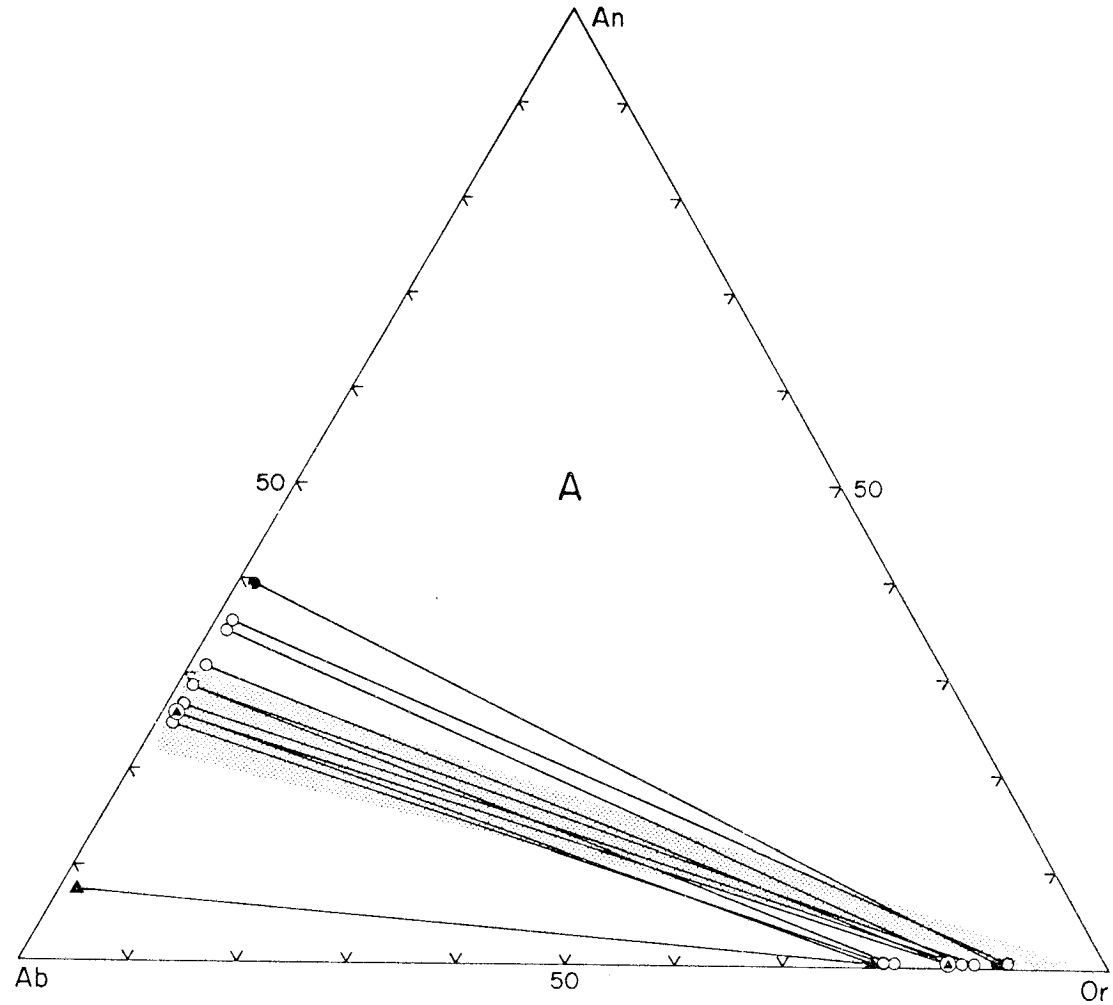
An
50
A
50
Ab
50
Or

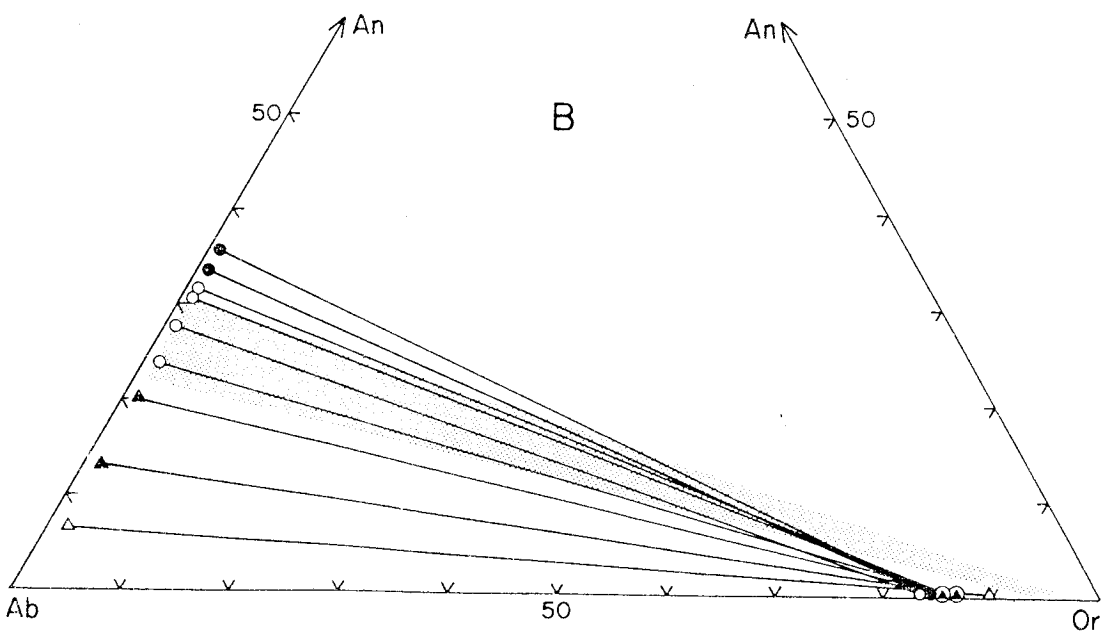
An
50
B
An
50
Ab
50
Or

compared to 0.6-1.3% Or and 0.1-0.6% An in the San José feldspars. In addition, Or contents of plagioclase grains in each case are constant from core to rim and independent of the An content of the rims. However, for comparable plagioclase rim compositions, K-feldspars in the Sierran and Wallowan rocks contain roughly 6-16% more Ab.

Most of the Sierran and Wallowan rocks examined are granodiorites, quartz monzonites, and granites in which both K-feldspar and plagioclase are major phases which presumably crystallized in magmatic equilibrium. Therefore, unless there has been appreciable subsolidus modification of compositions, tie lines for feldspar rim pairs in these rocks should be reasonably reliable indicators of the equilibrium partitioning of feldspar components at solidus conditions. Both Piwinskii and Piwinskii and Wyllie reported non-systematic variations of up to 10% Or in some K-feldspar crystals, implying some degree of disequilibrium as well as some uncertainty in the tabulated average compositions. However, apparent tie lines for contiguous feldspars in pegmatites from the Spruce Pine district of North Carolina (Orville, 1958) are quite similar to the Sierran and Wallowan data and support the interpretation that the compositions in all three cases represent a close approach to equilibrium.

In Figure 59, coexisting feldspar compositions determined in experiments by Yoder et al. (1957) on the Ab-Or-An-H_2O system at P_{H_2O} = 5 kb and by Piwinskii (1968a) and Piwinskii and Wyllie (1970) on natural Sierran and Wallowan plutonic rocks with excess water at 2 kb are superimposed on the range of apparent tie lines for K-feldspar and rim plagioclase in the San José tonalite. The experimental results agree

Figure 59. Comparison of the range of tie lines for K-feldspar and rim plagioclase in the San José pluton (stippled areas) with experimentally determined tie lines.

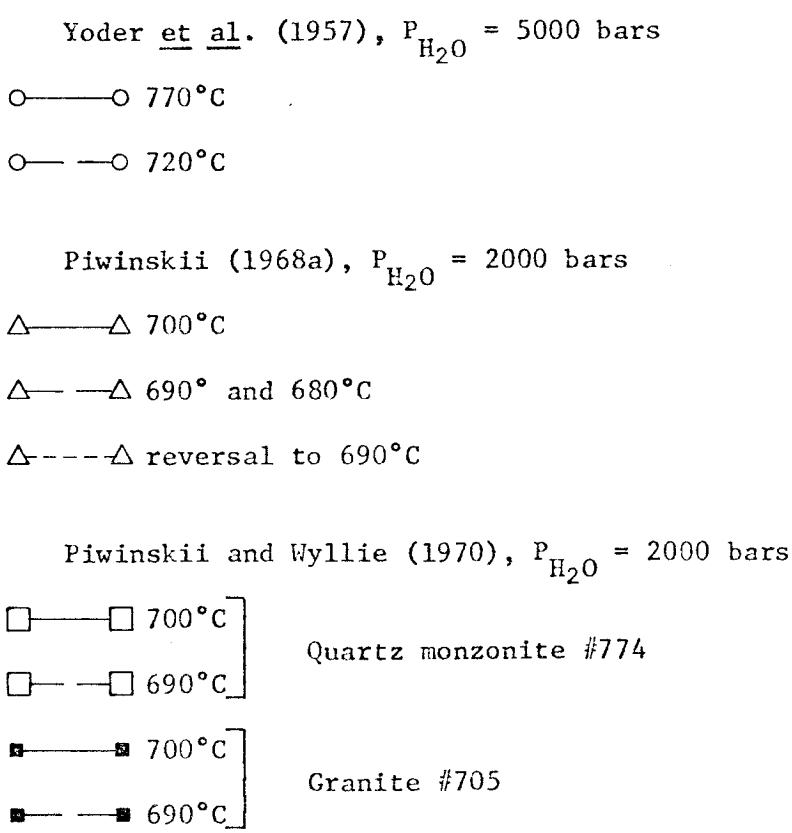

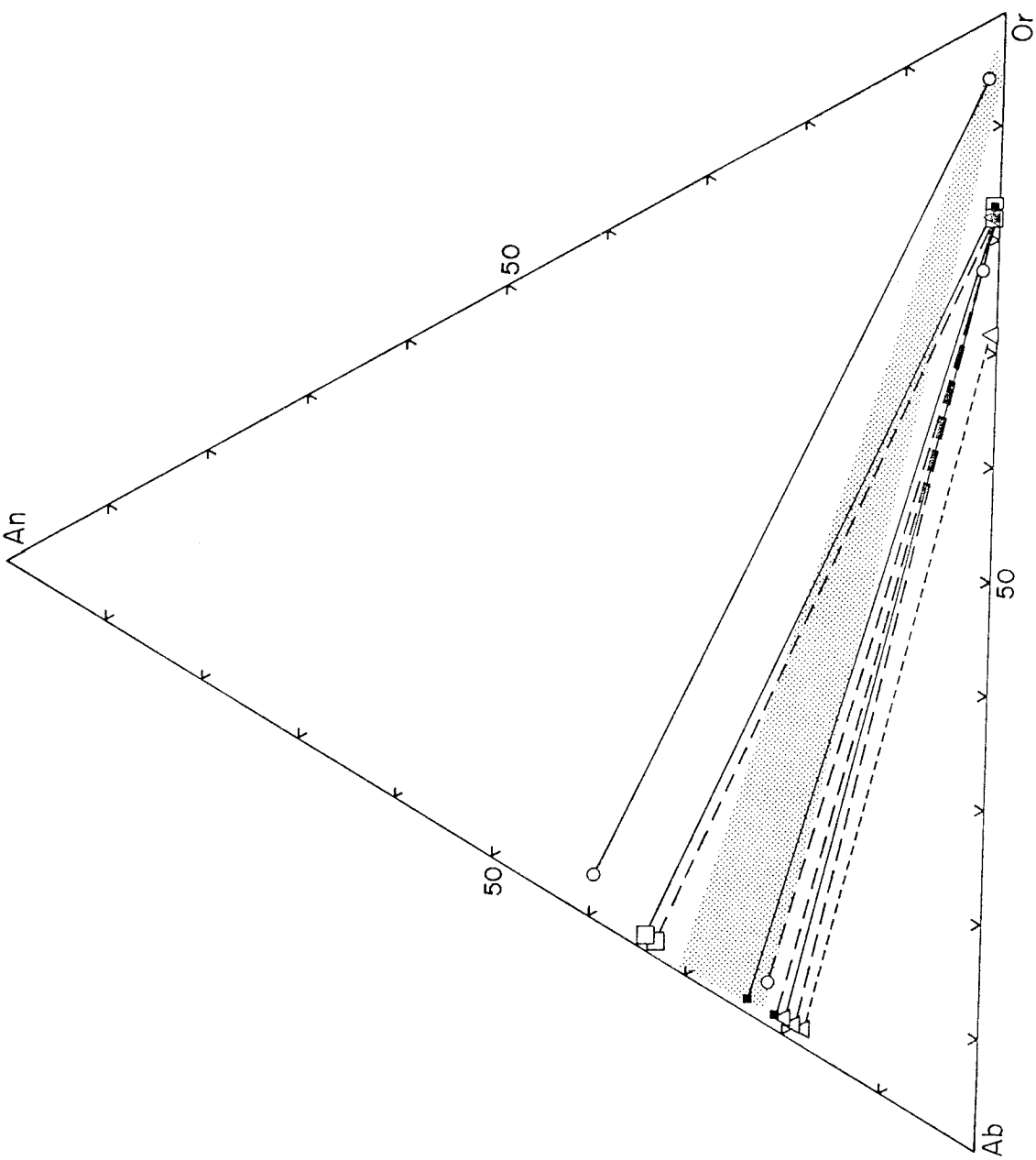
An
Or
Ab
50
50
50

closely with the data on natural feldspars in the Sierra Nevada and Wallowa batholiths, but they re-emphasize the unusually potassic compositions of K-feldspar in the San José pluton. Yoder et al. and Piwinskii both noted that attempts to reverse the reactions between feldspars yielded slightly different compositions; normal and reversed runs by Piwinskii at 690°C yielded similar plagioclase compositions, but a 10% disparity in Or content of K-feldspar. Piwinskii and Wyllie (1970) therefore concluded that the experimentally determined tie lines may not represent stable equilibrium values; nonetheless, the close agreement of their results with the experiments of Yoder et al. and with the natural Sierran and Wallowan feldspars is impressive.

Figure 60 shows the much different feldspar compositions predicted by the two-feldspar thermometer curve of Barth (1962) and by the more sophisticated thermodynamic partitioning model of Stormer (1975). Barth's thermometer curve, which plots ln $(X_{Ab}^{KF}/X_{Ab}^{Plag})$ against inverse temperature, is based upon analyses of natural feldspar pairs whose temperatures of equilibration were independently estimated. Barth's method is therefore limited by the uncertainty in the estimated equilibration temperatures of the natural feldspars used to calibrate the curve. Barth assumes, moreoever, that the effects of pressures and bulk composition on the partitioning of albite between coexisting feldspars are negligible.

In contrast, Stormer's curves account for the important effects of pressure and bulk composition and were established without recourse to measurements on natural rocks. However, the applicability of his curves to natural feldspars depends upon the validity of three

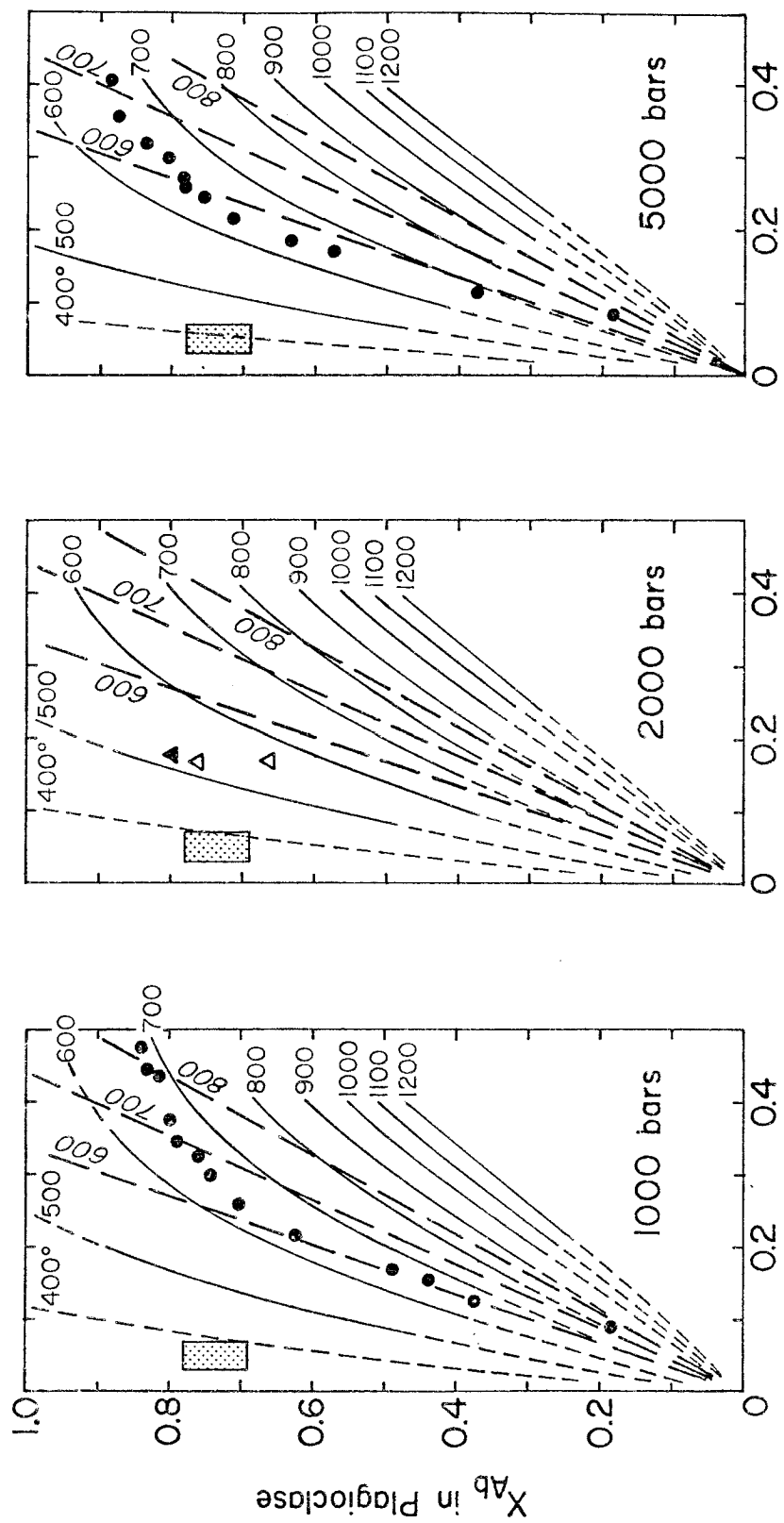

Figure 60. Partitioning of albite (mole fraction) between coexisting feldspars as a function of temperature (°C). Modified from Figure 3 of Stormer (1975).

——— Thermodynamic partitioning model of Stormer (1975); dashed where reliability is doubtful

—— — —— Empirical two-feldspar thermometer curves from Barth (1962)

● Experimental data of Seck (1971) at 650°C

▨ Range of plagioclase rim and K-feldspar compositions in the San José pluton

▲ Experimental data of Piwinskii (1968a) at 700°C

△ Experimental data of Piwinskii and Wyllie (1970) at 700°C

assumptions: (1) solid solution of Ab in plagioclase is ideal, (2) solid solution of Ab in alkali feldspar obeys the thermodynamic mixing model of Thompson and Waldbaum (1969) and Waldbaum and Thompson (1969) for the binary sanidine-high albite system, and (3) solid solution of Or in plagioclase and of An in alkali feldspar affects the activity of Ab only through inert dilution. The mixing model for the Ab-Or binary is based in turn upon the experiments of Orville (1963) and of Luth and Tuttle (1966).

Also shown in Figure 60 are the range of K-feldspar and rim plagioclase compositions in the San José pluton, plus the experimental results of Seck (1971) at 650°C and P_{H_2O} = 1000 and 5000 bars and those of Piwinskii (1968a) and Piwinskii and Wyllie (1970) at 680-700°C and P_{H_2O} = 2000 bars. Seck's results, based upon the synthesis of feldspars from dehydrated gels of stoichiometric feldspar composition, agree remarkably well with Stormer's model except in the region of Ab-poor bulk compositions, where the reliability of Stormer's curves is uncertain. Additional experiments by Seck at P_{H_2O} = 10,000 bars also agree well with Stormer's model. In contrast, the experiments of Piwinskii and of Piwinskii and Wyllie yielded feldspars whose compositions should, according to Stormer's curves, be in equilibrium at temperatures between 500 and 600°C rather than at 680-700°C; viewed in another way, Stormer's model predicts roughly 10-20% more Ab in alkali feldspar than was actually measured. Only the 690°C reversal run of Piwinskii approaches the partitioning expected from Stormer's model and Seck's data. Moreover, the experiments of Piwinskii and of Piwinskii and Wyllie yielded notably lower solid solution of Or in plagioclase (about 1.5% for An_{20-30})

than did the experiments of Seck (determined roughly by X-ray diffraction as 4% at 5 kb and 6% at 1 kb for An_{20-30}).

Stormer's curves imply that, if K-feldspar and rim plagioclase in the San José samples are equilibrium pairs, exchange occurred at temperatures below 450°C -- i.e., well below the solidus -- assuming reasonable pressures of 5 kb or less. Even for pressures up to 10 kb, the implied temperatures are below 500°C. Such temperatures seem inconsistent with the moderately disordered structural state of the K-feldspar indicated by the optical properties, unless the K-feldspar was structurally metastable. Stormer's curves also imply either disequilibrium or equilibration at temperatures of 500-600°C or less -- again notably subsolidus temperatures -- for all of the Sierran and Wallowan feldspar rim pairs in Figure 58, assuming $P \leq 5$ kb. Yet, as mentioned earlier, these feldspar pairs are probably as likely to record magmatic equilibrium as are those found in any plutonic rocks.

These inconsistencies point out the severe difficulty in interpreting two-feldspar data, both experimental and natural. Seck (1971) and Orville (1963) both demonstrated a close approach to reversible chemical equilibrium. In contrast, the single attempt by Piwinskii (1968a) to establish reversible equilibrium resulted in a 10% discrepancy in the Or content of the alkali feldspar. These results seem to imply that the data of Seck and Orville -- hence the calculated curves of Stormer -- are more reliable than the data of Piwinskii or Piwinskii and Wyllie. However, as pointed out by Seck, the feldspars synthesized in his experiments (and in those of Orville and of Luth and Tuttle, 1966, upon which Stormer's curves are ultimately based) have disordered, high-

temperature structures which are metastable under the P-T conditions of the experiments, and there is no guarantee that the more ordered feldspars structurally stable under these conditions would show the same partitioning of elements as observed in the metastable phases.

Experimental data on the binary Ab-Or system suggest that the influence of structural state on the compositions of coexisting plagioclase and alkali feldspar may be considerable. The solvus for metastable disordered feldspars of the sanidine-high albite series at 2 kb crests at about 675°C (Thompson and Waldbaum, 1969), whereas the solvus for metastable ordered feldspars of the microcline-low albite series at atmospheric pressure crests very roughly at 885°C (Bachinski and Müller, 1971).[12] Presumably, a rise in critical temperature results in an expansion of the solvus, i.e., in a shift of the solvus limbs towards the Ab and Or end members at any given temperature; the data of Bachinski and Müller show such a shift, at least for T >500°C, but the experimental difficulties in establishing reversible chemical equilibrium make the exact positions of the solvus limbs uncertain, especially for the microcline-low albite series.

Assuming that the effect of structural state observed in the Ab-Or binary also exists in An-bearing systems, the ternary feldspar solvus at a given temperature and pressure should be wider, i.e., approach closer to the Ab-An and Ab-Or sides of the Ab-An-Or triangle, for feldspars of low structural state than for those of high structural

---

[12]Because the critical temperature increases with increasing pressure, the disparity between the two solvi would be even greater if both data sets were at the same pressure.

state. This idea shown schematically in Figure 61; the magnitude of the effects is unknown, but is presumably proportional to the degree of disorder.

If valid, the foregoing conclusion implies that Stormer's curves may be applicable only to volcanic or hypabyssal intrusive rocks containing disordered alkali feldspar of the sanidine-high albite series; in plutonic rocks, coexisting feldspars of lower structural state should be characterized by (1) lesser amounts of Or in plagioclase and of An in alkali feldspar and (2) lesser amounts of Ab in alkali feldspar coexisting with plagioclase of a given Ab/An ratio. Thus, the feldspar rim pairs in the Sierran and Wallowan rocks may record magmatic equilibrium even though comparison with Stormer's curves and Seck's data suggests disequilibrium or subsolidus exchange. Similarly, the tie lines determined experimentally by Piwinskii (1968a) and Piwinskii and Wyllie (1970) may be more realistic for plutonic feldspars than are the tie lines predicted by Stormer or those determined by Seck.

Interpretation of experimental results and application to natural feldspars is further complicated by the results of Luth and Tuttle (1966; see also Luth and Fenn, 1973) showing that the experimentally determined sanidine-high albite solvus differs measurably depending upon whether the starting materials are of (1) stoichiometric alkali feldspar composition, (2) peraluminous composition (Al_2O_3 in excess of the amount in stoichiometric alkali feldspar), or (3) peralkaline composition (alkalies and silica in excess of the amount in stoichiometric alkali feldspar). Stormer noted that use of the various thermodynamic para-

Figure 61. Schematic illustration of the possible effect of variations in structural state on the ternary feldspar solvus. Solid lines: solvus and tie lines determined experimentally by Seck (1971) for synthetic feldspars of metastable high structural state at 650° and P_{H_2O} = 5000 bars. Dashed line: hypothetical solvus and tie lines for structurally-stable feldspars at the same pressure and temperature.

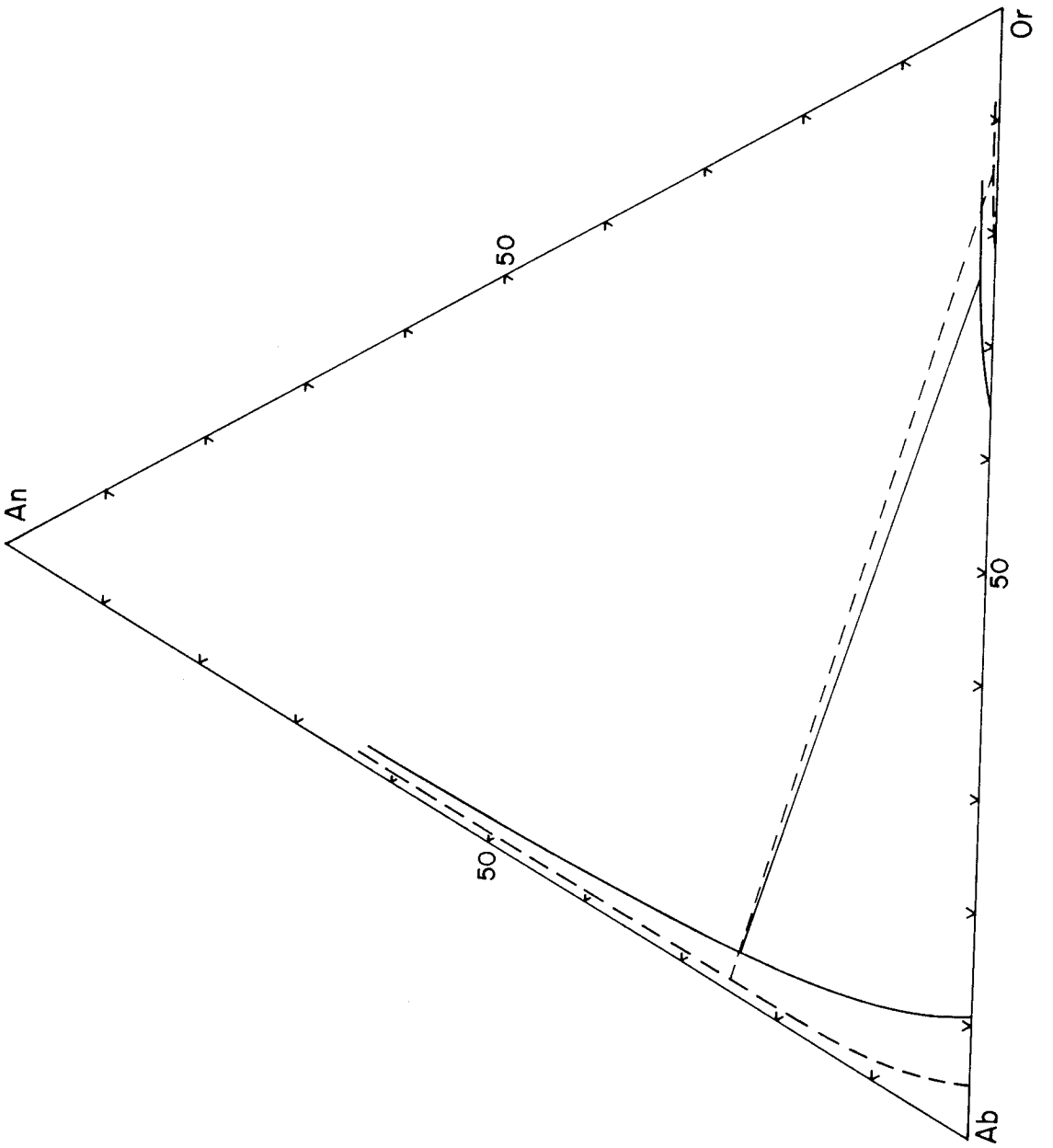
An
Or
Ab
50
50
50

meters reported by Luth and Fenn for the three different solvi in place of the parameters of Thompson and Waldbaum (1969) and Waldbaum and Thompson (1969) results in temperature differences of as much as 100°C in some parts of Figure 60.

In summary, the partitioning of components between coexisting plagioclase and alkali feldspar appears to be sensitive not only to pressure and temperature, but also to structural state and the bulk composition of the system. Consequently, evidence of *chemical* equilibrium in experimental systems is not necessarily a sufficient criterion to justify application to natural rocks. In particular, there is reason to suspect that application of Stormer's curves to coexisting feldspars in *plutonic* rocks may give erroneous results. Unfortunately, estimation of the equilibrium feldspar compositions which should be expected in plutonic rocks is extremely difficult.

From the preceding discussion it appears that the very limited solid solution of Or in plagioclase and of An in K-feldspar in the San José feldspars may not be incompatible with magmatic equilibrium. Certainly, it is not unusual for feldspars in batholithic rocks. The extremely high Or contents in K-feldspar are more difficult to reconcile with magmatic equilibrium. The hypothesized effects of structural state alone cannot readily explain the Or-rich compositions because, although the low 2V angles indicate a range in structural state from low or intermediate sanidine to orthoclase in the San José feldspars as compared with high sanidine in most experimental systems, the more Ab-rich alkali feldspars in many of the Sierran rocks exhibit grid twinning (Piwinskii, 1966a), and those in the Wallowan rocks have

2V angles ranging from 57 to 89° (Piwinskii and Wyllie, 1970; universal stage measurements). Thus, K-feldspars in the San José pluton have comparable to higher, rather than lower, structural states than those in the Sierran and Wallowan rocks.

The apparent tie lines in the San José feldspars therefore seem inconsistent with magmatic equilibrium, although the possibility remains that the combined effects of structural state, minor BaO contents, and/or additional unrecognized factors could shift magmatic equilibrium sufficiently to produce the observed compositions.

Post-crystallization exchange of the San José feldspars also appears unlikely for two reasons. (1) There is no textural evidence of perthitic or granular exsolution from either feldspar; nor is there evidence, in many cases, of reaction between adjacent K-feldspar and plagioclase grains. (2) The uniform composition of K-feldspar within individual grains and from grain to grain and rock to rock implies that, if significant post-crystallization exchange occurred, it was thorough; yet much K-feldspar retains moderately high-temperature optical properties. Furthermore, there is no apparent correlation of composition with optical properties (hence, with structural state) in the K-feldspar, such as would be expected if chemical exchange accompanied inversion to lower-temperature structural state.

The uniformly low Or contents in plagioclase throughout the pluton and from core to rim in each grain might be cited as evidence for post-crystallization equilibration. However, if such equilibration occurred, it left no residual Or-enriched areas in any of the analyzed grains, nor did it disrupt the Ab-An zoning in many grains. The Or contents

are the same in grains which preserve euhedral progressive and oscillatory zoning as in those whose original zoning has been extensively destroyed.

Thus, the compositional data are best explained by assuming disequilibrium between the K-feldspar and the plagioclase rims. This evidence of disequilibrium must be reconciled with the petrographic observations indicating that most of the K-feldspar has optical properties consistent with crystallization at or near magmatic temperatures and that much of the K-feldspar, especially in the SPT and western parts of the PHbT and SHbT, filled interstitial spaces and reacted little, if at all, with the adjacent minerals.

One possible explanation is that K-feldspar crystallized from a vapor phase which exsolved during the final stages of magmatic crystallization and which was not in equilibrium with plagioclase rims. Exsolution of the vapor phase from the magma rather than introduction of hydrothermal fluids from an external source readily accounts for the existence of the open spaces which the K-feldspar filled and for the dispersed distribution of the K-feldspar generally independent of fractures or alteration zones in the rock. Further support for this hypothesis comes from the observation that, in many SPT samples and in a few samples from the western parts of the PHbT and SHbT, minor amounts of primary chlorite, zeolite (chabazite?), muscovite, epidote, sphene, and rarely carbonate occupy similar interstitial areas between exceptionally euhedral plagioclase or hornblende faces. These primary interstitial phases, which in some cases are accompanied in apparent textural equilibrium by K-feldspar, appear to have crystallized in spaces

occupied either by melt or by a vapor phase (see Section 12.10 for a more detailed discussion). Inasmuch as several of the minerals are unlikely candidates for direct crystallization from the melt, subsolidus precipitation from a vapor phase is a much more reasonable interpretation. Plagioclase very rarely fills such interstitial spaces either as separate grains or as overgrowths on larger crystals and does not appear to be part of this assemblage.

Late magmatic or deuteric reactions involving biotite provide a reasonable source of Or component in the vapor phase. Alteration to chlorite is an obvious reaction. Another and possibly more important reaction is the equilibration of biotite to increasingly oxidizing conditions via the reaction

$$KFe_3AlSi_3O_{10}(OH)_2 + 1/2\ O_2 \rightleftharpoons KAlSi_3O_8 + Fe_3O_4 + H_2O.$$

Biotite remains a stable phase, but its composition must become progressively more magnesian (Wones and Eugster, 1965). Comparison of the compositions of coexisting biotite, magnetite, and K-feldspar with the experimental data of Wones and Eugster on this reaction suggest equilibration temperatures in the range 645-745°C, or possibly up to 50° higher (see Section 15.2.3), which compares with a solidus temperature estimated to be in the range 680-750°C (Section 15.2.1). Although there is no apparent spatial correlation of K-feldspar with biotite or chlorite, there is abundant evidence of recrystallization of biotite to varying degrees not only in the GBT, but also throughout much of the pluton. In the presence of a mobile vapor phase, the Or component released during either chloritization or oxidation and recrystallization of biotite need not have crystallized in direct

proximity to the biotite.

Deuteric alteration might provide a comparable source of Ab in the fluid phase. However, such alteration was generally very minor. Furthermore, equilibration of plagioclase to falling temperature should tend to consume rather than release Ab. It seems possible, therefore, that a late-magmatic or subsolidus vapor phase might develop a higher Or/Ab ratio than would result from magmatic crystallization and differentiation alone. Thus, vapor-phase crystallization of K-feldspar may account for the unusually potassic compositions of the K-feldspar and the apparent disequilibrium with plagioclase rims. However, neither equilibrium magmatic coprecipitation of K-feldspar and rim plagioclase nor subsolidus exchange can be unequivocally discounted.

Whatever the mechanism of formation, the optical properties of K-feldspar suggest crystallization at solidus or high subsolidus temperatures. Lower temperatures appear possible only if the K-feldspar crystallized or exchanged in a metastable disordered structure. Even if the hypothesis of vapor-phase crystallization of the Or-rich feldspar is correct, it is possible that an earlier generation of K-feldspar which crystallized in magmatic equilibrium with the plagioclase rims is also present locally. More analyses are needed of the feldspars in the west-central part of the pluton, where the likelihood of magmatic saturation in K-feldspar appears greatest. If two generations of K-feldspar with distinctly different Or contents could be identified, it would serve simultaneously as a test of the proposed vapor-phase crystallization of the high-Or feldspar and as a valuable source of data on the equilibrium compositions of coexisting feldspars in plutonic rocks.

12.5 Hornblende

12.5.1 Distribution and Petrographic Characteristics

Green hornblende is the principal mafic mineral in the tonalite. Concentrations range widely from 4-20% -- generally 6-14% -- but some mafic schlieren and lenses contain 40-50%. Concentrations generally decrease from east to west, but they also drop off markedly in the GBT, where biotite exceeds hornblende. Biotite also exceeds hornblende locally in the western parts of the PHbT and SPT. Replacement of hornblende by biotite is generally minor, but locally it is pronounced, especially in those parts of the PHbT and SPT where joint-controlled biotite tonalite layers are well developed or where conspicuously coarse poikilitic biotite books are disseminated through the tonalite. Chlorite, epidote, sphene, actinolitic amphibole and rarely carbonate, allanite, or white mica are minor alteration products.

Hornblende is pleochroic in shades of green: α = light grayish yellow-green or greenish yellow, β = medium yellow-green or slightly brownish green, γ = medium blue-green or grayish blue-green, sometimes with a slight brownish tinge. The 2V seems to be slightly variable in the estimated range 60-75° negative. Simple or multiple twinning on (100) is common.

Figure 62 compares the typical microscopic appearance of hornblende in both the PHbT and SPT, on the one hand, and in the SHbT on the other. The megascopic appearance can be seen in Figure 14 (pp. 108-110).

Hornblende in the former two units is characterized by the following features:

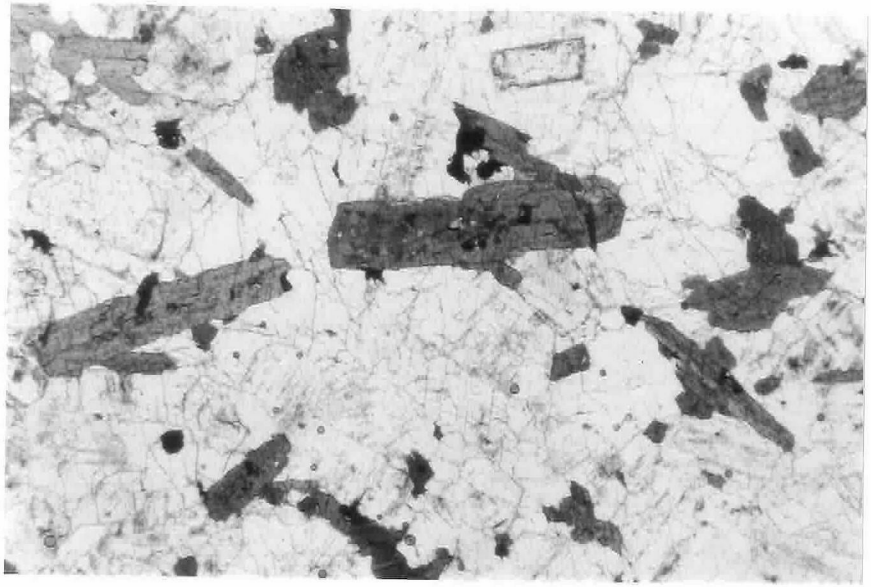

Figure 62A

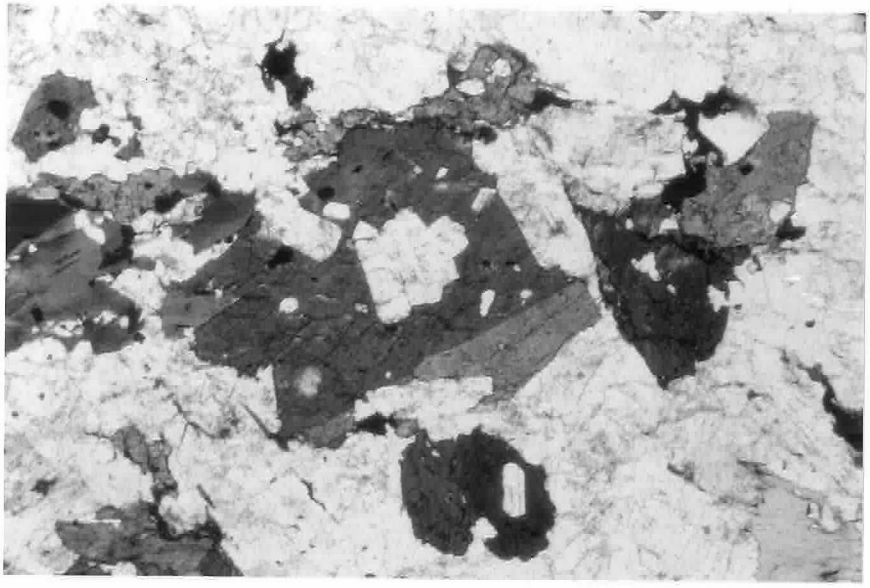

Figure 62B

Figure 62. Comparison of (A) the elongate subhedral, non-poikilitic forms of hornblende in the prismatic hornblende and seriate porphyritic tonalites, with (B) the anhedral, equant, molded and poikilitic forms characteristic of hornblende in the stubby hornblende tonalite. Samples (A) Ba-JM-639 from the arroyo called El Alisito, ∿320 m from the southeastern margin of the pluton (area R-8) and (B) Ba-JM-453 from Cañon Campo Buena Vista, 540 m from the northeastern margin of the pluton (area H-12).

(1) Subhedral and euhedral prisms elongate from 2:1 up to 5:1 parallel to the *c* axis predominate, although equant and anhedral grains are also common.

(2) Crystals 1-3 or 4 mm long are most common, but there is a seriate distribution of grain sizes from <<1 mm up to 5-6 mm or locally even 10 mm.

(3) Hornblende in the PHbT and SPT is blue-green or grayish blue-green with little or no brownish tinge; except for a very faint, fine-scale patchy distribution of lighter and darker areas in some grains, zoning is rare. A few crystals exhibit faint euhedral progressive or oscillatory zoning, an apparently magmatic rather than deuteric feature not seen in the SHbT or GBT.

(4) Hornblende is noticeably finer grained than plagioclase in the same rocks. Therefore, despite the subhedral or euhedral form of much of the hornblende, plagioclase largely controls the texture of the rocks, and hornblende tends to be distributed interstitially, often in small clusters with or without biotite, opaques or other accessory phases.

(5) Although hornblende in the PHbT and SPT commonly contains inclusions of other minerals -- especially opaques and apatite -- few crystals are conspicuously poikilitic. Inclusions of plagioclase occur in only a small proportion of grains and are usually very small ($\leq$0.1 mm). Inclusions of quartz, actinolite, cummingtonite, and clinopyroxene are notable rare with one exception: cummingtonite is slightly concentrated in the central and southern parts of the SPT, where it forms sparse homoaxial cores up to 1-2 mm long, in some cases with only thin hornblende rims.

Hornblende in the SHbT has a very different set of characteristics. (1) The grain-size distribution is more nearly equigranular than seriate. Although the average size varies from 2-3 mm in some parts of the unit to 6-8 mm in others, most of the crystals in a given hand specimen and commonly in a given outcrop or region fall within a 2 or 3 mm size range.

(2) Crystals are equant, usually anhedral, and commonly poikilitic. Grains elongate more than 1.5:1 are rare. Outlines of some grains are rounded, but more often the margins are molded around or between plagioclase crystals and occasionally quartz. The poikilitic appearance is due to the frequent occurrence of one or more moderately large (0.2-1 mm) inclusions of plagioclase and sometimes quartz; some inclusions of both minerals are euhedral or subhedral, but others are strongly corroded.

(3) Hornblende in the SHbT commonly shows an anhedral, geometrically irregular zoning from slightly brownish-green interiors to more blue-green margins (colors refer to vibration parallel to γ). The blue-green rims, which are similar to the typical hornblende in the PHbT and SPT, vary erratically in width from grain to grain and around the margins of individual crystals. Streaks and patches of blue-green color locally penetrate into the interiors of grains, especially along cleavage and microfractures. Foreign inclusions in the interiors of grains are commonly rimmed by a thin blue-green aureole which grades into the enclosing brownish-green core hornblende. These geometric relationships indicate that the zoning in the SHbT hornblendes resulted from deuteric reactions after the molded and poikilitic

morphologies had already developed; possibly some blue-green rim hornblende crystallized directly from the melt, but there is no clear evidence for this. Nor is there any evidence of recrystallization or changes in grain shape associated with the reactions.

(4) The average grain size of hornblende in the SHbT is comparable to that of plagioclase. Therefore, although the margins of hornblende grains are molded and interstitial, the grains as a whole are not, and hornblende plays as important a role as plagioclase in controlling the texture of the rock. Due to their large equant shapes, both hornblende and biotite in the SHbT commonly show little preferred orientation and tend, moreover, to disrupt preferred orientation of surrounding minerals.

(5) As in the PHbT and SPT, inclusions of opaques and apatite are common. However, unlike in those units, many hornblende crystals in the SHbT contain small, pale-colored patches or discrete included grains of cummingtonite and/or of actinolite ± fine-grained quartz; together the pale amphiboles comprise as much as 0.2-0.3% of a few rocks. One or more small anhedral relicts of clinopyroxene, generally separated from the enclosing hornblende by a reaction corona of actinolite plus fine-grained quartz, can also be found in many thin sections.

Despite the corrosion of some included crystals of plagioclase and quartz, the characteristically molded and interstitial margins of hornblende in the SHbT indicate growth into open spaces, with very little replacement of surrounding minerals. The patches of actinolite

plus quartz suggest that clinopyroxene was originally more abundant than at present. Likewise, it is possible, but not at all certain, that the patches of cummingtonite replaced orthopyroxene. Even so, there is no evidence that either pyroxene was ever a volumetrically significant phase in any of the tonalite.

Towards the margins of the SHbT, especially in the GBT, elongate subhedral, non-poikilitic prisms of hornblende become more prevalent despite the increasing intensity of protoclasis. Concurrently, hornblende becomes more uniformly blue-green, and zoning diminishes. Hornblende in the GBT is generally unzoned and similar in color to the blue-green rims of grains in the non-gneissose SHbT, although the interiors of some grains are faintly brownish green. This change in hornblende morphology and color correlates not only with increasing foliation intensity, but also with (1) increasing abundance of quartz, K-feldspar, and sphene; (2) increasing biotite/hornblende ratio; and (3) increasing prevalence of euhedral progressive and oscillatory zoning in plagioclase.

In the PHbT and SPT, the prevalence of euhedral hornblende faces is inversely proportional to the intensity of flow structure and protoclasis. Increasing euhedralism of hornblende also correlates with (1) increasing euhedralism and oscillatory zoning of plagioclase and (2) increasing prevalence of smooth interstitial textures in general and of smoothly interstitial K-feldspar, epidote, sphene, chlorite, zeolite, muscovite, and carbonate in particular. As for plagioclase, hornblende tends to be exceptionally euhedral against these late-stage interstitial minerals, suggesting unimpeded growth of hornblende into open spaces which were subsequently filled by

latest melt or vapor-phase crystallization. Again as for plagioclase, hornblende in the PHbT and SPT is more frequently euhedral against quartz than against plagioclase, biotite, or other hornblende crystals.

12.5.2 Compositions and Implications for Physico-Chemical Conditions of Crystallization and Deuteric Exchange

A total of 169 microprobe analyses were obtained on 38 grains in eight rocks. Table 12 shows the average compositions of hornblende in each sample; Tables 13 and 14 give the compositions of the cores and rims of zoned grains. The average composition of each grain is recorded in Appendix C (Table C-6).

12.5.2.1 Normalization of Analyses to Formula Proportions

The structural formula $A_{0-1}X_2Y_5Z_8O_{22}(OH)_2$ is assumed, where A can be occupied by Na and K; X (also denoted M4) by Na, Ca, and FM (defined as Fe + Mn + Mg); Y by Mg, Mn, Fe^{2+}, Fe^{3+}, Cr, Al^{VI}, and Ti; and Z by Al^{IV} and Si. Because microprobe analyses reveal neither the $Fe^{3+}/(Fe^{2+} + Fe^{3+})$ ratios nor the distribution of cations among the various sites, there is no unique method for normalization of the analyses to this formula. Various possible methods and their inherent assumptions and weaknesses have been discussed in detail by Laird (1977).

Four methods can be considered:

(1) cations - (Na + K) = (assumes $Na^{M4} = 0$)

(2) cations - K = (assumes $Na^{A} = 0$)

(3) cations - (Ca + Na + K) = (assumes $FM^{M4} = 0$)

(4) oxygen (exclusive of OH) = (assumes a specific $Fe^{3+}/(Fe^{2+} + Fe^{3+})$ ratio, in this case zero, and no substitution of $O \rightleftharpoons OH$)

Table 12

Average Microprobe Analyses of Hornblende in Individual Tonalite Samples*

Name of Unit	GBT	SHbT			PHbT		SPT		Pluton	
Sample #	Ba-JM 30a	Ba-JM 25a	Ba-JM 29	Ba-JM 68	Ba-JM 36a	Ba-JM 46a	Ba-JM 3a	Ba-JM 62a	Average	σ
Number of Grains	4	4	3	4	5	5	5	4		
SiO_2	49.24	48.62	48.44	47.92	49.32	49.59	49.50	49.32	48.93	0.69
TiO_2	0.96	1.15	1.18	1.14	1.07	0.73	0.83	0.80	0.98	0.18
Al_2O_3	6.17	7.54	7.05	6.98	7.08	5.90	6.44	6.11	6.66	0.58
Cr_2O_3	---	0.02	0.01	---	---	---	---	---	0.02	0.01
FeO_t	13.51	14.28	14.07	13.79	12.81	13.29	13.20	12.84	13.47	0.54
MnO	0.49	0.40	0.38	0.35	0.42	0.51	0.48	0.50	0.44	0.06
MgO	14.83	14.06	14.39	14.56	15.47	14.99	15.22	15.62	14.89	0.54
CaO	11.81	11.22	11.06	11.22	11.18	11.85	11.42	11.07	11.35	0.31
Na_2O	1.05	1.13	1.14	1.20	1.02	0.94	1.01	1.14	1.08	0.09
K_2O	0.35	0.31	0.28	0.33	0.19	0.28	0.22	0.20	0.27	0.06
"H_2O"	1.30	1.88	2.02	2.52	1.43	1.93	1.67	2.40	1.92	0.39
TOTAL	100.01	100.01	100.02	100.01	99.99	100.01	99.99	100.00	100.00	---
Formula Proportions Based on the Sum (Cations less Alkalies) = 15										
Si	7.130	6.992	7.054	7.010	7.075	7.176	7.134	7.152	7.090	0.068
Al(IV)	0.870	1.008	0.946	0.990	0.925	0.824	0.866	0.848	0.910	0.068
Al(VI)	0.181	0.286	0.264	0.212	0.271	0.181	0.227	0.198	0.228	0.042
Ti	0.104	0.123	0.130	0.123	0.116	0.079	0.090	0.088	0.107	0.020
Cr	---	0.002	0.001	---	---	---	---	---	0.002	0.001
Fe	1.632	1.738	1.717	1.686	1.537	1.607	1.590	1.557	1.633	0.074
Mn	0.059	0.050	0.046	0.044	0.051	0.062	0.059	0.062	0.054	0.007
Mg	3.195	3.051	3.117	3.173	3.307	3.232	3.270	3.376	3.215	0.104
Ca	1.828	1.750	1.726	1.760	1.719	1.838	1.764	1.720	1.763	0.047
Na	0.294	0.318	0.323	0.339	0.284	0.263	0.283	0.320	0.303	0.026
K	0.064	0.057	0.051	0.061	0.035	0.052	0.040	0.037	0.050	0.011
"OH"	1.442	1.818	1.949	2.347	1.370	1.864	1.610	2.336	1.841	0.366
Fe/(Fe + Mn + Mg)	0.334	0.359	0.352	0.344	0.314	0.328	0.323	0.312	0.333	0.017
Mn/(Fe + Mn + Mg)	0.012	0.010	0.009	0.009	0.010	0.013	0.012	0.012	0.011	0.002
Mg/(Fe + Mn + Mg)	0.654	0.631	0.639	0.647	0.676	0.660	0.665	0.676	0.656	0.016

*Grains included in plagioclase were omitted from the averages. Zoning in grains was accounted for by calculating average grain compositions based upon the "core"/"rim" ratio determined optically for each grain by point counting.

Table 13

Compositions of the "Cores" and "Rims" of Zoned Hornblende Crystals in the Stubby Hornblende Tonalite

	"Cores"					
Grain #	H-25a-2	H-29-1	H-29-5	H-68-1	H-68-2	H-68-4
Color*	brn-grn	brn-grn	brn-grn	brn-bl-grn	brn-grn	sl. brn-grn
# of Points	14	4	2	4	4	3
SiO_2	47.47	47.88	47.82	47.87	47.72	46.73
TiO_2	1.66	1.66	1.64	1.62	1.67	1.69
Al_2O_3	7.57	7.24	7.27	7.34	7.26	7.40
Cr_2O_3	0.02	0.01	n.a.	n.a.	n.a.	n.a.
FeO_t	13.15	13.31	13.83	13.72	13.39	13.25
MnO	0.28	0.30	0.33	0.35	0.30	0.28
MgO	14.71	14.61	14.64	14.58	14.78	14.88
CaO	11.05	10.82	10.78	10.82	10.99	10.94
Na_2O	1.32	1.39	1.32	1.38	1.43	1.48
K_2O	0.31	0.27	0.25	0.31	0.30	0.31
"H_2O"	2.48	2.51	2.14	2.02	2.16	3.05
TOTAL	100.02	100.00	100.02	100.01	100.00	100.01
Formula Proportions Based on the Sum (Cations less Alkalies) = 15						
Si	6.930	7.009	6.976	6.983	6.964	6.877
Al(IV)	1.070	0.991	1.024	1.017	1.036	1.123
Al(VI)	0.236	0.258	0.226	0.245	0.212	0.161
Ti	0.180	0.182	0.180	0.177	0.183	0.186
Cr	0.001	0.001	---	---	---	---
Fe	1.608	1.630	1.687	1.671	1.634	1.630
Mn	0.036	0.036	0.041	0.044	0.037	0.036
Mg	3.208	3.201	3.183	3.170	3.215	3.262
Ca	1.732	1.693	1.685	1.691	1.719	1.725
Na	0.368	0.393	0.372	0.390	0.404	0.421
K	0.057	0.050	0.047	0.057	0.056	0.058
"OH"	2.344	2.352	2.081	1.965	2.113	2.994
Fe/(Fe+Mn+Mg)	0.331	0.335	0.344	0.342	0.334	0.331
Mn/(Fe+Mn+Mg)	0.007	0.007	0.008	0.009	0.008	0.007
Mg/(Fe+Mn+Mg)	0.661	0.658	0.648	0.649	0.658	0.662

*Observed in thin section at maximum absorption (parallel to Y').
Abbreviations: bl-blue; brn-brownish; grn-green; sl-slightly; dp-deep.

Table 13 (continued)

	"Rims"				
Grain #	H-25a-2	H-25a-2i[b]	H-29-1	H-29-1f[c]	H-29-5
Color[a]	dp bl-grn	bl-grn	bl-grn	bl-grn	bl-grn
Number of Points	8	4	2	2	1
SiO_2	47.49	48.28	48.62	49.15	49.07
TiO_2	0.75	0.94	0.59	0.39	0.94
Al_2O_3	7.52	7.55	7.23	6.35	6.85
Cr_2O_3	n.a.	n.a.	n.a.	0.02	n.a.
FeO_t	14.24	14.27	13.98	13.44	14.20
MnO	0.35	0.38	0.36	0.31	0.41
MgO	14.07	13.93	14.53	14.22	14.64
CaO	11.51	11.46	11.59	11.68	10.97
Na_2O	1.10	1.06	1.01	0.81	1.08
K_2O	0.32	0.30	0.29	0.21	0.27
"H_2O"	2.65	1.82	1.81	3.42	1.57
TOTAL	100.00	99.99	100.01	100.00	100.00
Formula Proportions Based on the Sum (Cations less Alkalies) = 15					
Si	6.955	7.018	7.062	7.217	7.102
Al(IV)	1.045	0.982	0.938	0.783	0.898
Al(VI)	0.254	0.312	0.298	0.316	0.271
Ti	0.083	0.103	0.064	0.043	0.102
Cr	---	---	---	0.003	---
Fe	1.743	1.734	1.764	1.651	1.718
Mn	0.043	0.047	0.044	0.038	0.051
Mg	3.071	3.019	3.029	3.112	3.157
Ca	1.806	1.786	1.801	1.838	1.702
Na	0.312	0.299	0.284	0.231	0.303
K	0.060	0.055	0.054	0.039	0.050
"OH"	2.593	1.762	1.755	3.351	1.519
Fe/(Fe + Mn + Mg)	0.359	0.361	0.365	0.344	0.349
Mn/(Fe + Mn + Mg)	0.009	0.010	0.009	0.008	0.010
Mg/(Fe + Mn + Mg)	0.632	0.629	0.626	0.648	0.641

[a] Observed in thin section at maximum absorption (parallel to Y'). Abbreviations: bl-blue; brn-brownish; grn-green; sl-slightly; dp-deep.

[b] Interstitial branch off of the poikilitic margin of H-25a-2.

[c] Blue-green hornblende along a microfracture crossing the brownish-green interior of H-29-1.

Table 13 (concluded)

	"Rims"		
Grain #	H-68-1	H-68-2	H-68-4
		sl	sl
Color*	bl-grn	bl-grn	bl-grn
Number of Points	1	2	3
SiO_2	48.32	48.93	48.01
TiO_2	0.95	0.83	0.75
Al_2O_3	7.10	6.49	6.70
Cr_2O_3	n.a.	n.a.	n.a.
FeO_t	14.57	13.91	13.99
MnO	0.35	0.41	0.37
MgO	14.06	14.49	14.54
CaO	11.26	11.33	11.51
Na_2O	1.10	1.10	1.08
K_2O	0.28	0.35	0.36
"H_2O"	2.02	2.16	2.69
TOTAL	100.01	100.00	100.00
Formula Proportions Based on the Sum (Cations less Alkalies) = 15			
Si	7.045	7.133	7.028
Al(IV)	0.955	0.867	0.972
Al(VI)	0.265	0.248	0.183
Ti	0.104	0.092	0.082
Cr	---	---	---
Fe	1.776	1.695	1.712
Mn	0.043	0.051	0.046
Mg	3.054	3.147	3.172
Ca	1.759	1.769	1.805
Na	0.312	0.310	0.306
K	0.052	0.066	0.067
"OH"	1.964	2.111	2.640
Fe/(Fe + Mn + Mg)	0.364	0.346	0.347
Mn/(Fe + Mn + Mg)	0.009	0.010	0.009
Mg/(Fe + Mn + Mg)	0.627	0.643	0.643

*Observed in thin section at maximum absorption (parallel to γ').
Abbreviations: bl-blue; brn-brownish; grn-green; sl-slightly; dp-deep.

Table 14

Core and Rim Compositions of Rare Zoned Hornblende Crystals in the Prismatic Hornblende and Seriate Porphyritic Tonalites

	Cores		Rims		
Grain #	H-36a-2	H-62a-2	H-36a-2	H-62a-2	H-62a-2*
Number of Points	4	3	4	2	1
SiO_2	49.83	46.50	48.70	49.77	46.96
TiO_2	1.01	1.35	0.75	0.68	1.31
Al_2O_3	7.05	8.89	7.30	5.61	8.01
Cr_2O_3	n.a.	n.a.	n.a.	n.a.	n.a.
FeO_t	12.34	13.33	13.07	12.37	13.83
MnO	0.34	0.40	0.43	0.51	0.52
MgO	15.88	14.44	15.10	16.18	14.33
CaO	11.10	10.77	11.19	11.25	11.01
Na_2O	0.95	1.61	1.01	0.95	1.39
K_2O	0.20	0.19	0.21	0.24	0.18
"H_2O"	1.32	2.52	2.25	2.45	2.46
TOTAL	100.02	100.00	100.01	100.01	100.00
Formula Proportions Based on the Sum (Cations less Alkalies) = 15					
Si	7.115	6.802	7.048	7.190	6.869
Al(IV)	0.885	1.198	0.952	0.810	1.131
Al(VI)	0.302	0.335	0.293	0.144	0.249
Ti	0.109	0.148	0.082	0.074	0.144
Cr	---	---	---	---	---
Fe	1.473	1.630	1.581	1.494	1.691
Mn	0.041	0.050	0.053	0.062	0.064
Mg	3.378	3.149	3.257	3.484	3.124
Ca	1.699	1.689	1.736	1.742	1.726
Na	0.263	0.451	0.284	0.266	0.395
K	0.035	0.035	0.039	0.044	0.035
"OH"	1.268	2.460	2.177	2.356	2.401
Fe/(Fe + Mn + Mg)	0.301	0.338	0.323	0.296	0.347
Mn/(Fe + Mn + Mg)	0.008	0.010	0.011	0.012	0.013
Mg/(Fe + Mn + Mg)	0.691	0.652	0.666	0.691	0.640

*Unusual point in the rim zone, compositionally similar to the core.

Table 15

Comparison of Hornblende Formula Proportions
Calculated by Four Different Normalization Procedures

Sample #	Ba-JM-30a				Ba-JM-25a			
Normalization	1	2	3	4	1	2	3	4
Si	7.130	6.993	7.037	7.149	6.992	6.845	6.858	7.005
Al(IV)	0.807	1.007	0.963	0.851	1.008	1.155	1.142	0.995
Sum	8.000	8.000	8.000	8.000	8.000	8.000	8.000	8.000
Al(VI)	0.181	0.024	0.074	0.203	0.286	0.111	0.127	0.301
Ti	0.104	0.102	0.103	0.104	0.128	0.125	0.126	0.128
Cr	---	---	---	---	0.001	0.001	0.001	0.001
Fe	1.632	1.601	1.611	1.637	1.738	1.701	1.705	1.741
Mn	0.059	0.058	0.058	0.060	0.050	0.049	0.049	0.050
Mg	3.195	3.134	3.153	3.203	3.051	2.986	2.992	3.056
Sum	5.171	4.919	4.999	5.207	5.254	4.973	5.000	5.278
Ca	1.828	1.793	1.804	1.833	1.750	1.713	1.716	1.753
Na	0.294	0.288	0.290	0.294	0.318	0.312	0.312	0.319
K	0.064	0.063	0.063	0.064	0.057	0.056	0.056	0.057
Sum	2.186	2.144	2.157	2.191	2.125	2.081	2.084	2.129
"OH"	1.442	1.414	1.423	1.446	1.818	1.779	1.783	1.821
FM(M4)	0.171	0	0**	0.207	0.254	0	0**	0.278
Na(M4)	0**	0.288	0.196	0	0**	0.312	0.284	0
Na(A)	0.294	0**	0.094	0.294	0.318	0**	0.028	0.319
$Fe^{3+}/(Fe^{2+}+Fe^{3+})$*	0.077	0.627	0.449	0**	0.047	0.619	0.564	0**

*Fe apportioned between Fe^{2+} and Fe^{3+} such that total cation charge = 46.

**By assumption inherent in the normalization procedure.

Table 16

Comparison of the Range of Hornblende Compositions in the San José Pluton with the Compositions of Hornblende in Five Tonalites and Granodiorites from the Batholith in Southern California (Larsen and Draisin, 1950, Table 3). Data are presented as formula proportions based on the sum (cations less alkalies) = 15.

	SJP	BT	GVT	LT	BGd	WGd
Si	6.99-7.18	6.65	6.85	6.45	6.75	6.85
Al(IV)	0.82-1.01	1.45	1.15	1.55	1.65	1.15
Al(VI)	0.18-0.29	1.10	0.30	0.60	---	0.15
Ti	0.08-0.13	0.15	0.20	0.15	0.20	0.15
Fe	1.54-1.74	2.15	2.15	2.10	2.20	2.55
Mn	0.04-0.06	---	---	---	---	0.05
Mg	3.05-3.38	2.40	2.40	2.20	2.35	1.85
Ca	1.72-1.84	1.70	1.85	1.85	1.85	1.75
Na + K	0.30-0.40	0.45	0.50	0.40	0.55	0.55
Fe/(Fe + Mn + Mg)	0.31-0.36	0.47	0.47	0.49	0.48	0.58

SJP: San José pluton
BT: Bonsall tonalite
GVT: Green Valley tonalite
LT: Lakeview tonalite
BGd: Bonsall granodiorite
WGd: Woodson granodiorite

Each of the first three procedures permits an estimate of the Fe^{3+} content if one assumes that the cation charge must total 46, i.e., that there is no substitution of O for OH. Fe^{3+} contents can also be estimated from charge balance considerations related to substitutions (Papike et al., 1974): beginning from the simplest calcic amphibole formula $Ca_2FM_5Si_8O_{22}(OH)_2$, substitution of Na^+ for Ca^{2+} and of Al^{3+} for Si^{4+} must be balanced by substitution of Al^{3+}, Fe^{3+}, Cr^{3+}, and Ti^{4+} for FM^{2+} and of Na^+ and K^+ for a vacancy in the A site, i.e.,

$$Al^{IV} + Na^{M4} = Al^{VI} + Fe^{3+} + Cr + 2Ti + Na^{A} + K$$

If, for a given normalization scheme, the Fe^{3+} contents calculated by the two methods differ significantly, then that normalization scheme is clearly unacceptable. For all but a few of the analyses presented here, each normalization yields identical Fe^{3+} estimates by both methods.

Formula proportions presented in the tables and figures are all based upon normalization (1), cations - (Na + K) = 15. Table 15 compares the formula proportions calculated for two average hornblende analyses by all four methods. Large differences are apparent in the relative amounts of Al^{IV} and Al^{VI} and of Na^{A} and Na^{M4} and in the sum of Y cations; any excess over 5 in the Y position is assigned to FM^{M4}, whereas a deficiency in this position is interpreted as evidence that the normalization procedure is unacceptable. Calculated $Fe^{3+}/(Fe^{2+} + Fe^{3+})$ ratios are also widely divergent. Otherwise, the various procedures yield similar proportions for most constituents.

For all analyses in Table 12, normalization (4) yields Ca + FM^{M4} totals consistently above the theoretical limit of 2 in the M4 site. Both for this reason and because the assumption of no Fe^{3+} is un-

realistic, this normalization appears unacceptable.

Normalization (2), which assumes that all Na is in the M4 site, also seems inappropriate for magmatic hornblendes crystallized at low or moderate pressures; the two principal amphibole end member series which satisfy this requirement -- glaucophane, $Na_2FM_3^{2+}Al_2Si_8O_{22}(OH)_2$ and riebeckite, $Na_2FM_3^{2+}Fe_2^{3+}Si_8O_{22}(OH)_2$ -- are both characteristic of low temperature-high pressure metamorphic environments. Furthermore, normalization (2) yields a significant deficiency of cations in the Y site for many analyses (e.g., for Ba-JM-30a in Table 15), as well as a slight deficiency of Si + Al in the Z site, hence no Al^{VI}, for some Na-rich compositions. Finally, as discussed later, normalization (2) implies $Fe^{3+}/(Fe^{2+} + Fe^{3+})$ ratios which are consistently very high and seemingly unreasonable.

To help choose among the two remaining normalization procedures and to provide rough independent estimates of the Fe^{3+} contents and variations, optical to near-infrared absorption spectra (Figures 63 and 64) were obtained on two grains with the help of Professor G. R. Rossman and D. S. Goldman: a typical homogeneous grain in SPT sample 62a and a typical zoned grain in SHbT sample 510[13]. Goldman and Rossman (1977) have shown that an absorption band at about 1030 nm in the β

---

[13]Even qualitative estimation of Fe^{3+}/Fe^{2+} variations or of Fe^{2+} contents in the M4 site by optical and infrared spectroscopy requires a rare combination of appropriate grain orientation (thin section roughly parallel to the γ vibration direction for Fe^{3+} and the β direction for Fe^{M4}) and sufficiently large (>100 μm) relatively unfractured and inclusion-free areas. Zoned SHbT grains must have satisfactory areas of typical brownish-green core and blue-green rim zones, and the necessity of identifying these areas by color in thin section further restricts the choices to grains cut nearly parallel to both γ and α (color zonation is not visible in sections parallel to β). Unfortunately, none of the grains analyzed by microprobe, and very few grains in all thin sections together, satisfy these conditions even approximately.

Figure 63. Optical to near-infrared absorption spectra of a typical unzoned hornblende grain in SPT sample Ba-JM-62a. The spectra were measured in thin section on a grain which yields a nearly centered (5-10° off) BXA interference figure. Solid line: polarization approximately parallel to γ; dashed line: polarization approximately parallel to β.

Figure 64. Optical to near-infrared absorption spectra of the core and rim of a typical zoned hornblende grain in SHbT sample Ba-JM-510 (location: area N-11). The spectra were measured in thin section on a grain which gives a far off-centered optic axis interference figure. Solid line: brownish-green core hornblende; dashed line: blue-green rim hornblende.

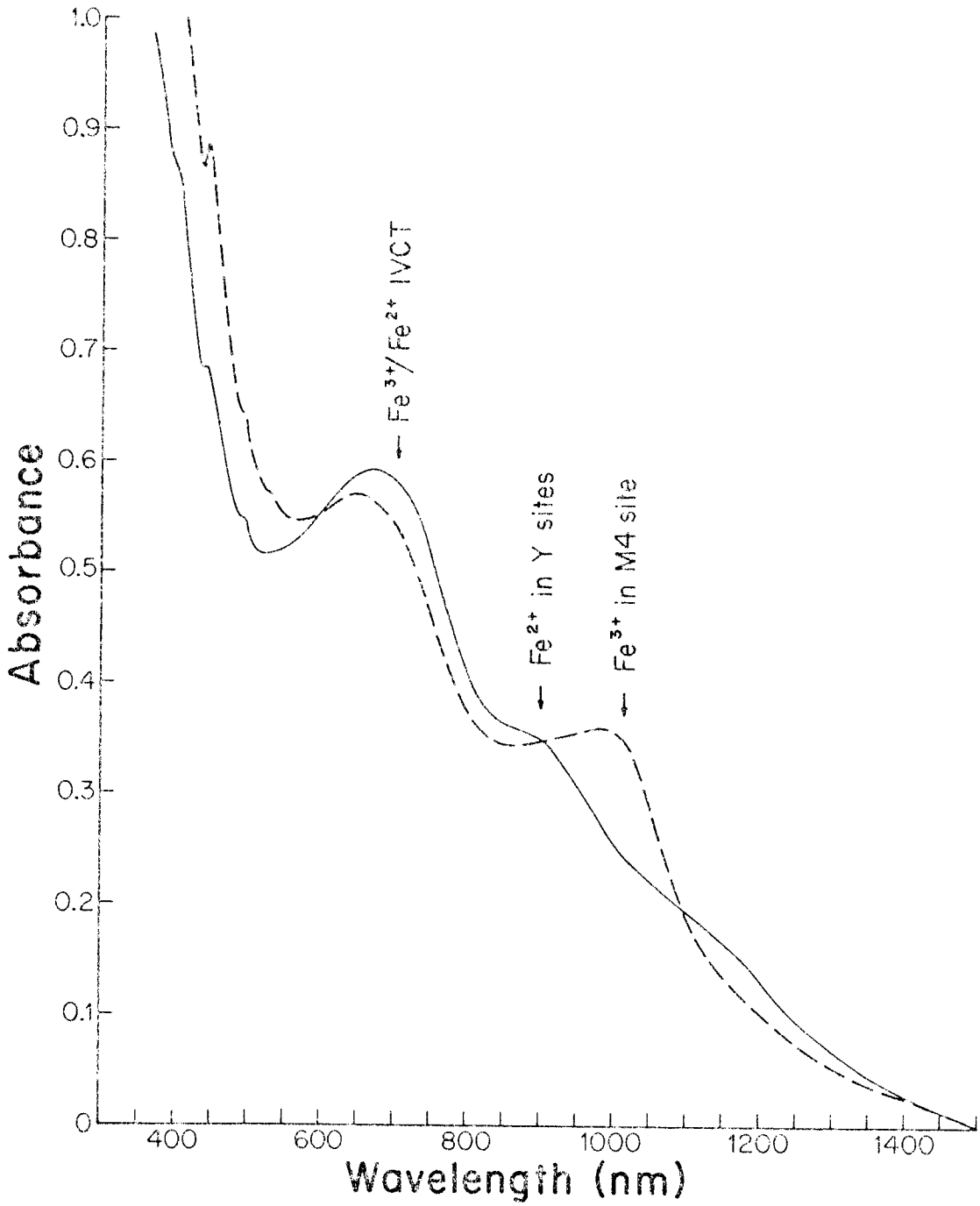
Absorbance
1.0
0.9
0.8
0.7
0.6
0.5
0.4
0.3
0.2
0.1
0
400
600
800
1000
1200
1400
Wavelength (nm)
← Fe3+/Fe2+ IVCT
← Fe2+ in Y sites
← Fe3+ in M4 site

Figure 63

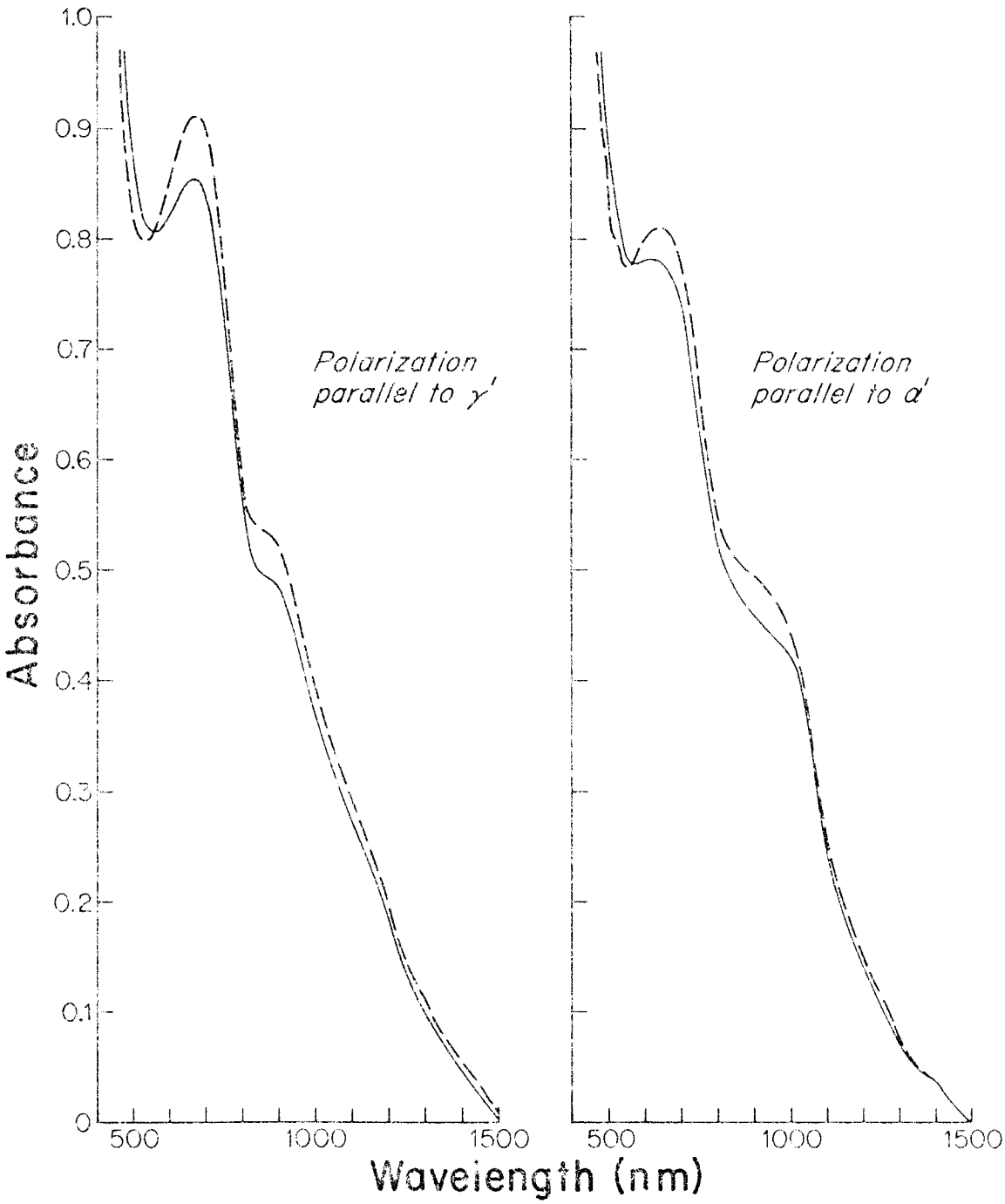
1.0
0.9
0.8
0.7
0.6
0.5
0.4
0.3
0.2
0.1
0
Absorbance
Polarization parallel to γ'
Polarization parallel to α'
500
1000
1500
500
1000
1500
Wavelength (nm)

Figure 64

spectrum of calcic amphiboles is diagnostic of Fe^{2+} in the M4 site. The presence of this band not only in the β spectrum of the SPT grain (Figure 63), but also in the α′ (approaching β) spectra of the zoned SHbT grain (Figure 64) indicates that the basic assumption behind normalization (3), that $FM^{M4} = 0$, is incorrect. From the height of this peak in Figure 63, Rossman's "best guess" is that there could be as much as 3.5 weight % FeO (corresponding to about 0.42 formula units Fe^{2+}) in the M4 site, which would be more than enough to fill the 0.25-0.31 M4 positions not occupied by Ca. Although this estimate is certainly crude, it suggests that normalization (1) is probably more reasonable than (3) and that much of the Na is probably in the A site.

Goldman (1977) has also shown that the Fe^{3+} content of calcic amphiboles can be estimated from the intensity of the Fe^{3+}/Fe^{2+} intervalance charge-transfer band at about 730 nm in the γ spectrum. This method yields a very rough estimate of $Fe^{3+}/(Fe^{2+} + Fe^{3+}) \approx 0.38$, with an uncertainty of perhaps ±0.10-0.15. In comparison, measured $Fe^{3+}/(Fe^{2+} + Fe^{3+})$ ratios of hornblende from 20 Sierra Nevadan granodiorites and quartz monzonites range from 0.120-0.292 (Dodge et al., 1968), and the ratios for hornblendes from 8 granodiorites and quartz diorites scattered along the San Andreas fault in central and southern California range from 0.201-0.314 (Dodge and Ross, 1971). In view of the high whole-rock $Fe_2O_3/(FeO + Fe_2O_3)$ ratios (Plates 9 and 9A) and the high Mg/(Fe + Mn + Mg) ratios of both biotite (Table 17) and hornblende in the San José pluton, the suggestion of higher $Fe^{3+}/(Fe^{2+} + Fe^{3+})$ ratios in the San José hornblendes seems very reasonable.

The γ′-α′ orientation of the zoned SHbT grain does not permit quantitative estimates, but the greater intensity of both the Fe^{3+}/

Fe^{2+} intravalence charge-transfer band and the Fe^{2+} band (at about 900 nm) in the γ' spectrum of the rim in comparison to the core demonstrates that not only the total Fe content, but also the $Fe^{3+}/(Fe^{2+} + Fe^{3+})$ ratio increases from core to rim. Petrographic and compositional characteristics of the Fe-Ti oxides also imply increasingly oxidizing conditions during late magmatic and subsolidus cooling (Section 12.7).

Normalizations (2) and (3) both imply extremely high and seemingly unrealistic $Fe^{3+}/(Fe^{2+} + Fe^{3+})$ ratios, ranging from 0.605-0.707 and 0.449-0.712, respectively, for the eight average compositions in Table 12. Both normalizations also imply $Fe^{3+}/(Fe^{2+} + Fe^{3+})$ ratios which decrease consistently from core to rim of zoned grains in the SHbT. In contrast, normalization (1) yields suspiciously low $Fe^{3+}/(Fe^{2+} + Fe^{3+})$ ratios (0.024-0.107) for the analyses in Table 12, but it implies consistently increasing $Fe^{3+}/(Fe^{2+} + Fe^{3+})$ ratios from core to rim of zoned SHbT grains, in agreement with the spectral data.

In summary, none of the four normalizations is wholly satisfactory. The true formula proportions are probably intermediate between those calculated by normalizations (1) and (3), with some Na^{A}, Na^{M4}, and FM^{M4} and with $Fe^{3+}/(Fe^{2+} + Fe^{3+})$ ratios probably in the range 0.30-0.45. The wet chemical hornblende analyses reported by Dodge et al. (1968) and Dodge and Ross (1971) all show both Na^{A} and Na^{M4} (generally $Na^{A} > Na^{M4}$) and generally some FM^{M4}. Regardless, as long as all analyses are normalized by the same method, in this case method (1), the data should be internally consistent. In fact, all normalizations yield nearly identical patterns of compositional zoning and variation from rock to rock, although the absolute values vary. Only the $Fe^{3+}/(Fe^{2+} + Fe^{3+})$

ratios, the assignment of A and M4 site occupancy, and the relative proportions (but not the relative variation) of Al^{IV} and Al^{VI} present any difficulties, and the conclusions reached in the following discussion should, in general, be valid regardless of these difficulties.

12.5.2.2 Discussion of the Compositional Data and Implications

The range of the hornblende compositions is relatively small throughout the pluton. Al^{IV}, Al^{VI}, Ti, and (Na + K) contents and the Fe/(Fe + Mn + Mg) ratios are consistently low (regardless of normalization) in comparison to the values reported by Larsen and Draisin (1950) for hornblendes from five tonalites and granodiorites in the batholith in southern California (Table 16). They also tend to be lower than for the majority of hornblende analyses reported by Dodge et al. (1968) and Dodge and Ross (1971). Wave-length scans of two grains revealed no elements other than those in the tables; thus, F and Cl contents must be very small.

As implied by the microscopic observations, compositional zoning is weak or absent in most analyzed grains in the GBT, PHbT, and SPT samples. Zoning is similarly weak in some analyzed grains in the SHbT samples, but those grains exhibiting appreciable color zonation all show consistent chemical zonation (Table 13). Quotation marks are used for the "cores" and "rims" of SHbT grains because, inasmuch as zoning is gradational and geometrically irregular, "core" and "rim" points were distinguished by color rather than by proximity to the grain margin. A few "rim" points are in the interiors of grains (generally along cracks or near inclusions).

Within individual zoned grains in the SHbT samples, the correlation

of compositional variations with color is very consistent. However, because the colors depend upon grain orientation as well as composition, the correlation appears less consistent from grain to grain. The brownish-green cores are richer in Ti, Na, Mg, Al^{IV}, and total Al, but poorer in Si, Al^{VI}, Fe, and Ca, relative to the blue-green rims of the same grains. Proportionally, the differences are most striking for Ti, but the relationships are consistent for all constituents, regardless of which normalization procedure is used. Mn contents are also slightly lower in the cores, but variations in K and total FM are small and non-systematic. As noted earlier, absorption spectra in Figure 64 indicate not only a higher total Fe content, but also a higher $Fe^{3+}/(Fe^{2+} + Fe^{3+})$ ratio, in the rim relative to the core.

A thin blue-green zone along a crack crossing the interior of grain H-29-1 (Table 13, H-29-1f) and blue-green aureoles surrounding foreign inclusions in the interior of H-25a-2 (left end of profile, Figure 65) have compositions similar to or approaching, respectively, those of the rims. Unzoned and weakly zoned crystals are similar in some cases to the core and in other cases to the rim compositions of zoned grains.

Figure 65 shows a step-scan across grain H-25a-2, beginning at the edges of slightly bluish, brownish-green aureoles surrounding inclusions of magnetite and plagioclase in the interior of the crystal (hence the tendency towards rim-type compositions at the inner end of the profile), and crossing normal brownish core hornblende grading to a thin blue-green rim. Additional core and rim points representing the extremes of the color range in this grain are plotted to the right of the profile. The profile shows all of the normal core-to-rim variations

Figure 65. Compositional profile across hornblende grain H-25a-2. The step-scan begins in the interior of the grain -- at the edges of two faintly bluish, brownish-green aureoles surrounding inclusions of plagioclase and magnetite -- and extends across normal brownish-green core-type hornblende grading to a thin blue-green rim. Average values (circles) and ranges (vertical bars) of additional analyses of the typical core and rim zones in this grain, and of a deep blue-green interstitial projection (I.P.) branching off the grain, are plotted to the right of the profile, with the number of additional analyses shown in parentheses.

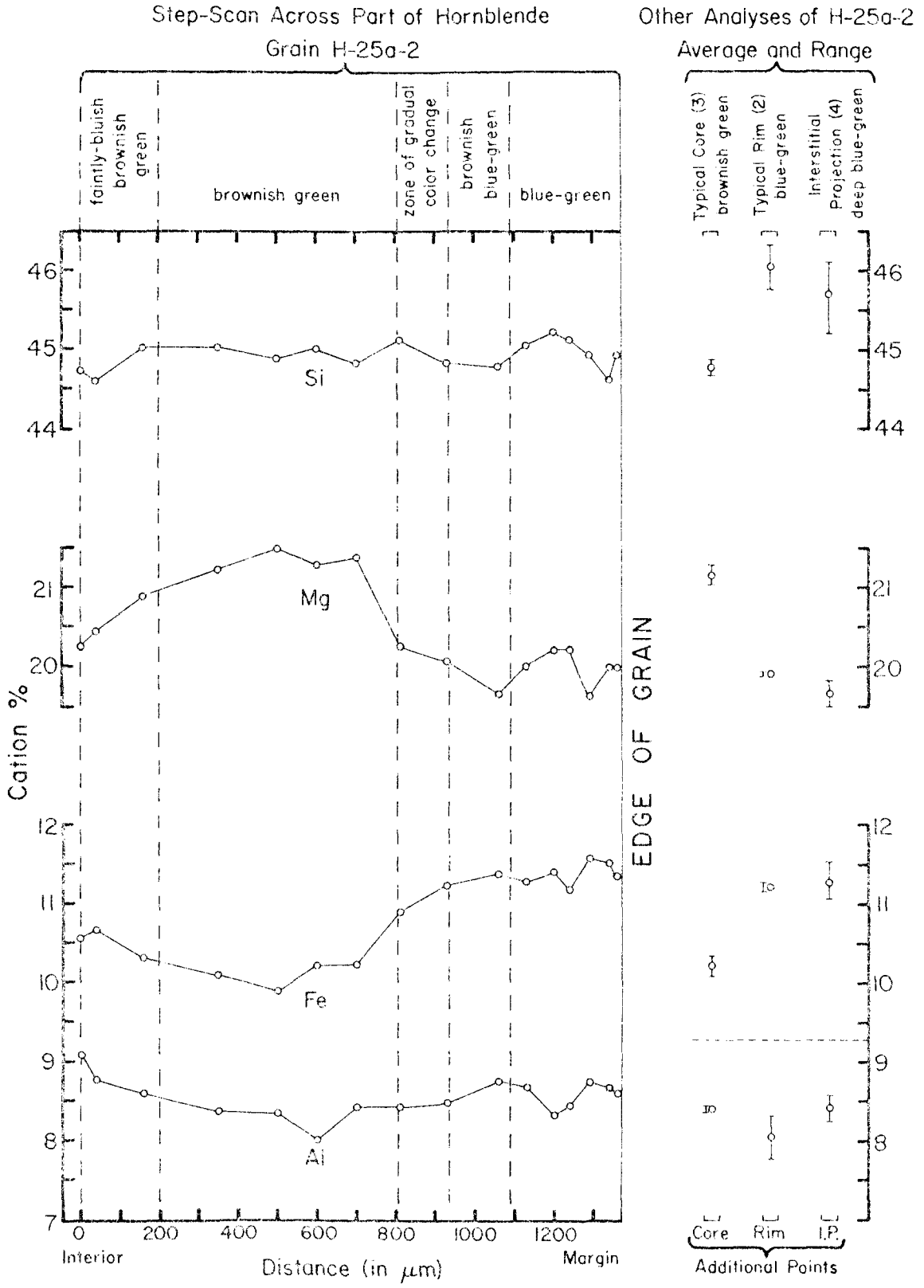
Step-Scan Across Part of Hornblende Grain H-25a-2
faintly-bluish brownish green
brownish green
zone of gradual color change
brownish blue-green
blue-green
Si
Mg
Fe
Al
Cation %
EDGE OF GRAIN
Interior
Distance (in μm)
Margin
Other Analyses of H-25a-2
Average and Range
Typical Core (3) brownish green
Typical Rim (2) blue-green
Interstitial Projection (4) deep blue-green
Core
Rim
I.P.
Additional Points

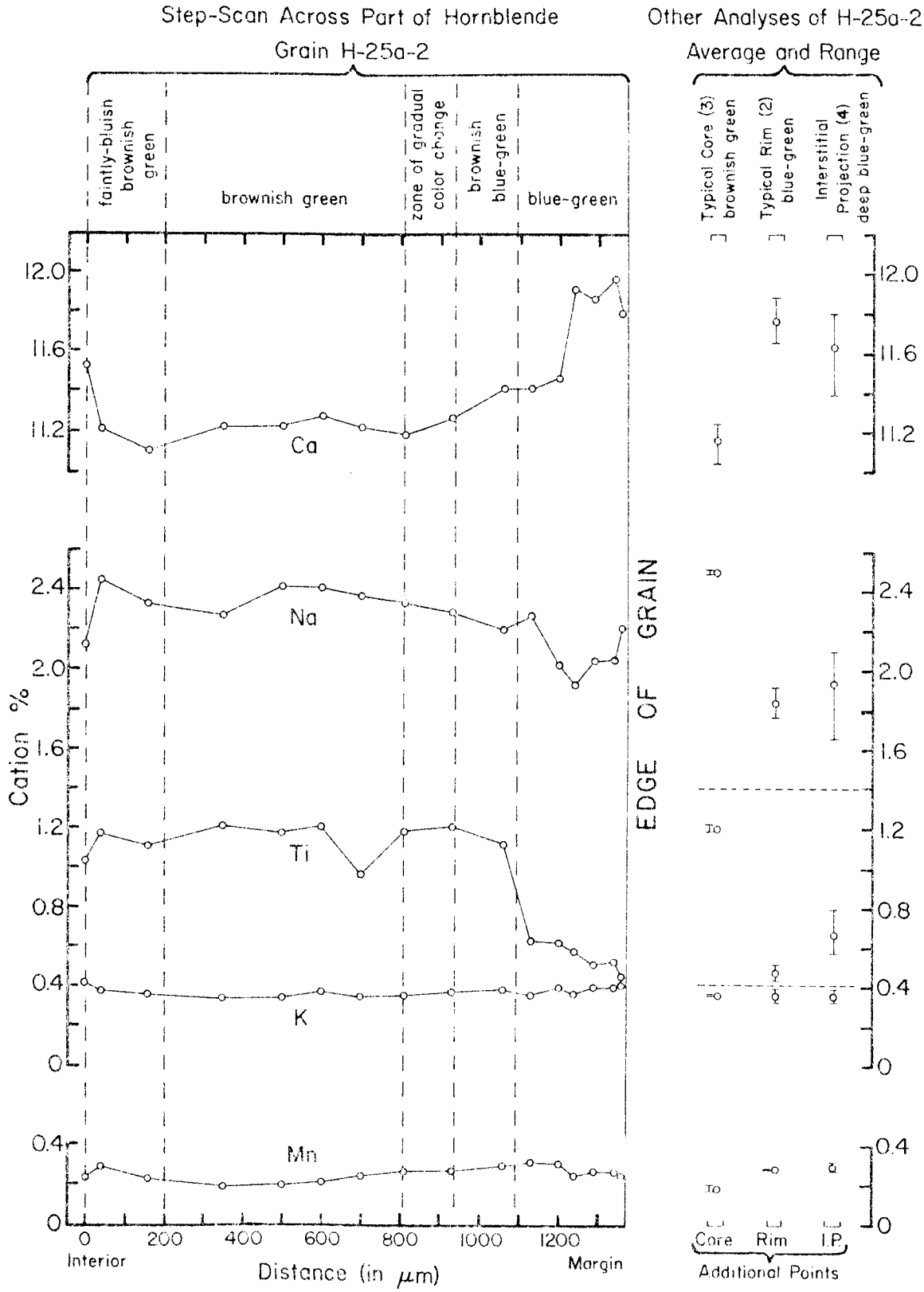
Step-Scan Across Part of Hornblende Grain H-25a-2
faintly-bluish brownish green
brownish green
zone of gradual color change
brownish blue-green
blue-green
Ca
Na
Ti
K
Mn
Cation %
12.0
11.6
11.2
2.4
2.0
1.6
1.2
0.8
0.4
0
0
200
400
600
800
1000
1200
Interior
Distance (in μm)
Margin
EDGE OF GRAIN
Other Analyses of H-25a-2
Average and Range
Typical Core (3) brownish green
Typical Rim (2) blue-green
Interstitial Projection (4) deep blue-green
Core
Rim
I.P.
Additional Points

except for the usual decrease in Al and increase in Si in the rims; however, an increase in Si, hence a decrease in Al^{IV}, is clearly shown by the additional rim points. The marginal decrease in Ti and increase in Ca are especially striking. The outward gradation towards more bluish-green color beginning at approximately 800 μm coincides with the rapidly increasing Fe/Mg ratio. The relatively abrupt disappearance of the brownish cast near the rim coincides with the sharp drop-off in Ti at nearly constant Fe/Mg.

A series of plots relating the Na, Ca, Ti, Al^{IV} (Si), and Al^{VI} contents of hornblende are presented in Figure 66. These plots include the average "core" and "rim" compositions for all zoned grains as well as the average compositions of hornblende in the GBT, PHbT, and SPT samples.

These plots emphasize the consistent compositional variations from cores (solid circles) to rims (open circles) of zoned grains in the SHbT. Consideration of the average slopes of core/rim joins for these grains suggests the approximate substitution reaction:

$$\underset{\text{cores}}{Na + Ti + 1.3\ Al^{IV}} \rightarrow \underset{\text{rims}}{0.7\ Ca + 0.3\ Al^{VI} + 1.3\ Si + 1.0\ o} \qquad (1)$$

where o denotes a vacancy. A plot of the formula proportions of reactants versus products, with the proportion of each constituent divided by the appropriate coefficient, yields 1:1 negative slopes for all SHbT zoned grains (Figure 67A); hence, the reaction appears to accurately describe the zonal variations for these constituents based upon normalization (1). The reaction does not attempt to account for the differences among these grains.

The corresponding reaction based upon normalization (3) -- and

Figure 66. Correlation plots for Na, Ca, Ti, Al^{IV} (Si), and Al^{VI} in hornblende.

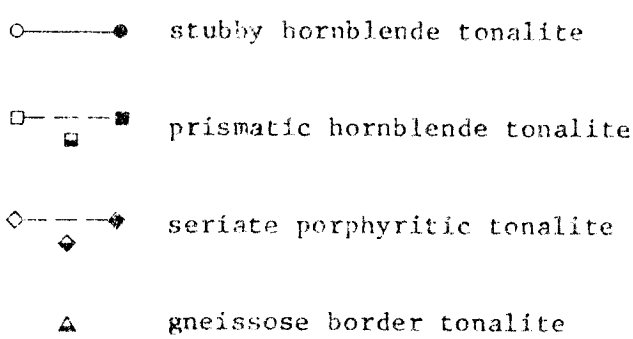

Solid or dashed lines join cores (solid symbols) and rims (open symbols) of zoned crystals. Half-filled symbols indicate average compositions of hornblende in individual samples (SHbT samples omitted). Short-dashed lines with indicated slopes of 1:1, 2:1 etc., are shown for reference.

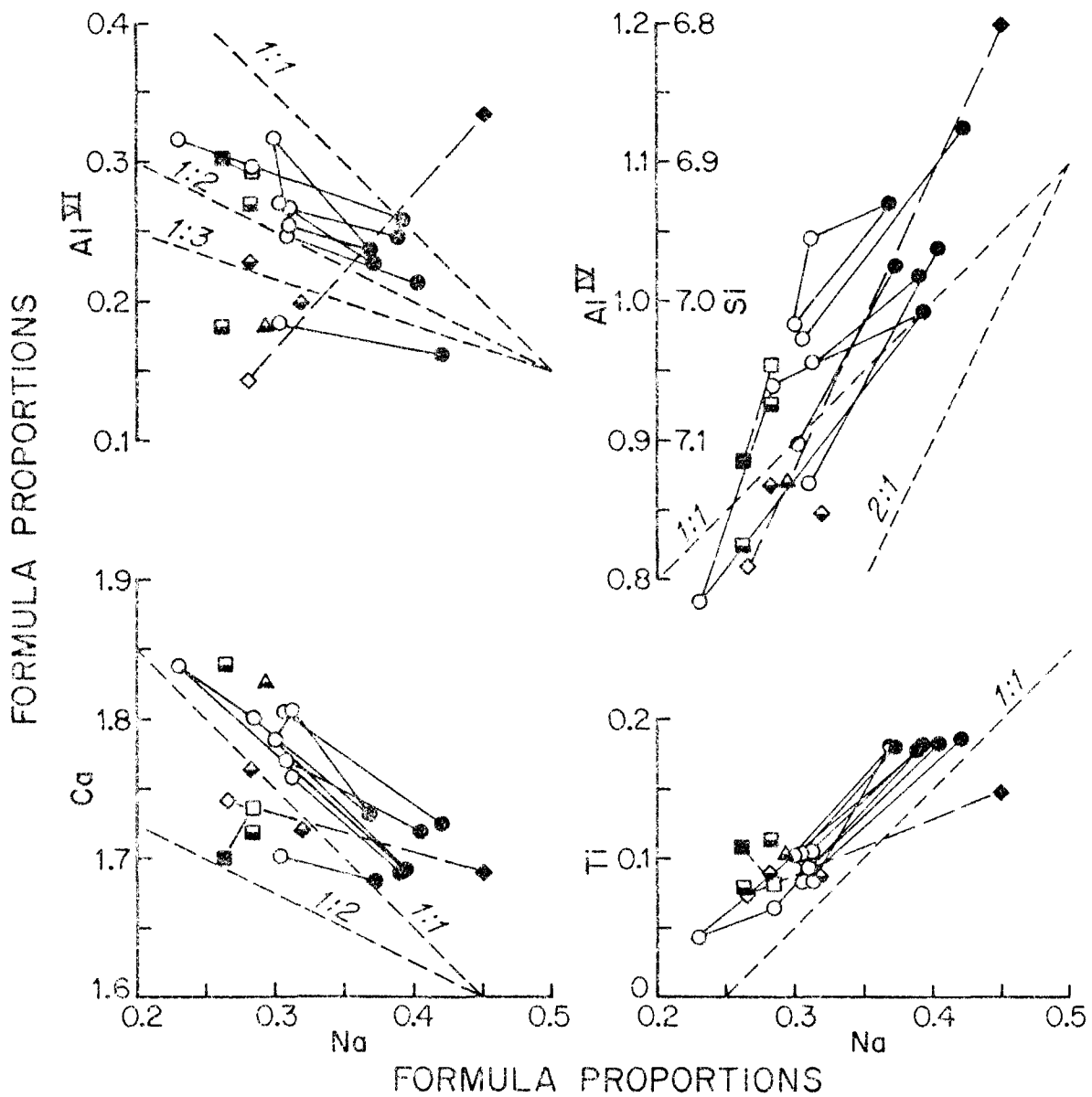
FORMULA PROPORTIONS
Al^{VI}
0.4
0.3
0.2
0.1
1:1
1:2
1:3
Al^{IV}
Si
1.2
1.1
1.0
0.9
0.8
6.8
6.9
7.0
7.1
1:1
2:1
Ca
1.9
1.8
1.7
1.6
1:2
1:1
Ti
0.2
0.1
0
1:1
0.2
0.3
0.4
0.5
Na
FORMULA PROPORTIONS

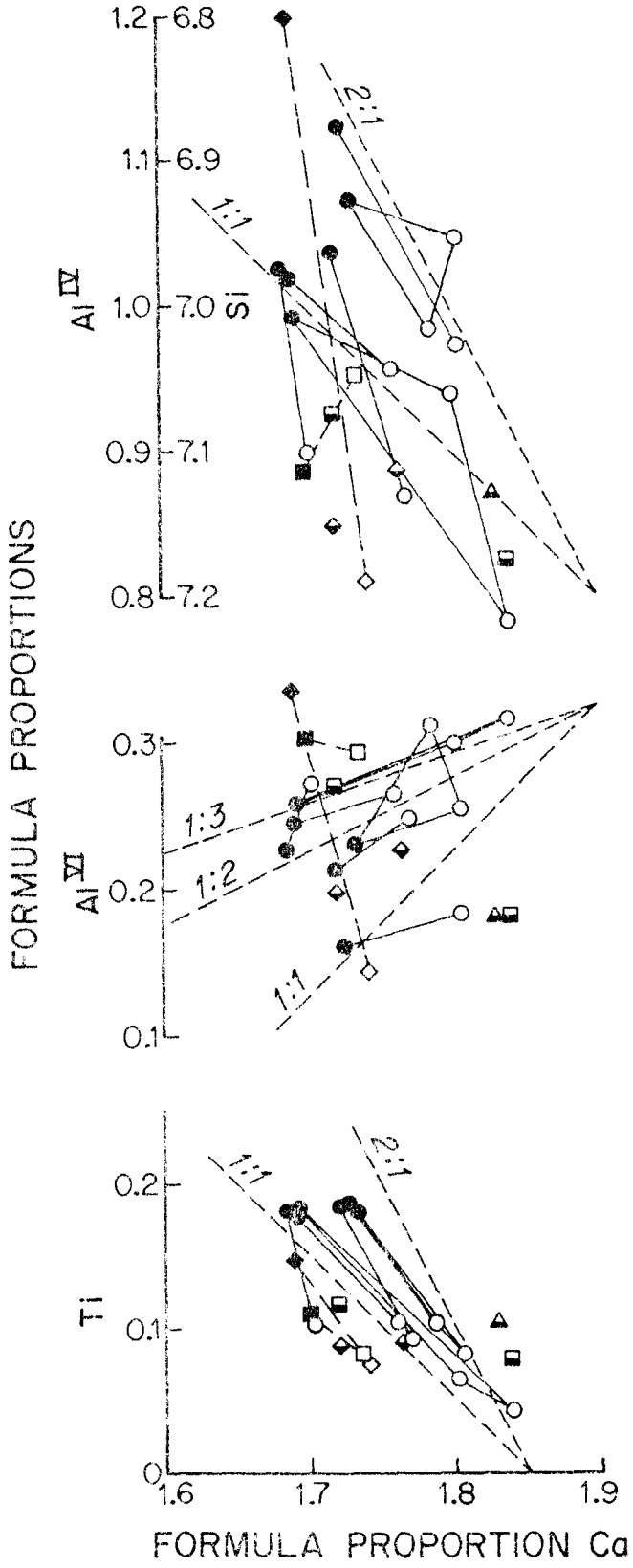
FORMULA PROPORTIONS
1.2
6.8
1.1
6.9
1.0
7.0
0.9
7.1
0.8
7.2
Al IV
Si
2:1
1:1
0.3
0.2
0.1
Al VI
1:3
1:2
1:1
0.2
0.1
0
Ti
1:1
2:1
1.6
1.7
1.8
1.9
FORMULA PROPORTION Ca

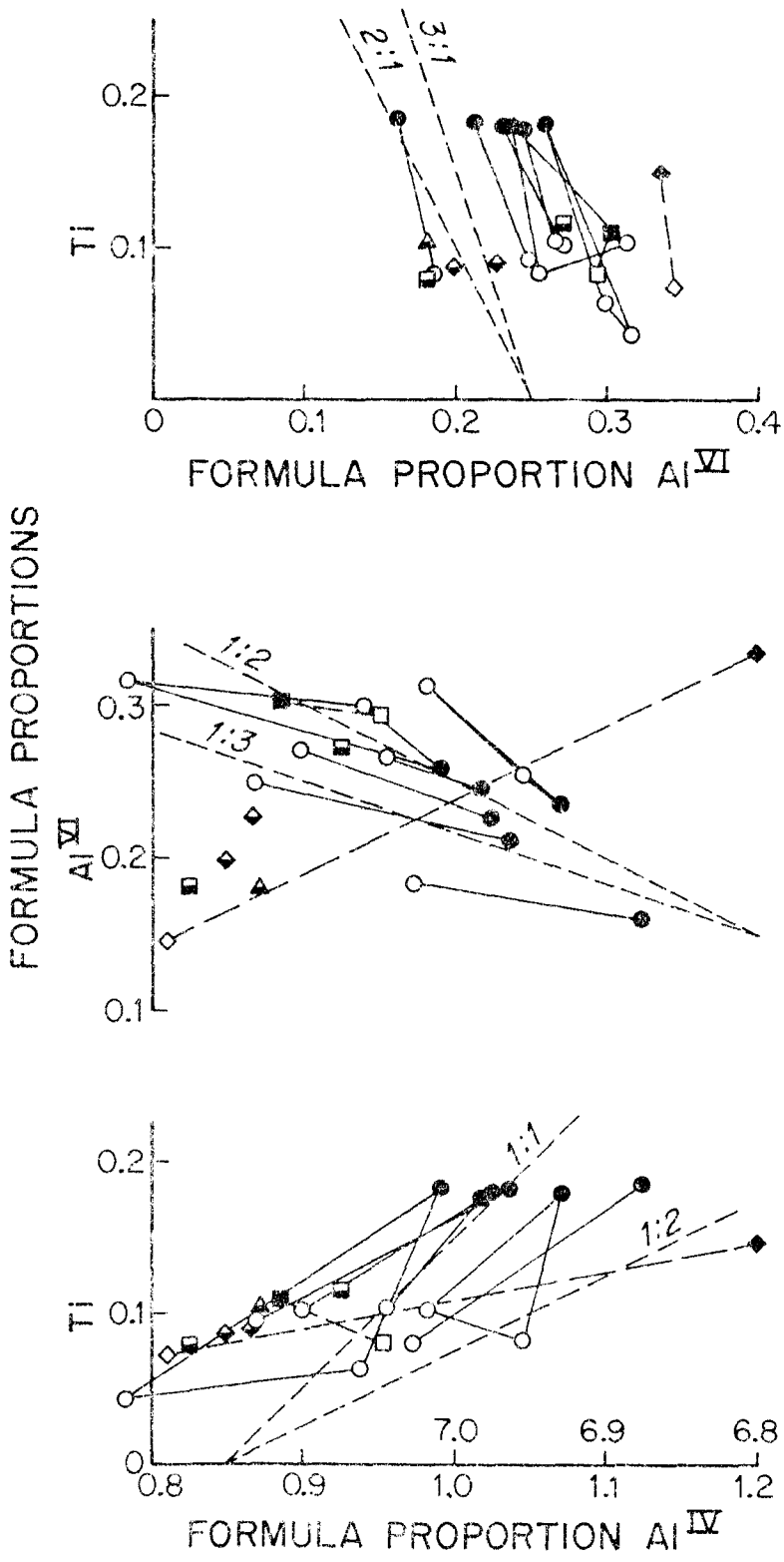
3:1
2:1
0.2
Ti 0.1
0
0.1
0.2
0.3
0.4
FORMULA PROPORTION AI VI
FORMULA PROPORTIONS
1:2
1:3
0.3
AI VI 0.2
0.1
1:1
1:2
0.2
Ti 0.1
0
7.0
6.9
6.8
0.8
0.9
1.0
1.1
1.2
FORMULA PROPORTION AI IV

Figure 67. Composite correlation plots for zoned hornblende grains in the stubby hornblende tonalite. (A) Formula proportions of reactants versus products appropriate to reaction(1) based on normalization (1). (B) Formula proportions of reactants versus products appropriate to reaction (2) based on normalization (3).

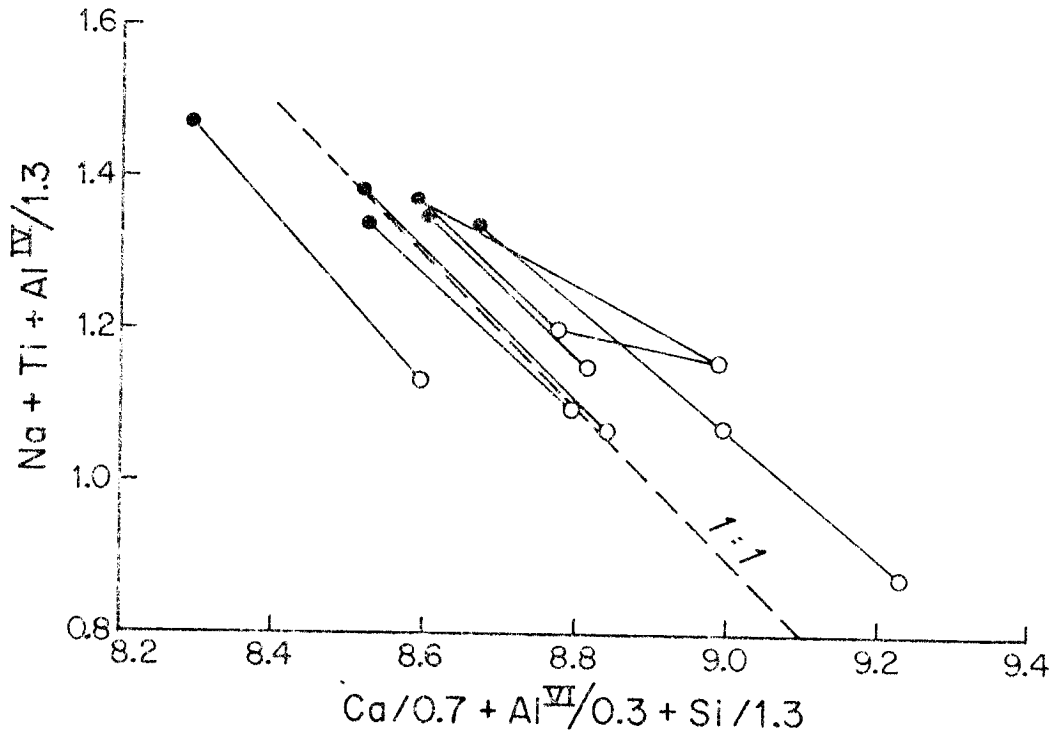
1.6
1.4
1.2
1.0
0.8
Na + Ti + AlIV/1.3
8.2
8.4
8.6
8.8
9.0
9.2
9.4
Ca/0.7 + AlVI/0.3 + Si/1.3
1:1

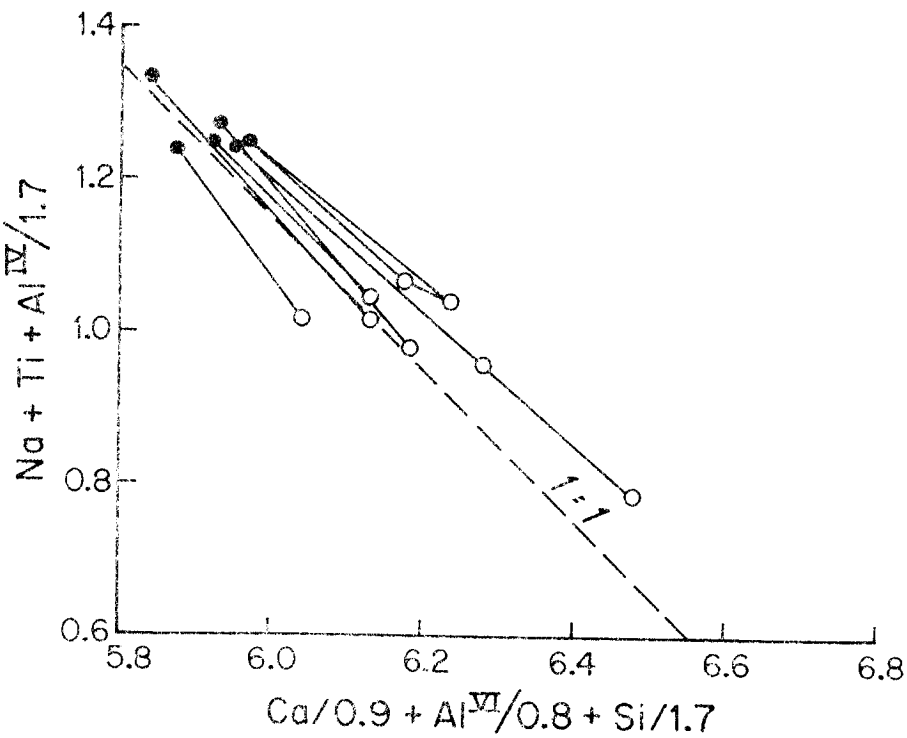
1.4
1.2
1.0
0.8
0.6
Na + Ti + AlIV/1.7
5.8
6.0
6.2
6.4
6.6
6.8
Ca/0.9 + AlVI/0.8 + Si/1.7
1:1

approximately valid for normalization (2) as well -- is:

$$\underbrace{Na + Ti + 1.7\ Al^{IV}}_{cores} \rightarrow \underbrace{0.9\ Ca + 0.8\ Al^{VI} + 1.7\ Si + 0.3\ o.}_{rims} \qquad (2)$$

This reaction also yields consistent 1:1 negative slopes (Figure 67B).

The Fe/(Fe + Mn + Mg) ratios also increase from core to rim in the zoned SHbT grains, but total FM contents are essentially constant. Charge balance considerations for reaction (1) imply the accompanying substitution $1.4\ FM^{2+}$ (cores) $\rightarrow 1.4\ Fe^{3+}$ (rims), which is consistent with the spectral evidence of higher $Fe^{3+}/(Fe^{2+} + Fe^{3+})$ in the rims. Reaction (2), in contrast, requires the reverse zonation -- $0.9\ Fe^{3+}$ (cores) $\rightarrow 0.9\ FM^{2+}$ (rims) -- and would therefore appear less reasonable.

The nearly 1:1 anticorrelation of Na to Ca in the zoned SHbT grains may indicate direct substitution of Na^{M4} (cores) $\rightarrow Ca^{M4}$ (rims). If so, normalization (1) and reaction (1) are inappropriate. However, the anticorrelation could also arise from a coupled substitution such as $Na^{A} + FM^{M4} + Ti^{Y}$ (cores) $\rightarrow o^{A} + Ca^{M4} + FM^{Y}$ (rims). With allowance for charge balance, reaction (1) could then be amended to:

$$\underbrace{Na^{A} + 0.7\ FM^{M4} + (Ti + 1.4\ Fe^{2+})^{Y} + 1.3\ Al^{IV}}_{cores} \rightarrow$$

$$\underbrace{o^{A} + 0.7\ Ca^{M4} + (0.3\ Al^{VI} + 0.7\ FM + 1.4\ Fe^{3+})^{Y} + 1.3\ Si.}_{rims} \qquad (1A)$$

Constant total FM content from core to rim is maintained simply by displacement of FM from the M4 site in the core to the Y site in the rim. This reaction may not be exactly correct, but considering the small amounts of FM^{M4} required -- only about 0.014-0.118 formula units, corresponding to 0.7-5.9% of the ideal M4 site occupancy -- an indirect Ca/Na correlation of this sort seems perfectly reasonable. The site

assignment of the Na involved in the reaction therefore remains ambiguous.

As implied by the bluish-green color and well shown in Figure 66, hornblende in the five GBT, PHbT and SPT samples is generally similar in composition to the blue-green rims in the SHbT samples. However, some differences exist. (1) Total Al contents of hornblende in four of the five samples are appreciably lower than in the rims of the SHbT hornblendes. (2) Na, Al^{IV}, and Al^{VI} contents average slightly lower in the GBT, PHbT, and SPT hornblendes, although they overlap with the SHbT rim values. (3) Fe/(Fe + Mn + Mg) ratios of hornblende in the GBT, PHbT, and SPT samples are comparable to or lower than the *core* values in the SHbT, hence considerably lower than rim values in that unit. Differences in the Na, Al^{IV}, Al^{VI}, and total Al contents are in the same direction as the core-to-rim zoning in the SHbT hornblendes, but slightly more extreme. In contrast, the differences in the Fe/(Fe + Mn + Mg) ratios are exactly the opposite of the zoning in the SHbT grains. Again, all of these characteristics are apparent regardless of which normalization scheme is used.

The microprobe results confirm the lack of appreciable zoning in most hornblende grains in the PHbT and SPT; there is no evidence that either unit ever contained significant amounts of brownish-green hornblende comparable to that in the SHbT. Sparse hornblende prisms in several samples preserve euhedral magmatic zoning, and the cores of these crystals are blue-green, with little or no brownish cast. Two of these zoned crystals were analyzed (Table 14) and plotted in Figure 66: relatively weak euhedral zoning in H-36a-2 (PHbT) bears no resemblance to the zoning in the SHbT hornblendes, whereas strong

euhedral zoning in H-62a-2 (SPT) is similar to the SHbT zoning in some respects, but differs greatly in others. In particular, both Na and Al^{IV} show a strong positive rather than negative correlation with Al^{VI} in H-62a-2; thus, both Al^{VI} and Al^{IV} are strongly concentrated in the core of that grain, and the total Al content of the core is unusually high. In addition, the FM content increases greatly from core to rim of H-62a-2 and therefore shows a strong inverse correlation with both Al^{IV} and Al^{VI}. These correlations imply that the coupled substitution of $Al^{IV} + Al^{VI}$ for Si + FM, not observed in the SHbT hornblendes, may have been important in H-62a-2.

Together the compositional and textural differences indicate that hornblende in the SHbT crystallized under conditions distinctly different from those prevailing during crystallization of hornblende in the PHbT and SPT, then underwent partial deuteric exchange which did not affect hornblende in the other units. Higher pressure might account for the higher Ti contents in the brownish-green cores (Holloway and Burnham, 1972). However, high pressure might also be expected to favor octahedral coordination of Al (e.g., Leake, 1971), yet Al^{VI} contents are lower in the Ti-rich cores than in the blue-green rims. Thus, with the exception of grain H-62a-2, which does have an Al^{VI}-rich core, pressure does not appear to have been the principal variable affecting the differences in hornblende composition.

Helz (1973), in her melting experiments on natural basalts, showed that hornblende compositions vary systematically as a function of temperature and oxygen fugacity at constant $P_{H_2O} = P_{total} = 5$ kb. Under conditions of the quartz + fayalite + magnetite (QFM) buffer,

Ti, Al^{IV}, and the amount of Na believed to be in the A site[14] increased steadily as temperature rose from 700 to 1000°C. The change was especially pronounced for Ti. Total Na concentrations increased in some experiments, but not in others. Helz emphasized the empirical observation that variations in Na^A were coupled in some way to the Ti and Al^{IV} variations; if the latter two increased or decreased, Na^A always varied correspondingly.

Helz also found that, at constant T, P_{H_2O}, and P_{total}, an increase in f_{O_2} from that of the QFM buffer to that of the HM (hematite-magnetite) buffer caused a decrease in the Fe/(Fe + Mg) ratios and in the Ti, Al^{IV}, and Na^A contents of the hornblende. Note that this effect on Ti, Al^{IV}, and Na^A contents is exactly opposite to the effect of increasing temperature under conditions of the QFM buffer. The effect of temperature on hornblende compositions appears to be much less pronounced for conditions of the HM buffer than for the QFM buffer; even so, the Al^{IV} contents increased appreciably and the amount of Na believed to be in the A site may have increased slightly as temperature rose.

Helz (p. 266) noted that, correlative with changing composition, the

> "QFM-buffered hornblendes change markedly in colour and habit as temperature increases. Hornblendes formed below 750°C are acicular in habit, pale green to blue green, and only faintly pleochroic. At higher temperatures, hornblende occurs in short stubby prisms and is strongly pleochroic (deep green to brown), becoming progressively browner, to reddish brown at 1000°C. The HM-buffered hornblendes are pale green and nonpleochroic at all temperatures."

---

[14] Helz normalized the hornblende analyses to 23 oxygens (i.e., total cation charge = 46), assuming all Fe is Fe^{2+}. Assignment of Na site distribution is therefore subject to the same ambiguities as in the present study.

Data on hornblendes from metamorphic rocks appear consistent with the temperature effects observed in the experiments. That is, Ti, Al^{IV}, and total alkali contents (ignoring site distribution) generally increase as metamorphic grade increases (Engel et al., 1964; Leake, 1965, 1971; Laird, 1977), whereas Al^{VI} and Na^{M4} contents increase as pressure increases (Leake, 1965, 1971; Laird, 1977).

The color and compositional variations produced experimentally by Helz are strikingly similar to the zoning observed in the SHbT hornblendes and to the differences between the hornblende cores in that unit and the typical hornblende in the PHbT and SPT. The higher Ti, Al^{IV}, and Na contents of the brownish-green cores of the SHbT hornblendes can apparently be explained by crystallization at higher temperature and/or less oxidizing conditions than for the blue-green hornblende in the other units. These conditions may be related in turn to lower water content in the SHbT magma. Numerous observations supporting this interpretation of differing T, f_{O_2}, and f_{H_2O} will be presented in the next several pages.

Three independent observations support the interpretation of more reducing conditions in the SHbT magma. First, although the Fe/(Fe + Mn + Mg) ratios increase from core to rim in the zoned SHbT grains, the Fe^{3+}/Fe^{2+} ratios also appear to increase. Secondly, the FeO_t/(FeO_t + MgO) ratios of the rocks (Plate 9) are slightly *lower* in the three SHbT samples (0.639-0.642) than in the four PHbT and SPT samples (0.646-0.662). Therefore, the consistently *higher* Fe/(Fe + Mn + Mg) ratios in both the cores and rims of the SHbT hornblendes compared to the values in the PHbT and SPT hornblendes cannot apparently be attributed to differing Fe and Mg contents in the magmas, whereas they

can be attributed reasonably to less oxidizing conditions in the SHbT magma. Thirdly, magnetite compositions are similar in all eight samples, but the proportion of hematite lamellae in the hematite-ilmenite intergrowths is generally lower in the SHbT samples than in the PHbT and SPT samples. Because the lamellae appear to be due primarily to exsolution rather than oxidative alteration, the differing proportions probably reflect, for the most part, differing Fe_2O_3 contents in the original homogeneous grains (see Section 12.7 for a discussion of the Fe-Ti oxides).

The evidence for lower water content in the SHbT magma is mainly textural. First, the anhedral molded and interstitial margins of hornblende imply that considerable growth of hornblende continued into the latest stages of magmatic crystallization. In contrast, the subhedral and euhedral prismatic forms of hornblende in the PHbT and SPT -- in particular, the absence of molded textures -- suggest that hornblende crystallization essentially ceased before competition for growth space became severe. Because the SHbT is just as mafic, in fact slightly more mafic, than most of the PHbT and SPT (Plates 9 and 9A), differing whole-rock composition apparently cannot account for the relatively late growth of hornblende in the SHbT, whereas differing water content can. That is, recent experiments have shown that the maximum stability temperature of amphiboles (Eggler, 1972; Holloway, 1973) and of biotite (Mallóe and Wyllie, 1975) in a melt increases only slightly and may eventually decrease as the H_2O content of the melt decreases progressively below the saturation limit. In contrast, the stability limits of the anhydrous phases plagioclase and quartz increase greatly as the H_2O content of the melt decreases (Robertson

and Wyllie, 1971; Maaløe and Wyllie, 1975).

Secondly, lower water content is consistent with the occurrence of sparse early-nucleated, subhedral quartz crystals (Section 12.2) and of relatively common small clinopyroxene relicts (or actinolite-quartz intergrowths suggestive of prior existence of clinopyroxene) as inclusions in the SHbT hornblendes, as compared with the apparent absence of the former and the extreme rarity of the latter in the PHbT and SPT hornblendes. Higher crystallization temperatures arising from lower water content in the SHbT magma are also implied by the abundance of rutile needles in some quartz crystals (mainly those partially or entirely enclosed in hornblende), by the characteristic occurrence of scattered hematite flakes in plagioclase, and by the slight clouding of some plagioclase crystals by minute specks of hematite, opaques, and unidentified material. These features, which probably formed by exsolution of components originally dissolved in the quartz and plagioclase at higher temperature, are all very poorly developed in the PHbT and SPT.

Thirdly, as discussed in Section 12.10, small, smoothly interstitial grains or aggregates of chlorite, muscovite, zeolite, and other relatively low-temperature, volatile-bearing minerals are common in some SPT samples and suggest filling of microcavities originally occupied by an exsolved vapor phase. Such interstitial grains and aggregates are relatively rare in the PHbT and extremely rare in the SHbT. Inasmuch as there is very little carbonate, fluorine, or sulfur in any of the rocks, the volatile phase was presumably water-rich, and the variable abundance of filled microcavities presumably reflects differences in the H_2O content of the magmas, the SHbT magma having

been driest.

At the close of magmatic crystallization or during early subsolidus cooling, a water-rich vapor phase appeared in the SHbT. Deuteric oxidation of the Fe-Ti oxides, producing hematite lamellae in magnetite and rutile + hematite intergrowths in ilmenite, indicates that the appearance of the vapor phase was accompanied by increasingly oxidizing conditions. The combination of these two changes resulted in extensive conversion of brownish-green hornblende to blue-green hornblende. It is interesting that hornblende in the GBT is generally blue-green and weakly zoned; brownish-green cores are rare, particularly along the northern and western contacts. Hornblende compositions in GBT sample 30a are quite uniform and similar to the rim hornblende in the other units. Possibly, thorough deuteric or late-magmatic exchange was responsible for the rarity of core-type hornblende in the GBT. However, it is also possible that interaction with the wall rocks resulted in higher f_{H_2O} and f_{O_2}, as well as lower temperatures at the margins of the SHbT magma; under these conditions, blue-green rather than brownish-green hornblende may have crystallized directly from the melt as in the PHbT and SPT. The tendency towards more elongate, euhedral, non-poikilitic hornblende morphologies and towards more pronounced euhedral progressive and oscillatory zoning in plagioclase in the GBT also suggests that conditions in the SHbT magma near contacts with country rocks approached those which prevailed throughout the PHbT and SPT, i.e., higher P_{H_2O}, hence lower temperature and higher f_{O_2}.

12.6 Biotite

Biotite and its minor alteration products -- mostly chlorite, plus some sphene, rutile, ilmenite, epidote, and white mica -- comprise variably 2 to 12% of the tonalite, averaging 4-8%. The abundance is greatest in the GBT and generally least in the eastern part of the PHbT. Biotite exceeds hornblende in the GBT, but elsewhere it is generally equal or subordinate to hornblende.

Biotite has a 2V of 0-10° and is pleochroic in the scheme: α = straw yellow or pale grayish gold, $\beta = \gamma$ = medium or dark grayish brown or orange-brown, locally grading to olive-green or greenish brown. Greener areas show a close spatial correlation to fine-grained anhedral sphene and rutile, indicating that the color change is related to deuteric reactions releasing TiO_2 from the biotite.[15]

A few scattered subhedral and euhedral biotite crystals are present in many thin sections of the SPT. Otherwise, except for flakes comprising recrystallized aggregates, biotite is consistently anhedral. Thin platy crystals characterize the PHbT and SPT. These flakes generally range from <1 mm up to 4-5 mm in diameter, but flakes 6-12 mm in diameter are locally conspicuous. In the SHbT, biotite is similar in size and shape to the hornblende in the same rocks, i.e., books are fat and roughly equant, and grain size is generally 2-5 mm, but locally averages as much as 5-8 mm.

Finer grained biotite exhibits relatively simple interstitial shapes, but most larger grains poikilitically enclose or are molded around and between the other minerals, especially plagioclase and horn-

---

[15] Microprobe analyses discussed later confirm this interpretation.

blende (Figure 68). Inclusions of apatite and opaque are common. Many biotite crystals penetrate raggedly into plagioclase and occasionally hornblende, yet many other grains occur side by side with or enclose euhedral or subhedral crystals of both mineral, especially hornblende, without obvious evidence of reaction. Although there is a slight tendency for biotite to be clustered with hornblende and opaques, much of the biotite is not spatially associated with hornblende at all.

In the western part of the PHbT and in the central and northwestern parts of the SPT, conspicuous poikilitic books of biotite 6-12 mm in diameter are uniformly disseminated not only through the tonalite, but in some cases through otherwise fine-grained, mafic, hornblende-plagioclase inclusions in the tonalite. The areas involved are shown in Figure 17 (p. 118). The books in the inclusions are apparently porphyroblasts whose indiscriminate growth in both the inclusions and host rock -- locally crossing inclusion-host rock contacts -- suggests crystallization when the tonalite was nearly solid.

Thus the textures clearly indicate that when biotite crystallized, the tonalite was already a crystal-rich system. Possibly some biotite crystallized from a subsolidus vapor phase. Although some biotite grew by replacement, the textural evidence seems to demonstrate conclusively that hornblende and biotite were coprecipitating phases during part of the crystallization history, rather than being strictly a reaction pair. Likewise, much biotite crystallized simultaneously with plagioclase. The degree of replacement growth, as opposed to to primary interstitial growth, of biotite varies from slight to so extensive as to partially obscure evidence of earlier interstitial growth. Both modes of growth are volumetrically important throughout

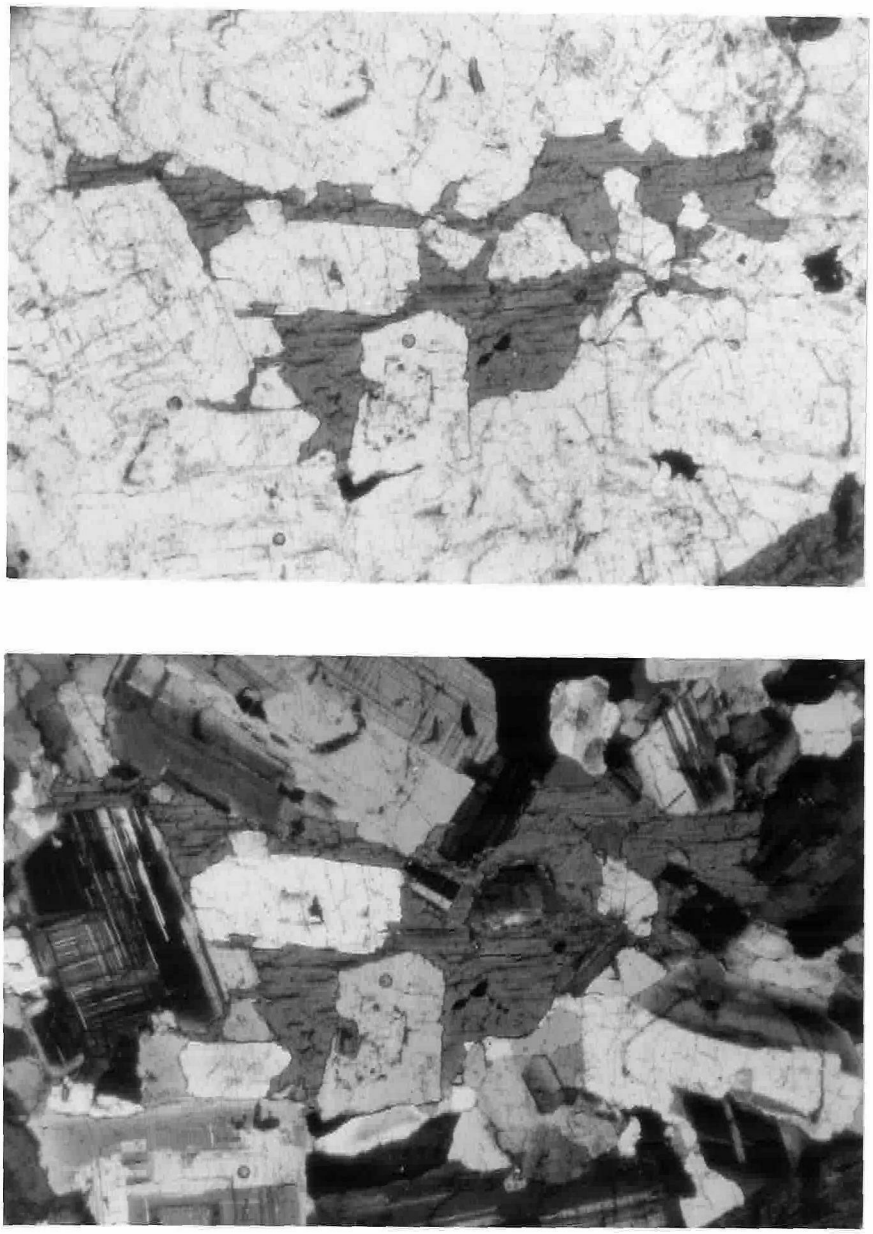

Figure 68. Large irregular biotite crystal in the seriate porphyritic tonalite. Upper photo, plane light; lower photo, same view in crossed nicols. This is an excellent example of the complex molded and poikilitic form commonly assumed by coarse biotite, especially in the PHbT and SPT. Although this biotite crystal has penetrated raggedly into plagioclase in some places, relatively smooth molded margins predominate and indicate growth mainly by filling of available interstitial space. In some cases, replacement of plagioclase and locally hornblende is much more extensive. Sample Ba-JM-639, from the arroyo called El Alisito, ∿320 m from the southeastern margin of the pluton (area R-8).

the pluton, but their relative contributions are difficult to determine. Disequilibrium apparently developed at the close of magmatic crystallization or during early subsolidus cooling, probably as an inevitable consequence of rapid changes in the composition of the residual melt and/or evolution of a water-rich vapor phase. As chemical exchange and communication among the decreasingly integrated areas of interstitial melt or vapor diminished, local variations in the melt and/or vapor-phase composition almost certainly developed, depending upon the proportions of the various phases in the immediate vicinity. Such variations in composition would have led to varying degrees of local disequilibrium and reaction. It is therefore not surprising that biotite replaced hornblende and plagioclase extensively in some areas, yet coexists in apparent textural equilibrium with these phases in other places.

Surprisingly, biotite generally appears to have replaced plagioclase more extensively than it did hornblende, perhaps because the Al:Si ratio of the biotite (about 0.50) is comparable to that of the plagioclase (0.48-0.53), but very different from that of the hornblende (about 0.16).

The preceding observations do not apply to the CBT, where thorough recrystallization of biotite into aggregates of euhedral to anhedral crystals destroyed original crystallization textures (Figures 31 and 32, pp. 192 and 193). The aggregates as a whole show strong preferred planar orientation and, in many cases, are smeared out into ellipses defining pronounced lineation. Within the plane of foliation, the crystals comprising the aggregates are less well oriented and locally appear randomly oriented. The crystals commonly show little or no deformation. Recrystallization therefore continued after deformation.

had largely or entirely ceased. Concentrations of very fine-grained sphene and rutile frequently occur between the flakes.

Partial recrystallization of biotite, producing small, variably oriented, subhedral and euhedral flakes within and at the margins of some larger grains, is also recognizable throughout the interior of the pluton. The larger (primary) grains may be bent or sharply kinked, but the smaller secondary flakes are undeformed. Concentrations of very fine-grained sphene and rutile are again common along the edges of the secondary flakes. The degree of recrystallization is directly proportional to the intensity of flow structure and protoclasis; thus very little recrystallization is apparent in the central and southern parts of the pluton, but partially recrystallized grains are common in the outer part of the PHbT and in much of the SHbT. Kinking and recrystallization of biotite both appear to be sensitive indicators of post-crystallization strain and recrystallization in the rocks.

In some parts of the pluton, especially in the SHbT, tiny grains of ilmenite, rutile, and sphene are locally concentrated along the margins of biotite crystals. The titaniferous phases are generally accompanied by tiny biotite flakes and are either intergrown with the rims of adjacent plagioclase crystals or occur in fine-grained aggregates with granular plagioclase and sometimes quartz. The textures indicate late magmatic or subsolidus release of Ti and Fe from the biotite and precipitation of the titaniferous phases and minor biotite preferentially along contacts with plagioclase. The release of Fe in turn implies breakdown of some of the annite component of biotite via the reaction

$$KFe_3AlSi_3O_{10}(OH)_2 \rightleftharpoons KAlSi_3O_8 + 3\ FeO + H_2O$$

or, if oxidation is involved,

$$KFe_3AlSi_3O_{10}(OH)_2 + 1/2\ O_2 \rightleftharpoons KAlSi_3O_8 + Fe_3O_4 + H_2O.$$

In some cases, the Fe released in the reaction combined with simultaneously-released Ti to produce hemo-ilmenite, but the K-feldspar component rarely occurs in association with the biotite or the titaniferous aggregates and must have been carried off in solution or crystallized elsewhere in the rock. In general, I recognized no spatial correlation of K-feldspar with biotite, even where partial chloritization indicates undeniable release of K_2O.

Biotite tonalite layers containing 10-20% biotite and only trace amounts of hornblende, are abundant in some outcrops in much the same areas as those characterized by coarse disseminated poikilitic biotite (Figure 17). The layers, generally 2-4 cm wide and several or more meters long, may be parallel to or at a low angle to foliation. Many are slightly wavy, but some are straight, and none are complexly contorted. They occur mainly in areas where foliation is very weak. Grain size averages 2-4 or up to 4-5 mm, that is, comparable to or perhaps slightly coarser than in the host rock, but, unlike in the host rock, biotite is more nearly equigranular than seriate. One layer was examined in thin section. It consists of 45% plagioclase, 35-40% quartz, 11-12% biotite, 3-4% interstitial and poikilitic K-feldspar, <<1% hornblende, and 2% accessory and deuteric minerals. This compares with 55-60% plagioclase, 20-25% quartz, 7-8% each of biotite and hornblende, 3-4% interstitial and poikilitic K-feldspar, and 1-2% accessory and deuteric minerals in the immediately adjacent host rock. Plagioclase is identical in the layer and host rock: average composition of An_{35-40}, with small cores, patches, and thin intermediate zones up to An_{55-60} and sharp rims of

An_{20-23}. Biotite is raggedly molded and poikilitic; it has replaced plagioclase to some extent, but it appears mainly to fill spaces between plagioclase and quartz grains. Direct textural evidence of replacement of hornblende by biotite is lacking in the layer -- most of the hornblende occurs as inclusions in plagioclase or quartz -- but there is abundant evidence of such replacement in the enclosing tonalite. The layers apparently developed along early-formed joint planes as a result of reaction of typical tonalite with residual melt or silica- and potash-rich fluids concentrated or injected along the fractures.

Average compositions of biotite in eight samples and in the pluton as a whole are given in Table 17. Compositions of individual grains are tabulated in Appendix C, Table C-7. The compositions are remarkably uniform throughout the pluton. Possibly, biotite contains slightly more TiO_2 and less Al_2O_3 in the SPT than in the rest of the tonalite; otherwise, there are no recognizable variations as a function of textural unit or of geographic position. The Fe/(Fe + Mn + Mg) ratio is similar in all samples, implying similar T-f_{O_2} conditions during *latest* equilibration throughout the pluton. Note that this conclusion is not inconsistent with the earlier conclusion of lower f_{O_2} in the SHbT during original crystallization of hornblende and opaques. Slight variations in this ratio appear to be independent of such indices of differentiation as the Thornton-Tuttle differentiation index of the rock and the An content of plagioclase rims. Na_2O concentrations are consistently very low, and CaO contents are negligible. No other elements were found in wave-length scans of two crystals, one each from samples 3a and 25a.

With the exception of the greenish-brown or olive-green areas mentioned earlier, individual grains are unzoned. Analysis of a

Table 17

Average Microprobe Analyses of Biotite in Individual Tonalite Samples

Name of Unit	GBT	SHbT			PHbT		SPT		Pluton	
Sample #	Ba-JM 30a	Ba-JM 25a	Ba-JM 29	Ba-JM 68	Ba-JM 36a*	Ba-JM 46a	Ba-JM 3a	Ba-JM 62a	Average	σ
# of Grains	4	5	2	4	4*	5	5	4		
SiO_2	37.49	36.81	37.27	37.27	36.74	36.76	37.02	37.55	37.11	0.33
TiO_2	2.14	2.27	2.51	2.13	2.31	2.54	3.27	3.05	2.53	0.42
Al_2O_3	16.11	16.22	15.87	15.98	15.99	15.56	15.27	14.77	15.72	0.49
FeO	16.82	16.83	17.64	16.88	16.22	17.17	16.83	16.80	16.90	0.40
MnO^t	0.33	0.10	0.16	0.17	0.13	0.33	0.17	0.19	0.20	0.09
MgO	12.81	12.94	12.36	12.86	13.52	13.08	13.20	13.86	13.08	0.46
CaO	0.03	0.05	0.04	0.01	0.10	0.06	0.04	0.06	0.05	0.03
Na_2O	0.08	0.11	0.13	0.10	0.09	0.06	0.10	0.19	0.11	0.04
K_2O	9.63	9.33	9.45	9.57	9.03	9.40	9.52	9.28	9.40	0.19
"H_2O"	4.57	5.34	4.57	5.[illegible]	5.86	5.04	4.58	4.27	4.91	0.52
TOTAL	100.00	100.00	100.00	100.[illegible]	99.99	100.00	100.00	100.00	100.00	--
Formula Proportions Based on the Sum (Cations less (K + Na + Ca)) = 14										
Si	5.734	5.655	5.721	5.726	5.636	5.643	5.671	5.705	5.686	0.040
Al(IV)	2.266	2.345	2.279	2.274	2.364	2.357	2.329	2.295	2.314	0.040
Al(VI)	0.638	0.592	0.592	0.620	0.528	0.458	0.427	0.349	0.526	0.104
Ti	0.246	0.262	0.289	0.246	0.267	0.293	0.377	0.349	0.291	0.048
Fe	2.151	2.161	2.263	2.168	2.080	2.203	2.155	2.133	2.164	0.053
Mn	0.042	0.013	0.020	0.022	0.016	0.043	0.023	0.024	0.025	0.011
Mg	2.920	2.962	2.828	2.944	3.092	2.993	3.013	3.139	2.986	0.098
Ca	0.004	0.009	0.007	0.002	0.017	0.011	0.007	0.007	0.008	0.005
Na	0.024	0.033	0.038	0.029	0.027	0.019	0.030	0.056	0.032	0.011
K	1.880	1.829	1.851	1.875	1.767	1.840	1.861	1.799	1.837	0.039
"OH"	4.666	5.473	4.675	5.174	6.001	5.166	4.679	4.328	5.020	0.541
Fe/(Fe+Mn+Mg)	0.421	0.421	0.443	0.422	0.401	0.421	0.415	0.403	0.418	0.013
Mn/(Fe+Mn+Mg)	0.008	0.003	0.004	0.004	0.003	0.008	0.004	0.005	0.005	0.002
Mg/(Fe+Mn+Mg)	0.571	0.577	0.553	0.574	0.596	0.571	0.580	0.593	0.577	0.014

*Analysis B-36a-7 (Table C-7, Appendix C) of an unusual greenish-brown part of a grain was omitted from the average.

greenish-brown area (B-36a-7; Table C-7) of one grain in sample 36a revealed that the greener biotite is significantly depleted in TiO_2 (1.81%) and slightly enriched in MgO (14.02%) relative to the four analyzed grains of typical grayish-brown biotite in this rock (TiO_2 = 2.21-2.49%; MgO = 13.26-13.81%). The Fe_2O_3/FeO ratio may also be different; otherwise, the greener biotite is compositionally similar to the other grains. Semi-quantitative analysis of a greenish-brown grain adjacent to sphene in sample 46a also showed low TiO_2 (roughly 1.4%) compared to the other grains in that rock (TiO_2 = 2.18-2.79%). These results confirm the petrographic interpretation that greenish color is correlated with deuteric loss of Ti.

In Section 15.2.3 I will discuss in detail the application of the experimental data on the reaction Fe-rich biotite + $O_2 \rightleftharpoons$ Mg-rich biotite + K-feldspar + magnetite + H_2O (Wones and Eugster, 1965), to the estimation of the T, f_{O_2}, and f_{H_2O} conditions of equilibration of the assemblage biotite + K-feldspar + magnetite. Suffice it to say here that the compositions of these phases indicate equilibration under conditions approximating those of the magnetite-hematite buffer curve at temperatures in the range 645-745°C or possibly as much as 50° higher, assuming $P_{H_2O} \approx$ 1-2 kb. Inasmuch as the solidus temperature of the tonalite is estimated to be in the range 680-750°C (p. 534), the compositional data are completely compatible with the petrographic observations indicating late magmatic and possibly high-temperature subsolidus crystallization of biotite. If the solidus temperature was closer to 800°C, the compositional data suggest the possibility of complete subsolidus equilibration of the biotite.

12.7 Fe-Ti Oxides

Magnetite and intergrowths of titano-hematite and ferrian-ilmenite are typically present in subequal amounts and together comprise 1-2% of all three textural units. Very tiny amounts of minute brassy sulfide (pyrite?) and rarely bornite and chalcocite (?) are the only opaques seen. The GBT differs from the rest of the tonalite in that sphene has taken the place of hematite-ilmenite as the principal titaniferous accessory mineral, and the opaques, which total only 0.3-0.7%, consist almost entirely of magnetite.

Magnetite is generally euhedral or subhedral and appears slightly brownish gray in reflected light. Alteration to patches and lamellae of hematite, concentrated especially at grain margins and along cracks, varies from nil to as much as 30%. Lamellae of ilmenite or of other spinel phases are entirely absent. Nor is there any alteration to rutile, sphene, or other titaniferous phases.

Hematite-ilmenite intergrowths are typically anhedral and rounded or slightly irregular in form. Some, however, are interstitial and molded, and rare grains are subhedral or euhedral. In reflected light the ilmenite is slightly brownish gray, with a faintly pinkish cast compared to magnetite. The hematite is nearly white. The intergrowths are often complex and vary considerably both in the relative proportions of the two minerals and in their mutual textural relationships. Most grains, such as those shown in Figures 69 to 72, consist of well-defined hematite and/or ilmenite lamellae oriented parallel to (0001) of the host phase, but in some grains the subordinate phase occurs as patches or rounded blebs scattered through the host.

The ratio of hematite to ilmenite is uniform from grain to grain

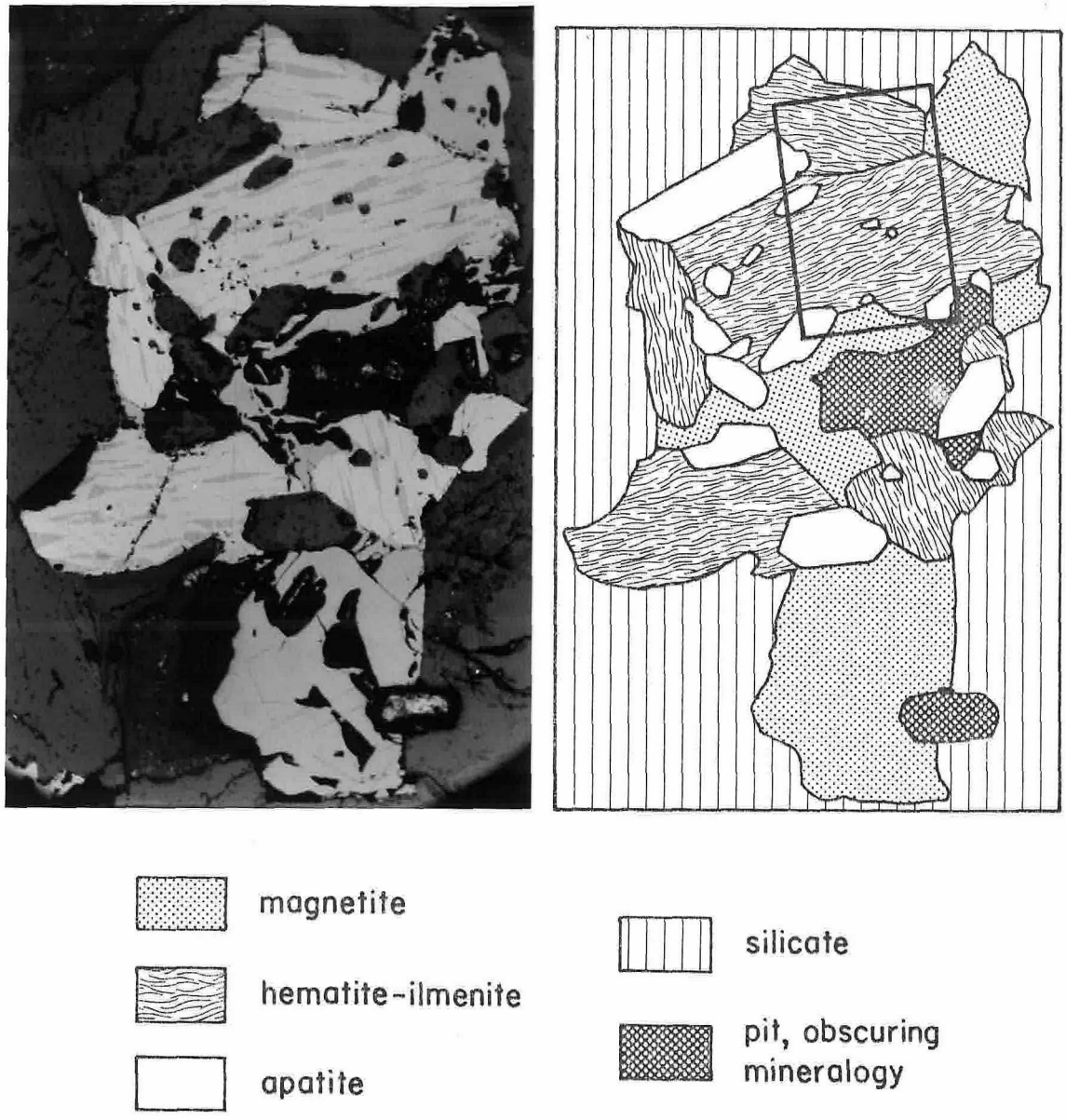

Figure 69. Aggregate of magnetite, hematite-rich hematite-ilmenite, and apatite in the seriate porphyritic tonalite. The drawing is traced directly from the photomicrograph; pits are shown only where the identity of the plucked phase(s) is unclear. In the hematite-ilmenite intergrowths, the brightest mineral (host phase) is hematite, and the slightly darker lamellae are ilmenite. Note the relatively uniform size and distribution of the ilmenite lamellae and the lack of evidence for reaction between the magnetite and hematite-ilmenite. The rectangle outlines the area shown in Figure 70. Sample Ba-JM-3a, from along the North-South road 340 m north of the intersection with the San José-San Telmo road (area (L-6).

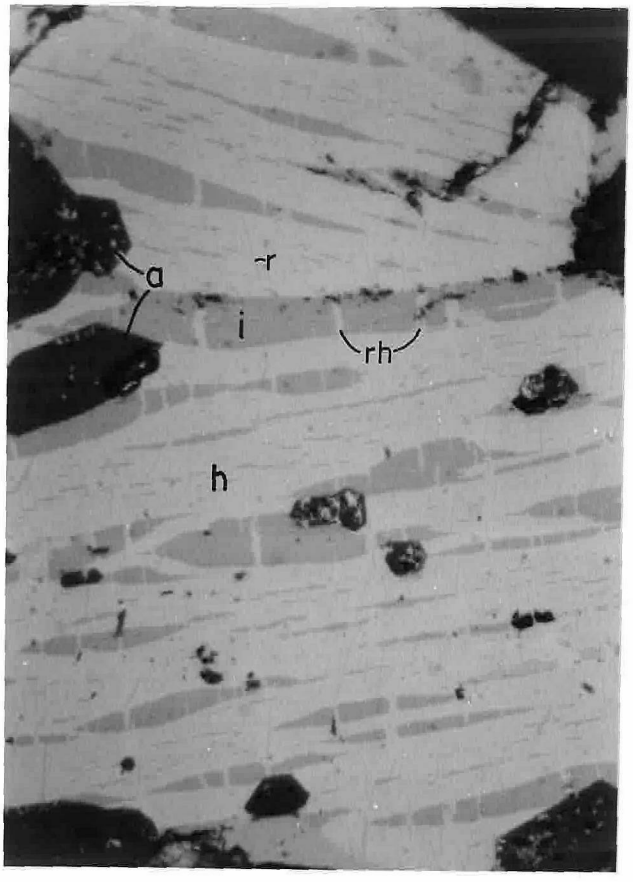

Figure 70. Close-up of hematite-ilmenite grains in the upper part of Figure 69. The narrow white swaths (rh) crossing the ilmenite lamellae (i) at right angles consist of rutile sheathed in hematite. Other extremely thin rutile lamellae (r) roughly normal to the ilmenite lamellae are visible in the hematite (h). A second generation of tiny hematite lamellae are barely resolvable in the ilmenite just below the two apatite crystals (a) in the upper right part of the photograph. The other dark euhedral crystals are also apatite.

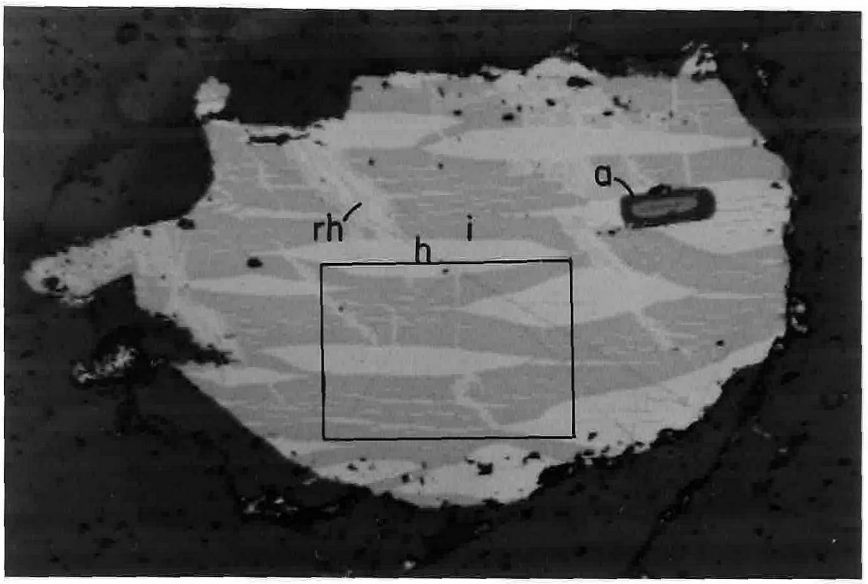

Figure 71A

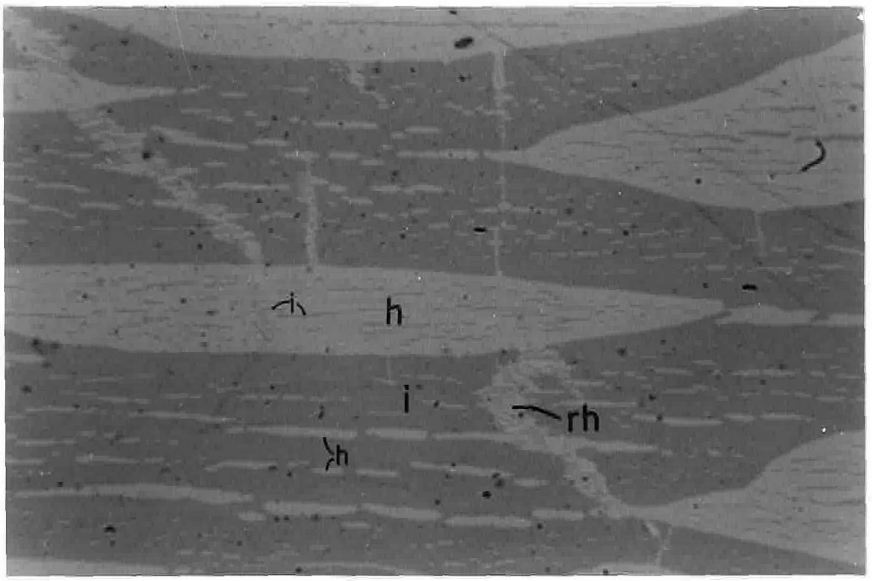

Figure 71B

Figure 71. Ilmenite-rich hematite-ilmenite grain occurring only 3 mm away from the aggregate in Figure 69. The rectangle in (A) outlines the area shown in (B). Symbols: h-hematite, i-ilmenite, rh-complex intergrowth of hematite (brightest areas) and rutile (intermediate in brightness between hematite and ilmenite), a-apatite. The distribution of hematite exsolution lamellae in the host ilmenite is relatively uniform and independent of the grain margins. Two generations of hematite and ilmenite exsolution lamellae are visible in (B), producing a "lamellae-within-lamellae" texture which is common in those grains consisting of 40% or more hematite.

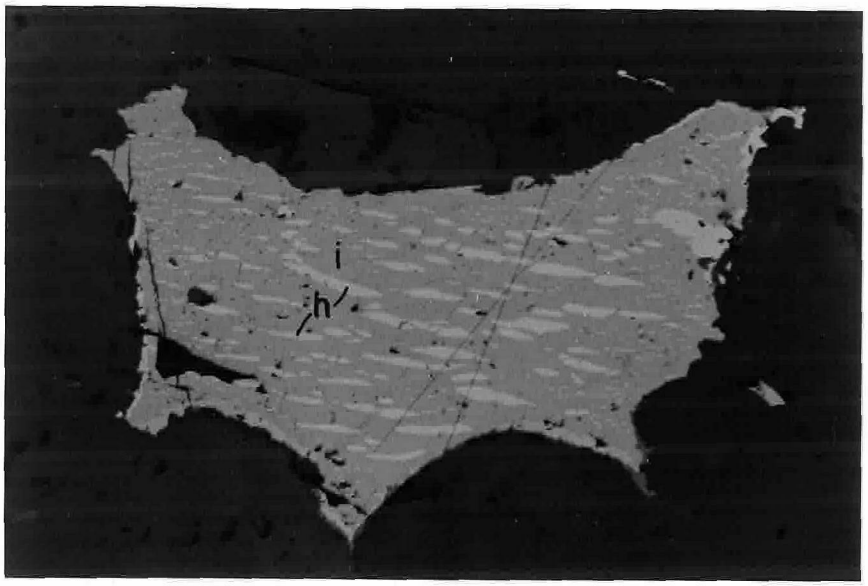

Figure 72A

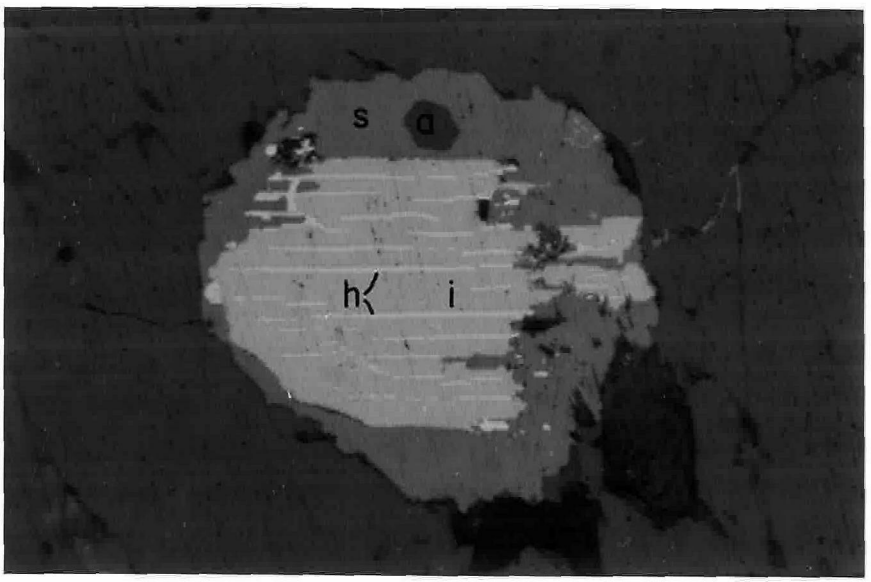

Figure 72B

Figure 72. Typical ilmenite-rich hematite-ilmenite intergrowths in the stubby hornblende tonalite. Symbols: h-hematite, i-ilmenite, s-sphene, a-apatite. Note that the corona of sphene in (B) replaced ilmenite preferentially to hematite; hematite lamellae locally control the position and geometry of the penetrating fingers of sphene, indicating that exsolution of hematite occurred before the alteration to sphene. The absence of either rutile or sphene in the interior of either opaque grain implies exsolution of hematite without accompanying oxidation of ilmenite. Samples: (A) Ba-JM-25a, from the northeastern part of the SHbT, 50 m west of Las Encinas Corral and 50 m south of the Concepción road (area D-9) and (B) Ba-JM-29, from the northwestern part of the SHbT, 15 m southwest of the Buena Vista-Coyote road, 670 m west-northwest of Rancho El Coyote (area D-5).

in some samples, but varies widely in others. Ilmenite containing 10-30% hematite (Figure 72) predominates in the SHbT and the southwestern part of the SPT. Rarely, hematite lamellae are not visible or can be seen only at high power. In contrast, intergrowths consisting of 20-60% of ilmenite as patches and lamellae in hematite (or vice versa) predominate throughout most of the PHbT and SPT. Grains in the latter rocks commonly show two generations of lamellae -- i.e., the host phase and the larger lamellae both contain abundant tiny lamellae of the other mineral (Figure 71B). These intergrowths also characteristically contain several percent rutile[16] in long thin lamellae oriented in one or more directions oblique or normal to the hematite or ilmenite lamellae. Rutile lamellae are most abundant in hematite; where they cross ilmenite lamellae, they are invariably separated from the ilmenite by a thin sheath of hematite. Most likely, this relationship resulted from direct oxidation of ilmenite to titano-hematite + rutile. Alternatively, oxidation of ilmenite may have initially produced lamellae of pseudobrookite solid solution ($FeTi_2O_5$ - Fe_2TiO_5) which subsequently broke down to produce the sheathed rutile lamellae. Formation of pseudobrookite solid solution would require oxidation at high temperature, since the pseudobrookite end-member (Fe_2TiO_5) is unstable below 1140°C (Lindsley, 1965).

Such well-oriented elongate rutile lamellae were not observed in ilmenite-rich intergrowths, although some of the latter have been partially oxidized to patches of irregularly intergrown hematite + rutile. Similar mottled patches too fine-grained to identify have

---

[16]Confirmed as pure TiO_2 by qualitative microprobe analysis.

been classified simply as "meta-ilmenite", a term proposed by Buddington and Lindsley (1964). The "meta-ilmenite" probably also consists of complexly intergrown hematite + rutile, but other Fe-Ti oxides, e.g., pseudobrookite, could be present. Sphene and sometimes pure rutile are other important alteration products of the hematite-ilmenite.

The Fe-Ti oxides occur both in scattered grains and in aggregates of up to 10-20 grains. The aggregates may consist of just magnetite, just hematite-ilmenite, or both. Individual grains seldom exceed 0.5 mm. Hematite-ilmenite is generally molded around or between euhedral magnetite crystals in the aggregates, but in a few cases the relationship is reversed. There is no evidence of reaction between the grains; nor is there evidence of external granular exsolution of ilmenite from magnetite or of either hematite or ilmenite from the hematite-ilmenite intergrowths.

Both types of opaques are commonly included in biotite and hornblende. Tiny grains are also common in plagioclase, but large inclusions are rare. A few examples of biotite partially rimming both magnetite and hematite-ilmenite were seen in the SPT. Magnetite inclusions rarely show evidence of reaction with the host minerals, whereas hematite-ilmenite inclusions in hornblende and especially in biotite are commonly rimmed by sphene and/or rutile. Euhedral inclusions of apatite are very common in hematite-ilmenite, but rare in magnetite.

Despite the evidence for oxidation, numerous observations indicate that many of the hematite-ilmenite intergrowths, including all of those in the photomicrographs, approach equilibrium high-

temperature exsolution assemblages. First, semiquantitative microprobe analysis indicates that the "hematite" in the intergrowths contains considerable TiO_2 in solid solution -- i.e., it is strictly titano-hematite -- whereas one would expect low-temperature disequilibrium oxidation to produce relatively pure Fe_2O_3 and free TiO_2. Likewise, the "ilmenite" contains dissolved Fe_2O_3 and is strictly ferrian-ilmenite. Secondly, the hematite/ilmenite ratio is relatively constant from grain to grain in many samples, although there are always exceptions. In a few other samples, there is a suggestion of a bimodal distribution of hematite/ilmenite ratios which, if real, implies subsolvus crystallization of both hematite-rich and hematite-poor solid solutions from the magma. Thirdly, the frequent absence of rutile (or sphene) in the ilmenite-rich intergrowths implies that the hematite lamellae in these grains formed by exsolution without oxidation, since oxidation of ilmenite to hematite must release free TiO_2 even if the hematite produced is itself titaniferous. Exsolution without oxidation in turn implies that the initial homogeneous phase crystallizing from the magma contained considerable Fe_2O_3 in solid solution. Fourthly, in some ilmenite-rich intergrowths, mainly in the SHbT, the hematite lamellae decrease rather than increase in size and abundance towards grain margins, which again seems inconsistent with oxidation and suggests compositional zoning in the original homogeneous solid solution. Finally, in most of the intergrowths, the size, shape, and distribution of lamellae are quite uniform and independent of grain shape or of proximity to grain boundaries. The frequently uniform appearance and distribution of the tiny second-generation lamellae provide a particularly persuasive argument for

approximate attainment of equilibrium as well as for two episodes of exsolution accompanied by oxidation. However, there are also many examples of disequilibrium oxidation producing patchy irregular intergrowths, with hematite sometimes concentrated near grain margins.

These observations discount low-temperature deuteric or hydrothermal alteration or weathering as the cause of the intergrowths. Low-temperature deuteric or hydrothermal alteration can also be ruled out because in low-grade metamorphic rocks the assemblage magnetite + rutile is stable relative to hematite + ilmenite (Lindsley, 1965). Weathering can also be ruled out because of the frequent alteration of the intergrowths to sphene -- in some cases clearly after development of the lamellar intergrowth texture (Figure 72B) -- and because the relative proportions and textures of the Fe-Ti oxides in four polished sections from different depths (66 to 230 m) in the drill core (locality 240, area I-7) are similar to those in the outcrop samples from that unit.

The intergrowths therefore formed by high-temperature exsolution, accompanied by varying degrees of oxidation. It is important to emphasize that oxidation and formation of rutile are not incompatible with equilibrium among the hematite, ilmenite, and rutile. Lindsley (1965) pointed out that these three phases may occur in equilibrium below the decomposition temperature of an intermediate $FeTi_2O_5$-Fe_2TiO_5 (pseudobrookite) solid solution, i.e., below perhaps 800-900°C. It is equally important to emphasize that the homogeneous solid solutions which initially crystallized from the magma contained considerable concentrations of both end members. Considering the low concentration (rarely >5%) of rutile lamellae in the oxidized intergrowths, it is

quite possible that some of the hematite-rich intergrowths formed from solid solutions initially containing as much or more Fe_2O_3 as $FeTiO_3$. Conceivably, the wide range of hematite-ilmenite ratios among grains in some samples records increasingly oxidizing conditions not just during subsolidus cooling, but also during magmatic crystallization. As mentioned earlier, coexisting hematite-rich and hematite-poor solid solutions may have crystallized locally from the melt in a solvus relationship.

Average compositions of magnetite in eight samples and in the pluton as a whole are given in Table 18. The averages are based on analysis of 119 points in 33 grains. Compositions of each grain are tabulated in Appendix C, Table C-8. Magnetite is remarkably pure and homogeneous, containing consistently 98-99% Fe_3O_4. V[17], Cr, and Al are the principal minor elements in order of decreasing abundance, but the concentrations are very low. Ti contents are almost negligible, and the ratio $Fe_2O_3/(Fe_2O_3 + Fe_2TiO_4)$ ranges from 0.996-0.999. No elements other than those in the table were detected in wave-length scans of two crystals. Analysis of one point adjacent to hematite-ilmenite in grain M-46a-2 gave 0.61% TiO_2 as compared with 0.07, 0.10, and 0.20% in other parts of the same grain. Otherwise, no gradients were detected in magnetite adjacent to hematite-ilmenite; nor do isolated magnetite grains differ in composition from those occurring in aggregates with hematite-ilmenite. Magnetite is also unzoned with respect to other minor constituents. Minor element concentrations, including Ti, in hematite patches and lamellae

---

[17] Contribution of TiKβ flux to the VKα count-rates is negligible due to the low Ti contents.

Table 18

Average Microprobe Analyses of Magnetite in Individual Tonalite Samples

Name of Unit	GBT	SHbT			PHbT		SPT		Pluton	
Sample #	Ba-JM 30a	Ba-JM 25a	Ba-JM 29	Ba-JM 68	Ba-JM 36a	Ba-JM 46a	Ba-JM 3a	Ba-JM 62a	Average	σ
Number of Grains	4	4	3	4	5	5	5	3		
SiO_2	0.06	0.05	0.04	0.06	0.04	0.04	0.04	0.06	0.05	0.01
TiO_2	0.03	0.12	0.05	0.06	0.04	0.12	0.06	0.06	0.07	0.04
Al_2O_3	0.14	0.12	0.13	0.12	0.09	0.16	0.11	0.12	0.12	0.02
V_2O_3	0.25	0.45	0.43	0.36	0.31	0.33	0.41	0.53	0.38	0.09
Cr_2O_3	0.11	0.30	0.23	0.25	0.10	0.14	0.13	0.18	0.18	0.07
Fe_2O_3	71.34	73.07	74.72	73.42	72.85	71.16	69.78	71.50	72.23	1.57
FeO	27.84	25.71	24.23	25.56	26.38	27.79	29.28	27.39	26.77	1.61
MnO	0.13	0.06	0.08	0.08	0.07	0.14	0.07	0.07	0.09	0.03
MgO	0.04	0.06	0.04	0.03	0.06	0.06	0.06	0.03	0.05	0.01
TOTAL	99.94	99.94	99.95	99.94	99.94	99.94	99.94	99.94	99.94	--
Formula Proportions based on Cation Sum = 3										
Si	0.002	0.002	0.002	0.002	0.001	0.001	0.002	0.002	0.002	0.000
Ti	0.001	0.003	0.002	0.002	0.001	0.004	0.002	0.002	0.002	0.001
Al	0.006	0.006	0.006	0.005	0.004	0.007	0.005	0.005	0.006	0.001
V	0.008	0.014	0.013	0.011	0.010	0.010	0.013	0.016	0.012	0.003
Cr	0.003	0.009	0.007	0.008	0.003	0.004	0.004	0.005	0.005	0.002
Fe^{3+}	2.074	2.128	2.181	2.139	2.121	2.068	2.025	2.079	2.102	0.049
Fe^{2+}	0.899	0.832	0.785	0.828	0.854	0.897	0.944	0.885	0.866	0.050
Mn	0.004	0.002	0.003	0.003	0.002	0.004	0.002	0.002	0.003	0.001
Mg	0.002	0.004	0.002	0.002	0.003	0.004	0.003	0.002	0.003	0.001
Total Fe as FeO	92.05	91.47	91.48	91.64	91.94	91.83	92.08	91.74	91.78	0.24
Mole % Fe_3O_4	98.80	98.02	98.39	98.39	98.90	98.40	98.57	98.20	98.46	0.29
Mole % Fe_2TiO_4	0.08	0.34	0.15	0.17	0.10	0.36	0.19	0.17	0.20	0.10
Mole % Other	1.12	1.64	1.45	1.44	0.99	1.23	1.24	1.61	1.34	0.23

replacing magnetite are comparable to those of the host magnetite.

Several factors make electron microprobe analysis of the hematite-ilmenite intergrowths extremely difficult. Although the larger lamellae and the host phase are commonly several times as broad as the minimum electron beam diameter (1-2 μm) few of these larger areas are entirely free either of tiny second-generation lamellae of the other phase or of tiny rutile lamellae. Furthermore, even the coarser lamellae are difficult to recognize microscopically through the thin conducting carbon coat applied to the microprobe sections prior to analysis. Consequently, efforts to obtain quantitative analyses of the lamellae were hindered by the difficulty of locating the electron beam on a homogeneous area of either phase. This problem could be reduced either by using the minimum electron beam diameter and averaging a large number of analyses of the most homogeneous-appearing areas of each mineral, or by using a defocused beam (up to 50 μm) and averaging a large number of analyses of composite multiphase areas in each grain. The first method should yield satisfactory average compositions for the hematite and ilmenite, but not for the intergrowths as a whole, whereas the latter method, which was used successfully by Rumble (1971a), should provide reasonable average bulk compositions for the intergrowths, but no data on the separate compositions of hematite and ilmenite.

Because both procedures would require a great deal of time and effort, detailed analysis of the hematite-ilmenite intergrowths was postponed in favor of obtaining more data on the other minerals. However, some useful qualitative and semiquantitative data were obtained on the intergrowths by means of wave-length scans, electron beam scans

(EBS), partial quantitative analysis for Fe, Ti, and Mg, and additional semiquantitative techniques. The hematite-ilmenite intergrowths consist principally of Fe, Ti, Mn, and V. Cr, Al, Si, Mg, and other potential constituents are all absent or present in only trace amounts. V is concentrated preferentially in hematite relative to the ilmenite[18], whereas Mn is concentrated strongly in the ilmenite (Figure 73). Mn must therefore be present primarily as Mn^{2+} substituting for Fe^{2+} rather than as Mn^{3+} substituting for Fe^{3+}, which implies crystallization and exsolution under f_{O_2}-T conditions below those of the MnO + Mn_3O_4 buffer.

Partial analyses for Fe, Ti, and Mg were obtained on seven hematite-ilmenite intergrowths in the SPT sample 3a using the minimum-beam-diameter method. Despite the difficulties discussed earlier, and despite a wide range in the relative proportions of hematite and ilmenite lamellae (40-75% hematite), the average K-values[19] for hematite and ilmenite (Table 19) are surprisingly constant from grain to grain,

---

[18]Estimates of V content are complicated by overlap of the TiKβ peak on the VKα peak. However, it is possible to estimate the TiKβ contribution by determining the ratio of the count-rates on a pure TiO_2 standard at the TiKα and VKα wave-lengths and then determining the TiKα and apparent "VKα" count-rates on the sample. Then the

$$\text{true } VK\alpha_{sam} = \text{"}VK\alpha\text{"}_{sam} - (TiK\alpha_{std}/\text{"}VK\alpha\text{"}_{std})TiK\alpha_{sam} .$$

Following this correction, the VKα count-rate on hematite is still several times the background rate, indicating that V is an important minor constituent, but the residual VKα peak on ilmenite is small and may not be significant. In fact, the uncorrected "VKα" count-rate is greater on hematite than on ilmenite, despite the much lower Ti content of the hematite.

[19]The K-value for an oxide is defined as the ratio of the count-rate (corrected for background and dead-time) for an element in the sample compared to that for the element in the pure oxide. It is a close approximation to the actual weight percent.

Figure 73. Electron beam scan (EBS) photographs showing the distribution of Fe, Ti, and Mn in a portion of the hematite-ilmenite intergrowth shown in Figures 69 and 70 (SPT sample Ba-JM-3a). Ti-rich areas are ilmenite lamellae, except in the case of two especially titaniferous areas which contain little or no Fe; the latter areas are rutile. Mn is very clearly concentrated in the ilmenite. (Note that the area covered by the Mn photograph is displaced very slightly relative to the areas in the Fe and Ti images.)

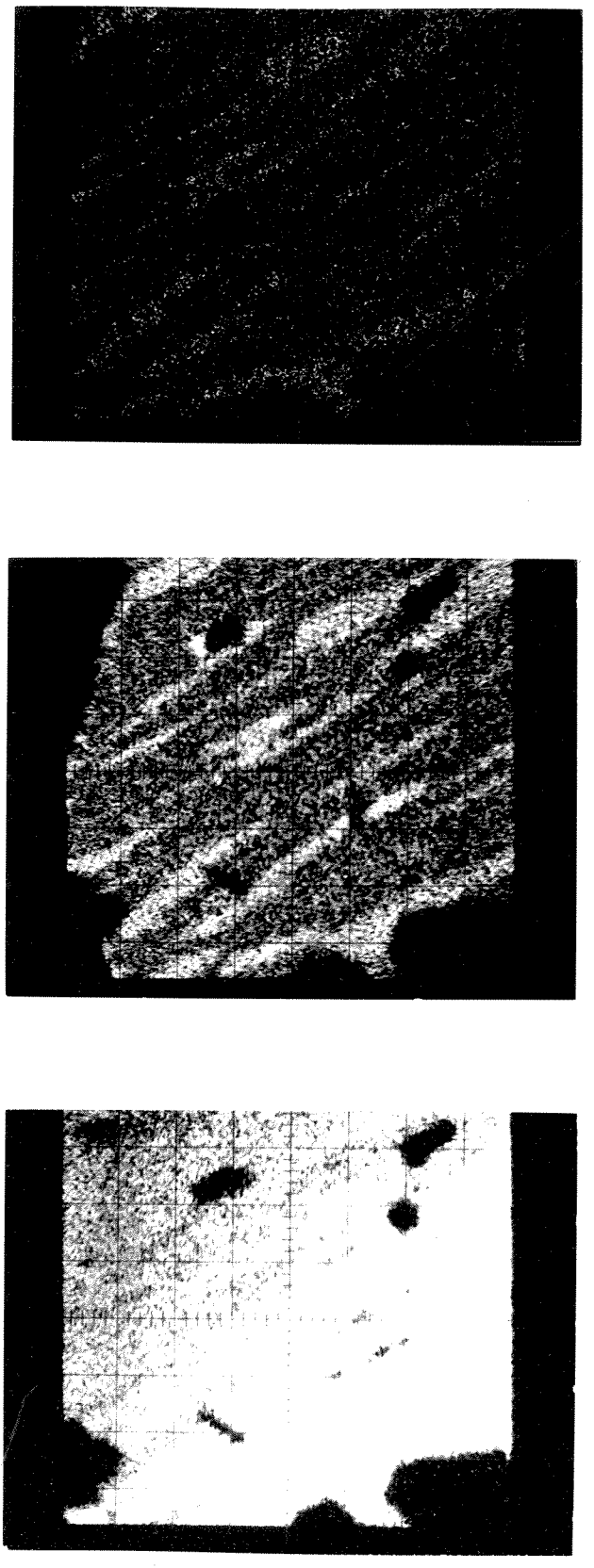
Mn
Ti
Fe
100 μm

Table 19

K-Values for FeO_t, TiO_2, and MgO

in Hematite and Ilmenite in SPT Sample Ba-JM-3a

Hematite

Point #	FeO_t K-value	FeO_t σ*	TiO_2 K-value	TiO_2 σ*	MgO K-value	MgO σ*
1	0.739	0.016	0.162	0.002	0.0005	0.0
2	0.747	0.007	0.157	0.005	0.0005	0.0
3	0.756	0.025	0.151	0.028	0.0005	0.0001
4	0.769	0.009	0.140	0.012	0.0004	0.0001
5	0.762	0.016	0.149	0.018	0.0003	0.0001
6	0.755	0.009	0.154	0.006	0.0004	0.0001
7	0.761	0.009	0.149	0.011	0.0004	0.0001
Average	0.756	0.010	0.152	0.007	0.0004	0.0001

Ilmenite

Point #	FeO_t K-value	FeO_t σ*	TiO_2 K-value	TiO_2 σ*	MgO K-value	MgO σ*
1	0.488	0.011	0.471	0.014	0.0013	0.0004
2	0.463	0.009	0.497	0.012	0.0016	0.0002
3	0.463	0.012	0.492	0.017	0.0015	0.0001
4	0.464	0.016	0.501	0.012	0.0014	0.0004
5	0.459	0.007	0.503	0.009	0.0023	0.0008
6	0.451	0.010	0.506	0.010	0.0011	0.0001
7	0.452	0.013	0.509	0.014	0.0014	0.0002
Average	0.463	0.012	0.497	0.012	0.0015	0.0004

*Standard deviation among five 10-second count-rates on each point.

which corroborates the petrographic evidence for a close approach to equilibrium in the intergrowths. Compared to the ideal K-value for FeO in pure hematite (0.89), the observed K-values indicate that the hematite contains considerable $FeTiO_3$ in solid solution, roughly 30-40 mole percent. Likewise, the ideal K-values for FeO (0.45) and TiO_2 (0.55) in pure ilmenite are slightly lower and considerably higher, respectively, than the measured values. Thus the ilmenite must contain considerable Fe_2O_3, roughly 10-20 mole percent, as well as perhaps several percent $MnTiO_3$, in solid solution. The overall compositions of the intergrowths appear to vary widely about an average of perhaps 40-50% Fe_2O_3.

12.7.1 T-f_{O_2} Conditions Implied by the Fe-Ti Oxides

In Figure 74 I have superimposed the stability curves for the compositions of coexisting magnetite-ulvospinel and hematite-ilmenite solid solutions (from Buddington and Lindsley, 1964) on the buffer curves for the assemblages magnetite + hematite (MH), MnO + Mn_3O_4, nickel + nickel oxide (NNO), and fayalite + magnetite + quartz (FMQ). Approximate stability curves for magnetite-ulvospinel solid solutions of compositions Mt_{92}, Mt_{94}, Mt_{96}, and Mt_{98} (long-dashed lines) in equilibrium with hematite-ilmenite have been interpolated from Figure 75 between the experimentally determined positions for Mt_{80} or Mt_{90} and that for Mt_{100}. Unfortunately, no experimental data exists for the stability limits of hematite-ilmenite compositions between $hem_{15}ilm_{85}$ and $hem_{100}ilm_0$, which is the range relevant to the San José tonalite. Buddington and Lindsley estimate an uncertainty of ±30° and one order of magnitude in f_{O_2} in the absolute positions of

Figure 74. Compositions of coexisting magnetite-ulvospinel and hematite-ilmenite solid solutions as a function of T and f_{O_2}. Compositional data are from the Appendix of Buddington and Lindsley (1964). The points are not actual experimental data points, but rather are points -- chosen by Buddington and Lindsley -- which allow construction of the experimentally determined T-f_{O_2} curves of constant magnetite-ulvospinel and hematite-ilmenite composition.

15---□---------- hematite-ilmenite; italicized numbers indicate the Fe_2O_3 content of the solid solution.

50——○——— — — magnetite-ulvospinel; non-italicized numbers indicate the Fe_3O_4 content of the solid solution. Long-dashed lines are interpolated from Figure 75.

MH: magnetite + hematite buffer curve (Wones and Eugster, 1965).

$MnO-Mn_3O_4$: buffer curve (Huebner and Sato, 1970).

NNO: nickel + nickel oxide buffer curve (Huebner and Sato, 1970).

FMQ: fayalite + magnetite + quartz buffer curve (Wones and Gilbert, 1969).

Stippled area: probable limits of the T-f_{O_2} conditions recorded by magnetite compositions in the San José pluton.

Hatchured area: approximate T-f_{O_2} field implied by the compositions and textures of hematite-ilmenite in the San José pluton.

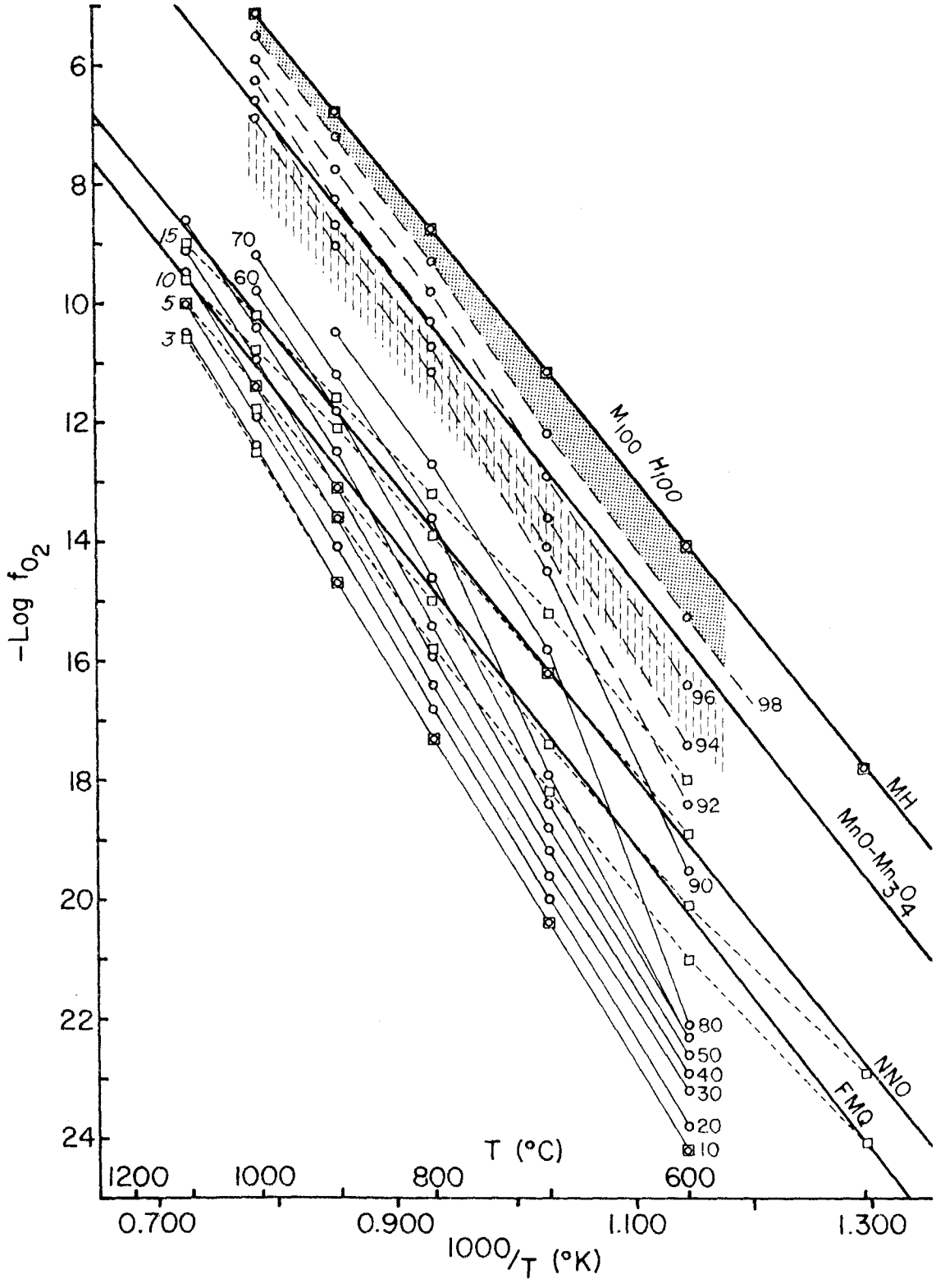
-Log f_{O_2}
6
8
10
12
14
16
18
20
22
24
T (°C)
1200
1000
800
600
0.700
0.900
1.100
1.300
1000/T (°K)
M100 H100
MH
MnO-Mn3O4
NNO
FMQ
98
96
94
92
90
80
50
40
30
20
10
70
60
15
10
5
3

Figures 75. Isothermal curves -- labelled in °C -- showing the change in composition of coexisting magnetite-ulvospinel and hematite-ilmenite solid solutions as a function of f_{O_2} at various temperatures. The compositional points are from the Appendix of Buddington and Lindsley (1964). The curves are hand-drawn by this writer.

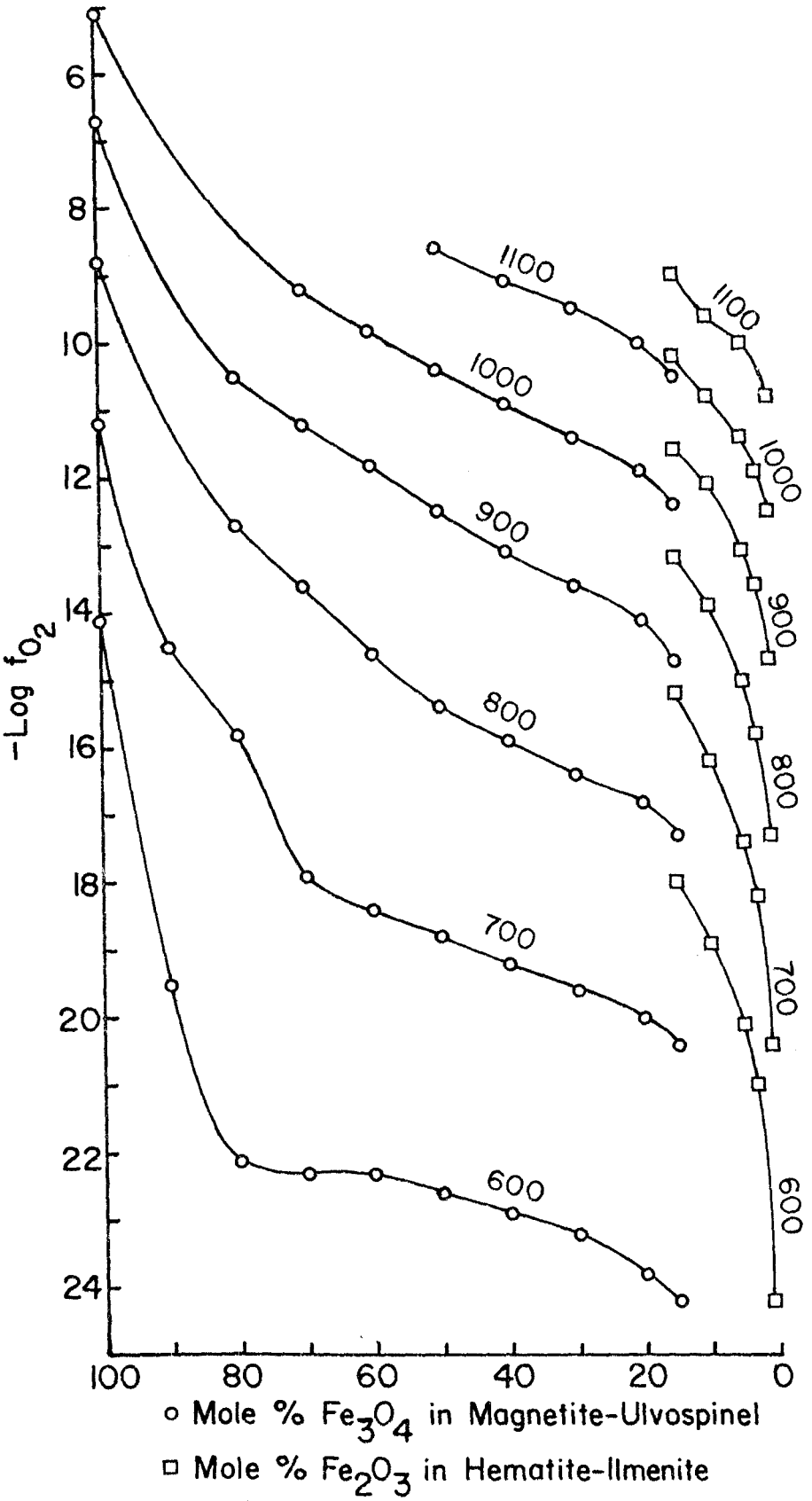
6
8
10
12
14
16
18
20
22
24
-Log f_{O_2}
1100
1000
900
800
700
600
100
80
60
40
20
0
o Mole % Fe_3O_4 in Magnetite-Ulvospinel
□ Mole % Fe_2O_3 in Hematite-Ilmenite

the determined portions of the curves. Additional errors introduced by interpolation are almost certainly less than ±1 in log f_{O_2} at any temperature. Lindsley (1963) detected no difference in the positions of the curves at pressures of 1000 and 2000 bars, and Rumble (1971b) concluded from thermodynamic calculations that the compositions of coexisting magnetite and ilmenite solid solutions should be effectively independent of pressure in the range 1-10 kb.

The extremely limited range of magnetite compositions -- X_{Mt} = 0.98-0.99 and $X_{Mt}/(X_{Mt} + X_{Usp})$ = 0.996-0.999 in all samples -- defines a very narrow band (stippled) of T-f_{O_2} conditions bounded on one side by the MH buffer curve and on the other by the stability curve for $Mt_{98}Usp_2$. The lower temperature limit (575°C) is based on the oxygen isotopic fractionation between plagioclase and magnetite in sample BC-I-12 (see Section 15.2.2).

Earlier I pointed out that strong concentration of Mn in ilmenite relative to hematite implies that Mn is in the 2+ state and therefore that crystallization and exsolution of hematite-ilmenite occurred under T-f_{O_2} conditions more reducing than those of the MnO + Mn_3O_4 buffer curve. Furthermore, the evidence for initial crystallization of hematite-ilmenite solid solutions of intermediate composition and for approximate equilibrium between the hematite, ilmenite, and rutile in the intergrowths indicates T-f_{O_2} conditions corresponding to those of the miscibility gap in the hematite-ilmenite system. Buddington and Lindsley (1964) and Lindsley (1973) have shown that this gap lies between the NNO and the MnO + Mn_3O_4 buffer curves, but closer to the latter. These considerations permit approximate delineation of the range of probable T-f_{O_2} conditions during initial crystallization and

later exsolution of the hematite-ilmenite (hatchured area in Figure 74). At these conditions, magnetite in equilibrium with the hematite-ilmenite should fall somewhere in the composition range Mt_{85} to Mt_{96}. Admittedly, the positions of the interpolated curves are only approximate, but it seems unlikely that the Mt_{98} curve could be lowered by the 1-2 orders of magnitude necessary to bring it much below the $MnO + Mn_3O_4$ buffer curve.

Thus, although the hematite, ilmenite, and rutile in many of the intergrowths appear to be approximately in equilibrium, the intergrowths are apparently not in equilibrium with the magnetite, but rather record earlier, slightly more reducing conditions. The Ti-free hematite patches and lamellae in magnetite are also clearly not in equilibrium with the titano-hematite of the hematite-ilmenite intergrowths, but may be in equilibrium with the host magnetite. Nor can hematite and ilmenite both be in equilibrium with rutile and with magnetite at the same time. Late magmatic and/or subsolidus oxidation of ilmenite to titano-hematite + rutile indicates increasingly oxidizing conditions during cooling and exsolution and is therefore consistent with this interpretation. So is the minor oxidation of magnetite to hematite. Alteration of ilmenite to sphene can also be interpreted as evidence for deuteric oxidation (Carmichael and Nicholls, 1967). It is important to emphasize that a trend towards increasingly oxidizing conditions does not require increasing or even constant f_{O_2} as temperature decreases. Increasingly oxidizing conditions result whenever the T-f_{O_2} path in the cooling magma or rock follows a positive slope more gentle than the slopes of the stability curves for the Fe-Ti oxides.

Two interpretations can account for the apparent disequilibrium. (1) Conditions may have become more oxidizing during magmatic crystallization, and magnetite may have crystallized later than hematite-ilmenite. (2) Magnetite may equilibrate more readily to changing conditions during cooling than does hematite-ilmenite. However, there are serious difficulties with both interpretations. Opposed to the first interpretation are the observations that (a) magnetite and hematite-ilmenite are commonly clustered and apparently grew simultaneously; (b) hematite-ilmenite is frequently molded around magnetite, but the reverse relationship is rare; and (c) the euhedral form of magnetite and rarely of hematite-ilmenite, the tendency for both phases to aggregate, the frequent occurrence of both phases as scattered inclusions in hornblende and biotite, and the lack of preferred spatial association of either phase with interstitial quartz, K-feldspar, etc., all suggest relatively early crystallization of most of the Fe-Ti oxides from the magma. Lesser amounts of magnetite and hematite-ilmenite are distributed interstitially and may have crystallized late. Opposed to the second interpretation are (a) the complete absence of alteration to or granular exsolution of titaniferous phases from the magnetite and (b) the absence of chemical gradients in magnetite next to hematite-ilmenite. There is simply no direct evidence that magnetite ever contained more Ti than is now present.

At present, I favor the second interpretation or some combination of the two. However, the problem is unresolved.

Regardless of the detailed relationships among the Fe-Ti oxides, two important conclusions can be drawn. First, both magnetite and hematite-ilmenite record crystallization under highly oxidizing

conditions approaching those of the MnO + Mn_3O_4 and MH buffer curves throughout the pluton. Conditions appear to have been slightly more reducing in the SHbT during crystallization and exsolution-oxidation of hematite-ilmenite, but apparently not during final equilibration of magnetite. Secondly, conditions became increasingly oxidizing (but f_{O_2} probably did not increase) during subsolidus cooling and possibly also during magmatic crystallization. As will be seen in the later discussions, the highly oxidizing conditions are unusual compared to most volcanic and plutonic rocks which have been studied, including other tonalites from the Peninsular Ranges batholith in southern California, and they have strongly influenced the compositions of the ferromagnesian phases as well as the Fe-Ti oxides.

In the GBT, sphene takes the place of hematite-ilmenite as the principal titaniferous accessory phase; the opposite opaque assemblage consists of magnetite plus a trace of titano-hematite containing only minor patches and lamellae of rutile and ilmenite. This assemblage, as compared to that in the non-gneissose SHbT, suggests crystallization (or equilibration) under more oxidizing conditions at the gneissose margin than in the interior of the unit. Perhaps the difference is due simply to continued equilibration at lower temperatures in the protoclastic border rocks. Alternatively, conditions may have been more oxidizing in the GBT due to influx of oxidizing fluids from the country rocks.

12.8 Pyroxene

Clinopyroxene occurs in trace amounts throughout the SHbT, but it is rare in the GBT (with the exception of minor lime-contaminated

rocks) and is extremely rare in the PHbT. None was seen in normal SPT, but again it occurs in lime-contaminated variants of that unit. Orthopyroxene was not identified in the tonalite.

In uncontaminated tonalite, clinopyroxene occurs exclusively as tiny round or irregularly shaped relicts in hornblende. It is colorless or very pale green, and pleochroism is weak or absent. The 2V is estimated by the method of Kamb (1958) as consistently about 60-63°. Simple or multiple twinning on (100) is rare, and exsolution lamellae are apparently absent. In all cases, a halo of colorless or pale green actinolite or actinolitic hornblende partially or wholly surrounds the clinopyroxene and separates it from the enclosing hornblende (Figure 76). Tiny inclusions of blebby or vermicular quartz are commonly abundant in this halo and sometimes in the adjacent hornblende as well, but inclusions of opaques are typically minor or absent.

Microprobe analyses of clinopyroxene from two rocks are given in Table 20. The compositions are uniform and correspond to an Al- and Ti-poor salite lying very close to the diopside-hedenbergite join. Optical properties of all of the clinopyroxene relicts are similar, suggesting that the compositional range is quite restricted.

Possible origins of the clinopyroxene relicts include: (1) minor early crystallization from the tonalite magma, (2) preservation as relicts of differentiation from a basaltic parental magma, (3) incorporation as xenocrysts from a refractory residue left over from partial melting, or (4) incorporation as xenocrysts from the country rocks, e.g., gabbro, calc-silicate rock, or meta-volcanic wacke.

The low Na, Ti, and Al contents suggest a low-pressure origin; hence, the third possibility is unlikely. Optical properties of

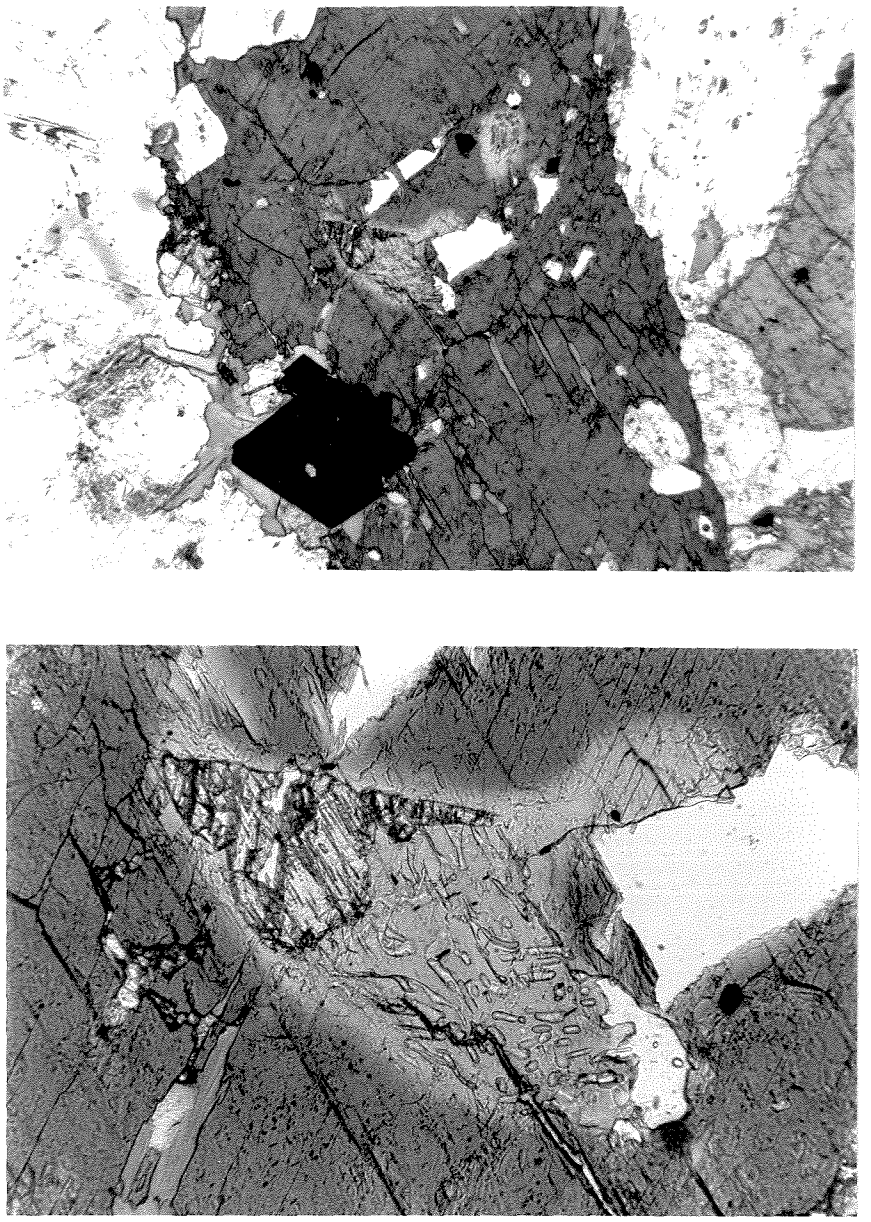

Figure 76. Relict clinopyroxene (salite) in hornblende in the prismatic hornblende tonalite. The lower photograph is a close-up of the central area in the upper photograph. Pyroxene (higher relief triangular grain) is surrounded and partially replaced by pale actinolitic amphibole (homoaxial with the hornblende) intergrown with fine-grained quartz. The irregularly shaped colorless grain along the lower right margin of the actinolite is quartz; the angular white areas just above and to the right of the pyroxene and actinolite are holes in the thin section. Sample Ba-JM-36a, 3.0 km east-northeast of Rancho San José 1.1 km west of the eastern margin of the PHbT (area K-10).

Table 20

Chemical Composition of Clinopyroxene Relicts in Hornblende in the Stubby Hornblende Tonalite

Sample #	Ba-JM-25a		Ba-JM-29
Grain #	Cp-25a-1	Cp-25a-3	Cp-29-1
Number of Points	2	3	2
SiO_2	53.50	52.92	52.47
TiO_2	0.19	0.43	0.20
Al_2O_3	0.98	0.96	1.13
Cr_2O_3	0.01	0.01	0.00
FeO_t	8.14	7.46	7.73
MnO	0.40	0.23	0.36
MgO	13.51	14.20	13.82
CaO	23.05	22.52	22.83
Na_2O	0.48	0.37	0.42
TOTAL	100.26	99.10	98.96
Formula Proportions Based on Cation Sum = 4			
Si	1.987	1.982	1.969
Al(IV)	0.013	0.018	0.031
Al(VI)	0.030	0.024	0.019
Ti	0.005	0.012	0.006
Cr	0.000	0.000	0.000
Fe	0.253	0.234	0.243
Mn	0.012	0.007	0.011
Mg	0.748	0.793	0.773
Ca	0.917	0.903	0.918
Na	0.034	0.027	0.031
Fe/(Fe + Mn + Mg)	0.250	0.226	0.236
Mn/(Fe + Mn + Mg)	0.012	0.007	0.011
Mg/(Fe + Mn + Mg)	0.738	0.767	0.753
Wo/(Wo + En + Fs)	0.474	0.464	0.469
En/(Wo + En + Fs)	0.388	0.411	0.399
Fs/(Wo + En + Fs)	0.138	0.125	0.131

magmatic clinopyroxenes in the lime-contaminated tonalite and of metamorphic clinopyroxenes in the skarns and meta-volcanic wackes, are all very similar to those of the relicts in the tonalite. The most nearly similar analyses tabulated by Deer et al. (1963, volume 2), are those of some diopsidic-hedenbergitic pyroxenes from calc-silicate rocks. However, Nishimori (oral communication, G.S.A. Cordilleran Section Meeting, 1975) reported similar low-Al, low-Ti salite in gabbroic plutons in southern California. Unfortunately, I know of no other chemical analyses of clinopyroxene from the Peninsular Ranges batholith.

If the clinopyroxene is derived from the country rocks, it and the actinolitic amphibole derived from it are so widespread as to indicate widely distributed minor crustal contamination of the magma, especially the SHbT magma. However, there is no independent evidence of appreciable contamination, and the modal and chemical data presented in Chapter 13 argue very strongly against such contamination. Hence, the pyroxene is most likely of magmatic origin. In the absence of other evidence for differentiation of the tonalite from basalt (see Chapter 16), it seems likely that clinopyroxene was a minor liquidus phase in the tonalite magma, especially in the SHbT magma.

12.9 Pale Amphiboles

Cummingtonitic and actinolitic amphibole occur as trace constituents throughout the tonalite, but together rarely exceed 0.1% by volume. The highest content observed in uncontaminated tonalite is 0.27% (SHbT sample 566). A sample from the hybridized mafic quartz diorite mass 1 km northeast of Rancho El Molino (area O-7) contains about 1-2% cummingtonite, occurring both as patches partially or wholly enclosed

in hornblende and as rare discrete grains. Otherwise, as for the pyroxene relicts, the pale amphiboles are invariably enclosed in hornblende. Uralitic overgrowths on hornblende were observed only in lime-contaminated tonalite.

Cummingtonite is colorless or very pale tan and rarely shows faint pleochoism (maximum absorption parallel to γ). The 2V is very near 90°, but where curvature of the isogyres can be recognized, the sign is always positive. In marked contrast to actinolite, cummingtonite rarely if ever contains quartz blebs and has not been recognized rimming clinopyroxene. Patches are usually homoaxial with the enclosing hornblende: most are sharply bounded, but some appear abruptly gradational into the hornblende.

In the SHbT and PHbT, cummingtonite occurs as small, round or irregularly shaped, anhedral relicts frequently containing abundant fine-grained opaques. Biotite, and rarely muscovite and quartz, may also be present. Some patches are finely twinned parallel to (100) or consist of parallel blades or needles, but most consist of a single uniformly extinguishing crystal. Actinolite locally occurs as rims and intergrowths, in some cases partially replacing the cummingtonite.

In the SPT, rare amphibole grains consist of up to 50% cummingtonite as cores and scattered patches rimmed by hornblende (Figure 77) This cummingtonite is generally inclusion-free and neither intergrown with nor rimmed by actinolite. Fine lamellar twinning is rare.

Analyses of cummingtonitic amphibole from two SHbT samples are given in Table 21. Analyses in columns 1 and 3 correspond to relatively pure cummingtonite. The high Ca content in the analysis in column 2 (intergrown with and indistinguishable from the low-Ca

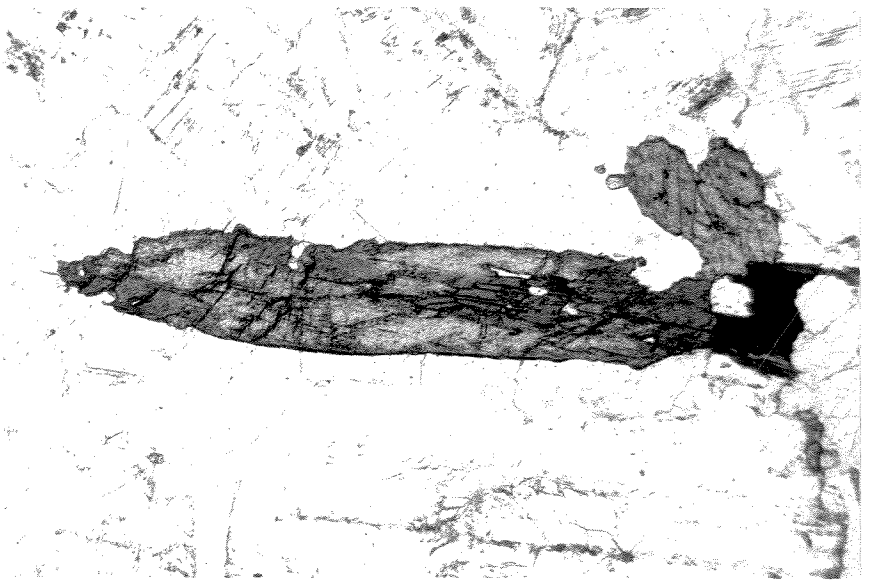

Figure 77. Composite cummingtonite-hornblende crystal in the seriate porphyritic tonalite. Cummingtonite (pale areas) comprises nearly half of the grain and is homoaxial with the enclosing hornblende. Sample Ba-JM-723, from the arroyo called El Alisito, ∿40 m east of the intersection with the north-south arroyo at the base of Cerro Hechicera (area R,S-7).

Table 21

Microprobe Analyses of Cummingtonitic Amphibole Enclosed in Hornblende

Name of Unit	SHbT		PHbT
Sample #	Ba-JM-25a		Ba-JM-36a
Grain #	Cu-25a-1*		Cu-36a-1
# of Points	4	2	2
SiO_2	54.89	54.68	54.79
TiO_2	0.06	0.15	0.15
Al_2O_3	0.59	1.25	1.24
Cr_2O_3	0.05	0.01	0.00
FeO_t	18.93	16.36	18.05
MnO	1.05	1.02	0.97
MgO	20.12	19.02	20.47
CaO	1.17	4.32	1.82
Na_2O	0.11	0.28	0.18
K_2O	0.01	0.02	0.00
"H_2O"	3.03	2.92	2.32
TOTAL	100.01	100.03	99.99
Formula Proportions Based on the Sum (Cations less Alkalies) = 15			
Si	7.940	7.901	7.844
Al(IV)	0.060	0.099	0.156
Al(VI)	0.041	0.114	0.053
Ti	0.007	0.016	0.017
Cr	0.006	0.001	0.000
Fe	2.298	1.978	2.163
Mn	0.129	0.124	0.118
Mg	4.338	4.098	4.371
Ca	0.182	0.669	0.279
Na	0.029	0.077	0.050
K	0.001	0.003	0.001
"OH"	2.922	2.809	2.221
Fe/(Fe + Mn + Mg)	0.340	0.319	0.325
Mn/(Fe + Mn + Mg)	0.019	0.020	0.018
Mg/(Fe + Mn + Mg)	0.641	0.661	0.657

*Intergrown low and high Ca areas in cummingtonite partially replaced by actinolitic amphibole (analyses 1 and 2, Table 22).

cummingtonite of column 1) may indicate appreciable solid solution with actinolite. If so, the cummingtonite is inhomogeneous and not internally equilibrated. Alternatively, the higher Ca content may be due to an unresolved intergrowth of actinolite in low-Ca cummingtonite. The Fe/(Fe + Mn + Mg) and Mg/(Fe + Mn + Mg) ratios are comparable to those of the host-rock hornblendes (Table 13), but the Mn/(Fe + Mn + Mg) ratios are significantly higher than those of hornblende.

Actinolitic amphibole covers a complete range in appearance and composition from nearly pure (i.e., low Na, Al, Ti) colorless actinolite to strongly pleochroic, aluminous actinolite only slightly paler in color than the enclosing hornblende. The 2V is negative and appears to vary from about 75°to nearly 90°. Typically, the actinolite occurs as round or irregular, anhedral patches homoaxial with and optically gradational into the hornblende. Less commonly, it occurs as single grains or aggregates of strongly pleochroic, green or blue-green crystals which are sharply bounded and not homoaxial with the enclosing hornblende. The aggregates of non-homoaxially included actinolite often contain abundant small inclusion of opaques. In contrast, the homoaxially included actinolite rarely contains opaques, but is commonly full of tiny blebs and vermicular grains of quartz and sometimes surrounds clinopyroxene relicts (Figure 76). In a few cases, quartz blebs are also present for a short distance into the enclosing hornblende. As mentioned earlier, actinolite also occurs as rims and intergrowths with cummingtonite, in some cases partially replacing the cummingtonite.

Chemical analyses in Table 22 show the variability of the actinolitic amphibole. Most analyses correspond to slightly aluminous actinolite but the full extent of gradation into hornblende may not

Table 22

Microprobe Analyses of Actinolitic Amphibole Enclosed in Hornblende in the Stubby Hornblende Tonalite

Analysis #	1	2	3	4	5	6	7	8	9	10	11
SiO_2	56.02	53.33	53.79	53.54	53.70	53.63	53.13	53.02	52.61	54.07	50.92
TiO_2	0.00	0.29	0.34	0.47	0.16	0.17	0.43	0.34	0.34	0.22	0.28
Al_2O_3	0.71	3.29	1.81	2.83	1.81	2.19	2.74	2.88	2.83	1.70	4.45
Cr_2O_3	0.00	0.01	0.02	0.02	0.01	0.01	0.01	0.02	0.02	0.02	0.00
FeO_t	9.33	11.06	10.34	10.10	10.05	10.82	9.78	11.17	11.05	10.65	12.50
MnO	0.38	0.31	0.39	0.18	0.43	0.35	0.33	0.34	0.32	0.53	0.39
MgO	18.94	16.47	17.29	17.45	18.08	17.53	16.32	16.82	16.81	17.58	15.27
CaO	12.37	11.97	12.19	11.72	11.34	11.44	12.11	11.98	11.79	11.17	11.51
Na_2O	0.16	0.56	0.29	0.52	0.30	0.40	0.39	0.47	0.46	0.35	0.69
K_2O	0.02	0.08	0.06	0.08	0.06	0.07	0.08	0.12	0.12	0.06	0.15
"H_2O"	2.08	2.63	3.49	3.12	4.04	3.38	4.68	2.86	3.68	3.65	3.86
TOTAL	100.01	100.00	100.01	100.03	99.98	99.99	100.00	100.02	100.03	100.00	100.02
Formula Proportions Based on the Sum (Cations less Alkalies) = 15											
Si	7.892	7.667	7.758	7.691	7.757	7.727	7.777	7.630	7.631	7.814	7.468
Al(IV)	0.108	0.333	0.242	0.309	0.243	0.273	0.223	0.370	0.369	0.186	0.532
Al(VI)	0.010	0.225	0.065	0.171	0.064	0.100	0.250	0.120	0.115	0.103	0.238
Ti	0.000	0.031	0.037	0.051	0.017	0.019	0.048	0.037	0.037	0.024	0.031
Cr	0.000	0.001	0.002	0.002	0.001	0.001	0.001	0.002	0.002	0.002	0.000
Fe	1.099	1.330	1.248	1.214	1.215	1.305	1.198	1.345	1.341	1.288	1.534
Mn	0.046	0.038	0.048	0.022	0.052	0.043	0.041	0.041	0.039	0.065	0.048
Mg	3.977	3.531	3.716	3.736	3.894	3.767	3.562	3.608	3.634	3.789	3.339
Ca	1.868	1.844	1.883	1.804	1.756	1.767	1.900	1.847	1.832	1.729	1.810
Na	0.043	0.155	0.080	0.145	0.089	0.113	0.110	0.130	0.129	0.099	0.194
K	0.003	0.015	0.010	0.015	0.011	0.014	0.015	0.023	0.023	0.010	0.029
"OH"	1.954	2.517	3.359	2.987	3.897	3.255	4.573	2.744	3.558	3.521	3.774
Fe/(Fe+Mn+Mg)	0.215	0.271	0.249	0.245	0.235	0.257	0.249	0.270	0.268	0.251	0.312
Mn/(Fe+Mn+Mg)	0.009	0.008	0.010	0.005	0.010	0.009	0.009	0.008	0.008	0.013	0.010
Mg/(Fe+Mn+Mg)	0.776	0.721	0.741	0.751	0.754	0.734	0.742	0.723	0.725	0.737	0.678

Table 22 (continued)

1. Single analysis of very pale green actinolite (A-25a-1) replacing cummingtonite (Cu-25a-1, Table 21); grades abruptly into enclosing hornblende. Part of same grain as analysis #2. Sample Ba-JM-25a.

2. Single analysis of pale blue-green aluminous actinolite (A-25a-1) replacing cummingtonite (Cu-25a-1, Table 21); part of same grain as analysis #1. Sample Ba-JM-25a.

3. Average of 2 analyses of very pale olive-green actinolite (A-25a-2) containing abundant tiny quartz grains; surrounds clinopyroxene and grades into enclosing hornblende. Sample Ba-JM-25a.

4. Average of 2 analyses of pale blue-green, aluminous actinolite (A-25a-4) containing abundant tiny quartz grains; surrounds clinopyroxene and grades into enclosing hornblende. Sample Ba-JM-25a.

5. Average of 3 analyses of pale yellowish-green, subhedral actinolite (A-29-1); neither homoaxial nor gradational with enclosing hornblende. Sample Ba-JM-29.

6. Average of 2 analyses of pale blue-green, aluminous actinolite (A-29-2); neither homoaxial nor gradational with enclosing hornblende. Sample Ba-JM-29.

7. Single analysis of very pale olive-green, aluminous actinolite (A-29-3) containing tiny quartz grains; surrounds clinopyroxene and grades into enclosing hornblende. Sample Ba-JM-29.

8. Average of 2 analyses of strongly pleochroic, yellowish-green, aluminous actinolite (A-68-1); neither homoaxial nor gradational with enclosing hornblende; rimmed and partially replaced by aluminous actinolite (column 9). Sample Ba-JM-68.

9. Average of 2 analyses of mottled green and pale-green, aluminous actinolite (A-68-2) surrounding and partially replacing aluminous actinolite (column 8); grades into enclosing hornblende. Sample Ba-JM-68.

10. Average of 2 analyses of very pale green actinolite (A-68-3) in an aggregate neither homoaxial nor gradational with hornblende; surrounded by actinolite which grades into enclosing hornblende. Sample Ba-JM-68.

11. Average of 2 analyses of strongly pleochroic, yellowish-green actinolitic hornblende (A-68-4) in an aggregate neither homoaxial nor gradational with enclosing hornblende. Sample Ba-JM-68.

be represented, because the palest-colored areas were preferentially chosen for analysis. Mg/(Fe + Mn + Mg) ratios are much higher than those of hornblende and cummingtonite. Mn/(Fe + Mn + Mg) ratios are comparable to those of hornblende and consistently lower than those of cummingtonite.

Pale amphiboles are present in most SHbT samples, but are rare in the PHbT. Actinolite is probably slightly more abundant than cummingtonite in both units.[20] In the SPT, actinolite is very rare, whereas cummingtonite occurs in nearly half of the samples.

12.9.1 Origin of the Pale Amphiboles

The frequent association of actinolitic amphibole -- generally containing fine-grained quartz -- as halos around relict inclusions of clinopyroxene in hornblende leaves little doubt that the actinolitic amphibole is genetically related to the clinopyroxene. Even where no pyroxene remains, the presence of pale patches of actinolitic amphibole plus fine-grained quartz in hornblende is probably indicative in most cases of the former presence of clinopyroxene. The nature of the replacement reactions, however, is uncertain.

Table 23 compares the compositions of associated hornblende, actinolitic amphibole, and clinopyroxene in three separate occurrences.

---

[20]Positive microscopic distinction between the two phases requires determination of the optic sign -- positive for cummingtonite, negative for actinolite -- which is difficult or impossible in many cases. However, other characteristics permit tentative identification, and semi-quantitative microprobe checks for Fe, Ca, and Al on a large number of grains generally confirmed the microscopic identification. Very pale tan color, the presence of abundant fine-grained opaques, and, in some cases, fine lamellar twinning generally indicate cummingtonite, whereas faintly greenish color and particularly the presence of blebby or vermicular quartz inclusions indicate actinolite.

Table 23

Comparison of Chemical Compositions of Associated Hornblende, Actinolite, and Clinopyroxene
Mole Percent Cations -- Anhydrous

Analysis #	1	2	3	4	5	6	7	8	9
Si	45.41	51.41	49.68	44.77	50.73	49.54	45.38	51.42	49.23
Ti	1.10	0.25	0.13	1.57	0.33	0.31	1.18	0.31	0.14
Al	8.30	2.04	1.08	8.42	3.17	1.06	8.09	3.13	1.25
Cr	n.a.	0.01	0.01	0.02	0.01	0.00	0.01	0.01	0.00
Fe	11.25	8.27	6.32	10.37	8.01	5.84	10.55	7.92	6.07
Mn	0.33	0.32	0.31	0.22	0.15	0.18	0.24	0.27	0.29
Mg	19.72	24.63	18.70	20.68	24.65	19.82	20.72	23.55	19.33
Ca	11.48	12.48	22.94	11.17	11.90	22.59	10.96	12.56	22.95
Na	2.00	0.53	0.85	2.41	0.96	0.67	2.55	0.73	0.76
K	0.41	0.07	n.a.	0.37	0.10	n.a.	0.33	0.10	n.a.

Ba-JM-25a, association 1; stubby hornblende tonalite

1. Brownish-green hornblende (H-25a-6) enclosing actinolite (A-25a-2) and clinopyroxene (Cp-25a-1).
2. Very pale olive-green actinolite (A-25a-2) containing abundant tiny quartz grains; surrounds clinopyroxene (Cp-25a-1) and grades into enclosing hornblende (H-25a-6).
3. Clinopyroxene (Cp-25a-1) separated from hornblende by actinolitic amphibole plus quartz.

Ba-JM-25a, association 2; stubby hornblende tonalite

4. Average brownish-green, core-type hornblende in rock 25a; similar to that enclosing actinolite (A-25a-4) and clinopyroxene (Cp-25a-3).
5. Pale blue-green, aluminous actinolite (A-25a-4) containing abundant tiny quartz grains; surrounds clinopyroxene (Cp-25a-3) and grades into brownish-green, core-type hornblende.
6. Clinopyroxene (Cp-25a-3) separated from hornblende by aluminous actinolite plus quartz.

Ba-JM-29; stubby hornblende tonalite

7. Average brownish-green, core-type hornblende in rock 29; similar to that enclosing actinolite (A-29-3) and clinopyroxene (Cp-29-1).
8. Very pale olive-green, aluminous actinolite (A-29-3) containing tiny quartz grains; surrounds clinopyroxene (Cp-29-1) and grades into brownish-green, core-type hornblende.
9. Clinopyroxene (Cp-29-1) separated from hornblende aluminous actinolite plus quartz.

The actinolitic amphibole is consistently intermediate in composition for Al, Fe, and Ca, but it contains in each case more Si and Mg than either of the adjacent minerals. The high Si content argues against two petrographically reasonable hypotheses for the origin of the actinolite + quartz assemblage: that is, both the direct uralitization of clinopyroxene and the reaction of clinopyroxene + hornblende to produce actinolite should consume rather than release silica. A third hypothesis, that actinolite replaced clinopyroxene, but has itself been partially replaced by hornblende + quartz, cannot account for the occurrence of quartz predominantly in the actinolite and only rarely in the surrounding hornblende.

A sequence which can explain both the petrographic and chemical relationships is magmatic replacement of clinopyroxene by hornblende + quartz, followed later by deuteric replacement of hornblende + quartz or of clinopyroxene + hornblende + quartz by actinolitic amphibole. That the quartz blebs were not entirely consumed during uralization implies that silica was readily available from the fluid phase.

The origin of the cummingtonitic amphibole is less clear. Several interpretations have been presented in the literature for different occurrences, chiefly, but not entirely, in gabbroic or dioritic rocks. Kuno (1938) described cummingtonitic amphibole, which he believed to be magmatic, enclosed in hornblende in dacites from Japan. The textural relationships are very similar to those of cummingtonite in the SPT. Seitsaari (1952) described complex homoaxial intergrowths of cummingtonite and hornblende in gabbro and diorite in Finland. He also concluded from textures and from the absence of hypersthene that

cummingtonite crystallized from the magma, but he suggested that influx of Fe and Mg from mafic country rocks created conditions permitting crystallization of cummingtonite. In the Garabal Hill-Glen Fyne complex in Scotland (Nockolds, 1941), cummingtonite in gabbro and diorite clearly replaced orthopyroxene, but cummingtonite in hybrid quartz diorite dikes occurs interstitially and molded around feldspar, as well as replacing orthopyroxene. Nockolds interpreted the interstitial cummingtonite as magmatic, but, like Seitsaari, he attributed magmatic crystallization of cummingtonite to conditions arising from contamination of the magma by the country rocks. Stewart (1947) found that cummingtonitic amphibole in uralitized mafic rocks from the gabbroic complex of Belhelvie in Aberdeenshire, Scotland, formed by replacement of both orthopyroxene and olivine. Deer (1935) likewise concluded that cummingtonite in gabbroic, dioritic, and tonalitic rocks from the Cairnsmore of Carsphairn igneous complex in Scotland was derived from orthopyroxene during hybridization of gabbro by fluids from adjacent tonalitic magma.

In the San José area, cummingtonitic amphibole occurs in trace amounts in tonalite and in quantities up to 1% or rarely several percent in mafic quartz diorite, diorite, and gabbro. Cummingtonite in the gabbronorite which comprises part of the mafic zone crossing Cañon Campo Buena Vista in the northeastern part of the SUbT (area H-11,12) all appears to be derived from hypersthene. However, orthopyroxene was not seen in any of the other cummingtonite-bearing rocks, except possibly for rare unidentified relicts in cummingtonite in the mafic rocks along and south of Willow Creek Canyon.

Considering the calcic character of the tonalite, it seems surprising that low-Ca amphibole would have crystallized from the magma. Never-

theless, the optically homogeneous, inclusion-free patches and cores of cummingtonite in hornblende in the SPT (e.g., Figure 77) show no sign of having replaced anything; they closely resemble the examples described and sketched by Kuno (1938) and are prime candidates for magmatic cummingtonite. In the mafic quartz diorite northeast of Rancho El Molino (area O-7) texturally similar, inclusion-free patches and cores in hornblende occur along with rare interstitial grains of cummingtonite which appear to be magmatic. Textures in that rock suggest stabilization of cummingtonite relative to hornblende in local environments next to quartz. By analogy, perhaps the high silica content of the tonalite permitted minor magmatic crystallization of cummingtonite despite the high Ca content of the rocks. On the other hand, the small, rounded, frequently opaque-rich relicts in the SHbT and PHbT are less convincingly magmatic and may rather be replacement products of orthopyroxene.

A third possibility, incorporation of cummingtonite as xenocrysts seems less likely. Cummingtonite has not been found in any of the metamorphic rocks surrounding the pluton. It is possible that interaction with wall rocks permitted magmatic crystallization of cummingtonite, particularly in the heterogeneous mafic rocks which are closely associated with the wall rocks. However, the distribution of cummingtonite in the tonalite bears no apparent correlation with the proximity to wall rocks. Moreover, the country rocks consist mainly of rather calcic assemblages of quartz, plagioclase, hornblende, biotite, and/or clinopyroxene; assimilation of such rocks would not logically lead to crystallization of a Ca-poor amphibole. Nevertheless, I cannot unequivocally discount possible interaction at depth with other metamorphic or mafic igneous rocks not exposed at the surface.

12.10 Other Accessory and Secondary Minerals

Fifteen additional phases were identified in the tonalite, altogether comprising 2-4% of most samples. White mica, clay minerals, apatite, epidote, sphene, chlorite, zircon, and rutile occur in all samples. Allanite, clinozoisite or zoisite, zeolite (chabazite?), carbonate, and prehnite are sporadic minor constituents. A single grain of tourmaline was identified in two or possibly three SHbT samples, and a single interstitial grain of garnet was seen in another SHbT sample.

Fine-grained white mica and unidentified clay minerals together comprise 0.5-2.5% of the typical tonalite, mostly as alteration products of plagioclase. A small amount of white mica occurs as alteration of biotite and, in some samples, as rare flakes in hornblende or rare interstitial primary[21] flakes. Subhedral muscovite flakes occur in recrystallized biotite aggregates in the GBT, presumably as a product of deuteric reactions accompanying protoclasis. Pale pinkish-brown patches of an extremely fine-grained clay mineral with low refractive indices occur interstitially and as a replacement of plagioclase in a few SPT samples.

Strongly pleochroic green chlorite is a ubiquitous secondary mineral replacing biotite and, to a slight degree, hornblende. In a few samples, mostly from the SPT, chlorite also occurs as rare interstitial primary patches. Interference colors are abnormal and vary widely among grains from grayish brown or greenish brown to

---

[21] "Primary" denotes crystals formed by direct precipitation from either the melt or a vapor phase, rather than by "secondary" replacement of pre-existing minerals.

blue or purple. The sign of elongation varies concomittantly from negative (length-fast) for brownish colors to positive (length-slow) for blue or purple. According to Albee (1962), this range of optical properties implies a broad compositional range from Mg>Fe to Fe>Mg, respectively. Many flakes are internally homogeneous, but others, especially those which have only partially replaced biotite, exhibit fine-scale interleaving of abnormal brown and abnormal blue or purple interference colors indicative of disequilibrium.

Epidote, varying from colorless to strongly pleochroic in shades of greenish yellow, generally constitutes 0.1-1% of the tonalite. Intensely epidotized areas up to tens of meters in dimension are scattered throughout the pluton, but are volumetrically minor. In the typical tonalite, epidote is fine-grained and generally anhedral, although subhedral or euhedral crystals occur locally. Most epidote is spatially associated with hornblende, biotite, and chlorite as an alteration product and possibly as a primary phase; in addition, colorless or pale yellow epidote also occurs, along with clinozoisite or zoisite (distinguished by positive 2V and low birefringence), as an alteration product of plagioclase and as occasional interstitial primary grains. Fine-grained anhedral allanite, often zoned outward to epidote, is an occasional trace constituent usually associated with hornblende or biotite; narrow dark pleochroic halos are common in hornblende or biotite adjacent to allanite.

Pale brown, weakly pleochroic sphene constitutes up to 1% of the tonalite. Concentrations are highest in the GBT and in minor lime-contaminated tonalite, both of which are characterized by

scattered subhedral or euhedral crystals up to 1 mm in size and by smaller anhedral grains and aggregates associated with biotite, chlorite, hornblende, and opaques.

In the rest of the tonalite, sphene rarely exceeds 0.5% and is generally anhedral and fine-grained. It occurs as a replacement product of hematite-ilmenite, as extremely fine-grained secondary material in recrystallized or chloritized biotite, as larger anhedral secondary (and primary?) grains associated with biotite and hornblende, and as interstitial primary grains. In the first two occurrences, it is commonly accompanied by rutile. Dark pleochroic halos occur rarely in hornblende and biotite adjacent to sphene.

Subhedral to euhedral apatite prisms generally <0.2 mm in maximum dimension comprise 0.1-0.5% of the tonalite. They occur as inclusions in each of the major minerals, but are especially common in and around hematite-ilmenite. Most crystals are clear and colorless or very pale greenish yellow; however, some grains in the SHbT are heavily clouded with extremely fine-grained unidentified material, especially in their cores. Many of the latter crystals are unusually large (up to 0.5 mm long) and sometimes corroded.

Apatite apparently grew throughout the crystallization history of the magma. That is, the abundance of euhedral inclusions in both the interiors and margins of plagioclase and hornblende grains suggests early nucleation, whereas occasional clustering of small crystals in interstitial quartz and especially in interstitial primary zeolite suggests late growth.

Subhedral to euhedral zircon is a ubiquitous trace constituent. Crystals are generally <0.2 mm in maximum dimension, except in many

SHbT samples, which are characterized by stout prisms 0.2-0.6 mm long. Pleochroic halos are faint or absent around most grains included in hornblende and biotite, implying low U and Th contents.[22]

Rutile is a trace constituent in all samples, occurring mainly as lamellae or alteration patches in hematite-ilmenite and as very fine-grained material associated with corroded, recrystallized, or chloritized biotite. Rutile also occurs as abundant hair-like needles in some quartz grains in the SHbT, almost exclusively in those grains which are partially or wholly enclosed in hornblende. The needles probably formed by exsolution of TiO_2 originally dissolved in the quartz at high temperature. Similar needles, probably rutile, occur rarely in plagioclase.

A colorless zeolite mineral with low relief and low birefringence occurs as an alteration of plagioclase, as small monomineralic veins, and as interstitial primary patches. It comprises nearly 0.5% of a few SPT samples, but is generally minor or absent. The 2V varies from small to moderate and from positive to negative. Most of the material was tentatively identified as chabazite but other zeolites -- e.g., heulandite or stilbite -- are possible. More than one zeolite may be present.

A uniaxial carbonate mineral, presumably calcite, is an occasional trace constituent of the tonalite. Most occurs as very fine-grained alteration of plagioclase, but several small interstitial primary grains were seen, as well as rare veinlets.

A platy mineral, almost certainly prehnite, occurs sporadically

---

[22]Whole-rock U and Th concentrations are also low (Table 25, p. 493).

as small lenticular bundles bulging apart the cleavage plates of biotite. The bundles, which are up to 0.5 mm long and 0.2 mm wide, were not seen in most samples, but comprise as much as 0.5% of others, especially samples which are slightly altered. The bundles frequently exhibit a feather-like texture of slightly curved plates diverging at low or moderate angles from a central axial line. The mineral is colorless (although often stained rusty), length-fast, and optically positive, with estimated 2V varying from 0° to about 30°. Rare crystals appear length-slow. Extinction is parallel, birefringence is moderate (ca. 0.020-0.025 on basis of maximum second-order blue interference colors in thin section), and refractive indices appear to be close to those of biotite, but are very difficult to determine due to the fine grain size and frequent rusty staining of the plates, as well as to frequent slight clouding of the immediately enclosing biotite.

These lenticular bundles are identical in almost every way to the "pods" of prehnite in biotite described by Phillips and Rickwood (1975) in the Mount Samson diorite from S. E. Queensland, Australia. These authors, who reviewed the scanty literature on the biotite-prehnite association, verified the optical identification of prehnite -- both in the Mount Samson diorite and in some actinolite schist from Antarctica -- by x-ray powder photography. All of the optical properties of the platy mineral in the San José samples are consistent with prehnite, except that the 2V is very small in comparison to the range of 50-60° determined by Phillips and Rickwood and the range of 65-69° listed by Deer et al. (1962, volume 3). However, Winchell and Winchell (1951) reported prehnite can also have a small 2V; hence the identification seems nearly certain.

Textures suggest nucleation and growth of prehnite between the cleavage plates of biotite, generally with very little replacement of the host phase. Deuteric alteration of plagioclase presumably supplied the Ca and Al required to form prehnite -- $Ca_2Al_2Si_3O_{10}(OH)_2$.

The primary interstitial textures exhibited by sphene, epidote, clinozoisite (or zoisite), chlorite, zeolite, white mica, and rarely carbonate are of considerable interest. The interstitial areas are 0.05-1 mm in size and consist of from one to several phases. Typical examples of interstitial chlorite, sphene, and K-feldspar are shown in Figures 78 and 79. The sphene, epidote, clinozoisite/zoisite, and carbonate occur generally as single smoothly bounded grains. The epidote and clinozoisite or zoisite are always colorless or very pale yellow; some grains show sharply defined repetitive zoning. Interstitial chlorite generally consists of a mosaic of many small fanning aggregates, as in the photographs, but single interstitial grains also occur; interference colors are invariably abnormal grayish brown or greenish brown. Interstitial zeolite occurs both as single grains and as aggregates sometimes with numerous centers of fanning extinction. Inclusions of apatite are common in the zeolite. Interstitial white mica occurs as single flakes, often with fanning extinction; the mica is frequently accompanied by interstitial K-feldspar, but does not appear to be replacing the latter.

I interpret these interstitial phases as primary because they show little or no evidence of reaction with adjacent minerals; in fact, hornblende and plagioclase crystals bounding or projecting into the interstitial areas commonly exhibit exceptionally smooth euhedral faces. The textures suggest uncontested growth of hornblende and

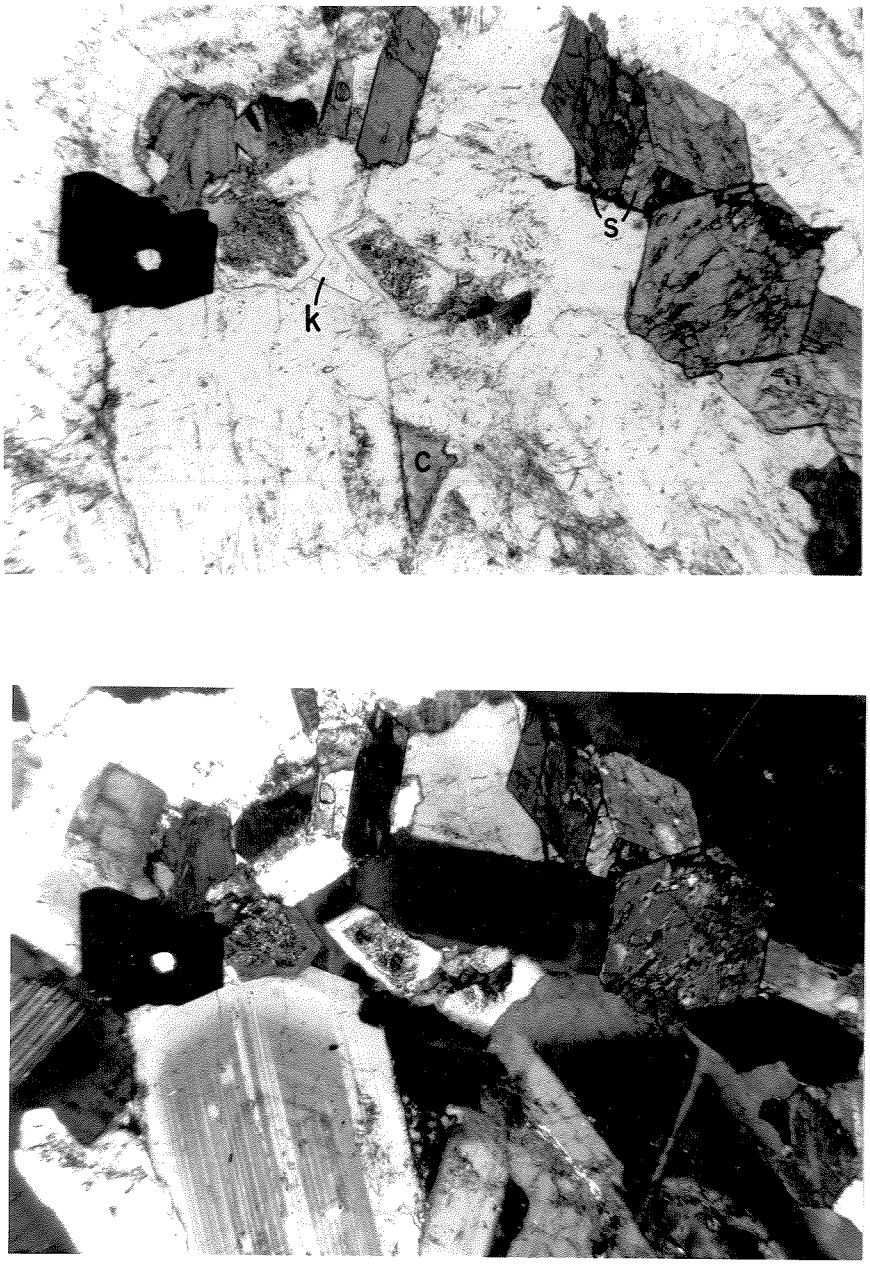

Figure 78. Interstitial sphene (s), chlorite (c), and K-feldspar (k) in the seriate porphyritic tonalite. Upper photo, plane light; lower photo, same view in crossed nicols. Note the mosaic character of the chlorite and the extremely smooth euhedral faces of plagioclase and hornblende bounding the interstitial phases. There is no evidence of replacement of the surrounding phases by the interstitial minerals. Sample Ba-JM-639, from the arroyo called El Alisito, ∿320 m from the southeastern margin of the pluton (area R-8).

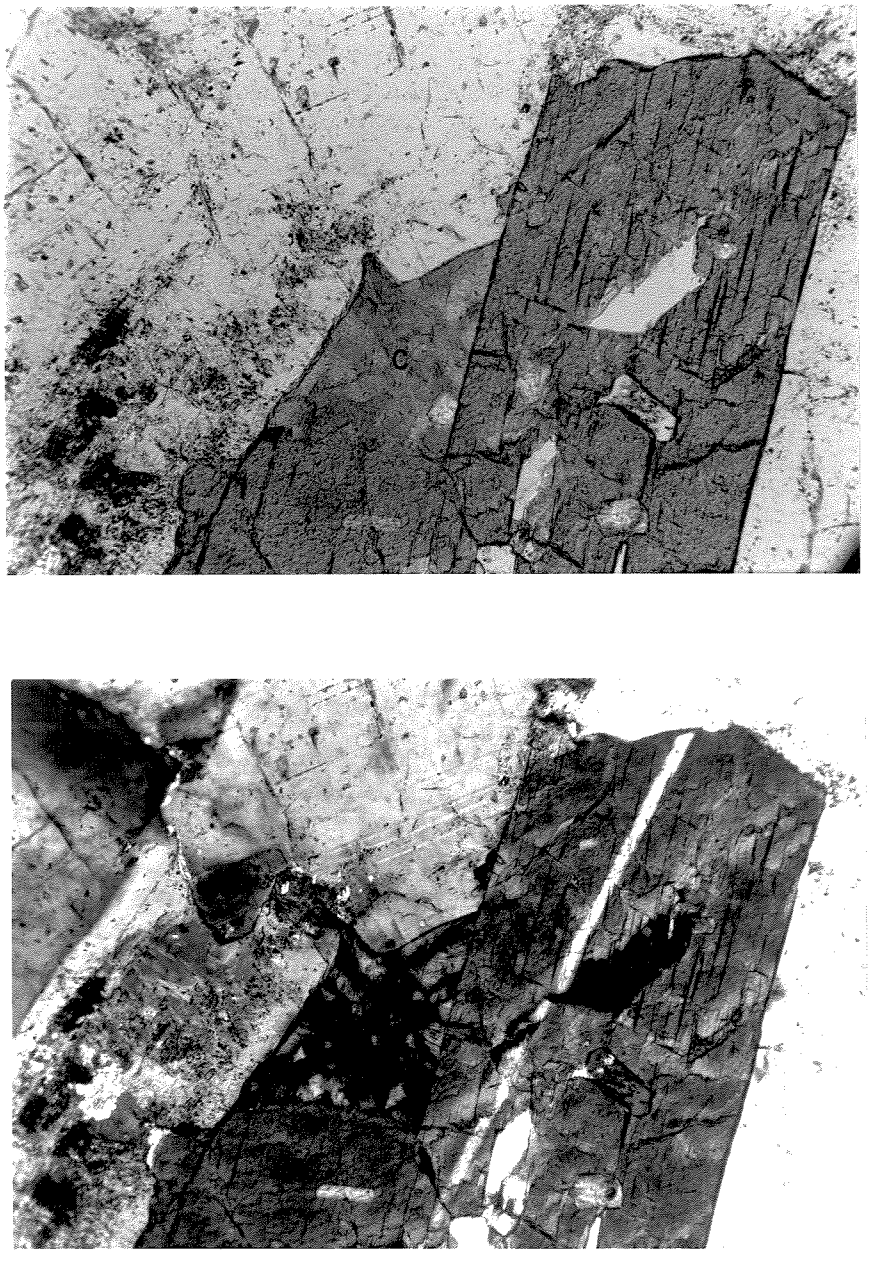

Figure 79. Interstitial mosaic of fanning chlorite aggregates (c) in the seriate porphyritic tonalite. Upper photo, plane light; lower photo, same view in crossed nicols. Note the smooth euhedral faces of the bounding hornblende and plagioclase crystals and the lack of evidence for replacement by the chlorite. Sample Ba-JM-639, from the arroyo called El Alisito, ∿320 m from the southeastern margin of the pluton (area R-8).

plagioclase into the interstitial spaces, followed later, after cessation of hornblende and plagioclase crystallization, by precipitation of the interstitial phases. Possibly some interstitial chlorite, particularly the single interstitial flakes, is secondary after biotite, but this origin can be ruled out in many cases, because examples of interstitial biotite grains bounded on all sides by comparably smooth hornblende and/or plagioclase crystals faces are very rare and because chlorite which has clearly replaced biotite (1) lacks the mosaic texture, (2) is raggedly bounded, (3) often contains relict patches of biotite as well as very fine-grained aggregates of secondary rutile and/or sphene, and (4) commonly exhibits abnormal blue or purple as well as brownish interference colors.

Whereas interstitial sphene, epidote, and possibly clinozoisite and zoisite are possible magmatic phases, chlorite, zeolite, white mica, and carbonate are unlikely candidates for crystallization from the melt. Subsolidus crystallization in microcavities occupied by an exsolved vapor phase is a much more likely origin for these volatile-rich phases and may likewise account for some or all of the interstitial sphene, epidote, and clinozoisite/zoisite. A similar but unfilled microcavity seen in one SPT sample supports this conclusion. Because interstitial K-feldspar often shows identical textural relationships to enclosing hornblende and/or plagioclase grains (e.g., Figure 78) and sometimes occurs with these other interstitial phases, and because the compositions of K-feldspar and rim plagioclase do not appear to be in equilibrium, I concluded earlier that some or all of the K-feldspar may have also crystallized from a vapor phase. The extreme rarity of carbonate and sulfides and the absence of fluorite imply that the vapor

phase consisted principally of H_2O.

With the exception of a trace of interstitial chlorite in SHbT sample 566, interstitial primary chlorite, zeolite, and carbonate are restricted to the SPT and a few PHbT samples. Interstitial sphene, epidote, and rarely white mica and clinozoisite occur throughout the pluton, but they too increase in abundance towards the southern end. Volatile-bearing, interstitial primary phases comprise 0.5-1% of the central and southern parts of the SPT, but they decrease in abundance northward even within that unit. This variation, which correlates with the southward decrease in the intensity of flow structures and protoclasis and with the outward increase in the frequency of smoothly euhedral hornblende and plagioclase faces and of smoothly interstitial quartz and K-feldspar textures, suggests concentration of volatiles towards the southern end of the pluton. Such concentration is consistent with, although it may not be the cause of, the greater fluidity of the magma implied by the stoping and discordance at the southern end of the pluton. However, the paucity and small size of the apparent cavity fillings implies exsolution of only a small amount of vapor. There is no evidence of saturation in volatiles prior to the latest stages of magmatic crystallization, even in the SPT. Indeed, there is no convincing evidence of the existence of a vapor phase in much of the SHbT prior to complete crystallization of the melt.

Chapter 13

MODAL AND CHEMICAL COMPOSITION OF THE TONALITE

13.1 Introduction

Major-element chemical analyses have been obtained on 24 tonalite samples representing all of the textural units in the pluton, including the GBT. Two of the analyses, BC-I-5 and BC-I-12, were kindly supplied by L. T. Silver. The others were obtained as part of the present study. Modal mineral proportions were measured on 23 of these samples and on 7 additional samples[23]. All samples selected for analysis were megascopically homogeneous and representative of the outcrops sampled.

Sr concentrations were determined by x-ray fluorescence on each of the chemically analyzed samples. In addition, T. O. Early and L. T. Silver (manuscript in preparation) determined Sr and Rb concentrations and the initial $^{87}Sr/^{86}Sr$ ratio on sample BC-I-12. Silver (unpubl. data) has also measured whole-rock U and Th concentrations and the Pb isotopic composition of this sample, as well as the U-Pb isotopic age of zircons from both this sample and sample BC-I-5, and B. W. Chappell at the Australian National University has obtained additional trace element concentration data on sample BC-I-12. Taylor and Epstein (1962) and Taylor (1968) reported oxygen isotopic compositions of the minerals in Sample BC-I-12, and L. P. Gromet is currently investigating the rare-earth element concentrations and patterns in this sample. Smith (1972) reported U, Th, and K concentrations and radioactive heat

---

[23]There is no modal data on samples BC-I-5 or Ba-JM-857; however, sample Ba-JM-30a, for which modal data exists, is from the same locality as BC-I-5.

generation values for 17 samples from 11 localities in the PHbT, as well as for a large number of samples from the Sierra San Pedro Mártir. Smith (1972, 1974) also reported the heat flow measured in a 254-m-deep drill hole in the center of the PHbT (heat flow site BA-1; my locality Ba-JM-240). Continuous core from this drill hole was kindly turned over to the author for petrologic study.

All sample locations for which chemical or modal data exist are plotted in Figure 80. Locations for the SJ series of samples (data of Smith, 1972) are approximate. All samples numbers for which letter prefixes have been omitted are part of the Ba-JM suite collected by the author.

13.2 Modal Analyses

Modal analyses of tonalite from 25 localities are presented in Plates 8 and 8A and treated graphically in Figures 81-85. The tabulated modes for samples 25a, 46a, and 240 are averages of two, two, and four hand specimens, respectively. The separate results for each hand specimen are compared in Appendix B, and plotted in Figure 84. All other modes are for single hand specimens.

The analyses fall into two categories -- "reconnaissance" modes and "detailed" modes -- depending upon the number of thin sections and the total thin-section area examined. Reconnaissance modes are each based upon three thin sections. Detailed modes each cover four thin sections, in the case of the relatively finer-grained GBT, and 7 or 8 thin sections for other samples. At least 3700 points, and generally more than 4500 points, were counted in each analysis; thus even the

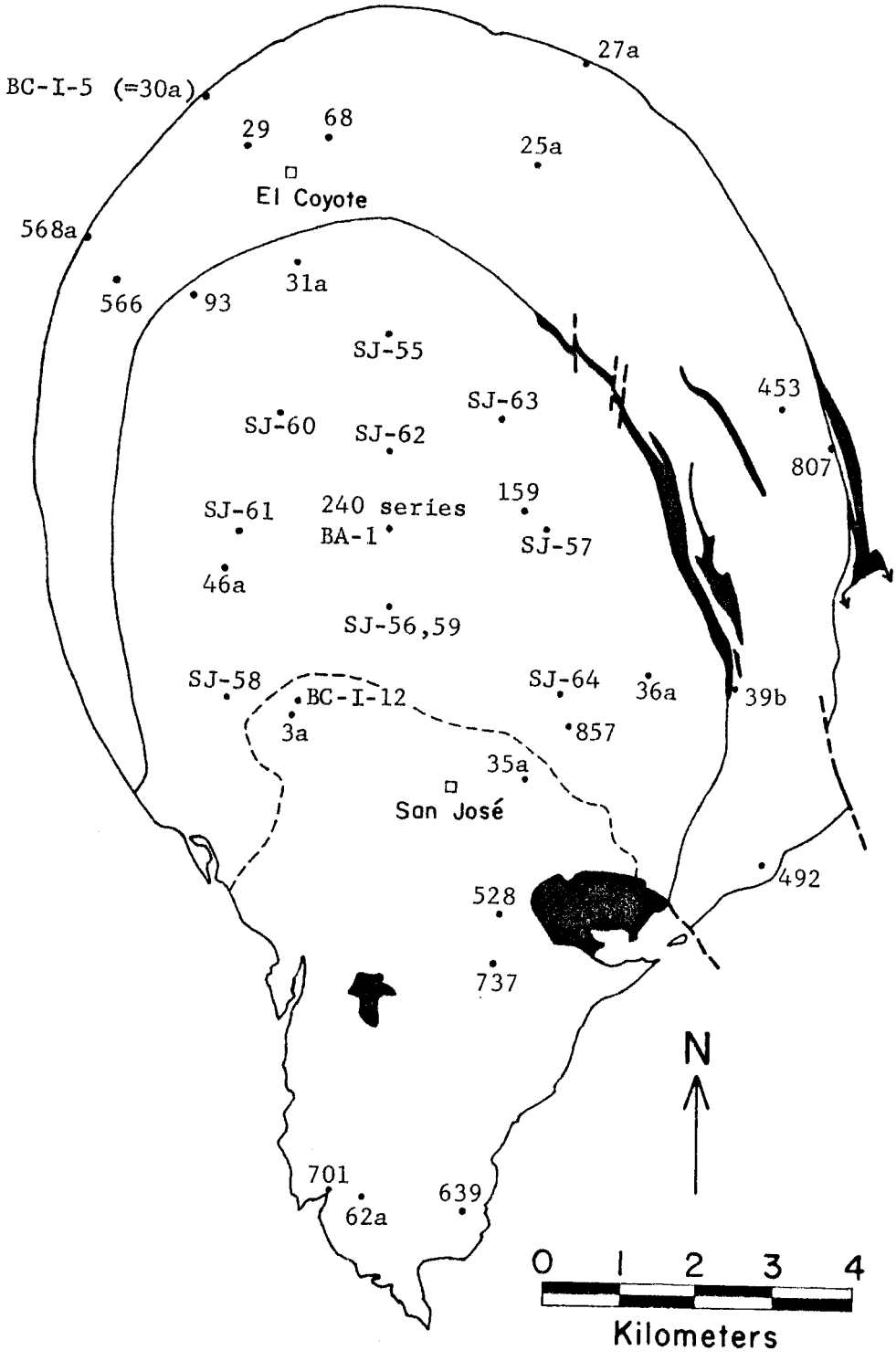

Figure 80. Locations of chemically and modally analyzed samples. Samples BC-I-5 and BC-I-12 were collected by L. T. Silver. BA-1 and the SJ series of samples, SJ-55 to SJ-64, are from Smith (1972). All other samples are part of the BA-JM series collected by the author.

"reconnaissance" modes are more detailed than most published modal analyses. For a discussion of the uncertainties in the results, see Appendix B.

Four minerals -- plagioclase, quartz, hornblende, and biotite -- plus their alteration products make up 95.6% or more of all samples; K-feldspar is minor everywhere and is only a trace constituent of most samples. The color index[25] falls consistently between 15 and 25%. Hornblende generally exceeds biotite, except in the GBT, where the relationship is reversed.

Triangular plots of modal quartz, color index, and plagioclase[26] (Figure 81) and of quartz, plagioclase, and K-feldspar (Figures 82 and 83) emphasize (1) the restricted compositional range of the pluton, especially if the GBT is omitted, (2) the similarity among the textural units, (3) the uniformly plagioclase-rich, relatively leucocratic nature of the rocks, and (4) the paucity of K-feldspar. In the classification system recommended by the International Union of Geological Sciences (IUGS: Streckeisen, 1973), all of the samples are biotite-hornblende tonalite or biotite-hornblende quartz diorite, except for the GBT samples, which are hornblende-biotite tonalites[27]. The ranges of modal compositions for the three main units overlap completely, and their average

---

[25] Modal color index is defined as the sum of the proportions of all mafic minerals: hornblende, biotite, chlorite, opaques, sphene, epidote, allanite, pyroxene, and pale amphibole.

[26] In all plots, the proportion of plagioclase includes the sum of its alteration products.

[27] By convention, the mineral modifiers in the rock name are listed in order of increasing abundance.

Figure 81. Relative modal proportions of quartz, plagioclase, and total mafic minerals (color index) in the San José pluton. All data are in volume percent.

▲ gneissose border tonalite

△ stubby hornblende tonalite

o prismatic hornblende tonalite

● seriate porphyritic tonalite

Figure 82. Average relative modal proportions of quartz, plagioclase, and K-feldspar in the principal textural phases of the tonalite. Symbols are the same as in Figure 81. The stippled area defines the total range of 25 analyzed samples from the pluton. Heavy dashed lines outline the area shown in Figure 83. The classification system is that proposed by the International Union of Geological Sciences (IUGS) for plutonic rocks containing <90% mafic minerals and containing plagioclase having an An content <50% (Streckeisen, 1973).

Figure 83. Enlargement of a small portion (outlined by the heavy dashed lines) of the quartz + plagioclase + K-feldspar triangle in Figure 82. Symbols are the same as in Figure 81.

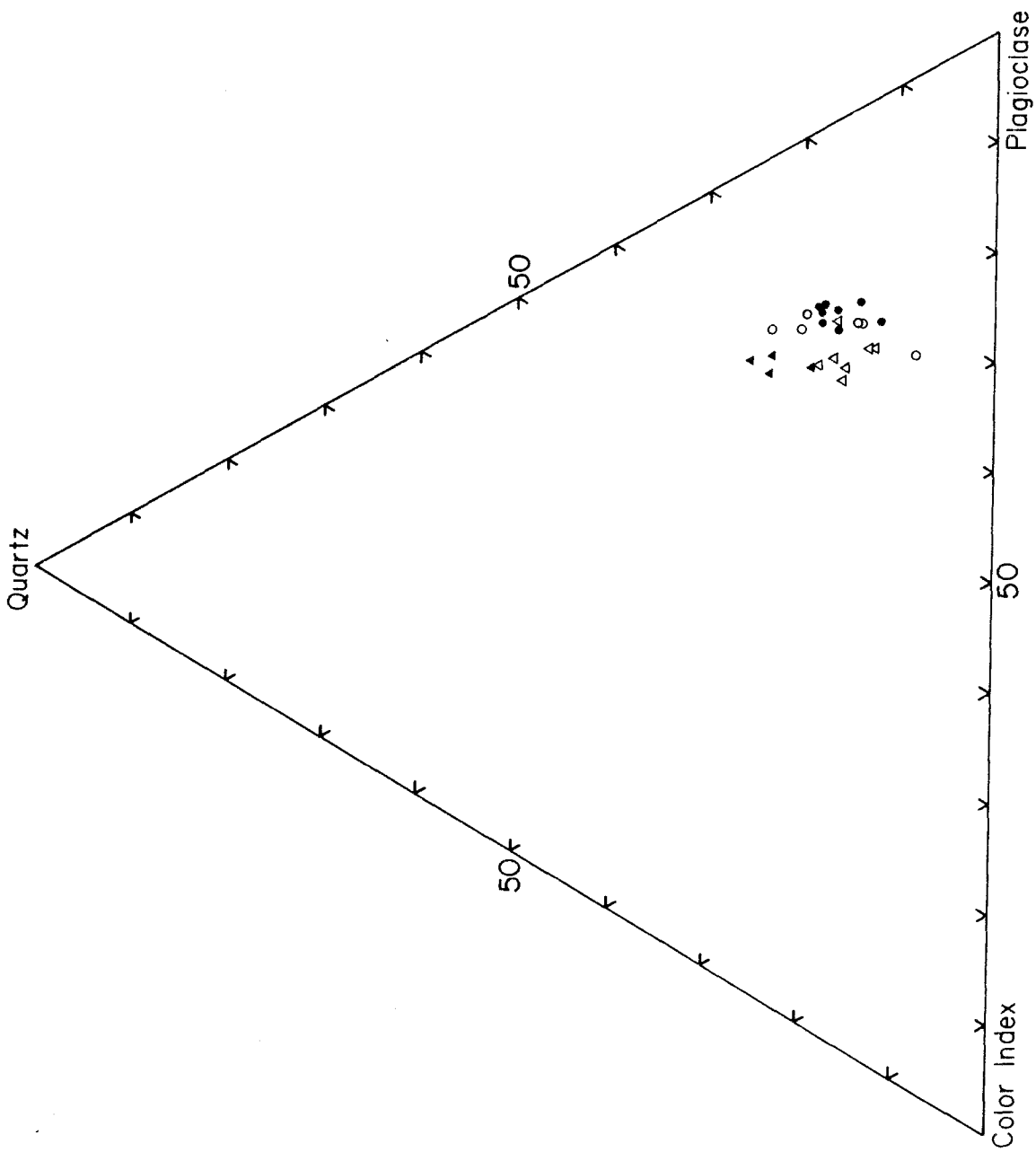

Figure 81

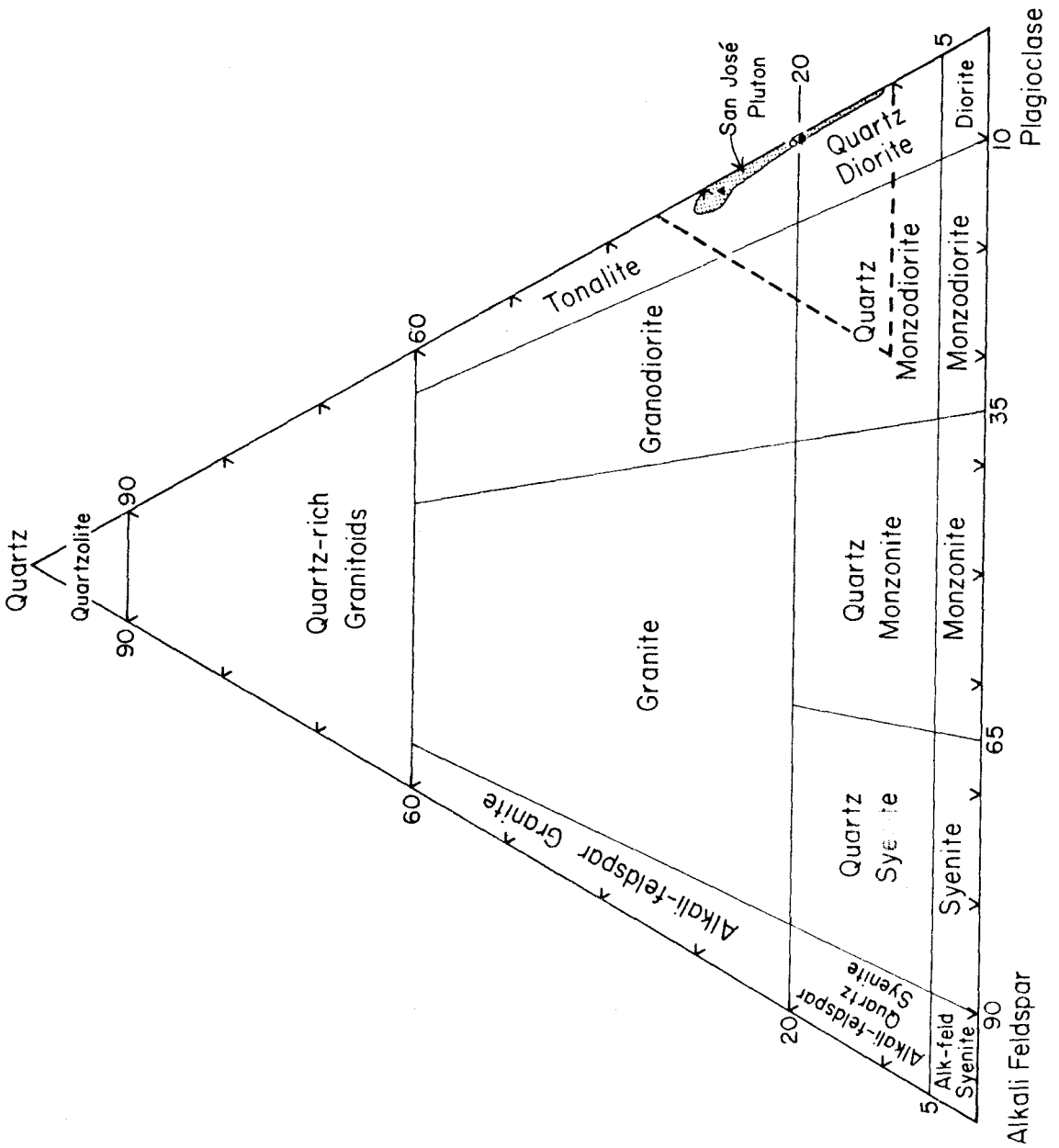
Quartz
Quartzolite
90
90
Quartz-rich Granitoids
60
60
Tonalite
Granodiorite
Granite
Alkali-feldspar Granite
San José Pluton
20
Quartz Diorite
Quartz Monzodiorite
Quartz Monzonite
Quartz Syenite
Alkali-feldspar Quartz Syenite
20
5
Diorite
Monzodiorite
Monzonite
Syenite
Alk-feld Syenite
5
10
35
65
90
Plagioclase
Alkali Feldspar

Figure 82

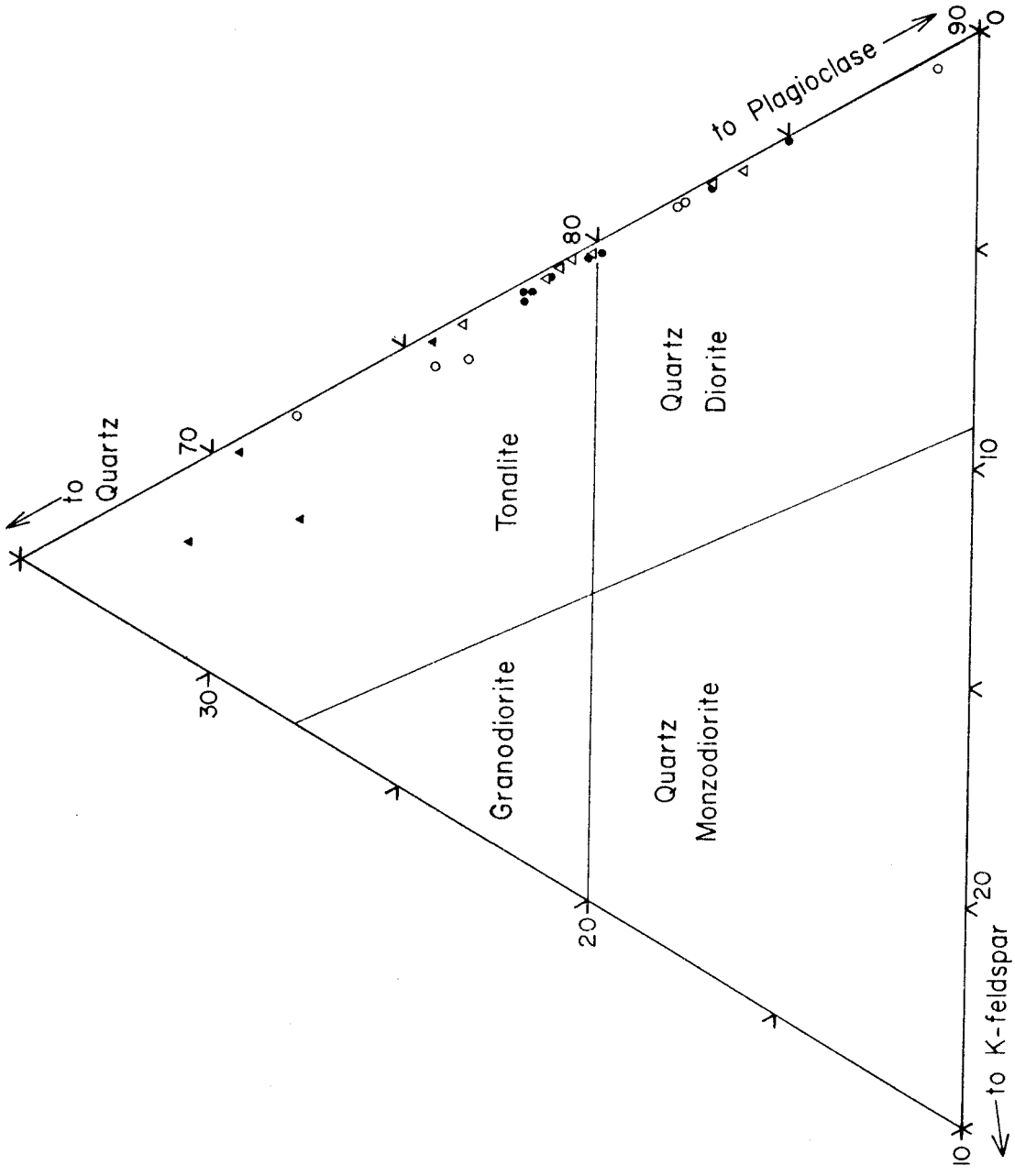
to Quartz
70
30
20
10
to Plagioclase
90
80
10
20
to K-feldspar
Tonalite
Quartz Diorite
Granodiorite
Quartz Monzodiorite

Figure 83

compositions, and that of the pluton as a whole, plot in an extremely tight cluster on the boundary between quartz diorite and tonalite. The GBT samples, however, are notably displaced towards the quartz apex. Because the modes show a continuous spread across the boundary, and the system as a whole is more closely allied to the granitic clan than to the diorite-gabbro clan. I have used the term tonalite for all of the rocks rather than dividing them artificially into tonalites and quartz diorites.

Despite the similarity among the textural units, slight systematic differences exist. For a given quartz content, the SHbT and GBT have a consistently higher content of hornblende (Figure 84A) and of biotite plus chlorite (Figure 84B), hence a higher color index (Figure 84C), and lower content of plagioclase (Figure 84D) than do the PHbT and SPT. Like the field, textural, and chemical evidence, the modes show that the pluton can be divided into two distinct petrologic units -- the SHbT and GBT, on one hand, and the PHbT and SPT on the other. The distinctions among the units are small and can only be recognized because of the internal consistency within the units and because of the large number of points counted and the large thin-section areas examined. The SHbT and SPT are especially homogeneous; standard deviations for the major minerals (Plate 8A) are very small. The PHbT shows slightly greater variability, principally because of a systematic east-to-west increase in quartz, biotite/hornblende ratio, and to a lesser degree K-feldspar, combined with a decrease in plagioclase, hornblende, and color index (compare modes of 36a, 159, and 240 from the eastern two thirds of the unit with those of 31a, 46a, and 93 from the western third).

Most often, modal analyses are used only for classification or characterization of a rock type or sometimes for recognizing variations within a rock unit or for correlating among units. However, detailed modal analyses can also provide valuable insight into the affinities and antipathies among minerals. In conjunction with textural observations, they can be used to test ideas on the crystallization and differentiation history of the magma.

Figure 84 shows the relationships among the major minerals in the San José pluton, and Figure 85 shows the modal variations as a function of the composition of plagioclase rims. Hornblende and plagioclase show a rough positive correlation (Figure 84F). As the volume percent quartz increases, hornblende, color index, plagioclase, and the An content of plagioclase rims all decrease (Figures 84A, 84C, 84D, and 85B). Concurrently, biotite + chlorite increases (Figure 84B). Thus hornblende and biotite vary antipathetically (Figure 84G), and the ratio (hb + pale amph)/(bio + chl) decreases rapidly with increasing quartz content (Figure 84J) and decreasing An content of plagioclase rims (Figures 85A and 85C). Implicit in these variations is the seemingly paradoxical fact that, as the percentage of biotite increases, color index actually decreases.

The decrease in hornblende, color index, and plagioclase with increasing quartz and biotite are in part simply dilution effects, but they cannot be accounted for entirely in this way. The positive correlations of hornblende with plagioclase and of biotite with quartz, the negative correlation between the two mineral pairs, and the respective positive and negative correlations of hornblende and quartz with the An

Figure 84. Correlation plots of modal mineral proportions and mineral ratios. Lines connect analyses of separate samples from the same locality. All data are in volume percent.

▲ gneissose border tonalite

△ stubby hornblende tonalite

○ prismatic hornblende tonalite

● seriate porphyritic tonalite

| denotes "reconnaissance" mode based on 3 thin sections

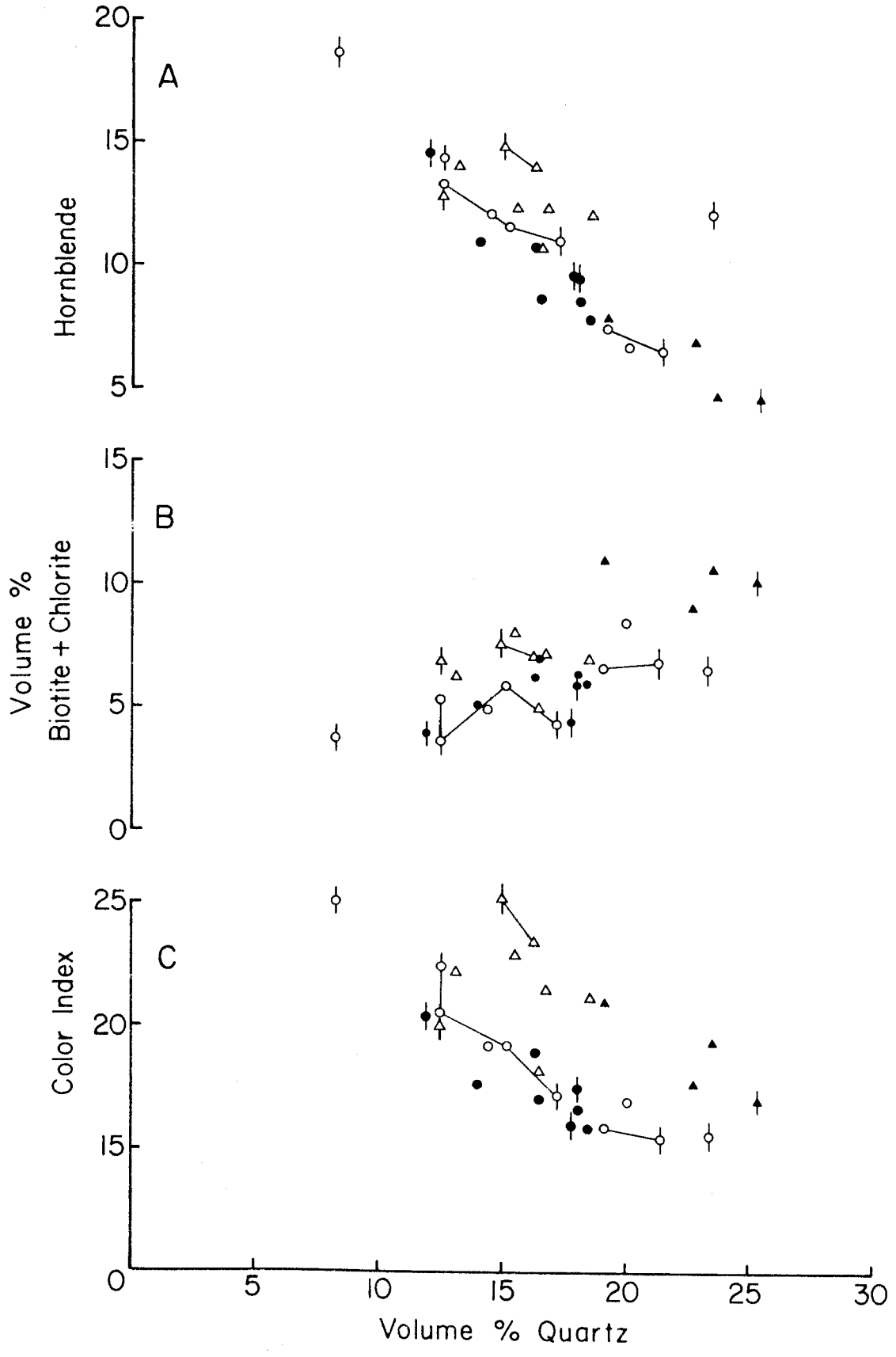
A
Hornblende
20
15
10
5
B
Volume %
Biotite + Chlorite
15
10
5
0
C
Color Index
25
20
15
0
5
10
15
20
25
30
Volume % Quartz

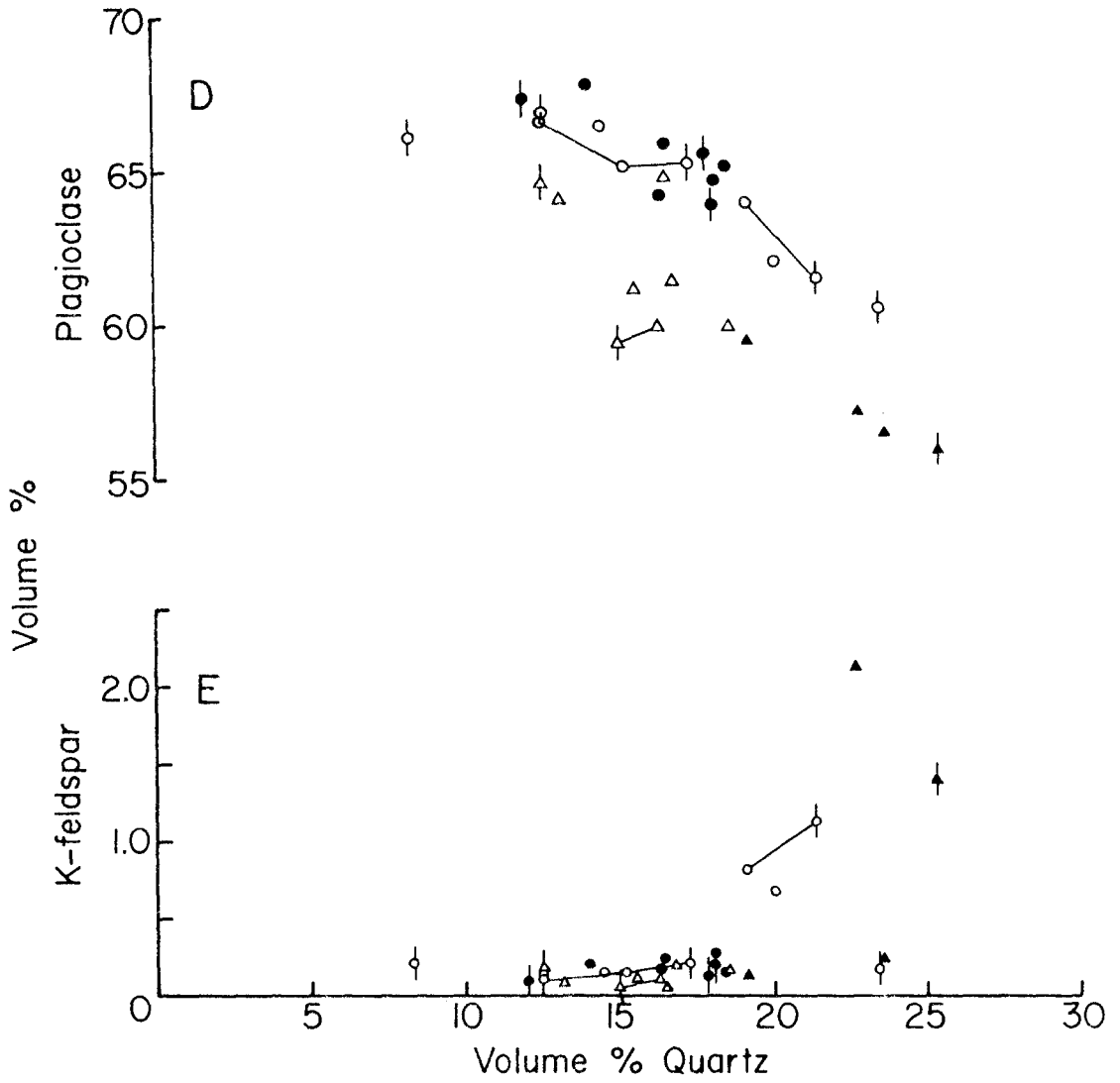
D
E
Plagioclase
K-feldspar
Volume %
Volume % Quartz
70
65
60
55
2.0
1.0
0
5
10
15
20
25
30

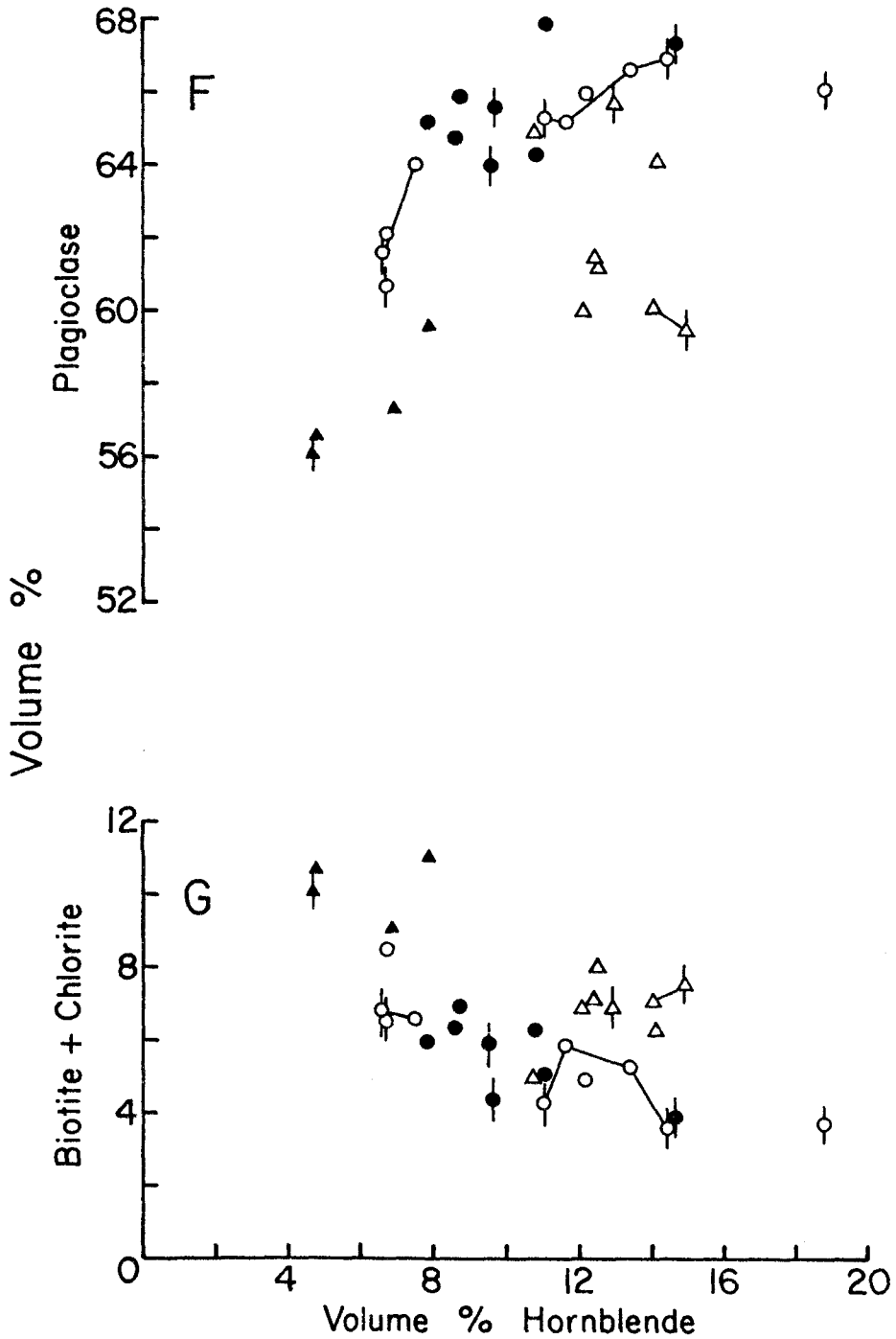
F
G
Plagioclase
Biotite + Chlorite
Volume %
Volume % Hornblende
68
64
60
56
52
12
8
4
0
4
8
12
16
20

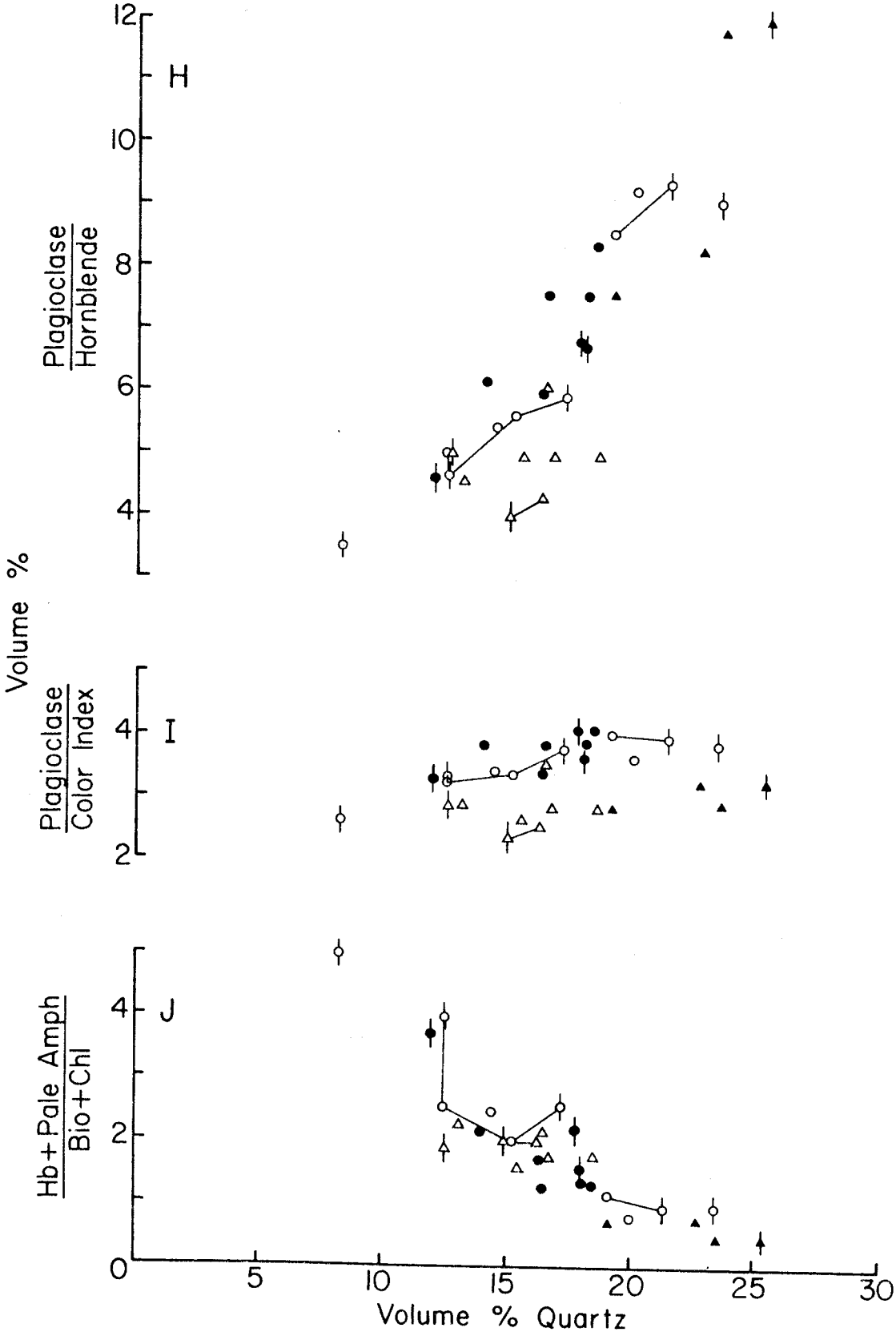
H
Plagioclase / Hornblende
12
10
8
6
4
I
Plagioclase / Color Index
4
2
J
Hb+Pale Amph / Bio+Chl
4
2
0
5
10
15
20
25
30
Volume % Quartz
Volume %

Figure 85. Correlation plots of hornblende, quartz, and biotite + chlorite against the An content of plagioclase rims. Symbols are the same as in Figure 84 except that:

(1) large symbols denote optical determination of plagioclase composition,

(2) small symbols denote microprobe analysis of plagioclase composition, and

(3) horizontal lines indicate the range of measured values.

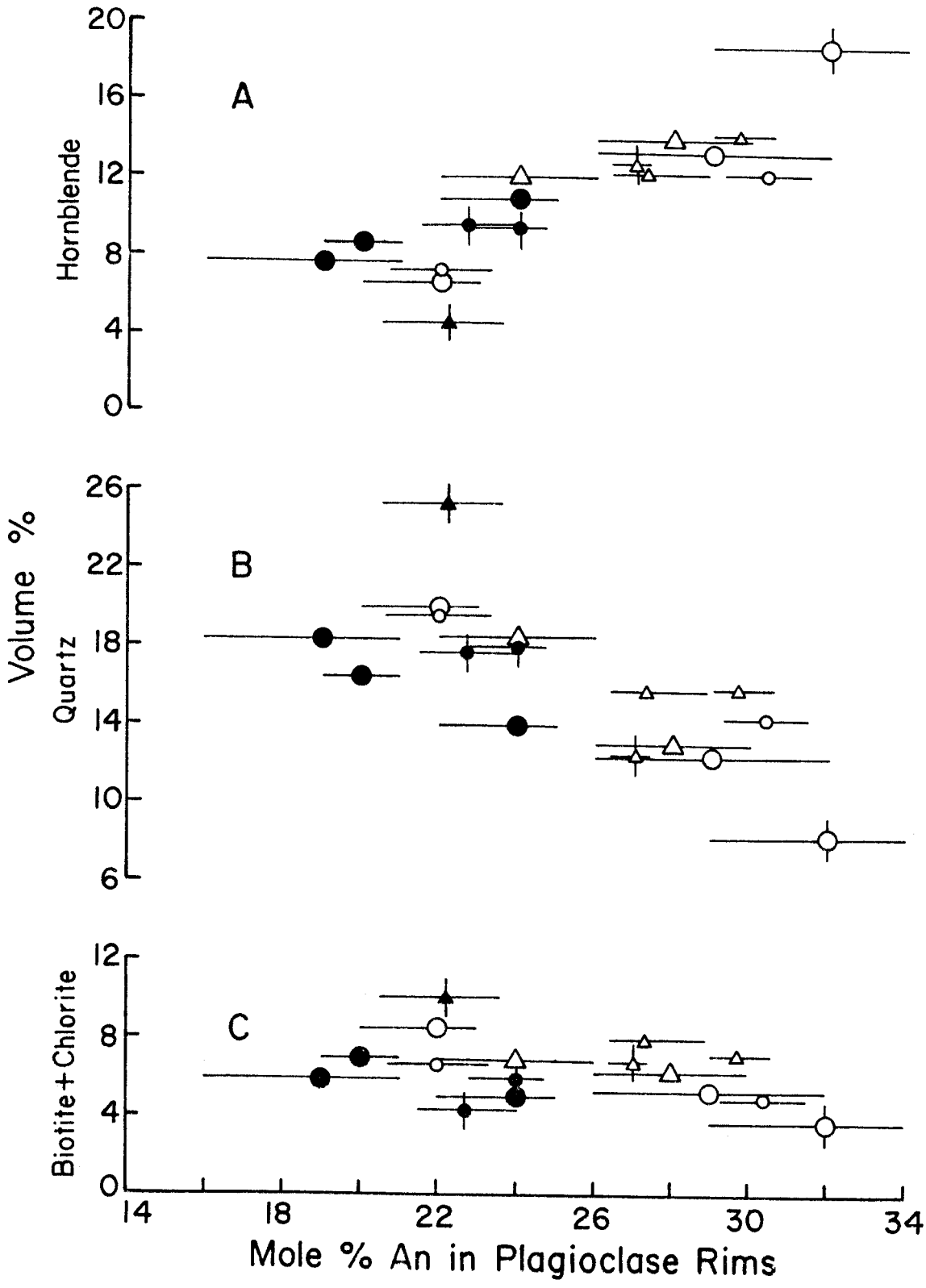
A
Hornblende
20
16
12
8
4
0
B
Quartz
26
22
18
14
10
6
Volume %
C
Biotite+Chlorite
12
8
4
0
14
18
22
26
30
34
Mole % An in Plagioclase Rims

content of plagioclase rims provide the principal modal evidence of differentiation. Biotite, although it is a ferromagnesian mineral, combined with quartz, rim plagioclase, and the trace amount of K-feldspar to form the granitic end of a differentiation trend whose mafic end is represented mainly by hornblende and the core plagioclase. Petrographic evidence that biotite grew during the later stages of crystallization supports this interpretation.

Surprisingly, the percentage of K-feldspar shows very little relationship to that of quartz (Figure 84E). Only samples 30a and 568a from the GBT and samples 46a#1, 46a#2 and 93 from the western side of the PHbT show a correlation of high K-feldspar and high quartz contents. Additional thin-section observations indicate that K-feldspar typically comprises about 0.5-2.0% of the rocks throughout most of the west-central part of the pluton, but elsewhere in the pluton conditions favored fixation of K_2O primarily in biotite, and to a lesser extent in plagioclase and hornblende, rather than in K-feldspar. On the average, 75-85% of the K_2O in the tonalite is present in biotite, 10-15% in plagioclase, 4-5% in hornblende, and only 2-7% in K-feldspar.

Once one recognizes that biotite behaved more as a salic than a mafic phase, the inverse correlation of biotite with color index becomes less paradoxical. Increase in the percentage of biotite reflects the increasing K_2O content (simultaneous with an increasing SiO_2 content) of the magma, which generally correlates with decreasing total mafic constituents in granitic systems.

Obviously, categorization of the minerals into early mafic and late granitic ends of a differentiation trend is a gross oversimplifi-

cation. In particular, plagioclase is strongly zoned and contains within it both early calcic and later sodic components. In fact, the percentage of plagioclase decreases less drastically than that of hornblende in response to increasing quartz and biotite contents, so that the plagioclase/hornblende ratio increases strikingly as quartz increases (Figure 84H), whereas the plagioclase/color index ratio remains nearly constant (Figure 84I). Quartz and biotite appear to increase principally at the expense of hornblende and only to a lesser extent of plagioclase. Yet petrographic evidence suggests co-precipitation of hornblende and biotite, with only limited replacement of the former. The systematic modal variations therefore appear to be the result of some process tending to separate early-formed crystals (with a high ratio of hornblende + plagioclase to biotite + quartz) from melt in the magma. That this process was very inefficient is clear from the limited range of modal variations observed. Except for sparse schlieren, the variations in crystal:melt ratio were apparently small and diffuse on a large scale.

Several of the modal relationships (especially Figure 84C,D,F,I) confirm the field evidence that the GBT is a marginal phase of the SHbT and that the two textural types form a petrologic unit distinctly different from the combined PHbT-SPT mass. Considering the proximity of the GBT to the country rocks, and considering the slightly greater abundance of mafic inclusions in the GBT relative to that in the interior of the SHbT, one might expect that the GBT forms a mafic shell surrounding the SHbT, but it actually forms a more granitic shell. The major differences between the GBT and SHbT are that the former:

(1) contains considerably more quartz and biotite, (2) contains considerably less plagioclase and hornblende, and (3) has a lower color index and a much lower ratio of (amph + cpx)/(bio + chl). GBT samples 30a and 568a from the northwestern margin of the pluton are comparatively rich in K-feldspar, but samples 27a and 807 from the northeastern and eastern margins are not. This west-to-east difference in K-feldspar contents also holds for all seven additional GBT samples examined in thin section.

Among the accessory minerals, the principal differences between the GBT and SHbT are that the former is enriched in sphene and depleted in opaques. In addition, actinolite, cummingtonite, and clinopyroxene are very rare in the GBT (excluding minor lime-contaminated rocks), whereas the former two occur in almost all thin sections of the SHbT, and clinopyroxene can be found in many. Sphene occurs in the GBT both as very fine-grained, anhedral deuteric material associated with opaques, biotite, and hornblende and as scattered anhedral to euhedral crystals up to 1 mm in size, especially in 30a and 807. Similar large, apparently primary, sphene crystals were not seen in the SHbT. Fine-grained magnetite is nearly the only opaque phase in the GBT; the few tiny hematite-ilmenite grains seen consist of nearly pure hematite, with minor intergrown ilmenite and rutile. In contrast, the SHbT is characterized by subequal amounts of magnetite and of hematite-ilmenite. The development of sphene in the GBT was thus balanced by the disappearance of the titaniferous opaque oxide phase; there is no petrographic evidence of higher TiO_2 contents in the GBT. In fact, Plates 9 and 9A show that the GBT has the lowest average TiO_2 content of any of the textural units.

13.3 Major-Element Chemical Analyses

Fourteen samples of tonalite were analyzed by standard wet chemical techniques. Four of these and ten additional samples were analyzed by electron microprobe using a technique adapted from x-ray spectrographic methods by R. L. Joesten (1974) and modified by myself.

In all cases, single homogeneous hand specimens weighing at least 600 g, generally >1 kg, were coarsely cut or broken, and numerous randomly chosen fragments totaling 220 g or more were crushed to pass a 5-mm mesh using a plattner mortar and a hydraulic press. The crushed samples were then ground to fine powders in a Spex Industries Shatterbox lined with tungsten carbide, and representative aliquots were obtained for analysis by repeatedly coring the powders with a thin glass tube. Aliquots for standard chemical analysis weighed about 20 g; those for microprobe analysis weighed about 1.5 g.

Aliquots for microprobe analysis were mixed with equal proportions of lithium tetraborate, fused in open graphite crucibles at 1100-1150°C in a muffle furnace, and mounted, polished, and coated with a carbon film following standard procedures for microprobe sample preparation. Nine oxides were analyzed, and the concentrations were normalized to 100%. Eight separate points were analyzed and averaged for each element on each glass. For all samples except Ba-JM-93, two glasses were analyzed, in each case on separate days. Glasses of known composition were prepared from U. S. Geological Survey standard rock powders G-2 (granite) and BCR-1 (basalt) and repeatedly analyzed to provide a calibration for the technique and an estimate of the reproducibility of the analyses. A more detailed discussion of the procedures for glass preparation and

analysis is presented in Appendix D, along with tables of duplicate analyses of each sample and a discussion of the precision and accuracy of the results.

Plate 9 lists the composition and CIPW norm of each rock. Average compositions of the major textural units and of the pluton as a whole are presented in Plate 9A. The average composition of the pluton was calculated from the average for each textural unit weighed in proportion to the outcrop area of the unit. To permit direct comparison with the microprobe analyses, wet chemical analyses have been normalized to total 100% for the nine major oxides, and total Fe is presented as FeO_t. However, the $FeO/(FeO + Fe_2O_3)$ ratios determined in the wet chemical analyses are also tabulated, and the norms were calculated using these ratios, or, in the case of the microprobe analyses, using an assumed $FeO/(FeO + Fe_2O_3)$ ratio equal to the average value given by wet chemical analyses of other samples of the same texutral unit. The complete wet chemical analyses -- including Fe_2O_3, FeO, MnO, and volatile contents -- are listed in Appendix D, Table D-1.

Wet chemical analyses of four samples -- 3a, 29, 62a, and 857 -- analyzed together at a different time and by a different analyst than the other samples, show unusually low Na_2O and high H_2O+ contents, high $FeO/(FeO + Fe_2O_3)$ ratios, and possibly low K_2O and high FeO_t contents inconsistent with their modal and petrographic characteristics and with the results for the other samples from the same textural units. Because of these discrepancies, which suggest serious analytical errors, these four analyses have been omitted from Plates 9 and 9A and from the following plots and discussions, but they are included in Table D-1.

For samples 25a, 46a, 93 and 240#52, the analyses in Plate 9 are the averages of wet chemical and microprobe results. Separate results of each technique are compared in Appendix D, Table D-9. Discrepancies are small and generally insignificant compared to the slight compositional variations among samples. As explained in the Appendix, the microprobe results for Na_2O may be consistently too high by about 0.1-0.2 (i.e., by about 2-4% of the amount present). Otherwise, the microprobe results appear to be very reliable.

The entire pluton is characterized by very low K_2O contents and high Na_2O contents, yet the CaO content is also relatively high. The intersection of the CaO and $Na_2O + K_2O$ variation trends versus SiO_2 (see Figure 86) yields an alkali-lime index (Peacock, 1931) of 63.3, making the tonalite a calcic rather than a calc-alkaline system. Except for the GBT samples, normative Or contents all fall in the range 2.95-5.60%, which is decidedly low for rocks containing 10-20% normative quartz. The $FeO/(FeO + Fe_2O_3)$ ratios are also uniformly low (0.408-0.515), which is consistent with the highly oxidizing conditions recorded by the Fe-Ti oxides and by the high Mg/(Mg + Fe) ratios in the mafic minerals.

As for the modes, the chemical composition of the tonalite is extremely uniform both within and among the textural units. Only the GBT differs from the other textural types by appreciably more than the standard deviations for the individual units (Plate 9A). The internal homogeneity of both the SHbT and the SPT is especially striking. Local, small-scale variations produced by schlieren and inclusions far exceed the regional variations. Yet, the small-scale variations are very minor

volumetrically. The slightly greater range of compositions in the PHbT compared to the SHbT and SPT reflects the same slight systematic, east-to-west variations noted in the discussion of the modal data. The three samples from the central and eastern parts of the PHbT (36a, 240#52, and 240#53) are all more mafic, less silicic, and less potassic than the two from the western part of the mass (46a and 93). Thin-section observations also indicate higher potash and perhaps higher silica contents in the southwestern part of the SHbT compared to the rest of that unit, although the increases are less consistent and less widespread than in the adjacent PHbT. Whatever the cause of the east-west variations, it affected both intrusive units to some degree.

Harker variation diagrams for the tonalite are shown in Figure 86. For all oxides, the variations in concentration as a function of increasing SiO_2 content are similar to those generally observed for calc-alkaline and calcic plutonic and volcanic rocks. The diagrams dramatically illustrate the extremely limited compositional range within the SHbT and SPT and the distinctly more felsic compositions of the GBT. Like the modal data, the Harker diagrams also clearly show two distinct variation trends, confirming the field-based conclusion that the pluton consists of two similar but distinct petrologic units. Together the PHbT and SPT define a trend which, for a given SiO_2 content, is characterized by slightly lower FeO_t, MgO, TiO_2, and possibly K_2O, but higher Al_2O_3, $FeO_t/(FeO_t + MgO)$, and possibly Na_2O than the combined trend of the SHbT and the GBT. For CaO the two trends coincide completely, whereas, for K_2O and possibly P_2O_5 the three main textural units define a single trend, but the GBT appears to be different. There is a

Figure 86. Harker variation diagrams of oxide concentrations (weight %) in the tonalite. The number 63.3 is the SiO_2 concentration at which the variation trends for CaO and $Na_2O + K_2O$ intersect. It was defined as the alkali-lime index by Peacock (1931).

▲ gneissose border tonalite

△ stubby hornblende tonalite

○ prismatic hornblende tonalite

● seriate porphyritic tonalite

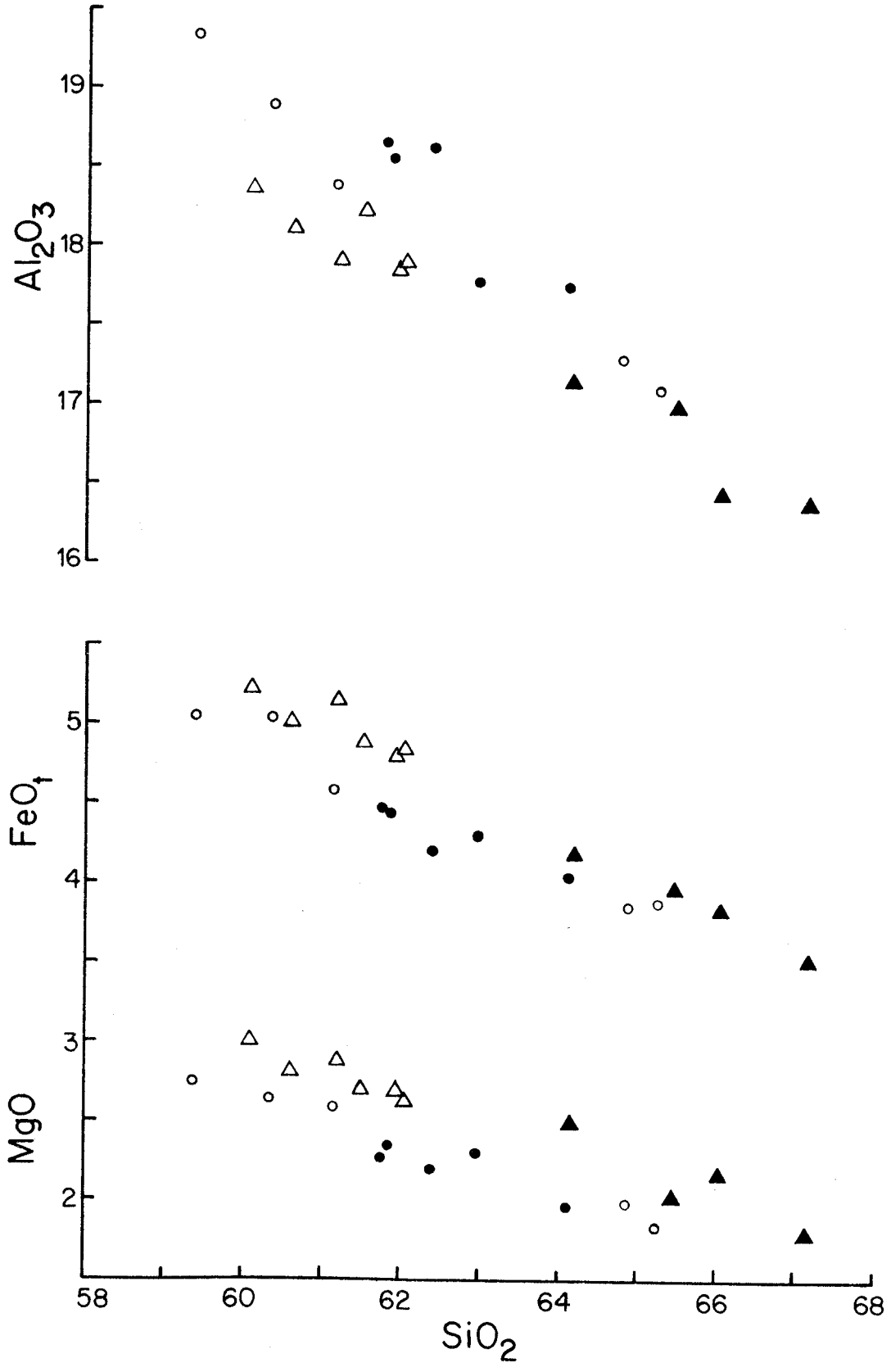
19
18
17
16
Al_2O_3
5
4
3
2
FeO_t
MgO
58
60
62
64
66
68
SiO_2

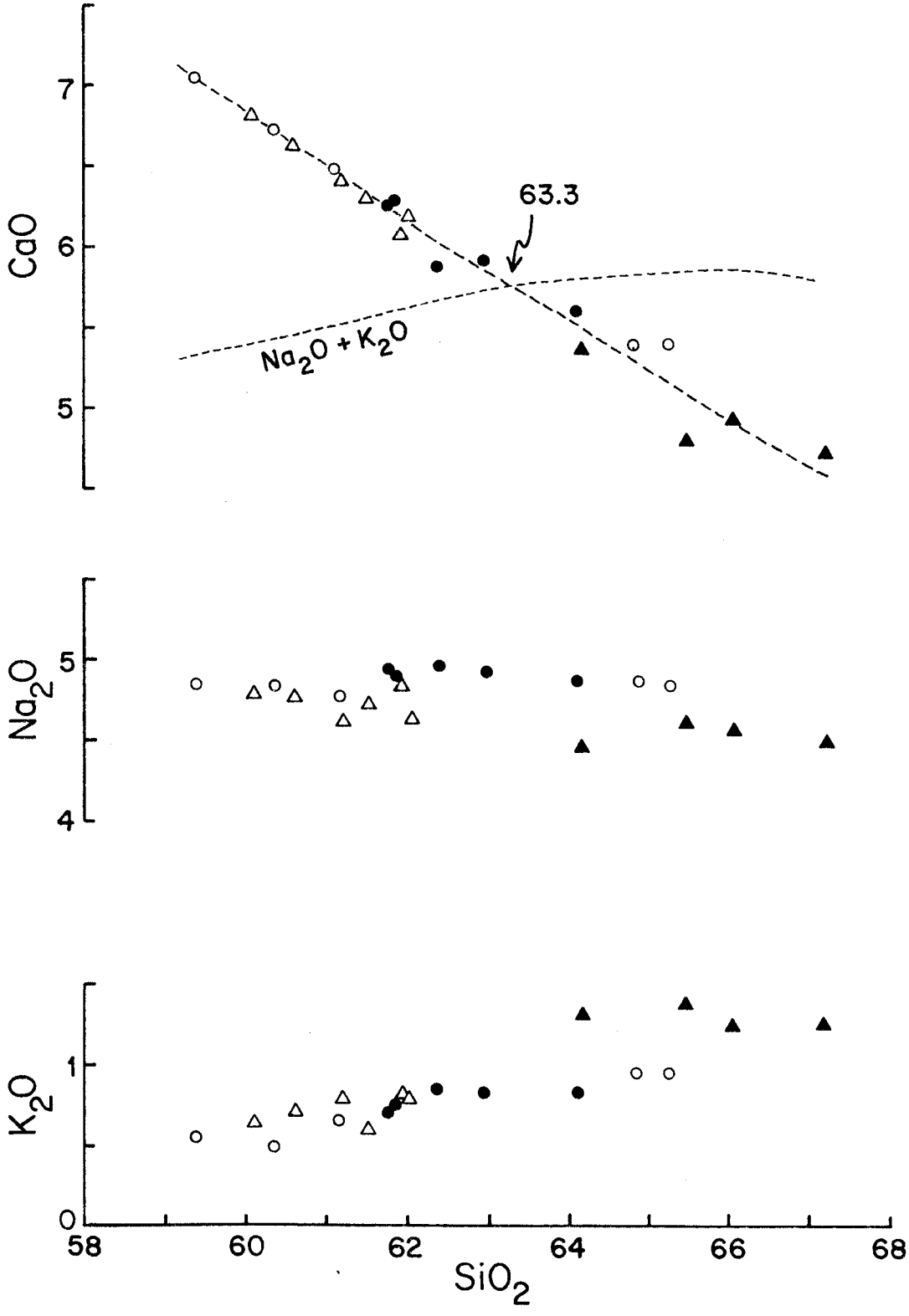
CaO
7
6
5
63.3
$Na_2O + K_2O$
Na_2O
5
4
K_2O
1
0
58
60
62
64
66
68
SiO_2

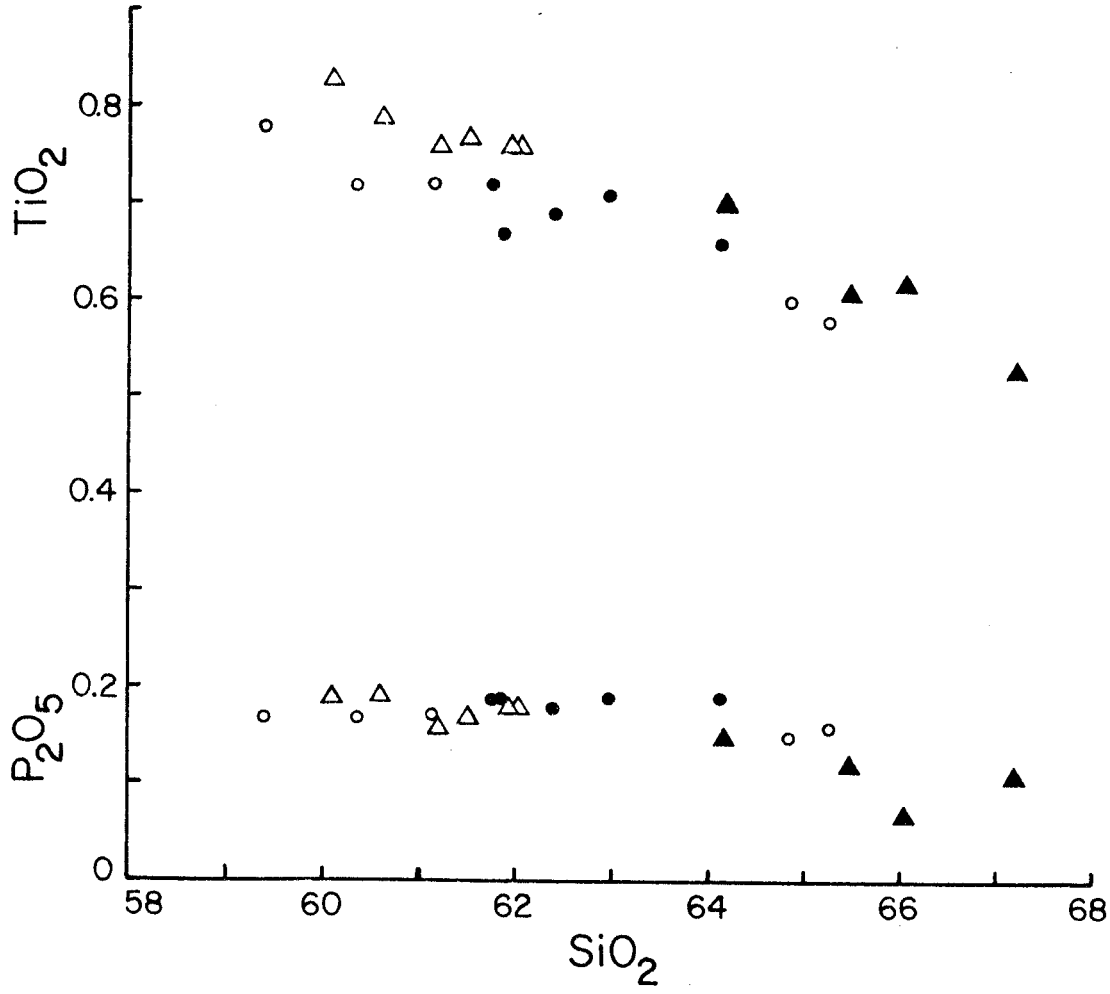
TiO2
P2O5
SiO2
0.8
0.6
0.4
0.2
0
58
60
62
64
66
68

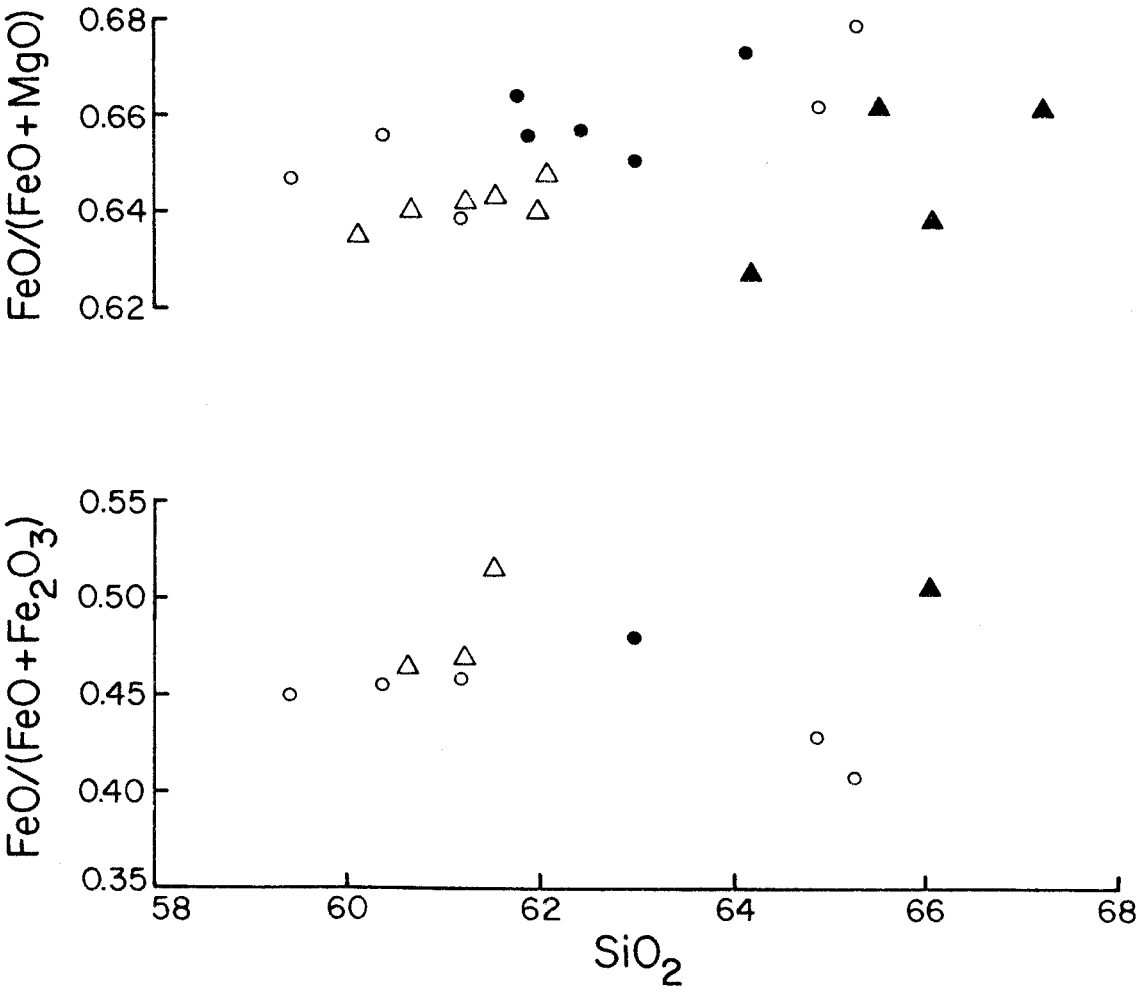
FeO/(FeO+MgO)
0.68
0.66
0.64
0.62
FeO/(FeO+Fe2O3)
0.55
0.50
0.45
0.40
0.35
58
60
62
64
66
68
SiO2

suggestion that the $FeO/(FeO + Fe_2O_3)$ ratios in the SHbT and GBT are slightly higher than the ratios in the other units. Such a difference, if real, is consistent with the arguments from hornblende and the Fe-Ti oxides that the SHbT crystallized under more reducing conditions.

Note that Na_2O is constant and, with the exception of the GBT, K_2O increases only very slightly with increasing SiO_2. The trend of differentiation was towards a siliceous and leucocratic melt having not only a high Na_2O/CaO ratio, but also a relatively high Na_2O/K_2O ratio. The ratio $FeO_t/(FeO_t + MgO)$ also increases very slightly with increasing SiO_2 within the three main units.

Although for most oxides, the GBT and SHbT appear to define a single variation trend, for K_2O and possibly for the $FeO_t/(FeO_t + MgO)$ ratios, the gneissose rocks do not appear to fall on any simple variation trend involving the other rocks. This suggests the possibility that concentration of K_2O in the GBT was to some degree independent of the variations in SiO_2 and the other oxides.

It is important to re-emphasize the chemical similarity among the units. As will be seen in the next chapter, the differences among the units and the total range of compositions in the pluton are very small compared to the total range of compositions in the batholith.

13.4 Trace Element and Isotopic Data

Trace element and isotopic data obtained on sample BC-I-12 by L. T. Silver and T. O. Early are shown in Table 24, along with x-ray fluorescence (XRF) analyses obtained by B. W. Chappell at the Australian National University in Canberra. Less accurate and less precise XRF

Table 24

Selected Minor and Trace Element Concentrations and Elemental and Isotopic Ratios in Sample BC-I-12

Concentrations in ppm

Sr^a:	623 ± 12	Sr^d:	620
Rb^a:	11.9 ± 0.2	Rb^d:	12.5
K^b:	6800 ±500	K^d:	6400
U^c:	0.38 ± 0.01	Ni^d:	31
Th^c:	1.14 ± 0.02	Cu^d:	5
Pb^c:	3.02 ± 0.04	Zn^d:	69
		Ga^d:	21.5
Rb/Sr:	0.019	Y^d:	6
K/Rb:	572	Zr^d:	71
Th/U:	3.00	Nb^d:	3
K/U:	17900	Pb^d:	4

$^{87}Sr/^{86}Sr$ initial[a]: 0.7036 ± 0.0001

$^{206}Pb/^{204}Pb^c$: 18.56 ± 0.02

$^{207}Pb/^{204}Pb^c$: 15.58 ± 0.02

$^{208}Pb/^{204}Pb^c$: 38.19 ± 0.03

[a]T. O. Early and L. T. Silver (manuscript in preparation). Concentrations measured by isotope dilution. Sr isotopic ratio normalized relative to a value of 0.7080 for $^{87}Sr/^{86}Sr$ in the Eimer and Amend standard $SrCO_3$.

[b]From wet chemical analysis (Table D-1, Appendix D).

[c]L. T. Silver (unpublished data). Concentrations measured by isotope dilution.

[d]X-ray fluorescence analyses by B. W. Chappell, the Australian National University, Canberra. Compare the Sr, Rb, K, and Pb values with those in the column to the left.

analyses for Sr and Rb were obtained at Caltech on all chemically analysed samples: the Sr concentrations, included in Plate 9, are averages of 2 to 5 different determinations each; Rb concentrations are consistently below the detection level (30-40 ppm). Reproducibility for the Caltech XRF analyses for Sr is ± 5% at worst for the higher concentrations, and appreciably better for lower concentrations; relative differences between samples are therefore considered reliable to about this precision. However, comparison of replicate Caltech XRF determinations for BC-I-12 (746 and 754 ppm) with the isotope dilution value (623 ppm) and the A.N.U. XRF determination (620 ppm) suggests that the Caltech XRF values are probably all too high by roughly 20%.

Table 25 shows gamma ray spectrometric analyses for U, Th, and K and the heat generation values calculated from the concentrations for seven samples of the drill core from heat-flow hole BA-1 in the center of the PHbT (my locality 240; Figure 80 and Plate 2, area I-7) and for ten additional PHbT outcrop samples collected at approximately specified distances and directions from the drill hole. These data, taken from Smith (1972), exhibit the same remarkable uniformity as the other chemical data. Again, the slight differences define an east-west asymmetry; that is, U, Th, and K concentrations increase from east to west. K_2O concentrations calculated from the spectrometric analyses are notably lower than both the wet chemical and microprobe results for other drill core and surface samples from comparable parts of the PHbT, suggesting

Table 25

Gamma Ray Spectrometric Analyses of U, Th, and K from the Prismatic Hornblende Tonalite[a]

Samples from Drill Core BA-1[b]

Sample Number	Depth in Core (m)[c]	U ppm	Th ppm	K ppm	K %	hgu[d]	Th/U	K/U
48	230-254	0.30	0.76	4200	0.51	0.38	2.5	14000
49	200-225	0.30	0.73	4400	0.53	0.38	2.4	14700
50	150-175	0.33	0.86	4400	0.53	0.41	2.6	13300
51	120-145	0.35	0.83	4500	0.54	0.43	2.4	12900
52	91-115	0.35	0.88	4700	0.57	0.44	2.5	13400
53	60-85	0.34	0.82	5100	0.61	0.43	2.4	15000
54	180-188	0.45	0.92	4700	0.57	0.50	2.0	10400
Average	---	0.35	0.83	4600	0.55	0.42	2.4	13100

Surface Samples and Drill Core Average

Sample Number	Location[e]	U ppm	Th ppm	K ppm	K %	hgu[d]	Th/U	K/U
BA-1 ave	0 km	0.35	0.83	4600	0.55	0.42	2.4	13100
SJ-55	2.5 km N	0.28	0.66	4400	0.53	0.36	2.4	15700
SJ-56	1 km S	0.38	0.91	5400	0.65	0.47	2.4	14200
SJ-57	2 km E	0.30	0.76	4300	0.52	0.38	2.5	14300
SJ-58	3 km SW	0.36	0.96	5400	0.65	0.48	2.7	15000
SJ-59	1 km S	0.33	0.98	5900	0.71	0.46	3.0	17900
SJ-60	2 km NW	0.31	0.93	6000	0.72	0.45	3.0	19400
SJ-61	2 km W	0.38	1.21	6100	0.74	0.53	3.2	16100
SJ-62	1 km N	0.27	0.87	5000	0.60	0.39	3.2	18500
SJ-63	2 km NE	0.21	0.70	3900	0.47	0.31	3.3	18600
SJ-64	3 km SE	0.23	0.76	4800	0.58	0.35	3.3	20900
Average	---	0.31	0.87	5100	0.61	0.42	2.8	16500

[a]Data from D. L. Smith (1972). Analyst: A. Smith, Lawrence Radiation Laboratory. Uncertainty reported as ±5%.

[b]Drill hole site BA-1 corresponds to my locality and sample series Ba-JM-240; center of the PHbT (Plate 2, area I-7).

[c]Each sample from the drill core is a 1 kg composite of material spread over the depth interval indicated

[d]Heat generation units (1 hgu = 10^{-13} cal/cm^{3}sec) calculated from the total abundances of U, Th, and K.

[e]Approximate direction and distance from the drill hole site.

that the absolute values in Table 25 may be in error, but the relative values appear to be reliable to the ± 5% reported.

Compared to the granitic rocks in the Sierra San Pedro Mártir farther east, the U, Th, and K concentrations and heat generation values in the San José pluton are unusually low. Among more than 150 analyzed tonalite and granodiorite samples from the sierra (Smith, 1972), approximately 82% have U concentrations in the range 1-2.5 ppm, approximately 84% have Th concentrations in the range 3-9 ppm, approximately 95% have K_2O concentrations in the range 1-2.5%, and approximately 93% have heat generation values in the range 1.5-4 hgu. Only one of the many tonalite samples gave concentrations and heat generation values comparable to those of the San José samples. The Rb and Pb concentrations in BC-I-12 are also very low, whereas the Sr concentrations are unusually high, compared to most other Peninsular Ranges tonalites analyzed by Early and Silver. Among the other elements analyzed by Chappell, Ni and Ga concentrations are relatively high, Zn is moderate, and Cu, Y, Zr, and Nb are low compared to other Peninsular Ranges tonalites.

The heat flow measured in the drill hole is also very low, 0.84 $\mu cal/cm^2sec$ (0.84 hfu; Smith, 1972, 1974). Assuming a uniform distribution of heat generation in the rocks to a depth of 4 km (the assumed thickness of the tonalite), Smith calculated that only 0.04 hfu is contributed by radioactivity in the upper 4 km, whereas 0.80 hfu originates at a depth >4 km. The latter value, called the "reduced heat flow" is considered "normal", and the low total heat flow is attributed to the extremely low U, Th, and K concentrations in the tonalite.

The $^{87}Sr/^{86}Sr$ initial ratio (0.7036) is near the low end of the spectrum for plutonic rocks in the Peninsular Ranges (0.7027-0.7080; Early and Silver, 1973, and manuscript in preparation) and in Alta California north of the Garlock fault (0.7032-0.7094; Kistler and Peterman, 1973). However, values in the range 0.7027-0.7045 appear to be characteristic of the western part of the Peninsular Ranges batholith and of the few analyzed plutons in the western foothills of the Sierra Nevada. A great deal of data have shown that values of 0.7030-0.7045 also characterize most of the volcanic rocks from many Mesozoic and Cenozoic volcanic arcs both in the ocean basins and along continental margins (e.g., Gill and Compston, 1973; Hedge et al., 1970; Pushkar, 1968). Basaltic rocks from oceanic islands also show a rather narrow distribution about a mean value of 0.7037 ± 0.0001 (Faure and Powell, 1972).

The lead isotopic ratios in plagioclase also fall towards the low end of the spectrum for plutonic rocks from the Peninsular Ranges (Silver, pers. comm., 1977) and are lower than the few published values in K-feldspar from granitic rocks in the Sierra Nevada (Doe and Delevaux, 1973), although the BC-I-12 ratios plot nearly along an approximate pseudo-isochron (2900 m.y.) drawn by Doe and Delevaux for the Sierran data. Compared to oceanic rocks, the $^{206}Pb/^{204}Pb$ and $^{208}Pb/^{204}Pb$ ratios are near the more radiogenic end of the spectrum for ocean floor (abyssal or mid-ocean ridge) basalts, but the $^{207}Pb/^{204}Pb$ ratio is slightly high and more similar to the values for some oceanic islands (Doe and Delevaux, 1973; Sun, 1973; Church and Tatsumoto, 1975; Vollmer, 1977).

Finally rare earth element concentrations measured by L. P. Gromet are relatively low and show a moderately fractionated pattern. The light rare earths Ce and Nd are enriched by factors of 24 and 20 times chondrites, respectively, whereas the heavy rare earths Er and Yb are enriched by only 3 and 2 times chondrites. There is a slight (about 15%) positive Eu anomaly.

Chapter 14

SUMMARY OF THE PETROGRAPHIC AND CHEMICAL CHARACTERISTICS OF THE TONALITE, COMPARISON WITH OTHER PLUTONIC ROCKS IN BAJA AND ALTA CALIFORNIA, AND ORIGIN OF THE TEXTURAL VARIATIONS

The pluton consists essentially of four minerals: plagioclase, quartz, hornblende, and biotite. K-feldspar contents are extremely low. Plagioclase is by far the dominant phase, and quartz is second in abundance. Hornblende generally exceeds biotite.

Textures indicate that plagioclase was an early-crystallizing phase. In the PHbT and SPT, hornblende and possibly opaques probably accompanied plagioclase on the liquidus, whereas, in the SHbT and locally in the PHbT, salitic clinopyroxene was apparently the first mafic mineral to crystallize, but was later replaced almost entirely by hornblende and actinolitic amphibole. Cummingtonitic amphibole, or possibly orthopyroxene now converted to cummingtonite, was an additional minor

parts of the SPT. Cummingtonite in the SPT appears to be a primary magmatic phase, but that in the other units is of uncertain origin.

Plagioclase is strongly zoned, particularly in the PHbT and SPT. It grew throughout the crystallization history of the magma. The thin, regular oscillatory zoning most strikingly developed in the southern part of the pluton, especially in the largest crystals, probably formed by a repetitive diffusion-controlled mechanism similar to that proposed by Bottinga et al. (1966). However, the few thin, especially calcic zones in many crystals most likely record abrupt perturbations in the magma, possibly resulting from sudden pulses of intrusion

Partial obliteration of original zoning by internal re-equilibration and by conversion of core plagioclase to rim compositions was minor except in the SHbT, where grains with euhedral zoning patterns are subordinate to those with mottled or weak diffuse anhedral zoning.

Except for differences in the zoning patterns and in the degree or euhedralism of crystal margins, plagioclase varies only slightly from unit to unit. Rims are distinctly more sodic in the SPT and the western part of the PHbT, but core and average grain compositions are similar throughout the pluton. Rims of many grains in the west-central part of the pluton and in some parts of the SPT appear to be abrupt overgrowths which differ in An content by 5-10% from the immediately adjacent interior plagioclase. Overgrowths of K-feldspar also partially mantle plagioclase in one sample from the southwestern part of the PHbT.

The subhedral and euhedral forms of hornblende in the PHbT and SPT suggest cessation of hornblende growth before the proportion of crystals in the magma became sufficient to cause much competition for growth space. In contrast, the molded shapes of hornblende margins in the SHbT imply considerable growth of hornblende up to the latest stages of magmatic crystallization.

Some quartz crystallized early in the SHbT and is now preserved as anhedral to euhedral inclusions in hornblende, but most quartz in this unit crystallized late in interstices. There is no clear evidence of when quartz began to crystallize in the PHbT and SPT; large inclusions of quartz are absent in hornblende and occur only near the margins of plagioclase. Much quartz in the latter units is coarse and

must have begun to crystallize early, but the margins are interstitial and grew late.

Biotite was a late phase in all units. In part it filled interstices, and in part it replaced plagioclase and, to a lesser degree, hornblende. Possibly some biotite crystallized from a subsolidus vapor phase. The abundance of biotite is directly proportional to that of quartz, but is inversely proportional to the abundance of hornblende and to color index. Being the principal potassic phase in the tonalite, biotite must be treated as part of the granitic rather than the mafic end of a differentiation trend. Compositions of biotite are very uniform throughout the pluton.

K-feldspar grew extremely late, both interstitially and as a minor replacement of plagioclase. Optical properties imply crystallization in a moderately high-temperature structural state (sanidine and perhaps locally orthoclase), yet the compositions appear too Or-rich to have been in equilibrium with plagioclase rims at solidus temperatures. Possibly most or all of the K-feldspar crystallized from a vapor phase at solidus or slightly subsolidus temperatures.

Rare primary interstitial chlorite, zeolite, muscovite, and carbonate almost certainly crystallized from an exsolved vapor phase. Possibly some or all of the interstitial epidote and sphene also formed in this way. Interstitial primary grains and patches of the first four phases are most abundant, although still very sparse, in the central and southern parts of the SPT. They also occur sporadically in the PHbT, especially in the western part, but are extremely rare

in the SHbT. Smoothly interstitial epidote, sphene, and K-feldspar occur throughout the pluton, but are also least abundant in the SHbT and most abundant in the central and southern parts of the SPT. These observations suggest slight concentration of volatiles and possibly of residual melt towards the southern (shallower?) end of the pluton and towards the western part of the PHbT. Both the more sodic compositions and the common overgrowth relationships of plagioclase rims in these areas compared to the rest of the pluton are consistent with this interpretation. Except in one sample (566 from the northwestern part), there is no good evidence for the existence of a vapor phase in the SHbT prior to complete crystallization of the melt.

Hornblende in the SHbT is zoned from slightly brownish-green cores richer in Na, Ti, Mg, Al^{IV}, and total Al, to blue-green margins richer in Si, Al^{VI}, Ca, and Fe. Fe^{3+}/Fe^{2+} ratios appear to increase from core to rim. The zoning resulted from essentially pseudomorphic replacement of the brownish-green cores by blue-green hornblende during subsolidus cooling. Hornblende in the rest of the pluton, including the GBT, is generally unzoned and similar both in color and in composition to the rim hornblende in the SHbT.

Comparison with the experimental data of Helz (1973) suggests that the brownish-green hornblende in the SHbT crystallized at higher temperature and/or lower f_{O_2} than the blue-green hornblende in the other units. Both the generally lower proportion of hematite in the hematite-ilmenite intergrowths and the suggestion of slightly lower whole-rock $Fe_2O_3/(FeO + Fe_2O_3)$ ratios in the SHbT compared to the other major units are consistent with crystallization under more reducing conditions,

whereas the abundance of rutile needles in early-formed quartz and of hematite flakes in plagioclase, both probably the result of exsolution, are consistent with higher crystallization temperatures in the SHbT.

The molded shapes of hornblende margins -- indicating extensive late growth of hornblende -- and the general absence of interstitial primary volatile-rich phases such as chlorite, zeolite, and white mica, suggest that the apparently higher crystallization temperatures of plagioclase and quartz in the SHbT were due to lower P_{H_2O}. The greater abundance of relict clinopyroxene -- and of actinolitic amphibole secondary after clinopyroxene -- in the SHbT than in the rest of the pluton is also consistent with lower P_{H_2O}. However, because experimental data show that the maximum stability temperature of hornblende increases only slightly as the amount of water in a melt decreases below the saturation limit (Eggler, 1972; Holloway, 1973), and because hornblende must have crystallized over a wide range of temperature in all three textural units, it is difficult to conceive how the crystallization temperatures of hornblende could have been significantly higher in the SHbT than in the other units. Hence, variations in f_{O_2} and possibly P_{H_2O} are the most likely explanations for the differences in hornblende compositions.

Thus the petrographic distinctions between the SHbT, on the one hand, and the PHbT and SPT, on the other, appear to be due to differences primarily in P_{H_2O} and f_{O_2} and secondarily in temperature during crystallization and subsolidus cooling. The similarity of whole-rock compositions among the units seems to preclude the possibility that any other chemical variations are responsible for the distinctions. P_{H_2O} and f_{O_2} conditions in the SHbT became very similar to those in the

PHbT and SPT during subsolidus cooling and possibly during the latest stages of magmatic crystallization. Varying intensity of late-magmatic and subsolidus flow contributed to variations in the euhedralism of crystal faces. Also, protoclastic deformation in the SHbT probably facilitated deuteric modification of hornblende compositions, partial obliteration of zoning in plagioclase, and exsolution of hematite from plagioclase (thereby contributing to the characteristic tannish tint of the SHbT. However, the basic textural distinctions between the units cannot be explained in terms of varying intensity of flow and deformation.

I do not know why hornblende and biotite in the SHbT tend to be equant and equigranular as well as molded and poikilitic, whereas, in the other two units, they have a seriate size distribution and occur as elongate prisms and thin plates, respectively. Helz (1973) observed such a variation in shape of hornblende as a function of temperature in her melting experiments on natural basalts. Possibly higher P_{H_2O} and/or lower temperature favor more acicular shapes, although again temperature is a doubtful factor.

Despite the textural variations and the evidence for emplacement in two or possibly three intrusive pulses, the range of chemical and modal variations in the pluton is very limited. The SHbT and SPT are especially uniform internally. Yet zoning in plagioclase and the textural evidence for extensive late crystallization of quartz and biotite and minor late crystallization of K-feldspar all attest to considerable change in the composition of the melt as crystallization proceeded. The implications of this chemical and modal homogeneity in terms of both the mechanisms and efficiency of differentiation and the possible origins

of the tonalite magma will be discussed in the following chapters.

Although the textural units are very similar in composition, both the Harker diagrams and the correlation plots of modal minerals reveal slight systematic differences among the units, which permit the pluton to be divided into two distinctive but similar petrologic units: the PHbT and SPT, on the one hand, and the SHbT and GBT on the other. Thus the chemical and modal data lead to the same fundamental subdivisions of the pluton as do the field observations. Although the SPT cannot be distinguished from the PHbT on the basis of chemical and modal data, the extremely limited compositional range of the former is consistent with its recognition as a mappable entity closely related in composition and genesis to the PHbT. The GBT is remarkable in being more granitic rather than more mafic than the rest of the pluton.

The mineralogy and modal composition of the pluton is basically similar to that of other tonalites in the batholith; megascopically, the pluton appears quite ordinary. The chemical variation trends, as displayed on Harker diagrams, are also similar to those of most batholithic rocks. The relatively high alkali-lime index (63.3) makes this a calcic pluton in the classification system of Peacock (1931).

Closer examination shows that there are numerous second-order modal and chemical characteristics which distinguish this pluton from most other Peninsular Ranges tonalites yet studied. Some of these characteristics are shown in Tables 26 and 27 and Figure 87. In comparison to the limited published modal data for northern Baja California and southern Alta California (Table 26), the San José pluton has an unusually high hornblende/biotite ratio and low K-feldspar content, as well as a

Table 26

Comparison of the Average Modal Composition of the San José Pluton with That of Other Tonalites from the Peninsular Ranges Batholith

	San José Area			Northern B. Cal.	Southern Alta California			
	SJP	PP	WCP	EPT	LMP	GVT-1	GVT-2	BT
Quartz	16.27	18.4	7.4	24	22.2	18	15	20-25
Plagioclase*	63.65	62.2	66.1	52	50.3	58	62	55-60
K-feldspar	0.26	0.1	0.2	3	tr	7	3	"few %"
Hornblende	11.31	8.3	17.0	21	12.1	8	9	10
Biotite + chlorite	6.20	9.2	5.5		14.4	7	10	5-15
Opaque	1.27	0.6	1.7		1.1	1	1	---
Other accessories	1.05	1.3	2.1			--	--	---

tr: trace constituent

*includes alteration phases

SJP: San José pluton

PP: Potrero pluton. Average of 14 samples, one thin section per sample. See Appendix G for sample locations and individual analyses.

WCP: Willow Creek pluton. Average of 2 samples, one thin section per sample. See Appendix G for sample locations and individual analyses.

EPT: El Pinal tonalite (Duffield, 1968, Figure 4). Approximate average estimated by the present author from a generalized plot of the modal variations across the pluton. Based upon 142 stained slabs.

LMP: Lakeview Mountains pluton (Morton et al., 1969). Average of 16 samples, one thin section per sample.

GVT-1: Green Valley tonalite north of Escondido Creek (Larsen, 1948). Average or typical composition as reported by Larsen rather than an average of tabulated modal analyses.

GVT-2: Green Valley tonalite, other parts (Larsen, 1948). Same significance as for GVT-1.

BT: Bonsall tonalite (Larsen, 1948). Same significance as for GVT-1.

Table 27

Comparison of the Average Chemical Composition of the San José Pluton with those of Tonalites from the Batholith in Southern California

	SJP	LMP	GVT	BT
SiO_2	62.00	60.11	66.9	62.7
TiO_2	0.72	--	0.6	0.7
Al_2O_3	18.16	18.37	14.9	16.9
FeO_t	4.63	6.70	5.1	5.9
MnO	0.07	--	0.06	0.06
MgO	2.49	3.60	2.2	2.7
CaO	6.23	7.04	4.5	5.9
Na_2O	4.82	2.68	3.5	3.4
K_2O	0.74	1.49	2.1	1.6
P_2O_5	0.17	--	0.05	0.09
TOTAL	100.03	99.99	99.9	100.0
$FeO/(FeO + Fe_2O_3)$	0.46	0.78	0.73	0.76
$FeO_t/(FeO_t + MgO)$	0.65	0.65	0.70	0.68
$Na_2O/(Na_2O + K_2O)$	0.87	0.64	0.62	0.68
An/(Ab + An) (norm)	0.39	0.60	0.38	0.47
Color Index (norm)	13.82	21.80	15.15	17.32
Fe/(Fe + Mg) (biotite)	0.42	0.56*	0.50*	0.49*
Fe/(Fe + Mg) (hornblende)	0.34	0.49*	0.47*	0.47*

SJP: San José pluton
LMP: Lakeview Mountains pluton (Morton et al., 1969)
GVT: Green Valley tonalite (Larsen, 1948)
BT: Bonsall tonalite (Larsen, 1948)

*Larsen and Draisin (1950)

Figure 87. Larsen variation diagrams comparing the San José pluton with other plutonic rocks of the Peninsular Ranges batholith.

- – – ——— variation trend for plutonic rocks of the batholith in southern Alta California (Larsen, 1948)
- ——— —— variation trend for plutonic rocks of Baja California (data of Hirschi and de Quervain, 1927-1933, as plotted by Larsen, 1948)
- o plutonic rocks of Baja California (data of Gastil et al., 1975)
- · ·· · San José pluton

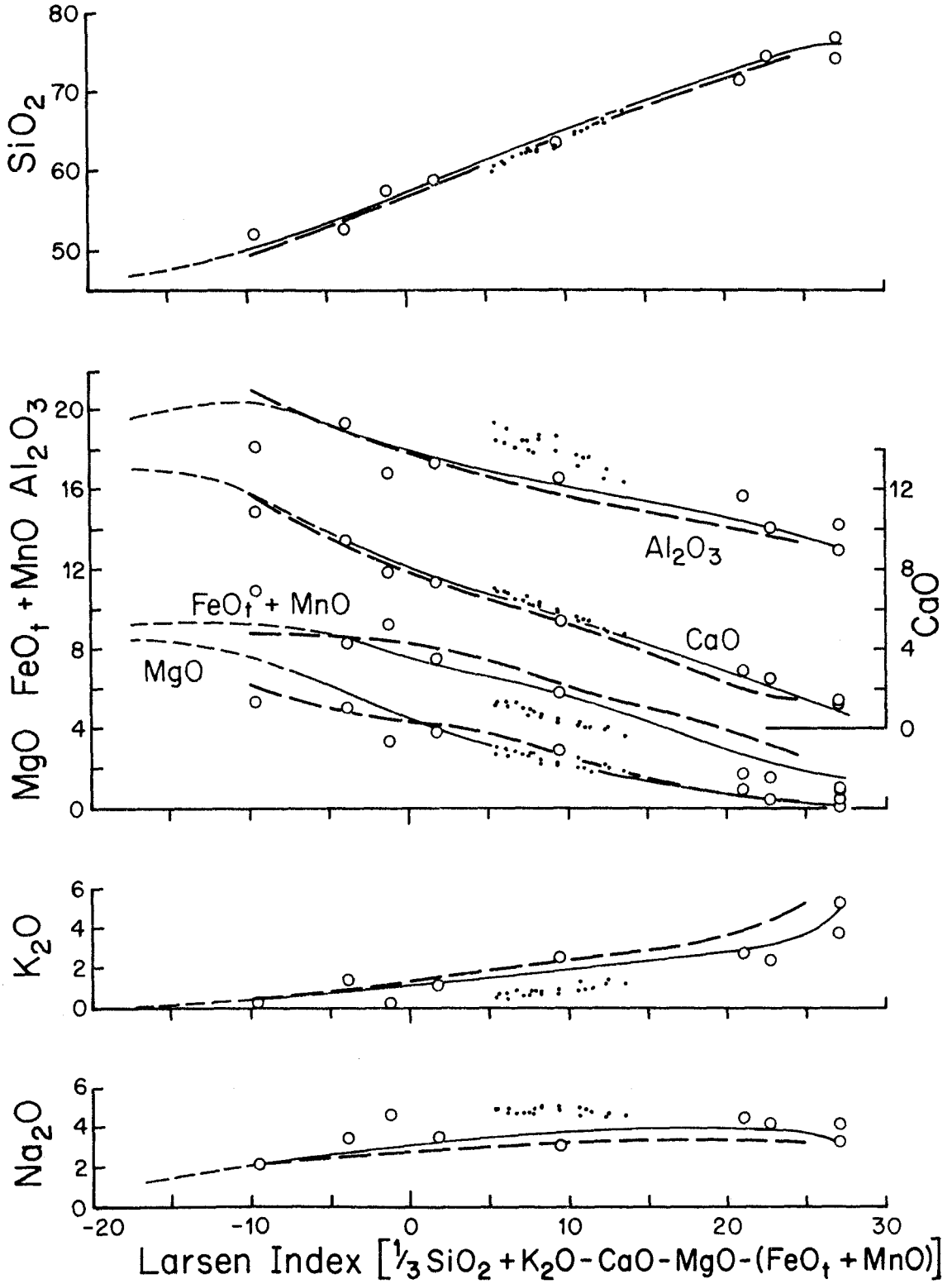
SiO2
80
70
60
50
MgO FeOt + MnO Al2O3
20
16
12
8
4
0
Al2O3
FeOt + MnO
MgO
CaO
12
8
4
0
K2O
6
4
2
0
Na2O
6
4
2
0
-20
-10
0
10
20
30
Larsen Index [⅓ SiO2 + K2O - CaO - MgO - (FeOt + MnO)]

high plagioclase and slightly low quartz content. Approximate modes reported by Smith (1972; based on 400-900 points in one thin section per sample), plus thin-section observations by the author, reveal similar differences from most of the tonalites in the Sierra San Pedro Mártir; some of the latter rocks approach granodiorite in modal composition. Also shown in Table 26 are the average modal compositions of two nearby plutons. The Potrero pluton (southeastern corner of Plate 1) is very similar to the San José pluton, except for having a notably lower hornblende/biotite ratio and a lower content of opaques. In contrast, the small Willow Creek pluton located immediately southeast of the San José pluton (Plate 2, area N,0-12) is richer in hornblende and possibly plagioclase, but much poorer in quartz; it consists of biotite-hornblende quartz diorite rather than tonalite.

A comparison of chemical data in Table 27 and Figure 87 shows that the San José pluton is unusually rich in Na_2O and Al_2O_3, but poor in K_2O and FeO_t. The Na_2O/K_2O ratio is therefore very high. Normative Or contents fall between 3.0 and 5.6% for all analyses except those of the GBT, for which the range is 7.3-8.1%. CaO is only slightly high, which, together with the high Na_2O and Al_2O_3, reflects the high proportion, but relatively sodic composition, of plagioclase in the rocks. The normative color index is relatively low.

The whole-rock $FeO/(FeO + Fe_2O_3)$ ratios are strikingly low, as are the atomic Fe/(Fe + Mg) ratios in biotite and hornblende. These differences imply crystallization under unusually oxidizing conditions. The compositions and petrographic characteristics of the Fe-Ti oxides indicate T-f_{O_2} conditions ranging from slightly below those of the $MnO + Mn_3O_4$

buffer up to those of the HM buffer. Conditions became increasingly oxidizing, although f_{O_2} may not have actually increased, as crystallization and cooling proceeded. A more precise estimate of the T-f_{O_2} conditions of equilibration of the assemblage biotite + magnetite + K-feldspar will be presented in the next chapter.

Inasmuch as the average $FeO_t/(FeO_t + MgO)$ ratio is similar in the San José tonalite to that in the three major tonalite types in southern Alta California, a higher proportion of Fe must be fixed in opaques in the San José pluton. This difference is again attributable to higher oxygen fugacities in the San José magmas.

Figure 88, a ternary plot of the normative proportions of quartz, albite + anorthite, and color index (CI) shows very strikingly the more leucocratic and plagioclase-rich nature of the San José pluton compared not only to most other Peninsular Ranges plutonic rocks for which data have been published, but also to the average hornblende-biotite tonalite of Nockolds (1954) and the average Cenozoic andesite of Chayes (1969). Only one of the other rocks, the La Sierra tonalite (LST), has comparably high normative Ab + An. As seen in Figure 89, this rock has a considerably higher Or content than the San José pluton and is thus not comparable. Figure 88 also emphasizes the extremely tight clustering of compositions within each textural unit and the distinctly more leucocratic and plagioclase-rich compositions of the PHbT and SPT compared to the SHbT and GBT.

Ternary plots of the normative proportions of albite, anorthite, and orthoclase (Figure 89A) and of quartz, albite + anorthite, and orthoclase (Figure 89B) both emphasize the low K_2O content of the San José pluton

Figure 88. Comparison of the normative proportions of quartz, albite + anorthite, and color index in the San José pluton with those in other plutonic rocks of the Peninsular Ranges batholith.

San José pluton (norms were calculated using the measured or assumed $FeO/(FeO + Fe_2O_3)$ ratios)

- ▲ gneissose border tonalite
- △ stubby hornblende tonalite
- o prismatic hornblende tonalite
- ● seriate porphyritic tonalite

southern Alta California

- ■ SCB = average of plutonic rocks in a five-quadrangle area
- ⊞ SMG = average San Marcos gabbro
- ⊞ BT = average Bonsall tonalite
- ⊞ GVT = average Green Valley tonalite
- ⊞ WMG = average Woodson Mountain granodiorite

(Larsen, 1948)

- □ = single analyses of other rocks
  - LST = La Sierra tonalite
- ⊠ LMP = average Lakeview Mountains pluton (Morton et al., 1969)

- ▽ = single analyses of other plutonic rocks in Baja California (Gastil et al., 1975)

- ⊗ CA = average Cenozoic andesite (Chayes, 1969)

- ○ N = average hornblende-biotite tonalite (Nockolds, 1954)

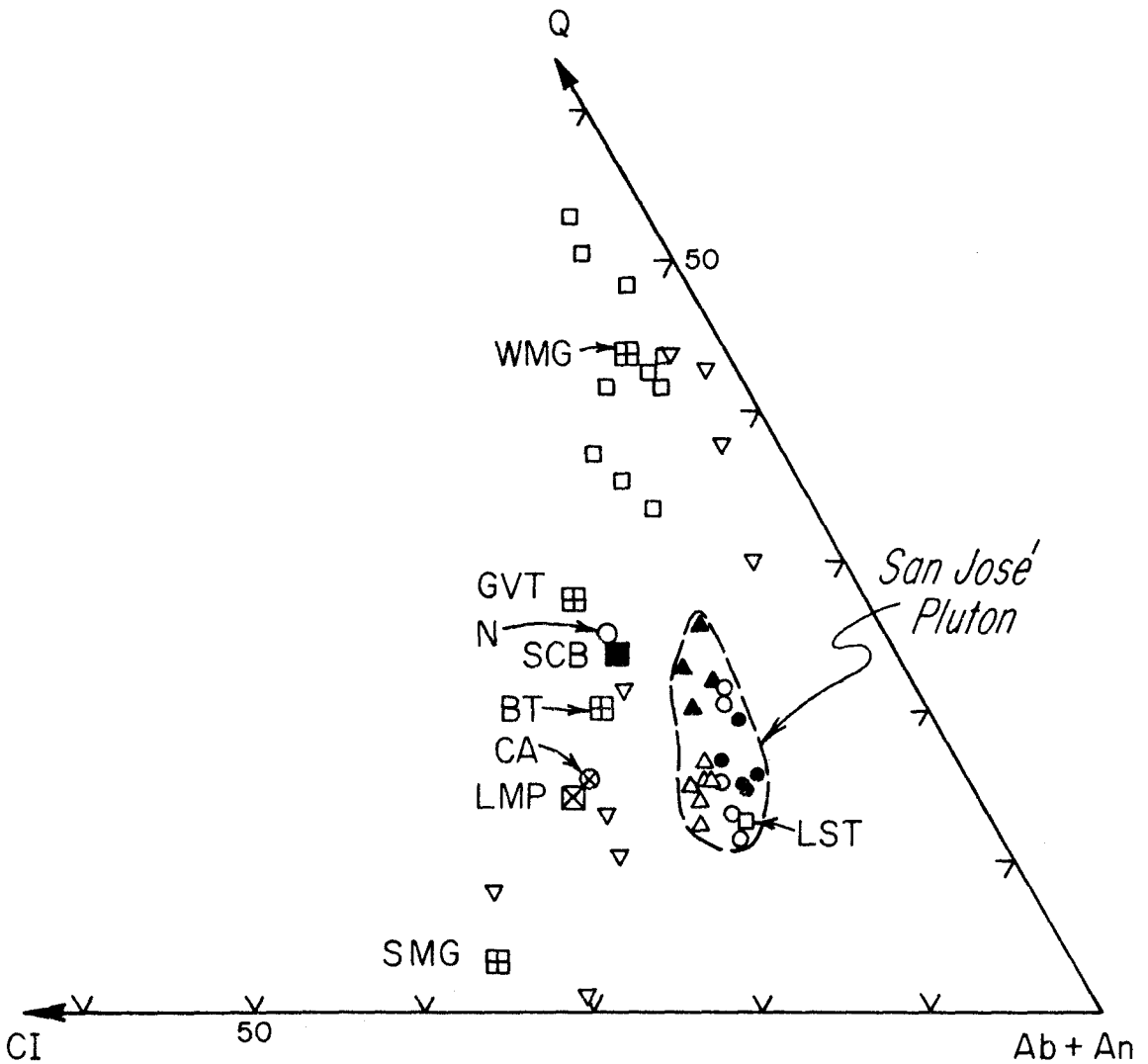
Q
50
WMG
GVT
N
SCB
BT
CA
LMP
San José
Pluton
LST
SMG
CI
50
Ab + An

Figure 89. Comparison of the normative proportions of (A) albite, anorthite, and orthoclase and (B) quartz, albite + anorthite, and orthoclase in the San José pluton with those in other plutonic rocks of the Peninsular Ranges and Sierra Nevada batholith.

Sierra Nevada batholith (Presnall and Bateman, 1973)
SN = composite trend for granitic rocks from the central Sierra Nevada
\+ = plutonic rocks from the western foothills (shown only in (B))

Other symbols and data sources are the same as in Figure 88.

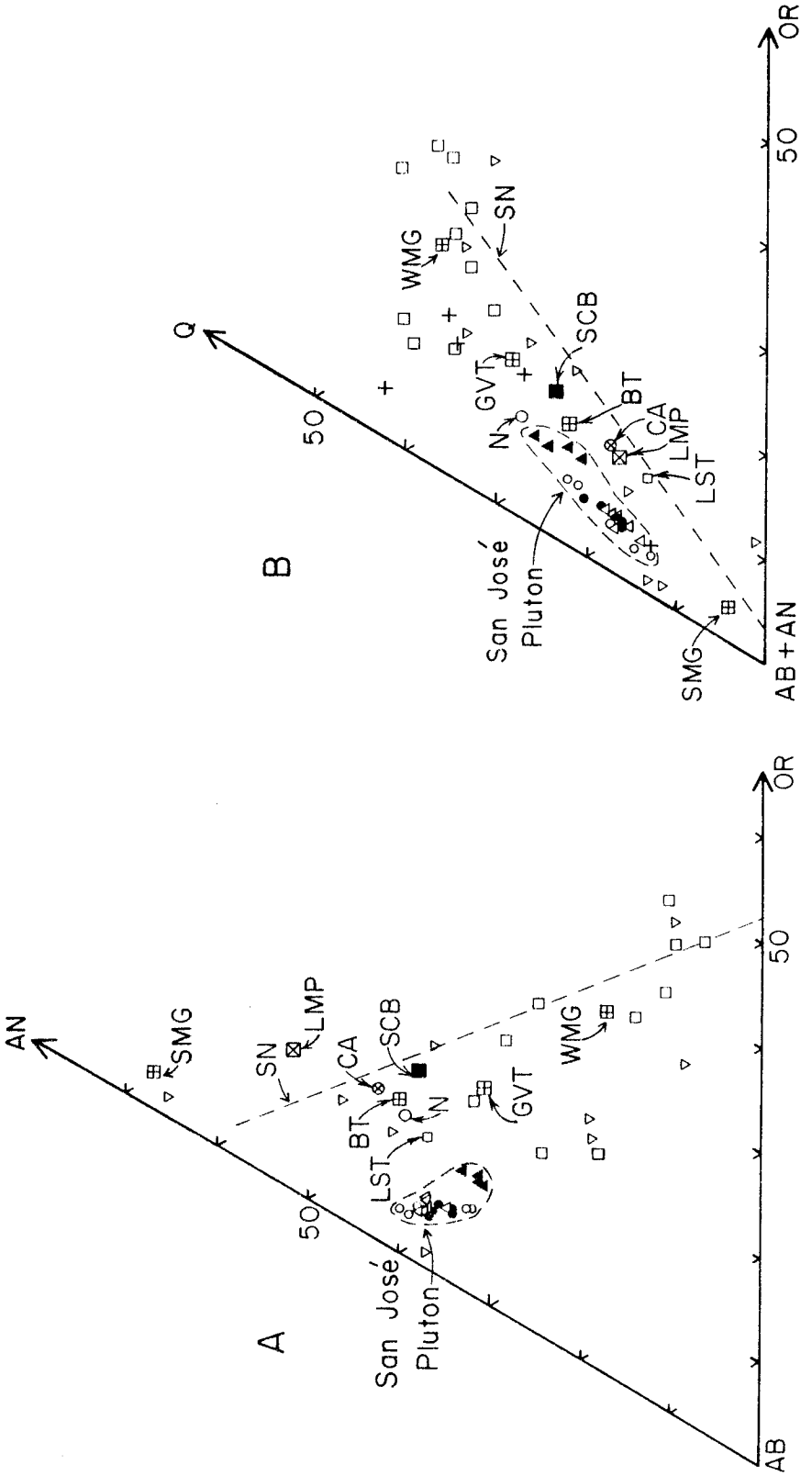
A
AN
AB
OR
50
50
SMG
SN
LMP
CA
SCB
BT
N
LST
GVT
WMG
San José
Pluton
B
Q
AB+AN
OR
50
50
WMG
SN
SCB
GVT
N
BT
CA
LMP
LST
San José
Pluton
SMG

and the very limited increase in K_2O as differentiation proceeded. If the GBT is excluded, the San José analyses define short variation trends characterized by only a slight increase in the Or/Ab ratio as the An/Ab ratio decreases and an even smaller increase in the Or/(Ab + An) ratio as quartz increases. All three ternary diagrams also emphasize the limited compositional range of the pluton, exclusive of the GBT, and the distinctly different compositions of the latter rocks, particularly their higher SiO_2 and K_2O contents.

The Q-(Ab + An)-Or triangle shows that, whereas most of the plutonic rocks from the Sierra Nevada are comparatively rich in Or, all five from the western foothills plot well towards the (Ab + An)-Q side of the main trend. The San José pluton is likewise located towards the western side of the Peninsular Ranges batholith, so the low K_2O content suggests a possible analogy with the western foothills rocks of the Sierra Nevada. However, four of the five western foothills rocks in Figure 89B have trondhjemitic rather than tonalitic compositions -- i.e., they have much less CaO and more SiO_2 than the San José tonalite (Bateman and Dodge, 1970) -- and are therefore not strictly comparable. The fifth western foothills rock in Figure 89B, which plots at the plagioclase-rich end of the San José field, appears from the data of Bateman and Dodge to be a quartz gabbro, not a tonalite or quartz diorite.

Sr concentrations are high, whereas U, Th, Rb, and Pb levels are low in the San José pluton compared to the levels in most tonalites and granodiorites throughout the batholith. The Th/U ratio (3.0) in BC-I-12 is also low, whereas the K/Rb ratio (574) is high. Rare earth elements show a moderately fractionated pattern, with moderate enrichment

relative to chondrites in the lighter elements, but very little enrichment at the heavy end.

The $^{87}Sr/^{86}Sr$ initial ratio of 0.7036 is near the low end of the spectrum for plutonic rocks in the Peninsular Ranges (0.7027-0.7080; Early and Silver, 1973, and manuscript in preparation), and in Alta California north of the Garlock fault (0.7032-0.7094; Kistler and Peterman, 1973). However, values less than 0.7045 appear to be characteristic of plutons in the western parts of both batholiths. The Pb isotopic ratios in plagioclase are also less radiogenic than the ratios both in granitic rocks from the Sierra Nevada (Doe and Delevaux, 1973) and in most other analyzed tonalites in the Peninsular Ranges (L. T. Silver, personal communication).

In summary, the San José pluton is, on the whole, petrographically and chemically similar to the rest of the tonalite in the Peninsular Ranges, yet it has many recognizable distinguishing characteristics:

(1) high plagioclase content and hornblende/biotite ratio, but low K-feldspar content and color index;

(2) high Na_2O, Al_2O_3, and Na_2O/K_2O ratio, but low K_2O, FeO_t, and $FeO/(FeO + Fe_2O_3)$ ratio, and low $Fe/(Fe + Mg)$ ratios in hornblende and biotite;

(3) high Sr and low U, Th, Rb, and Pb concentrations and high K/Rb ratio;

(4) relatively low concentrations and moderately fractionated pattern of rare earth elements; and

(5) relatively unradiogenic $^{87}Sr/^{86}Sr$ initial and Pb isotopic ratios.

Differentiation trended towards a siliceous leucocratic composition maintaining a relatively high Na_2O/K_2O ratio despite slight increase in K_2O; however, the compositional range throughout the pluton is very limited. Surprisingly, the outer gneissose phase has been enriched in K_2O and SiO_2 relative to the rest of the SHbT.

Some of these characteristics may be related to the position of the pluton in the western part of the batholith, well south of the area for which extensive published data exists, but whether all of the distinctive characteristics can be attributed to geographic and tectonic position is unclear.

Chapter 15

FACTORS CONTROLLING COMPOSITIONAL VARIATIONS AND MAGMATIC DIFFERENTIATION

15.1 Origin of the Compositional Variations in the Tonalite

In discussing the origin of the compositional variations, it is necessary to consider not only the trend of chemical change, but also the extremely limited degree of chemical variation, especially within the individual textural units. Critical factors include: (1) the extent of assimilation or chemical interaction with wall rocks, (2) the relative proportions of different phases crystallizing from the melt at any time, (3) the effectiveness of processes tending to separate crystals from melt, and (4) the extent to which various components, especially alkalies and SiO_2, may have been transferred through the pluton via a vapor phase. The latter three factors depend, in turn, upon the bulk compositions of the magmas and upon T, P, f_{H_2O}, and f_{O_2}.

(1) Wall-Rock Contamination.

Evidence of contamination of the tonalite is minor and local. Inclusions generally constitute 1% or less of the tonalite, and it is possible that many are autoliths rather than reconstituted fragments of wall rocks. The remarkable modal and chemical homogeneity within and among the three main textural units seems completely incompatible with extensive contamination unless, of course, the contamination occurred at much greater depths, and the inhomogeneities inevitably produced were effectively eliminated by thorough mixing during continued emplacement. Whereas such extremely effective rehomogenization cannot

be ruled out, it is conceptually difficult to accept. As will be discussed at the end of this section, the distinctly more granitic composition of the GBT may be due to *selective* contamination of this narrow border zone with a felsic component from the wall rocks, but it could also be due to differentiation processes within the pluton.

The Sr data also suggest little if any contamination. Certainly, the low $^{87}Sr/^{86}Sr$ initial ratio (0.7036) rules out involvement of old sialic crust, or of sediments derived from such crust, as either a contaminant or a parental material for the magma. If significant contamination occurred and affected more than just a thin outer skin of the pluton, the contaminant either contained very little Sr or had an isotopic composition not much different from 0.7036. The distribution of Sr contoured in Figure 90 also rules out a net gain in Sr from the wall rocks. The lower Sr contents of the GBT may indicate contamination with Sr-poor material from the country rocks, but, if so, the effect appears to have been restricted to the narrow gneissose zone. Concentrations within the interior of the SHbT are considerably higher and quite uniform. Furthermore, there is little change either in Sr or in major-element concentrations towards the non-gneissose margins around the southern third of the pluton. The distribution of Sr closely parallels the distributions of CaO, of modal and normative plagioclase, and of modal and normative color index, but is almost exactly opposite to the distributions of SiO_2, K_2O, and modal biotite/hornblende ratio. There is no evidence of migration of Sr independent of other elements, either within the

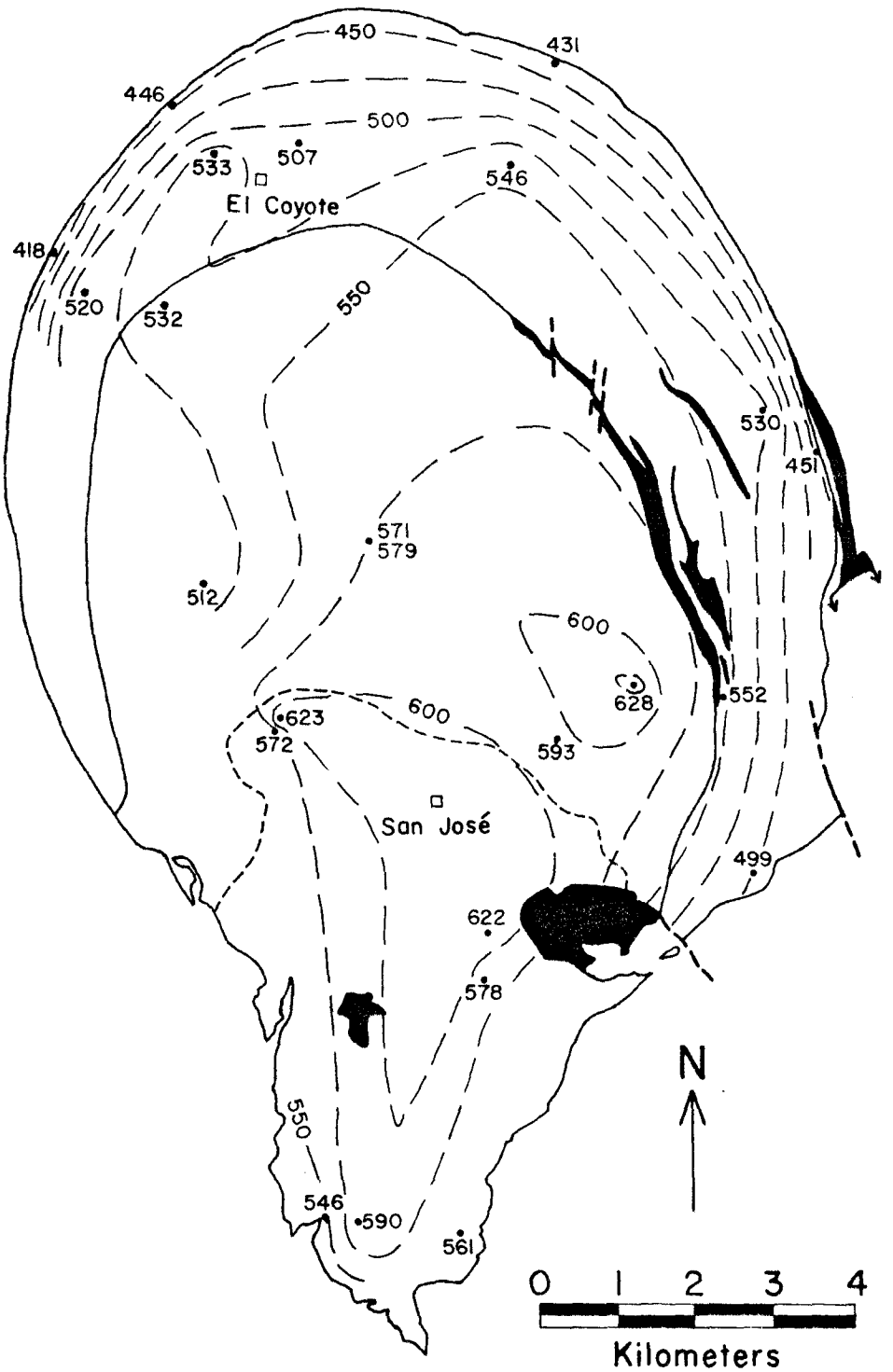

Figure 90. Spatial distribution of whole-rock Sr concentrations in the tonalite. All values are normalized to an assumed value of 623 ppm in sample BC-I-12. Contour interval is 25 ppm.

pluton or between the pluton and wall rocks.

The relatively unradiogenic Pb isotopic ratios likewise rule out any significant contribution from old granitic crust or related sedimentary rocks. According to L. T. Silver (personal communication, 1977), zircons in GBT sample BC-I-5 contain a small amount of inherited Pb, but those in SPT sample BC-I-12 from the interior of the pluton contain little or none.

(2) Sequence and Proportions of Crystallizing Phases.

The relative proportions and compositions of the minerals crystallizing at any time was obviously an important factor controlling the changing composition of the melt. Early crystallization of hornblende and of moderately calcic plagioclase (An_{40-45}) must have led to enrichment of the residual melt in Na_2O, K_2O, and SiO_2. However, once the melt became saturated in quartz, SiO_2 enrichment must have been severely curtailed. Similarly, once biotite began to crystallize, K_2O enrichment must have been restricted.

At the same time, the initial bulk composition of the magma must also have influenced the manner and extent to which crystallization of the different phases changed the residual melt composition. Consider K_2O. The average K_2O content of the tonalite is 0.74%. Prior to deuteric alteration, about 75% of this was fixed in biotite, about 15% in plagioclase, 5% in K-feldspar, and 4% in hornblende. Even though the absolute concentrations of K_2O in plagioclase and hornblende are very low (0.18 and 0.27%, respectively), the total concentration

of K_2O in the tonalite is so low that crystallization of these two minerals must still have consumed a significant proportion of that total. Consequently, eventual crystallization of only a small proportion of biotite was sufficient to prevent strong K_2O enrichment. In contrast, in a magma initially containing more K_2O -- e.g., 1.5-1.6% as in the average Bonsall tonalite and the Lakeview Mountains pluton -- crystallization of hornblende and plagioclase would consume a much smaller fraction of the total K_2O and would therefore lead to a more rapid and proportionally greater increase in K_2O in the melt. In this case, much more biotite would have to crystallize in order to restrict K_2O enrichment as effectively, and a residual K_2O-rich melt is more likely to result.

A similar conclusion was reached years ago by Lipman (1963, p. 1279), who pointed out the "tendency for differentiation to reinforce initially small contrasts in composition of the parental material", particularly in terms of controlling whether differentiation leads towards a "trondhjemitic trend characterized by a nearly constant alkali ratio" (i.e., K_2O/Na_2O ratio) or towards a "normal calc-alkaline trend" of progressive K_2O enrichment and increasing K_2O/Na_2O ratio. The K_2O/Na_2O trend in the San José pluton increases only slightly as a function of SiO_2 content and therefore approaches the "trondhjemitic trend" as defined by this criterion, but the CaO content of the rocks is much higher than in true trondhjemites.

Similar considerations can be made for SiO_2. The early-formed minerals hornblende and plagioclase (An_{40-45}) contain about 49% and 57-58% SiO_2, respectively, compared to 62% in the tonalite. Because

much more plagioclase crystallized than hornblende, progressive enrichment in SiO_2 must have been modest even before nucleation of quartz. Crystallization of biotite (37% SiO_2) was potentially capable of producing strong SiO_2 enrichment in the melt, but its contribution was counteracted by simultaneous crystallization of quartz. The plagioclase-rich, leucocratic nature of the tonalite was therefore a factor in limiting SiO_2 enrichment in the residual melt. Had the magma contained more Fe and Mg and therefore crystallized more hornblende (or biotite if enough K_2O were available), the potential for SiO_2 enrichment would have been greater.

(3) Separation of Crystals from the Melt.

Despite the above-mentioned factors tending to restrict differentiation of the melt, the zoning of plagioclase and the evidence for extensive late crystallization of quartz and biotite prove that the composition of the residual melt did change considerably as crystallization proceeded. Therefore, the principal factor limiting the range of chemical variation in the pluton must have been the ineffectiveness of processes tending to separate crystals from melt. The two potentially most important processes are gravitational settling (or floating) and flow differentiation.

I have recognized no structures or textures suggestive of gravity-dependent sorting of crystals. Layering in the small area of mafic-layered tonalite at locality 532 in the SPT is more readily explained by flow-dependent sorting of crystals in a crystal-rich magma than by gravitational processes (see Section 7.6). Rock compositions within

each textural unit appear to be independent of elevation, although the greatest range of elevation within any of the units, about 550 m in the PHbT, is small, as is the number of samples available to text the correlation.

Possibly, the more mafic compositions of the eastern two thirds of the PHbT as compared both to the western part of that unit and to the SPT is due to gravitational accumulation of early-formed dark minerals and perhaps plagioclase prior to emplacement. Likewise, large plagioclase crystals may have accumulated in the SPT by crystal settling, again prior to final emplacement.[28] However, there is no corresponding concentration of dark minerals in the SPT; in fact, the SPT has the lowest average modal and normative color indices of the three main textural units. Whatever their cause, these spatial variations are small and provide no indication that gravitational segregation of crystals was an important process.

It is possible that the low FeO_t content of the tonalite as a whole compared to the rocks in southern Alta California (Table 27 and Figure 87) resulted from early crystallization and settling out of Fe-Ti oxides in response to the unusually oxidizing conditions in the San José magmas. Only 1.3% by weight (0.7% by volume) of magnetite need settle out to account for the low FeO_t. I have recognized no textural or modal evidence of settling out of opaques, yet the amount of settling required is sufficiently small compared to the range of modal opaque contents in the pluton (0.85-1.92% by volume, even

---

[28]Density considerations discussed in Appendix F apparently rule out floatation of plagioclase in the magma.

excluding the opaque-poor GBT) that the evidence might not be recognizable. However, there are alternative explanations for the low FeO_t content as, for example, initial formation of the magma by partial melting under relatively oxidizing conditions or partial melting of an iron-poor material.

Flow differentiation was locally effective on a small scale (schlieren and mafic-layered tonalite); it is also one of several possible explanations for the K_2O and SiO_2 enrichment in the GBT, as explained later in this chapter. Otherwise, flow-dependent sorting of crystals from melt failed to produce major modal or chemical variations. Certainly, the east-to-west variations in the PHbT, being apparently independent of flow patterns and contact geometry, would seem to require a different explanation.

High viscosity of the magma is the most obvious factor which could have restricted separation of crystals from melt. A high proportion of crystals in the magma, particularly a proportion sufficient to produce a mutually interfering meshwork of crystals, should have effectively curtailed gravitational separation and flow differentiation, except in local environments of high shear flow. Without better knowledge of the viscosity of the magma under various conditions, I cannot rule out the possibility of separation of crystals during earlier stages of crystallization.

(4) Vapor-phase Transfer of Components.

This process may have contributed to the higher K_2O and SiO_2 contents of the rocks and the more sodic compositions of plagioclase rims in

the west-central part of the pluton, particularly within the PHbT. The distribution both of joint-controlled biotite tonalite layers, which apparently formed by reaction of the host tonalite with silica- and potash-rich solutions, and of late-formed, coarse, highly poikilitic biotite locally disseminated through mafic inclusions as well as through the tonalite is consistent with this suggestion. So is the apparent compositional disequilibrium between K-feldspar and plagioclase rims and the textural evidence suggesting possible vapor-phase crystallization of K-feldspar. It is possible that the abrupt overgrowth relationships of the sodic rims on many plagioclase grains in this part of the pluton were also due to late introduction of Na_2O via a vapor phase; alternatively, these overgrowths may be attributable to a sudden decrease in pressure, assuming that the magma was saturated or nearly saturated in water at that stage of crystallization.

The presence of biotite tonalite layers, of thin sodic overgrowths on plagioclase, and of interstitial primary, volatile-bearing minerals interpreted as cavity fillings suggest that vapor-phase transfer may also have occurred in some parts of the SPT.

All of this evidence is only permissive; there is no concrete evidence of vapor-phase transfer as a major process. In fact, even in the SPT and PHbT, there is no evidence of the existence of a water-rich vapor phase prior to the latest stages of crystallization, whereas the SHbT was even drier. If operative at all, vapor-phase transfer of

components appears to have resulted in only small chemical variations.[29]

15.1.1 Origin of the SiO_2 and K_2O Enrichment in the Gneissose Border Rocks

Plutons are commonly zoned near their margins to more mafic, inclusion-rich rock. This type of zoning occurs to a minor degree around the northeastern and eastern margins of the PHbT, but a different and unusual type of zoning characterizes the gneissose outer margin of the SHbT. Despite a slightly greater abundance of mafic inclusions and a slightly darker appearance, the GBT is actually the most silicic and potassic phase of the tonalite[30] and is notably more leucocratic than the typical non-gneissose SHbT.

Four mechanisms can be proposed to explain the SiO_2 and K_2O enrichment in the GBT:

(1) bulk assimilation of wall rocks,

(2) selective assimilation of a silicic and potassic component derived from the wall rocks either by partial melting or by chemical exchange via a fluid phase,

(3) magmatic flow differentiation, producing a greater concentration of residual interstitial melt relative to suspended crystals in the zone of intense shear flow near the contact

---

[29] One may speculate that the very low K_2O contents of the tonalite are due to vapor-phase transfer of K_2O to higher levels now eroded away. Although this is possible, the lack of greater concentration of K_2O in the central and southern parts of the SPT, where evidence of lower pressure and exsolution of a vapor phase is greatest, argues against this suggestion.

[30] Possibly some of the tonalite in the southwestern part of the PHbT has comparable, but probably not higher, SiO_2 and K_2O contents.

with wall rocks, and

(4) late introduction of residual melt or magmatic fluids into the highly sheared gneissose rocks.

Figure 91 shows a two-end-member mixing model for calculating the range of possible compositions of a hypothetical component X which could be mixed with the average composition of the SHbT to produce the average composition in the GBT. Sample 807 from the eastern margin of the pluton has been omitted from the GBT average because it is intermediate both in textural characteristics and in modal and chemical composition between the typical non-gneissose SHbT and the other three analyzed GBT samples. Inclusion of 807 has little effect on the mixing model.

Possible compositions of component X obviously vary linearly as a function of the amount added, the smaller the amount, the more extreme the composition would have to be. Whatever the proportion added, the hypothetical component would have to have higher SiO_2 and K_2O contents, lower Al_2O_3, CaO, FeO_t, MgO, and TiO_2 contents, and comparable Na_2O contents relative to the SHbT. P_2O_5 and SrO contents would also have to be lower in the added component.

The dashed line labelled X(MgO = 0) in Figure 91 shows the composition of the most silicic material which could be added to the SHbT to produce the composition of the GBT without simultaneous subtraction of one or more other oxides, i.e., without a process of chemical exchange rather than simple addition of material. Thus, for addition of a component X with $SiO_2 > 78.7\%$, MgO would have to be

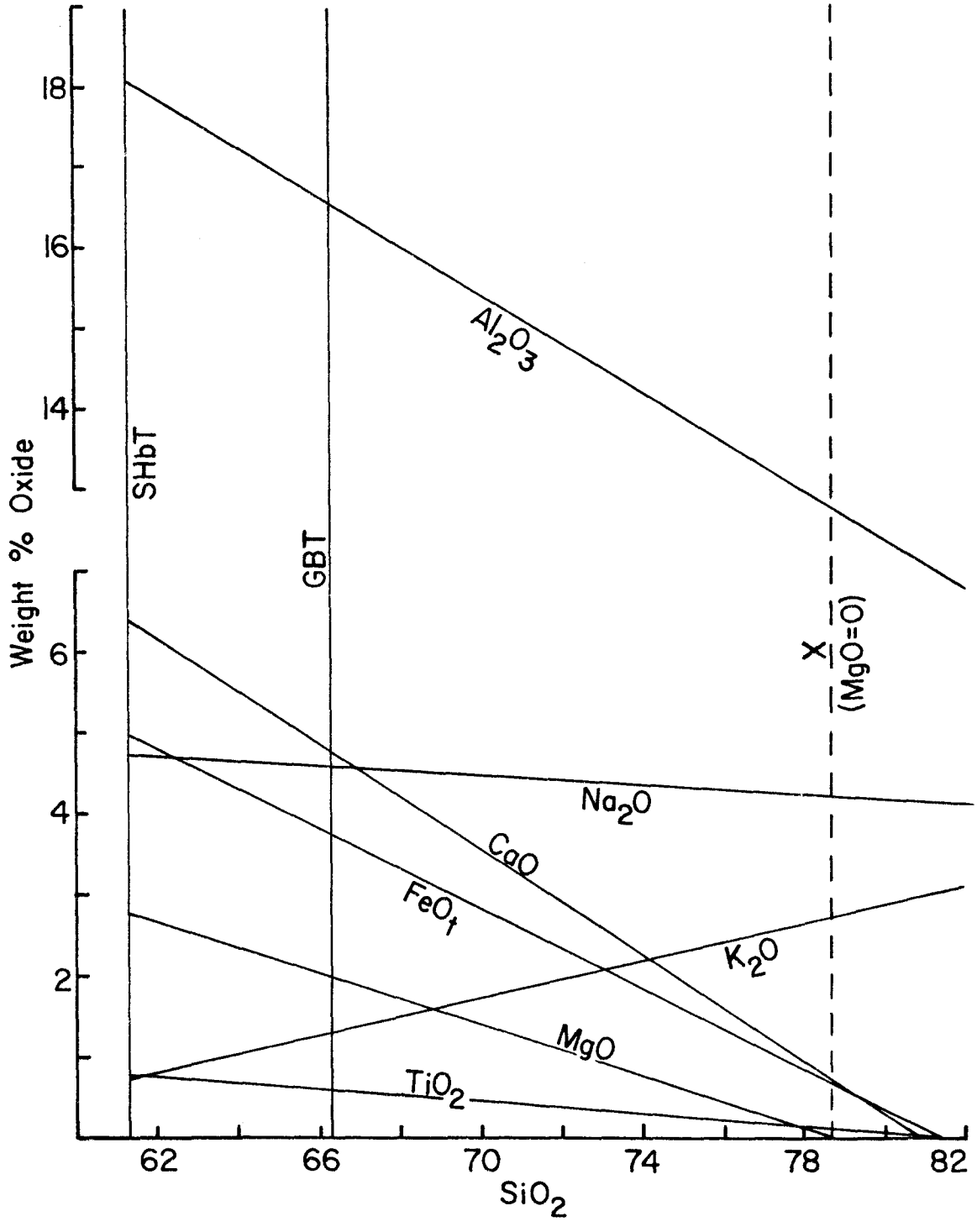

Figure 91. Hypothetical two-end-member mixing model to account for the more felsic composition of the gneissose border phase of the stubby hornblende tonalite.

simultaneously removed from the mixture, and for addition of component X with SiO_2 > 81%, FeO_t, CaO, and TiO_2 would also have to be removed. The composition represented by the line X(MgO = 0) is therefore the most felsic composition of any *melt* which could be added to the SHbT to alone produce the composition of the GBT, regardless of the source of the melt.

This extreme felsic "melt" and a second arbitrarily chosen composition corresponding to a mixture of 40% component X and 60% SHbT are compared in Table 28 with the compositions of four leucocratic granitic rocks from the batholith in southern Alta California and with the average alkali rhyolite + rhyolite-obsidian of Nockolds (1954). Both model compositions are characterized by high SiO_2, comparatively low K_2O, FeO_t, and MgO, and high $Na_2O/(Na_2O + K_2O + CaO)$ ratios. The extreme felsic "melt" is very similar to the two leucogranodiorites, whereas the 40% X composition is similar to the two leucogranites and the average alkali rhyolite, although the latter compositions are higher in K_2O and FeO_t. Obviously, the model compositions are not unreasonable for real melt or magma compositions.

The range of possible compositions indicated by the mixing model seems to rule out bulk assimilation of wall rocks; strata of appropriate leucocratic composition comprise an extremely minor part of the pre-batholithic section both immediately around the pluton and throughout this part of the peninsula. Field observations also rule out extensive assimilation.

Each of the other hypotheses is possible. However, hypothesis (4) seems least reasonable, because introduction of residual melt or

Table 28

Comparison of Two Possible Compositions of Component X
with Selected Natural Rocks and Average Rock Compositions

	40% X	LWLGd	ECLGd	X(MgO=0)	RLG	MRLG	ARRO
SiO_2	73.69	75.33	73.81	78.69	77.23	75.84	75.20
TiO_2	0.28	0.15	0.29	0.12	0.19	0.11	0.17
Al_2O_3	14.43	13.92	14.49	12.86	11.97	12.98	12.69
FeO_t	1.97	1.86	2.61	0.67	1.77	1.58	2.21
MgO	0.81	0.21	0.27	---	0.30	0.16	0.11
CaO	2.42	2.28	2.84	0.75	1.11	0.85	0.62
Na_2O	4.28	4.14	3.94	4.22	3.09	3.50	4.16
K_2O	2.13	2.03	1.75	2.69	4.33	4.98	4.77
P_2O_5	---	0.09	---	---	0.02	---	0.07
TOTAL	100.01	100.01	100.00	100.00	100.01	100.00	100.00

40% X: calculated composition of component X assuming 40% X and 60% SHbT
X(MgO=0): calculated composition of component X assuming no addition or removal of MgO
LWLGd: Lake Wohlford leucogranodiorite (Larsen, 1948)
ECLGd: Escondido Creek leucogranodiorite (Larsen, 1948)
RLG: Roblar leucogranite (Larsen, 1948)
MRLG: fine-grained leucogranite of Rubidoux Mountain (Larsen, 1948)
ARRO: average alkali rhyolite + rhyolite-obsidian (Nockolds, 1954)

magmatic fluids into solid or nearly solid rocks necessarily characterized by non-uniform fracturing and permeability would seem likely to result in considerable inhomogeneity, with abundant leucocratic segregations and dikes or veins, yet the GBT is remarkably homogeneous on a hand specimen, outcrop, and regional scale. Such homogeneity seems more consistent with chemical exchange or addition of material while the tonalite was still a relatively mobile magma.

As mentioned earlier, I have recognized no field or petrographic evidence of partial melting of the wall rocks. Thus, if assimilation of a partial melt from the wall rocks was responsible for the more felsic composition of the GBT, this assimilation apparently occurred at greater depths. Subsequent flow accompanying continued rise of the pluton might then have distributed the contaminating material uniformly through the outer part of the magma.

It is interesting that the marginal K_2O and SiO_2 enrichment is restricted to areas where the rocks are gneissose. Unfoliated rocks around the margins of the southern third of the pluton differ very little from their counterparts in the interior of the SPT. Possibly this correlation exists because the SHbT magma was hotter and more capable of partially melting the wall rocks, or because the intense flow and shearing in the GBT facilitated assimilation of melt or exchange with fluids from the wall rocks. Alternatively, if the SiO_2 and K_2O enrichment is genetically related to the intensity of shear flow, flow differentiation would seem to be a reasonable explanation. The range of possible compositions of component X, particularly the high SiO_2 contents and the relatively high Na_2O/K_2O

and Na_2O/CaO ratios, are consistent with the apparent trend of changing melt composition during crystallization of the SHbT.

In summary, flow-induced concentration of interstitial melt in the zone of intense shear flow around the outer margin of the SHbT can readily account for the observed compositional zoning. However, chemical interaction with the wall rocks either by assimilation of a partial melt or by chemical exchange via a fluid phase are reasonable alternative hypotheses. If assimilation of a partial melt from the wall rocks was the actual mechanism, assimilation apparently occurred prior to emplacement of the pluton to its present level relative to the wall rocks. Whatever the mechanism responsible for the zoning, its effects are recognizable only in the thin gneissose shell around the SHbT.

15.2 Estimation of Intensive Parameters During Emplacement and Crystallization

Two assemblages in the tonalite are particularly useful for estimating T, f_{O_2}, and, to a lesser degree of confidence, P_{H_2O}: (1) magnetite + hematite-ilmenite, and (2) biotite + magnetite + K-feldspar. The oxygen isotopic data reported by Taylor and Epstein (1962) and Taylor (1968) permit an independent estimate of temperature. Also, liquidus and solidus temperatures can be estimated by analogy with melting experiments on natural tonalites and granodiorites (Piwinskii, 1968a, 1973a, 1973b; Piwinskii and Wyllie, 1968). In contrast, P_{total} is extremely difficult to estimate; the best estimate arises from recognition that the magmas, at least the PHbT and SPT magmas, were saturated in volatiles during the latest stages of

crystallization, and from very rough estimation of f_{H_2O} and P_{H_2O} accompanying late-magmatic or high-temperature deuteric equilibration of the biotite + magnetite + K-feldspar assemblage. Unfortunately, this assemblage, as well as the Fe-Ti oxides and the oxygen isotopic data, record only the conditions of latest equilibration or some disequilibrium combination of these and earlier conditions. Conditions prevailing during the earlier history of the magma are difficult to estimate.

15.2.1 Liquidus and Solidus Temperatures of the Tonalite

Piwinskii (1968a) and Piwinskii and Wyllie (1968) carried out melting experiments on three natural tonalites and five granodiorites under conditions of excess water at 1-3 kb. Piwinskii (1973a, 1973b) extended the data to 10 kb on three of these rocks and presented data on three additional tonalites and quartz diorites up to 10 kb, again with excess water. The range of solidus temperatures for the tonalites and quartz diorites is: 765-795°C at 1 kb, 705-745°C at 2 kb, and 690-725°C at 3 kb, declining gradually to about 655-660°C at 10 kb. Solidus temperatures for the granodiorites are typically about 20-30° lower at 1 kb, but only 5-20° lower at higher pressures. Small differences in rock composition therefore have only a small influence on the solidus temperature. *Approximate* liquidus temperatures for the tonalites and quartz diorites are 950-990°C at 2-5 kb and decrease slightly to 925-950°C at 10 kb. For the granodiorites, the temperatures are about 930-950°C at 2-5 kb, decreasing to about 905°C at 10 kb for the one rock studied at these conditions.

Thus, if the San José magmas were initially saturated in H_2O, the liquidus temperature would apparently have been near 950-1000°C. However, the magmas probably were saturated only near the end of crystallization, and the liquidus temperature may well have been appreciably greater than 1000°C. Given the evidence for saturation in volatiles towards the end of crystallization, especially in the PHbT and SPT magmas, and the absence of evidence for appreciable concentrations of volatile components other than H_2O, a solidus temperature in the range 680-750°C seems likely. Structural and textural data indicate intrusion as crystal-rich magmas; hence the temperatures during emplacement were probably somewhere in the range 800-900°C, possibly slightly higher.

15.2.2 Application of Oxygen Isotope Geothermometry

Oxygen isotopic data obtained by Taylor and Epstein (1962) and Taylor (1968) for one sample (BC-I-12) from the interior of the San José pluton are given in Table 29. Assuming isotopic equilibrium, fractionation of ^{18}O and ^{16}O among the phases is an indicator of the temperature of equilibration and is effectively independent of pressure. The relationship of the plagioclase-magnetite fractionation to temperature (in °K) is given by the experimentally calibrated equation (Anderson et al., 1971)

$$\Delta_{Plag-Mt} = (4.72 - 1.19\beta)10^6\ T^{-2},$$

where $\Delta_{Plag-Mt} = 1000 \ln \alpha_{Plag-Mt}$, $\alpha_{Plag-Mt} = \frac{\delta_{Plag} + 1000}{\delta_{Mt} + 1000}$, and β is the mole fraction of anorthite in the feldspar. For sample

Table 29

Oxygen Isotopic Compositions for Sample BC-I-12

	$\delta^{18}O$ ‰*	Range of Values	Number of Analyses
quartz[a]	9.3	0.2	3
plagioclase[a]	7.6	0.0	2
hornblende[a]	6.2	0.3	3
biotite[a]	4.8	0.0	2
sphene[a]	5.9	---	1
whole rock (calculated)[a]	7.4	---	-
magnetite[b]	1.6	---	1

$$*\delta = \left[\frac{(^{18}O/^{16}O)_{sample}}{(^{18}O/^{16}O)_{standard}} - 1 \right] \times 1000$$

[a]from Taylor and Epstein (1962)

[b]from Taylor (1968)

following Taylor (1977, personal communication), all values were lowered by 0.4‰ from the previously reported values to make them directly comparable with post-1968 data.

BC-I-12, $\beta \approx 0.35$, giving T = 575°C.[31] Comparison with the estimated solidus temperature of 680-750°C clearly indicates that isotopic exchange continued during subsolidus cooling. This does not necessarily imply continued cation exchange down to this low temperature. Certainly the preservation of magmatic oscillatory zoning patterns in plagioclase precludes the possibility of significant subsolidus cation redistribution in this mineral, at least in the PHbT and SPT. As discussed later in this chapter, the biotite + magnetite + K-feldspar assemblage suggests final equilibration at higher, but possibly still subsolidus temperatures in the range 645-730°C or perhaps as much as 50° higher.

15.2.3 Conditions Indicated by the Fe-Ti Oxides and the Assemblage Biotite + Magnetite + K-Feldspar

In Section 12.7.1 I outlined the ranges of T-f_{O_2} conditions recorded by magnetite and by the hematite-ilmenite intergrowths and showed that magnetite and hematite-ilmenite were not in equilibrium. Magnetite equilibrated under T-f_{O_2} conditions approximating those of the MH buffer curve, whereas the hematite-ilmenite intergrowths imply crystallization and exsolution under earlier, slightly more reducing conditions between those of the NNO and MnO + Mn_3O_4 buffer

---

[31] Taylor (1968) reported 650°C for this mineral pair. Because accurate curves for the temperature dependence of fractionation between minerals had not yet been determined, his temperature estimates were based on an arbitrarily assumed equation for plagioclase-magnetite pair, which equation was chosen because it "gives 'reasonable' temperatures of formation for a variety of feldspar-magnetite pairs in igneous and metamorphic rocks" (p. 23). He considered that the actual temperature values are "not particularly meaningful", but that the relative temperatures for different rocks have significance. There is therefore no conflict between the two temperature estimates.

curves, but closer to the latter. Both sets of conditions are unusually oxidizing. Conditions became progressively more oxidizing as crystallization and cooling proceeded, but there is no evidence that conditions in the magma were ever substantially more reducing than those estimated for the hematite-ilmenite intergrowths.

The T-f_{O_2} conditions of equilibration of the assemblage biotite + magnetite + K-feldspar can be estimated more precisely. Wones and Eugster (1965) determined the compositions of biotite coexisting with magnetite + sanidine + vapor over a wide range of T and f_{O_2} at 1 kb and 2 kb pressure. As oxygen fugacity increases, biotite in equilibrium with magnetite and K-feldspar must become progressively less iron-rich because of the reaction

$$KFe_3AlSi_3O_{10}(OH)_2 \text{ (Annite)} + 1/2\ O_2 \rightleftharpoons KAlSi_3O_8 + Fe_3O_4 + H_2O.$$

For rocks in which magnetite coexists with hematite-ilmenite and with biotite + K-feldspar, intersection of the stability curves for the analyzed compositions of the biotite and magnetite closely defines T and f_{O_2} for a given f_{H_2O}.

Before continuing, it is important to consider whether or not the requirements of coexistence are met in the San José samples. Magnetite and hematite-ilmenite are not in equilibrium, but they are reasonably close. Textural observations show that biotite is more nearly in equilibrium with magnetite than with hematite-ilmenite. That is, hematite-ilmenite grains included in biotite are commonly corroded and often rimmed with sphene and/or rutile. In contrast, biotite rarely shows slight evidence of reaction with magnetite; microprobe checks revealed no chemical gradients in two biotite

crystals next to inclusions of magnetite.[32] In general, the chemical homogeneity of both minerals in all eight analyzed rocks argues strongly for equilibrium. The evidence therefore suggests that similar T-f_{O_2} conditions apply to both biotite and magnetite compositions. Modal and textural relationships are compatible with the assumption of equilibrium between biotite, magnetite, and K-feldspar in samples 3a, 30a, 46a, 62a, and possibly 36a, but SHbT samples 25a, 29, and 68 all contain only tiny amounts of K-feldspar which may not be in equilibrium with the other phases. Thus, for the latter three rocks and possibly for 36a as well, only maximum f_{O_2} estimates can be made, and the temperature estimates could be either too high or too low. Nevertheless, the similarity of biotite and magnetite compositions in these rocks to those in the other four samples suggests that all eight rocks record a relatively uniform set of physico-chemical conditions.

There are two ways to determine the T-f_{O_2} conditions of equilibration for the San José assemblages. The first approach, shown in Figure 93, involves graphical superposition of the stability curves determined by Wones and Eugster for biotites of various Fe/(Fe + Mg) ratios onto the field of possible T-f_{O_2} conditions estimated for magnetite in the samples (from Figure 74, pp. 428-429), followed by plotting of the appropriate compositional parameters of biotite and magnetite in each of the tonalite samples. This approach

---

[32]Slight gradients could exist within about 10 microns of the magnetite grains. Due to the extreme difference in hardness between the biotite and magnetite, the biotite immediately adjacent to magnetite polishes very poorly, precluding precise analysis.

ignores the oxidation state of the iron in both the experimental and natural biotites. However, because the method compares synthetic and natural biotites which formed under similar T-f_{O_2} conditions and which should therefore have similar Fe^{3+}/Fe^{2+} ratios, ignoring the oxidation state of iron should introduce little error.

This approach also assumes that components not present in the experimental system -- e.g., Ti, Mn, and excess Al (more than 1.0 atoms per formula unit) in biotite, V and Cr in magnetite, and Na, Ba, and Ca in K-feldspar -- do not appreciably affect the equilibrium Fe/(Fe + Mg) ratio of the biotite. Mueller (1972) summarized data showing that, in general, the distribution of Fe and Mg between biotite and coexisting ferromagnesian silicates (except garnet) in natural assemblages is nearly ideal and that the Fe/(Fe + Mg) ratios are affected very little by the presence of other components in the biotite. Ideality may not hold for biotites with very high Al contents. However, Al concentrations in the San José biotites (1.3-1.5 atoms per formula unit) are only slightly greater than the ideal concentration. These excesses are less than those in biotites from tonalites in southern Alta California (Larsen and Draisin, 1950, Table 2), which latter excesses Mueller (p. 306) considered to be relatively unimportant. Likewise, because the San José K-feldspar and magnetite are nearly pure (X_{Or} = 0.905-0.948 and $X_{Mt} \geq 0.98$), the assumption that minor impurities in these phases do not appreciably affect the Fe/(Fe + Mg) ratios of coexisting biotite seems reasonable.

The second approach involves estimation of the mole fraction of the Fe^{2+} end member ($X_{Annite} = X_1$)[33] in the biotites and calculation of T and f_{O_2} for an assumed f_{H_2O} by simultaneous solution of the equation for the MH buffer curve (corresponding to the T-f_{O_2} conditions implied by magnetite compositions in the tonalite) and the empirical equation obtained by Wones and Eugster (1965, p. 1249) and modified by Wones (1972, p. 317) relating the compositions of the synthetic biotites to T, f_{O_2}, and f_{H_2O}. The revised expression of Wones (1972) is

$$\log f_{H_2O} = \frac{7409}{T} + 4.25 + 1/2 \log f_{O_2} + 3 \log X - \log a_{Or} - \log a_{Mt}, \quad (1)$$

where X is as defined $X_1/3$. Wones and Eugster showed that the effects of total pressure (as opposed to P_{H_2O}) are negligible. The equation for the MH buffer curve is (Wones and Eugster, p. 30)

$$\log f_{O_2} = 14.41 - \frac{24912}{T} + 0.019 \frac{(P - 1)}{T}. \quad (2)$$

Again, the pressure term is negligible.[34] Because $a_{Mt} = 1$ along the

---

[33]The symbols used in the following discussion are adopted from Wones and Eugster (1965):

X_1 = mole fraction annite: $KFe_3^{2+}AlSi_3O_{10}(OH)_2$

X_2 = mole fraction phlogopite: $KMg_3AlSi_3O_{10}(OH)_2$

X_3 = mole fraction "oxybiotite" (hypothetical impossible end member): $KFe_3^{3+}AlSi_3O_{12}(H_{-1})$

$X = X_1/3$

[34]Including the pressure term raises the calculated temperatures by 3-4°C.

the MH buffer curve, combination of equations (1) and (2) yields

$$\log f_{H_2O} = -\frac{5047}{T} + 11.46 + 3 \log X - \log a_{Or}. \qquad (3)$$

X and a_{Or} can be determined approximately from the microprobe data so that T and f_{O_2} can be readily calculated for a given f_{H_2O}.

Equations (1) and (3) assume ideal behavior of biotite solid solutions; components not present in the synthetic biotites are assumed to behave as inert dilutants decreasing X_1 and X. As mentioned earlier, this assumption appears to be essentially valid for most natural biotites, but may break down for biotites containing very high Al contents (Mueller, 1972). Mueller also points out that high Fe^{3+} contents, which are most likely present in the San José biotites, may also introduce nonideality and may therefore lead to small errors in the calculated T and f_{O_2}. I have also assumed ideal solid solution for K-feldspar, so that $a_{Or} = X_{Or}$.

Lack of data on the oxidation state of iron in the biotite introduces a second, more serious uncertainty in the application of equations (1) and (3) in that X_1 and X must be estimated indirectly. The procedure for estimating X_1 is shown in Figure 92, along with a sample calculation. Biotite is constrained by the composition of coexisting magnetite to plot approximately along the dashed curve representing the compositions of all biotites buffered by the MH assemblages. However, the position of that curve is, in the words of Wones and Eugster (p. 1232), "little more than an 'educated guess'". Because of this uncertainty, I favor the T-f_{O_2} estimates obtained from the Fe/(Fe + Mg) ratios over those calculated from the equations.

Figure 92. Biotite compositional triangle illustrating the procedure for estimating the mole percent annite (X_1) from microprobe analyses. The diagram is modified from Figure 1 of Wones and Eugster (1965). The stippled area designates biotite compositions which are theoretically impossible. Open circles and the heavy hand-drawn line (MH) indicate estimated compositions of synthetic biotites buffered by the assemblage magnetite + hematite (from Table 4 of Wones and Eugster). Dashed lines bracket the range of $Fe/(Fe + Mg)$ and $X_1/(X_1 + X_3)$ ratios of biotite in the San José samples. For a given sample, the intersection of the MH curve with the appropriate line of constant $Fe/(Fe + Mg)$ defines the ratio $X_1/(X_1 + X_3)$. The latter, in combination with the measured ratio of Fe to total octahedral cations, i.e., $Fe/(Fe + Mg + Mn + Ti + Al^{VI})$, fixes X_1.

Example of calculation of X_1 (sample 46a):

From the microprobe analysis:

$$Fe/(Fe + Mg) = 0.424$$

$$Fe/(Fe + Mg + Mn + Ti + Al^{VI}) = 0.367$$

From the intersection of the MH curve and the 0.424 line:

$$X_1/(X_1 + X_3) \approx 0.633$$

Therefore:

$$X_1 \approx 0.633 \cdot (0.367)$$

$$X_1 \approx 0.232$$

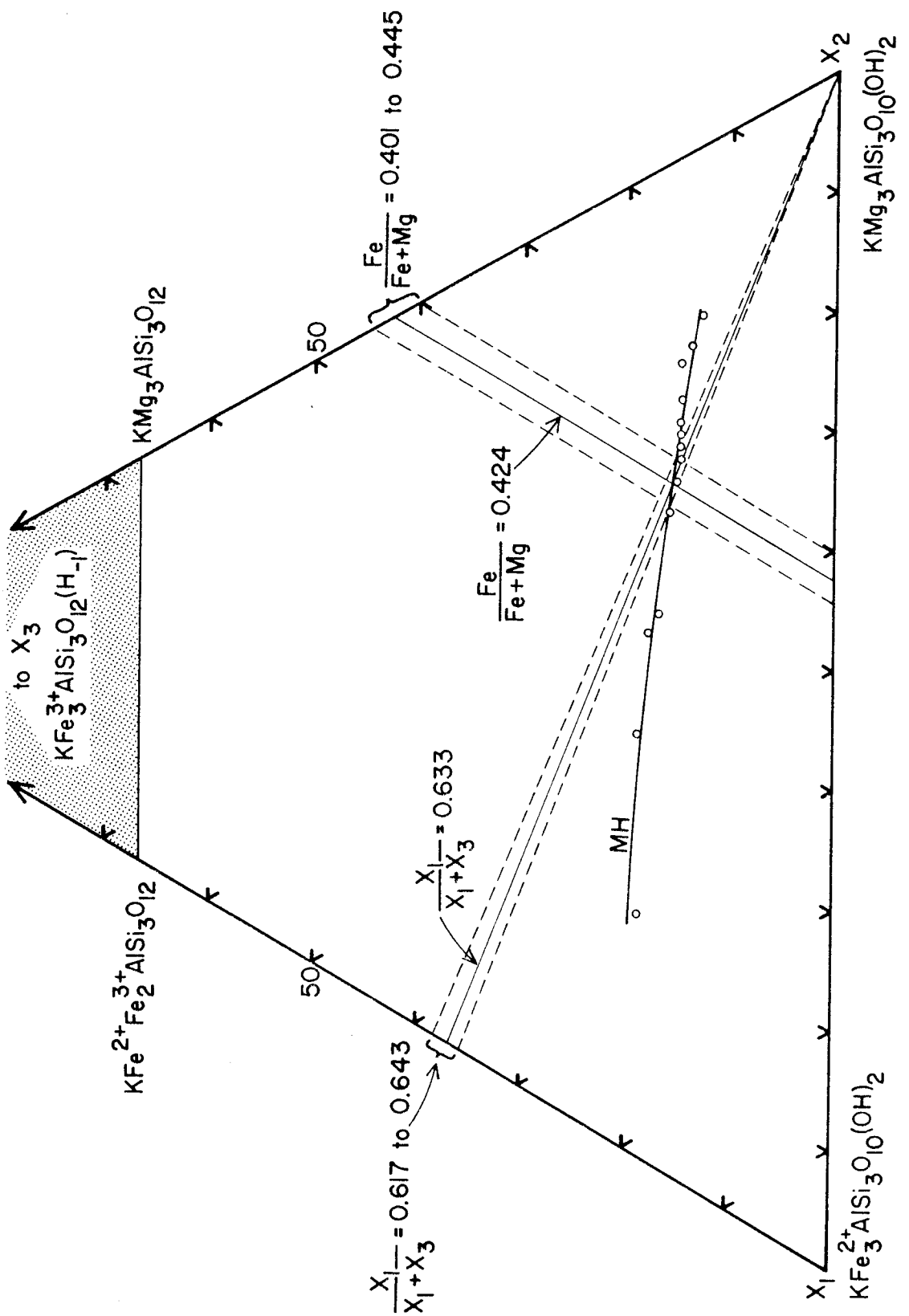
to X3
KFe3+3AlSi3O12(H-1)
KMg3AlSi3O12
KFe2+Fe2 3+AlSi3O12
X2
KMg3AlSi3O10(OH)2
X1
KFe2+3AlSi3O10(OH)2
50
50
Fe/(Fe+Mg) = 0.401 to 0.445
Fe/(Fe+Mg) = 0.424
X1/(X1+X3) = 0.633
X1/(X1+X3) = 0.617 to 0.643
MH

Figure 93. Fe/(Fe + Mg) ratios as a function of T and f_{O_2} for biotite in equilibrium with magnetite + sanidine + vapor at P_{H_2O} = 1035 bars and 2070 bars and corresponding T-f_{O_2} conditions (heavily stippled areas) implied by this assemblage in the San José pluton. The biotite compositional data are from Wones and Eugster (1965); biotite with a given Fe/(Fe + Mg) ratio is stable below the line designated by that ratio. The lightly stippled areas (taken from Figure 74, pp. 428-429) delimit the range of T-f_{O_2} conditions compatible with the composition of magnetite in the San José pluton. Heavy solid lines are the magnetite + hematite (MH), MnO-Mn_3O_4, and nickel + nickel oxide (NNO) buffer curves.

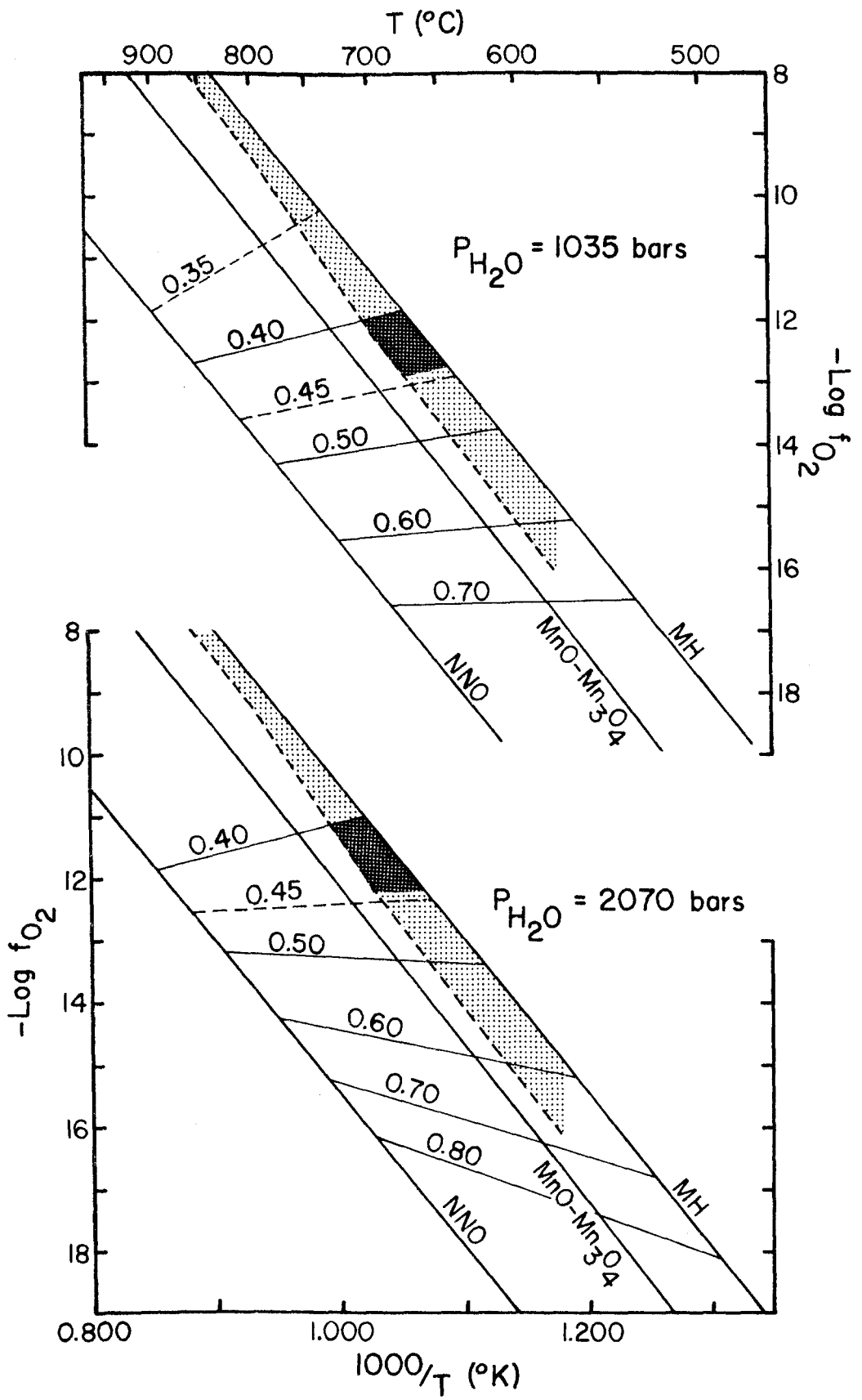
T (°C)
900
800
700
600
500
8
10
12
14
16
18
-Log f_{O_2}
P_{H_2O} = 1035 bars
0.35
0.40
0.45
0.50
0.60
0.70
NNO
MnO-Mn_3O_4
MH
P_{H_2O} = 2070 bars
0.40
0.45
0.50
0.60
0.70
0.80
NNO
MnO-Mn_3O_4
MH
0.800
1.000
1.200
1000/T (°K)

Table 30

Important Compositional Parameters in the Assemblage
Biotite - Magnetite + K-Feldspar

	Biotite			Magnetite		K-feldspar
	$Fe/(Fe+Mg)$	$Fe/Sum(Y)$[a]	X_1	X_{Mt}	$X_{Mt}/(X_{Mt}+X_{Usp})$	X_{Or}
Ba-JM-3a	0.417	0.359	0.225	0.986	0.998	0.930
Ba-JM-25a[b]	0.422	0.361	0.227	0.980	0.996	0.920[c]
Ba-JM-29[b]	0.445	0.377	0.242	0.984	0.998	0.920[c]
Ba-JM-30a	0.424	0.359	0.227	0.988	0.999	0.905
Ba-JM-36a[b]	0.401	0.348	0.215	0.989	0.999	0.933
Ba-JM-46a	0.424	0.367	0.232	0.984	0.996	0.907
Ba-JM-62a	0.404	0.356	0.221	0.982	0.998	0.948
Ba-JM-68[b]	0.425	0.361	0.229	0.984	0.998	0.920[c]

[a] $Sum(Y)$ = sum of octahedral cations: Fe, Mn, Mg, Ti, and Al^{VI}.

[b] Sample contains very little K-feldspar which may not be in equilibrium with biotite and magnetite. Estimated f_{O_2} conditions are therefore maximum values.

[c] Assumed value; no analysis available.

Table 31

Estimated T-f_{O_2} Conditions for the Assemblage Biotite + Magnetite + K-Feldspar

T is in °C, log f_{O_2} in bars

	Graphical Solutions								Calculated Solutions			
	P_{H_2O} = 1035 bars				P_{H_2O} = 2070 bars				f_{H_2O} = 760 bars[b]		f_{H_2O} = 1400 bars[b]	
	for X_{Mt}		for $X_{Mt}/(X_{Mt}+X_{Usp})$		for X_{Mt}		for $X_{Mt}/(X_{Mt}+X_{Usp})$		for X_{Mt} = 1.0		for X_{Mt} = 1.0	
	T	log f_{O_2}	T	log f_{O_2}	T	log f_{O_2}	T	log f_{O_2}	T	log f_{O_2}	T	log f_{O_2}
Ba-JM-3a	685	-12.3	668	-12.2	712	-11.5	691	-11.4	691	-11.4	742	-10.1
Ba-JM-25a[a]	690	-12.5	662	-12.3	716	-11.7	689	-11.6	688	-11.5	739	-10.2
Ba-JM-29[a]	667	-12.9	645	-12.8	690	-12.2	665	-12.2	673	-11.9	722	-10.6
Ba-JM-30a	675	-12.5	657	-12.4	700	-11.7	681	-11.7	687	-11.5	737	-10.3
Ba-JM-36a[a]	691	-12.0	675	-11.9	721	-11.1	707	-11.0	702	-11.1	754	- 9.8
Ba-JM-46a	681	-12.5	662	-12.4	706	-11.7	688	-11.7	682	-11.7	732	-10.4
Ba-JM-62a	700	-12.1	673	-12.0	729	-11.2	704	-11.1	697	-11.3	749	-10.0
Ba-JM-68[a]	685	-12.5	660	-12.4	706	-11.7	683	-11.7	686	-11.6	737	-10.3

[a] Sample contains very little K-feldspar which may not be in equilibrium with biotite and magnetite. Estimated f_{O_2} conditions are therefore maximum values.

[b] f_{H_2O} = 760 and 1400 bars corresponds to P_{H_2O} = 1000 and 2100 bars respectively at 700 °C (Burnham et al., 1969).

An additional uncertainty common to both approaches arises from the difference in structural state of the K-feldspar in the experiments (high sanidine) and in the San José samples (initially sanidine and possibly orthoclase). I will discuss the effect of variable structural state after presenting the results.

Consider the first approach. In Figure 93 the Fe/(Fe + Mg) ratios as a function of T and f_{O_2} for synthetic biotites in equilibrium with magnetite + sanidine + gas at P_{H_2O} = 1 kb and 2 kb have been superimposed on the buffer curves and on the field (lightly stippled) of T-f_{O_2} conditions compatible with the compositions of magnetite in the tonalite (from Figure 74). An upper temperature limit (800°C) has been placed on the possible T-f_{O_2} conditions of equilibration of magnetite in this assemblage based upon the maximum reasonable solidus temperature of the tonalite. That is, because textures indicate crystallization of K-feldspar from the last bit of melt remaining and/or from a late interstitial vapor phase, magnetite and biotite could not have been in equilibrium with K-feldspar at conditions significantly above the solidus. The lower temperature limit (575°C) is based upon the plagioclase-magnetite oxygen isotopic fractionation. Magnetite could not have equilibrated below this temperature. In fact, as mentioned earlier, oxygen isotopic exchange may well have continued to lower temperatures than did major cation exchange, so the lower T and f_{O_2} limits on the lightly stippled field are likely to be excessively low.

Plotted on Figure 93, the relevant compositional parameters for the eight tonalite samples (Table 30) define a very restricted range

of T-f_{O_2} conditions (heavily shaded area) at each pressure. The precise T and f_{O_2} estimates are tabulated under "Graphical Solutions" in Table 31. Conditions were estimated for two possible choices of the magnetite compositional parameter, that is, X_{Mt}, or $X_{Mt}/(X_{Mt} + X_{Usp})$. The latter parameter is the one which Buddington and Lindsley considered appropriate. Regardless of which parameter is used, all eight samples fall within the range T = 645-700°C and $f_{H_2O} = 10^{-11.9}$-$10^{-12.9}$ bars for P_{H_2O} = 1035 bars, or T = 665-729°C and $f_{H_2O} = 10^{-11.0}$-$10^{-12.2}$ bars for P_{H_2O} = 2070 bars.

Temperatures and oxygen fugacities calculated from equation (3) are slightly higher: T = 673-702°C and $f_{H_2O} = 10^{-11.1}$-$10^{-11.9}$ bars at f_{H_2O} = 760 bars ($P_{H_2O} \approx$ 1000 bars), or T = 722-754°C and $f_{H_2O} = 10^{-9.8}$-$10^{-10.6}$ bars at f_{H_2O} = 1400 bars ($P_{H_2O} \approx$ 2100 bars). However, as explained earlier, I place less confidence in these values than in those obtained by the graphical approach, because the calculated values are based on necessarily rough estimates of the Fe^{3+}/Fe^{2+} ratios in the biotites.

Because the uncertainty in the microprobe analyses for Fe and Mg is about ±2% of the amount present, corresponding to ±0.01 in the Fe/(Fe + Mg) ratio and to about ±10° and ±0.2-0.3 in log f_{O_2}, error in the microprobe analyses is relatively unimportant. However, examination of the experimental data indicates that the uncertainty in the positions of the biotite stability curves is probably about ±50°C and ±1-1.5 in log f_{O_2}. In addition, the effect of crystallization of sanidine in the San José samples as opposed to high sanidine in the experimental system should be to raise the stability limits of the

biotites, possibly by as much as 50° and 1-1.5 in log f_{O_2} as discussed in the following paragraphs. Consequently it is not possible to distinguish definitively between equilibration at solidus or slightly subsolidus conditions. Equilibration clearly did not continue to nearly as low a temperature as did oxygen isotopic exchange between magnetite and plagioclase (575°C); at that temperature the equilibrium Fe/(Fe + Mg) ratios would fall between 0.62-0.75 at either pressure.

I have referred several times to the importance of the structural state of K-feldspar. K-feldspar in the tonalite is generally untwinned, with $2V_\alpha$ varying from 5-10° up to about 50°. Based upon Figure 28 in Deer et al. (1963, vol. 4), these properties, together with the very high Or content, indicate a present range in structural state from sanidine to orthoclase. Some grid-twinned microcline was seen in samples 30a and 46a, but not in the other six samples. The feldspar apparently crystallized as sanidine and perhaps locally as orthoclase -- but not as high sanidine -- and has inverted to varying degrees to a more ordered state.

It is not possible to evaluate exactly the effect this difference in structural state would have on the biotite stability curves, but an estimate can be made from the thermodynamic considerations. As before, I have assumed that biotite solid solutions behave ideally. For the reaction

$$KFe_3^{2+}AlSi_3O_{10}(OH)_2 + 1/2\ O_2 \rightleftharpoons KAlSi_3O_8 + Fe_3O_4 + H_2O,$$

the equilibrium constant K is given by

$$K = \frac{a_{Or}\ a_{Mt}\ f_{H_2O}}{X^3\ (f_{O_2})^{1/2}}. \qquad (4)$$

Because $\Delta G_r^o = -2.303\ RT \log K$, therefore

$$\Delta G_r^o = -2.303\ RT\ (\log a_{Or} + \log a_{Mt} + \log f_{H_2O} - 3 \log x - 1/2 \log f_{O_2}). \quad (5)$$

Solving for $\log f_{H_2O}$ gives

$$\log f_{H_2O} = \frac{-\Delta G_r^o}{2.303\ RT} + 1/2 \log f_{O_2} + 3 \log X - \log a_{Or} - \log a_{Mt}. \quad (5a)$$

Comparison with the empirical equation (1) of Wones (1972) shows that

$$\frac{-\Delta G_r^o}{2.303\ RT} = \frac{7409}{T} + 4.25. \quad (6)$$

Substituting R = 1.99 cal/mole-deg and rearranging gives

$$\Delta G_r^o = -33955 - 19.478\ T. \quad (6a)$$

Equations (6) and (6a) apply to the actual experimental system involving high sanidine. To account for the different feldspar structural states, it is necessary only to add in the free energy change for the transition from high sanidine to the polymorph in question, i.e.,

$$\Delta G_r^o = -33955 - 19.478\ T + G^o\ (\text{polymorph}) - G^o\ (\text{high sanidine}) \quad (7)$$

Substitution of the values obtained from equation (7) into equation (5a) allows calculation of the biotite compositions which would have been produced in the experiments if the feldspar had crystallized in a different structural state. Unfortunately, high-temperature thermodynamic data are available only for high sanidine, microcline, and adularia. The relevant data are given in Table 32, along with the calculated biotite compositions for assemblages equilibrated along the

Table 32

Thermodynamic Properties of K-Feldspar Polymorphs and Calculated Compositions of Biotite in Equilibrium with the Assemblage K-Feldspar Polymorph + Magnetite + Vapor at P_{H_2O} = 2100 bars and T-f_{O_2} Conditions of the MH Buffer Curve

Data from Robie and Waldbaum (1968)
T is in °K, $\bar{V}$ in cc/mole, and G^o in cal/mole

	$\bar{V}_{298,1\ atm}$	$G^o_{T,1\ atm}$			$\Delta\bar{V}(P-1)$		
		900°	1000°	1100°	900°	1000°	1100°
High Sanidine	109.05	-786280	-768733	-750182	0	0	0
Microcline	108.72	-784144	-766150	-747152	-17	-17	-17
Adularia	108.29	-786047	-768405	-749759	-39	-39	-39

	$\Delta G^o_{T,2100\ atm}$ (polymorph - high sanidine)[a]			X_1			Fe/(Fe + Mg)[b]		
	900°	1000°	1100°	900°	1000°	1100°	900°	1000°	1100°
High Sanidine	0	0	0	0.35	0.24	0.18	0.52	0.39	0.33
Microcline	2119	2566	3013	0.52	0.38	0.29	0.71	0.55	0.45
Adularia	194	289	384	0.36	0.26	0.19	0.53	0.41	0.34

[a] $\Delta G^o_{T,2100\ atm} = \Delta G^o_{T,1\ atm} + \Delta\bar{V}(P-1)$. $\Delta\bar{V}$ is assumed to be constant and equal to $\Delta\bar{V}_{298,1\ atm}$.

[b] Determined from Table 4 of Wones and Eugster (1965) using the calculated value of X_1.

MH buffer curve ($a_{Mt} = 1$) at 623, 723, and 823°C and $P_{H_2O} = 2100$ bars. For adularia, the experimental biotite stability curves would be essentially unchanged. Indeed, the free energy differences between adularia and high sanidine under these conditions are less than the uncertainty in the values of $G^{o}_{f,298}$ (about 1000 cal/mole). However, if microcline had crystallized, the stability limits of biotites of given Fe/(Fe + Mg) ratios would have risen by about 100-170°C and 2-4 orders of magnitude in f_{O_2}. Thus the structural state of the feldspar is an extremely important variable whose influence is only roughly known. Since most or all of the K-feldspar in the tonalite crystallized as sanidine, the estimated T and f_{O_2} conditions given in Table 31 may be slightly low, but probably by no more than 50°.

In summary, the assemblage biotite + magnetite + K-feldspar apparently equilibrated at solidus or possibly slightly subsolidus temperatures in the range 650-750°C, or possibly as much as 50° higher. Prevailing oxygen fugacities were unusually high for these temperatures, approximating those of the MH buffer curve in the range 10^{-10}-10^{-13} bars, or possibly as much as 1-1.5 orders of magnitude higher. Much of the range in estimated T and f_{O_2} arises from uncertainties in the estimation procedures; actual variations in conditions throughout the pluton were apparently very limited. The estimates assume water pressures of 1-2 kb, which are reasonable on the basis of geologic evidence. A crude direct estimate of the water pressure prevailing at or just below the solidus will be made in the next section.

15.2.4 Crude Estimation of P_{H_2O} and the Depth of Emplacement

In the last section the biotite + magnetite + K-feldspar assemblage was used to estimate T and f_{O_2} conditions at assumed values of P_{H_2O} and f_{H_2O}. The procedure can also be reversed, and equation (1) can be used to calculate limits on possible values of the latter parameters (assuming ideal mixing in the vapor phase) for the maximum range of T and f_{O_2} compatible with this assemblage in the tonalite. In Figure 94, values calculated for sample 46a are plotted for a range of temperatures and oxygen fugacities corresponding to the MH buffer curve ($a_{Mt} = 1$) and to the estimated stability curve for $Mt_{98}Usp_2$ ($a_{Mt} = 0.98$). The results are exceedingly sensitive to the assumed T and f_{O_2}; the apparent sensitivity to a_{Mt} is an indirect effect arising entirely from the dependence of f_{O_2} estimates on magnetite composition rather than from the log a_{Mt} term in the equation. The results also depend greatly on the assumed structural state of the K-feldspar. The curves shown apply to assemblages containing high sanidine; for microcline the calculated curves drop considerably. For example, at T = 727°C and $a_{Mt} = 1$, f_{H_2O} = 1300 bars for high sanidine, but only 355 bars for microcline. The curves in Figure 94 would therefore be displaced towards slightly lower water pressures if corrected for the actual structural state of the K-feldspar.

A variety of arguments suggest that P_{H_2O} during equilibration of this assemblage was almost certainly somewhere in the range 500-3500 bars, and most likely within the limits 1000-2300 bars. As mentioned earlier, the assemblage could not have equilibrated at temperatures

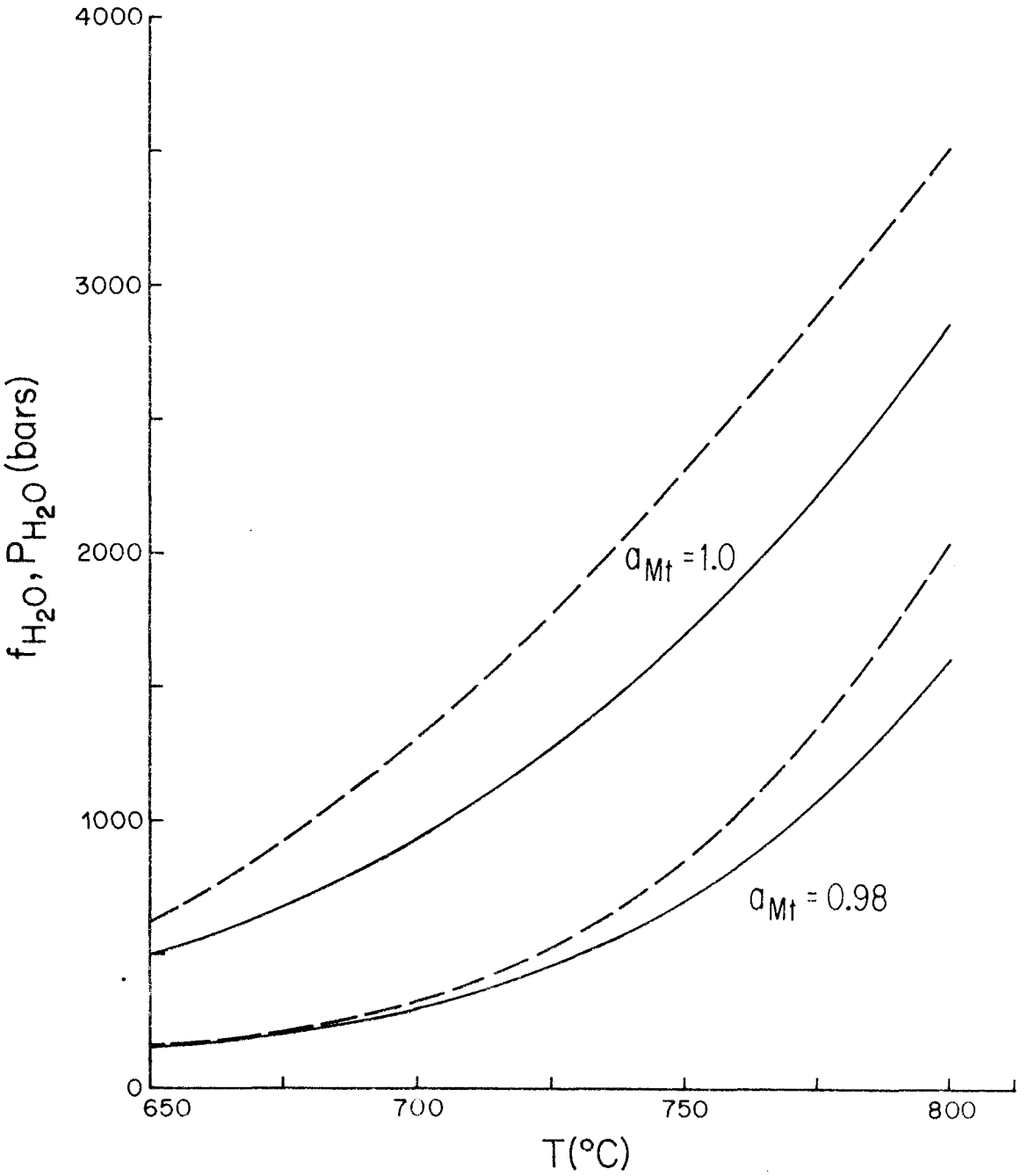

Figure 94. Calculated values of f_{H_2O} (solid curves) and P_{H_2O} (dashed curves as a function of temperature for the assemblage biotite + magnetite + sanidine + vapor in sample Ba-JM-46a. Values are calculated for $a_{Mt} = 1.0$ and $a_{Mt} = 0.98$, corresponding to the two extreme possible choices of the magnetite compositional parameter. Values of P_{H_2O} are interpolated from Table 5 of Burnham et al. (1969) assuming ideal mixing in the vapor phase.

significantly above the solidus, because K-feldspar was not stable. The extreme upper limit, P_{H_2O} = 3500 bars, corresponds to equilibration at the maximum reasonable solidus temperature, 800°C. The more likely upper limit of 2300 bars corresponds to equilibration at the more probable maximum solidus temperature of 750°C. The extreme lower limit corresponds to the approximate minimum P_{H_2O} (500-600 bars) at which biotite is stable at or above the solidi of all of the tonalites studied experimentally by Piwinskii (1968a, 1973a, 1973b) and Piwinskii and Wyllie (1968). The more probable minimum P_{H_2O} (1000 bars) is based on an assumed depth of emplacement $\geq$ 3-4 km for the rocks at the present level of exposure, together with the evidence for the presence of a water-rich vapor phase at the close of magmatic crystallization.

Unfortunately, geologic evidence for the depth of emplacement is very limited. The original thickness of the country-rock cover over the pluton cannot be estimated because of a lack of sufficient data on the stratigraphic thickness of the Alisitos formation in the San José area and because the strata are steeply dipping and were deformed and possibly eroded prior to emplacement. The presence of andalusite at locality 850 (area D-11; 730 m northeast of the pluton contact) indicates a maximum pressure below that of the kyanite-sillimanite-andalusite triple point, but estimates of the P-T position of this triple point vary widely. Recent reconstructions of the phase diagram by Richardson et al. (1969) and Holdaway (1971) place it at 5.5 kb (about 17-20 km) and 3.76 kb (about 12-14 km) respectively, whereas other workers have suggested even higher pressures. Obviously, the

presence of andalusite does not define the maximum depth of metamorphism very precisely. Regional metamorphic grade outside the contact aureole of the pluton is very low to the west and northwest and drops locally to the conditions of the low greenschist facies 2-6 km east of the pluton as well. In general, there is a lack of evidence for deep burial.

Consideration of the probable pre-erosion geometry of the pluton provides an additional conceptual argument for the minimum likely depth of emplacement. The exposed outline of the body is 16 km long and 10 km wide; contacts are steep and generally smoothly dipping, and there is little or no petrographic or chemical variation as a function of elevation over the exposed vertical range of 630 m. The pattern of flow structures is remarkably regular and generally steeply dipping throughout most of the pluton. Except perhaps at the southern end, there is no structural evidence for proximity to the roof. Similarly, except for the widespread, very minor occurrence in the SPT of small interstitial patches of chlorite, zeolites, or other minerals which may be subsolidus fillings of tiny vapor cavities, there is no petrographic evidence of shallow emplacement, i.e., no macroscopic miarolitic cavities, finer-grained groundmass, or notable decrease in grain size near contacts (except for the slightly finer grain size of the gneissose rocks). All of these structural and petrographic observations seem incompatible with a hypothetical reconstruction placing the ground surface at the time of intrusion significantly <1500 m above the present level of exposure. Even a depth of 3-4 km requires an abrupt change in the upward-projected

geometry of the pluton, that is, a very flat roof.

In summary, the biotite + magnetite + K-feldspar assemblage in sample 46a apparently equilibrated at water pressures most likely in the range 1000-2300 bars, but conceivably as low as 500 bars or as high as 3500 bars. Assuming $P_{H_2O} \approx P_{total}$, the depth of emplacement at locality 46 in the west-central part of the pluton was probably somewhere in the range 3-9 km, but possibly as shallow as 1.5-2 km or as deep as 12-14 km. The southern end of the pluton may have risen to a slightly shallower level than the northern end.

Chapter 16

CONSIDERATIONS ON THE ORIGIN OF THE MAGMA

Any model offering a potential source area and mechanism for producing the tonalite magma must satisfy an extensive, reasonably well-defined set of conditions. First of all, it must be able to account for the generation of two or three successive pulses of nearly identical, homogeneous magmas rising through the same conduit, without accompanying emplacement of magmas of different character. Secondly, the model must be consistent with the low $^{87}Sr/^{86}Sr$ initial and Pb isotopic ratios; the high normative plagioclase content, particularly the high Na_2O; the very low K_2O content, hence high Na_2O/K_2O ratio; the very low U, Th, Rb, and rare earth element contents and high Sr content and K/Rb ratio; the low FeO_t content; and the low $FeO/(FeO + Fe_2O_3)$ ratio.

The relatively unradiogenic $^{87}Sr/^{86}Sr$ initial and Pb isotopic ratios and low K, Rb, U, Th, and rare earth element concentrations almost certainly rule out significant contribution either from older sialic crust or from sediment derived from such crust. Assuming that K, Rb, U, and Th all partition largely or entirely into the melt during partial fusion, and assuming about 50% melting, the source material apparently contained at most about 0.40% K_2O, 6 ppm Rb, 0.2 ppm U, and 0.6 ppm Th. For 25% melting, the apparent limits are half of the above values.

Possibly, the high Na_2O and normative plagioclase contents are indicative of a source material rich in modal or normative plagioclase of intermediate composition. Such a source could account in turn for the high Sr concentrations. However, these high contents could also be

attributed either to partial melting of a less plagioclase-rich source material under conditions at which plagioclase is unstable or largely disappears after small or moderate degrees of partial melting, or to gravitational accumulation of relatively sodic plagioclase in the magma, although the latter process seems unlikely to have given rise to such uniform whole-rock compositions and modal plagioclase contents throughout the pluton.

Likewise, the low $FeO/(FeO + Fe_2O_3)$ ratio in the tonalite may be evidence of derivation from a relatively oxidized source material -- e.g., from subducted or deeply buried volcanic rocks which were oxidized by exposure to the atmosphere and hydrosphere. Alternatively, interaction of an initially reduced magma with water derived from the wall rocks during emplacement might also account for the high oxidation state. The latter suggestion is consistent with the evidence for increasingly oxidizing conditions as crystallization and cooling proceeded; although there is no indication, either from the Fe-Ti oxide assemblage or from the Fe/(Fe + Mg) ratios of hornblende and biotite, that the magma was ever as reduced as the three southern California tonalites in Table 27, conditions during the early history are uncertain. Assuming initially oxidizing conditions, the low FeO_t content of the tonalite may be attributed to early crystallization and settling of the Fe-Ti oxide minerals from the magma and/or to high concentrations of these phases in the residuum after partial melting. Again, partial melting of a Fe-poor source material is an alternative interpretation.

Figure 95 compares the Sr, K, and Rb concentrations of sample BC-I-12 with the range of concentrations in plutonic rocks from central

and northern Alta California (Kistler and Peterman, 1973). Also shown are the average concentrations in four types of basalt from oceanic, island arc, and continental margin regions as compiled by Hart et al. (1970). These plots reveal a striking difference between the San José tonalite, which plots along trends defined by the average oceanic and island arc and continental margin basalts, and nearly all of the granitic rocks from the Sierra Nevada batholith. Plots of data from the Peninsular Ranges batholith yield similar patterns; among the many Peninsular Ranges plutonic rocks analyzed by Early and Silver, only the San José tonalite and some gabbros plot along or near the trends defined by the average oceanic and volcanic arc basalts.

Five plutonic rocks from central and northern California also plot along the basalt trends. Three (square symbols) are quartz diorite or trondhjemite from the western Sierran foothills or Klamath Mountains; they have low initial $^{87}Sr/^{86}Sr$ ratios comparable to those of the San José tonalite. The other two (triangles) are a gabbro from the Lucia Range west of the San Andreas fault near the coast and a quartz-bearing monzodiorite from the Inyo Mountains east of the Sierra Nevada, both of which have high $^{87}Sr/^{86}Sr$ initials (0.708-0.709) and bear little resemblance to the San José tonalite.

The Sr, K, and Rb concentrations and ratios, like the initial Sr isotopic ratio, the Pb isotopic ratios, and the low U, Th, and rare earth element concentrations, suggest that the ultimate source of the tonalite was an upper mantle similar in composition to the oceanic upper mantle (or a lower crust with trace element and isotopic properties similar to the oceanic upper mantle). Five basic hypotheses

Figure 95. Sr-K, Rb-K, and Rb-Sr plots comparing the San José pluton with plutonic rocks from central and northern California and with average oceanic, island arc, and continental margin basalts.

⊕ SJP San José pluton

Central and northern California (Kistler and Peterman, 1973)

R_i = initial $^{87}Sr/^{86}Sr$ isotopic composition

□ R_i = 0.7030-0.7039

○ R_i = 0.7040-0.7049

● R_i = 0.7050-0.7059

△ R_i = $\geq$0.7060

The dashed-line envelopes are drawn to emphasize the ranges of concentrations characteristic of most analyzed plutonic rocks in the Sierra Nevada batholith. The solid lines labelled 200 to 700 in (B) are lines of constant K/Rb ratio.

Average oceanic and island arc basalts (Hart et al., 1970)

AB average oceanic alkali basalt

TB average oceanic and island arc tholeiitic basalt

■ LKT average of 8 low-potassium basalts from Japan, California, Hawaii, and Iceland

OFB average ocean floor (ridge) basalt

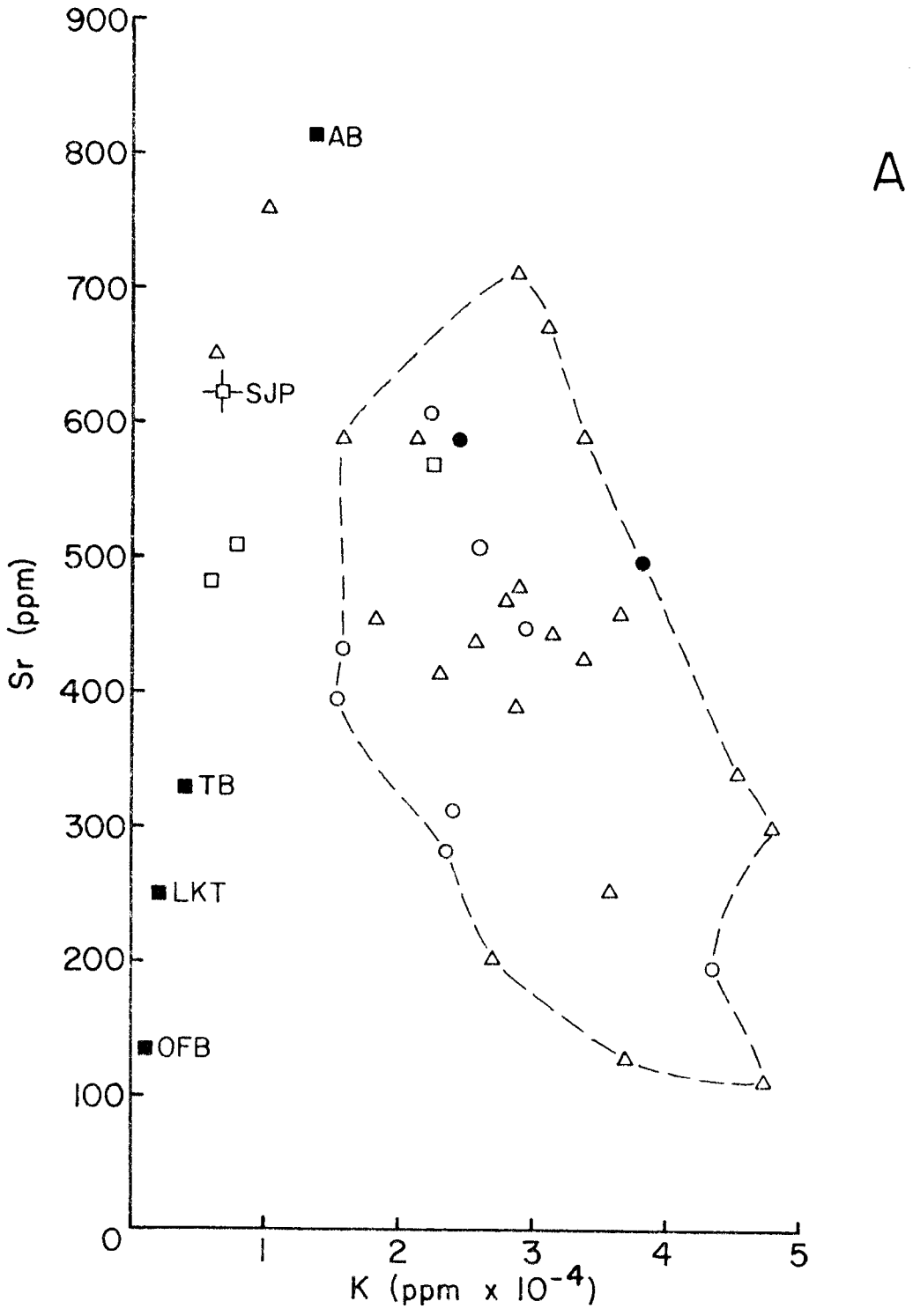
900
800
700
600
500
400
300
200
100
0
Sr (ppm)
AB
SJP
TB
LKT
OFB
1
2
3
4
5
K (ppm x 10⁻⁴)
A

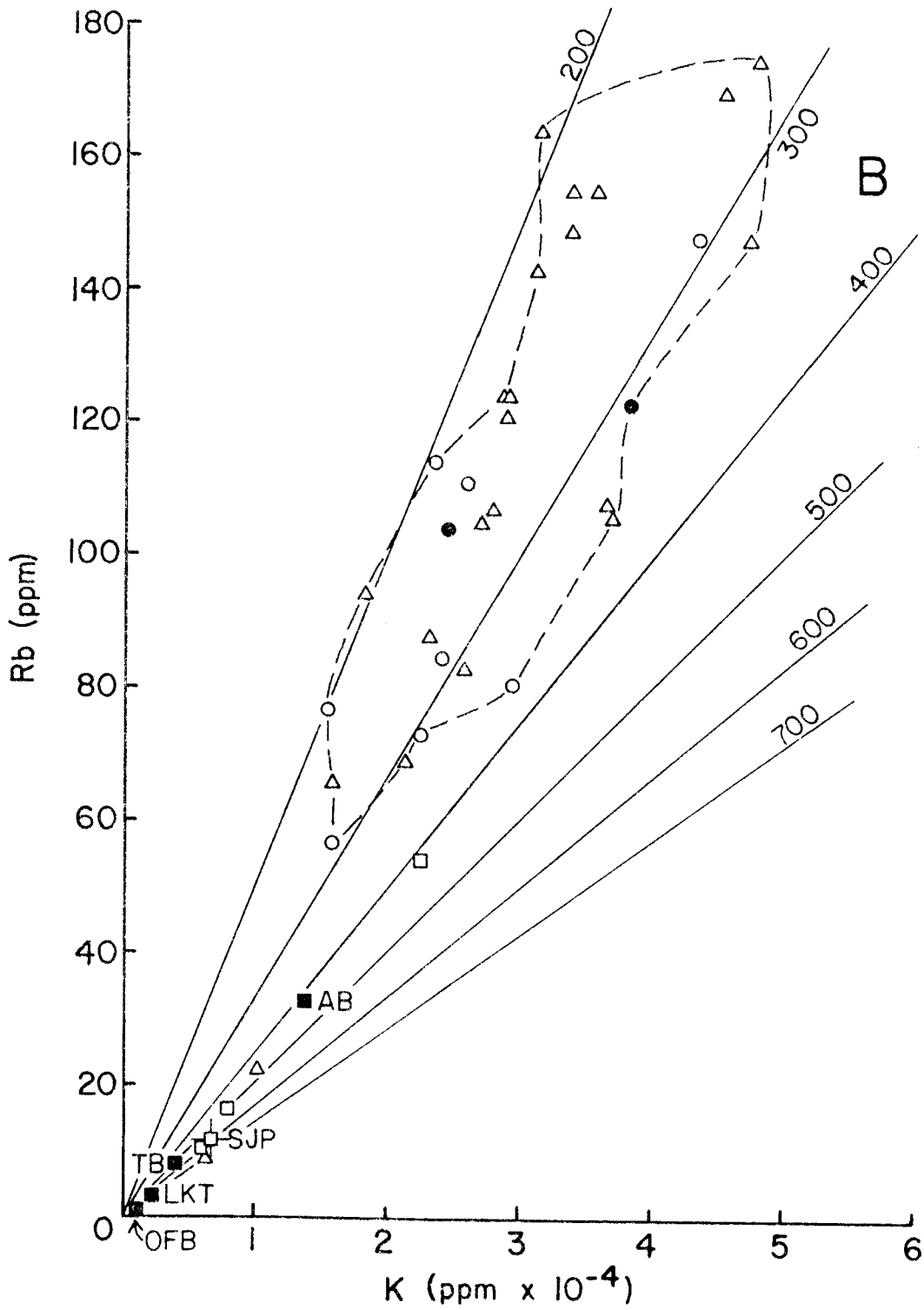
180
160
140
120
100
80
60
40
20
0
Rb (ppm)
200
300
400
500
600
700
B
AB
SJP
TB
LKT
OFB
1
2
3
4
5
6
K (ppm x 10⁻⁴)

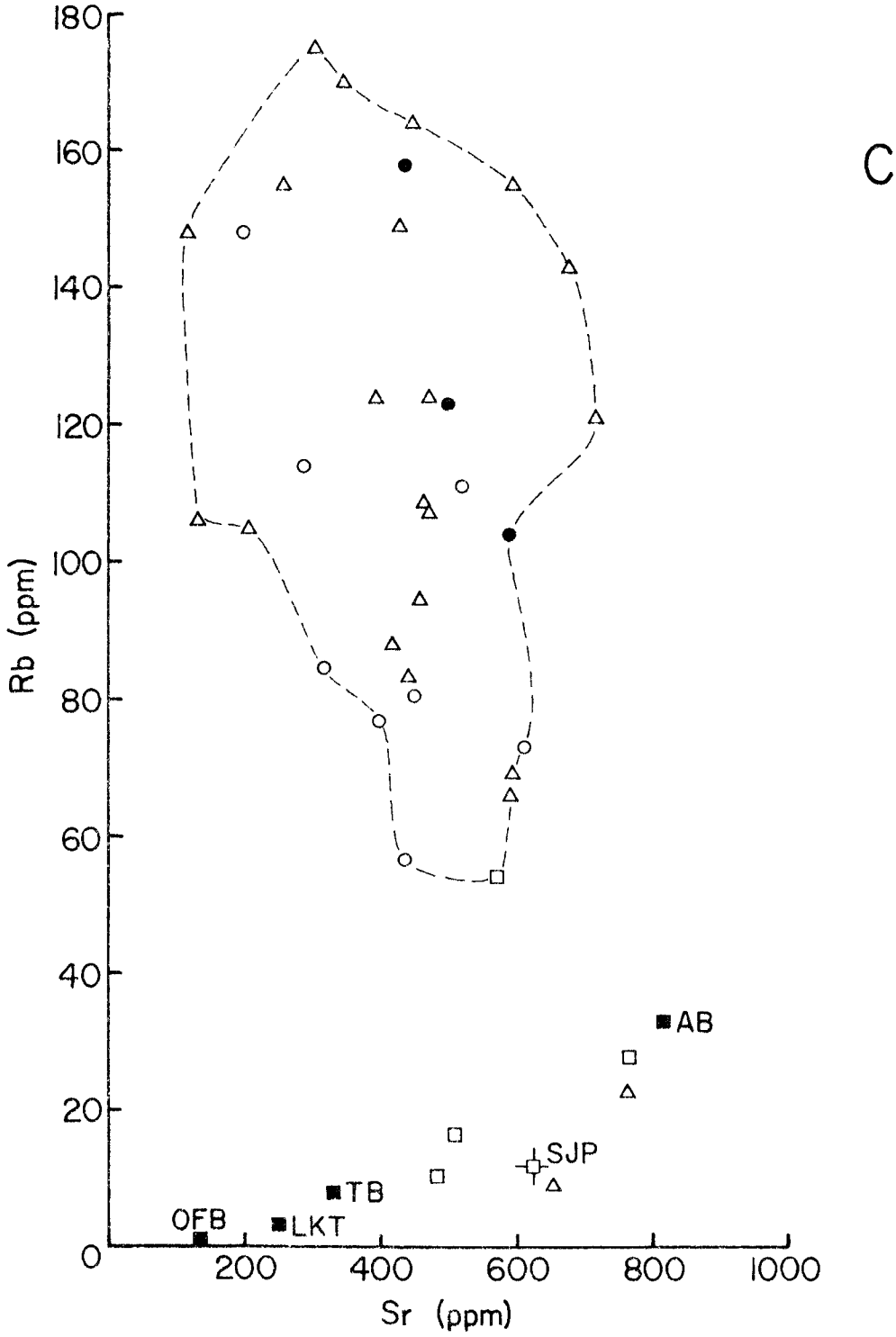
C
Rb (ppm)
Sr (ppm)
180
160
140
120
100
80
60
40
20
0
200
400
600
800
1000
AB
SJP
TB
OFB
LKT

may be considered: (1) formation of primary tonalite magma by hydrous partial melting of mantle peridotite; (2) differentiation of basaltic magma, itself formed by partial melting of mantle peridotite; (3) partial melting of non-peridotitic (e.g., amphibolitic or eclogitic) areas in the upper mantle or lower crust; (4) partial melting of mantle-derived oceanic basalts (amphibolite or eclogite) in a subduction zone; and (5) partial melting of young mantle-derived island arc volcanic rocks. More elaborate models involving combinations of these mechanisms are also possible.

It is important to emphasize that the tonalite may never have been entirely liquid. White and Chappell (1977) have argued that the batholithic rocks of southeastern Australia were emplaced as suspensions of various proportions of residual crystals in a minimum or near-minimum melt. Other workers (e.g., Piwinskii and Wyllie, 1968, 1970; Presnall and Bateman, 1973) have proposed similar models for the Sierra Nevada and other Cordilleran batholiths. This interpretation is conceptually attractive; that is, there is no reason to assume that partial melts would necessarily segregate cleanly from the residual material before gravitational instability caused upwelling and emplacement. However, unequivocal evidence of relict source material in the tonalite is lacking; the relatively low Al, Ti, and Na contents of both the hornblende and the trace amounts of relict clinopyroxene imply crystallization (or thorough equilibration) at moderate or low pressures. Inasmuch as the mafic inclusions are the best candidates for possible relict source material, it would be useful to analyze the phases in these inclusions for possible traces of higher pressure origin; unfortunately, it is

quite possible that such traces, if they existed, could have been entirely destroyed by subsequent re-equilibration.

On the basis of hydrous melting experiments on natural peridotites and simplified synthetic systems at high pressures, several workers (e.g., Kushiro et al., 1968, 1972; Kushiro, 1972; Mysen and Boettcher, in Mysen et al., 1974; Yoder, 1969), have proposed that silica-oversaturated magmas of andesitic and dacitic character can be derived by hydrous melting of mantle peridotite at high pressures (up to at least 25 kb). The theoretical basis for this suggestion is that, at high pressures, the presence of H_2O expands the stability field of liquidus olivine relative to the dry system (Kushiro et al., 1968; Nicholls and Ringwood, 1973), thereby raising the possibility that incongruent melting of orthopyroxene at high pressures could produce silica-saturated or oversaturated liquids in equilibrium with hydrous peridotite. In dry systems, incongruent melting of enstatite is restricted to pressures definitely <5.4 kb, probably ≤ 2.3 kb (Boyd et al., 1964), so partial melting of dry peridotite cannot yield silica-saturated or oversaturated melts at mantle depths. However, Green (1973) and Nicholls and Ringwood (1973; also in Mysen et al., 1974) concluded that the siliceous glasses of broadly andesitic and dacitic composition produced by Mysen and Boettcher (Mysen et al., 1974) and by Kushiro et al. (1972) from a spinel lherzolite at 7.5, 19.5, and 26 kb and by Green (1973) from an olivine-deficient pyrolite composition at 10 and 20 kb were not in equilibrium with the residual phases (olivine or olivine + pyroxene). Green showed that the glasses he produced (and, by implication, the glasses produced by the other workers) owed their

siliceous character to metastable growth of one or more of the phases olivine, clinopyroxene, amphibole, and mica during quenching. He concluded (p. 52) that the glasses "do not constitute evidence for the genesis of siliceous (>55% SiO_2) liquids by partial melting of peridotite under water-saturated conditions at P > 10 kb" and that "water saturated, magnesian quartz tholeiites and basaltic andesites may be derived by direct partial melting of *pyrolite* at ∿10 kb but that water-saturated olivine tholeiites are the least undersaturated magmas which may be derived by partial melting of pyrolite at ∿20 kb". Experimental evidence therefore suggests that the first mechanism of formation of the tonalite magma is probably not viable.

No certain choice can be made among the other hypotheses. However, several arguments lead me to favor partial melting either of areas of basaltic composition in the upper mantle or lower crust (hypothesis 3) or of subducted oceanic crust (hypothesis 4). Ocean floor (ocean ridge or abyssal) tholeiitic basalts, which are by far the most abundant igneous rocks in the ocean basins (Engel et al., 1965) have compositions appropriate to be parent materials for the tonalite magma. In particular, the concentrations of K (500-3000 ppm), Rb (0.2-5 ppm), U (0.10 ppm), Th (0.15 ppm), and rare earth elements (nearly flat relative-abundance patterns at typically 10-20 times chondrites) in these rocks are very low (Hart et al., 1970; Kay et al., 1970; Jakeš and Gill, 1970). In comparison, the San José tonalite has concentrations of about 5000-7000 ppm K, 11.9 ppm Rb, 0.2-0.4 ppm U, and 0.7-1.2 ppm Th and a fractionated pattern of rare earth element relative abundances ranging from 23 times chondrites for Ce to 3 times chondrites for Yb. Ocean floor basalts also

have high Na_2O/K_2O ratios in the range 10-15, compared to 2-3 for typical calc-alkaline volcanic rocks (Jakeš and Gill, 1970) and a range of 3.4-9.7 (average 6.5) for the tonalite. Assuming that K, Rb, U, Th, and at least the light rare earth elements all partition largely or entirely into the liquid, partial melting of such basaltic compositions could readily produce the tonalite magma.

On the other hand, the low K, Rb, U, Th, and rare earth element concentrations of the tonalite present a serious objection to the hypothesis of partial melting of young island arc volcanic rocks. Very little data have been published on the compositions of pre-batholithic volcanic and volcanogenic sedimentary rocks from the Peninsular Ranges, but the "average ANDESITE" of Taylor (1969) has notably higher concentrations of these elements: 13,300 ppm K, 31 ppm Rb, 0.69 ppm U, 2.2 ppm Th, and chondrite-normalized rare earth element abundances ranging from 28 for Ce to about 10 for Yb. The concentrations in Taylor's average low-K andesite and low-Si andesite are much lower -- 5900 and 9100 ppm K, 10 and 14 ppm Rb, 0.4 and 0.43 ppm U, and 1.3 and 1.34 ppm Th, respectively -- but the Na_2O/K_2O ratios (3.76 and 3.21, respectively) are also relatively low compared to the average of 6.5 for the tonalite. Chondrite-normalized rare earth element abundances in these rocks are also lower: about 8 and 18 for Ce and Yb in the low-K andesite and about 16 and 9 for Ce and Yb in the low-Si andesite.

Rocks of the island arc tholeiitic series, which commonly occur in large volumes on the side of an arc nearest to the trench, have similarly low concentrations of K (3000-10,000 ppm), Rb (3-10 ppm), U (0.3 ppm), Th (0.5 ppm), and rare earth elements (generally flat

patterns at about 5-25 times chondrites), as well as high Na_2O/K_2O ratios (4-6) (Jakeš and Gill, 1970), and it is possible that rocks of this type comprise a large portion of the volcanic pile on the western side of the Peninsular Ranges. However, because K, Rb, U, Th, and at least the light rare earth elements should partition strongly into the melt during fusion, these or any other volcanic arc rocks would have to have unusually low concentrations of these elements in order to generate a magma with the composition of the tonalite. Similarly, derivation of the tonalite magma by partial fusion of a lower crust of andesitic to dacitic average composition, as proposed by Presnall and Bateman (1973) for the granitic magmas of the Sierra Nevada batholith, would require the same unusual compositional characteristics. (This constraint does not apply, however, to generation of the more felsic Sierran rocks.) On the other hand, the general compositional similarity of the tonalite to many volcanic arc rocks, particularly the low-K or island arc tholeiitic series, suggests derivation from a similar source. The tonalite appears to be a plutonic manifestation of the same magmatism which generated the surrounding volcanic pile and may itself have contributed to this pile.

Larsen (1948) interpreted the tonalites and more felsic rocks of the batholith in southern Alta California as differentiates from gabbroic (basaltic) parental magma. Although this mechanism certainly could yield a tonalitic magma, there is no direct evidence to suggest this origin for the San José pluton. Calcic cores are extremely rare in the plagioclase, yet the preservation of delicate zoning patterns and of thin highly calcic intermediate zones, especially in the PHbT and SPT,

suggests that remnants of such cores would have persisted if they had formed. Relatively early nucleation of quartz, at least in the SHbT, also argues against differentiation from gabbroic magma. The trace amount of clinopyroxene can be interpreted as evidence in favor of this model, but clinopyroxene can also be readily explained as a minor liquidus phase of the tonalite, particularly of the apparently hotter and drier SHbT magma, where it was most abundant.

The homogeneity and large volume of the tonalite seem to be particularly persuasive arguments against differentiation from a gabbroic magma. Processes tending to separate crystals from melt were clearly ineffective, at least during the intermediate and later stages of crystallization. If extensive separation occurred earlier, by what mechanism was the magma so thoroughly homogenized? The low Al, Ti, and Na contents of the pyroxene argue against crystallization at high pressures; therefore, if the pyroxene is interpreted as evidence of differentiation from a parental gabbroic magma, one seems led to conclude that differentiation occurred at crustal depths, probably not too much greater than that at which the pluton was emplaced. If so, the opportunity for homogenization of the tonalite magma during intrusion would seem to have been very limited -- much more so than if the tonalite magma were tapped from a deep source. Furthermore, could a differentiating gabbroic magma supply such large volumes of magma of uniform composition in two or possibly three successive pulses without also supplying appreciable quantities of more or less differentiated material?

From these considerations it appears most likely that the tonalite magmas were primary magmas formed by partial melting of a material

similar in composition to ocean floor basalt. Whether this material was, in fact, subducted oceanic crust, or whether it was basaltic material in the overlying mantle or lower crust is an open question. Likewise, whether the mineralogy of the source material was amphibolitic (plagioclase-hornblende), eclogitic (pyroxene-garnet), or a combination of these assemblages is uncertain. The moderately fractionated pattern of rare earth element concentrations in BC-I-12 suggests that garnet was probably an important residual mineral in the source material after partial melting. However, other interpretations are possible: e.g., partial melting of a non-garnetiferous source, itself having a fractionated pattern.

Green and Ringwood (1968) produced aluminous, siliceous liquids quite similar in composition to the San José tonalite (Table 33) by roughly 45-55% melting of a high-alumina quartz tholeiite composition under "wet" conditions at 10 kb ($P_{H_2O} < P_{total}$). From these and additional experiments on this and three more-felsic compositions, they proposed partial melting of hydrated basalt (amphibolite) at depths of 30-40 km ($P_{H_2O} < P_{total}$) as one model for the origin of calc-alkaline (or calcic) magmas. Holloway and Burnham (1972) produced tonalitic melts of very similar composition (except for unusually low MgO contents) by 30-35% partial melting of an Hawaiian olivine tholeiite at lower pressures (5-8 kb), with $f_{H_2O} = 0.6\ f^{\circ}_{H_2O}$. Thus the experimental data suggest that partial melting of hydrated oceanic crust (amphibolite) or other basaltic material of similar composition at moderate to shallow depths is a reasonable hypothesis. Plagioclase-rich normative compositions result because high P_{H_2O} greatly depresses the stability

Table 33

Comparison of the Composition of the San José Tonalite with the Compositions of Glasses[a] Produced by Partial Melting or Partial Crystallization of Basaltic Compositions at 5-10 kb ($P_{H_2O} < P_{total}$)

	Green and Ringwood (1968)[b]			Holloway and Burnham (1972)[c]				San José Tonalite
	Initial Composition	Compositions of Partial Melts		Initial Composition	Compositions of Partial Melts			
Pressure	--	10 kb	10 kb	--	5.2 kb	7.8 kb	7.96 kb	--
Temperature	--	960°C	920°C	--	999°C	995°C	1050°C	--
% melt	--	55	45	--	30	30	35	--
SiO_2	53.0	59.9	65.0	49.91	64.2	63.6	63.6	62.13
TiO_2	1.5	0.4	0.1	2.55	1.2	1.0	1.2	0.72
Al_2O_3	16.9	20.3	20.0	12.79	18.7	20.1	20.4	18.20
FeO_t	8.2	6.3	4.3	11.48	4.3	3.0	3.0	4.64
MgO	7.0	2.1	2.0	9.36	0.7	0.2	0.3	2.49
CaO	10.0	6.7	3.9	11.27	6.9	6.4	7.4	6.24
Na_2O	2.7	3.4	3.6	2.15	2.8	4.7	3.0	4.83
K_2O	0.6	0.9	1.0	0.48	1.0	1.0	0.9	0.74
TOTAL	99.9	100.0	99.9	99.99	99.8	100.0	99.8	99.99

[a]All compositions are normalized to 100% for the oxides listed.

[b]Starting material: synthetic glass with composition corresponding to high-alumina quartz tholeiite. P_{H_2O} was uncontrolled. Liquid compositions were calculated by mass balance. FeO_t contents were corrected for significant loss of Fe to the platinum capsule during the experiments.

[c]Starting material: olivine tholeiite from the 1921 flow of Kilauea Volcano, Hawaii: $f_{H_2O} = 0.6\ f^{\circ}_{H_2O}$. Liquid compositions are based upon electron microprobe analyses of the glass, except for the alkali contents, which were calculated by mass balance.

limits of plagioclase, causing it to disappear after only small to moderate degrees of melting, and because the pressures are lower than those at which aluminous garnet becomes an important residual phase (18 kb or higher: Green and Ringwood, 1968; Nicholls and Ringwood, 1973). Yet garnet may have been an important residual phase in the source area of the tonalite. Except for the possible difficulty in producing aluminous melts from a garnet-bearing source, there appears to be no evidence against generation of the magma by hydrous partial melting of basaltic material at pressures significantly greater than 10 kb. In fact, Green and Ringwood suggest that silica-rich, potash-poor dacitic or granodioritic compositions with low K_2O/Na_2O ratios may be derived by partial melting under wet conditions at pressures of 27-36 kb ($P_{H_2O} < P_{total}$).

Green and Ringwood proposed a second model for the origin of the calc-alkaline suite: transformation of basalt to quartz eclogite under dry conditions, followed by partial melting of the eclogite at depths of 100-150 km. As under wet conditions, garnet is a major residual phase at these pressures, and the liquids produced from high-alumina olivine tholeiite and high-alumina quartz tholeiite compositions at 18, 27, and 36 kb show little or no enrichment in Al_2O_3 relative to the starting materials. At lower pressures under dry conditions, garnet disappears, but plagioclase remains as an important residual phase along with pyroxene; hence generation of siliceous, plagioclase-rich liquids by this mechanism at pressures <18 kb is unlikely. Furthermore, calculated liquid compositions plotted on a triangular diagram of alkalies + FeO_t + MgO define essentially calc-alkaline trends at 27 and

36 kb, but follow trends of marked iron enrichment at 18 kb. Obviously, these trends must be sensitive to f_{O_2}, and Fe enrichment should be restricted under more oxidizing conditions; f_{O_2} was not controlled in the experiments. Nevertheless, melting of basaltic compositions under dry conditions at pressures <25 kb appears less likely as a source for the tonalite magma. Partial melting of dry quartz eclogite at higher pressures seems possible if the eclogite was rich in normative plagioclase.

In summary, the homogeneity of the tonalite, the evidence against effective separation of crystals from melt during at least the intermediate and later stages of crystallization, the early nucleation of quartz, the paucity of relict evidence of a gabbroic parental magma, and the multiple emplacement of magmas of essentially identical composition without appreciable amounts of more or less differentiated material seem to be powerful arguments in favor of primary tonalitic magmas. The most reasonable origin would seem to be partial melting of a hydrated basaltic material similar in composition to ocean floor or oceanic island basalt at depths of 30-40 km or greater. This material may have been either subducted oceanic crust or basaltic areas in the overlying mantle or lower crust; an eclogitic or garnet-bearing amphibolitic mineralogy seems likely, but a garnet-free source cannot be ruled out. Dry partial melting of a similar composition at higher pressures (>18 kb) is also a possibility, whereas dry partial melting at pressures <18 kb, where plagioclase would be a major residual phase, seems inconsistent with the plagioclase-rich composition of the tonalite, unless the source was unusually plagioclase-rich or unless residual plagioclase was

carried up in suspension in the magma. Formation of the tonalite magma as a mixture of melt plus residual source material is possible, but evidence of moderate or high pressure phases or mineral compositions is lacking. Microprobe analysis of the mineral compositions in the mafic inclusions would be useful in this respect.

Partial melting of typical volcanic arc rocks does not appear to satisfy all of the constraints imposed by the composition of the tonalite, unless the volcanic rocks had unusually low concentrations of the incompatible elements. The same compositional constraint applies to derivation from a hypothetical lower crust of andesitic to dacitic composition. Partial melting or assimilation of old sialic crust or of sedimentary rocks derived from such crust can be definitely ruled out, unless some mechanism exists for selectively assimilating silica and plagioclase components without simultaneously incorporating notable amounts of other incompatible elements such as K, Rb, U, Th, and rare earth elements or notably increasing the radiogenic character of the Sr and Pb isotopic compositions. Differentiation of the tonalite magma from a parental basaltic magma cannot be ruled out, but there is no direct evidence in support of this hypothesis.

It is possible that generation of the magma involved much more complex processes and multiple sources: e.g., mixing of andesitic or basaltic magma derived from subducted oceanic crust with magma generated in the overlying crust (Presnall and Bateman, 1973; Gastil, 1975) or mixing of felsic magmas generated from subducted oceanic crust with overlying mantle peridotite, followed by diapiric upwelling and eventual differentiation of the mixed system (Ringwood, 1975). Such

elaborate models seem feasible, but probably unnecessary. In particular, as mentioned earlier, there appears to be no need to invoke formation of the plutonic tonalite magma by processes different in any fundamental way from those which generate calc-alkaline or calcic volcanic magmas. In particular, the mixing mechanisms suggested by Chayes (1956b) for tonalites in southern Alta California and by Piwinskii (1968a) and Piwinskii and Wyllie (1968, 1970) for the Sierra Nevada and Wallowa batholiths -- specifically, mixing of granodioritic or near-minimum melt with pre-existing gabbro -- seems not only unnecessary, but also inconsistent with both the homogeneity of the tonalite and the compositions of the minerals. Moreover, to yield a composition like that of the San José tonalite would require mixing of gabbro not with typical Peninsular Ranges granodiorite, as suggested by Chayes, or with a melt approaching the low-pressure minimum melting composition in the Q-Or-Ab or Q-Or-Ab-An system as suggested by Piwinskii and Wyllie, but rather with a siliceous, leucocratic melt of unusually low K_2O content and high Na_2O/K_2O ratio. Plutonic bodies approaching this sort of trondhjemitic composition are rare in the Peninsular Ranges and not known in the San José area.

16.1 Some Comments on a Model by R. C. Gastil for the Origin of the Batholith

Gastil (1975) presented a model for the origin of the Peninsular Ranges batholith as a whole which warrants particular consideration. The model invokes accumulation of a thick pile of Jurassic-Cretaceous volcanic rocks primarily on the western half of a giant, westward-thinning wedge of Paleozoic-to-Jurassic, continentally-derived clastic

sedimentary strata. The clastic wedge is assumed to rest directly on oceanic crust in the western and central parts of the Peninsular Ranges and on sialic continental crust in the eastern Peninsular Ranges and farther east. Gastil divided the volcanic arc into five longitudinal belts:

(1) an outer continental borderland belt characterized by exclusively basaltic magmas derived from subducted oceanic crust or overlying mantle;

(2) an inner continental borderland belt characterized by basalt and andesite derived from the above sources as well as from the older oceanic crust underlying the clastic wedge;

(3) a belt of basalt + andesite + dacite underlying the western half of the Peninsular Ranges (Gastil's depth zones A and B, including the San José area) and characterized by magmas generated primarily within the autocthonous oceanic crust and the lower part of the overlying clastic wedge, with some contribution from subducted oceanic crust or overlying mantle;

(4) a belt of andesite + dacite in the eastern Peninsular Ranges (Gastil's depth zone C) consisting of magmas generated by partial fusion of older sialic crust and related clastic rocks, again with some contribution directly from subducted oceanic crust or overlying mantle; and

(5) a belt of predominantly dacite + rhyolite in Sonora, Mexico derived from the same sources as for (4), but involving greater contribution directly from older sialic crust.

Accompanying volcanism, partial melting of the underlying older

crust and probably the lower part of the clastic wedge is assumed to have generated "huge welts of tonalitic magma" from which diapiric masses rose through the sedimentary wedge and, in many cases, penetrated into the overlying volcanic pile and locally vented to the surface to contribute to that pile. As for the volcanic belts, the source material is assumed to have varied across the batholith from primarily older oceanic crust along the western margin to oceanic crust + Paleozoic-Jurassic sedimentary rocks under most of the western half of the ranges (Gastil's depth zones A and B), then to primarily older sialic crust + sedimentary rocks under the eastern side of the ranges and farther east, with additional eastward-decreasing contribution of basaltic (or andesitic?) melt from subducted oceanic crust or overlying mantle. Granodioritic and more felsic magmas are assumed to have been produced in some areas by differentiation of the tonalite welt, particularly in areas where older sialic rocks were partially incorporated into the melt. Eventually, the entire central part of the magmatic welt rose *en masse* isostatically and pushed aside the sedimentary and volcanic rocks to produce the large tonalite and granodiorite masses in the central and eastern parts of the ranges (i.e., Sierra San Pedro Mártir, Sierra Juárez, and their extensions in southern Alta California. Generation and removal of the tonalitic magmas is assumed to have created a residual amphibolitic lower crust under the present ranges.

In terms of the San José pluton alone, many aspects of this model are plausible. Generation of the San José magmas by partial fusion of older oceanic crust, with or without additional contribution from subducted oceanic crust or overlying mantle, can satisfy the constraints

imposed by the composition of the tonalite. However, as emphasized earlier, significant contribution from continentally-derived clastic rocks of Paleozoic to Jurassic age is inconsistent with both the very low concentrations of K, Rb, U, Th, Pb, and rare earth elements and the relatively unradiogenic Sr initial and Pb isotopic ratios. Furthermore, existence of such a sedimentary wedge under the San José area has not been verified. The unusually low heat flow (0.84 $\mu cal/cm^2 sec$) measured in the center of the pluton (Smith, 1972, 1974) also argues against the existence of a thick section of continentally-derived clastic rocks, unless the heat flow from the mantle is very low.

In terms of the batholith as a whole, there are several objections to this model. Again, the proposed existence of a thick wedge of Paleozoic to Jurassic clastic rocks underlying the volcanic pile throughout the western half of the ranges is unverified. Although the highly metamorphosed schists and gneisses throughout the eastern part of the ranges (Gastil's depth zone C) appear to be largely of sedimentary parentage, documented evidence of pre-Jurassic age exists only in a few localities along the eastern margin of the Peninsular Ranges and in the Gulf of California Trough (Gastil et al., 1975). In fact, strata unequivocally of Jurassic age have not yet been identified in most of northern Baja California. The relatively low $^{87}Sr/^{86}Sr$ initial ratios (<0.7045) characteristic of the plutonic rocks in all but the easternmost part of the ranges (Early and Silver, 1973) imply that, if this wedge of older clastic rocks underlies most or all of the Peninsular Ranges, it contributed little, if at all, to the batholithic magmas.

Secondly, biotite-hornblende tonalite or low-K granodiorite are

the dominant rock types across the entire width of the Peninsular Ranges and recur across the Gulf in Sonora as well; hence a major west-to-east change in source-rock composition from oceanic crust to sialic crust + sedimentary strata seems unlikely.

Thirdly, Gastil's model implies that the large plutonic bodies exposed in the Sierra San Pedro Mártir, Sierra Juárez, and eastern Peninsular Ranges in southern Alta California (depth zone C of Gastil) have been tectonically uplifted along with the surrounding metamorphic rocks from depths of perhaps 25-40 km. If so, pressures must have been in the range 8-13 kb during metamorphism and magmatic crystallization. Metamorphic grade is indeed much higher in the wall rocks in zone C than it is farther west, but evidence of high pressures is lacking. Sillimanite is the principal alumino-silicate polymorph, but andalusite also occurs locally, for example, in the Sierra San Pedro Mártir. Kyanite has not been found. Cordierite occurs in many areas, including the Sierra San Pedro Mártir (Appendix E). The mineral assemblages imply moderate- to low-pressure metamorphism -- certainly not pressures >8 kb. Likewise, there are no obvious petrographic differences in the plutonic rocks in zone C, e.g., in the optical properties of hornblende, compared to the San José and many other B-zone plutons; admittedly though, petrographic characteristics may not vary sufficiently to provide obvious evidence of differing pressures. Finally, Gastil's model implies that the plutons in zone C formed for the most part by *in situ* accumulation and crystallization of magma rather than by upward intrusion into the metamorphic rocks, yet it is not clear that there is any fundamental difference in the structural characteristics or relationships

to wall rocks of these plutons compared to those in zone B. As pointed out by Gastil, the plutons in zone C may be larger and more irregular in shape on the average than those in zone B, and they certainly comprise a larger proportion of the exposed area than in zone B; they may indeed represent a deeper level of emplacement and crystallization than those in zone B, or particularly in Pacific coastal zone A, but depths of 25-40 km or more as implied by Gastil's model appear unreasonable. Perhaps the scarcity of conspicuous circular intrusive bodies in zone C, as contrasted with their abundance in zone B, is due not to initial generation of the upwelling circular masses at the top of zone C, as suggested by Gastil, but rather to frequent juxtaposition of intrusive bodies against each other in zone C; many of the circular plutons in zone B are isolated bodies emplaced into stratified rocks. It is also possible that the suggested scarcity of circular intrusive structures in zone C is in part more apparent than real, because in many cases the geometry of individual intrusive units in zone C may be difficult to recognize without detailed mapping.

In summary, to the extent that Gastil's model emphasizes partial melting of oceanic crust or compositionally similar material without contribution from older sialic crust or related sedimentary rocks, the model provides a plausible but unproven mechanism for generating the San José magmas. However, there are serious objections to his model for the volcano-sedimentary arc and the batholith as a whole. At present, the structural, petrographic, and geochemical data are sufficient to allow important constraints to be placed on models of magma genesis, but a unique interpretation of the origin of either the San José magmas or the batholith as a whole is not yet possible.

LIST OF REFERENCES

Abbott, P. L., G. L. Peterson, and J. A. Minch, 1973, "Pre-Eocene Weathering in Southwestern California and Northwestern Baja California", Geol. Soc. Amer. Abs. with Programs, vol. 5, no. 1, p. 1.

Akella, J. and H. G. F. Winkler, 1966, "Orthorhombic Amphibole in some Metamorphic Reactions", Contr. Mineral. Petrol., vol. 12, pp. 1-12.

Albee, A. L., 1962, "Relationships between Mineralogical Association, Chemical Composition, and Physical Properties of the Chlorite Series", Amer. Mineral., vol. 47, pp. 851-870.

Albee, A. L. and L. Ray, 1970, "Correction Factors for Electron Probe Microanalysis of Silicates, Oxides, Carbonates, Phosphates, and Sulfates", Anal. Chem., vol. 42, pp. 1408-1414.

Allen, C. R., L. T. Silver, and F. G. Stehli, 1960, "Agua Blanca Fault -- A Major Transverse Structure of Northern Baja California, Mexico", Geol. Soc. Amer. Bull., vol. 71, pp. 457-482.

Allison, E. C., 1955, "Middle Cretaceous Gastropoda from Punta China, Baja California, Mexico", Journ. Paleon., vol. 29, pp. 400-432.

----------, 1964, "Geology of Areas Bordering Gulf of California, in Marine Geology of the Gulf of California, ed. T. H. van Andel and G. G. Shor, Jr., Amer. Assoc. Petrol. Geol. Memoir 3, pp. 3-29.

----------, 1974, "The Type Alisitos Formation (Cretaceous, Aptian-Albian) of Baja California and its Bivalve Fauna", in Geology of Peninsular California, ed. G. Gastil and J. Lillegraven, Guidebook for the Pacific Sections of AAPG, SEPM, and SEG, pp. 20-59.

Althaus, E., 1966a, "Die Bildung von Pyrophyllit und Andalusit Zwischen 2000 und 7000 Bar H_2O-Druck", Naturwiss, vol. 53, pp. 105-106.

----------, 1966b, "Der Stabilitätsbereich des Pyrophyllits Unter dem Einfluss von Säuren; I. Mitteilung, Experimentelle Untersuchungen", Contr. Mineral. Petrol., vol. 13, pp. 31-50.

----------, 1967, "The Triple Point Andalusite-Sillimanite-Kyanite. An Experimental and Petrologic Study", Contr. Mineral. Petrol., vol. 16, pp. 29-44.

Althaus, E., E. Karotke, K. H. Nitsche, and H. G. F. Winkler, 1970, "An Experimental Re-examination of the Upper Stability Limit of Muscovite Plus Quartz", Neues Jb. Mineral. Monat., no. 7, pp. 325-336.

Anderson, A. T., Jr., R. N. Clayton, and T. K. Mayeda, 1971, "Oxygen Isotope Thermometry of Mafic Igneous Rocks", Journ. Geol., vol. 79, pp. 715-729.

Anderson, T. H., L. T. Silver, and D. A. Cordoba, 1969, "Mesozoic Magmatic Events of the Northern Sonora Coastal Region, Mexico", Geol. Soc. Amer. Abs. with Programs for 1969, part 7, pp. 3-4.

Anonymous, 1924, "Informe Sobre la Exploración Geológica de la Baja California por la Marland Oil Company de Mexico", Bol. de Petrol., vol., 17, no. 6, pp. 417-453; vol. 18, no. 1, pp. 14-53.

Armstrong, R. L. and J. Suppe, 1973, "Potassium-Argon Geochronometry of Mesozoic Igneous Rocks in Nevada, Utah, and Southern California", Geol. Soc. Amer. Bull., vol. 84, pp. 1375-1392.

Bachinski, S. W. and G. Müller, 1971, "Experimental Determinations of the Microcline-Low Albite Solvus", Journ. Petrol., vol. 12, pp. 329-356.

Bailey, E. H., W. P. Irwin, and D. L. Jones, 1964, "Franciscan and Related Rocks, and their Significance in the Geology of Western California", Cal. Div. Mines Geol. Bull. 183, 177 pp.

Balk, R., 1937, "Structural Behavior of Igneous Rocks", Geol. Soc. Amer. Memoir 5, 177 pp.

Balk, R. and F. F. Grout, 1934, "Structural Study of the Snowbank Stock", Geol. Soc. Amer. Bull., vol. 45, pp. 621-636.

Banks, P. O. and L. T. Silver, 1966, "Evaluation of the Decay Constant of Uranium 235 from Lead Isotope Ratios", Journ. Geophys. Res., vol. 71, pp. 4037-4046.

Banks, P. O. and L. T. Silver, 1969, "U-Pb Isotope Analyses of Zircons from Cretaceous Plutons of the Peninsular and Transverse Ranges, Southern California", (abs.), Geol. Soc. Amer. Spec. Paper 121, pp. 17-18.

Barth, T. F. W., 1962, "The Feldspar Geologic Thermometers", Norsk. Geol. Tidsskr., vol. 42, part II (Feldspar Volume), pp. 330-339.

Bateman, P. C. and F. C. W. Dodge, 1970, "Variations of Major Chemical Constituents across the Central Sierra Nevada Batholith", Geol. Soc. Amer. Bull., vol. 81, pp. 409-420.

Beal, C. H., 1948, "Reconnaissance Geology and Oil Possibilities of Baja California, Mexico", Geol. Soc. Amer. Memoir 31, 138 pp.

Bence, A. E. and A. L. Albee, 1968, "Empirical Correction Factors for the Electron Microanalysis of Silicates and Oxides", Journ. Geol., vol. 76, pp. 382-403.

Bhattacharji, S., 1967, "Mechanics of Flow Differentiation in Ultramafic and Mafic Sills", Journ. Geol., vol. 75, pp. 101-112.

Bhattacharji, S., and C. H. Smith, 1964, "Flowage Differentiation", Science, vol. 145, pp. 150-153.

Billings, M. P., 1972, Structural Geology, 3rd edition, Prentice-Hall, Inc., Englewood Cliffs, New Jersey, 606 pp.

Birch, F., 1966, "Compressibility; Elastic Constants", in Handbook of Physical Constants, ed. S. P. Clark, Jr., Geol. Soc. Amer. Memoir 97, pp. 97-173.

Birkbahn, P., 1969, "Structure and Petrology of a Pluton in Baja California", Undergrad. Research Report, vol. 13, San Diego State Univ., 16 pp.

Bottinga, Y., A. Kudo, and D. Weill, 1966, "Some Observations on Oscillatory Zoning and Crystallization of Magmatic Plagioclase", Amer. Mineral., vol. 51, pp. 792-806.

Boyd, F. R., J. L. England, and B. T. C. Davis, 1964, "Effects of Pressure on the Melting and Polymorphism of Enstatite, $MgSiO_3$", Journ. Geophys. Res., vol. 69, pp. 2101-2109.

Buddington, A. F. and D. H. Lindsley, 1964, "Iron-Titanium Oxide Minerals and Synthetic Equivalents", Journ. Petrol., vol. 5, pp. 310-357.

Burnham, C. W., J. R. Holloway, and N. F. Davis, 1969, "Thermodynamic Properties of Water to 1000°C and 10,000 Bars", Geol. Soc. Amer. Spec. Paper 132, 96 pp.

Carmichael, I. S. E. and J. Nicholls, 1967, "Iron-Titanium Oxides and Oxygen Fugacities in Volcanic Rocks", Journ. Geophys. Res., vol. 72, pp. 4665-4687.

Champion, D. E., A. L. Albee, and A. A. Chodos, 1975, "Reproducibility and Operator Bias in a Computer-Controlled System for Quantitative Electron Microprobe Analysis", Proc. Nat. Conf. Electron Probe Analyses (10th), Las Vegas, Nevada.

Chayes, F., 1956a, Petrographic Modal Analysis -- An Elementary Statistical Appraisal, John Wiley and Sons, Inc., New York, 113 pp.

----------, 1956b, "Modal Composition of the Major Members of the Southern California Batholith", Carn. Inst. Wash. Year Book 55, pp. 214-216.

----------, 1969, "The Chemical Composition of Cenozoic Andesite", in Proceedings of the Andesite Conference, ed. A. R. McBirney, Oregon Dept. Geol. and Min. Industries Bull. 65, pp. 1-11.

Choudhuri, A. and H. G. F. Winkler, 1967, "Anthophyllit und Hornblende in Einigen Metamorphen Reaktionen", Contr. Mineral. Petrol., vol. 14, pp. 293-315.

Church, S. E. and M. Tatsumoto, 1975, "Lead Isotope Relations in Oceanic Ridge Basalts from the Juan de Fuca-Gorda Ridge Area, N. E. Pacific Ocean", Contr. Mineral. Petrol., vol. 53, pp. 253-279.

Cloos, E., 1935, "Mother Lode and the Sierra Nevada Batholith", Journ. Geol.,vol. 43, pp. 225-249.

---------, 1937, "The Application of Recent Structural Methods in the Interpretation of the Crystalline Rocks of Maryland", Maryland Geol. Surv., vol. 13, pp. 37-108.

Cohen, L. H., K. C. Condie, L. J. Kuest, Jr., G. S. MacKenzie, F. H. Meister, P. Pushkar, and A. M. Stueber, 1963, "Geology of the San Benito Islands, Baja California, Mexico", Geol. Soc. Amer. Bull., vol. 74, pp. 1355-1369.

Compton, R. R., 1955, "Trondhjemite Batholith near Bidwell Bar, California", Geol. Soc. Amer. Bull., vol. 66, pp. 9-44.

Deer, W. A., 1935, "The Cairnsmore of Carsphairn Igneous Complex", Quart. Journ. Geol. Soc., vol. 91, pp. 47-76.

Deer, W. A., R. A. Howie, and J. Zussman, 1962, Rock-Forming Minerals, Vol. 3, John Wiley and Sons, Inc., New York, 270 pp.

Deer, W. A., R. A. Howie, and J. Zussman, 1963, Rock-Forming Minerals, Vol. 2, John Wiley and Sons, Inc., New York, 379 pp.

Deer, W. A., R. A. Howie, and J. Zussman, 1963, Rock-Forming Minerals, Vol. 4., John Wiley and Sons, Inc., New York, 435 pp.

Deer, W. A., R. A. Howie, and J. Zussman, 1966, An Introduction to the Rock-Forming Minerals, John Wiley and Sons, Inc., New York, 528 pp.

Dodge, F. C. W., J. J. Papike, and R. E. Mays, 1968, "Hornblendes from Granitic Rocks of the Central Sierra Nevada Batholith, California", Journ. Petrol., vol. 9, pp. 378-410.

Dodge, F. C. W. and D. C. Ross, 1971, "Coexisting Hornblendes and Biotites from Granitic Rocks near the San Andreas Fault, California", Journ. Geol., vol. 79, pp. 158-172.

Doe, B. R. and M. H. Delevaux, 1973, "Variations in Lead-Isotopic Compositions in Mesozoic Granitic Rocks of California: A Preliminary Investigation", Geol. Soc. Amer. Bull., vol. 84, pp. 3513-3526.

Duffield, W. A., 1968, "The Petrology and Structure of the El Pinal Tonalite, Baja California, Mexico", Geol. Soc. Amer. Bull., vol. 79, pp. 1351-1374.

Durham, J. W. and E. C. Allison, 1960, "The Geologic History of Baja California and its Marine Faunas", in Symposium: The Biogeography of Baja California and Adjacent Seas, Part I, Geologic History, Syst. Zoology, vol. 9, pp. 47-91.

Early, T. O. and L. T. Silver, 1973, "Rb-Sr Isotopic Systematics in the Peninsular Ranges Batholith of Southern and Baja California", EOS, Trans. Amer. Geophys. Union, vol. 54, p. 494.

Eggler, D. H., 1972, "Amphibole Stability in H_2O-Undersaturated Calc-Alkaline Melts", Earth Planet. Sci. Lett., vol. 15, pp. 28-34.

Eggler, D. H. and C. W. Burnham, 1973, "Crystallization and Fractionation Trends in the System Andesite-H_2O-CO_2-O_2 at Pressures to 10 Kb", Geol. Soc. Amer. Bull., vol. 84, pp. 2517-2532.

Engel, A. E. J. and C. G. Engel, 1962, "Hornblendes Formed During Progressive Metamorphism of Amphibolites, Northwest Adirondack Mountains, New York", Geol. Soc. Amer. Bull., vol. 73, pp. 1499-1514.

Engel, A. E. J., C. G. Engel, and R. G. Havens, 1964, "Mineralogy of Amphibolite Layers in the Gneiss Complex, Northwest Adirondack Mountains, New York", Journ. Geol., vol. 72, pp. 131-156.

Engel, A. E. J., C. G. Engel, and R. G. Havens, 1965, "Chemical Characteristics of Oceanic Basalts and the Upper Mantle", Geol. Soc. Amer. Bull., vol. 76, pp. 719-734.

Evernden, J. F. and R. W. Kistler, 1970, "Chronology of Emplacement of Mesozoic Batholithic Complexes in California and Western Nevada", U. S. Geol. Surv. Prof. Paper 623, 42 pp.

Faure, G. and J. L. Powell, 1972, Strontium Isotope Geology, Springer-Verlag, New York, 188 pp.

Fife, D., J. A. Minch, and P. J. Crampton, 1967, "Late Jurassic Age of the Santiago Peak Volcanics, California", Geol. Soc. Amer. Bull., vol. 78, pp. 299-304.

Flanagan, F. J., 1969, "U.S. Geological Survey Standards -- II. First Compilation of Data for the New U.S.G.S. Rocks", Geochim. et Cosmochim. Acta, vol. 33, pp. 81-120.

Fries, C., Jr. and E. Schmitter, 1945, "Scheelite Deposits in the Northern Part of the Sierra de Juárez, Northern Territory, Lower California, Mexico", U. S. Geol. Surv. Bull. 946-C, pp. 73-101.

Gastil, G., 1961, "The Elevated Erosion Surfaces", in Guidebook for Field Trips, 57th Ann. Meeting, Cordilleran Sect., Geol. Soc. Amer., ed. T. E. Blakemore, pp. 1-3.

Gastil, R. G., 1975, "Plutonic Zones in the Peninsular Ranges of Southern California and Northern Baja California", Geology, vol. 3, pp. 361-363.

Gastil, R. G. and E. C. Allison, 1966, "An Upper Cretaceous Fault-Line Coast", (abs.), Amer. Assoc. Petrol. Geol. Bull., vol. 50, pp. 647-648.

Gastil, R. G., D. Krummenacher, J. Doupont, and J. Bushee, 1974, "The Batholithic Belt of Southern California and Western Mexico", Pac. Geol., vol. 8, pp. 73-78.

Gastil, R. G., D. V. LeMone, and W. J. Stewart, 1973a, "Permian Fusilinids from near San Felipe, Baja California", Amer. Assoc. Petrol. Geol. Bull., vol. 57, pp. 746-747.

Gastil, R. G., R. P. Phillips, and E. C. Allison, 1973b, "Reconnaissance Geologic Map of the State of Baja California", Geol. Soc. Amer. Map and Chart Series MC-3.

Gastil, R. G., R. P. Phillips, and E. C. Allison, 1975, "Reconnaissance Geology of the State of Baja California", Geol. Soc. Amer. Memoir 140, 170 pp.

Gastil, R. G., R. P. Phillips, and R. Rodriguez-Torres, 1972, "The Reconstruction of Mesozoic California", Internat. Geol. Congr., Report of the 24th Session, Montreal, Sec. 3, pp. 217-229.

Gastil, R. G., D. Stickney, and A. Terry, 1971, "Pluton Sizes in the Peninsular Ranges of Baja California and the Sierra Nevada", Geol. Soc. Amer. Abs. with Programs, vol. 3, p. 123.

Gill, J. and W. Compston, 1973, "Strontium Isotopes in Island Arc Volcanic Rocks", in The Western Pacific. Island Arcs, Marginal Seas, Geochemistry, ed. P. J. Coleman, Crane, Russack, and Company, Inc., New York, pp. 483-496.

Goldman, D. S., 1977, "Crystal-Field and Mössbauer Applications to the Study of Site Distribution and Electronic Properties of Ferrous Iron in Minerals with Emphasis on Calcic Amphiboles, Orthopyroxene and Cordierite", Ph.D. Thesis, California Institute of Technology, 295 pp.

Goldman, D. S. and G. R. Rossman, 1977, "The Identification of Fe^{2+} in the M(4) Site of Calcic Amphiboles", Amer. Mineral., vol. 62, pp. 205-216.

Green, D. H., 1973, "Experimental Melting Studies on a Model Upper Mantle Composition at High Pressure Under Water-Saturated and Water-Undersaturated Conditions", Earth Planet. Sci. Lett., vol. 19, pp. 37-53.

Green, T. H. and A. E. Ringwood, 1968, "Genesis of the Calc-Alkaline Igneous Rock Suite", Contr. Mineral. Petrol., vol. 18, pp. 105-162.

Greenwood, H. J., 1967, "Wollastonite Stability in H_2O-CO_2 Mixtures and Occurrence in a Contact Metamorphic Aureole Near Salmo, British Columbia, Canada", Amer. Mineral., vol. 52, pp. 1669-1680.

Hanna, M. A., 1926, "Geology of the La Jolla Quadrangle, California", Univ. Calif. Dept. Geol. Sci. Bull., vol. 16, pp. 187-246.

Harker, R. I. and O. F. Tuttle, 1956, "Experimental Data on the P_{CO_2}-T Curve for the Reaction: Calcite + Quartz $\rightleftharpoons$ Wollastonite + Carbon Dioxide", Amer. Journ. Sci., vol. 254, pp. 239-256.

Hart, S. R., C. Brooks, T. E. Krogh, G. L. Davis, and D. Nava, 1970, "Ancient and Modern Volcanic Rocks: A Trace Element Model", Earth Planet. Sci. Lett., vol. 10, pp. 17-28.

Hawkins, J. W., 1970, "Metamorphosed Late Jurassic Andesites and Dacites of the Tijuana-Tecate Area, Baja California", in Pacific Slope Geology of Northern Baja California and Adjacent Alta California, Guidebook for the Pacific Sections of AAPG, SEPM, and SEG, pp. 25-29.

Hedge, C. E., R. A. Hildreth, and W. T. Henderson, 1970, "Strontium Isotopes in some Cenozoic Lavas from Oregon and Washington", Earth Planet. Sci. Lett., vol. 8, pp. 434-438.

Helz, R. T., 1973, "Phase Relations of Basalts in their Melting Range at P_{H_2O} = 5 kb as a Function of Oxygen Fugacity. Part I. Mafic Phases", Journ. Petrol., vol. 14, pp. 249-302.

Higgins, M. W., 1971, "Cataclastic Rocks", U. S. Geol. Surv. Prof. Paper 687, 97 pp.

Hirschi, H. and F. de Quervain, 1927, "Beiträge zur Petrographie von Baja California (Mexiko). Fortsetzung.", Schweiz. Min. Pet. Mitt., vol. 7, pp. 142-164.

Hirschi, H. and F. de Quervain, 1928, "Beiträge zur Petrographie von Baja California (Mexiko)", Schweiz. Min. Pet. Mitt., vol. 8, pp. 323-356.

Hirschi, H. and F. de Quervain, 1930, "Beiträge zur Petrographie von Baja California", Schweiz. Min. Pet. Mitt., vol. 10, pp. 228-272.

Hirschi, H. and F. de Quervain, 1933, "Beiträge zur Petrographie von Baja California (Mexico) (Fortsetzung und Schluss)", Schweiz. Min. Pet. Mitt., vol. 13, pp. 232-277.

Hoefs, J. and S. Epstein, 1969, "O^{18}/O^{16} Ratios of Minerals from Migmatites, Rapakivi Granites, and Orbicular Rocks", Lithos, vol. 2, pp. 1-8.

Holdaway, M. J., 1971, "Stability of Andalusite and the Aluminum Silicate Phase Diagram", Amer. Journ. Sci., vol. 271, pp. 97-131.

Holloway, J. R., 1973, "The System Pargasite - H_2O-CO_2: a Model for Melting of a Hydrous Mineral with a Mixed-Volatile Fluid -- I. Experimental Results to 8 Kbar", Geochim. et Cosmochim. Acta, vol. 37, pp. 651-666.

Holloway, J. R. and C. W. Burnham, 1972, "Melting Relations of Basalt with Equilibrium Water Pressure Less than Total Pressure", Journ. Petrol., vol. 13, pp. 1-29.

Hudson, F. S., 1922, "Geology of the Cuyamaca Region of California with Special Reference to the Origin of the Nickeliferous Pyrrhotite", Univ. of Calif. Publ. Geol. Sci., vol. 13, pp. 175-252.

Huebner, J. S. and M. Sato, 1970, "Compositions of the Relationships of Manganous Oxide and Nickel Oxide Buffers", Amer. Mineral., vol. 55, pp. 934-952.

Imlay, R. W., 1964, "Middle and Upper Jurassic Fossils from Southern California", Journ. Paleon., vol. 38, pp. 505-509.

Jahns, R. H., 1954, "Geology of the Peninsular Range Province, Southern California and Baja California", Calif. Div. Mines Bull. 170, Ch. 2, pp. 29-52.

Jakeš, P. and J. Gill, 1970, "Rare Earth Elements and the Island Arc Tholeiitic Series", Earth Planet. Sci. Lett., vol. 9, pp. 17-28.

Joesten, R. L., 1974, "Metasomatism and Magmatic Assimilation at a Gabbro-Limestone Contact, Christmas Mountains, Big Bend Region, Texas" Ph.D. Thesis, California Institute of Technology, 397 pp.

Kamb, W. B., 1958, "Isogyres in Interference Figures", Amer. Mineral., vol. 43, pp. 1029-1067.

Kay, R., N. J. Hubbard, and P. W. Gast, 1970, "Chemical Characteristics and Origin of Oceanic Ridge Volcanic Rocks", Journ. Geophys. Res., vol. 75, pp. 1585-1613.

Kistler, R. W. and Z. E. Peterman, 1973, "Variations in Sr, Rb, K, Na, and Initial Sr^{87}/Sr^{86} in Mesozoic Granitic Rocks and Intruded Wall Rocks in Central California", Geol. Soc. Amer. Bull., vol. 84, pp. 3489-3512.

Komar, P. D., 1972a, "Mechanical Interactions of Phenocrysts and the Flow Differentiation of Igneous Dikes and Sills", Geol. Soc. Amer. Bull., vol. 83, pp. 973-988.

----------, 1972b, "Flow Differentiation in Igneous Dikes and Sills", Geol. Soc. Amer. Bull., vol. 83, pp. 3443-3448.

Krummenacher, D., R. G. Gastil, J. Bushee, and J. Doupont, 1975, "K-Ar Apparent Ages, Peninsular Ranges Batholith, Southern California and Baja California", Geol. Soc. Amer. Bull., vol. 86, pp. 760-768.

Kuno, H., 1938, "On the Occurrence of Primary Cummingtonitic Hornblende in some Dacites from Japan", Proc. Imp. Acad. Tokyo, vol. 14, pp. 221-224.

Kushiro, I., 1972, "Effect of Water on the Composition of Magmas Formed at High Pressures", Journ Petrol., vol. 13, pp. 311-334.

Kushiro, I., N. Shimizu, and Y. Nakamura, 1972, "Composition of Coexisting Liquid and Solid Phases Upon Melting of Natural Garnet and Spinel Lherzolites at High Pressures: A Preliminary Report", Earth Planet. Sci. Lett., vol. 14, pp. 19-25.

Kushiro, I., K. Syono, and S. Akimoto, 1968, "Melting of a Peridotite Nodule at High Pressures and High Water Pressures", Journ. Geophys. Res., vol. 73, pp. 6023-6029.

Laird, J., 1977, "Phase Equilibria in Mafic Schist and the Polymetamorphic History of Vermont", Ph.D. Thesis, California Institute of Technology, 445 pp.

Larsen, E. S., 1938, "Some New Variation Diagrams for Groups of Igneous Rocks", Journ. Geol., vol. 46, pp. 505-520.

Larsen, E. S., Jr., 1948, "Batholith and Associated Rocks of Corona, Elsinore, and San Luis Rey Quadrangles, Southern California", Geol. Soc. Amer. Memoir 29, 182 pp.

Larsen, E. S., Jr. and W. Draisin, 1950, "Composition of the Minerals in the Rocks of the Southern California Batholith", Internat. Geol. Congr., Report of the 18th Session, Great Britain, Part 2, pp. 66-77.

Larsen, E. S., Jr., D. Gottfried, H. W. Jaffe, and C. L. Waring, 1958, "Lead-Alpha Ages of the Mesozoic Batholiths of Western North America", U. S. Geol. Surv. Bull. 1070-B, 62 pp.

Leake, B. E., 1965, "The Relationship Between Composition of Calciferous Amphibole and Grade of Metamorphism", in Controls of Metamorphism, ed. W. S. Pitcher and G. W. Flynn, Oliver and Boyd, Ltd., Edinburgh and London, pp. 299-318.

----------, 1971, "On Aluminous and Edenitic Hornblendes", Mineral. Mag., vol. 38, pp. 389-407.

Lindsley, D. H., 1963, "Fe-Ti Oxides in Rocks as Thermometers and Oxygen Barometers", Carn. Inst. Wash. Year Book 62, pp. 60-66.

----------, 1965, "Lower Thermal Stability of $FeTi_2O_5$-Fe_2TiO_5 (Pseudobrookite) Solid Solution Series", (abs.), Geol. Soc. Amer. Spec. Paper 87, p. 97.

----------, 1973, "Delimitization of the Hematite-Ilmenite Miscibility Gap", Geol. Soc. Amer. Bull., vol. 84, pp. 657-662.

Lipman, P. W., 1963, "Gibson Peak Pluton: A Discordant Composite Intrusion in the Southeastern Trinity Alps, Northern California", Geol. Soc. Amer. Bull., vol. 74, pp. 1259-1280.

Luth, W. C. and P. M. Fenn, 1973, "Calculation of Binary Solvi with Special Reference to the Sanidine-High Albite Solvus", Amer. Mineral., vol. 58, pp. 1009-1015.

Luth, W. C. and O. F. Tuttle, 1966, "The Alkali Feldspar Solvus in the System Na_2O-K_2O-Al_2O_3-SiO_2-H_2O", Amer. Mineral., vol. 51, pp. 1359-1373.

Maaløe, S. and P. J. Wyllie, 1975, "Water Content of a Granite Magma Deduced from the Sequence of Crystallization Determined Experimentally with Water-Undersaturated Conditions", Contr. Mineral. Petrol., vol. 52, pp. 175-191.

McEldowney, R. C., 1970, "An Occurrence of Paleozoic Fossils in Baja California, Mexico", (abs.), Geol. Soc. Amer. Abs. with Programs, vol. 2, no. 2, p. 117.

Metz, P., 1966, "Untersuchungen Eines Heterogenen Bivarianten, Gleichgewichts mit CO_2 und H_2O als Fluider Phase bei Hohen Drucken", Ber. Bunsen. Ges. Physik. Chem., vol. 70, pp. 1043-1045.

Metz, P. and V. Trommsdorff, 1968, "On Phase Equilibria in Metamorphosed Siliceous Dolomites", Contr. Mineral. Petrol., vol. 18, pp. 305-309.

Metz, P. and H. G. F. Winkler, 1964, Naturwiss, vol. 51, p. 400.

Miller, W. J., 1935, "A Geologic Section Across the Southern Peninsular Range of California", Calif. Journ. Mines Geol., vol. 31, pp. 115-142.

Minch, J. A., 1967, "Stratigraphy and Structure of the Tijuana-Rosarito Beach Area, Northwestern Baja California, Mexico", Geol. Soc. Amer. Bull., vol. 78, pp. 1155-1178.

----------, 1969, "A Depositional Contact Between the Pre-Batholithic Jurassic and Cretaceous Rocks in Baja California, Mexico", Geol. Soc. Amer. Abs. with Programs for 1969, Part 3, pp. 42-43.

----------, 1970, "Early Tertiary Paleogeography of a Portion of the Northern Peninsular Range", in Pacific Slope Geology of Northern Baja California and Adjacent Alta California, Guidebook for the Pacific Sections of AAPG, SEPM, and SEG, pp. 83-87.

Minch, J. A., K. C. Schulte, and G. Hofman, 1970, "A Middle Miocene Age for the Rosarito Beach Formation in Northwestern Baja California, Mexico", Geol. Soc. Amer. Bull., vol. 81, pp. 3149-3154.

Miyashiro, A., 1958, "Regional Metamorphism of the Gosaisyo-Takanuki District in the Central Abukuma Plateau", Journ. Fac. Sci. Univ. Tokyo, Sec. II, vol. 11, pp. 219-272.

Moore, G. W. and M. P. Kennedy, 1970, "Coastal Geology of the California-Baja California Border Area", in Pacific Slope Geology of Northern Baja California and Adjacent Alta California, Guidebook for the Pacific Sections of AAPG, SEPM, and SEG, pp. 4-9.

Morton, D. M., 1969, "The Lakeview Mountains Pluton, Southern California Batholith. Part I: Petrology and Structure", Geol. Soc. Amer. Bull., vol. 80, pp. 1539-1552.

Morton, D. M., A. K. Baird, and K. W. Baird, 1969, "The Lakeview Mountains Pluton, Southern California Batholith. Part II: Chemical Composition and Variation", Geol. Soc. Amer. Bull., vol. 80, pp. 1553-1564.

Mueller, R. F., 1972, "Stability of Biotite: A Discussion", Amer. Mineral., vol. 57, pp. 300-316.

Murase, T. and A. R. McBirney, 1973, "Properties of Some Common Igneous Rocks and Their Melts at High Temperatures", Geol. Soc. Amer. Bull., vol. 84, pp. 3563-3592.

Mysen, B. O., I. Kushiro, I. A. Nicholls, and A. E. Ringwood, 1974, "A Possible Mantle Origin for Andesitic Magmas: Discussion of a Paper by Nicholls and Ringwood", Earth Planet. Sci. Lett., vol. 21, pp. 221-229.

Nicholls, I. A. and A. E. Ringwood, 1973, "Effect of Water on Olivine Stability in Tholeiites and the Production of Silica-Saturated Magmas in the Island Arc-Environment", Journ. Geol., vol. 81, pp. 285-300.

Nockolds, S. R., 1941, "The Garabal Hill-Glen Fyne Igneous Complex", Quart. Journ. Geol. Soc., vol. 96, pp. 451-511.

----------, 1954, "Average Chemical Compositions of Some Igneous Rocks", Geol. Soc. Amer. Bull., vol. 65, pp. 1007-1032.

Orville, P. M., 1958, "Feldspar Investigations", Carn. Inst. Wash. Year Book 57, pp. 206-209.

----------, 1963, "Alkali Ion Exchange Between Vapor and Feldspar Phases", Amer. Journ. Sci., vol. 261, pp. 201-237.

Pabst, A., 1928, "Observations on Inclusions in Granitic Rocks of the Sierra Nevada", Univ. Calif. Publ. Geol. Sci., vol. 17, pp. 325-386.

Papike, J. J., K. L. Cameron, and K. Baldwin, 1974, "Amphiboles and Pyroxenes: Characterization of Other than Quadrilateral Components and Estimates of Ferric Iron from Microprobe Data", Geol. Soc. Amer. Abs. with Programs, vol. 6, pp. 1053-1054.

Peacock, M. A., 1931, "Classification of Igneous Rock Series", Journ. Geol., vol. 39, pp. 54-67.

Phillips, E. R. and P. C. Rickwood, 1975, "The Biotite-Prehnite Association", Lithos, vol. 8, pp. 275-281.

Pitcher, W. S. and A. R. Berger, 1972, The Geology of Donegal. A Study of Granite Emplacement and Unroofing, Wiley-Interscience, New York, 435 pp.

Piwinskii, A. J., 1968a, "Experimental Studies of Igneous Rock Series: Central Sierra Nevada Batholith, California", Journ. Geol., vol. 76, pp. 548-570.

----------, 1968b, "Studies of Batholithic Feldspars: Sierra Nevada, California", Contr. Mineral. Petrol., vol. 17, pp. 201-223.

----------, 1973a, "Experimental Studies of Igneous Rock Series, Central Sierra Nevada Batholith, California: Part II", Neues Jb. Mineral. Monat., H. 5, pp. 193-215.

----------, 1973b, "Experimental Studies of Granitoids from the Central and Southern Coast Ranges, California", Tschermaks Mineral. Petrog. Mitt., vol. 20, pp. 107-130.

Piwinskii, A. J. and P. J. Wyllie, 1968, "Experimental Studies of Igneous Rock Series: A Zoned Pluton in the Wallowa Batholith, Oregon", Journ. Geol., vol. 76, pp. 205- 234.

Piwinskii, A. J. and P. J. Wyllie, 1970, "Experimental Studies of Igneous Rock Series: Felsic Body Suite from the Needle Point Pluton, Wallowa Batholith, Oregon", Journ. Geol., vol. 78, pp. 52-76.

Presnall, D. C. and P. C. Bateman, 1973, "Fusion Relations in the System $NaAlSi_3O_8$-$CaAl_2Si_2O_8$-$KAlSi_3O_8$-SiO_2-H_2O and Generation of Granitic Magmas in the Sierra Nevada Batholith", Geol. Soc. Amer. Bull., vol. 84, pp. 3181-3202.

Pushkar, P., 1968, "Strontium Isotope Ratios in Volcanic Rocks of Three Island Arc Areas", Journ. Geophys. Res., vol. 73, pp. 2701-2714.

Ramberg, H., 1967, Gravity, Deformation, and the Earth's Crust, Academic Press, Inc., New York, 214 pp.

----------, 1970, "Model Studies in Relation to Intrusion of Plutonic Bodies", in Mechanisms of Igneous Intrusion, ed. G. Newall and N. Rast, Gallery Press, Liverpool, pp. 261-286.

Richardson, S. W., M. C. Gilbert, and P. M. Bell, 1969, "Experimental Determination of Kyanite-Andalusite and Andalusite-Sillimanite Equilibria; the Aluminum Silicate Triple Point", Amer. Journ. Sci., vol. 267, pp. 259-272.

Ringwood, A. E., 1975, Composition and Petrology of the Earth's Mantle, McGraw-Hill, Inc., New York, 618 pp.

Robertson, J. K. and P. J. Wyllie, 1971, "Experimental Studies on Rocks from the Deboullie Stock, Northern Maine, Including Melting Relations in the Water-Deficient Environment", Journ. Geol., vol. 79, pp. 549-571.

Robie, R. A. and D. R. Waldbaum, 1968, "Thermodynamic Properties of Minerals and Related Substances at 298.15°K (25.0°C) at One Atmosphere (1.013 bars) Pressure and at Higher Temperatures", U. S. Geol. Surv. Bull. 1259, 256 pp.

Rumble, D., 1971a, "Fe-Ti Oxide Minerals and the Behavior of Oxygen During Regional Metamorphism", Carn. Inst. Wash. Year Book 70, pp. 157-165.

----------, 1971b, "Thermodynamic Analysis of Phase Equilibria in the System Fe_2TiO_4-Fe_3O_4-TiO_2", Carn. Inst. Wash. Year Book 69, pp. 198-207.

Santillán, M. and T. Barrera, 1930, "Las Posibilidades Petrolíferas en la Costa Occidental de la Baja California, Entre los Paralelos 30° y 32° de Latitud Norte", Anales de Inst. Geol. de México, vol. V, pp. 1-37.

Schwarcz, H. P., 1969, "Pre-Cretaceous Sedimentation and Metamorphism in the Winchester Area, Northern Peninsular Ranges, California", Geol. Soc. Amer. Spec. Paper 100, 63 pp.

Seck, H. A., 1971, "Der Einfluss des Drucks auf die Zusammensetzung Koexistierender Alkalifeldspäte und Plagioklase im System $NaAlSi_3O_8$-$KAlSi_3O_8$-$CaAl_2Si_2O_8$-H_2O", Contr. Mineral. and Petrol., vol. 31, pp. 67-86.

Seitsaari, J., 1952, "On Association of Cummingtonite and Hornblende", Ann. Acad. Sci. Fennicae, ser. A., III, no. 30, 20 pp.

Shaw, H. R., D. L. Peck, T. L. Wright, and R. Okamura, 1968, "The Viscosity of Basaltic Magma: An Analysis of Field Measurements in Makaopuhi Lava Lake, Hawaii", Amer. Journ. Sci., vol. 266, pp. 225-264.

Silberling, N. J., J. E. Schoellhamer, C. H. Gray, Jr., and R. W. Imlay, 1961, "Upper Jurassic Fossils from Bedford Canyon Formation, Southern California", Amer. Assoc. Petrol. Geol. Bull., vol. 45, pp. 1746-1748.

Silver, L. T., C. R. Allen, and F. G. Stehli, 1969, "Geological and Geochronological Observations on a Portion of the Peninsular Range Batholith of Northwestern Baja California, Mexico", (abs.), Geol. Soc. Amer. Spec. Paper 121, pp. 279-280.

Silver, L. T., T. O. Early, and T. H. Anderson, 1975, "Petrological, Geochemical, and Geochronological Asymmetries of the Peninsular Ranges Batholith", Geol. Soc. Amer. Abs. with Programs, vol. 7, no. 3, pp. 375-376.

Silver, L. T., F. G. Stehli, and C. R. Allen, 1956, "Lower Cretaceous Pre-Batholithic Rocks of Northern Baja California, Mexico". (abs.), Internat. Geol. Congr., Report of the 20th Session, Mexico City, Resumenes de los Trabajos Presentados, p. 30.

Silver, L. T., F. G. Stehli, and C. R. Allen, 1963, "Lower Cretaceous Pre-Batholithic Rocks of Northern Baja California, Mexico", Amer. Assoc. Petrol. Geol. Bull., vol. 47, pp. 2054-2059.

Skinner, B. J., 1966, "Thermal Expansion", in Handbook of Physical Constants, ed. S. P. Clark, Jr., Geol. Soc. Amer. Memoir 97, pp. 75-96.

Smith, D. L., 1972, "The Vertical Distribution of Heat Production and Heat Flow in Northwestern Mexico", Ph.D. Thesis, University of Minnesota, 174 pp.

----------, 1974, "Heat Flow, Radioactive Heat Generation, and Theoretical Tectonics for Northwestern Mexico", Earth Planet. Sci. Lett., vol. 23, pp. 43-52.

Smith, T. E., 1975, "Layered Granitic Rocks at Chebucto Head, Halifax County, Nova Scotia", Can. Journ. Earth Sci., vol. 12, pp. 456-463.

Stern, C. R., W. L. Huang, and P. J. Wyllie, 1975, "Basalt-Andesite-Rhyolite-H_2O: Crystallization Intervals with Excess H_2O and H_2O-Undersaturated Liquidus Surfaces to 35 Kilobars, with Implications for Magma Genesis", Earth Planet. Sci. Lett., vol. 28, pp. 189-196.

Stewart, F. H., 1947, "The Gabbroic Complex in Belhevie in Aberdeenshire", Quart. Journ. Geol. Soc., vol. 102, pp. 465-498.

Stormer, J. C., Jr., 1975, "A Practical Two-Feldspar Geothermometer", Amer. Mineral., vol. 60, pp. 667-674.

Streckeisen, A. L., 1973, "Plutonic Rocks: Classification and Nomenclature Recommended by the IUGS Subcommission on the Systematics of Igneous Rocks", Geotimes, vol. 18, no. 10, pp. 26-30.

Sun, S. S., 1973, "Lead Isotope Studies of Young Volcanic Rocks from Oceanic Islands, Mid-Ocean Ridges, and Island Arcs", Ph.D. Thesis, Columbia University.

Taylor, H. P., Jr., 1968, "The Oxygen Isotope Geochemistry of Igneous Rocks", Contr. Mineral. Petrol., vol. 19, pp. 1-71.

Taylor, H. P., Jr. and S. Epstein, 1962, "Relationship Between O^{18}/O^{16} Ratios in Coexisting Minerals of Igneous and Metamorphic Rocks. Part I: Principles and Experimental Results", Geol. Soc. Amer. Bull., vol. 73, pp. 461-480.

Taylor, S. R., 1969, "Trace Element Chemistry of Andesites and Associated Calc-Alkaline Rocks", in Proceedings of the Andesite Conference, ed. A. R. McBirney, Oregon Dept. Geol. and Min. Industries Bull. 65, pp. 43-63.

Thompson, J. B., Jr. and D. R. Waldbaum, 1969, "Mixing Properties of Sanidine Crystalline Solutions: III. Calculations Based on Two-Phase Data", Amer. Mineral., vol. 54, pp. 811-838.

Thornton, C. P. and O. F. Tuttle, 1960, "Chemistry of Igneous Rocks I. Differentiation Index", Amer. Journ. Sci., vol. 258, pp. 664-684.

Tuttle, O. F., 1952, "Optical Studies of Alkali Feldspars", Amer. Journ. Sci., Bowen Volume, pp. 553-567.

Tuttle, O. F. and N. L. Bowen, 1958, "Origin of Granite in the Light of Experimental Studies", Geol. Soc. Amer. Memoir 74, 153 pp.

Vance, J. A., 1961, "Polysynthetic Twinning in Plagioclase", Amer. Mineral. vol. 46, pp. 1097-1119.

----------, 1969, "On Synneusis", Contr. Mineral. Petrol., vol. 24, pp. 7-29.

Vollmer, R., 1977, "Terrestrial Lead Isotopic Evolution and Formation Time of the Earth's Core", Nature, vol. 270, pp. 144-147.

von Platen, H., 1965, "Kristallisation Granitischer Schmelzen", Beitr. Mineral. Petrog. (Contr. Mineral. Petrol.), vol. 11, pp. 334-381.

Waldbaum, D. R. and J. B. Thompson, Jr., 1969, "Mixing Properties of Sanidine Crystalline Solutions: IV. Phase Diagrams from Equations of State", Amer. Mineral., vol. 54, pp. 1274-1298.

Waters, A. C. and K. Krauskopf, 1941, "Protoclastic Border of the Colville Batholith", Geol. Soc. Amer. Bull., vol. 52, pp. 1355-1418.

Webb, R. W., 1939, "Evidence of the Age of a Crystalline Limestone, Southern California", Journ. Geol., vol. 47, pp. 198-201.

White, A. J. R. and B. W. Chappell, 1977, "Ultrametamorphism and Granitoid Genesis", Tectonophysics, vol. 43, pp. 7-22.

Whitney, J. A., 1975, "The Effect of Pressure, Temperature, and X_{H_2O} on Phase Assemblage in Four Synthetic Rock Compositions", Journ. Geol., vol. 83, pp. 1-31.

Wilshire, H. G., 1969, "Mineral Layering in the Twin Lakes Granodiorite, Colorado", in Igneous and Metamorphic Geology (Arie Poldervaart volume), Geol. Soc. Amer. Memoir 115, pp. 235-261.

Wilson, J. C., 1961, "Geology of the Alta Stock, Utah", Ph.D. Thesis, California Institute of Technology, 236 pp.

Winchell, H., 1965, Optical Properties of Minerals -- A Determinative Table, Academic Press, Inc., New York, 91 pp.

Winchell, A. N. and H. Winchell, 1951, Elements of Optical Mineralogy, Part II: Description of Minerals, 4th edit., John Wiley and Sons, Inc., New York, 551 pp.

Winkler, H. G. F., 1967, Petrogenesis of Metamorphic Rocks, rev. 2nd edit., trans. by N. D. Chatterjee and E. Froese, Springer-Verlag New York, Inc., 237 pp.

Wisser, E., 1954, "Geology and Ore Deposits of Baja California, Mexico", Econ. Geol., vol. 49, pp. 44-76.

Wones, D. R., 1972, "Stability of Biotite: A Reply", Amer. Mineral., vol. 57, pp. 316-317.

Wones, D. R. and H. P. Eugster, 1965, "Stability of Biotite: Experiment, Theory and Application", Amer. Mineral., vol. 50, pp. 1228-1272.

Wones, D. R. and W. C. Gilbert, 1969, "The Fayalite-Magnetite-Quartz Assemblage Between 600° and 800°C", Amer. Journ. Sci., Schairer Volume, vol. 267-A, pp. 480-488.

Woodford, A. O., 1925, "The San Onofre Breccia; its Nature and Origin", Univ. Calif. Dept. Geol. Sci. Bull., vol. 15, pp. 159-280.

----------, 1928, "The San Quintín Volcanic Field, Lower California", Amer. Journ. Sci., 5th Series, vol. 15, pp. 337-345.

Woodford, A. O. and T. F. Harriss, 1938, "Geological Reconnaissance Across Sierra San Pedro Mártir, Baja California", Geol. Soc. Amer. Bull., vol. 49, pp. 1297-1336.

Wyllie, P. J., W. L. Huang, C. R. Stern, and S. Maaløe, 1976, "Granitic Magmas: Possible and Impossible Sources, Water Contents, and Crystallization Sequences", Can. Journ. Earth Sci., vol. 13, pp. 1007-1019.

Yeats, R. S., J. A. Minch, and J. A. Forman, 1971, "Paired Basement Terranes in Baja California Sur, Mexico", Geol. Soc. Amer. Abs. with Programs, vol. 3, no. 7, p. 760.

Yoder, H. S., Jr., 1969, "Calcalkalic Andesites: Experimental Data Bearing on the Origin of their Assumed Characteristics", in Proceedings of the Andesite Conference, ed. A. R. McBirney, Oregon Dept. Geol. and Min. Industries Bull. 65, pp. 77-89.

Yoder, H. S., D. B. Stewart, and J. R. Smith, 1957, "Ternary Feldspars", Carn. Inst. Wash. Year Book 56, pp. 206-214.

APPENDIX A

THIN-SECTION DESCRIPTIONS OF TONALITE SAMPLES ANALYZED FOR WHOLE-ROCK AND/OR MINERAL CHEMICAL COMPOSITION

The following descriptions are arranged into four groups corresponding to the four major textural phases of the tonalite; within each group, descriptions are presented in sequence of increasing sample number. The first sample in each group is described in full detail. Descriptions of other samples are more brief and simply refer back to the first (or another) description in that group wherever possible. Unless otherwise noted, plagioclase compositions are based upon optical determination; the latter agree well with microprobe analyses from the same rocks. The term "primary" denotes grains which formed by direct crystallization rather than by replacement of a pre-existing solid phase. Primary minerals may have formed by crystallization either from the melt or from a vapor phase.

Abbreviations used:

Rock units:

GBT: gneissose border tonalite
SHbT stubby hornblende tonalite
PHbT: prismatic hornblende tonalite
SPT: seriate porphyritic tonalite

Mineral names:

actin: actinolite, actinolitic
ab: albite
amph: amphibole
An: anorthite content
ap: apatite
bio: biotite
chab: chabazite
chl: chlorite
cpx: clinopyroxene
cumm: cummingtonite, cummingtonitic
ep: epidote
hem: hematite
hb: hornblende
ilm: ilmenite
Kfld: K-feldspar
"meta-ilm": "meta-ilmenite"
micr: microcline
mt: magnetite
op: opaque
orth: orthoclase
plag: plagioclase
qtz: quartz
rut: rutile
san: sanidine
sph: sphene
w mica: white mica
zeol: zeolite
zir: zircon

Abbreviations used (continued):

Textural and other terms

abrd: abraded
adj: adjacent
agg(s): aggregate(s)
alt: alteration
anal: analyses
anh: anhedral
anom: anomalous
App: Appendix
approx: approximately
assoc: associated
ave: average
bl: blue, bluish
brn: brown, brownish
Carls: Carlsbad
cg: course-grained
chem: chemical
comp: composition
conc: concentrated, concentration
contam: contamination
defm: deformation
discont: discontinuous
distrib: distribution
elong: elongate
equigran: equigranular
esp: especially
euh: euhedral
ext: extinction
fg: fine-grained
fol: foliated, foliation
frag(s): fragment(s)
gen: generally
gn: gneissose
gran: granular
granobl: granoblastic
grn: green, greenish
hyp: hypidiomorphic
interf: interference
interst: interstitial
irreg: irregular
med: medium
mg: medium-grained
min(s): mineral(s)
mod: moderate
myrm: myrmekite
occas: occasional, occasionally
olv: olive
ora: orange
oscil: oscillatory
per: pericline
photomic(s): photomicrograph(s)
pleo: pleochroic, pleochroism
poik: poikilitic
polygran: polygranular
prep: preparation
procl: protoclasis, protoclastic
progr: progressive
prpl: purple
reg: regular
rel(s): relict(s)
rxld: recrystallized
rxltn: recrystallization
scat: scattered
ser: seriate
sl: slight, slightly
spec(s): specimen(s)
struc: structural
subh: subhedral
synn: synneusis
temp: temperature
tr: trace
undul: undulatory
unfol: unfoliated
unident: unidentified
utw: untwinned
vfg: very fine-grained
w/: with
w/in: within
w/out: without
xl(s): crystal(s)
xltn: crystallization
yel: yellow
+ve: positive
-ve: negative

Samples of the Gneissose Border Phase of the Stubby Hornblende Tonalite

BC-I-5 (collected by L. T. Silver) and Ba-JM-30a (collected by the author) same locality; gneissose border phase of stubby hornblende tonalite

Location: ∿35 m from the NW margin of pluton, 610 m NE of Buena Vista-Coyote road at base of E wall of Arroyo El Tepetate (Plate 2, area D-3,4)

Textures and general description: med to light gray flaser gneiss; hyp gran, mg (0.3-3 mm), ser, modified by mod procl and rxltn; sparse plag and hb xls up to 10 mm; 5% mortar (≤0.1 mm), largely rxld; mod to strong planar orientation of plag; mafics mainly fg, in wavy stringers and aggs between plag xls; oval platy bio aggs 1 cm across give spotty or streaked appearance to surfaces parallel to fol (photo, Fig 15).

Mineralogy

25.4	quartz: thin polygran stringers of anh 0.01-1 mm xls w/ interlocking mutual contacts; stringers up to 3 mm long parallel to fol; weak to mod undul ext
54.4	plagioclase: (anal, Tables 7 and 8; also App C, Table C-4) 0.5-3 mm, plus some vfg mortar and sparse xls up to 10 mm; anh-subh, occas euh, stout tablets; strongly abrd; some bending and breaking; mod euh progr and oscil zoning; some patchy zoning and veining by rim comp; ave interiors, An = 37-42; rims, 21-24; rare gran rxltn; Carls, ab, and per twinning common; many composite synn xls; tr myrm; tr alt to ep, w mica, Kfld, and clay(?)
1.4	K-feldspar: (anal, Table 11; also App C, Table C-5) orth (utw, 2V∿35-45°), plus some micr; 0.01-1 mm, anh, interst and irreg branching, often polygran; tr alt of plag
4.7	hornblende: (anal, Table 12; also App C, Table C-6) 0.3-2.5 mm, plus some vfg mortar and sparse xls up to 10 mm; anh, broken and abrd; some rel elong prisms, not esp poik; unzoned, α=grn-yel, β=sl brn-grn, γ=sl bl-grn
10.0	biotite: (anal, Table 17; also App C, Table C-7) 0.05-1.5 mm, anh-subh, in thin platy aggs; α=gray-gold, β=γ=olv-brn; tr olv-grn color near sph; tr alt to chl
0.7	magnetite: (anal, Table 18; also App C, Table C-8) ≤0.3 mm, subh, euh, equant; aggs, often assoc w/sph and bio
tr	hematite-ilmenite: ≤0.05 mm, anh, subequant; hem-rich intergrowths w/5-10% rut lamellae; much alt to sph
tr	sulfide(?): ≤0.01 mm; possibly brass contam from thin section prep
tr	hematite: ≤0.03 mm, euh, red-brn flakes in plag

BC-I-5 and Ba-JM-30a (continued)

1.1 sphene: 0.2-0.8 mm, subh-euh, scat xls; also ≤0.1 mm, anh-subh, aggs gen assoc w/bio and op; light to med brn, weakly pleo; occas weak pleo halos in adj hb

0.5 epidote: ≤1 mm, anh; colorless to weakly pleo in shades of grn-yel; assoc w/hb and bio; also alt of plag and raggedly interst

0.7 white mica: ≤1 mm, anh-subh; alt of plag; also scat xls and aggs assoc w/bio

1.0 clay(?): vfg unident alt of plag

0.006 apatite: 0.06 mm, subh-euh, colorless to very pale yel-grn

0.1 chlorite: alt of bio and rarely of hb and plag; mostly α=β=bright grn, γ=light grn-yel, w/anom light brn interf color; some is α=light grn-yel, β=γ=bright grn, w/anom bl or prpl interf color

tr zircon: ≤0.05 mm, subh-euh, rare weak pleo halos in adj hb and bio

tr rutile: tiny exsolved lamellae in hem-ilm; also ≤0.02 mm, anh xls assoc w/bio and chl

tr actinolitic(?) amphibole: rare tiny anh, pale grn, homoaxial patches in hb

Notable characteristics: typical of GBT, but w/distinct differences (besides procl) from typical SHbT; abundance of qtz, bio, and Kfld; non-poik elong prismatic form of least broken and abrd hb; mod euh zoning of plag; abundance and frequently coarse subh-euh form of sph in place of hem-ilm. Other characteristics: mortar partially rxld to granobl aggs; strain in qtz largely annealed; delicate branching form and mod high-temp struc state of Kfld; vfg sph conc between bio flakes and bio aggs.

Ba-JM-27a: gneissose border phase of stubby hornblende tonalite

Location: ∿15 m from NE margin of pluton on Concepción road ∿40 m E of Rancho Cerro Costilla (Plate 2, area C-9)

Textures and general description: (photomics, Fig. 31) med gray gneiss very similar to BC-I-5, except gn layering is quite smooth and reg; min orientation very strong

Mineralogy

23.6 quartz: same as in BC-I-5, but w/more complex interlocking and sutured qtz-qtz contacts; strong undul ext; also occas 0.1-1 mm, anh-subh xls included in hb, some rutilated; rare similar inclusions in plag

54.2 plagioclase: grain size, textures, zoning, and twinning same as in BC-I-5; ave interiors, An = 33-40, w/calcic patches and discont zones 42-52; rims, 21-23; tr local rims, veins, and patches 18-20; sl alt to ep, w mica, Kfld, and clay(?)

0.2 K-feldspar: same as in BC-I-5, but more fg (≤0.3 mm)

4.8 hornblende: same as in BC-I-5, except that larger xls commonly include 1 or 2 anh-subh, 0.1-1 mm plag and/or qtz grains

Ba-JM-27a (continued):

10.6	biotite: same as in BC-I-5
0.4	magnetite: same as in BC-I-5
tr	hematite-ilmenite: same as in BC-I-5
tr	sulfide(?): same as in BC-I-5
tr	hematite: same as in BC-I-5
1.0	sphene: same as in BC-I-5
2.5	epidote: same as in BC-I-5; also occas subh xls
0.6	white mica: same as in BC-I-5
1.7	clay(?): same as in BC-I-5
0.13	apatite: same as in BC-I-5
0.09	chlorite: same as in BC-I-5
tr	zircon: same as in BC-I-5
tr	actinolitic amphibole: small, anh, pale grn, homoaxial patches in hb, locally containing tiny qtz blebs
tr	clinopyroxene(?): one 0.15 mm, anh, pale grn rel in hb, partially rimmed and replaced by actin + qtz
tr	rutile: same as in BC-I-5; also minute needles in a few qtz xls included in hb and plag

Notable characteristics: same distinctive features as in BC-I-5 except: less Kfld; crushing and strain of qtz is less annealed by rxltn; the larger, least broken hb xls have elong prismatic forms as in BC-I-5, but also commonly include one or more plag and/or qtz grains as in typical SHbT

Ba-JM-568a: gneissose border phase of stubby hornblende tonalite

Location: NW margin of pluton in Arroyo de las Parritas, 45 m from pluton contact (Plate 2, area F-3)

Textures and general description: light to med gray gneiss very much like BC-I-5, but sl less procl and sl stronger planar min orientation; 2-3% mortar

Mineralogy

22.7	quartz: same as in BC-I-5, also occas 0.1-0.3 mm, anh-subh, equant inclusions in hb, commonly rutilated
55.4	plagioclase: grain size, textures, zoning and twinning same as in BC-I-5; ave interiors, An=33-40, w/rel calcic patches, zones, and rare cores 49-52; rims, 21-25; tr myrm as rims (photomic, Fig. 56) and separate grains; minor alt to clay(?), w mica, ep, and Kfld
2.1	K-feldspar: same as in BC-I-5 (photomic, Fig 33)
6.9	hornblende: like that in BC-I-5, but w/weak patchy zoning (γ= sl brn-grn to sl bl-grn); also commonly includes one or more 0.1-0.4 mm, anh-subh plag and/or qtz xls
8.7	biotite: same as in BC-I-5
0.6	magnetite: same as in BC-I-5
tr	hematite-ilmenite: same as in BC-I-5
tr	hematite: same as in BC-I-5
0.7	sphene: anh-subh; otherwise same as in BC-I-5
0.3	epidote: same as in BC-I-5
0.4	white mica: same as in BC-I-5
1.5	clay(?): same as in BC-I-5

Ba-JM-568a (continued):

0.2 apatite: same as in BC-I-5
0.4 chlorite: same as in BC-I-5
tr zircon: same as in BC-I-5
tr rutile: same as in BC-I-5; also minute needles in a few qtz grains included in hb
tr actinolitic amphibole: same as in Ba-JM-27a
tr allanite: small aggs of vfg, anh, strongly pleo, ora-brn xls in hb; pleo halos in hb

Notable characteristics: same as those of BC-I-5, except for weak zoning and mod poik character of hb, which are features characteristic of the non-gneissose SHbT

Ba-JM-807: gneissose border phase of stubby hornblende tonalite

Location: E margin of pluton ∿900 m S of Cañon Campo Buena Vista; ∿30 m from pluton contact (Plate 2, area H-13)

Textures and general description: med gray flaser gneiss; hyp gran, mg (1-4 mm), ser, modified by mod procl and rxltn; 5% mortar <0.1 mm, largely rxld to granobl aggs; mod to strong planar min orientation; hb and plag abrd; hb xls commonly broken; many 1-2.5 mm subequant, sl poik, abrd hb grains; bio fg, conc in thin planar aggs 1 cm or more across in the plane of fol

Mineralogy

19.2 quartz: an, interst 0.05-2 mm aggs of interlocking xls; most aggs strongly elong parallel to fol, but numerous subequant patches up to 2 mm; mod undul ext; rare anh, equant, 0.1-0.2 mm inclusions in hb
58.3 plagioclase: same grain size, textures, and twinning as in BC-I-5; some mod to strong euh progr and oscil zoning, but more than half of xls show only weak zoning, often wavy or sl mottled; some veining or patchy replacement of interiors by rim comp; ave interiors, An=37-42, w/occas cores and patches = 50; rims, 23-26; sl alt to clay(?), ep, w mica, Kfld, and zeol (chab?)
0.13 K-feldspar: orth (and san?); ≤0.1 mm, anh, interst and replacing plag; utw, small to mod 2V
7.9 hornblende: 0.3-2.5 mm, plus minor vfg grains; anh to rarely subh, abrd and often broken, commonly contains one or more 0.1-0.5 mm, anh-subh plag inclusions; weak patchy zoning as in Ba-JM-568a; many grains are clearly frags or larger anh, poik, initially-equant(?), weakly zoned grains like those characteristic of SHbT; also some elong prisms as in BC-I-5
10.8 biotite: 0.05-1.5 mm, subh-euh xls in aggs up to 5 mm long and gen 0.2-0.5 mm thick; xls are undeformed and vary from strongly aligned to randomly oriented (photomic, Fig 32); pleo same as in BC-I-5; sl alt to chl
0.3 magnetite: same as in BC-I-5
tr hematite-ilmenite: same as in BC-I-5
tr sulfide: ≤0.01 mm, anh-euh; brassy, weakly anisotropic pyrite(?) and rare composite bornite-chalcocite(?) xls
tr hematite: same as in BC-I-5

Ba-JM-807 (continued)

0.7 sphene: same as in BC-I-5

1.1 epidote: same as in BC-I-5, but w/occas subh-euh xls up to 1 mm assoc w/bio and hb; rare skeletal branching grains up to 1.5 mm

0.13 white mica: ≤0.5 mm, anh-subh, alt of plag

1.1 clay(?): vfg unident alt of plag

0.13 apatite: ≤0.3 mm, subh-euh

0.2 chlorite: same as in BC-I-5

tr zircon: ≤0.3 mm, subh-euh

tr rutile: tiny exsolved lamellae in hem-ilm

tr zeolite: chabazite(?); 0.05-0.3 mm, anh, alt of plag; also raggedly interst (primary?)

tr allanite: single 0.2 mm, anh, ragged interst grain w/thin ep rim

tr actinolitic amphibole: single 0.35 mm, anh xl in hb; mottled light to med grn; not homoaxial w/enclosing hb

tr prehnite: colorless to rusty sheaths of platy xls in bio; in part replacing and in part bulging apart cleavage plates of bio

Notable characteristics: similar to those of BC-I-5, but w/sl less qtz and much less Kfld; also less euh zoning in plag; less gn and procl, and qtz less strung out; bio completely rxld, but aggs are less flattened than in other GBT samples; undeformed subh-euh bio flakes indicate rxltn after defm ceased; weak zoning of hb like that in Ba-JM-568a and in SHbT; some elong hb xls; some relatively cg zir and ap xls. All of these features make this rock transitional between the other GBT samples and typical SHbT, but closer to former; textures suggest xltn of ep and sph concurrently w/rxltn of bio, but some sph is abrd or broken and grew before defm ceased

Samples of the Stubby Hornblende Tonalite

Ba-JM-25a: stubby hornblende tonalite

Location: center of SHbT in NNE; S bank of Arroyo Cerro Costilla, ∿50 m W of Las Encinas corral, ∿100 m S of Concepción road (Plate 2, area D-9)

Textures and general description: light tan-gray, mg (2-5 mm), hyp gran, w/mod fol and weak procl; plag and qtz have ser grain-size distrib, hb and bio more nearly equigran; occas plag, hb, and bio xls up to 10 mm; mafics subequant, mod poik, w/margins commonly molded around plag; mod planar orientation of plag, weak orientation of mafics; grain margins gen sl ragged, but sparse smooth euh plag faces; sl bending and breaking of grains; tr mortar (≤0.05 mm) partially rxld to granobl aggs

Mineralogy

15.9 quartz: anh, interst, single grains and aggs 0.05-4 mm, ave 1-2.5 mm; often sl elong parallel to fol; mod undul ext; qtz-qtz contacts often interlocking

58.7 plagioclase: (anal, Tables 7, 8 and 10; also App C, Table C-4) 0.5-6 mm, rarely up to 10 mm, ser, ave 1.5-3 mm; anh-subh, w/sparse euh faces, gen against qtz; margins gen sl ragged or rounded; occas bent and fractured xls; Carls, ab, and per twinning common; weak to mod zoning; ave interiors, An=37-41, w/calcic cores, patches, and zones 45-58; rims, 26-33; some xls show mod to strong euh oscil or progr zoning, but many appear unzoned or weakly zoned, and many others show mottled zoning due to partial internal homogenization and/or to replacement of interior zones by more sodic outer-zone comps; occas composite synn xls; sl alt to clay(?), ep, w mica, and rare Kfld

0.10 K-feldspar: ≤0.05 mm, anh, interst and replacing plag; utw

14.3 hornblende: (anal, Tables 12 and 13; also App C, Table C-6) 0.5-6 mm, mostly 2-4 mm; rare xls up to 10 mm; anh, poik, gen subequent (elong ≤1.5-1), w/margins commonly molded around and between plag and occas qtz xls; rare sub xls, still approx equant; margins sl ragged or smooth; most xls contain 1-10 anh-subh, often rounded, 0.1-1 mm inclusions of plag; op, ap, bio, and actin inclusions also common; occas qtz, cumm, zir, sph, ep, and cpx inclusions; weak to mod zoning most visible parallel to γ; α=grn-yel; β=brn-grn or yel-grn; γ=sl brn-grn in interior to bl-grn at margin; zoning is anh, patchy, and gradational, w/bl-grn rim comp extending varying distances inward from xl margins, sometimes farthest along cleavages or cracks; bl-grn hb also forms thin aureoles around included grains of other mins; some patchy zoning w/out clear core-rim pattern; zoning formed by post-xltn reactions w/out modification of primary textures

Ba-JM-25a (continued)

6.7 biotite: (anal, Table 17; also App C, Table C-7) 0.5-6 mm, ave 1-3 mm, rarely up to 10 mm; anh; thick, irreg-shaped books, sl poik, w/molded interst margins; commonly penetrates raggedly into plag; minor replacement of hb; frequent inclusions of op, ap and occas plag; minor bending and some rxltn into aggs of fg to mg subh xls; α=light gray-yel, β=γ=variably ora-brn to grn-brn or olv-brn; sl alt to chl ± sph and/or rut

1.3 opaque: approx equal amounts of magnetite and hematite-ilmenite; tr sulfide

magnetite: (anal, Table 18; also App C, Table C-8) ≤0.5 mm, subh-euh, single xls and aggs, often w/hem-ilm; commonly included in bio and hb; sl to mod alt to hem, mostly as lamellae parallel to (111)

hematite-ilmenite: (photomic, Fig 72A ≤0.5 mm, anh, single xls and aggs, often w/mt; rare subh-euh xls; commonly included in bio and hb; consists of ilm w/ widely varying proportions (tr up to >50% but gen 10-30%) of hem as lamellae parallel to (0001); occas 2 generations of lamellae, i.e., lamellae w/in lamellae; up to a few % of tiny rut lamellae in some xls; euh inclusions of ap common; mod alt to sph, plus some "meta-ilm" and rut

sulfide: pyrite(?); ≤0.01 mm, brassy, weakly(?) anisotropic

tr hematite: many ≤0.03 mm, thin euh flakes in most plag xls

0.2 sphene: ≤0.4 mm, anh, rarely subh; replacing hem-ilm; also assoc w/hb, bio, and chl; most, if not all, appears secondary

0.8 epidote: 0.05-0.7 mm, anh, rarely subh; colorless to pale grn-yel, weakly pleo; replacing plag and assoc w/ bio and hb; most, if not all, appears secondary

0.04 white mica: ≤0.2 mm, anh alt of plag

1.2 clay(?): vfg unident alt of plag

0.2 apatite: ≤0.5 mm, subh, euh; gen clear, very pale grn-yel, but many of larger xls are clouded w/vfg brn alt, esp in cores; clouded xls are gen corroded

0.5 chlorite: alt of bio and rarely of hb; mostly α=β=bright grn, γ=light grn-yel, w/anom light brn or grn-brn interf color; some is α=light grn-yel, β=γ=bright grn, w/anom bl or prpl interf color

0.06 pale amphibole: actinolitic amph more abundant than cummingtonitic amph

actinolitic amphibole: (anal, Table 22) two modes of occurrence: (1) very pale grn, anh, homoaxial patches ≤0.2 mm in hb, commonly containing abundant small blebs of qtz, and sometimes forming aureoles around rel cpx, cumm, or second type of actin amph; (2) pale to med grn or bl-grn, anh-subh, gen corroded, rel single xls and aggs ≤0.5 mm enclosed in hb, but not homoaxial w/hb; type-2 actin often contains abundant vfg op grains, but

Ba-JM-25a (continued):

no qtz, and is sometimes surrounded by a thin aureole of type-1 actin; also occas aggs of type-2 actin up to 2 x 5 mm not enclosed in hb

cummingtonitic amphibole: (anal, Table 21) 0.05-0.8 mm, anh, rounded, rel inclusions in hb; very pale tan, 2V large +ve, often w/fine lamellar (100) twinning; gen homoaxial w/enclosing hb; often contains abundant vfg op; sometimes partially replaced by actin

tr clinopyroxene: (anal, Table 20) ≤0.1 mm, anh, corroded rels in hb; very pale grn salite; gen separated from host hb by aureole of actin ± qtz blebs

tr zircon: 0.1-0.5 mm, euh, no particular assoc w/any min; no pleo halos in adj hb or bio

tr rutile: alt and rare tiny exsolved lamellae in hem-ilm; also minute needles in a few qtz xls included in hb; rare minute needles in plag; occas vfg, anh xls in and adj to bio

tr allanite: rare ≤0.2 mm, anh grains rimming and replacing hb; zoned to ep rims

Notable characteristics: typical of SHbT. Characterized by: equant, anh, poik, and molded form of hb; thick, anh, molded and sl poik bio books; patchy zoning of hb; predominance of weak or mottled zoning over strong progr or oscil zoning in plag; abundant tiny hem flakes in plag, giving plag a sl brn or ora color; presence of rel cpx and relatively abundant pale amph in hb; relatively cg zir and ap. Other notable features: paucity of Kfld; penetration and replacement of plag by bio; euh form and lack of alt of mt, compared to anh form and mod alt of hem-ilm to sph, "meta-ilm", and rut

Ba-JM-29b: stubby hornblende tonalite

Location: interior of SHbT in NNW, ∿15 m SW of Buena Vista-Coyote road, 670 m WNW of Rancho El Coyote (Plate 2, area D-5)

Textures and general description: light tan-gray, mg (2-5 mm), hyp gran, w/weak fol and very little procl; occas hb, bio, and plag xls up to 10 mm; very similar to Ba-JM-25a, but sl less deformed; plag light gray or gray-brn; very weak planar orientation of mafics; weak to mod orientation of plag; grain margins gen sl ragged and some grains broken, but some nearly smooth euh plag faces; mafics subequant, gen anh and poik, w/margins commonly molded around plag; sl tr mortar; rare bending of plag and bio

Mineralogy

12.5 quartz: similar to Ba-JM-25a, but aggs rarely >2.5 mm; some xls contain abundant rut needles and rare hem flakes

62.7 plagioclase: (anal, Tables 7, 8, and 9; also App C, Table C-4) grain size, textures, twinning, and zoning patterns similar to Ba-JM-25a; ave interiors, An=40-45 w/some patches and zones >45; rims, 25-31; some xls are complexly veined by and/or have patches or local thin rims of sodic plag (probe anal, An=17-20, Table 9);

Ba-JM-29 (continued):

minor alt to clay(?), w mica, ep, and Kfld

<0.2 K-feldspar: same as in Ba-JM-25a; much material counted as Kfld in the mode was later identified as sodic plag; actual Kfld content probably <0.1%

12.9 hornblende: (anal, Tables 12 and 13; also App C, Table C-6) same as in Ba-JM-25a

6.2 biotite: (anal, Table 17; also App C, Table C-7) same as in Ba-JM-25a

1.6 opaque: about twice as much magnetite (anal, Table 18; also App C, Table C-8) as hematite-ilmenite; tr sulfide; min characteristics same as in Ba-JM-25a; photomic of hem-ilm rimmed by sph, Fig 72B

tr hematite: tiny euh flakes in plag and rarely qtz

0.4 sphene: same as in Ba-JM-25a

0.5 epidote: same as in Ba-JM-25a; also rare 0.1 mm, anh, primary(?) interst grains

0.4 white mica: same as in Ba-JM-25a; also rare 0.1-0.2 mm, anh, primary(?) interst grains locally assoc w/interst Kfld

1.5 clay(?): vfg unident alt of plag

0.2 apatite: same as in Ba-JM-25a

0.7 chlorite: same as in Ba-JM-25a; also single 0.15 mm, anh, primary(?) interst flake w/inclusion of sph

tr pale amphibole: actinolitic amph (anal, Table 22) more abundant than cummingtonitic amph; characteristics and occurrence same as in Ba-JM-25a

tr clinopyroxene: (anal, Table 20) same as in Ba-JM-25a

tr zircon: same as in Ba-JM-25a

tr rutile: same as in Ba-JM-25a

tr allanite: single 0.4 mm, anh grain w/thin ep rim; replacing plag and bio

Notable characteristics: essentially indistinguishable from Ba-JM-25a except for sl weaker procl and sl greater development and preservation of euh xl outlines and of euh progr and oscil zoning in plag; typical SHbT

Ba-JM-39b: stubby hornblende tonalite

Location: inner margin of SHbT, ∿20 m E of San José-Observatorio road, 4 km ENE of Rancho San José; ∿15 m E of contact w/zone MZ-1 of diorite plus inclusion-rich PHbT (Plate 2, area K-11)

Textures and general description: light tan-gray, mg (2-5 mm), hyp gran, w/weak fol and procl; very similar to Ba-JM-25a, but sl less deformed and sl more leucocratic; occas subh hb faces; many plag xls sl brn or ora; minor rxltn of bio into aggs

Mineralogy

16.5 quartz: 0.5-3 mm, anh, interst, but w/numerous subequant xls or aggs of several xls; weak undul ext; rare anh-subh, 0.2-1 mm, rutilated inclusions in hb

64.0 plagioclase: grain size, textures, twinning, and zoning patterns same as in Ba-JM-25a; ave interiors, An=35-44; rims, 27-30; sl alt to clay(?), w mica, Kfld, and ep

Ba-JM-39b (continued):

0.05 K-feldspar: same as in Ba-JM-25a
10.8 hornblende: same as in Ba-JM-25a; perhaps sl less poik, and a few more subh xls
4.6 biotite: same as in Ba-JM-25a
1.9 opaque: same as in Ba-JM-25a
tr hematite: ≤0.03 mm, euh flakes in most plag xls and rarely in qtz
0.09 sphene: same as in Ba-JM-25a
0.4 epidote: same as in Ba-JM-25a
0.09 white mica: ≤0.05 mm, anh, replacing plag and bio; also occas thin rims around hem-ilm inclusions in plag
0.8 clay(?): vfg unident alt of plag
0.3 apatite: same as in Ba-JM-25a, except no corrosion or alt
0.4 chlorite: same as in Ba-JM-25a
0.05 pale amphibole: actinolitic amph more abundant than cummingtonitic amph; characteristics same as in Ba-JM-25a; most of actin amph is type-1
tr clinopyroxene: same as in Ba-JM-25a
tr zircon: same as in Ba-JM-25a; perhaps sl preference to occur w/op
tr rutile: same as in Ba-JM-25a
tr: allanite: same as in Ba-JM-25a

Notable characteristics: very similar to Ba-JM-25a, but sl weaker fol; 1-3 mm subequant xls and aggs of qtz sl more common than in 25a

Ba-JM-68: stubby hornblende tonalite

Location: north-central part of SHbT; ~700 m NE of Rancho El Coyote (100 m N of an abandoned road from Rancho El Coyote to the Tepetate road) (Plate 2, area D-6)

Textures and general description: (photomics, Fig 45A,B) light gray, mg (2-6 mm), hyp gran, w/weak fol and tr of procl; very similar to Ba-JM-25a, but sl weaker fol, mafics sl more cg (ave 3-6 mm), and plag has less brn tinge; grain margins gen sl irreg, but not notably abrd; mod planar orientation of plag much more pronounced than orientation of mafics; occas 6-10 mm plag, hb, and bio xls

Mineralogy

15.5 quartz: like that in Ba-JM-25a, but w/only weak undul ext; also rare anh-subh rutilated inclusions in hb
59.3 plagioclase: (anal, Tables 7, 8 and 10; also App C, Table C-4) 0.5-6 mm, ser, ave 2-4 mm; sparse xls up to 10 mm; subh, w/occas euh faces, esp against qtz, but gen w/sl irreg margins; zoning patterns and twinning same as in Ba-JM-25a; ave interiors, An=37-42; rims, 26-27, occas cores and patches, 45 and possibly greater; minor bending and fracturing; some xls complexly veined by rim comp or by plag which is sl more sodic than typical rim plag; minor alt to clay(?), w mica, ep, Kfld, and zeol
0.11 K-feldspar: same as in Ba-JM-25a

Ba-JM-68 (continued):

12.4	hornblende: (anal, Tables 12 and 13; also App C, Table C-6; photomics, Fig 45A,B) same as in Ba-JM-25a
7.5	biotite: (anal, Table 17; also App C, Table C-7; photomics, Fig 45A, B) very similar to Ba-JM-25a, but sl more cg (many 3-5 mm books) and commonly w/one or more 0.2-1 mm, anh-subh, ragged inclusions of plag; aggs of vfg, anh ilm + sph + rut in or adj to many xls -- bio often has grn tinge near these aggs
1.2	opaque: magnetite (anal, Table 18; also App C, Table C-8) sl more abundant than hem-ilm; tr sulfide (pyrite?); characteristics of mins same as in Ba-JM-25a, except very little alt of mt to hem
tr	hematite: same as in Ba-JM-25a
0.2	sphene: same as in Ba-JM-25a; also rare primary interst xls
1.0	epidote: 0.05-1.5 mm, anh-subh, rarely euh; color, pleo, and occurrence same as in Ba-JM-25a; also rare primary interst grains
0.5	white mica: $\leq$0.2 mm, anh-subh; alt of plag and rarely rimming hem-ilm xls included in plag
1.5	clay(?): vfg unident alt of plag
0.3	apatite: same as in Ba-JM-25a
0.5	chlorite: same as in Ba-JM-25a
0.13	actinolitic amphibole: (anal, Table 22) same as in Ba-JM-25a, except no aggs of type-2 actin seen
tr	clinopyroxene: same as in Ba-JM-25a
tr	zircon: same as in Ba-JM-25a
tr	rutile: vfg alt of hem-ilm and rare tiny exsolved lamellae in hem-ilm; vfg anh grains and aggs assoc w/ sph in chl and assoc w/sph and ilm in and adj to bio; rare minute needles in a few qtz xls included in hb
tr	allanite: rare vfg, anh patches in ep
tr	zeolite: tiny vein; colorless, low relief, low biref 2V $\sim$ 70° -ve

Notable characteristics: same as those of Ba-JM-25a; typical of SHbT

Ba-JM-453: stubby hornblende tonalite

Location: interior of eastern prong of SHbT in Cañon Campo Buena Vista, $\sim$540 m W of pluton margin (Plate 2, area H-12)

Textures and general description: (photomics, Fig 45G,H) light to med gray, mg (2-4 mm), hyp gran, w/mod fol and procl; plag light gray to med gray-brn; mafics anh-subh, subequant, poik, approaching equigran, commonly w/molded margins; strong planar orientation of plag, weak to mod planar orientation of mafics; grain margins sl irreg and abrd; rare smooth euh plag faces; 2-3% mortar; minor fracturing and microfaulting of grains; plag commonly bent; sl to mod rxltn of bio and incipient rxltn of plag and hb; rare veining of plag and hb by qtz

Ba-JM-453 (continued)

Mineralogy

13.1 quartz: anh, interst, 0.5-2 mm aggs of interlocking grains w/strong undul ext; rare anh-subh, 0.1-0.5 mm inclusions in hb, some rutilated

63.6 plagioclase: 0.5-4 mm, ser, anh-sub, gen w/abrd and corroded margins; rare smooth euh faces; mod to strong planar orientation; many xls bent, and some fractured, fragmented, rarely veined w/qtz; twinning and zoning patterns like those in Ba-JM-25a, but well-preserved oscil zoning is rare; ave interiors, An=40-47; rims, 27-30; occas calcic cores, patches, and zones, 48-53; interiors of many xls faintly clouded ora-brn w/minute needles and flakes of hem(?); larger (up to 0.03 mm) euh hem flakes and op xls also common; minor rxltn into aggs; sl alt to clay(?), w mica, ep, zeol, and Kfld

0.08 K-feldspar: same as in Ba-JM-25a

14.1 hornblende: (photomic, Fig 62B) very similar to Ba-JM-25a, but occas elong prisms; 0.5-4 mm, ave 1.5-3 mm; margins often sl ragged and abrd; some xls broken or rarely veined by qtz; minor replacement by bio, chl, and ep

5.6 biotite: texturally very similar to Ba-JM-25a, but gen ora-brn, rarely w/grn tinge; sl alt to chl; occas included sheaths of prehnite

1.2 opaque: magnetite sl more abundant than hematite-ilmenite; tr sulfide

magnetite: same as in Ba-JM-25a

hematite-ilmenite: similar in grain size, texture, and occurrence to Ba-JM-25a; ilm-rich intergrowths, w/ 5-25% hem lamellae; tr rut lamellae; ∿25% alt to "meta-ilm" and minor alt to sph and rut

sulfide: pyrite(?); same as in Ba-JM-25a

tr hematite: ≤0.03 mm, euh flakes in plag; frequently abundant, causing faint clouding of plag interiors

0.14 sphene: same as in Ba-JM-25a

0.4 epidote: same as in Ba-JM-25a; also rarely interst

0.08 white mica: vfg alt of plag; also rarely interst

0.5 clay(?): vfg unident alt of plag

0.4 apatite: ≤0.5 mm, subh-euh unaltered, rarely corroded

0.7 chlorite: same as in Ba-JM-25a

0.10 pale amphibole: actinolitic amph more abundant than cummingtonitic amph; characteristics and occurrence same as in Ba-JM-25a, except no aggs of type-2 actin seen

tr clinopyroxene: same as in Ba-JM-25a

tr zircon: rare 0.05-0.3 mm, subh-euh xls

tr rutile: same as in Ba-JM-25a

tr allanite: rare vfg patches in ep; also single 0.05 mm, euh inclusion in hb; pleo halos in adj hb

tr zeolite: chabazite(?) or heulandite(?); replacing plag

tr tourmaline: single 0.3 mm, anh, rel partially replaced by bio; mod pleo, ε=med gray-bl, ω=dark gray-bl

Ba-JM-453 (continued)

tr prehnite: sheaths of platy colorless to rusty xls bulging apart cleavage of bio and partially replacing bio; sheaths ave 0.1-0.5 mm; 2nd order bl interf color; parallel ext; 2V variable, 0° to ∿30°, +ve

tr garnet(?): single anh, interst, high-relief, colorless, isotropic grain

Notable characteristics: very similar to Ba-JM-25a, but sl more fg, more fol, and more procl; faint clouding of plag w/hem(?)

Ba-JM-492: stubby hornblende tonalite

Location: SE part of SHbT, ∿160 m SW of San José-Observatorio road and ∿200 m NW of pluton margin (Plate 2, area M-12)

Textures and general description: light gray, mg (2-5 mm), bio-hb tonalite similar to Ba-JM-25a, but w/sl differences; mod to strong planar orientation of plag, weak orientation of mafics, and sl procl (photomics, Fig 45E,F); grain margins sl abrd, but occas smooth euh plag faces; tr mortar; occas sl bending of plag; plag light gray, w/out brn tinge; mafics mostly equant, anh, sl poik, some w/margins molded around plag; occas subh hb prisms elong up to 2:1; minor rxltn of bio

Mineralogy

16.7 quartz: 0.05-3 mm, anh; some small interst grains and aggs, but many large single xls or aggs of several xls gen elong parallel to fol; margins of large aggs are molded and interst; mod to strong undul ext; embays plag and hb sl

61.1 plagioclase: 0.5-5 mm, ave 2-3 mm; subh, w/occas anh grains and occas euh faces; sl abrasion and occas sl bending; twinning and zoning patterns same as in Ba-JM-25a; ave interiors, An=37-41; rims, 24-26, rarely 22; common calcic patches and occas cores 43-50, and maybe higher; a few xls veined by sodic plag (An<24); sl alt to clay(?), ep, w mica, and Kfld

0.2 K-feldspar: same as in Ba-JM-25a

12.4 hornblende: gen very similar to Ba-JM-25a, but w/occas subh prisms elong up to 2:1; also margins less consistently molded, and sl larger proportion (∿20%) of hb xls lack plag inclusions; minor veining by qtz and alt to chl and ep

6.6 biotite: texturally like that in Ba-JM-25a, but consistently ora-brn; minor rxltn into aggs; very sl alt to chl

0.9 opaque: same as in Ba-JM-25a

tr hematite: occas tiny euh flakes in plag

0.08 sphene: ≤0.2 mm, anh, alt of hem-ilm and assoc w/hb, bio, and chl (mostly secondary?); also occas primary interst and subh-euh xls up to 0.5 mm

0.08 epidote: same as in Ba-JM-25a; also occas primary interst grains 0.1-0.4 mm

0.02 white mica: rare vfg alt of plag

Ba-JM-492 (continued)

0.4 clay(?): vfg unident alt of plag

0.15 apatite: same as in Ba-JM-25a, except not clouded

0.6 chlorite: alt of hb and bio; also rare primary(?) interst aggs w/multiple centers of fanning ext ("mosaic" chl); same optical properties as in Ba-JM-25a

0.08 pale amphibole: actinolitic amph more abundant than cummingtonitic amph; same characteristics as in Ba-JM-25a, but no aggs of type-2 actin

tr clinopyroxene: same as in Ba-JM-25a

tr zircon: same as in Ba-JM-25a

tr rutile: alt and rare lamellae in hem-ilm; also tiny anh xls assoc w/sph in chl and assoc w/sph and ilm in and adj to bio

tr allanite: rare 0.1-0.3 mm grains assoc w/hb; thin ep rims

tr zeolite: chabazite(?); ≤0.1 mm, anh, interst and alt of plag

Notable characteristics: much like Ba-JM-25a and other SHbT samples, but plag lacks brn tinge (few included hem flakes), and hb is sl less poik and occas subh; also occas primary interst ep, sph, and possibly chl

Ba-JM-566: stubby hornblende tonalite

Location: center of SHbT in NW, along Arroyo de las Parritas, ~660 m from both the pluton contact and the SHbT-PHbT contact zone (Plate 2, area F-3)

Textures and general description: light gray, mg (2-4 mm), hyp gran, w/weak to mod fol and very sl procl; sl tr mortar; grain margins gen sl ragged, but occas smooth euh plag faces; plag light gray, w/out brn tinge; mafics subequant, poik, mostly anh, w/molded margins common; occas subh hb faces; sl rxltn of bio into aggs and strong rxltn of qtz into aggs

Mineralogy

18.5 quartz: anh, interst aggs 0.5-5 mm; large aggs may be subequant or elong parallel to fol; most aggs consist of 10-50 or more ext domains, but sutured contacts are rare; weak to mod undul ext; some large aggs contain several subh-euh plag xls

58.8 plagioclase: 0.5-5 mm, ave 2-3 mm; subh, occas anh or euh; margins gen sl ragged, occas smoothly euh, esp against qtz; rare bending; twinning and zoning patterns same as in Ba-JM-25a, but xls w/mod to strong subh-euh progr and sl oscil zoning are as common or more common than mottled xls, and weakly zoned xls are minor; ave interiors, An=40-46, sometimes partially replaced by 34-35; rims, 22-26; occas calcic zones and patches, 50 or possibly higher; minor alt to clay(?), w mica, ep, and Kfld

0.2 K-feldspar: same as in Ba-JM-25a

Ba-JM-566 (continued)

12.1	hornblende: very similar to Ba-JM-25a, but w/occas subh xls; minor alt to chl and ep
6.5	biotite: very similar to Ba-JM-25a; most large xls contain one or more ragged inclusions of plag
1.3	opaque: sl more magnetite than hematite-ilmenite; tr sulfide
	magnetite: similar to Ba-JM-25a, but only tr of alt to hem; also many anh-subh interst xls and aggs
	hematite-ilmenite: grain size, textures, and occurrence similar to Ba-JM-25a; ilm-rich intergrowths w/15-20%, rarely up to 40%, hem lamellae, gen very small; tr rut lamellae; sl to mod alt to sph, "meta-ilm", and rut
	sulfide: pyrite(?); same as in Ba-JM-25a
tr	hematite: occas $\leq$0.03 mm euh flakes in plag
0.4	sphene: same as in Ba-JM-25a; also occas primary interst xls
0.2	epidote: like that in Ba-JM-25a, except gen $\leq$0.2 mm; also occas primary interst xls
0.4	white mica: $\leq$0.3 mm, anh-subh, alt of plag and intergrown w/chl ± sph as alt of bio; also rare primary(?) interst flakes
0.7	clay(?): vfg unident alt of plag
0.12	apatite: same as in Ba-JM-25a, except not clouded
0.5	chlorite: alt of bio and hb; also rare primary interst aggs w/multiple centers of fanning ext ("mosaic" chl)
tr	pale amphibole: actinolitic amph and possibly rare cummingtonite amphibole; same as in Ba-JM-25a
tr	clinopyroxene: same as in Ba-JM-25a
tr	zircon: same as in Ba-JM-25a
tr	rutile: same as in Ba-JM-25a

Notable characteristics: very similar to Ba-JM-25a and other SHbT samples, but w/several sl differences: less procl; ~10-20% of the hb xls have one or more subh faces, but these xls are still poik and approx equant; smooth euh plag faces and smooth interst textures are more abundant than in most SHbT samples, but still subordinate; euh progr and oscil zoning better developed or preserved in plag; rims of plag are sl more sodic; relatively few hem flakes in plag; large, frequently poik aggs of qtz probably rxld from large single xls; rare primary interst sph, ep, chl, and possibly w mica. These characteristics suggest sl conc of residual melt and volatiles in otherwise typical SHbT

Samples of the Prismatic Hornblende Tonalite

Ba-JM-36a: prismatic hornblende tonalite

Location: east-central part of PHbT, 3 km ENE of Rancho San José, 1.1 km W of the E margin of the PHbT (Plate 2, area K-10)

Textures and general description: light gray, mg (1-4 mm), hyp gran, w/weak to mod fol, weak lineation, and very little procl; rare plag and mafic xls up to 10 mm; all mins show ser size distrib; abundant mafic xls in all sizes from <1 mm to 4 mm, but mafics ave sl more fg than plag, and distrib of mafics is partially controlled by coarser plag; occas clustering of several mafic xls; grain margins gen sl ragged, but some smooth euh hb and plag faces; bio anh and platy; hb prisms subh, gen elong 2 or 3:1; some hb xls poik, but margins very rarely molded or interst; plag light gray, subh-euh, tabular parallel (010); mafics and plag show comparable preferred orientation

Mineralogy

13.9 quartz: 0.05-3 mm, ave 0.5-1.5 mm, anh, interst grains and aggs of several xls; also some 1.5-3 mm subequant grains and aggs w/molded or interst margins and occas w/one or more plag inclusions; some grains embay hb and plag sl; mod to strong undul ext

65.5 plagioclase (anal, Tables 7, 8, and 10, also App C, Table C-4) 0.1-5 mm, ser, ave 1.5-3mm; rare 6-10 mm xls; subh-euh, occas anh; margins gen sl ragged, but some smooth euh faces, esp against qtz; ragged margins appear due to competing growth and occas embayment by qtz rather than to abrasion; well-developed Carls, ab, and per twinning; strong euh progr and oscil zoning; also some mottled zoning as in Ba-JM-25a; few composite synn xls; ave interiors, An=37-43; rims, 29-33; thin calcic zones, patches, and cores, 40-47 and probably higher; sl alt to clay(?), zeol(?), w mica, ep, and Kfld

0.2 K-feldspar: (anal, Table 11; also App C, Table C-5) <0.05 mm, anh, interst and replacing plag; utw, small $\overline{2}V$ -ve

12.2 hornblende: (anal, Tables 12 and 14; also App C, Table C-6) 0.1-5 mm, ser, ave 1-2.5 mm; rare 6-10 mm xls; anh-subh, w/occas smooth euh faces; margins very rarely molded; some equant xls, but most are elong 2 or 3:1; some xls contain one or more ≤0.5 mm, anh-subh inclusions of plag, but many xls lack plag inclusions; op inclusions also common; occas weak subh-euh or patchy anh zoning visible parallel to γ similar in color to that in Ba-JM-25a and typical SHbT, but less pronounced; α=sl grn-tan, β=yel-grn or sl brn-grn γ=bl-grn, w/occas interiors or scat patches sl brn-grn; minor alt to chl and ep

Ba-JM-36a (continued)

3.8	biotite: (anal, Table 17; also App C, Table C-7) 0.1-4 mm, ave 0.5-2 mm, thin anh plates commonly w/molded or interst margins; rare 5-10 mm xls; frequent inclusions of plag and op; margins penetrate raggedly into and replace plag and occas hb; α= light gold-brn, β=γ=ora-brn or sl gray-brn, locally w/grn tinge; sl rxltn into aggs; 10-20% alt to chl ± sph or rut
1.2	opaque: sl more magnetite than hematite-ilmenite; tr sulfide
	magnetite: (anal, Table 18; also App C, Table C-8) ≤0.5 mm, in aggs up to 1 mm, often w/hem-ilm; variably anh to euh, mostly equant; gen included in or adj to hb or bio; some xls and aggs are interst; very sl alt to hem
	hematite-ilmenite: ≤0.5 mm, anh, equant or irreg; rare sub-euh xls; occurrence same as for mt; consists of lamellar and occas patchy intergrowths of hem and ilm, often w/several % rut lamellae; hem/(hem + ilm) variably 0.2-0.8, but usually 0.5-0.6; often two generations of hem and ilm lamellae, i.e., lamellae w/in lamellae; inclusions of ap common; sl to mod alt to sph, rut, "meta-ilm", and patchy intergrowths of hem + rut
	sulfide: ≤0.01 mm, anisotropic(?), brassy pyrite(?)
tr	hematite: sparse ≤0.03 mm, euh flakes in some plag xls
0.5	sphene: ≤0.5 mm, anh, alt of hem-ilm and assoc w/bio, hb, and chl (mostly or entirely secondary); rare primary(?) interst grains
0.4	epidote: 0.05-1 mm, anh-subh, replacing plag and assoc w/bio, hb, and chl (mostly or entirely secondary); variably colorless to pleo in shades of grn-yel
tr	clinozoisite or zoisite: single 0.1 mm, anh, primary(?) interst grain; colorless, 2V large +ve
0.09	white mica: ≤0.2 mm, anh-subh, replacing plag; also rare primary(?) interst grains occurring w/interst Kfld
1.0	clay(?): vfg unident alt of plag
0.2	apatite: ≤0.3 mm, subh-euh, colorless or very pale grn-yel
1.0	chlorite: alt of bio and occas of hb and plag; also rare primary(?) interst grains; mostly α=β=bright grn, γ=light grn-yel, w/anom light brn or grn-brn interf color; rarely α=light grn-yel, β=γ=bright grn, w/anom bl or prpl interf color
tr	actinolitic amphibole: rare ≤0.5 mm, anh patches in hb, gen homoaxial w/the hb; very pale grn, weakly pleo; some patches contain abundant tiny blebs or vermicular grains of qtz; rarely encloses rel cpx inclusions in hb (photomics, Fig 76)
tr	cummingtonitic amphibole: (anal, Table 21) very rare ≤0.3 mm, anh patches in hb; same as in Ba-JM-25a and other SHbT samples

Ba-JM-36a (continued)

tr clinopyroxene: (photomics, Fig 76) very rare ≤0.2 mm, anh, corroded rels in hb, surrounded by halos of actin amph ± vfg qtz; very pale grn

tr zircon: few 0.05-0.1 mm, subh-euh xls commonly included in bio, hb, or op; occas faint pleo halos in adj bio or hb

tr rutile: tiny exsolved lamellae and patchy alt of hem-ilm

tr allanite: ≤0.3 mm, anh, vfg, replacing plag; zoned to ep rims

tr zeolite: anh fg alt of plag

Notable characteristics: most characteristics typical of PHbT unit; plag light gray, w/mod to strong euh progr and oscil zoning and gen few if any included flakes of hem; hb subh, occas euh, elong prisms lacking molded margins; bio anh and platy; mafics show ser grain-size distrib, w/abundant xls in all sizes from <1 to 4 mm; preferred orientation of mafics comparable to that of plag; hem ≥ ilm in hem-ilm intergrowths; 2-3 mm subequant grains and aggs of qtz more common than in most SHbT samples; characteristic of eastern part of PHbT, but differs sl from western part in having less qtz, Kfld, and bio, but higher color index, hb/bio ratio, and An content in plag rims; weak zoning (occas subh-euh) and abundance of plag inclusions in some hb xls and presence of relict cpx are unusual for PHbT

Ba-JM-46a: prismatic hornblende tonalite

Location: west-central part of PHbT, ∿40 m W of Quatal road, 1.3 km N of Rancho Quatal (Plate 2, area J-5)

Textures and general description: light gray, mg (1-4 mm), ser, hyp gran, w/weak to mod fol and very little procl; similar in most respects to Ba-JM-36a; hb prisms subh, elong 2 or 3:1; bio anh, platy, and sl poik, w/molded or interst margins, abundant mafic xls <1 mm; also numerous conspicuous 6-12 mm poik bio books and rare 6-12 mm euh plag tablets; grain margins gen sl ragged or rounded, but occas smooth euh plag and hb faces, esp against qtz and Kfld

Mineralogy

19.6 quartz: anh; 0.1-5 mm; continuous range from small interst grains to large subequant, single grains and aggs w/ molded interst margins; some large grains and aggs enclose several anh-euh plag and hb xls, but many are inclusion-free; most aggs consist of only a few ext domains; weak undul ext; some xls embay plag or hb sl

62.1 plagioclase: (anal, Tables 7 and 8; also App C, Table C-4) 0.1-6 mm, ser, ave 1.5-3 mm, mostly subh-euh; rare xls up to 12 mm; textures, twinning, and zoning patterns similar to Ba-JM-36a, but oscil zoning esp pronounced: ave interiors, An=37-44, w/common zones, patches, and occas cores 45-58 and possibly higher; rims, 19-21; rims on some xls are thin abrupt overgrowths on sodic andesine; few composite synn xls; tr myrm overgrowths against Kfld;

Ba-JM-46a (continued)

locally heavy alt of calcic zones to clay(?); minor alt to w mica, ep, Kfld, and zeol

0.9 K-feldspar: (anal, Table 11; also App C, Table C-5) ≤1 mm, rarely up to 3 mm, anh, interst and replacing plag; interst grains vary from smoothly bounded to extremely irreg; larger xls are highly poik (inclusions mostly plag and hb); mostly utw orth and san w/2V variable from <20 to 50°, -ve; some grid-twinned micr

7.3 hornblende (anal, Table 12; also App C, Table C-6) same as in Ba-JM-36a, except sl more fg (ave 0.5-2 mm long) and seldom poik; also patchy zoning rare and very weak, euh zoning not seen; minor embayment by qtz and replacement by bio

6.2 biotite: (anal, Table 17; also App C, Table C-7) same as in Ba-JM-36a, except many thin, ragged, poik flakes 6-12 mm wide

0.9 opaque: approx equal amounts of magnetite, and hematite-ilmenite; tr sulfide

magnetite: (anal, Table 18; also App C, Table C-8) same as in Ba-JM-36a

hematite-ilmenite: hem-rich intergrowths w/5-10% rut lamellae; grain size, textures, and occurrence same as in Ba-JM-36a; hem/(hem + ilm) ratio 0.6-1, gen 0.8-0.9; extensive alt to sph and some rut

sulfide: same as in Ba-JM-36a

tr hematite: rare tiny euh flakes in plag

0.6 sphene: 0.01-1 mm, anh, rarely subh, alt of hem-ilm and assoc w/bio and chl as alt of bio; also many interst grains gen adj to op, hb, and bio; interst grains appear partly primary and partly alt of hem-ilm

0.3 epidote: same as in Ba-JM-36a; also rare primary interst xls

0.4 white mica: ≤0.5 mm, anh-subh, alt of plag and assoc w/ chl as alt of bio; rare primary interst grains

1.0 clay(?): vfg unident alt of plag

0.15 apatite: same as in Ba-JM-36a

0.4 chlorite: same as in Ba-JM-36a, except no interst grains seen

tr cummingtonitic amphibole: one 0.5 mm, pale yel-grn, anh xl zoned to thin hb rim; 2V large +ve

tr zircon: ≤0.1 mm, euh; often assoc w/bio or op; faint pleo halos in bio

tr rutile: tiny exsolved lamellae and patchy alt in hem-ilm

tr zeolite: chabazite(?); alt of plag and interst (primary?): 2V = 10-20° +ve

Notable characteristics: the ser size distrib of mafics; the elong, subh-euh, non-poik, unzoned hb; the thin platy bio; the strong progr and oscil zoning and paucity of hem flakes in plag; and the absence of cpx and paucity of pale amph in hb are all typical of PHbT. The abundance and relatively coarse size of qtz and Kfld, the fairly low hb-bio ratio, and the relatively sodic comp

Ba-JM-46a (continued)
and frequent abrupt overgrowth relationship of plag rims are all characteristic of the western third of the PHbT. Other notable features: abundant cg bio, rare cg plag, hem-rich hem-ilm intergrowths, relatively cg interst sph, rare primary interst w mica, and possible primary interst zeol

Ba-JM-93: prismatic hornblende tonalite

Location: NW part of PHbT, along E bank of Arroyo de las Parritas, ∿230 m from contact zone with the SHbT (Plate 2, area G-4)
Textures and general characteristics: light gray, mg (2-3 mm), ser, hyp gran, w/mod fol, weak lineation, and weak procl; occas plag and hb xls up to 8 mm; textures very similar to Ba-JM-36a, except grain margins sl more rounded and abrd; smooth euh xl faces are sparse; minor rxltn of bio into aggs; <1% mortar, partially rxld to granobl aggs; occas subequant, poik hb xls w/molded margins; mod replacement of hb and plag by bio
Mineralogy

20.0	quartz: same as in Ba-JM-36a except undul ext gen weak
60.9	plagioclase: similar to Ba-JM-36a, except few xls >3 mm; also margins commonly sl abrd and rims more sodic: ave interiors, An=35-42, w/thin calcic zones and some patches and cores 42-51 and possibly higher; rims, 20-23; minor alt to clay(?), w mica, ep and Kfld
0.7	K-feldspar: ≤0.3 mm, anh, interst and replacing plag; complex branching and poik grains common; utw, but wavy ext common; 2V ∿45-70°; orth
6.7	hornblende: similar to Ba-JM-36a except for following characteristics - ave 0.5-2 mm; only rare weak zoning, always anh and patchy; margins commonly sl abrd, and smooth euh faces are rare; many xls partially replaced by bio; occas anh-subh, subequant xls w/margins molded around plag (atypical of PHbT)
8.3	biotite: similar to Ba-JM-36a, except marginal or patchy replacement of hb common; minor alt to chl ± sph
1.0	opaque: sl more magnetite than hematite-ilmenite magnetite: same as in Ba-JM-36a; occas rimmed by sph hematite-ilmenite: consistently hem-rich intergrowths; usually 75-85% hem, 10-20% ilm, and ∿5% rut; other characteristics similar to Ba-JM-36a
tr	hematite: rare tiny euh flakes in plag
0.5	sphene: same as in Ba-JM-36a
0.2	epidote: same as in Ba-JM-36a
0.2	white mica: ≤0.3 mm, anh-subh, replacing plag and assoc w/bio, hb, chl, and ep; rare thin rims around op; entirely secondary
1.0	clay(?): vfg unident alt of plag
0.2	apatite: same as in Ba-JM-36a, but rarely >0.1 mm
0.2	chlorite: same as in Ba-JM-36a, except no primary(?) interst grains seen

Ba-JM-93 (continued)

tr pale amphibole: ≤0.1 mm, anh patches in hb, gen homoaxial w/hb; mostly actinolitic amph ± vfg qtz blebs; rare cummingtonitic(?) amph

tr zircon: same as in Ba-JM-36a

tr rutile: tiny exsolved lamellae and patchy alt in hem-ilm

Notable characteristics: very similar to Ba-JM-46a and other samples in western third of PHbT, but distinguished by: weak procl and <1% mortar, bio > hb, sl to mod replacement of hb as well as plag by bio, and occas subequant, poik hb xls w/molded margins (similar to hb in SHbT, but atypical of PHbT)

Ba-JM-240#52: prismatic hornblende tonalite

Location: from a depth of 66 m in the drill core from center of the PHbT, 3.7 km N of Rancho San José (Plate 2, area I-7)

Textures and general description: light gray, mg (1-4 mm), ser, hyp gran, w/weak fol and very weak procl (photomics, Figs 43 and 44); rare hb and plag xls up to 8 mm; grain margins gen sl irreg, but seldom visibly abrd; also many smooth euh plag and hb faces; hb prisms subh-euh, gen elong 2 or 3:1; bio platy and poik, w/molded or interst margins; abundant mafic xls in all sizes from <1 mm to 4 mm; minor clustering of mafics; minor bending and rare fracturing of xls

Mineralogy

15.2 quartz: same as in Ba-JM-46a

63.8 plagioclase: textures, grain size, twinning, and zoning patterns same as in Ba-JM-36a; ave interiors, An=37-44, w/calcic patches, thin zones, and rare cores gen 45-52, but up to 63 and possibly higher; rims, 25-31; sl alt to clay(?), w mica, ep, carb, and Kfld

0.15 K-feldspar: ≤0.05 mm, anh, interst and replacing plag; utw; 2V gen small (<30°), but up to ∿45°; san and possibly orth

11.6 hornblende: similar to that in Ba-JM-36a, except rarely poik; also lacks anh patchy zoning, but occas xls show repetive euh zoning; clustering of several xls common

5.4 biotite: same as in Ba-JM-36a, except only sl alt to chl

1.3 opaque: ∿1/4 magnetite and 3/4 hematite-ilmenite w/same characteristics as in Ba-JM-36a; tr sulfide (pyrite?) ≤0.01 mm, anh-euh, brassy, weakly(?) anisotropic

tr hematite: rare tiny euh flakes in plag

0.14 sphene: ≤0.5 mm, anh; alt of hem-ilm and assoc w/hb, bio, and chl; also occas primary interst grains

0.3 epidote: ≤0.5 mm, anh; replacing plag and assoc w/hb, bio, and chl; also occas primary interst grains

tr clinozoisite or zoisite: rare ≤0.1 mm, anh, primary interst grains

0.4 white mica: ≤0.2 mm, anh-subh; alt of plag; also occas primary interst flakes gen occurring w/, but not visibly replacing interst Kfld

Ba-JM-240#52 (continued)

1.0	clay(?): vfg unident alt of plag
0.2	apatite: same as in Ba-JM-36a
0.4	chlorite: same as in Ba-JM-36a
0.05	carbonate: vfg alt of plag and rare tiny primary(?) interst grains
tr	zircon: same as in Ba-JM-36a
tr	rutile: tiny exsolved lamellae and patchy alt of hem-ilm; also rare tiny xls in and adj to bio, hb, and chl
tr	allanite: ≤0.2 mm, anh; also w/hb and ep
tr	zeolite: chabazite(?); ≤0.5 mm, anh, primary(?) interst aggs w/fanning ext

Notable characteristics: typical of weakly fol PHbT, w/subh, non-poik, elong hb prisms and platy, poik bio w/ragged molded and interst margins often penetrating and replacing plag and occas hb; weak to mod planar min orientation w/out defm or rxltn; occas primary interst w mica, sph, ep, and clinozo or zo; also primary(?) interst zeol, chl, and carb; no pale amph or cpx seen

Ba-JM-240#53: prismatic hornblende tonalite

Location: from a depth of 226 m in the drill core from center of the PHbT, ∿3.7 km N of Rancho San José (Plate 2, area I-7)

Textures and general description: extremely similar megascopically and in thin section to Ba-JM-240#52

Mineralogy (except for specifically noted characteristics, the min descriptions for Ba-JM-240#52 apply)

12.5	quartz
64.3	plagioclase: ave interiors, An=38-45, w/thin calcic zones and patches gen 46-50, but up to 63 and possibly higher; rims, 26-29; locally heavy alt to clay(?), w mica, ep, zeol(?), Kfld(?), and rare carb
0.14	K-feldspar
13.4	hornblende: many xls show very weak irreg zoning from sl brn-grn interiors to bl-grn rims (like zoning in Ba-JM-36a and SHbT samples) as well as occas faint repetitive euh zoning; otherwise same as in Ba-JM-240#52
4.8	biotite
1.5	opaque: ∿1/3 magnetite and 2/3 hematite-ilmenite; tr of vfg sulfide (pyrite? and rare bornite?)
tr	hematite
0.2	sphene
0.2	epidote
0.3	white mica
2.0	clay(?)
0.2	apatite
0.5	chlorite
tr	pale amphibole: tiny anh patches in hb; actinolitic amph ± qtz blebs and rare cummingtonitic(?) amph
tr	carbonate: vfg alt of plag; no interst grains seen
tr	zircon
tr	rutile
tr	allanite

Ba-JM-240#53 (continued)

tr zeolite(?): vfg alt of plag; no interst grains seen

tr prehnite: sheaths of platy, colorless to rusty xls bulging apart cleavage of bio and partially replacing bio, same as in Ba-JM-453

Notable characteristics: same as for Ba-JM-240#52; typical PHbT

Samples of the Seriate Porphyritic Tonalite

BC-I-12 (collected by L. T. Silver): transitional between prismatic hornblende tonalite and seriate porphyritic tonalite; mapped as part of the latter

Location: west-central part of pluton, from gradational contact zone between PHbT and SPT; SW base of prominent hill ∿130 m NE of intersection of North-South road with old by-passed segment of San José-San Telmo road (Plate 2, area K-6)

Textures and general description: light gray, mg (1-4 mm), ser, hyp gran, w/weak fol and lineation and no procl; sparse (<1 per 30 x 30 cm area) 8-12 mm plag xls; otherwise similar to typical weakly fol PHbT; abundant mafic xls in all sizes from <1 mm to 4 mm, but mafic mins ave sl more fg than plag, and distrib of mafic mins partially controlled by plag; hb prisms subh, elong 2 or 3:1, rarely poik and almost never molded; bio anh, platy, and poik, often w/ragged molded or interst margins; occas clustering of several mafic xls; grain margins gen sl irreg, but occas smooth euh plag and hb faces

Mineralogy

18.2 quartz: anh, 0.1-4 mm; continuous range from small interst grains to large subequent patches w/molded interst margins; larger patches gen consist of only 1 to 3 ext domains; some larger patches contain several subh-euh plag and/or hb inclusions, but many are inclusions-free; very weak undul ext; some grains embay plag or hb sl

63.0 plagioclase: continuous range from 0.1-12 mm, ave 1.5-3 mm; very few xls >5 mm; subh-euh; most margins sl irreg, but also many smooth euh faces, esp against qtz; no visible abrasion; strong oscil and progr zoning; well-developed Carls, ab, and per twinning; ave interiors An=36-40, commonly w/calcic patches and thin zones 45-60 and probably sl higher; rims, 23-25, locally down to 18-20; sl alt to clay(?), w mica, ep, Kfld, and zeol

0.3 K-feldspar: ≤0.3 mm, anh; mostly interst, but also replacing plag; 2V gen 5-20° but up to 35°; utw: san and possibly orth

8.6 hornblende: 0.1-6 mm; ave 1-2.5 mm; subh, w/some anh and euh xls; prisms elong 2 or 3:1; few inclusions, gen of op or plag; α=sl grn-tan, β=yel-grn, γ=bl-grn; rare weak anh zoning to sl brn-grn patches and cores; frequent aggs of several xls ± bio; tr alt to bio and chl

5.8 biotite: 0.1-6 mm, ave 1-2.5 mm; thin anh plates gen w/ molded margins often raggedly penetrating plag; minor rxltn into aggs of anh-euh xls; rare bent xls; occas inclusions, gen of plag, ap, op, or hb; α=light brn-gold; β=γ=ora-brn, locally w/grn tinge, esp adj to vfg sph, rut, or op; minor alt to chl + sph and/or rut; occas included sheaths of prehnite

BC-I-12 (continued)

1.4 opaque: 0.01-0.3 mm, anh-subh, occas euh, gen subequant; scat xls and aggs up to 1 mm, often w/ap; textures suggest hem-ilm >> mt, but not examined in polished section; minor alt to sph

tr hematite: rare ≤0.03 mm euh flakes in plag

0.2 sphene: ≤0.4 mm, anh, alt of op and assoc w/chl as alt of bio; also as occas primary interst xls and as vfg aggs between bio xls in rxld bio aggs

0.3 epidote: ≤0.5 mm, anh-subh, assoc w/hb and bio and replacing plag; also occas primary interst grains; variably colorless to pleo in shades of grn-yel

tr clinozoisite or zoisite: rare ≤0.1 mm, anh primary interst grains; 2V small or mod, +ve

0.4 white mica: ≤0.5 mm, anh, alt of plag; occas w/chl as alt of bio

1.0 clay(?): vfg unident alt of plag

0.2 apatite: ≤0.2 mm, subh-euh, colorless or very pale grn-yel

0.6 chlorite: alt of bio and occas of hb; mostly α=β=bright grn, γ=light grn-yel, w/anom light brn or brn-grn interf color; some is α=light grn-yel, β=γ=bright grn, w/anom bl or prpl interf color

tr pale amphibole: rare ≤0.05 mm, anh pale patches in hb; probably both actinolitic and cummingtonitic amph

tr zircon: ≤0.1 mm, subh-euh

tr allanite: very rare, tiny anh patches in ep

tr zeolite: chabazite(?); ≤0.2 mm, anh, replacing plag and raggedly interst (primary?)

tr prehnite: occas sheaths of platy colorless to rusty xls bulging apart cleavage of bio and partially replacing bio

Notable characteristics: indistinguishable from weakly fol PHbT except for very sparse conspicuous 8-12 mm plag xls; fewer large plag xls than in typical SPT

Ba-JM-3a: seriate porphyritic tonalite

Location: NW part of SPT, along the North-South road, ∿340 m N of the intersection w/the San José-San Telmo road; w/in southern part of the gradational contact zone w/PHbT (Plate 2, area L-6)

Textures and general description: light gray, mg (1-4 mm), ser, hyp gran, w/weak fol and no procl; ∿1 conspicuous 8-12 mm plag xl per 30 x 30 cm area and many thin 5-10 mm bio plates; otherwise very similar to weakly fol PHbT samples (e.g., Ba-JM-46a and 240#52); euh plag and hb faces common, but still subordinate to sl irreg margins; clustering of several mafic xls common

Mineralogy

18.0 quartz: same as in BC-I-12

59.8 plagioclase: (anal, Tables 7 and 8; also App C, Table C-4) grain size, textures, twinning, and zoning patterns same as in BC-I-12, but 6-12 mm xls are sl more common; smooth euh faces common; ave interiors, An=38-43, w/

Ba-JM-3a (continued)

calcic patches and thin zones 45 and higher; rims, 21-24; locally heavy alt, mostly of calcic zones, to clay(?), w mica, and some ep and Kfld

0.2 K-feldspar: (anal, Table 11; also App C, Table C-5) ≤0.5 mm, anh, mostly interst, some replacing plag; utw; 2V gen 5-15°, few xls zoned to rims of 20-30°; san

9.5 hornblende: (anal, Table 12; also App C, Table C-6) very similar to BC-I-12, but subh-euh rather than subh

5.0 biotite: (anal, Table 17; also App C, Table C-7) same as in BC-I-12, except many 5-10 mm wide poik flakes

1.5 opaque: sl less magnetite than hematite-ilmenite (photomics, Figs 69, 70, and 71); tr sulfide

magnetite: (anal, Table 18; also App C, Table C-8) ≤0.5 mm, subh-euh, subequant, scat xls and aggs up to 1 mm, often w/hem-ilm; no alt to hem

hematite-ilmenite: (semi-quantitative anal, Table 19) ≤0.5 mm, anh, rarely subh, gen subequant, scat xls and aggs up to 1 mm, often w/mt and ap; hem/(hem + ilm) variable, 0.25-0.75, ave 0.5; gen several % rut lamellae; 2 generations of hem and ilm lamellae common; minor alt to sph and occas rut and "meta-ilm"

sulfide: ≤0.01 mm brassy pyrite(?)

tr hematite: rare tiny euh flakes in plag

0.3 sphene: ≤0.7 mm, anh-subh; alt of hem-ilm and assoc w/hb, bio, and chl (gen secondary); also occas primary interst grains

0.3 epidote: ≤0.5 mm, anh-subh; replacing plag and assoc w/ hb, bio, and chl; also occas primary interst grains

0.14 white mica: ≤0.2 mm, anh-subh; alt of plag and assoc w/ chl as alt of bio; also rare primary interst flakes gen assoc w/interst Kfld

4.1 clay(?): vfg unident alt of plag; also occas (<1%) light pinkish-brn, homog patches ≤0.3 mm of extremely fg clay(?); some of latter patches are interst and appear primary

0.3 apatite: same as in BC-I-12; often in aggs w/hem-ilm

0.9 chlorite: alt of bio and occas hb and plag; also rare primary interst aggs w/multiple centers of fanning ext ("mosaic" chl)

tr zircon: few 0.05-0.1 mm, subh-euh xls

tr rutile: tiny lamellae and patchy alt of hem-ilm

tr carbonate: rare ≤0.3 mm, primary interst grains (calcite?)

Notable characteristics: typical of the N part of SPT transitional into PHbT; sparse 8-12 mm plag xls are only feature distinct from weakly fol PHbT; notably heavier alt of plag plus presence of primary(?) interst clay(?) are probably related to abundant auriferous qtz veins and local hydrothermal alt in this area; smooth euh plag and hb faces, smoothly bounded interst areas, and primary interst sph, ep, w mica, chl, and carb are all more abundant than in most of the PHbT, but less so than in central and southern part of SPT

Ba-JM-62a: seriate porphyritic tonalite

Location: SW part of SPT in the arroyo called El Alisito, ∿2.5 km SSE of Rancho El Molino (Plate 2, area R-7)

Textures and general description: light gray, mg (1-4 mm), ser, hyp gran, w/very weak fol and no procl; 2 or 3 conspicuous 8-12 mm plag xls per 30 x 30 cm area; abundant mafic xls in all sizes from <1 mm up to 4 mm; mafic mins, esp hb, ave sl more fg than plag and are often clustered between plag xls; hb prisms gen elong 2 or 3:1; plag and hb both subh-euh, but most faces are sl irreg

Mineralogy

17.8 quartz: same as in BC-I-12

63.5 plagioclase: (anal, Tables 7 and 8; also App C, Table C-4) complete range from 0.2-12 mm, ave 1-3 mm; subh-euh, most faces sl irreg, but occas smooth euh faces, esp against qtz, Kfld, and other interst mins; strong progr and oscil zoning, minor patchy zoning; well-developed Carls, ab, and per twinning; aveinteriors An=34-35, w/calcic zones, patches, and cores up to 60 and possibly higher; rims, 22-24; locally mod alt to clay(?), w mica, ep, Kfld, and chl

0.14 K-feldspar: (anal, Table 11; also App C, Table C-5) similar to BC-I-12; 2V gen 5-20°, but up to 45°

9.6 hornblende: (anal, Tables 12 and 14; also App C, Table C-6) subh-euh prisms 0.1-6 mm long, ave 1-2.5 mm; gen elong 2 or 3:1; often clustered w/ or w/out bio: minor replacement by bio; pleo same as in BC-I-12; minor alt to chl

3.7 biotite: (anal, Table 17; also App C, Table C-7) 0.1-6 mm, ave 1-3 mm; thin anh, sl poik plates w/molded and interst margins; pleo same as in BC-I-12; ∿10% alt to chl ± vfg sph and/or rut; occas included sheaths of prehnite

1.6 opaque: subequal amounts of magnetite and hematite-ilmenite; tr sulfide (pyrite?)

- magnetite: (anal, Table 18; also App C, Table C-8) same as in Ba-JM-3a, except sl alt to hem
- hematite-ilmenite: ≤0.5 mm, anh, rarely subh-euh; scat xls and aggs often w/mt and ap; hem/(hem + ilm) variably 0(?) to 0.7, commonly 0.2-0.4; 0-5% rut lamellae; locally heavy alt to sph and minor "meta-ilm"
- sulfide: ≤0.01 mm brassy anisotropic pyrite(?)

tr hematite: rare ≤0.03 mm euh flakes in plag

0.4 sphene: ≤0.8 mm, anh, occas subh-euh; mostly primary interst grains; also alt of hem-ilm and assoc w/hb, bio, and chl

0.07 epidote: ≤0.5 mm, anh, alt of plag and assoc w/mafics; rare primary interst grains

0.2 white mica: ≤0.2 mm, anh-subh, alt of plag and rare primary interst grains

1.9 clay(?): vfg unident of plag and rarely Kfld

0.4 apatite: ≤0.5 mm, subh-euh

Ba-JM-62a (continued)

0.6 chlorite: alt of bio and occas hb and plag; also sparse primary interst "mosaic" chl; pleo and interf colors same as in BC-I-12

tr pale amphibole: ≤0.2 mm, anh patches homoaxially included in hb; both(?) cummingtonitic and actinolitic amph

tr zircon: ≤0.2 mm, subh-euh; occas weak pleo halos in adj hb or bio

tr rutile: tiny lamellae in hem-ilm and vfg aggs in chl as alt of bio

tr prehnite: sparse sheaths of colorless to rusty platy xls bulging apart cleavage in bio and partially replacing bio

Notable characteristics: gen typical of least fol parts of SPT; paucity of hem in hem-ilm is unlike most of SPT, but is similar to Ba-JM-701, collected only 500 m to the W

Ba-JM-528: seriate porphyritic tonalite

Location: NE part of SPT, ∿190 m E of Arroyo San José, 1.8 km SSE of Rancho San José (Plate 2, area N-8)

Textures and general description: light gray, mg (1-4 mm), ser, hyp gran, w/very weak fol and no procl; sparse (∿1 per 30 x 30 cm area) conspicuous 8-12 mm plag xls; abundant mafic xls in all sizes from <1 mm to 4 mm; also abundant highly poik bio plates 6-12 mm wide and occas hb prisms 5-8 mm long; hb prisms subh-euh, elong 2:1 up to 5:1; smooth euh hb and plag xl faces both common, but sl irreg faces still prevail; plag averages sl coarser than hb; mafics, esp hb, often clustered between plag xls

Mineralogy

16.3 quartz: same as in BC-I-12

62.9 plagioclase: very similar to BC-I-12, but sl more cg (ave 2-4 mm); numerous composite synn xls; ave interiors, An=38-43, w/frequent calcic patches and thin zones, 45-65 and possibly higher; rims, 22-26; rare local very thin sharp deuteric(?) rims down to 10, esp against qtz; minor alt to clay(?), w mica, ep, Kfld, zeol, and chl

0.2 K-feldspar: same as in BC-I-12

10.8 hornblende: 0.1-8 mm, ser; ave 1.5-3 mm, but many smaller xls; subh-euh prisms often elong 3 or 4:1, even 5:1

5.4 biotite: 0.1-12 mm, ave 2-4 mm; thin anh, highly poik plates w/molded interst margins; occas fg subh xls; sl replacement of plag and hb; inclusions mainly plag and op, lesser hb and ap; pleo same as in BC-I-12; little or no rxltn into aggs; minor alt to chl; occas included sheaths of prehnite

1.4 opaque: ∿1/3 magnetite and 2/3 hematite-ilmenite; tr sulfide (pyrite?); numerous clusters up to 1 mm of mt + hem-ilm

Ba-JM-528 (continued)

magnetite: same as in Ba-JM-3a, except gen 10% alt to hem

hematite-ilmenite: same as in Ba-JM-3a, except hem/(hem + ilm) uniformly ∿0.8

sulfide: ≤0.01 mm brassy pyrite(?)

tr hematite: rare ≤0.03 mm euh flakes in plag

0.2 sphene: ≤0.5 mm, anh, replacing hem-ilm and assoc w/hb, bio, and chl (probably secondary); also occas primary interst grains

0.3 epidote: ≤0.5 mm, anh-subh; assoc w/hb, bio, and chl (entirely secondary?) and alt of plag; also occas primary interst grains

tr clinozoisite or zoisite: rare ≤0.1 mm, anh primary interst grains; colorless; 2V small to mod, +ve

0.4 white mica: ≤0.2 mm, anh-subh; alt of plag and occas assoc w/chl as alt of bio; also sparse primary interst grains, often w/Kfld

0.9 clay(?): vfg unident alt of plag

0.2 apatite: ≤0.3 mm, subh-euh

0.9 chlorite: alt of bio and occas hb and plag; rare primary(?) interst mosaic chl; pleo same as in BC-I-12

tr actinolitic(?) amphibole: rare ≤0.01 mm, anh patches of pale amph + qtz blebs in hb

tr zircon: ≤0.1 mm, subh-euh

tr allanite: rare patches and thin rims in ep; weak pleo halos in adj hb

tr zeolite: (chabazite?) ≤0.03 mm, anh, alt of plag; also primary(?) interst grains and aggs; 2V ≈ 15-25°, variably +ve and -ve

tr prehnite: sheaths of platy, colorless or rusty xls bulging apart cleavage in bio and partially replacing bio; sheaths ≤0.5 mm, biref ∿0.020-0.025, parallel ext, 2V variably 0°(?) to ∿30° +ve

Notable characteristics: subh-euh elong form of hb; abundance of smooth euh plag and hb faces; cg poik bio w/only minor replacement of plag and hb; minor primary interst ep, cz or zo, sph, w mica, and possibly chl and zeol; relatively few large conspicuous plag xls; most characteristics typical of unfol or weakly fol SPT and PHbT

Ba-JM-639: seriate porphyritic tonalite

Location: SE part of SPT in the arroyo called El Alisito, ∿320 m W of pluton contact (Plate 2, area R-8)

Textures and general description: (photomics, Figs 42 and 62A) light gray, mg (1-4 mm), ser, hyp gran, w/very weak fol and no procl; ∿1 large (6-12 mm) conspicuous plag xl per 30 x 30 cm area; abundant mafic xls in all sizes from <1 mm to 4 mm; also abundant highly poik bio plates 5-12 mm wide; hb averages sl more fg than plag, and mafic mins, esp hb, often clustered between plag xls; hb prisms subh-euh, gen elong 2:1 to 4:1: smooth euh plag and hb faces both common, esp against qtz, Kfld,

Ba-JM-639 (continued)

and other interst phases

Mineralogy

18.4 quartz: same as in BC-I-12

63.5 plagioclase: complete range from 0.1-12 mm, ave 1.5-4 mm; few xls >6 mm; subh-euh, w/most xls showing at least one smooth euh face; strong progr and oscil zoning, esp in largest xls; Carls, Ab, and per twinning well developed; occas composite synn xls; ave interiors, An= 37-43, w/calcic patches, thin intermed zones, and rare cores, 45-75, commonly 60-65; rims 19-22, w/local thin sharp overgrowths down to 16; minor alt to clay(?), w mica, ep, zeol, and Kfld

0.3 K-feldspar: similar to BC-I-12; 2V gen 0(?)-15°, but up to 50°

7.8 hornblende: (photomics, Figs 42 and 62A) 0.1-5 mm, ave 1-2.5 mm; subh-euh prisms elong 2:1 to 4:1; most xls show at least one smooth euh face, esp against qtz, Kfld, and other interst phases, and some are entirely euh; unzoned; other characteristics same as in BC-I-12

5.5 biotite: (photomics, Fig 68) 0.1-12 mm, ave 1.5-3.5 mm; thin, anh, highly poik plates w/molded interst margins; occas subh xls mostly fg; sl replacement of plag and hb; inclusions mainly plag and op, less hb and ap; little or no rxltn; pleo same as in BC-I-12; minor alt to chl ± sph or rut

1.5 opaque: sl more magnetite than hematite-ilmenite; occas aggs of 10-20 or more xls ± hb, ap, and sph

magnetite: same as in Ba-JM-3a, except 5-10% alt to hem

hematite-ilmenite: textures same as in Ba-JM-3a; hem/(hem + ilm) gen 0.6-0.8, but down to 0.3; minor rut lamellae; minor alt to sph

tr hematite: rare ≤0.03 mm euh flakes in plag

0.4 sphene: 0.05-1 mm, anh, occas subh-euh; mostly primary interst grains (photomics, Fig 78); minor alt of hem-ilm and assoc w/chl as alt of bio or hb

0.12 epidote: ≤0.5 mm, anh-subh; primary interst grains, alt of plag, and assoc w/hb, bio, and chl (probably secondary)

tr clinozoisite or zoisite: ≤0.5 mm, anh, primary interst grains; colorless, 2V mod to small +ve

0.3 white mica: ≤0.2 mm, anh-subh; alt of plag and occas assoc w/chl as alt of bio; also occas primary interst grains and rare flakes of hb

1.4 clay(?): vfg unident alt of plag

0.2 apatite: ≤0.3 mm, subh-euh

0.5 chlorite: alt of bio and occas hb; also occas primary interst aggs w/many centers of fanning flakes ("mosaic" chl; photomics, Figs 78 and 79); pleo and interf colors same as in BC-I-12

tr pale amphibole: single 0.8 mm, subh xl consisting of

Ba-JM-639 (continued)

very pale grn, weakly pleo, cummingtonite(?) core zoned to hb rim

0.02 zircon: ≤0.1 mm, subh-euh; occas strong pleo halos in adj bio or hb

tr rutile: minor lamellae and patchy alt of hem-ilm; also vfg aggs in chl as alt of bio

tr zeolite: (chabazite?) anh, primary interst grains and aggs up to 1 mm; also minor alt of plag; low relief, low biref (~0.005-0.010); 2V ≈ 10-30°, variably +ve and -ve; parallel ext, length slow; inclusions of ap common; local mod alt to vfg w mica or clay(?)

Notable characteristics: typical of least fol central and southern parts of SPT; no defm despite proximity to pluton contact; sparse conspicuous 8-12 mm plag xls; strong progr and oscil plag zoning, esp in largest xls; abundance of euh plag and hb xls; elong, non-poik form and frequent clustering of hb; anh, highly poik and molded form of bio; abundance (0.5-1% total) of primary interst accessory mins (sph, ep, chl, and zeol, plus minor w mica and cz or zo) suggestive of vapor phase xltn

Ba-JM-701: seriate porphyritic tonalite

Location: SW part of SPT, 2.3 km S of Rancho El Molino; ≤30 m from poorly exposed pluton contact (Plate 2, area B-6)

Textures and general description: light gray, mg (1-4 mm), ser, hyp gran, w/extremely weak fol and no procl; ~1 conspicuous 8-10 mm plag xl per 30 x 30 cm area; abundant mafic xls in all sizes from <1 mm to 4 mm, but ave sl more fg than plag and often clustered between plag xls; hb prisms subh-euh, gen elong 2:1 to 4:1; smooth euh plag and hb faces both common, esp against qtz, Kfld, and other interst phases; sl to mod replacement of hb by bio

Mineralogy

16.5 quartz: same as in BC-I-12

64.7 plagioclase: very similar to Ba-JM-639; ave interiors, An=38-45, w/calcic patches and thin zones commonly 62-70; rims, 19-21; sl alt to clay(?), w mica, ep, cz or zo, Kfld, and zeol

0.2 K-feldspar: same as in BC-I-12

8.7 hornblende: 0.1-6 mm, ave 1-2.5 mm; subh-euh prisms elong gen 2:1 to 4:1; pleo and other characteristics same as in BC-I-12; locally mod replacement by bio; sl alt to chl

6.5 biotite: 0.1-6 mm, ave 1.5-3 mm; thin, anh, poik plates w/molded margins; inclusions mostly plag, hb, op, and ap; locally mod replacement of hb; pleo same as in BC-I-12; minor alt to chl ± sph or rut and to vfg clay(?)

1.2 opaque: subequal amounts of magnetite and hematite-ilmenite; occas aggs of 10-20 or more xls ± hb, bio, ap, and sph

magnetite: same as in Ba-JM-3a, except 5-10% alt to hem

Ba-JM-701 (continued)

hematite-ilmenite: textures same as in Ba-JM-3a, but hem/(hem + ilm) gen 0.05-0.2; hem lamellae abundant, but tiny, no rut lamellae seen; paucity of hem probably indicates relatively limited exsolution rather than relatively reduced bulk comp; sl alt to sph

tr hematite: rare ≤0.03 mm euh flakes in plag

0.08 sphene: ≤0.3 mm, rarely up to 1 mm, anh, occas subh-euh: mostly primary interst grains; also replacing hem-ilm intergrown w/hb, and assoc w/chl as alt of bio; occas weak pleo halos in adj hb

0.10 epidote: same as in BC-I-12

tr clinozoisite or zoisite: ≤0.1 mm, anh; alt of plag and primary interst grains

0.2 white mica: ≤0.2 mm, anh, alt of plag or w/chl as alt of bio; rare flakes in hb

1.1 clay(?): vfg unident alt of plag and rarely bio

0.3 apatite: ≤0.5 mm, subh-euh; notably coarse and abundant

0.4 chlorite: alt of bio and occas of hb; also sparse primary interst "mosaic" chl; pleo same as in BC-I-12

tr pale amphibole: rare ≤0.2 mm, anh-subh patches in hb: probably cummingtonitic amph

tr zircon: ≤0.3 mm, subh-euh; mod pleo halos in adj hb or bio

tr rutile: tiny aggs of minute xls in chl as alt of bio

tr allanite: single 0.1 mm subh core in primary interst ep

tr zeolite: (chabazite?) anh primary interst aggs up to 0.5 mm; occas inclusions of ap; also alt of plag; 2V ≈ 0-10°, +ve

Notable characteristics: very similar to Ba-JM-639, except bio xls rarely >6 mm across and relatively little primary interst sph, ep, chl, zeol, and cz or zo; also paucity and small size of hem lamellae in hem-ilm is unusual for most SPT samples, but similar to Ba-JM-62a collected only ∿500 m to the E

Ba-JM-737: seriate porphyritic tonalite

Location: central part of SPT, 2.4 km SSE of Rancho San José (Plate 2, area O-8)

Textures and general description: light gray, mg (1-4 mm), ser, hyp gran, w/very weak fol and no procl; ∿2 conspicuous 8-12 mm plag xls per 30 x 30 cm area; abundant mafic xls in all sizes from <1 mm to 4 mm; also numerous bio plates 5-6 mm across and sparse hb prisms 5-6 mm long; hb elong 2 or 3:1; mafics, esp hb, ave sl more fg than plag and often clustered between plag xls; local weak subporphyritic texture, w/3-10 mm plag xls in a 0.5-2 mm groundmass; smooth euh plag and hb faces common, esp against qtz, Kfld, and other interst phases, but sl irreg faces are more common

Mineralogy

14.0 quartz: same as in BC-I-12

66.2 plagioclase: similar to Ba-JM-639; largest xls show

Ba-JM-737 (continued)

spectacular oscil zoning (photomic, Fig 55); ave interiors, An=36-41, w/calcic patches, thin zones, and rare cores varying widely from 45 to ∿75; rims, 22-25, w/rare very thin discont deuteric rims and occas microveinlets down to ∿10; minor alt to clay(?), w mica, ep, Kfld, and zeol

0.2 K-feldspar: same as in BC-I-12

11.0 hornblende: subh-euh prisms 0.5-8 mm long, ave 1-2.5 mm; elong 2 or 3:1; common clustering w/bio and minor replacement by bio; pleo and other characteristics same as in BC-I-12

4.5 biotite: thin plates 0.1-7 mm wide, ave 1-2 mm, but also many 4-5 mm plates; gen anh, w/molded and interst margins, but many fg subh xls; minor replacement of hb; pleo same as in BC-I-12; minor alt to chl and w mica

1.1 opaque: 1/5 magnetite, 4/5 hematite-ilmenite; tr sulfide (pyrite?); occas aggs of 10-20 or more mt and hem-ilm xls

magnetite: same as in Ba-JM-3a, except 5-10% alt to hem

hematite-ilmenite: same as in Ba-JM-3a, except hem/(hem + ilm) uniformly ∿0.8

sulfide: rare <0.01 mm brassy pyrite(?)

tr hematite: rare ≤0.03 mm euh flakes in plag

0.3 sphene: 0.5 mm, anh, alt of hem-ilm and assoc w/hb, bio, and chl; also occas primary interst grains

0.2 epidote: same as in BC-I-12

tr clinozoisite or zoisite: same as in BC-I-12

0.2 white mica: ≤0.5 mm, anh-subh, alt of plag and intergrown w/bio and chl; also rare primary interst flakes

1.4 clay(?): vfg unident alt of plag

0.3 apatite: ≤0.5 mm, subh-euh

0.6 chlorite: alt of bio and occas hb; also occas primary "mosaic" chl; pleo and interf colors same as in BC-I-12

0.03 cummingtonitic amphibole: anh rounded or irreg patches up to 1.5 mm in hb; very pale grn-yel; 2V large +ve

tr actinolitic amphibole: ≤0.03 mm, anh, pale grn, weakly pleo patches in hb

tr zircon: ≤0.2 mm, subh-euh; weak pleo halos in adj hb or bio

tr rutile: tiny lamellae in hem-ilm; also vfg aggs in chl as alt of bio

tr allanite: ≤0.1 mm, anh; rare patches in ep and irreg grains w/weak pleo halos in hb and bio

tr zeolite: (chabazite?) anh primary interst aggs up to 0.5 mm, gen w/inclusions of ap; also minor alt of plag; 2V small, +ve

Notable characteristics: very similar to Ba-JM-639, but large plag xls sl more common; also bio is rarely >7 mm and not esp poik, and primary interst sph, ep, and w mica are minor; typical of central and soutnern parts of SPT; one unfilled microcavity 0.05-0.2 mm, bounded by smooth euh plag faces implies existence of a free vapor phase during final stages of magmatic xltn

APPENDIX B

RELIABILITY OF MODAL ANALYSES

Three separate methods were used to test the reliability of the modal analyses. Tables B-1 and B-2 show the variability among thin sections of individual samples. In no case does the standard deviation for any mineral exceed ±3.9% for "detailed" modes or ±4.6% for "reconnaissance" modes. Expressed as percentage of the amount present, the standard deviations for the four principal minerals in both types of modes average about ±11-12% for quartz, ±3.5-4% for plagioclase (including alteration), ±13-17% for hornblende, and ±21-22% for biotite.

Table B-3 compares replicate analyses of two or three thin sections of each of three samples. The replicate analyses cover the same areas, but with the grid spacing offset or changed to ensure that the results of the two measurements are entirely independent. The deviations from the mean for each constituent in the replicate pairs are consistently less than half of the average standard deviations observed among thin sections in the detailed modes (exceptions: opaques in BC-I-12 and chlorite in Ba-JM-36a).

These results suggest that real variations among thin sections are the greatest source of uncertainty in the modes. Uncertainty in the mode for a given thin section appears to be much smaller. Hence, the standard deviations in Table B-1 should be reasonably reliable measures of the accuracy of the detailed modes of each sample. The reconnaissance modes are obviously less reliable, but the uncertainties are less well

determined.

Table B-4 compares results for two or more samples from individual localities. The Ba-JM-240 drill core series actually consists of two localities: first, #39 and #52 from a depth of 66-70 m and second, #6 and #53 from a depth of 226-230 m. Deviations from the mean between samples from each locality are consistently smaller than the average standard deviations among thin sections in Table B-1. Thus, in outcrops which appear megascopically homogeneous, much -- perhaps most -- of the modal variability apparently occurs on a scale of centimeters rather than meters. This conclusion strongly supports the field observation that the analyzed samples are all representative of their respective localities.

Table B-1

Variability of Modal Mineral Proportions Among Thin Sections of Individual Samples: "Detailed" Modes

± 1 σ Standard Deviation Expressed as Percentage of the Rock

	Qtz	Pl+Alt	K-feld	Hb	Bio	Op	Sph	Ep	Ap	Chl	Pale Amph	Other
BC-I-12	1.65	0.84	0.06	1.12	0.91	0.47	0.09	0.11	0.14	0.18	0.00	0.07
Ba-JM-25a#2	2.24	2.99	0.09	3.74	2.30	0.43	0.11	0.29	0.19	0.38	0.09	0.05
Ba-JM-27a*	2.34	1.96	0.17	1.32	0.79	0.15	0.21	0.64	0.11	0.12	0.00	0.08
Ba-JM-36a**	0.82	1.81	0.20	1.40	1.01	0.29	0.34	0.21	0.14	0.49	0.00	0.08
Ba-JM-39b	3.30	2.98	0.07	2.64	0.52	0.69	0.14	0.26	0.29	0.24	0.08	0.08
Ba-JM-46a#2	2.51	3.49	0.42	1.14	2.68	0.14	0.34	0.17	0.10	0.28	0.00	0.08
Ba-JM-68	1.35	2.42	0.05	2.00	2.61	0.33	0.16	0.38	0.13	0.35	0.11	0.06
Ba-JM-93	1.60	2.18	0.24	1.53	1.74	0.25	0.20	0.09	0.19	0.12	0.00	0.00
Ba-JM-240#52	3.83	3.91	0.12	2.01	1.18	0.40	0.07	0.12	0.15	0.30	0.00	0.07
Ba-JM-240#53	1.26	2.73	0.10	2.89	1.13	0.50	0.19	0.15	0.16	0.18	0.00	0.00
Ba-JM-453	1.45	2.22	0.07	1.36	0.69	0.52	0.16	0.21	0.28	0.30	0.16	0.12
Ba-JM-492	2.20	1.80	0.15	1.89	1.60	0.15	0.07	0.23	0.10	0.19	0.10	0.05
Ba-JM-528	2.29	2.92	0.10	1.96	1.29	0.57	0.19	0.21	0.11	0.29	0.00	0.10
Ba-JM-566	1.95	3.00	0.17	3.08	1.21	0.54	0.29	0.16	0.16	0.22	0.22	0.00
Ba-JM-568a*	1.34	1.42	0.32	1.12	0.67	0.14	0.10	0.19	0.19	0.20	0.00	0.04
Ba-JM-639	3.23	3.18	0.09	0.94	1.35	0.40	0.09	0.07	0.12	0.18	0.00	0.03
Ba-JM-701	1.78	2.38	0.17	1.22	1.58	0.64	0.11	0.10	0.26	0.15	0.00	0.08
Ba-JM-737	0.94	1.58	0.09	1.27	1.00	0.22	0.18	0.05	0.17	0.30	0.05	0.03
Ba-JM-807*	0.88	2.26	0.11	0.74	0.51	0.17	0.27	0.20	0.06	0.09	0.00	0.00
AVERAGE	1.95	2.42	0.15	1.76	1.30	0.37	0.17	0.20	0.16	0.24	0.04	0.05

*Denotes modes of finer-grained GBT, based upon 4 thin sections.

**Based upon 8 thin sections.

Table B-2

Variability of Modal Mineral Proportions Among Thin Sections of Individual Samples: "Reconnaissance" Modes

± 1 σ Standard Deviation Expressed as Percentage of the Rock

	Qtz	Pl+Alt	K-feld	Hb	Bio	Op	Sph	Ep	Ap	Chl	Pale Amph	Other
Ba-JM-3a	1.22	1.24	0.12	0.91	0.99	0.10	0.10	0.13	0.08	0.36	0.00	0.00
Ba-JM-25a#1	0.62	1.89	0.04	1.53	3.64	0.09	0.08	0.23	0.16	0.15	0.04	0.06
Ba-JM-29	1.73	4.18	0.10	2.10	0.30	0.32	0.13	0.13	0.19	0.09	0.00	0.08
Ba-JM-30a	1.35	2.51	0.26	1.57	0.37	0.12	0.23	0.27	0.01	0.04	0.00	0.03
Ba-JM-31a	1.12	0.48	0.16	1.27	1.26	0.05	0.24	0.16	0.06	0.25	0.00	0.00
Ba-JM-35a	2.36	3.80	0.08	1.08	0.25	0.35	0.07	0.10	0.03	0.14	0.00	0.04
Ba-JM-46a#1	3.57	3.18	0.49	0.64	1.90	0.58	0.38	0.08	0.17	0.12	0.00	0.11
Ba-JM-62a	2.26	1.90	0.03	0.40	1.26	0.82	0.20	0.07	0.21	0.26	0.00	0.09
Ba-JM-159	1.84	0.18	0.10	1.83	0.75	0.24	0.11	0.15	0.03	0.21	0.00	0.03
Ba-JM-240#6	1.35	4.56	0.05	1.94	1.57	0.30	0.08	0.09	0.12	0.20	0.00	0.05
Ba-JM-240#39	3.53	2.02	0.14	1.59	0.15	0.76	0.11	0.08	0.10	0.18	0.00	0.00
AVERAGE	1.74	2.36	0.14	1.35	1.13	0.34	0.16	0.14	0.11	0.18	0.00	0.04

Table B-3

Replicate Modal Analyses of Selected Thin Sections

	BC-I-12		Ba-JM-36a		Ba-JM-46a#2	
Quartz	18.89	18.43	13.96	15.89	21.64	20.61
Plagioclase	62.71	64.50	65.17	63.28	59.92	61.45
K-feldspar	0.30	0.30	0.35	0.09	0.41	0.48
Hornblende	8.05	8.12	13.31	12.81	7.04	6.48
Biotite	5.52	4.96	3.00	3.10	7.39	7.09
Opaque	1.78	0.93	1.15	1.23	0.93	1.03
Sphene	0.15	0.19	0.55	0.59	0.70	0.67
Epidote	0.32	0.19	0.50	0.32	0.23	0.24
Apatite	0.15	0.22	0.20	0.29	0.17	0.24
Chlorite	0.68	0.71	0.90	1.38	0.35	0.30
Pale amphibole[a]	0.00	0.00	0.00	0.00	0.00	0.00
White mica + clay[b]	1.37	1.38	0.85	0.94	1.16	1.39
Other	0.06	0.10	0.05	0.09	0.06	0.00
TOTAL	99.98	100.03	99.99	100.01	100.00	99.98
Plag + alteration	64.08	65.88	66.02	64.22	61.08	62.84
Color index	16.50	15.10	19.41	19.43	16.64	15.81
Amph/(bio + chl)	1.28	1.43	3.41	2.86	0.91	0.88
Total # of points	5267	5383	1998	3418	1719	1650
Total area (mm^2)	2130		2000		1680	
# of thin sections	3		3		2	

[a]Actinolitic or cummingtonitic amphibole or both.

[b]Almost entirely alteration of plagioclase; clay includes all very fine-grained alteration of plagioclase.

Table B-4

Comparison of Modal Mineral Compositions
of Multiple Samples from the Same Locality

	Ba-JM-25a			Ba-JM-46a		
	#1	#2	Average[a]	#1	#2	Average[a]
Quartz	14.95	16.25	15.92	21.37	19.11	19.59
Plagioclase	58.56	58.75	58.70	59.89	62.68	62.09
K-feldspar	0.06	0.11	0.10	1.24	0.80	0.89
Hornblende	14.95	14.03	14.26	6.59	7.50	7.31
Biotite	6.96	6.64	6.72	6.47	6.12	6.19
Opaque	1.59	1.23	1.32	1.19	0.88	0.94
Sphene	0.13	0.22	0.19	0.55	0.60	0.59
Epidote	0.90	0.74	0.78	0.29	0.30	0.30
Apatite	0.22	0.16	0.18	0.21	0.14	0.15
Chlorite	0.58	0.47	0.50	0.36	0.48	0.45
Pale amphibole[b]	0.04	0.07	0.06	0.00	0.00	0.00
White mica + clay[c]	0.94	1.32	1.22	1.72	1.36	1.44
Other	0.08	0.02	0.04	0.12	0.04	0.06
TOTAL	99.96	100.01	99.99	100.00	100.01	100.00
Color index	25.15	23.40	23.83	15.45	15.88	15.78
Plag + alteration	59.50	60.07	59.92	61.61	64.04	63.53
Amph/(bio + chl)	1.99	1.98	1.98	0.96	1.14	1.10
Total # of points	4641	5544	---	4189	5013	---
Total area (mm^2)	1485	4435	5920	1340	5013	6353
# of thin sections	3	7	10	3	7	10

[a]Averages are weighted in proportion to the total thin-section area represented by each analysis. Samples 25a#1 and 25a#2 were collected within 20 m of each other. Samples 46a#1 and 46a#2 were collected approximately 3-4 m apart.

[b]Actinolitic or cummingtonitic amphibole or both.

[c]Almost entirely alteration of plagioclase; "clay" includes all very fine-grained unidentified alteration.

Table B-4 (concluded)

	Ba-JM-240				
	#6	#39	#52	#53	Average[a]
Quartz	12.52	17.19	15.17	12.50	14.18
Plagioclase	64.21	60.78	63.80	64.31	63.49
K-feldspar	0.11	0.21	0.15	0.14	0.15
Hornblende	14.41	11.04	11.63	13.37	12.60
Biotite	3.08	3.63	5.42	4.80	4.46
Opaque	1.81	1.43	1.30	1.47	1.47
Sphene	0.08	0.19	0.14	0.20	0.16
Epidote	0.16	0.29	0.27	0.20	0.23
Apatite	0.19	0.05	0.17	0.22	0.17
Chlorite	0.53	0.66	0.45	0.48	0.51
Pale amphibole[b]	0.00	0.00	0.00	0.00	0.00
White mica + clay[c]	2.74	4.52	1.34	2.32	2.50
Other	0.16	0.00	0.15	0.00	0.08
TOTAL	100.00	99.99	99.99	100.01	100.00
Color index	20.07	17.24	19.21	20.52	19.43
Plag + alteration	66.95	65.30	65.19	66.63	65.99
Amph/(bio + chl)	3.99	2.57	1.98	2.53	2.54
Total # of points	3761	3776	5828	5041	---
Total area (mm^2)	2257	2266	3730	4033	12286
# of thin sections	3	3	7	7	20

[a]Averages are weighted in proportion to the total thin-section area represented by each analysis. The 240 series of samples was taken from a continuous drill core at depths of 70 and 66 m for #39 and #52, respectively, and 230 and 226 m for #6 and #53, respectively.

[b]Actinolitic or cummingtonitic amphibole or both.

[c]Almost entirely alteration of plagioclase; "clay" includes all very fine-grained unidentified alteration.

APPENDIX C

MICROPROBE ANALYSES OF MINERALS

Mineral compositions were determined by electron microprobe analysis of grains in polished thin sections. Several points were analyzed from each of several grains in each section to provide a measure of the homogeneity within grains as well as the variation from grain to grain and from rock to rock. All elements detected in wavelength scans of selected grains were analyzed quantitatively. A few analyses include several additional elements. Most analyses were obtained using an Applied Research Laboratories (ARL) model EMX electron microprobe; others were obtained using a Materials Analysis Company (MAC) model 5-SA-3 electron microprobe. The accelerating potential was 15 kV for all analyses. Amphiboles, pyroxene, and magnetite were run at a sample current of 0.05 microamps (measured on brass) and an electron beam spot size of 1-10 microns. Biotite and feldspars were run at 0.01-0.02 microamps, with a 5-15 micron spot size, or at 0.05 microamps, with a 20 micron spot size. These conditions were carefully tested to verify that no decrease in x-ray intensity (e.g., for Na or K) occurred during an analysis. For the ARL probe, beam-current drift was compensated for by counting x-rays generated for a fixed flux of electrons rather than for a fixed time. For the MAC probe, drift was compensated for by normalizing the x-ray intensity to the beam current averaged over a fixed counting time.

Data reduction and correction procedures followed the method of

Bence and Albee (1968; Albee and Ray, 1970). The method involves calculation of the ratio (K-value) of x-ray intensity (minus background) in the sample to that in a standard of known composition. With the exception of vanadium metal, all of the standards used (Table C-1) are synthetic oxides or silicates or natural minerals of well-determined composition. Two or more additional minerals were analyzed as secondary standards during all runs. K-values are converted to weight percent oxides by correcting for the absorption-enhancement effects of other oxides on each radiation using a matrix of correction factors computed by Albee and Ray (1970) for binary oxide systems.

The ARL probe was set up to run three elements at a time on each of a large number of points, and the data were punched onto paper tape. Data for a single nine-element analysis were thus accumulated in three runs on different days. The paper tape output was processed by an IBM 360/75 computer which edited the data, corrected for background and dead-time, and calculated K-values. A second program converted the K-values to oxide concentrations and mineral formulae.

The MAC probe was interfaced to a DEC PDP-8/L computer which calculated K-values, oxide concentrations, and mineral formulae using FOCAL-8 programs written by A. A. Chodos. Successive sets of three elements were run on a single point, and the complete analysis was calculated and typed out before moving the sample to a new point.

Table C-1

Primary Standards Used for Microprobe Analysis of Minerals

Si	quartz (Brazil) or kyanite
Ti	synthetic TiO_2
Al	kyanite or synthetic Al_2O_3
V	vanadium metal
Cr	chromite or synthetic Cr_2O_3
Fe	synthetic ferrosilite or synthetic fayalite
Mn	rhodonite or garnet (Nuevo)
Mg	synthetic pyrope or synthetic MgO
Ba	benitoite
Ca	wollastonite
Na	albite (Amelia)
K	microcline (Asbestos)
P	fluor-apatite (Durango)

For hydroxyl-bearing minerals, the deficiency of the oxide summation from 100% was assigned to "H_2O", and the oxide concentrations were recalculated to correct for the absorption-enhancement effects of the "H_2O". For magnetite, the deficiency of the oxide summation from 100% was assigned to "excess oxygen", and the oxide concentrations were corrected for the absorption-enhancement effects of the oxygen. Sufficient Fe was then assigned to Fe^{3+} and Fe_2O_3 to account for the "excess oxygen". The remaining Fe was assigned to Fe^{2+} and FeO.

Note that these procedures for determining OH contents and Fe_2O_3/FeO ratios are inherently weak in that they incorporate all analytical errors and assume the absence of measurable amounts of all elements not counted in the analysis. Wave-length scans indicate that the assumption of insignificant concentrations of unanalyzed components is justified -- in particular, there is no detectable F or Cl in the two biotite and hornblende grains and the one actinolite grain scanned. Nevertheless, the "H_2O" and "OH" contents in amphiboles and biotite and

the Fe_2O_3/FeO ratios in magnetite are less reliable than other oxide concentrations.

For the ARL runs numerous minerals were analyzed as secondary standards, generally for one to several elements. Reproducibility was consistently better than ±2% for the amount present for oxide concentrations >5% and no worse than ±6% for concentrations down to 0.8%.

Two secondary standards now run routinely in this laboratory -- Leilenkopf sanidine and McGetchin garnet -- were analyzed before and generally during each run with the MAC microprobe. Reproducibilities for these analyses (Table C-2) are comparable to or only slightly poorer than those reported by Champion et al. (1975) for a large number analyses of these standards in this laboratory 18-30 months after most of my work, by five different analysts using more standardized and refined techniques. Reproducibility does not exceed 2.4% of the amount present for oxide concentrations >4.5% and is generally <8% for concentrations down to 0.4%. Hornblende standard P-328 (Engel and Engel, 1962, sample AE 338) was also analyzed during some MAC runs; Table C-3 shows that these results agree closely with the wet chemical analysis reported by Engel and Engel and with the great number of microprobe analyses of this standard by Laird (1977); CaO is slightly lower, but the error overlaps considerably with the results of Laird. Laird pointed out that the relatively large σ for Al_2O_3 may indicate slight inhomogeneity in the standard; perhaps the lower CaO in my results is also due to inhomogeneity.

Mineral grains are coded in the tables by mineral name, rock number, and grain number. For example, B-3a-1 is biotite grain #1 in rock

Ba-JM-3a. Mineral abbreviations are: P, plagioclase; KF, K-feldspar; H, hornblende; B, biotite; M, magnetite, Cp, clinopyroxene; Cu, cummingtonitic amphibole; and A, actinolitic amphibole.

Table C-2

Analyses of Leilenkopf Sanidine and McGetchin Garnet

	Leilenkopf Sanidine 22[a] analyses			McGetchin Garnet 24[b] analyses		
	Average	σ	σ(%)[c]	Average	σ	σ(%)[c]
SiO_2	64.10	0.55	0.9	42.68	0.53	1.2
TiO_2	0.03	0.02	67	0.15	0.04	27
Al_2O_3	18.42	0.41	2.2	22.94	0.54	2.4
Cr_2O_3	n.a.	--	--	1.39[b]	0.04	2.9
FeO_t	0.15	0.05	33	9.26	0.14	1.5
MnO	n.a.	--	--	0.40	0.03	7.5
MgO	0.01	0.01	100	19.98	0.45	2.3
BaO	1.16[a]	0.13	11	n.a.	--	--
CaO	0.02	0.02	100	4.64	0.08	1.7
Na_2O	2.39	0.09	3.8	n.a.	--	--
K_2O	12.81	0.15	1.2	n.a.	--	--

[a]Fewer than 22 analyses for BaO (8).

[b]Fewer than 24 analyses for Cr_2O_3 (7) and MnO (11).

[c]Standard deviation in % of the amount present.

Table C-3

Analyses of Hornblende Standard P-328[a]

		MAC Microprobe					
	Wet	This study (11 analyses)			Laird (202 analyses)		
	Chemical[a]	Average	σ	σ(%)[c]	Average	σ	σ(%)[c]
SiO_2	42.18	41.82	0.34	0.8	41.52	0.49	1.2
TiO_2	1.30	1.18	0.08	6.7	1.18	0.08	6.7
Al_2O_3	13.09	12.80	0.45	3.5	12.80	0.47	3.7
FeO_t	18.68	18.46	0.23	1.2	18.60	0.27	1.5
MnO	0.32	0.34	0.02	5.9	0.33	0.02	6.1
MgO	8.65	8.89	0.19	2.1	8.81	0.19	2.2
CaO	11.37	10.97	0.37	3.4	11.26	0.23	2.0
Na_2O	1.33	1.37	0.04	2.9	1.39	0.04	2.9
K_2O	0.96	0.96	0.02	2.1	0.99	0.08	8.1

[a]From Engel and Engel (1962), sample AE 338.

[b]Laird (1977).

[c]Standard deviation in % of the amount present.

Table C-4

Microprobe Analyses of Plagioclase

Textural Unit	Gneissose Border Tonalite					
Sample #	Ba-JM-30a					
	Cores			Rims		
Grain #	P-30a-1	P-30a-2	P-30a-3	P-30a-1	P-30a-2	P-30a-3
Number of Points	3	3	3	3	3	3
SiO_2	n.a.	n.a.	n.a.	n.a.	n.a.	n.a.
Al_2O_3	n.a.	n.a.	n.a.	n.a.	n.a.	n.a.
FeO_t	n.a.	n.a.	n.a.	n.a.	n.a.	n.a.
CaO	8.90	8.87	8.32	4.73	4.80	5.10
Na_2O	6.63	6.61	6.99	9.05	9.02	9.03
K_2O	0.24	0.30	0.31	0.20	0.21	0.11
TOTAL	--	--	--	--	--	--
Formula Proportions Based on Cation Sum = 5						
Si	--	--	--	--	--	--
Al	--	--	--	--	--	--
Fe	--	--	--	--	--	--
Ca	0.420	0.418	0.390	0.222	0.224	0.236
Na	0.566	0.565	0.593	0.777	0.764	0.757
K	0.014	0.017	0.017	0.011	0.012	0.006
Or/(Or + Ab + An)	0.014	0.017	0.017	0.011	0.012	0.006
Ab/(Or + Ab + An)	0.566	0.565	0.593	0.777	0.764	0.757
An/(Or + Ab + An)	0.420	0.418	0.390	0.222	0.224	0.236

Table C-4

Plagioclase (continued)

Textural Unit	Stubby Hornblende Tonalite							
Sample #	Ba-JM-25a							
	Cores			Rims			Inclusions in Hornblende	
Grain #	P-25a-1	P-25a-2	P-25a-3	P-25a-1	P-25a-2	P-25a-3	P-25a-4c*	P-25a-4r*
Number of Points	3	3	3	3	3	3	1	1
SiO_2	56.30	57.06	56.27	61.21	60.55	60.90	58.60	60.52
Al_2O_3	27.78	27.37	27.82	24.90	25.04	24.99	26.22	24.86
FeO_t	0.15	0.10	0.12	0.10	0.10	0.09	0.00	0.28
CaO	9.75	9.18	9.85	6.22	6.49	6.32	8.10	6.54
Na_2O	6.16	6.49	6.14	8.37	8.05	8.25	6.73	7.74
K_2O	0.13	0.10	0.13	0.11	0.11	0.10	0.11	0.10
TOTAL	100.28	100.30	100.32	100.91	100.34	100.64	99.76	100.04
Formula Proportions Based on Cation Sum = 5								
Si	2.519	2.549	2.517	2.692	2.683	2.687	2.631	2.697
Al	1.465	1.440	1.467	1.291	1.308	1.299	1.388	1.307
Fe	0.006	0.004	0.004	0.004	0.004	0.003	0.0	0.010
Ca	0.468	0.439	0.472	0.293	0.308	0.299	0.390	0.312
Na	0.535	0.562	0.532	0.714	0.692	0.705	0.586	0.669
K	0.007	0.006	0.007	0.006	0.006	0.006	0.006	0.006
Or/(Or + Ab + An)	0.007	0.006	0.007	0.006	0.006	0.006	0.006	0.006
Ab/(Or + Ab + An)	0.530	0.558	0.526	0.704	0.688	0.698	0.597	0.678
An/(Or + Ab + An)	0.463	0.436	0.467	0.290	0.306	0.296	0.397	0.317

*Letters "c" and "r" in the grain numbers designate core and rim zones.

Table C-4

Plagioclase (continued)

Textural Unit	Stubby Hornblende Tonalite							
Sample #	Ba-JM-29							
	Cores			Rims			Microveinlets	
Grain #	P-29-1	P-29-3	P-29-4	P-29-1	P-29-3	P-29-4	P-29-3	P-29-4
Number of Points	3	9	3	3	3	3	3	2
SiO_2	n.a.	n.a.	n.a.	n.a.	n.a.	n.a.	n.a.	n.a.
Al_2O_3	n.a.	n.a.	n.a.	n.a.	n.a.	n.a.	n.a.	n.a.
FeO_t	n.a.	n.a.	n.a.	n.a.	n.a.	n.a.	n.a.	n.a.
CaO	8.69	9.25	8.51	8.42	8.38	8.49	4.26	3.69
Na_2O	6.73	6.34	6.92	0.15	0.16	0.11	9.35	9.70
K_2O	0.11	0.14	0.15	5.54	5.73	5.85	0.10	0.09
TOTAL	--	--	--	--	--	--	--	--
Formula Proportions Based on Cation Sum = 5								
Si	--	--	--	--	--	--	--	--
Al	--	--	--	--	--	--	--	--
Fe	--	--	--	--	--	--	--	--
Ca	0.414	0.432	0.401	0.264	0.272	0.274	0.200	0.173
Na	0.580	0.560	0.590	0.727	0.719	0.720	0.795	0.822
K	0.006	0.008	0.008	0.008	0.009	0.006	0.005	0.005
Or/(Or + Ab + An)	0.006	0.008	0.008	0.008	0.009	0.006	0.005	0.005
Ab/(Or + Ab + An)	0.580	0.560	0.590	0.727	0.719	0.720	0.795	0.822
An/(Or + Ab + An)	0.414	0.432	0.401	0.264	0.272	0.274	0.200	0.173

Table C-4

Plagioclase (continued)

Textural Unit	Stubby Hornblende Tonalite							
Sample #	Ba-JM-68							
	Cores			Rims			Inclusions in Hornblende	
Grain #	P-68-1	P-68-2	P-68-3	P-68-1	P-68-2	P-68-3	P-68-4	P-68-5
Number of Points	3	3	3	3	3	3	2	1
SiO_2	n.a.	n.a.	n.a.	n.a.	n.a.	n.a.	58.12	56.62
Al_2O_3	n.a.	n.a.	n.a.	n.a.	n.a.	n.a.	26.57	27.04
FeO_t	n.a.	n.a.	n.a.	n.a.	n.a.	n.a.	0.16	0.18
CaO	9.03	9.59	9.21	5.62	5.67	6.07	8.32	8.90
Na_2O	6.46	6.19	6.42	8.58	8.57	8.17	6.54	6.46
K_2O	0.22	0.18	0.17	0.13	0.15	0.13	0.09	0.09
TOTAL	--	--	--	--	--	--	99.80	99.29
Formula Proportions Based on Cation Sum = 5								
Si	--	--	--	--	--	--	2.162	2.555
Al	--	--	--	--	--	--	1.408	1.439
Fe	--	--	--	--	--	--	0.006	0.007
Ca	0.430	0.456	0.438	0.264	0.266	0.289	0.400	0.430
Na	0.557	0.534	0.552	0.729	0.726	0.704	0.570	0.565
K	0.012	0.010	0.010	0.007	0.008	0.007	0.005	0.005
Or/(Or + Ab + An)	0.012	0.010	0.010	0.007	0.008	0.007	0.005	0.005
Ab/(Or + Ab + An)	0.557	0.534	0.552	0.729	0.726	0.704	0.585	0.565
An/(Or + Ab + An)	0.430	0.456	0.438	0.264	0.266	0.289	0.410	0.430

Table C-4

Plagioclase (continued)

Textural Unit	Prismatic Hornblende Tonalite									
Sample #	Ba-JM-36a									
	Cores			Rims			Inclusions in Hornblende			
Grain #	P-36a-1	P-36a-2	P-36a-3	P-36a-1	P-36a-2	P-36a-3	P-36a-4c*	P-36a-4r*	P-36a-5	P-36a-6
Number of Points	3	3	3	3	3	3	1	1	2	2
SiO_2	58.74	57.52	56.63	60.88	60.54	60.28	55.64	59.30	56.50	57.71
Al_2O_3	26.42	27.08	27.69	25.05	25.22	25.42	28.24	25.62	27.60	26.40
FeO_t	0.08	0.08	0.13	0.10	0.10	0.11	0.16	0.20	0.19	0.11
CaO	8.03	8.70	9.64	6.28	6.45	6.80	10.80	7.28	9.83	8.39
Na_2O	7.10	6.71	6.42	8.30	8.09	8.10	5.37	7.48	5.93	6.87
K_2O	0.14	0.13	0.14	0.10	0.11	0.12	0.07	0.09	0.06	0.09
TOTAL	100.51	100.21	100.64	100.69	100.52	100.83	100.28	99.97	100.11	99.57
Formula Proportions Based on Cation Sum = 5										
Si	2.611	2.568	2.521	2.684	2.677	2.656	2.503	2.645	2.537	2.593
Al	1.384	1.425	1.453	1.301	1.314	1.320	1.498	1.348	1.461	1.398
Fe	0.003	0.003	0.005	0.004	0.004	0.004	0.006	0.007	0.007	0.004
Ca	0.382	0.416	0.460	0.297	0.306	0.321	0.521	0.348	0.473	0.403
Na	0.612	0.581	0.554	0.709	0.694	0.692	0.468	0.647	0.516	0.597
K	0.008	0.007	0.008	0.005	0.006	0.006	0.004	0.005	0.004	0.005
Or/(Or + Ab + An)	0.008	0.007	0.008	0.005	0.006	0.006	0.004	0.005	0.004	0.005
Ab/(Or + Ab + An)	0.610	0.579	0.542	0.702	0.690	0.679	0.472	0.647	0.520	0.594
An/(Or + Ab + An)	0.382	0.414	0.450	0.293	0.304	0.315	0.525	0.348	0.477	0.401

*Letters "c" and "r" in the grain number designate core and rim zones.

Table C-4

Plagioclase (continued)

Textural Unit	Prismatic Hornblende Tonalite						
Sample #	Ba-JM-46a						
	Cores		Rims		Intermediate Zones		
Grain #	P-46a-1	P-46a-2	P-46a-1	P-46a-3	P-46a-1[a]	P-46a-2[b]	P-46a-3[c]
Number of Points	3	3	1	3	3	3	3
SiO_2	58.33	57.00	62.25	63.70	59.42	58.70	61.06
Al_2O_3	26.69	27.94	24.05	23.55	26.14	26.51	24.93
FeO_t	0.13	0.09	0.14	0.10	0.12	0.12	0.15
CaO	8.27	9.77	4.92	4.45	7.51	8.01	6.35
Na_2O	6.87	6.18	8.75	9.35	7.45	7.10	8.12
K_2O	0.22	0.13	0.31	0.13	0.24	0.21	0.30
TOTAL	100.51	101.11	100.43	101.27	100.88	100.71	100.91
Formula Proportions Based on Cation Sum = 5							
Si	2.596	2.531	2.746	2.779	2.626	2.604	2.690
Al	1.400	1.462	1.250	1.211	1.361	1.389	1.294
Fe	0.005	0.003	0.005	0.004	0.004	0.004	0.005
Ca	0.394	0.465	0.233	0.208	0.356	0.381	0.300
Na	0.593	0.532	0.749	0.791	0.638	0.610	0.693
K	0.012	0.007	0.017	0.007	0.014	0.012	0.017
Or/(Or + Ab + An)	0.012	0.007	0.017	0.007	0.014	0.012	0.017
Ab/(Or + Ab + An)	0.594	0.530	0.750	0.787	0.633	0.609	0.686
An/(Or + Ab + An)	0.394	0.463	0.233	0.206	0.353	0.380	0.297

[a]Rim along a slightly embayed part of the grain margin.
[b]Outer part of a plagioclase grain largely enclosed in grain P-46a-1. Indicates the composition which was crystallizing when the two grains came into contact and shortly thereafter.
[c]Interior of a grain whose core is not cut by the thin section.

Table C-4

Plagioclase (continued)

Textural Unit	Seriate Porphyritic Tonalite					
Sample #	Ba-JM-3a					
	Cores			Rims		
Grain #	P-3a-1	P-3a-2	P-3a-3	P-3a-1	P-3a-2	P-3a-3
Number of Points	3	3	3	3	3	3
SiO_2	58.37	58.34	57.32	62.57	62.09	61.79
Al_2O_3	26.56	26.41	27.06	23.64	24.17	24.57
FeO_t	0.14	0.12	0.17	0.14	0.13	0.20
CaO	8.21	7.81	9.12	4.87	5.19	5.21
Na_2O	6.96	7.10	6.35	9.00	8.62	8.60
K_2O	0.22	0.16	0.22	0.19	0.22	0.29
TOTAL	100.46	99.93	100.24	100.41	100.42	100.66
Formula Proportions Based on Cation Sum = 5						
Si	2.597	2.607	2.565	2.758	2.742	2.721
Al	1.393	1.391	1.427	1.228	1.258	1.275
Fe	0.005	0.004	0.006	0.005	0.005	0.007
Ca	0.391	0.374	0.438	0.230	0.246	0.246
Na	0.601	0.615	0.551	0.769	0.738	0.735
K	0.013	0.009	0.012	0.011	0.012	0.016
Or/(Or + Ab + An)	0.013	0.009	0.012	0.010	0.012	0.016
Ab/(Or + Ab + An)	0.597	0.616	0.551	0.762	0.741	0.737
An/(Or + Ab + An)	0.390	0.375	0.437	0.228	0.247	0.247

Table C-4

Plagioclase (concluded)

Textural Unit	Seriate Porphyritic Tonalite							
Sample #	Ba-JM-62a							
	Cores				Rims			
Grain #	P-62a-1	P-62a-2	P-62a-3	P-62a-4*	P-62a-1	P-62a-2	P-62a-3	P-62a-4
Number of Points	3	3	3	3	3	3	3	3
SiO_2	n.a.	n.a.	n.a.	n.a.	n.a.	n.a.	n.a.	n.a.
Al_2O_3	n.a.	n.a.	n.a.	n.a.	n.a.	n.a.	n.a.	n.a.
FeO_t	n.a.	n.a.	n.a.	n.a.	n.a.	n.a.	n.a.	n.a.
CaO	9.90	9.13	9.24	6.84	4.66	5.09	4.57	5.00
Na_2O	6.07	6.40	6.39	7.83	9.22	8.73	9.02	8.86
K_2O	0.17	0.25	0.21	0.26	0.14	0.30	0.28	0.23
TOTAL	--	--	--	--	--	--	--	--
Formula Proportions Based on Cation Sum = 5								
Si	--	--	--	--	--	--	--	--
Al	--	--	--	--	--	--	--	--
Fe	--	--	--	--	--	--	--	--
Ca	0.470	0.434	0.439	0.321	0.217	0.240	0.215	0.234
Na	0.521	0.551	0.549	0.665	0.776	0.744	0.769	0.753
K	0.010	0.014	0.012	0.015	0.008	0.016	0.016	0.013
Or/(Or + Ab + An)	0.010	0.014	0.012	0.015	0.008	0.016	0.016	0.013
Ab/(Or + Ab + An)	0.521	0.551	0.549	0.665	0.775	0.744	0.769	0.753
An/(Or + Ab + An)	0.470	0.434	0.439	0.321	0.217	0.240	0.215	0.234

*The unusually low An content of the "core" of P-62a-4 suggests that the thin section does not transect the actual core of this grain. This analysis was therefore omitted from the calculated averaged core composition for this rock given in Table 7.

Table C-5

Microprobe Analyses of K-Feldspar

Textural Unit	Gneissose Border Tonalite			
Sample #	Ba-JM-30a			
Grain #	KF-30a-1	KF-30a-2	KF-30a-3	KF-30a-4
Number of Points	3	3	4	3
SiO_2	65.04	64.94	64.27	64.15
TiO_2	n.a.	n.a.	n.a.	n.a.
Al_2O_3	18.39	18.61	18.72	18.72
FeO_t	0.08	0.07	0.07	0.06
MnO	0.00	0.00	0.00	0.00
MgO	0.04	0.03	0.03	0.04
BaO	0.76	1.42	1.79	1.89
CaO	0.03	0.02	0.02	0.03
Na_2O	0.65	0.66	0.76	0.89
K_2O	15.57	15.25	15.07	14.82
TOTAL	100.56	100.01	100.74	100.60
Formula Proportions Based on Cation Sum = 5				
Si	3.003	2.998	2.979	2.978
Ti	--	--	--	--
Al	1.001	1.013	1.023	1.024
Fe	0.003	0.003	0.003	0.002
Mn	0.0	0.0	0.0	0.0
Mg	0.003	0.002	0.002	0.003
Ba	0.014	0.026	0.032	0.034
Ca	0.002	0.001	0.001	0.002
Na	0.058	0.059	0.069	0.080
K	0.917	0.899	0.891	0.878
Or/(Or + Ab + An + Ce)	0.926	0.913	0.897	0.884
Ab/(Or + Ab + An + Ce)	0.059	0.060	0.069	0.080
An/(Or + Ab + An + Ce)	0.002	0.001	0.001	0.002
Ce/(Or + Ab + An + Ce)	0.014	0.026	0.033	0.035
2V (estimated)	35 ± 10°	35 ± 20°	--	40 ± 10°

Table C-5

K-Feldspar (continued)

Textural Unit	Prismatic Hornblende Tonalite			
Sample #	Ba-JM-36a		Ba-JM-46a	
Grain #	KF-36a-1*	KF-36a-2	KF-46a-1	KF-46a-2
Number of Points	1	1	4	4
SiO_2	63.45	61.91	64.66	64.87
TiO_2	0.00	0.01	n.a.	n.a.
Al_2O_3	17.79	19.26	18.89	18.79
FeO_t	0.00	0.13	0.10	0.02
MnO	n.a.	n.a.	0.00	0.00
MgO	0.00	0.01	0.04	0.03
BaO	0.56	2.78	1.93	0.75
CaO	0.09	0.11	0.02	0.03
Na_2O	0.19	0.44	0.84	0.63
K_2O	14.92	14.40	14.66	15.43
TOTAL	97.00	99.06	101.14	100.55
Formula Proportions Based on Cation Sum = 5				
Si	3.046	2.943	2.989	2.995
Ti	0.0	0.0	--	--
Al	1.007	1.079	1.029	1.022
Fe	0.0	0.005	0.004	0.001
Mn	--	--	0.0	0.0
Mg	0.0	0.001	0.003	0.002
Ba	0.011	0.052	0.035	0.014
Ca	0.005	0.006	0.001	0.001
Na	0.017	0.041	0.075	0.056
K	0.914	0.873	0.865	0.909
Or/(Or + Ab + An + Ce)	0.966	0.899	0.886	0.928
Ab/(Or + Ab + An + Ce)	0.018	0.042	0.077	0.057
An/(Or + Ab + An + Ce)	0.005	0.006	0.001	0.001
Ce/(Or + Ab + An + Ce)	0.011	0.053	0.036	0.014
2V (est.)	--	--	<20° near 0°?	35 ± 15°

*Extremely small grain, both the oxide sum (97.00) and the sum Na + K + Ba + Ca (0.947) are low.

Table C-5

K-Feldspar (continued)

Textural Unit	Seriate Porphyritic Tonalite			
Sample #	Ba-JM-3a			
Grain #	KF-3a-1	KF-3a-2	KF-3a-3	KF-3a-4
Number of Points	2	3	2	2
SiO_2	64.34	64.11	62.88	63.76
TiO_2	0.01	0.00	0.02	0.01
Al_2O_3	19.00	18.53	18.59	18.50
FeO_t	0.00	0.06	0.06	0.05
MnO	n.a.	n.a.	n.a.	n.a.
MgO	0.02	0.01	0.01	0.00
BaO	0.83	0.42	1.35	1.01
CaO	0.03	0.01	0.02	0.00
Na_2O	0.60	0.57	0.61	0.57
K_2O	15.74	15.87	15.48	15.64
TOTAL	100.57	99.58	99.02	99.54
Formula Proportions Based on Cation Sum = 5				
Si	2.968	2.981	2.957	2.978
Ti	0.0	0.0	0.001	0.0
Al	1.034	1.016	1.031	1.019
Fe	0.0	0.002	0.002	0.002
Mn	--	--	--	--
Mg	0.001	0.001	0.0	0.0
Ba	0.015	0.008	0.025	0.018
Ca	0.001	0.001	0.001	0.0
Na	0.053	0.051	0.055	0.051
K	0.926	0.941	0.929	0.932
Or/(Or + Ab + An + Ce)	0.930	0.940	0.920	0.930
Ab/(Or + Ab + An + Ce)	0.054	0.051	0.055	0.051
An/(Or + Ab + An + Ce)	0.001	0.001	0.001	0.0
Ce/(Or + Ab + An + Ce)	0.015	0.008	0.025	0.018
2V (est.)	<10°	<10°	<20°	<30°

Table C-5

K-Feldspar (concluded)

Textural Unit	Seriate Porphyritic Tonalite		
Sample #	Ba-JM-62a		
Grain #	KF-62a-1	KF-62a-2	KF-62a-3
Number of Points	1	3	2
SiO_2	63.50	63.55	63.64
TiO_2	0.01	0.02	0.03
Al_2O_3	17.64	18.01	18.28
FeO_t	0.03	0.07	0.00
MnO	n.a.	n.a.	n.a.
MgO	0.00	0.02	0.00
BaO	0.49	0.61	1.06
CaO	0.04	0.04	0.02
Na_2O	0.22	0.56	0.45
K_2O	16.24	15.77	15.89
TOTAL	98.17	98.65	99.37
Formula Proportions Based on Cation Sum = 5			
Si	3.004	2.987	2.990
Ti	0.0	0.001	0.001
Al	0.984	0.998	0.999
Fe	0.001	0.003	0.001
Mn	--	--	--
Mg	0.0	0.001	0.001
Ba	0.009	0.011	0.017
Ca	0.002	0.002	0.001
Na	0.020	0.051	0.041
K	0.980	0.946	0.950
Or/(Or + Ab + An + Ce)	0.969	0.936	0.940
Ab/(Or + Ab + An + Ce)	0.020	0.051	0.040
An/(Or + Ab + An + Ce)	0.002	0.002	0.001
Ce/(Or + Ab + An + Ce)	0.009	0.011	0.019
2V (est.)	35 ± 10°	--	45 ± 15°

Table C-6

Microprobe Analyses of Hornblende

Textural Unit	Gneissose Border Tonalite			
Sample #	Ba-JM-30a			
	Unzoned and Weakly Zoned Grains			
Grain #	H-30a-1	H-30a-2	H-30a-3	H-30a-4
# of Points	3	3	3	3
SiO_2	49.61	49.11	50.10	48.54
TiO_2	0.88	1.12	1.12	0.70
Al_2O_3	6.02	6.33	5.80	6.54
Cr_2O_3	n.a.	n.a.	n.a.	n.a.
FeO_t	13.42	14.00	12.31	14.32
MnO	0.52	0.52	0.42	0.49
MgO	15.06	14.30	15.92	14.03
CaO	11.73	11.89	11.46	12.14
Na_2O	1.04	1.08	1.14	0.92
K_2O	0.31	0.34	0.25	0.50
"H_2O"	1.42	1.31	1.48	1.80
TOTAL	100.01	100.00	100.00	99.98
Formula Proportions Based on the Sum (Cations less Alkalies) = 15				
Si	7.153	7.110	7.196	7.062
Al(IV)	0.847	0.890	0.804	0.938
Al(VI)	0.176	0.189	0.178	0.184
Ti	0.095	0.122	0.121	0.077
Cr	---	---	---	---
Fe	1.617	1.694	1.478	1.742
Mn	0.063	0.064	0.051	0.060
Mg	3.237	3.086	3.409	3.043
Ca	1.812	1.845	1.764	1.893
Na	0.291	0.304	0.318	0.261
K	0.056	0.062	0.046	0.093
"OH"	1.368	1.265	1.416	1.747
Fe/(Fe+Mn+Mg)	0.329	0.350	0.299	0.360
Mn/(Fe+Mn+Mg)	0.013	0.013	0.010	0.012
Mg/(Fe+Mn+Mg)	0.658	0.637	0.690	0.628

Table C-6

Hornblende (continued)

Textural Unit	Stubby Hornblende Tonalite					
Sample #	Ba-JM-25a					
	"Cores"	"Rims"		Weakly Zoned Grains		
Grain #	H-25a-2	H-25a-2	H-25a-2i†	H-25a-5	H-25a-6	H-25a-7
Color*	brn-grn	bl-grn	dp bl-grn	sl brn-bl-grn	brn-grn	bl-grn
# of Points	14	8	4	4	3	4
SiO_2	47.47	47.49	48.28	48.29	48.00	48.23
TiO_2	1.66	0.75	0.94	0.88	1.54	0.93
Al_2O_3	7.57	7.52	7.55	7.58	7.44	7.59
Cr_2O_3	0.02	n.a.	n.a.	n.a.	n.a.	n.a.
FeO_t	13.13	14.24	14.27	14.46	14.22	14.75
MnO	0.28	0.35	0.38	0.46	0.42	0.41
MgO	14.71	14.07	13.93	13.96	13.98	13.92
CaO	11.05	11.51	11.46	11.23	11.33	11.05
Na_2O	1.32	1.10	1.06	1.11	1.09	1.11
K_2O	0.31	0.32	0.30	0.30	0.34	0.28
"H_2O"	2.48	2.65	1.82	1.74	1.64	1.72
TOTAL	100.02	100.00	99.99	100.01	100.00	99.99
Formula Proportions Based on the Sum (Cations less Alkalies) = 15						
Si	6.930	6.955	7.018	7.020	6.980	7.015
Al(IV)	1.070	1.045	0.982	0.980	1.020	0.985
Al(VI)	0.236	0.254	0.312	0.318	0.256	0.316
Ti	0.180	0.083	0.103	0.097	0.169	0.102
Cr	0.001	---	---	---	---	---
Fe	1.608	1.743	1.734	1.756	1.729	1.793
Mn	0.036	0.043	0.047	0.056	0.051	0.051
Mg	3.208	3.071	3.019	3.024	3.031	3.017
Ca	1.732	1.806	1.786	1.748	1.765	1.722
Na	0.368	0.312	0.299	0.313	0.307	0.314
K	0.057	0.060	0.055	0.055	0.063	0.052
"OH"	2.344	2.593	1.762	1.683	1.586	1.672
Fe/(Fe+Mg+Mg)	0.331	0.359	0.361	0.363	0.359	0.369
Mn/(Fe+Mn+Mg)	0.007	0.009	0.010	0.012	0.011	0.010
Mg/(Fe+Mn+Mg)	0.661	0.632	0.629	0.625	0.630	0.621

*Observed in thin section at maximum absorption (parallel to γ').
Abbreviations: bl-blue; brn-brownish; grn-green; sl-slightly; dp-deep.

†Interstitial branch off of the poikilitic margin of H-25a-2.

Table C-6

Hornblende (continued)

Textural Unit	Stubby Hornblende Tonalite					
Sample #	Ba-JM-29					
	"Cores"		"Rims"		Weakly Zoned Grains	
Grain #	H-29-1	H-29-5	H-29-1	H-29-5	H-29-3	H-29-4†
Color*	brn-grn	brn-grn	bl-grn	bl-grn	sl bl-brn-grn	sl br-bl-grn
# of Points	4	2	4	1	3	3
SiO_2	47.88	47.82	48.89	49.07	48.05	48.86
TiO_2	1.66	1.64	0.49	0.94	1.55	0.86
Al_2O_3	7.24	7.27	6.79	6.85	7.23	6.90
Cr_2O_3	0.01	n.a.	0.02	n.a.	n.a.	n.a.
FeO_t	13.31	13.83	13.71	14.20	14.16	14.58
MnO	0.30	0.33	0.33	0.41	0.42	0.40
MgO	14.61	14.64	14.37	14.64	14.38	14.03
CaO	10.82	10.78	11.63	10.97	10.92	11.21
Na_2O	1.39	1.32	0.91	1.08	1.19	1.04
K_2O	0.27	0.25	0.25	0.27	0.30	0.28
"H_2O"	2.51	2.14	2.61	1.57	1.81	1.84
TOTAL	100.00	100.02	100.00	100.00	100.01	100.00
Formula Proportions Based on the Sum (Cations less Alkalies) = 15						
Si	7.009	6.976	7.140	7.102	6.993	7.109
Al(IV)	0.991	1.024	0.860	0.898	1.007	0.891
Al(VI)	0.258	0.226	0.308	0.271	0.234	0.293
Ti	0.182	0.180	0.054	0.102	0.169	0.094
Cr	0.001	---	0.003	---	---	---
Fe	1.630	1.687	1.708	1.718	1.723	1.774
Mn	0.036	0.041	0.041	0.051	0.052	0.049
Mg	3.201	3.183	3.071	3.157	3.118	3.043
Ca	1.693	1.685	1.820	1.702	1.704	1.748
Na	0.393	0.372	0.258	0.303	0.336	0.292
K	0.050	0.047	0.047	0.050	0.055	0.053
"OH"	2.352	2.081	2.551	1.519	1.754	1.791
Fe/(Fe+Mn+Mg)	0.335	0.344	0.354	0.349	0.352	0.364
Mn/(Fe+Mn+Mg)	0.007	0.008	0.009	0.010	0.011	0.010
Mg/(Fe+Mn+Mg)	0.658	0.648	0.637	0.641	0.637	0.625

*Observed in thin section at maximum absorption (parallel to γ').
Abbreviations: bl-blue; brn-brownish; grn-green; sl-slightly; dp-deep.

†Small inclusion in plagioclase.

Table C-6

Hornblende (continued)

Textural Unit	Stubby Hornblende Tonalite						
Sample #	Ba-JM-68						
	"Cores"			"Rims"			Weakly Zoned Grain
Grain #	H-68-1	H-68-2	H-68-4	H-68-1	H-68-2	H-68-4	H-68-3
Color*	brn bl-grn	brn-grn	sl brn-grn	bl-grn	sl bl-grn	sl bl-grn	sl brn-grn
# of Points	4	4	3	1	2	3	3
SiO_2	47.87	47.72	46.73	48.32	48.93	48.01	47.87
TiO_2	1.62	1.67	1.69	0.95	0.83	0.75	0.82
Al_2O_3	7.34	7.26	7.40	7.10	6.49	6.70	6.76
Cr_2O_3	n.a.	n.a.	n.a.	n.a.	n.a.	n.a.	n.a.
FeO_t	13.72	13.39	13.25	14.57	13.91	13.99	13.72
MnO	0.35	0.30	0.28	0.35	0.41	0.37	0.37
MgO	14.58	14.78	14.88	14.06	14.49	14.54	14.56
CaO	10.82	10.99	10.94	11.26	11.33	11.51	11.46
Na_2O	1.38	1.43	1.48	1.10	1.10	1.08	1.01
K_2O	0.31	0.30	0.31	0.28	0.35	0.36	0.37
"H_2O"	2.02	2.16	3.05	2.02	2.16	2.69	3.06
TOTAL	100.01	100.00	100.01	100.01	100.00	100.00	100.00
Formula Proportions Based on the Sum (Cations less Alkalies) = 15							
Si	6.983	6.964	6.877	7.045	7.133	7.028	7.025
Al(IV)	1.017	1.036	1.123	0.955	0.867	0.972	0.975
Al(VI)	0.245	0.212	0.161	0.265	0.248	0.183	0.195
Ti	0.177	0.183	0.186	0.104	0.092	0.082	0.090
Cr	---	---	---	---	---	---	---
Fe	1.671	1.634	1.630	1.776	1.695	1.712	1.684
Mn	0.044	0.037	0.036	0.043	0.051	0.046	0.045
Mg	3.170	3.215	3.262	3.054	3.147	3.172	3.184
Ca	1.691	1.719	1.725	1.759	1.769	1.805	1.802
Na	0.390	0.404	0.421	0.312	0.310	0.306	0.287
K	0.057	0.056	0.058	0.052	0.066	0.067	0.070
"OH"	1.965	2.113	2.994	1.964	2.111	2.640	3.000
Fe/(Fe+Mn+Mg)	0.342	0.334	0.331	0.364	0.346	0.347	0.343
Mn/(Fe+Mn+Mg)	0.009	0.008	0.007	0.009	0.010	0.009	0.009
Mg/(Fe+Mn+Mg)	0.649	0.658	0.662	0.627	0.643	0.643	0.648

*Observed in thin section at maximum absorption (parallel to Y').
Abbreviations: bl-blue; brn-brownish; grn-green; sl-slightly; dp-deep.

Table C-6

Hornblende (continued)

Textural Unit	Prismatic Hornblende Tonalite					
Sample #	Ba-JM-36a					
	Unzoned and Weakly Zoned Grains					
Grain #	H-36a-1	H-36a-3	H-36a-4	H-36-5	H-36a-6*	H-36a-7*
# of Points	3	4	4	4	2	2
SiO_2	49.49	49.63	48.64	49.30	50.58	49.20
TiO_2	1.11	0.88	1.08	1.33	0.22	0.62
Al_2O_3	6.94	6.98	7.40	6.96	6.16	7.39
Cr_2O_3	n.a.	n.a.	n.a.	n.a.	0.01	0.02
FeO_t	12.69	13.05	13.30	12.50	12.85	13.22
MnO	0.37	0.48	0.47	0.41	0.55	0.45
MgO	15.93	15.31	14.74	15.70	15.06	14.14
CaO	10.88	11.50	11.34	11.08	10.88	11.47
Na_2O	1.08	0.98	1.04	1.04	0.96	0.99
K_2O	0.17	0.19	0.21	0.19	0.14	0.21
"H_2O"	1.35	1.00	1.75	1.50	2.60	2.28
TOTAL	100.01	100.00	99.97	100.01	100.01	99.99
Formula Proportions Based on the Sum (Cations less Alkalies) = 15						
Si	7.082	7.092	7.027	7.072	7.342	7.151
Al(IV)	0.918	0.908	0.973	0.928	0.658	0.849
Al(VI)	0.252	0.267	0.287	0.248	0.396	0.417
Ti	0.120	0.095	0.118	0.143	0.024	0.068
Cr	---	---	---	---	0.001	0.002
Fe	1.518	1.559	1.607	1.500	1.561	1.608
Mn	0.045	0.058	0.058	0.049	0.067	0.056
Mg	3.397	3.260	3.175	3.357	3.259	3.063
Ca	1.668	1.761	1.755	1.703	1.692	1.786
Na	0.299	0.270	0.291	0.290	0.269	0.279
K	0.032	0.035	0.039	0.034	0.026	0.040
"OH"	1.289	0.952	1.690	1.435	2.515	2.210
Fe/(Fe+Mn+Mg)	0.306	0.320	0.332	0.306	0.319	0.318
Mn/(Fe+Mn+Mg)	0.009	0.012	0.012	0.010	0.014	0.010
Mg/(Fe+Mn+Mg)	0.685	0.668	0.656	0.684	0.667	0.672

*Small inclusions in plagioclase.

Table C-6

Hornblende (continued)

Textural Unit	Prismatic Hornblende Tonalite	
Sample #	Ba-JM-36a	
	Core	Rim
Grain #	H-36a-2	H-36a-2
# of Points	4	4
SiO_2	49.83	48.70
TiO_2	1.01	0.75
Al_2O_3	7.05	7.30
Cr_2O_3	n.a.	n.a.
FeO_t	12.34	13.07
MnO	0.34	0.43
MgO	15.88	15.10
CaO	11.10	11.19
Na_2O	0.95	1.01
K_2O	0.20	0.21
"H_2O"	1.32	2.25
TOTAL	100.02	100.01
Formula Proportions Based on the Sum (Cations less Alkalies) = 15		
Si	7.115	7.048
Al(IV)	0.885	0.952
Al(VI)	0.302	0.293
Ti	0.109	0.082
Cr	---	---
Fe	1.473	1.581
Mn	0.041	0.053
Mg	3.378	3.257
Ca	1.699	1.736
Na	0.263	0.284
K	0.035	0.039
"OH"	1.268	2.177
Fe/(Fe+Mn+Mg)	0.301	0.323
Mn/(Fe+Mn+Mg)	0.008	0.011
Mg/(Fe+Mn+Mg)	0.691	0.666

Table C-6

Hornblende (continued)

Textural Unit	Prismatic Hornblende Tonalite					
Sample #	Ba-JM-46a					
	Unzoned and Weakly Zoned Grains					
Grain #	H-46a-1	H-46a-2	H-46a-3	H-46a-4	H-46a-5	H-46a-6*
# of Points	4	4	4	4	4	2
SiO_2	49.81	49.88	50.27	48.81	49.19	48.53
TiO_2	0.70	0.66	0.70	0.81	0.77	1.31
Al_2O_3	5.86	5.63	5.74	6.12	6.12	7.26
Cr_2O_3	n.a.	n.a.	n.a.	n.a.	n.a.	0.01
FeO_t	13.32	13.11	12.93	13.78	13.30	12.57
MnO	0.52	0.52	0.49	0.51	0.50	0.39
MgO	14.95	15.16	15.36	14.56	14.90	14.95
CaO	11.76	11.81	11.73	11.92	12.04	11.21
Na_2O	1.00	0.90	0.90	0.97	0.93	1.43
K_2O	0.28	0.24	0.29	0.28	0.31	0.19
"H_2O"	1.79	2.10	1.59	2.24	1.94	2.17
TOTAL	99.99	100.01	100.00	100.00	100.00	100.02
Formula Proportions Based on the Sum (Cations less Alkalies) = 15						
Si	7.205	7.219	7.233	7.105	7.120	7.053
Al (IV)	0.795	0.781	0.767	0.895	0.880	0.947
Al (VI)	0.204	0.180	0.207	0.154	0.164	0.296
Ti	0.076	0.072	0.076	0.089	0.084	0.143
Cr	---	---	---	---	---	0.001
Fe	1.611	1.586	1.555	1.676	1.609	1.528
Mn	0.064	0.063	0.060	0.063	0.061	0.048
Mg	3.223	3.269	3.295	3.159	3.215	3.238
Ca	1.823	1.831	1.808	1.859	1.868	1.746
Na	0.280	0.052	0.251	0.273	0.260	0.403
K	0.052	0.045	0.054	0.053	0.057	0.035
"OH"	1.727	2.027	1.523	2.175	1.877	2.103
Fe/(Fe+Mn+Mg)	0.329	0.322	0.317	0.342	0.329	0.318
Mn/(Fe+Mn+Mg)	0.013	0.013	0.012	0.013	0.012	0.010
Mg/(Fe+Mn+Mg)	0.658	0.665	0.671	0.645	0.658	0.672

*Small inclusions in plagioclase.

Table C-6

Hornblende (continued)

Textural Unit	Seriate Porphyritic Tonalite				
Sample #	Ba-JM-3a				
	Unzoned and Weakly Zoned Grains				
Grain #	H-3a-2	H-3a-3	H-3a-5	H-3a-6	H-3a-9
# of Points	3	3	3	4	4
SiO_2	50.17	48.57	49.36	49.66	49.72
TiO_2	0.76	1.08	0.84	0.74	0.74
Al_2O_3	6.08	7.20	6.52	6.20	6.18
Cr_2O_3	n.a.	n.a.	n.a.	n.a.	n.a.
FeO_t	12.77	13.34	13.29	13.40	13.18
MnO	0.51	0.46	0.49	0.46	0.48
MgO	15.69	14.89	15.17	15.08	15.29
CaO	11.46	11.44	11.44	11.62	11.17
Na_2O	1.03	1.12	1.04	0.87	1.01
K_2O	0.23	0.24	0.22	0.19	0.20
"H_2O"	1.29	1.65	1.63	1.77	2.03
TOTAL	99.99	99.99	100.00	99.99	99.99
Formula Proportions Based on the Sum (Cations less Alkalies) = 15					
Si	7.189	7.015	7.115	7.160	7.189
Al(IV)	0.811	0.985	0.885	0.840	0.811
Al(VI)	0.216	0.241	0.223	0.213	0.243
Ti	0.082	0.117	0.091	0.080	0.080
Cr	---	---	---	---	---
Fe	1.530	1.611	1.601	1.614	1.592
Mn	0.061	0.057	0.060	0.057	0.059
Mg	3.351	3.205	3.259	3.241	3.295
Ca	1.760	1.770	1.766	1.795	1.730
Na	0.285	0.315	0.290	0.244	0.283
K	0.042	0.045	0.040	0.036	0.036
"OH"	1.234	1.589	1.568	1.705	1.962
Fe/(Fe+Mn+Mg)	0.310	0.331	0.326	0.329	0.322
Mn/(Fe+Mn+Mg)	0.012	0.012	0 012	0.012	0.012
Mg/(Fe+Mn+Mg)	0.678	0.658	0.662	0.660	0.666

Table C-6

Hornblende (concluded)

Textural Unit	Seriate Porphyritic Tonalite					
Sample #	Ba-JM-62a					
	Core	Rim	Atypical Rim Point	Unzoned and Weakly Zoned Grains		
Grain #	H-62a-2*	H-62a-2*	H-62a-2*	H-62a-1	H-62a-4	H-62a-5
# of Points	3	2	1	3	6	2
SiO_2	46.50	49.77	46.96	50.61	48.71	49.26
TiO_2	1.35	0.68	1.31	0.67	0.90	0.75
Al_2O_3	8.89	5.61	8.01	5.06	6.66	6.03
Cr_2O_3	n.a.	n.a.	n.a.	n.a.	n.a.	n.a.
FeO_t	13.33	12.37	13.83	12.48	12.84	13.35
MnO	0.40	0.51	0.52	0.52	0.46	0.57
MgO	14.44	16.18	14.33	16.03	15.54	15.31
CaO	10.77	11.25	11.01	11.34	10.92	10.93
Na_2O	1.61	0.95	1.39	0.93	1.28	1.16
K_2O	0.19	0.24	0.18	0.22	0.20	0.18
"H_2O"	2.52	2.45	2.46	2.15	2.50	2.47
TOTAL	100.00	100.01	100.00	100.01	100.01	100.01
Formula Proportions Based on the Sum (Cations less Alkalies) = 15						
Si	6.802	7.190	6.869	7.302	7.079	7.167
Al(IV)	1.198	0.810	1.131	0.698	0.921	0.833
Al(VI)	0.335	0.144	0.249	0.162	0.220	0.202
Ti	0.148	0.074	0.144	0.072	0.098	0.082
Cr	---	---	---	---	---	---
Fe	1.630	1.494	1.691	1.505	1.560	1.623
Mn	0.050	0.062	0.064	0.063	0.056	0.070
Mg	3.149	3.484	3.124	3.446	3.366	3.320
Ca	1.689	1.742	1.726	1.752	1.700	1.703
Na	0.457	0.266	0.395	0.261	0.361	0.328
K	0.035	0.044	0.035	0.041	0.037	0.032
"OH"	2.460	2.356	2.401	2.071	2.421	2.395
		0				
Fe/(Fe+Mn+Mg)	0.338	0.296	0.347	0.300	0.313	0.324
Mn/(Fe+Mn+Mg)	0.010	0.012	0.013	0.013	0.011	0.014
Mg/(Fe+Mn+Mg)	0.652	0.691	0.640	0.687	0.676	0.662

*Zoning is defined by a discontinuous band of very fine-grained oriented opaque laths outlining a euhedral core comprising 33% of the grain and containing large corroded plagioclase inclusions, plus much chlorite and some sphene. Both the core and especially the rim are inhomogeneous, but optical properties vary very little with composition.

Table C-7

Microprobe Analyses of Biotite

Textural Unit	Gneissose Border Tonalite			
Sample #	Ba-JM-30a			
Grain #	B-30a-1	B-30a-2	B-30a-3	B-30a-4
# of Points	3	3	3	3
SiO_2	37.39	37.34	37.31	37.91
TiO_2	2.44	2.16	2.24	1.71
Al_2O_3	15.86	16.29	15.98	16.32
FeO_t	17.09	16.81	16.68	16.70
MnO	0.36	0.32	0.32	0.30
MgO	12.69	12.80	12.58	13.16
CaO	0.01	0.04	0.03	0.03
Na_2O	0.08	0.11	0.08	0.06
K_2O	9.76	9.42	9.61	9.74
"H_2O"	4.33	4.71	5.18	4.08
TOTAL	100.01	100.00	100.01	100.01
Formula Proportions Based on the Sum (Cations less (Ca + Na + K)) = 14				
Si	5.725	5.707	5.752	5.751
Al(IV)	2.275	2.293	2.248	2.249
Al(VI)	0.587	0.640	0.656	0.668
Ti	0.281	0.248	0.259	0.195
Fe	2.188	2.148	2.149	2.118
Mn	0.046	0.042	0.042	0.039
Mg	2.897	2.916	2.889	2.977
Ca	0.001	0.006	0.005	0.004
Na	0.024	0.032	0.022	0.018
K	1.908	1.838	1.890	1.885
"OH"	4.420	4.804	5.330	4.124
Fe/(Fe+Mn+Mg)	0.426	0.421	0.423	0.413
Mn/(Fe+Mn+Mg)	0.009	0.008	0.008	0.008
Mg/(Fe+Mn+Mg)	0.565	0.571	0.569	0.580

Table C-7

Biotite (continued)

Textural Unit	Stubby Hornblende Tonalite				
Sample #	Ba-JM-25a				
Grain #	B-25a-1	B-25a-2	B-25a-5	B-25a-6	B-25a-7
# of Points	4	4	4	4	4
SiO_2	36.69	36.96	36.36	36.84	37.18
TiO_2	2.14	2.22	2.21	2.57	2.21
Al_2O_3	16.04	16.24	16.30	16.28	16.24
FeO_t	16.98	16.49	17.37	16.56	16.74
MnO	0.11	0.12	0.08	0.11	0.10
MgO	12.58	12.96	12.71	13.21	13.22
CaO	0.06	0.05	0.10	0.02	0.04
Na_2O	0.10	0.10	0.13	0.12	0.11
K_2O	9.12	9.35	9.24	9.57	9.37
"H_2O"	6.18	5.51	5.50	4.73	4.78
TOTAL	100.00	100.00	100.00	100.01	99.99
Formual Proportions Based on the Sum (Cations less (K + Na + Ca)) = 14					
Si	5.687	5.684	5.602	5.631	5.670
Al(IV)	2.313	2.316	2.398	2.369	2.330
Al(VI)	0.617	0.628	0.562	0.563	0.589
Ti	0.250	0.257	0.256	0.295	0.254
Fe	2.201	2.120	2.237	2.116	2.134
Mn	0.015	0.016	0.010	0.014	0.012
Mg	2.908	2.971	2.919	3.008	3.005
Ca	0.010	0.008	0.016	0.004	0.006
Na	0.029	0.030	0.038	0.034	0.034
K	1.804	1.836	1.816	1.865	1.824
"OH"	6.391	5.652	5.653	4.820	4.869
Fe/(Fe+Mn+Mg)	0.430	0.415	0.433	0.412	0.414
Mn/(Fe+Mn+Mg)	0.003	0.003	0.002	0.003	0.002
Mg/(Fe+Mn+Mg)	0.568	0.582	0.565	0.586	0.583

Table C-7

Biotite (continued)

Textural Unit	Stubby Hornblende Tonalite					
Sample #	Ba-JM-29		Ba-JM-68			
Grain #	B-29-1	B-29-2	B-68-1	B-68-2	B-68-3	B-68-4
# of Points	3	4	3	3	4	3
SiO_2	37.01	37.53	37.55	37.36	37.02	37.14
TiO_2	2.38	2.64	2.67	1.79	1.78	2.27
Al_2O_3	15.86	15.88	15.82	15.96	16.12	16.02
FeO_t	17.98	17.30	16.84	16.55	16.95	17.18
MnO	0.16	0.15	0.18	0.16	0.17	0.16
MgO	12.12	12.60	12.75	12.77	13.10	12.81
CaO	0.04	0.04	0.00	0.00	0.01	0.02
Na_2O	0.12	0.14	0.11	0.08	0.11	0.10
K_2O	9.52	9.39	9.59	9.61	9.62	9.45
"H_2O"	4.82	4.32	4.50	5.73	5.13	4.84
TOTAL	100.01	99.99	100.01	100.01	100.01	99.99
Formula Proportions Based on the Sum (Cation less (K + Na + Ca)) = 14						
Si	5.709	5.733	5.749	5.780	5.683	5.692
Al(IV)	2.291	2.267	2.251	2.220	2.317	2.308
Al(VI)	0.592	0.592	0.604	0.689	0.600	0.586
Ti	0.275	0.303	0.307	0.208	0.205	0.262
Fe	2.318	2.209	2.155	2.140	2.175	2.201
Mn	0.021	0.020	0.023	0.020	0.021	0.021
Mg	2.787	2.869	2.910	2.943	2.997	2.926
Ca	0.007	0.007	0.001	0.0	0.002	0.004
Na	0.035	0.042	0.032	0.024	0.031	0.029
K	1.873	1.830	1.873	1.897	1.885	1.847
"OH"	4.954	4.401	4.593	5.909	5.250	4.954
Fe/(Fe+Mn+Mg)	0.452	0.433	0.424	0.419	0.419	0.428
Mn/(Fe+Mn+Mg)	0.004	0.004	0.004	0.004	0.004	0.004
Mg/(Fe+Mn+Mg)	0.544	0.563	0.572	0.577	0.577	0.568

Table C-7

Biotite (continued)

Textural Unit	Prismatic Hornblende Tonalite				
Sample #	Ba-JM-36a				
Grain #	B-36a-1	B-36a-2	B-36a-3	B-36a-5	B-36a-7*
# of Points	4	4	4	4	4
SiO_2	37.26	36.77	36.75	36.17	36.30
TiO_2	2.49	2.29	2.21	2.27	1.81
Al_2O_3	15.87	16.04	15.97	16.10	16.14
FeO_t	16.22	16.51	16.21	15.95	16.08
MnO	0.14	0.15	0.12	0.09	0.11
MgO	13.45	13.26	13.81	13.55	14.02
CaO	0.08	0.11	0.15	0.08	0.07
Na_2O	0.08	0.10	0.10	0.08	0.06
K_2O	9.38	8.69	8.75	9.29	9.04
"H_2O"	5.03	6.08	5.91	6.42	6.36
TOTAL	100.00	100.00	99.98	100.00	99.99
Formula Proportions Based on the Sum (Cations less (K + Na + Ca)) = 14					
Si	5.692	5.644	5.615	5.593	5.572
Al(IV)	2.308	2.356	2.385	2.407	2.428
Al(VI)	0.549	0.545	0.491	0.526	0.493
Ti	0.286	0.264	0.254	0.264	0.209
Fe	2.071	2.118	2.070	2.062	2.064
Mn	0.018	0.019	0.016	0.012	0.014
Mg	3.063	3.035	3.145	3.123	3.209
Ca	0.012	0.018	0.024	0.013	0.012
Na	0.022	0.030	0.031	0.025	0.018
K	1.828	1.703	1.706	1.832	1.772
"OH"	5.128	6.232	6.025	6.620	6.517
Fe/(Fe+Mn+Mg)	0.402	0.410	0.396	0.397	0.390
Mg/(Fe+Mn+Mg)	0.004	0.004	0.003	0.002	0.003
Mn/(Fe+Mn+Mg)	0.595	0.587	0.601	0.601	0.607

*Unusual greenish-brown margin of a grayish-brown grain. Note low TiO_2.

Table C-7

Biotite (continued)

Textural Unit	Prismatic Hornblende Tonalite				
Sample #	Ba-JM-46a				
Grain #	B-46a-1	B-46a-2	B-46a-3	B-46a-4	B-46a-5
# of Points	3	4	4	4	4
SiO_2	36.71	36.58	36.96	36.82	36.73
TiO_2	2.79	2.61	2.49	2.62	2.18
Al_2O_3	15.46	15.63	15.64	15.23	15.85
FeO_t	17.43	17.08	17.23	16.97	17.13
MnO	0.29	0.32	0.33	0.34	0.36
MgO	12.84	13.06	12.92	13.17	13.41
CaO	0.05	0.07	0.03	0.09	0.08
Na_2O	0.04	0.07	0.06	0.07	0.08
K_2O	9.64	9.12	9.72	9.27	9.23
"H_2O"	4.75	5.47	4.62	5.43	4.94
TOTAL	100.00	100.01	100.00	100.01	99.99
Formula Proportions Based on the Sum (Cations less (K + Na + Ca)) = 14					
Si	5.646	5.625	5.672	5.668	5.604
Al(IV)	2.354	2.375	2.328	2.332	2.396
Al(VI)	0.449	0.458	0.500	0.431	0.454
Ti	0.322	0.301	0.287	0.304	0.250
Fe	2.241	2.196	2.210	2.183	2.185
Mn	0.038	0.041	0.043	0.044	0.047
Mg	2.942	2.993	2.955	3.022	3.050
Ca	0.008	0.011	0.005	0.015	0.014
Na	0.013	0.021	0.018	0.020	0.024
K	1.892	1.789	1.902	1.820	1.798
"OH"	4.874	5.615	4.731	5.577	5.035
Fe/(Fe+Mn+Mg)	0.429	0.420	0.424	0.416	0.414
Mn/(Fe+Mn+Mg)	0.007	0.008	0.008	0.008	0.009
Mg/(Fe+Mn+Mg)	0.564	0.572	0.567	0.576	0.578

Table C-7

Biotite (continued)

Textural Unit	Seriate Porphyritic Tonalite				
Sample #	Ba-JM-3a				
Grain #	B-3a-1	B-3a-3	B-3a-5	B-3a-6	B-3a-7
# of Points	4	4	4	4	4
SiO_2	36.98	36.97	37.02	37.18	36.96
TiO_2	2.98	3.38	3.21	3.33	3.46
Al_2O_3	15.22	15.05	15.43	15.45	15.17
FeO_t	17.31	16.85	16.90	16.85	16.25
MnO	0.18	0.19	0.18	0.16	0.16
MgO	12.80	13.38	12.97	13.15	13.68
CaO	0.07	0.05	0.04	0.0	0.02
Na_2O	0.12	0.10	0.08	0.10	0.10
K_2O	9.51	9.53	9.53	9.59	9.47
"H_2O"	4.84	4.51	4.65	4.16	4.74
TOTAL	100.01	100.01	100.01	99.99	100.01
Formula Proportions Based on the Sum (Cations less (K + Na + Ca)) = 14					
Si	5.693	5.657	5.679	5.674	5.651
Al(IV)	2.307	2.343	2.321	2.326	2.349
Al(VI)	0.455	0.372	0.468	0.452	0.385
Ti	0.345	0.389	0.370	0.382	0.397
Fe	2.228	2.155	2.167	2.150	2.077
Mn	0.023	0.024	0.024	0.021	0.021
Mg	2.937	3.052	2.965	2.992	3.116
Ca	0.012	0.008	0.006	0.004	0.003
Na	0.034	0.029	0.025	0.030	0.031
K	1.868	1.860	1.865	1.867	1.847
"OH"	4.975	4.603	4.756	4.230	4.835
Fe/(Fe+Mn+Mg)	0.429	0.412	0.420	0.416	0.398
Mn/(Fe+Mn+Mg)	0.004	0.005	0.005	0.004	0.004
Mg/(Fe+Mn+Mg)	0.566	0.583	0.575	0.580	0.598

Table C-7

Biotite (concluded)

Textural Unit	Seriate Porphyritic Tonalite			
Sample #	Ba-JM-62a			
Grain #	B-62a-1	B-62a-2	B-62a-3	B-62a-4
# of Points	3	3	3	3
SiO_2	37.93	37.62	37.40	37.26
TiO_2	3.32	3.28	2.84	2.78
Al_2O_3	14.46	14.52	15.07	15.01
FeO_t	16.21	16.14	17.27	17.55
MnO	0.16	0.18	0.21	0.20
MgO	14.22	14.41	13.40	13.42
CaO	0.03	0.07	0.04	0.04
Na_2O	0.22	0.20	0.16	0.17
K_2O	9.18	9.18	9.32	9.44
"H_2O"	4.27	4.40	4.29	4.13
TOTAL	100.00	100.00	100.00	100.00
Formula Proportions Based on the Sum (Cations less (K + Na + Ca)) = 14				
Si	5.749	5.700	5.696	5.674
Al(IV)	2.251	2.300	2.304	2.326
Al(VI)	0.332	0.294	0.401	0.368
Ti	0.379	0.373	0.325	0.318
Fe	2.054	2.045	2.199	2.235
Mn	0.021	0.023	0.027	0.026
Mg	3.211	3.253	3.042	3.046
Ca	0.005	0.012	0.006	0.007
Na	0.065	0.059	0.048	0.051
K	1.775	1.774	1.812	1.833
"OH"	4.313	4.449	4.358	4.198
Fe/(Fe+Mn+Mg)	0.389	0.384	0.417	0.421
Mn/(Fe+Mn+Mg)	0.004	0.004	0.005	0.005
Mg/(Fe+Mn+Mg)	0.608	0.611	0.577	0.574

Table C-8

Microprobe Analyses of Magnetite

Textural Unit	Gneissose Border Tonalite				Stubby Hornblende Tonalite			
Sample #	Ba-JM-30a				Ba-JM-25a			
Grain #	M-30a-1	M-30a-2	M-30a-3	M-30a-4	M-25a-1	M-25a-2	M-25a-3	M-25a-4
# of Points	3	3	3	3	4	4	4	4
SiO_2	0.09	0.04	0.06	0.05	0.04	0.08	0.05	0.05
TiO_2	0.04	0.02	0.02	0.02	0.07	0.08	0.20	0.12
Al_2O_3	0.23	0.12	0.11	0.11	0.13	0.14	0.09	0.13
V_2O_3	0.31	0.27	0.28	0.15	0.31	0.58	0.56	0.36
Cr_2O_3	0.13	0.17	0.07	0.09	0.45	0.23	0.31	0.20
Fe_2O_3	71.36	67.51	74.76	71.53	73.60	73.09	70.94	74.64
FeO	27.59	31.63	24.46	27.85	25.21	25.62	27.67	24.33
MnO	0.17	0.14	0.14	0.11	0.06	0.07	0.06	0.06
MgO	0.03	0.05	0.04	0.04	0.06	0.06	0.07	0.06
TOTAL	99.95	99.95	99.94	99.95	99.94	99.94	99.94	99.94
Formula Proportions Based on Cation Sum = 3								
Si	0.003	0.002	0.002	0.002	0.002	0.003	0.002	0.002
Ti	0.001	0.001	0.001	0.001	0.002	0.002	0.006	0.004
Al	0.011	0.005	0.005	0.005	0.006	0.006	0.004	0.006
V	0.009	0.008	0.009	0.005	0.010	0.018	0.017	0.011
Cr	0.004	0.005	0.002	0.003	0.014	0.007	0.009	0.006
Fe^{3+}	2.073	1.954	2.181	2.080	2.145	2.129	2.062	2.177
Fe^{2+}	0.891	1.017	0.793	0.900	0.816	0.829	0.894	0.789
Mn	0.005	0.004	0.005	0.004	0.002	0.002	0.002	0.002
Mg	0.002	0.003	0.002	0.002	0.003	0.003	0.004	0.003
Total Fe as FeO	91.81	92.39	91.74	92.23	91.45	91.40	91.52	91.51
Mole % Fe_3O_4	98.35	98.83	98.88	99.12	98.15	97.91	97.71	98.30
Mole % Fe_2TiO_4	0.10	0.07	0.07	0.07	0.20	0.23	0.59	0.36
Mole % Other	1.53	1.10	1.04	0.80	1.65	1.86	1.70	1.34
Mt/(Mt + Usp)	0.999	0.999	0.999	0.999	0.998	0.998	0.994	0.996
Usp/(Mt + Usp)	0.001	0.001	0.001	0.001	0.002	0.002	0.006	0.004

Table C-8

Magnetite (continued)

Textural Unit	Stubby Hornblende Tonalite						
Sample #	Ba-JM-29			Ba-JM-68			
Grain #	M-29-1	M-29-2	M-29-3	M-68-1	M-68-2	M-68-3	M-68-4
# of Points	3	3	3	3	3	4	3
SiO_2	0.04	0.04	0.04	0.06	0.05	0.06	0.07
TiO_2	0.04	0.07	0.04	0.03	0.11	0.04	0.05
Al_2O_3	0.11	0.13	0.14	0.10	0.12	0.12	0.13
V_2O_3	0.42	0.34	0.53	0.34	0.40	0.26	0.45
Cr_2O_3	0.20	0.28	0.20	0.28	0.22	0.23	0.26
Fe_2O_3	75.53	76.20	72.50	73.14	73.30	74.01	73.22
FeO	23.48	22.78	26.38	25.88	25.65	25.10	25.64
MnO	0.08	0.06	0.09	0.08	0.07	0.08	0.09
MgO	0.04	0.04	0.03	0.03	0.03	0.03	0.04
TOTAL	99.94	99.94	99.95	99.94	99.95	99.93	99.95
Formula Proportions Based on Cation Sum = 3							
Si	0.001	0.002	0.002	0.002	0.002	0.002	0.003
Ti	0.001	0.002	0.001	0.001	0.003	0.001	0.002
Al	0.005	0.006	0.006	0.005	0.006	0.005	0.006
V	0.013	0.010	0.016	0.011	0.012	0.008	0.014
Cr	0.006	0.009	0.006	0.009	0.007	0.007	0.008
Fe^{3+}	2.206	2.227	2.111	2.131	2.136	2.158	2.133
Fe^{2+}	0.762	0.740	0.853	0.838	0.831	0.813	0.830
Mn	0.003	0.002	0.003	0.002	0.002	0.002	0.003
Mg	0.002	0.002	0.002	0.002	0.002	0.002	0.002
Total Fe as FeO	91.46	91.36	91.63	91.71	91.62	91.71	91.54
Mole % Fe_3O_4	98.49	98.37	98.28	98.49	98.27	98.59	98.19
Mole % Fe_2TiO_4	0.12	0.22	0.12	0.08	0.31	0.11	0.15
Mole % Other	1.35	1.41	1.59	1.43	1.41	1.26	1.66
Mt/(Mt + Usp)	0.999	0.998	0.999	0.999	0.997	0.999	0.998
Usp/(Mt + Usp)	0.001	0.002	0.001	0.001	0.003	0.001	0.002

Table C-8

Magnetite (continued)

Textural Unit	Prismatic Hornblende Tonalite				
Sample #	Ba-JM-36a				
Grain #	M-36a-1	M-36a-2	M-36a-3	M-36a-4	M-36a-5
# of Points	4	4	4	4	4
SiO_2	0.04	0.04	0.04	0.04	0.02
TiO_2	0.04	0.03	0.03	0.02	0.05
Al_2O_3	0.08	0.08	0.10	0.08	0.11
V_2O_3	0.22	0.27	0.37	0.25	0.44
Cr_2O_3	0.01	0.06	0.10	0.10	0.23
Fe_2O_3	74.26	73.41	71.62	73.30	71.67
FeO	25.18	25.93	27.52	26.00	27.28
MnO	0.05	0.05	0.08	0.09	0.07
MgO	0.05	0.06	0.06	0.06	0.06
TOTAL	99.93	99.93	99.92	99.94	99.93
Formula Proportions Based on Cation Sum = 3					
Si	0.002	0.002	0.002	0.002	0.001
Ti	0.001	0.001	0.001	0.001	0.002
Al	0.004	0.004	0.004	0.004	0.005
V	0.007	0.009	0.012	0.008	0.013
Cr	0.0	0.002	0.003	0.003	0.007
Fe^{3+}	2.166	2.139	2.083	2.135	2.084
Fe^{2+}	0.816	0.840	0.889	0.841	0.882
Mn	0.002	0.002	0.003	0.003	0.002
Mg	0.003	0.003	0.003	0.004	0.004
Total Fe as FeO	92.01	92.00	91.98	91.97	91.78
Mole % Fe_3O_4	99.18	99.05	98.76	99.04	98.47
Mole % Fe_2TiO_4	0.11	0.09	0.09	0.06	0.16
Mole % Other	0.70	0.87	1.12	0.89	1.37
Mt/(Mt + Usp)	0.999	0.999	0.999	0.999	0.998
Usp/(Mt + Usp)	0.001	0.001	0.011	0.001	0.002

Table C-8

Magnetite (continued)

Textural Unit	Prismatic Hornblende Tonalite				
Sample #	Ba-JM-46a				
Grain #	M-46a-1	M-46a-2	M-46a-3	M-46a-4	M-46a-5
# of Points	4	4	4	4	4
SiO_2	0.04	0.04	0.04	0.03	0.05
TiO_2	0.05	0.25	0.09	0.06	0.17
Al_2O_3	0.22	0.21	0.16	0.07	0.12
V_2O_3	0.39	0.38	0.36	0.21	0.33
Cr_2O_3	0.14	0.07	0.11	0.13	0.22
Fe_2O_3	69.64	70.37	72.58	72.57	70.66
FeO	29.20	28.39	26.42	26.72	28.20
MnO	0.16	0.15	0.13	0.10	0.13
MgO	0.08	0.07	0.06	0.04	0.06
TOTAL	99.92	99.93	99.95	99.93	99.94
Formula Proportions Based on Cation Sum = 3					
Si	0.001	0.002	0.001	0.001	0.002
Ti	0.002	0.007	0.003	0.002	0.005
Al	0.010	0.010	0.007	0.003	0.006
V	0.012	0.012	0.011	0.006	0.010
Cr	0.004	0.002	0.003	0.004	0.007
Fe^{3+}	2.020	2.043	2.112	2.113	2.053
Fe^{2+}	0.941	0.916	0.854	0.865	0.910
Mn	0.005	0.005	0.004	0.003	0.004
Mg	0.005	0.004	0.003	0.002	0.004
Total Fe as FeO	91.88	91.72	91.74	92.03	91.79
Mole % Fe_3O_4	98.35	97.93	98.50	99.01	98.20
Mole % Fe_2TiO_4	0.16	0.73	0.25	0.18	0.50
Mole % Other	1.48	1.33	1.23	0.81	1.31
Mt/(Mt + Usp)	0.998	0.993	0.998	0.998	0.995
Usp/(Mt + Usp)	0.002	0.007	0.002	0.002	0.005

Table C-8

Magnetite (concluded)

Textural Unit	Seriate Porphyritic Tonalite							
Sample #	Ba-JM-3a					Ba-JM-62a		
Grain #	M-3a-1	M-3a-4	M-3a-5	M-3a-6	M-3a-7	M-62a-1	M-62a-3	M-62a-4
# of Points	4	4	4	4	4	3	3	3
SiO_2	0.03	0.05	0.04	0.02	0.06	0.06	0.07	0.06
TiO_2	0.06	0.15	0.06	0.04	0.05	0.07	0.06	0.04
Al_2O_3	0.14	0.08	0.12	0.12	0.09	0.12	0.10	0.14
V_2O_3	0.43	0.54	0.36	0.35	0.39	0.53	0.50	0.50
Cr_2O_3	0.13	0.16	0.11	0.10	0.15	0.17	0.19	0.17
Fe_2O_3	69.90	71.20	69.12	69.64	68.74	70.59	71.69	72.15
FeO	29.12	27.63	30.02	29.55	30.36	28.24	27.22	26.76
MnO	0.06	0.09	0.06	0.07	0.05	0.06	0.10	0.06
MgO	0.06	0.05	0.05	0.06	0.06	0.03	0.02	0.04
TOTAL	99.93	99.95	99.94	99.95	99.95	99.92	99.95	99.92
Formula Proportions Based on Cation Sum = 3								
Si	0.001	0.002	0.001	0.001	0.002	0.002	0.003	0.002
Ti	0.002	0.004	0.002	0.001	0.001	0.002	0.002	0.001
Al	0.006	0.004	0.005	0.005	0.004	0.005	0.005	0.007
V	0.013	0.017	0.011	0.011	0.012	0.018	0.016	0.015
Cr	0.004	0.005	0.003	0.003	0.004	0.005	0.006	0.005
Fe^{3+}	2.029	2.070	2.005	2.021	1.993	2.051	2.086	2.099
Fe^{2+}	0.939	0.892	0.967	0.953	0.978	0.912	0.880	0.865
Mn	0.002	0.003	0.002	0.002	0.002	0.002	0.003	0.002
Mg	0.004	0.003	0.003	0.003	0.003	0.002	0.001	0.002
Total Fe as Feo	92.03	91.71	92.23	92.23	92.23	91.77	91.74	91.69
Mole % Fe_3O_4	98.52	98.12	98.67	98.83	98.62	98.09	98.26	98.24
Mole % Fe_2TiO_4	0.16	0.43	0.19	0.11	0.14	0.22	0.17	0.13
Mole % Other	1.32	1.45	1.14	1.06	1.24	1.66	1.56	1.60
Mt/(Mt + Usp)	0.998	0.996	0.998	0.999	0.999	0.998	0.998	0.999
Usp/(Mt + Usp)	0.002	0.004	0.002	0.001	0.001	0.002	0.002	0.001

APPENDIX D

WHOLE-ROCK CHEMICAL ANALYSIS

Whole-rock chemical analyses have been obtained on twenty-four samples of the tonalite. Twelve rocks were analyzed by wet chemical techniques at the Japan Analytical Chemical Research Institute (JACRI), Tamiya Asari, Director. Four of those twelve, plus ten additional samples, were analyzed by myself at Caltech, using an electron microprobe technique described below. The remaining two analyses, kindly supplied by L. T. Silver, were done prior to this study by W. Blake at Caltech, using wet chemical techniques. CIPW norms were calculated using a FOCAL-8 computer program written by C. M. Conway.

In all cases, single homogeneous hand specimens chosen for analysis weighed at least 600 g, generally >1 kg. Hand specimens were cut or coarsely broken, and randomly chosen fragments totaling 220 g or more were reduced to fragments $\leq$5 mm in size using a plattner mortar and hydraulic press, then ground to fine powders in a Shatterbox (Spex Industries, Inc.) lined with tungsten carbide. Representative aliquots for analysis were obtained by repeated coring of the powders with a thin glass tube.

The wet chemical analyses, complete with Fe_2O_3, FeO, MnO, and volatile contents are presented in Table D-1. Of the twelve analyses from the Japan Laboratory, eight were done by S. Imai in June, 1970 and four by Tadashi Asari in March, 1974. The latter analyses (samples 3a, 29, 62a and 857), together with those of a large number of additional plutonic rock samples submitted at the same time, are all unusually low

in Na_2O, high in H_2O+, and possibly low in K_2O and Fe_2O_3/FeO. The discrepancies in these four analyses, relative to the other twenty San José results, cannot be explained by differences in either the modal mineral proportions or the compositions of the minerals determined by electron microprobe for three of the samples. Thus the discrepancies are apparently due to analytical error, and these four analyses have therefore been omitted from Plates 9 and Plates 9A and from all petrologic discussion in the text.

Electron Microprobe Whole-Rock Analysis

R. L. Joesten (1974) initiated a procedure of electron microprobe analysis of glasses prepared by fusion of rock powders fluxed with lithium tetraborate. I have used his procedure, with slight modification, to analyze fourteen samples from the San José pluton. In addition, I carefully prepared glasses of known composition from U. S. Geological Survey standard rocks G-2 (granite) and BCR-1 (basalt). These were used both for secondary standards during each run and for establishing empirical correction factors for the absorption-enhancement effects of the flux on all radiations. Although this discussion will be restricted almost entirely to the U. S. G. S. and San José samples, C. M. Conway, L. P. Gromet, and I have analyzed many additional samples ranging in composition from gabbro to granite with excellent results.

Preparation of Glasses: Approximately 1.5 g of each rock powder and $Li_2B_4O_7$ were mixed in a Mixer-Mill (Spex Industries, Inc.) for about one minute. Two supplies of flux were used: Baker and Adamson $Li_2B_4O_7$

Table D-1

Wet Chemical Analyses of Tonalite from the San José Pluton

Name of Unit	GBT	SHbT				PHbT	
Sample #	BC-I 5[a]	Ba-JM 25a[b]	Ba-JM 29[c]	Ba-JM 39b[b]	Ba-JM 68[b]	Ba-JM 36a[b]	Ba-JM 46a[a]
SiO_2	65.66	59.44	58.64	60.96	60.33	59.83	63.95
TiO_2	0.62	0.78	0.74	0.76	0.75	0.71	0.60
Al_2O_3	16.35	17.77	18.37	18.08	17.67	18.74	17.34
Fe_2O_3	1.98	2.84	2.47	2.47	2.85	2.87	2.38
FeO	2.04	2.46	3.27	2.62	2.52	2.41	1.78
MnO	0.08	0.07	0.07	0.07	0.07	0.07	0.06
MgO	2.16	2.83	3.11	2.68	2.84	2.62	2.00
CaO	4.90	6.66	6.53	6.25	6.33	6.68	5.47
Na_2O	4.54	4.62	4.26	4.69	4.55	4.82	4.81
K_2O	1.24	0.71	0.64	0.60	0.80	0.50	0.93
P_2O_5	0.07	0.17	0.18	0.17	0.16	0.17	0.13
H_2O^+	0.54	0.96	1.56	0.88	0.87	0.89	0.70
H_2O^-	0.03	0.69	0.33	0.36	0.62	0.21	0.41
CO_2	---	0.20	0.04	0.14	0.33	0.11	0.14
F	---	0.00	---	0.02	0.00	0.01	0.02
S	---	0.06	---	0.06	0.04	0.05	0.01
TOTAL	100.21	100.28	100.21	100.81	100.73	100.69	100.73
		CIPW Normative Minerals					
Quartz	21.20	12.94	12.65	14.54	14.14	12.61	18.69
Orthoclase	7.35	4.27	3.85	3.57	4.78	2.97	5.53
Albite	38.56	39.76	36.66	39.95	38.95	41.03	40.93
Anorthite	20.66	26.10	29.63	26.70	25.73	28.20	23.12
Corundum	---	---	---	---	---	---	---
Diopside	2.61	5.03	1.71	2.70	3.93	3.18	2.60
Hypersthene	5.40	5.83	9.98	7.09	6.47	6.08	4.21
Magnetite	2.88	4.19	3.65	3.60	4.18	4.18	3.47
Ilmenite	1.18	1.51	1.43	1.45	1.44	1.36	1.15
Apatite	0.16	0.39	0.44	0.39	0.37	0.39	0.30
Ab + An	59.22	65.85	66.29	66.65	64.68	69.23	64.05
An/(Ab + An)	0.349	0.396	0.447	0.401	0.398	0.407	0.361
Color Index	12.07	16.55	16.77	14.85	16.03	14.80	11.43

a Analyst: W. Blake, Caltech.

b Analyst: S. Imai, JACRI, June, 1970.

c Analyst: Tadashi Asari, JACRI, March, 1974; the accuracy of these analyses (3a, 29, 62a, and 857) is suspect, particularly for Na_2O, H_2O^+, and perhaps K_2O and Fe_2O_3/FeO.

Table D-1 (continued)

Name of Unit	PHbT				SPT		
Sample #	Ba-JM 93[b]	Ba-JM 240#52[b]	Ba-JM 240#53[b]	Ba-JM 857[c]	Ba-JM 3a[c]	BC-I 12[a]	Ba-JM 62a[c]
SiO_2	64.03	61.16	58.55	58.87	61.36	62.54	62.55
TiO_2	0.59	0.73	0.77	0.70	0.60	0.70	0.58
Al_2O_3	17.34	18.16	19.07	18.77	17.88	17.66	17.76
Fe_2O_3	2.44	2.59	2.90	2.83	2.33	2.36	2.18
FeO	1.68	2.19	2.37	2.60	2.46	2.16	2.38
MnO	0.06	0.07	0.07	0.07	0.06	0.08	0.06
MgO	1.85	2.62	2.71	2.90	2.50	2.29	2.35
CaO	5.34	6.50	6.95	6.82	5.65	5.87	5.64
Na_2O	4.70	4.70	4.78	4.41	4.30	4.90	4.46
K_2O	0.94	0.65	0.54	0.45	0.60	0.82	0.61
P_2O_5	0.14	0.15	0.17	0.17	0.17	0.19	0.16
H_2O^+	0.85	0.78	1.00	1.25	1.18	0.53	1.26
H_2O^-	0.61	0.20	0.47	0.33	0.45	0.04	0.26
CO_2	0.13	0.13	0.20	0.02	0.07	---	0.08
F	0.02	0.00	0.03	---	---	---	---
S	0.04	0.07	0.04	---	---	---	---
TOTAL	100.76	100.70	100.62	100.19	99.61	100.14	100.33
	CIPW Normative Minerals						
Quartz	19.82	14.64	10.91	13.15	18.30	15.93	18.65
Orthoclase	5.61	3.86	3.23	2.70	3.62	4.87	3.65
Albite	40.13	39.97	40.91	37.83	37.15	41.65	38.21
Anorthite	23.66	26.68	29.33	30.53	27.49	23.89	26.99
Corundum	---	---	---	----	0.30	---	---
Diopside	1.68	3.74	3.48	2.11	---	3.26	0.23
Hypersthene	4.08	5.61	6.01	7.76	8.11	5.20	7.56
Magnetite	3.57	3.77	4.25	4.16	3.45	3.44	3.20
Ilmenite	1.13	1.39	1.48	1.35	1.16	1.34	1.12
Apatite	0.32	0.34	0.39	0.42	0.42	0.43	0.39
Ab + An	63.80	66.65	70.24	68.36	64.64	65.54	65.20
An/(Ab + An)	0.371	0.400	0.418	0.447	0.425	0.364	0.414
Color Index	10.45	14.51	15.23	15.38	12.72	13.23	12.11

a Analyst: W. Blake, Caltech.

b Analyst: S. Imai, JACRI, June, 1970.

c Analyst: Tadashi Asari, JACRI, March, 1974; the accuracy of these four analyses (3a, 29, 62a, and 857) is suspect, particularly for Na_2O, H_2O^+, and perhaps K_2O and Fe_2O_3/FeO.

and Spex Industries high-purity lithium tetraborate #6005. Concentrations of impurities are given below.

Baker and Adamson (in wt %)[1]		Spex Industries (in ppm)[2]	
SiO_2	0.030	Si	5-20
TiO_2	0.004		
Al_2O_3	0.052	Al	1- 5
FeO_t	0.010	Fe	10-20
MgO	0.009	Mg	5-20
CaO	0.042		
Na_2O	0.009		
K_2O	0.014		
P_2O_5	0.022		
TOTAL	0.192		

The rock-flux mixtures were then fused in 7/8"-deep, 1"-diameter open graphite crucibles (National Brand, Union Carbide Corporation) at 1100°-1150°C in a muffle furnace.

Upon removal from the furnace, the melts were quickly poured onto an aluminum sheet held at about 200-300°C on a hot plate. After about 10 minutes the resultant glass beads were transferred to clean asbestos pads and allowed to cool. The beads were then finely crushed in a steel mortar and remelted for 12 additional minutes. This procedure of grinding and remelting yields glasses which are considerably more homogeneous than those produced by a single fusion step, especially for siliceous compositions. Following fusion, the glasses were broken into small chips, and 10-20 chips were mounted with epoxy in 1"-diameter brass mounts, then polished and coated with a carbon film. Each mount contained three chambers, permitting three glasses per mount.

Glasses of U.S.G.S. standard rocks G-2 and BCR-1 were prepared

---

[1]Mean values of microprobe analyses of 3 glasses (Joesten, 1974, p. 311).

[2]Semi-quantitative spectroscopic analysis reported by Spex Industries.

from precise 1:1 mixtures of rock powder and flux. In order to ensure accurate knowledge of the compositions of these glasses, the flux was dried, prior to weighing and mixing with the rock powders, for about five hours in a furnace at 500°C; similarly, the rock powders were dried for about 15 hours in an oven at 105°C. Weighing was precise to four decimal places. Rock powders and flux were then mixed and fused following the procedure described earlier, and the glass beads were mounted unbroken, each in a separate brass mount.

Analytical Procedures: Two glasses were prepared and analyzed, in each case on different days, for all San José samples except Ba-JM-93 (one glass, one analysis). In addition, at least one glass of either G-2 or BCR-1 or both was run on each day. Analyses were carried out on a Materials Analysis Company (MAC) model 5-SA-3 electron microprobe interfaced to a DEC PDP-8/L computer, using a FOCAL-8 program written specifically for borosilicate glass analysis.

Elements were run in successive sets of three (Ca-Si-Na, P-Ti-Mg, and Fe-K-Al) on one glass at a time. For a given triad, 60-second counts were taken on eight points, each from a separate glass chip. Backgrounds were measured by counting for 30 seconds both before and after each group of eight points and combining the results. The average count-rate (minus background) and the standard deviation among the eight points were then calculated for each element before proceeding to the next triad. Operating conditions -- accelerating potential of 15 kV, specimen current of 0.037 microamps (measured on brass), electron

beam spot size of 50 microns, and counting time of 60 seconds -- were carefully selected to optimize count-rates without loss of K or Na x-ray intensity during the run. Further, to avoid possible deleterious effects of repeated exposure to the electron beam, no point was analyzed more than once.

After counting for all elements, the average count-rates were converted to weight percent oxides following the method of Bence and Albee (1968; Albee and Ray, 1970), as discussed briefly in the section on mineral analyses (Appendix C). The standards used are listed in Table D-2. The presence of roughly 50% $Li_2B_4O_7$ in the glasses was accounted for by a reiterative calculation procedure analogous to that used for hydroxyl-bearing minerals and magnetite. That is, the K-values were converted to preliminary oxide concentrations by correcting for the absorption-enhancement effects of all components (except the flux) on each radiation. These preliminary concentration estimates were summed, and the deficiency of the total from 100% was assigned to flux. Oxide concentrations were then recalculated to correct for the absorption-enhancement effects of the flux, using correction factors determined by the procedure discussed in the next paragraph, and the oxide summation was normalized to 100%.

Correction factors (A-factors) for the effects of the $Li_2B_4O_7$ flux on the radiations of each element were determined by repeatedly analyzing the glasses of U.S.G.S. standard rocks G-2 and BCR-1 and fitting the results to the known compositions of the two standards (from the compilation of Flanagan, 1969). Each analysis provides

Table D-2

Standards Used for Microprobe Analysis
of Whole-Rock Compositions

Si:	quartz (Brazil)
Ti:	synthetic TiO_2
Al:	kyanite or synthetic Al_2O_3
Fe:	synthetic fayalite
Mg:	synthetic periclase
Ca:	wollastonite
Na:	albite (Amelia)
K:	microcline (Asbestos)
P:	fluor-apatite (Durango)

a separate estimate of the correction factor for each element. The following procedure for calculating the factors is based upon the discussion in Albee and Ray (1970). If the actual concentrations of all oxides in a multicomponent glass are known, the correction factor α^A_{AN} for element A in a binary glass consisting of the oxide AO + flux can be calculated from the relationships:

$$\beta^A_{ABC\ldots N} = \frac{C^A_{ABC\ldots N}}{K^A_{ABC\ldots N}} \qquad \text{(by definition)} \qquad \text{(D-1)}$$

$$\beta^A_{ABC\ldots N} = \frac{C^A_{ABC\ldots N}\alpha^A_{AA} + C^B_{ABC\ldots N}\alpha^A_{AB} + \ldots + C^N_{ABC\ldots N}\alpha^A_{AN}}{C^A_{ABC\ldots N} + C^B_{ABC\ldots N} + \ldots + C^N_{ABC\ldots N}} \qquad \text{(D-2)}$$

where the flux plus any unanalyzed oxides are treated as a single component N; $\beta^A_{ABC\ldots N}$ is the correction factor for element A in the multicomponent glass; $C^A_{ABC\ldots N}$, $C^B_{ABC\ldots N}$, etc., are the concentrations of the oxides in the glass; $K^A_{ABC\ldots N}$ is the ratio of the background-corrected intensity for element A in the glass relative to that in pure

oxide AO; α^{A}_{AA} is the correction factor for element A in pure oxide AO ($\alpha^{A}_{AA} = 1$); α^{A}_{AB} is the correction factor for A in binary oxide AO-BO; etc. Substituting for β and solving for α^{A}_{AN}:

$$\alpha^{A}_{AN} = \frac{C^{A}_{ABC\ldots N}\left(C^{A}_{ABC\ldots N} + C^{B}_{ABC\ldots N} + \ldots + C^{N}_{ABC\ldots N}\right)}{K^{A}_{ABC\ldots N} C^{N}_{ABC\ldots N}} - \frac{C^{A}_{ABC\ldots N}\alpha^{A}_{AA} + C^{B}_{ABC\ldots N}\alpha^{A}_{AB} + \ldots + C^{N-1}_{ABC\ldots N}\alpha^{A}_{A(N-1)}}{C^{N}_{ABC\ldots N}} \qquad \text{(D-3)}$$

All A-factors except α^{A}_{AN} are known. Because the ratio of rock to flux was carefully controlled for these glasses, all oxide concentrations are known. For those elements (Mg, Si, Ti, and in some cases Al) for which pure oxides are used as working standards, the measured K-values can be used directly in equation D-3. For the other elements, working standards other than the pure oxide were used, and the K-values measured relative to the working standards must be converted to K-values relative to the pure oxide before calculation of the A-factors. The relationship is

$$K^{A}_{ABC\ldots N} = \frac{k^{A}_{ABC\ldots N} C^{A}_{WS}}{k^{A}_{WS}\beta^{A}_{WS}} \qquad \text{(D-4)}$$

where $k^{A}_{ABC\ldots N}$ is the measured count-rate in the sample, k^{A}_{WS} is the measured count-rate in the working standard, C^{A}_{WS} is the concentration of oxide AO in the working standard, and β^{A}_{WS} is the ratio C/K for the working standard.

The average A-factors calculated from the G-2 and BCR-1 analyses are given in Table D-3, along with the final factors used in calculating all analyses. Because MgO, P_2O_5, CaO, and TiO_2 are present in very low concentrations in G-2 glasses, estimates of A-factors for these elements in G-2 glasses are poor and are very sensitive to slight errors in the assumed concentrations. For these oxides, the average BCR-1 A-factors were chosen in preference to the G-2 values; for the other oxides, the A-factors from both standards were averaged.

Table D-3

Element-Flux A-Factors Calculated from Analyses of U.S.G.S. Standard Rock Powders G-2 and BCR-1

	G-2 (11 analyses)		BCR-1 (13 analyses)		Final Values
	Average	σ	Average	σ	
Na	1.681	0.073	1.605	0.054	1.65
Mg	1.473	0.069	1.196	0.069	1.20*
Al	1.223	0.044	1.257	0.051	1.24
Si	1.100	0.031	1.090	0.028	1.10
P	1.357	0.347	1.103	0.111	1.20
K	1.197	0.028	1.128	0.042	1.18
Ca	1.145	0.037	1.090	0.035	1.10
Ti	1.451	0.237	1.190	0.095	1.19*
Fe	1.256	0.085	1.239	0.040	1.24

*Final A-factors for Mg and Ti are based entirely on BCR-1, because G-2 contains too little of either oxide to yield reliable A-factor estimates.

Results: Analyses of the G-2 and BCR-1 glasses are given in Tables D-4 and D-5, respectively; those of the tonalite samples from the San José pluton are listed in Table D-6. Table D-7, listing the maximum, minimum, and average standard deviations of the count-rates among the eight points for each element in the G-2, BCR-1, and San José analyses shows that the individual glasses are very homogeneous. For highly siliceous rocks

Table D-4

Analyses of U.S.G.S. Standard Granite G-2

Glass #	1						2			
SiO_2	69.35	70.03	69.94	69.89	69.82	69.83	69.54	69.89	70.32	70.03
TiO_2	0.67	0.45	0.05	0.51	0.49	0.51	0.43	0.50	0.54	0.49
Al_2O_3	15.93	15.85	15.61	15.47	15.67	15.79	16.05	15.80	15.13	15.24
FeO_t	2.61	2.51	2.61	2.57	2.42	2.50	2.65	2.44	2.49	2.57
MgO	0.73	0.72	0.69	0.68	0.71	0.71	0.72	0.70	0.74	0.71
CaO	2.06	(1.75)	1.96	2.04	1.99	1.96	1.99	1.96	1.95	1.97
Na_2O	4.36	4.11	4.08	4.10	4.24	4.12	4.30	4.04	4.17	4.26
K_2O	(4.21)	4.44	4.49	4.60	4.55	4.48	(4.19)	4.52	4.53	4.60
P_2O	0.09	0.15	0.11	0.15	0.11	0.12	0.14	0.16	0.14	0.14
TOTAL	100.01	100.01	99.99	100.01	100.00	100.02	100.01	100.01	100.01	100.01

Glass #	2			Probe Average*	Flanagan Average
SiO_2	70.19	70.06	70.00	69.86	69.80
TiO_2	0.56	0.44	0.43	0.50	0.54
Al_2O_3	15.48	15.56	15.83	15.63	15.48
FeO_t	2.53	2.39	2.35	2.51	2.51
MgO	0.71	0.72	0.70	0.71	0.79
CaO	1.95	1.99	1.91	1.97	2.01
Na_2O	3.98	4.20	4.16	4.16	4.19
K_2O	4.44	4.51	4.50	4.53	4.55
P_2O	0.16	0.13	0.12	0.13	0.14
TOTAL	100.00	100.00	100.00	100.00	100.01

*Calculated from the average K-values rather than from the weight percents; values enclosed in parentheses (two for K_2O and one for CaO) are anomalously low and have been omitted from the average.

Table D-5

Analyses of U.S.G.S. Standard Basalt BCR-1

SiO_2	56.07	55.15	55.00	55.50	55.77	55.76	55.94	55.40	55.49
TiO_2	(1.70)	2.22	2.32	2.33	2.34	2.30	2.27	2.42	2.11
Al_2O_3	13.59	14.17	14.12	14.19	13.51	13.51	13.27	13.72	14.16
FeO_t	12.53	12.38	12.45	12.19	12.53	12.36	12.34	12.45	12.09
MgO	3.29	3.46	3.44	3.12	3.25	3.30	3.34	3.38	3.38
CaO	7.26	7.07	7.16	7.13	7.15	7.19	7.20	7.13	7.04
Na_2O	3.38	3.45	3.38	3.40	3.32	3.40	3.44	3.37	3.55
K_2O	1.79	1.74	1.75	1.75	1.75	1.77	1.80	1.73	1.78
P_2O_5	0.39	0.36	0.38	0.39	0.39	0.41	0.40	0.40	0.41
TOTAL	100.00	100.00	100.00	100.00	100.01	100.00	100.00	100.00	100.01

					Probe Average*	Flanagan Average
SiO_2	55.58	55.07	55.44	55.66	55.46	55.41
TiO_2	2.17	2.34	2.23	2.29	2.28	2.28
Al_2O_3	14.10	13.89	13.68	13.61	13.83	13.95
FeO_t	12.16	12.50	12.49	12.52	12.38	12.41
MgO	3.44	3.45	3.40	3.30	3.35	3.36
CaO	7.04	7.14	7.18	7.11	7.13	7.10
Na_2O	3.41	3.48	3.42	3.39	3.42	3.39
K_2O	1.73	1.76	1.78	1.76	1.76	1.72
P_2O_5	0.37	0.38	0.39	0.36	0.39	0.37
TOTAL	100.00	100.01	100.01	100.00	100.00	99.99

*Calculated from the average K-values rather than from the weight percents; the TiO_2 value enclosed in parentheses is anomalously low and has been omitted from the average.

Table D-6

Replicate Analyses of San José Tonalite

Sample #	Ba-JM-25a			Ba-JM-27a			Ba-JM-46a		
Glass #	1	2	Average	1	2	Average	1	2	Average
SiO_2	61.28	61.07	61.18	66.98	67.44	67.21	65.07	65.38	65.22
TiO_2	0.80	0.77	0.78	0.51	0.55	0.53	0.58	0.57	0.58
Al_2O_3	18.10	18.20	18.15	16.54	16.25	16.39	17.24	16.96	17.10
FeO_t	4.90	4.93	4.92	3.53	3.52	3.52	3.76	3.79	3.78
MgO	2.71	2.77	2.74	1.89	1.71	1.80	1.92	1.94	1.93
CaO	6.42	6.52	6.47	4.71	4.70	4.71	5.38	5.37	5.38
Na_2O	4.86	4.83	4.85	4.47	4.50	4.48	4.94	4.88	4.91
K_2O	0.71	0.72	0.71	1.25	1.23	1.24	0.94	0.95	0.95
P_2O_5	0.22	0.18	0.20	0.12	0.10	0.11	0.16	0.16	0.16
TOTAL	100.00	100.00	100.00	100.00	100.00	99.99	99.99	100.00	100.01

Sample #	Ba-JM-240#52			Ba-JM-453			Ba-JM-492		
Glass #	1	2	Average	1	2	Average	1	2	Average
SiO_2	61.47	61.62	61.55	60.04	60.20	60.12	62.20	61.72	61.96
TiO_2	0.75	0.66	0.70	0.81	0.84	0.83	0.75	0.77	0.76
Al_2O_3	18.61	18.43	18.52	18.55	18.21	18.38	17.72	18.00	17.86
FeO_t	4.62	4.63	4.63	5.27	5.19	5.23	4.72	4.89	4.81
MgO	2.51	2.56	2.54	2.89	3.14	3.01	2.62	2.78	2.70
CaO	6.38	6.46	6.42	6.81	6.80	6.81	6.13	6.02	6.07
Na_2O	4.83	4.81	4.82	4.80	4.77	4.79	4.87	4.80	4.84
K_2O	0.64	0.64	0.64	0.65	0.65	0.65	0.82	0.82	0.82
P_2O_5	0.20	0.17	0.19	0.19	0.19	0.19	0.16	0.20	0.18
TOTAL	100.01	99.98	100.01	100.01	99.99	100.01	99.99	100.00	100.00

Table D-6 (continued)

Sample #	Ba-JM-528			Ba-JM-566			Ba-JM-568a		
Glass #	1	2	Average	1	2	Average	1	2	Average
SiO_2	62.16	61.60	61.88	62.11	61.99	62.05	65.25	65.75	65.50
TiO_2	0.67	0.67	0.67	0.75	0.77	0.76	0.59	0.63	0.61
Al_2O_3	18.25	18.89	18.57	17.97	17.87	17.92	17.24	16.75	17.00
FeO_t	4.49	4.41	4.45	4.77	4.93	4.85	3.97	3.97	3.97
MgO	2.34	2.32	2.33	2.61	2.65	2.63	2.04	2.02	2.03
CaO	6.23	6.31	6.27	6.19	6.16	6.17	4.74	4.82	4.78
Na_2O	4.93	4.87	4.90	4.61	4.67	4.64	4.65	4.57	4.61
K_2O	0.74	0.73	0.74	0.80	0.78	0.79	1.39	1.37	1.38
P_2O_5	0.19	0.19	0.19	0.18	0.18	0.18	0.13	0.11	0.12
TOTAL	100.00	99.99	100.00	99.99	100.00	99.99	100.00	99.99	100.00

Sample #	Ba-JM-639			Ba-JM-701			Ba-JM-737		
Glass #	1	2	Average	1	2	Average	1	2	Average
SiO_2	63.56	64.65	64.11	62.22	62.60	62.41	61.41	62.15	61.78
TiO_2	0.66	0.65	0.66	0.70	0.68	0.69	0.74	0.70	0.72
Al_2O_3	18.23	17.29	17.76	18.82	18.46	18.64	19.06	18.29	18.68
FeO	4.05	4.04	4.04	4.19	4.23	4.21	4.50	4.46	4.48
MgO	2.03	1.89	1.96	2.19	2.21	2.20	2.27	2.26	2.27
CaO	5.53	5.65	5.59	5.90	5.83	5.86	6.21	6.28	6.24
Na_2O	4.94	4.82	4.88	4.94	5.00	4.97	4.94	4.97	4.96
K_2O	0.80	0.83	0.81	0.86	0.83	0.84	0.70	0.70	0.70
P_2O_5	0.20	0.17	0.19	0.20	0.16	0.18	0.17	0.18	0.18
TOTAL	100.00	99.99	100.00	100.02	100.00	100.00	100.00	99.99	100.01

Table D-6 (concluded)

Sample #	Ba-JM-807		
Glass #	1	2	Average
SiO_2	63.98	64.39	64.19
TiO_2	0.68	0.72	0.70
Al_2O_3	17.34	16.97	17.16
FeO_t	4.20	4.19	4.19
MgO	2.53	2.45	2.49
CaO	5.32	5.40	5.36
Na_2O	4.49	4.45	4.47
K_2O	1.32	1.29	1.30
P_2O_5	0.16	0.14	0.15
TOTAL	100.02	100.00	100.01

Table D-7

Oxide Concentration and Standard Deviation (in %) of the Count-Rates of Each Element for Analyses of G-2, BCR-1, and San José Tonalite

	G-2 (11 Analyses)			
		Minimum	Maximum	Average
	Wt %	σ	σ	σ
SiO_2	69.81	0.4	0.9	0.5
TiO_2	0.50	6.3	15.4	10.9
Al_2O_3	15.64	0.8	3.5	2.0
FeO_t	2.51	2.0	4.5	3.3
MgO	0.71	2.2	6.4	4.1
CaO	1.98	2.4	4.6	3.2
Na_2O	4.17	0.9	3.0	1.9
K_2O	4.54	0.6	2.2	1.4
P_2O_5	0.13	10.2	26.0	17.5

	BCR-1 (13 Analyses)			
		Minimum	Maximum	Average
	Wt %	σ	σ	σ
SiO_2	55.40	0.3	0.9	0.5
TiO_2	2.29	3.2	6.5	4.7
Al_2O_3	13.83	0.6	4.0	2.0
FeO_t	12.40	0.7	2.2	1.4
MgO	3.37	1.4	3.9	2.3
CaO	7.14	1.1	2.0	1.6
Na_2O	3.43	1.1	2.7	1.7
K_2O	1.76	0.6	2.6	1.3
P_2O_5	0.38	3.5	10.0	6.9

	San José Tonalite (27 Analyses)			
		Minimum	Maximum	Average
	Wt %	σ	σ	σ
SiO_2	63.10	0.4	2.1	0.9
TiO_2	0.68	3.8	17.7	10.5
Al_2O_3	17.82	0.6	3.8	2.3
FeO_t	4.36	1.4	4.8	2.8
MgO	2.33	1.3	4.4	2.7
CaO	5.83	0.8	2.9	1.8
Na_2O	4.82	0.9	2.5	1.6
K_2O	0.90	0.7	2.2	1.9
P_2O_5	0.17	6.0	18.9	11.0

such as rhyolite and granite, glass inhomogeneity can be a serious problem if the glass beads are not finely powdered between the two fusion steps.

Variations in the results for individual samples from day to day and from glass to glass are slightly greater. Because oxide totals are about 50% in the glasses and must be normalized to 100%, errors in one oxide are distributed with opposite sign to all other oxides, particularly those in highest concentration. Prior to normalization, the greatest variability is in Al_2O_3, and much of the range in SiO_2 is a reflection of that in alumina. Nevertheless, in comparison to the range in the results compiled by Flanagan (1969) for the U.S.G.S. rocks, the reproducibility of the microprobe analyses is very satisfactory. The reproducibility of the San José samples is likewise very satisfactory, and both the glasses and the rock powders are obviously homogeneous.

Two additional analyses of U.S.G.S. standard rocks are presented in Table D-8 -- one of a 1:3 rock:flux mixture of BCR-1 and the other of a roughly 1:1 glass of GSP-1 (granodiorite) prepared and analyzed by L. P. Gromet. The results agree quite closely with the average composition reported for these rocks by Flanagan.

In Table D-9, microprobe results for four of the San José samples and one unrelated granite sample are compared with wet chemical analyses of the same rocks. Na_2O is consistently slightly higher, and MgO and CaO slightly lower, in the microprobe results than in the wet chemical analyses. Also, SiO_2 is generally higher and FeO lower in the microprobe analyses. However, these discrepancies are small and do not affect the petrologic conclusions reached in this study. In particular,

there is no suggestion of alkali loss during fusion or analysis; if anything, the microprobe results may be biased towards slightly high Na_2O concentrations. In any case, it is important to note that these discrepancies are small compared to the inter-laboratory scatter in the analyses compiled by Flanagan (1969) for the U.S.G.S. standards. The quality of the microprobe results appear to be excellent.

Table D-8

Additional Analyses of U.S.G.S. Standard Rocks

	GSP-1		BCR-1	
	a	b	a	b
SiO_2	68.30	68.21	55.24	55.46
TiO_2	0.68	0.71	2.30	2.28
Al_2O_3	15.13	15.32	13.88	13.83
FeO_t	4.13	3.96	12.84	12.38
MgO	0.93	0.97	3.21	3.35
CaO	2.06	2.06	7.14	7.13
Na_2O	2.82	2.92	3.21	3.42
K_2O	5.69	5.56	1.78	1.76
P_2O_5	0.28	0.29	0.40	0.39
TOTAL	100.02	100.00	100.00	100.00

Columns headed "a" give microprobe results -- one analysis each.
GSP-1 (granodiorite): Analyst - L. P. Gromet
BCR-1 (rock:flux ratio of 1:3): Analyst - J. D. Murray
Columns headed "b" give average compositions tabulated by Flanagan (1969).

Table D-9

Comparison of Microprobe and Wet Chemical Analyses of the Same Samples

	Ba-JM-25a		Ba-JM-240#52		Ba-JM-93	
	a	b	a	b	a*	b
SiO_2	61.18	60.65	61.55	61.66	65.67	64.81
TiO_2	0.78	0.80	0.70	0.74	0.55	0.60
Al_2O_3	18.15	18.13	18.52	18.31	16.66	17.55
FeO_t	4.92	5.12	4.63	4.55	3.86	3.92
MgO	2.74	2.89	2.54	2.64	1.81	1.87
CaO	6.47	6.80	6.42	6.55	5.38	5.40
Na_2O	4.85	4.71	4.82	4.74	4.94	4.75
K_2O	0.71	0.72	0.64	0.65	0.95	0.95
P_2O_5	0.20	0.17	0.19	0.15	0.17	0.14
TOTAL	100.00	99.99	100.01	99.99	99.99	99.99

	Ba-JM-46a		Gr-1A	
	a	b	a**	b
SiO_2	65.22	64.49	74.52	74.18
TiO_2	0.58	0.61	0.19	0.15
Al_2O_3	17.10	17.49	13.26	13.75
FeO_t	3.78	3.95	0.98	1.09
MgO	1.93	2.02	0.20	0.25
CaO	5.38	5.51	0.10	0.18
Na_2O	4.91	4.85	0.46	0.39
K_2O	0.95	0.94	10.26	9.98
P_2O_5	0.16	0.13	0.02	0.02
TOTAL	100.01	99.99	99.99	99.99

Columns "a" give microprobe results. Except where noted, analyses are averages of one analysis of each of two glasses.
Analyst: for GR-1A, C. M. Conway;
for all others, J. D. Murray.
Columns "b" give wet chemical results.
Analyst: S. Imai, Japan Analytical Chemistry Research Institute.

*Single analysis using 30-second rather than 60-second counting times.

**Average of two analyses of one glass.

APPENDIX E

METAMORPHIC MINERAL ASSEMBLAGES FROM THE SIERRA SAN PEDRO MÁRTIR

Minerals are listed in order of decreasing abundance. Those comprising ≥10% of the rock are capitalized; those comprising ≥1% are underlined. Abbreviations are explained on the next page.

Ba-JM-19a: QTZ-PLAG (An≈25)-BIO-alk feld-op-musc-cord (?)-ap-zir

Ba-JM-19b: QTZ-ORTH/MICR-HB-PLAG (An≥45)-ep-bio-sph-op-ap-zir (R: chl)

Ba-SPM-9: QTZ-MUSC-BIO-plag-op (R?: hem)

Ba-SPM-12d: QTZ-BIO-PLAG-MUSC-sill-cord(?)-op-zir (R: chl)

Ba-SPM-13a: QTZ-ORTH PERTH-BIO-MUSC-sill-op-tourm

Ba-SPM-13c: QTZ-ORTH-BIO-MUSC-sill-plag-op-tourm

Ba-SPM-14a: QTZ-BIO-PLAG-op-musc-alk feld (R: chl)

Ba-SPM-19a: QTZ-ORTH/MICR-bio-musc-ga-zir (R: chl)

Ba-SPM-64c: QTZ-bio-cord-musc-sill-plag-ga-op-zir (R: pin)

Locations of Samples:

Ba-JM-19a:
Ba-JM-19b: San José-Observatorio road just above the base of the western escarpment of Sierra San Pedro Mártir; ∿10 km east of Rancho San José.

Ba-SPM-9: Southwestern margin of the observatory roof pendant or septum; roughly 400 m northeast of Cienega Vallecitos on the road to the observatory.

Ba-SPM-12d: At the observatory at the eastern rim of the Sierra San Pedro Mártir; near the middle of the observatory pendant or septum.

Ba-SPM-13a:
Ba-SPM-13c: Roughly 0.5 km west of the observatory, near the center of the observatory pendant or septum.

Ba-SPM-14a: Cañon Venado Blanco 5 km northwest of the observatory; near the center of the observatory pendant or septum.

APPENDIX E (continued)

Location of samples (continued)

Ba-SPM-19a: Cañon Tinaja about 6.5 km northwest of the observatory; western margin of the observatory pendant or septum.

Ba-SPM-64c: Roughly 1.5 km east of Alcatraz; about 1.3 km southeast of Cienaga La Grulla.

Abbreviations:

Alk feld:	alkali feldspar
micr:	microcline
orth:	orthoclase
orth perth:	orthoclase perthite
An:	anorthite content of plagioclase
ap:	apatite
bio:	biotite
chl:	chlorite
cord:	cordierite
ep:	epidote
ga:	garnet
hem:	hematite
hb:	hornblende
musc:	muscovite
op:	opaque
pin:	pinite
plag:	plagioclase
qtz	quartz
R:	retrograde mineral
sill:	sillimanite
sph:	sphene
tourm:	tourmaline
zir:	zircon

APPENDIX F

COMPARISON OF CALCULATED DENSITIES OF PLAGIOCLASE AND MAGMA IN THE SERIATE PORPHYRITIC TONALITE

The room-temperature density of plagioclase having the composition of the large crystals in the SPT ($\sim An_{40}$ if the late-crystallizing sodic rims are excluded) is 2.67 gm/cc (Deer et al., 1966, Figure 122). According to Skinner (1966), thermal expansion increases the volume of plagioclase of composition An_{44} by 1.32% at 800°C and 1.75% at 1000°C. The corresponding densities are 2.63 and 2.62, respectively.

Very little data are available on the density of natural magmas Murase and McBirney (1973) reported measurements on a recent andesite flow from Mount Hood, Oregon. Their data, measured in air in the temperature range 800-1500°C, are believed to be accurate to ±0.5%. At 800°C, ρ = 2.50; at 1000°C, ρ = 2.45. Because the composition of the Mount Hood sample is similar to, although slightly more mafic than, the average composition of the SPT (Table F-1), the low-pressure density of an SPT magma should be comparable or perhaps slightly lower. The compressibilities of plagioclase and of natural and synthetic rock glasses are sufficiently small and similar that they can be neglected for pressures <10 kb (Birch, 1966). These data suggest that plagioclase should have tended to sink, rather than float, in the SPT magma if gravitational separation was at all significant.

Table F-1

Comparison of Mount Hood Andesite with Average Seriate Porphyritic Tonalite from the San José Pluton

	Mount Hood Andesite*	Seriate Porphyritic Tonalite
SiO_2	61.08	62.58
TiO_2	0.93	0.69
Al_2O_3	17.57	18.19
FeO_t	5.81	4.30
MnO	0.10	0.07
MgO	3.37	2.25
CaO	5.56	5.98
Na_2O	4.25	4.98
K_2O	1.18	0.79
P_2O_5	0.16	0.18
TOTAL	100.01	100.01

*Reported by Murase and McBirney (1973); Analyst - K. Aoki. Normalized to 10 oxides totaling 100%.

APPENDIX G

MODAL MINERAL COMPOSITIONS OF ADJACENT PLUTONS

Table G-1

Modal Mineral Analyses of Tonalite from the Potrero Pluton

Sample Number	Ba-JM 76	Ba-JM 77a	Ba-JM 78b	Ba-JM 79	Ba-JM 80	Ba-JM 891b	Ba-JM 892	Ba-JM 893	Ba-JM 894
Quartz	17.96	20.08	18.69	18.29	18.58	20.96	14.40	14.20	16.61
Plagioclase	66.67	60.14	58.18	58.45	61.38	57.85	65.84	60.68	61.95
K-feldspar	0.23	0.20	0.00	0.31	0.18	0.05	0.05	0.08	0.00
Hornblende	5.52	8.03	12.15	4.34	10.20	11.12	11.15	13.90	7.51
Biotite	5.87	9.64	4.44	11.94	5.74	8.09	6.24	8.08	10.63
Opaque	0.59	0.50	0.23	1.09	1.09	0.52	0.57	1.05	0.54
Sphene	0.47	0.00	0.23	0.62	0.36	0.05	0.05	0.04	0.09
Epidote	0.94	0.10	0.93	2.17	0.18	0.38	0.05	0.34	0.50
Apatite	0.00	0.30	0.23	0.16	0.18	0.09	0.31	0.46	0.27
Chlorite	0.59	0.30	1.64	1.09	0.91	0.47	0.26	0.54	0.59
Pale Amphibole[a]	0.00	0.00	0.00	0.00	0.00	0.00	0.00	0.00	0.05
White Mica + Clay[b]	0.70	0.60	3.04	1.40	1.18	0.43	0.88	0.63	0.90
Other	0.47	0.10	0.23	0.16	0.00	0.00	0.20	0.00	0.37
TOTAL	100.01	99.99	99.99	100.02	99.98	100.01	100.02	100.00	100.01
Color Index (CI)	13.98	18.57	19.62	21.25	18.48	20.63	18.42	23.95	19.96
Pl + Alteration	67.37	60.74	61.22	59.85	62.56	58.28	66.72	61.31	62.85
Amph/(Bio + Chl)	0.85	0.81	2.00	0.33	1.53	1.30	1.72	1.61	0.67
Number of Points	852	996	428	645	1098	2114	1938	2388	2210
Area (mm^2)	408	478	205	310	527	761	698	860	796

[a]Cummingtonitic and actinolitic amphibole.

[b]Mostly alteration of plagioclase; includes some fine-grained unidentified alteration.

Table G-1 (continued)

Sample Number	Ba-JM 900	Ba-JM 905	Ba-JM 906	Ba-JM 907	Ba-JM 908a	Pluton Average[c]
Quartz	19.14	21.87	24.07	17.31	17.11	18.35
Plagioclase	59.67	62.47	58.27	59.65	63.61	61.12
K-feldspar	0.10	0.16	0.20	0.04	0.09	0.10
Hornblende	7.36	3.13	3.00	7.33	9.23	8.28
Biotite	9.47	6.86	10.13	11.42	7.32	8.56
Opaque	0.60	0.05	0.46	0.67	0.65	0.61
Sphene	0.20	0.27	0.31	0.51	0.14	0.21
Epidote	0.90	1.30	1.48	0.93	0.23	0.67
Apatite	0.30	0.27	0.15	0.29	0.14	0.24
Chlorite	0.75	0.38	0.81	0.59	0.60	0.60
Pale Amphibole[a]	0.00	0.00	0.00	0.00	0.05	0.01
White Mica + Clay[b]	1.35	2.00	1.06	1.18	0.74	1.03
Other	0.15	1.24	0.05	0.08	0.10	0.22
TOTAL	99.99	100.00	99.99	100.00	100.01	100.00
Color Index (CI)	19.33	11.99	16.19	21.49	18.27	18.94
Pl + Alteration	61.02	64.47	59.33	60.83	64.35	62.15
Amph/(Bio + Chl)	0.72	0.43	0.27	0.61	1.17	0.91
Number of Points	1996	1852	1965	2374	2157	23013
Area (mm^2)	719	667	707	855	777	8768

[a]Cummingtonitic and actinolitic amphibole.

[b]Mostly alteration of plagioclase; includes some fine-grained unidentified alteration.

[c]Calculated on the basis of the combined number of points in all thin sections.

Table G-2

Modal Mineral Analyses of Quartz Diorite from the Willow Creek Pluton

Sample Number	Ba-JM 172a	Ba-JM 495	Pluton Average[c]
Quartz	7.83	7.05	7.43
Plagioclase	63.43	65.90	64.71
K-feldspar	0.14	0.20	0.17
Hornblende	16.29	17.64	16.99
Biotite	4.69	3.85	4.26
Opaque	2.10	1.31	1.69
Sphene	0.91	0.20	0.54
Epidote	1.12	1.37	1.25
Apatite	0.35	0.00	0.17
Chlorite	1.68	0.85	1.25
Pale Amphibole[a]	0.00	0.00	0.00
White Mica + Clay[b]	1.26	1.50	1.38
Other	0.21	0.13	0.17
TOTAL	100.01	100.00	100.01
Color Index (CI)	26.79	25.22	25.98
Pl + Alteration	64.69	67.40	66.09
Amph/(Bio + Chl)	2.56	3.75	3.08
Number of Points	1430	1531	2961
Area (mm^2)	686	735	1421

[a]Cummingtonitic and actinolitic amphibole.

[b]Mostly alteration of plagioclase; includes some fine-grained unidentified alteration.

[c]Calculated on the basis of the combined number points in both thin sections.

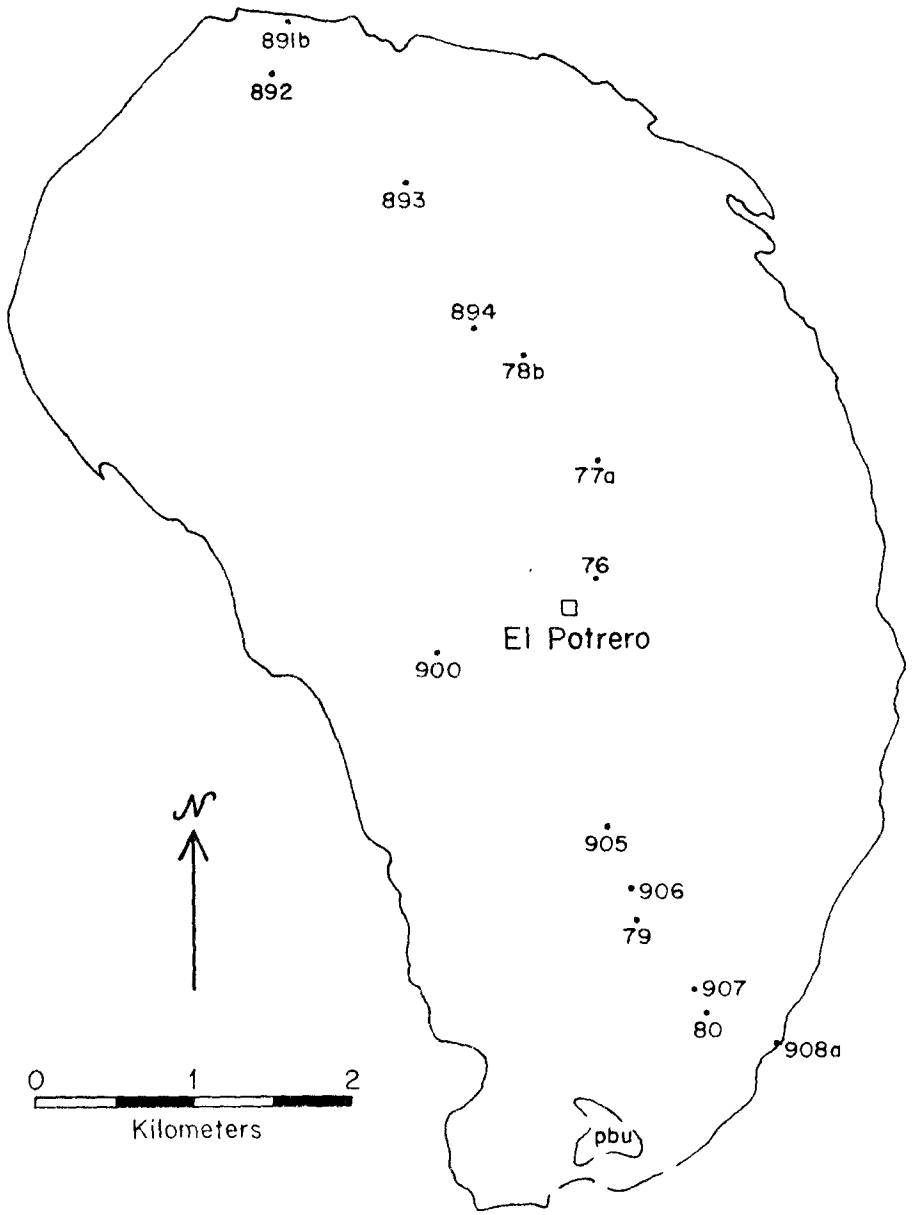

Figure G-1. Outline map of the Potrero pluton showing the locations of samples analyzed for modal mineral composition. The rocks are biotite-hornblende and hornblende-biotite tonalites similar to the San José tonalite, but with a more pronounced seriate porphyritic texture. The proportions of quartz and non-opaque accessories (mainly sphene, epidote, apatite, and zeolite) and the quartz/plagioclase ratio generally increase from north to south through the interior of the body, whereas the hornblende content, color index, and amphibole/(biotite + chlorite) ratio generally decrease.

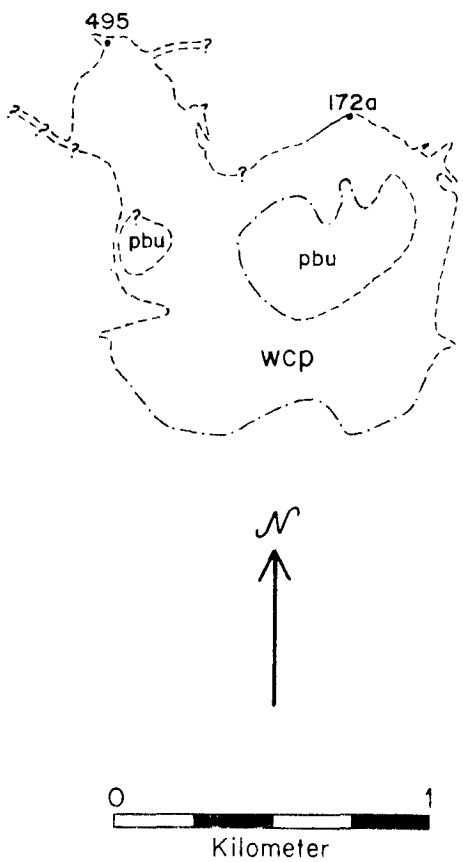

Figure G-2. Outline map of the Willow Creek pluton showing the locations of samples analyzed for modal mineral composition. The entire body appears to consist of hornblende-biotite quartz diorite similar to the analyzed samples, but exposures are scarce and generally deeply weathered. The body appears to be a ring structure at the roof of a small pluton. The ring geometry resulted from intrusion along the intersecting planes of bedding (northeast-southwest) and regional fracture systems (primarily northwest-southeast, subparallel to the Willow Creek fault zone) rather than by intrusion along arcuate fractures.